

ANL-85-51

ANL-85-51

**FLOW-INDUCED VIBRATION OF
CIRCULAR CYLINDRICAL STRUCTURES**

by

Shoei-Sheng Chen

BASE TECHNOLOGY



MASTER

ARGONNE NATIONAL LABORATORY, ARGONNE, ILLINOIS

Operated by THE UNIVERSITY OF CHICAGO

for the U. S. DEPARTMENT OF ENERGY

under Contract W-31-109-Eng-38

Distribution Category:
LMFBR--Components: Base
Technology (UC-79k)

ANL-85-51

ANL--85-51

DE86 003981

ARGONNE NATIONAL LABORATORY
9700 South Cass Avenue
Argonne, Illinois 60439

FLOW-INDUCED VIBRATION OF
CIRCULAR CYLINDRICAL STRUCTURES

by

Shoei-Sheng Chen

Components Technology Division

DISCLAIMER

This report was prepared as an account of work sponsored by an agency of the United States Government. Neither the United States Government nor any agency thereof, nor any of their employees, makes any warranty, express or implied, or assumes any legal liability or responsibility for the accuracy, completeness, or usefulness of any information, apparatus, product, or process disclosed, or represents that its use would not infringe privately owned rights. Reference herein to any specific commercial product, process, or service by trade name, trademark, manufacturer, or otherwise does not necessarily constitute or imply its endorsement, recommendation, or favoring by the United States Government or any agency thereof. The views and opinions of authors expressed herein do not necessarily state or reflect those of the United States Government or any agency thereof.

June 1985

CONTENTS

	<u>Page</u>
FIGURES.....	9
TABLES.....	19
NOMENCLATURE.....	21
ACKNOWLEDGMENTS.....	27
CREDITS.....	28
ABSTRACT.....	33
1. INTRODUCTION.....	1-1
1.1 Examples of Flow-Induced Vibration Problems.....	1-2
1.2 Nondimensional Parameters.....	1-5
1.3 Fluid-Force Components.....	1-8
1.4 Mechanisms of Flow-Induced Vibration.....	1-12
References--Sec. 1.....	1-16
2. A SINGLE CYLINDER IN QUIESCENT FLUID.....	2-1
2.1 Introduction.....	2-1
2.2 A Simple Example--A Single Circular Cylinder Oscillating in an Infinite Perfect Fluid.....	2-i
2.3 A Circular Cylinder Near a Wall.....	2-5
2.4 A Circular Cylinder in an Annular Region of Compressible Inviscid Fluid.....	2-7
2.5 A Circular Cylinder in an Infinite Compressible Inviscid Fluid.....	2-10
2.6 A Circular Cylinder in a Concentric Annular Incompressible Viscous Fluid.....	2-17
2.7 A Circular Cylinder in an Eccentric Annular Incompressible Viscous Fluid.....	2-27
2.8 A Circular Cylinder in a Concentric Annular Two-Phase Flow...	2-27
2.9 Free Vibration of a Circular Cylinder Supported at Both Ends in a Fluid.....	2-29
2.10 Nonlinear Effects of a Circular Cylinder Oscillating in an Infinite Fluid.....	2-34
2.11 Three-Dimensional Effect on a Circular Cylinder Oscillating in Fluid.....	2-35

2.12	A Circular Cylinder in a Finite-Length Annular Viscous Region.....	2-36
2.13	Examples of Applications.....	2-39
2.14	Closing Remarks.....	2-46
	References--Sec. 2.....	2-47
3.	MULTIPLE CYLINDERS IN QUIESCENT FLUID.....	3-1
3.1	Introduction.....	3-1
3.2	A Simple Example--Two Parallel Circular Cylinders Oscillating in an Infinite Perfect Fluid.....	3-2
3.2.1	Equations of Motion.....	3-2
3.2.2	Free Vibration.....	3-5
3.3	Added Mass Matrices for a Group of Cylinders Oscillating in a Fluid Based on the Two-Dimensional Potential Flow Theory....	3-8
3.3.1	Formulation and Solution	3-8
3.3.2	Reciprocal Relations.....	3-14
3.3.3	Coordination Transformation.....	3-17
3.3.4	Composite Motion of Cylinder Array.....	3-20
3.3.5	Numerical Examples.....	3-22
3.4	Dynamics of a Group of Cylinders in a Perfect Fluid.....	3-23
3.4.1	Equations of Motion.....	3-23
3.4.2	Free Vibration.....	3-30
3.4.3	Forced Vibration.....	3-34
3.5	Natural Frequencies of a Group of Identical Continuous Cylinders Vibrating in a Fluid.....	3-38
3.5.1	Natural Frequencies of a Cylinder on Multiple Supports with Equal Spans.....	3-38
3.5.2	Natural Frequencies of an Array of Cylinders on Multiple Supports in Fluid.....	3-44
3.6	Two Coaxial Cylinders Coupled by a Perfect Fluid.....	3-46
3.6.1	Statement of the Problem.....	3-46
3.6.2	Frequency Equation.....	3-49
3.7	Two Coaxial Circular Cylinders Separated by Viscous Fluid.....	3-54
3.7.1	Added Mass and Fluid Damping Matrices.....	3-54
3.7.2	Vibration of Two Coaxial Tubes.....	3-60
3.8	Added Mass and Damping of an Array of Cylinders in a Compressible Inviscid Fluid.....	3-67
3.9	Added Mass and Damping of an Array of Cylinders in an Incompressible Viscous Fluid.....	3-72
3.10	Closing Remarks.....	3-73
	References--Sec. 3.....	3-74
4.	CIRCULAR CYLINDRICAL SHELLS CONTAINING FLUID.....	4-1
4.1	Introduction.....	4-1

4.2	Free Vibration of Circular Cylindrical Shells in Air.....	4-1
4.3	Free Vibration of Circular Cylindrical Shells Containing Compressible Inviscid Fluid.....	4-5
4.4	Dynamics of Two Shells Coupled by a Compressible Inviscid Fluid.....	4-12
4.5	Two Shells Coupled by Viscous Fluid.....	4-23
4.6	Closing Remarks.....	4-33
	References--Sec. 4.....	4-34
5.	PIPES CONVEYING FLUID.....	5-1
5.1	Introduction.....	5-1
5.2	Hamilton's Principle for Pipes Conveying Fluid.....	5-1
5.3	Straight Pipes Conveying Fluid.....	5-6
5.3.1	Equations of Motion.....	5-6
5.3.2	Free Vibration and Stability Analysis.....	5-13
5.3.3	Frequency Characteristics.....	5-19
5.3.4	Stability Boundaries.....	5-27
5.3.5	Effects of Various Parameters.....	5-34
5.3.6	Experimental Studies.....	5-40
5.4	Curved Pipes.....	5-51
5.4.1	Equations of Motion.....	5-51
5.4.2	Out-of-Plane Vibration and Stability Analysis.....	5-56
5.4.3	In-plane Vibration and Stability.....	5-67
5.5	Circular Cylindrical Shells Conveying Fluid.....	5-73
5.6	Closing Remarks.....	5-74
	References--Sec. 5.....	5-75
6.	CIRCULAR CYLINDERS IN AXIAL FLOW.....	6-1
6.1	Introduction.....	6-1
6.2	Equation of Motion of a Circular Cylinder in Axial Flow.....	6-1
6.3	Analysis for a Single Cylinder in Axial Flow.....	6-9
6.4	Dynamic Behavior.....	6-16
6.5	Nearfield Flow Noise.....	6-22
6.6	Cylinder Response to Nearfield Flow Noise.....	6-36
6.7	Empirical Correlations for Subcritical Vibration.....	6-41
6.8	Effects of Different Flow Conditions.....	6-45
6.8.1	Fluid Compressibility.....	6-45
6.8.2	Towed Cylinders.....	6-45
6.8.3	Pulsating Flow.....	6-46
6.8.4	Combined Internal and External Flows.....	6-46
6.8.5	Confined Region.....	6-46

6.8.6	Two-Phase Flow.....	6-47
6.9	Multiple Cylinders in Axial Flow.....	6-47
6.9.1	Equations of Motion of a Group of Circular Cylinders in Axial Flow.....	6-48
6.9.2	Dynamic Characteristics of an Array of Cylinders in Axial Flow.....	6-49
6.10	Leakage Flow-Induced Vibration.....	6-51
6.11	Closing Remarks.....	6-54
	References--Sec. 6.....	6-58
	A SINGLE CYLINDER IN CROSSFLOW.....	7-1
7.1	Introduction.....	7-1
7.2	Flow Regimes.....	7-1
7.3	Strouhal Number.....	7-5
7.4	Steady Fluid-Force Coefficients.....	7-10
7.5	Fluctuating Fluid-Force Coefficients.....	7-14
7.6	High Reynolds Numbers.....	7-20
7.7	Turbulent Excitation.....	7-20
7.8	Equations of Motion in Crossflow.....	7-29
7.9	Response of a Circular Cylinder in Crossflow.....	7-34
7.10	Prediction Methods for Lock-in Responses.....	7-44
7.10.1	Lock-in Region for In-line Vibration.....	7-44
7.10.2	Lock-in Region for Crossflow Vibration.....	7-48
7.11	Effects of Different System Parameters.....	7-55
7.12	Response of Circular Cylindrical Shells in Crossflow.....	7-59
7.13	Closing Remarks.....	7-61
	References--Sec. 7.....	7-63
8.	AN ARRAY OF CIRCULAR CYLINDERS IN CROSSFLOW.....	8-1
8.1	Introduction.....	8-1
8.2	Flow Regimes.....	8-3
8.3	Vortex Shedding Frequency.....	8-3
8.4	Pressure and Flow Velocity Distributions.....	8-7
8.5	Fluid Excitation Force Coefficients.....	8-10
8.6	Analysis of Flow-Induced Vibration.....	8-22
8.7	Response of Cylinder Arrays.....	8-28

8.8	Acoustic Resonance.....	8-35
8.8.1	Propagation of Sound Waves along Fluid Cylinders.....	8-35
8.8.2	Criteria for Acoustic Resonance.....	8-39
8.8.3	Avoidance of Acoustic Resonances.....	8-41
8.9	Closing Remarks.....	8-41
	References--Sec. 8.....	8-42
9.	TWO CYLINDERS IN CROSSFLOW.....	9-1
9.1	Introduction.....	9-1
9.2	Fluid-Force Components.....	9-1
9.3	Flow Regimes.....	9-3
9.3.1	Two Cylinders Side-by-Side.....	9-3
9.3.2	Two Cylinders in Tandem.....	9-13
9.3.3	Two Cylinders in Staggered Arrangement.....	9-22
9.4	Response of Two Cylinders in Flow.....	9-24
9.4.1	Two Cylinders Side by Side.....	9-26
9.4.2	Two Cylinders in Tandem.....	9-35
9.5	Wake-induced Flutter.....	9-43
9.5.1	Motion-dependent Fluid Forces on the Downstream Cylinder.....	9-43
9.5.2	Stability Analysis.....	9-50
9.6	Interference Galloping.....	9-52
9.7	Closing Remarks.....	9-56
	References--Sec. 9.....	9-57
10.	FLUIDELASTIC INSTABILITY OF A GROUP OF CIRCULAR CYLINDERS IN CROSSFLOW.....	10-1
10.1	Introduction.....	10-1
10.2	Definition of Critical Flow Velocity and System Parameters..	10-1
10.3	Empirical Stability Criteria.....	10-6
10.4	Mathematical Models.....	10-10
10.5	Fluid Force Coefficients.....	10-12
10.6	Prediction of the Critical Flow Velocity	
10.6.1	Analysis.....	10-21
10.6.2	Two Instability Mechanisms.....	10-27
10.6.3	Numerical Examples.....	10-28
10.6.4	Comparison of Theoretical and Experimental Results..	10-36
10.7	Stability Maps.....	10-41
10.7.1	A Row of Cylinders.....	10-49
10.7.2	Square Array (90°).....	10-49
10.7.3	Rotated Square Array (45°).....	10-50
10.7.4	Triangular Array (30°).....	10-50

10.7.5	Rotated Triangular Arrays (60°).....	10-50
10.8	Effect of Various Parameters on Dynamic Instability.....	10-51
10.8.1	Detuning.....	10-51
10.8.2	Upstream Turbulence.....	10-53
10.8.3	Nonuniform Flow Distribution.....	10-54
10.8.4	Tube Location.....	10-55
10.9	Closing Remarks.....	10-55
	References--Sec. 10.....	10-57
11.	DESIGN CONSIDERATIONS.....	11-1
11.1	Introduction.....	11-1
11.2	Assessment of Flow-Induced Vibration.....	11-1
11.3	Methods of Suppressing Vibration.....	11-3
11.4	Closing Remarks.....	11-6
	References--Sec. 11.....	11-7
	APPENDIX A: VIBRATION OF DAMPED LINEAR SYSTEMS.....	A-1
A.1	Classical Normal Modes.....	A-1
A.2	Forced Vibration of System with Classical Normal Modes.....	A-2
A.3	Forced Vibration of System with Nonclassical Normal Modes....	A-3
	APPENDIX B: GENERAL FLUID EQUATIONS.....	B-1
B.1	Incompressible Fluid.....	B-2
B.2	Linearized Compressible Viscous Fluid.....	B-3
B.3	Linearized Incompressible Fluid Equations.....	B-4
B.4	Linearized Compressible Inviscid Fluid.....	B-4
	APPENDIX C: CHARACTERISTIC EQUATIONS, EIGENFUNCTIONS, AND ADJOINT EIGENFUNCTIONS.....	C-1
	APPENDIX D: AMASS--FLUID DYNAMIC MASS COEFFICIENTS OF A GROUP OF CIRCULAR CYLINDERS IN A FLUID.....	D-1

FIGURES

<u>Figure</u>		<u>Page</u>
1.1	Steam Generator Tube Bank Damaged by Vibration	1-4
1.2	Tube Arrangements.....	1-6
1.3	A Group of Cylinders in Flow.....	1-11
2.1	A Circular Cylinder Oscillating in an Infinite Perfect Fluid	2-2
2.2	Added Mass Coefficients for a Cylinder Vibrating Near a Wall	2-6
2.3	A Circular Cylinder Vibrating in a Compressible Fluid Annulus	2-8
2.4	Added Mass Coefficient for a Circular Cylinder Inside a Compressible Fluid Annulus.....	2-12
2.5	Acoustically Induced Vibration of a Circular Cylinder.....	2-13
2.6	Added Mass Coefficient and Fluid Damping Coefficient for a Circular Cylinder in a Compressible Inviscid Fluid.....	2-18
2.7	Fluid Radiation Damping at Resonance.....	2-19
2.8	Real Values of H as a Function of Diameter Ratio and Kinetic Reynolds Number.....	2-24
2.9	Imaginary Values of H as a Function of Diameter Ratio and Kinetic Reynolds Number.....	2-25
2.10	Real and Imaginary Values of H for a Cylinder Vibrating in an Infinite Incompressible Viscous Fluid.....	2-26
2.11	Added Mass and Damping Coefficients as a Function of Eccentricity.....	2-28
2.12	Effective Density for Two-phase Flow as a Function of Void Fraction.....	2-30
2.13	Two-phase Flow Damping Coefficient.....	2-31
2.14	A Circular Cylinder Vibrating in a Fluid.....	2-32
2.15	Three-dimensional Effect on the Added Mass Coefficient.....	2-37
2.16	A Circular Cylinder in a Fluid-filled Annular Region.....	2-38
2.17	Real and Imaginary Values of H for a Cylinder Vibrating in a Finite-length Annular Viscous Fluid.....	2-40
2.18	A Simply Supported Tube with a Baffle Plate Support.....	2-41

2.19	Different Modes for a Tube with Motion-limiting Gap.....	2-45
3.1	Two Parallel Circular Cylinders Vibrating in a Fluid.....	3-3
3.2	Four Normal Modes of Two Identical Cylinders Vibrating in a Fluid.....	3-9
3.3	A Group of N Circular Cylinders Vibrating in a Fluid.....	3-10
3.4	Coordination Transformation.....	3-18
3.5	Theoretical and Experimental Values of Added-mass Coefficients α_{11} and β_{11} for Seven and Nine Cylinders	3-24
3.6	Tube Bank Arranged in a Hexagonal Pattern.....	3-25
3.7	Added-mass Coefficients as Functions of Pitch-to-diameter Ratio.....	3-26
3.8	Upper and Lower Bounds of Effective Added-mass Coefficients as Functions of Pitch-to-diameter Ratio.....	3-27
3.9	A Group of Circular Cylinders Vibrating in a Fluid.....	3-28
3.10	Frequency Bands for an Array of Cylinders in Fluid.....	3-33
3.11	Normal Modes of Three and Four Identical Cylinders Vibrating in a Fluid.....	3-35
3.12	Natural Frequencies of a Group of Three Cylinders as a Function of Pitch Ratio.....	3-36
3.13	Transient Response of a Tube Bank.....	3-37
3.14	Steady-state Response of a Row of Five Tubes to Excitation of Tube 5 in the y Direction.....	3-39
3.15	A Continuous Cylinder with Intermediate Supports.....	3-40
3.16	Propagation Constant for a Periodically Supported Cylinder...	3-42
3.17	Propagation Constant and Frequency Curves for a Cylinder, First and Second Propagation Bands.....	3-43
3.18	Frequency Factor of a Four-span Cylinder Hinged at the Two Extreme Ends.....	3-45
3.19	A Cylindrical Rod Coupled to a Cylindrical Shell by a Perfect Fluid.....	3-47
3.20	Dimensionless Natural Frequency as a Function of the Uncoupled Frequency Ratio	3-56

3.21	Mode Shapes of Two Coupled Cylinders.....	3-57
3.22	Natural Frequencies of Two Coaxial Tubes as a Function of Fluid Gap.....	3-63
3.23	Modal Damping Ratio of Two Coaxial Tubes as a Function of Fluid Gap.....	3-65
3.24	Comparison of Natural Frequency and Modal Damping Ratio of Coupled Modes for Different Scale Models for $\zeta_{vj} = 0.01$	3-66
4.1	Vibration Form for Circular Cylindrical Shells.....	4-4
4.2	Frequency Spectra of Empty and Fluid-filled Shells for $n = 0$, $\delta = 0.01$, $\rho_s R/\rho h = 12.8$, and $\gamma = 0.257$	4-7
4.3	Frequency Spectra of Empty and Fluid-filled Shells for $n = 1$, $\delta = 0.01$, $\rho_s R/\rho h = 12.8$, and $\gamma = 0.257$	4-8
4.4	Amplitude Ratios of a Fluid-filled Shell for $n = 0$, $\delta = 0.01$, $\rho_s R/\rho h = 12.8$ and $\gamma = 0.257$	4-9
4.5	Values of the Added Mass Coefficient for $n = 1$ to 5.....	4-13
4.6	Two Circular Cylindrical Shells Coupled by a Fluid.....	4-14
4.7	Natural Frequencies of Out-of-phase and In-phase Modes of a Coupled Shell System and Related Cases.....	4-22
5.1	Definition of Control Volume R under Specified Conditions....	5-3
5.2	A Cantilevered Pipe Conveying Fluid.....	5-5
5.3	A Pipe Conveying Fluid.....	5-8
5.4	A Vertical Pipe Conveying Fluid and Forces and Moments Acting on Elements of the Fluid and Pipe.....	5-12
5.5	Nonconservative and Gyroscopic Conservative Systems.....	5-14
5.6	Real and Imaginary Components of Dimensionless Frequency Ω as Functions of Dimensionless Flow Velocity for the Lowest Three Modes of a Pipe with $\beta = 0.1$	5-20
5.7	Real and Imaginary Components of Dimensionless Frequency Ω as Functions of Dimensionless Flow Velocity for the Lowest Three Modes of a Pipe with $\beta = 0.8$	5-21
5.8	Dimensionless Complex Frequency of a Pipe Fixed at the Upstream End and Supported by a Spring at the Downstream End for $\bar{a} = 10$, $\beta = 0.2$	5-23
5.9	Dimensionless Complex Frequency of a Pipe Fixed at the Upstream End and Supported by a Spring at the Downstream End for $\bar{a} = 100$, $\beta = 0.6$	5-24

5.10	Coriolis Force for Gyroscopic Conservative and Non-conservative Systems.....	5-26
5.11	Variation of Amplitudes of Fundamental and Second Modes during a Period of Oscillation.....	5-28
5.12	Fundamental Natural Frequency vs. Nondimensional Flow Velocity.....	5-30
5.13	Dimensionless Critical Flow Velocity as a Function of β for a Cantilevered Pipe.....	5-31
5.14	Dimensionless Critical Frequency as a Function of β for a Cantilevered Pipe.....	5-32
5.15	Mode Shape for Flutter of a Cantilevered Pipe for $\beta = 0.4$ (fractions indicate time period).....	5-33
5.16	Pipe Fixed at Upstream End and Supported by Rotational Spring and Displacement Spring at Downstream End.....	5-36
5.17	Stability Maps in $\bar{\alpha} - v^2$ plane.....	5-37
5.18	Stability Map in $\bar{\alpha} - \bar{\beta}$ Plane.....	5-39
5.19	Static Deformation Shapes for a Polyethylene Tube.....	5-43
5.20	Displacement and Dominant Response Frequency of an Excited Polyethylene Tube.....	5-44
5.21	Displacement and Dominant Response Frequency of an Unexcited Polyethylene Tube.....	5-45
5.22	Critical Flow Velocities for a Pipe Fixed at the Upstream End and a Knife-Edge Support Movable along the Pipe.....	5-47
5.23	Static Deformation Shapes for a Polyethylene Tube.....	5-48
5.24	Flutter Modes of a Polyethylene Tube.....	5-49
5.25	Time History of Tube Oscillations at Various Velocities for a Polyethylene Tube.....	5-50
5.26	Definition of Coordinates and Displacements of a Uniformly Curved Pipe Conveying Fluid.....	5-52
5.27	Natural Frequency of a Fixed-Fixed Pipe as a Function of Flow Velocity.....	5-61
5.28	Complex Frequencies of a Fixed-Free Pipe.....	5-62
5.29	Dimensionless Critical Flow Velocities Under Fixed-Fixed Conditions.....	5-63

5.30	Dimensionless Critical Flow Velocities Under Hinged-Hinged Conditions.....	5-64
5.31	Dimensionless Critical Flow Velocities Under Fixed-Hinged Conditions.....	5-65
5.32	Dimensionless Critical Flow Velocities and Associated Frequencies as Functions of Mass Ratio β for a Cantilevered Pipe.....	5-66
5.33	Dimensionless Critical Flow Velocities for Fixed-Fixed Pipes.....	5-71
5.34	Asymmetric and Symmetric Mode Shapes for $\alpha/2\pi = 0.8$ for Fixed-Fixed Pipes.....	5-72
6.1	Circular Cylinder in Axial Flow.....	6-2
6.2	Forces and Moments Acting on an Element of the Cylinder.....	6-3
6.3	Complex Frequencies of the First Three Modes of a Hinged-Hinged Cylinder in Axial Flow.....	6-18
6.4	Complex Frequencies of the First Three Modes of a Cantilevered Cylinder in Axial Flow.....	6-19
6.5	Second-mode Flutter of Fixed-Free Cylinder and Pinned-Pinned Cylinder in Axial Flow.....	6-20
6.6	Fundamental Natural Frequency of Fixed-Fixed Rods.....	6-24
6.7	Fundamental Natural Frequency of Fixed-Free Cylinders.....	6-25
6.8	Modal Damping Ratio of Fixed-Fixed Cylinders.....	6-26
6.9	Modal Damping Ratio of Fixed-Free Cylinders.....	6-27
6.10	Circular Cylinder Subject to Turbulent Pressure Fluctuations	6-28
6.11	Dependence of Convection Velocity on Dimensionless Frequency	6-30
6.12	Magnitude of Longitudinal Cross-spectral Density of Turbulent Wall Pressure.....	6-31
6.13	Magnitude of Lateral Cross-spectral Density of Turbulent Wall Pressure.....	6-32
6.14	Turbulent Wall Pressure Power Spectra.....	6-33
6.15	Nondimensional Nearfield Turbulent Wall Pressure Power Spectra.....	6-35

6.16	RMS Displacement of Fixed-Fixed Cylinders at Midspan.....	6-38
6.17	RMS Displacement of Cantilevered Rods 2 ft from Fixed End....	6-39
6.18	Typical Probability Density Representation of Displacement of Flexible Cylinder Vibrating in Parallel-flowing Fluid.....	6-40
6.19	Agreement Between Measured and Predicted Amplitudes of Vibration According to Paidoussis' Empirical Expression.....	6-44
6.20	Buckling Modes of Four- and Three-cylinder Systems.....	6-50
6.21	Generation of Positive and Negative Damping in Leakage Flow.....	6-52
6.22	Leakage Flow Geometries.....	6-53
6.23	Vibration Modes.....	6-55
6.24	Limit Cycle of Unstable Motion.....	6-56
7.1	Regimes of Flow Across a Circular Cylinder.....	7-2
7.2	Flow Regimes.....	7-3
7.3	Typical Traces in a Karman Vortex Street Behind a Circular Cylinder.....	7-7
7.4	A Pattern of Vortices in the Clouds Downstream from the Island of Guadalupe, West of Baja California.....	7-8
7.5	Envelope of Strouhal/Reynolds Number Relationship for Circular Cylinders.....	7-9
7.6	Drag Coefficient for a Circular Cylinder in Crossflow.....	7-11
7.7	Ratio of Vibrating to Stationary Cylinder Drag Coefficient...	7-13
7.8	Fluctuating Lift Coefficients versus Amplitudes of Oscillation.....	7-17
7.9	Fluctuating Drag Coefficients vs. Amplitudes of Oscillation.....	7-18
7.10	Correlation Coefficient for Fluctuating Pressures Measured on a Cylinder.....	7-21
7.11	RMS Lift Coefficient, Strouhal Number and Steady Drag Coefficient at High Reynolds Numbers.....	7-22
7.12	Power Spectra of the Lift Fluctuations at Various Reynolds Numbers.....	7-23

7.13	Steady Drag Force Coefficient as a Function of Reynolds Number for Various Turbulence Intensities.....	7-25
7.14	Fluctuating Drag Coefficient as a Function of Reynolds Number for Various Turbulence Intensities.....	7-26
7.15	Fluctuating Lift Coefficient as a Function of Reynolds Number for Various Turbulence Intensities.....	7-27
7.16	Strouhal Number as a Function of Reynolds Number for Various Turbulence Intensities.....	7-28
7.17	Drag and Lift Force Components Acting on a Cylinder.....	7-30
7.18	Tube Displacement and Spectral Density of Tube Displacement in Water.....	7-36
7.19	Tube Response Characteristics.....	7-37
7.20	Vortex-excited Displacement of a Cylinder in the In-line Direction.....	7-39
7.21	Symmetric and Alternate Vortex Shedding.....	7-40
7.22	Oscillation Characteristics for a Circular Cylinder.....	7-42
7.23	Lift Coefficient vs. Reduced Flow Velocity for Forced Oscillation of a Circular Cylinder.....	7-43
7.24	Response Amplitude of a Cylinder in In-Line Direction.....	7-49
7.25	Synchronization Range in Crossflow Direction.....	7-52
7.26	Response Amplitude of a Cylinder in Crossflow Direction.....	7-53
7.27	Maximum Vortex-excited Crossflow Displacement Amplitude $2a/D$ of Circular Cylinder.....	7-54
7.28	Universal Strouhal Number Plotted Against Wake Reynolds Number.....	7-56
7.29	Crossflow Displacement Amplitude as a Function of U_r for Full-scale Marine Piles.....	7-57
7.30	Maximum Amplitude and Frequency Response vs. Reduced Flow Velocity of a Circular Cylinder for Different Gap to Diameter Ratios.....	7-60
7.31	Measured Vibration and Wake Characteristics of a Clamped-Free Shell in Crossflow.....	7-62
8.1	Typical Response Curves of a Cylinder Array in Crossflow.....	8-2
8.2	Flow Patterns for In-Line and Staggered Arrays.....	8-4

8.3	Strouhal Number for In-Line Arrays.....	8-5
8.4	Strouhal Number for Staggered Arrays.....	8-6
8.5	Fluctuating and Time-Average Pressure Distribution Around the Tubes in Rows 1-6.....	8-8
8.6	Time-Average Pressure Distribution in First Three Rows.....	8-9
8.7	Velocity and Turbulence Profiles Between Rows Along One Pitch.....	8-11
8.8	Turbulence Intensity vs. Depth Into Array.....	8-12
8.9	Row-by-Row Fluctuating Lift Coefficient for an Equilateral Staggered Array.....	8-17
8.10	Fluctuating Lift Coefficient for an In-Line Array.....	8-18
8.11	Fluctuating Drag Coefficient for an In-Line Array.....	8-19
8.12	Form Drag Coefficient for Tube Bank.....	8-21
8.13	Power Spectra of Turbulent Fluid Force for the Front Row.....	8-23
8.14	Power Spectra of Turbulent Fluid Force for Different Rows.....	8-24
8.15	Response of the Second Row Tube.....	8-29
8.16	Tube Response Spectra of the Second Row	8-30
8.17	Flow Field for $0 < U < 0.45$ m/s.....	8-31
8.18	Flow Field for $U \approx 0.75$ m/s.....	8-33
8.19	Flow Field for $U = 1.32$ m/s.....	8-34
9.1	Two Cylinders in Crossflow.....	9-2
9.2	Interference Regions for Two Cylinders.....	9-4
9.3	Interference Drag Coefficient for Side-by-Side Arrangement...	9-6
9.4	Strouhal Number for Side-by-Side Arrangement.....	9-7
9.5	Steady Drag and Lift Coefficients for Side-by-Side Arrangement.....	9-8
9.6	Steady Drag Force Coefficient for Side-by-Side Arrangement...	9-9
9.7	Steady Lift Force Coefficient for Side-by-Side Arrangement...	9-10
9.8	Fluctuating Drag Force Coefficient for Side-by-Side Arrangement.....	9-11


9.9	Fluctuating Lift Force Coefficient for Side-by-Side Arrangement.....	9-12
9.10	Classification of Flow Regimes in Side-by-Side and Tandem Arrangements for Stationary Cylinders.....	9-14
9.11	Interference Drag Coefficient for Tandem Cylinders.....	9-15
9.12	Strouhal Number Behind Cylinders in Tandem Arrangement.....	9-17
9.13	Steady Drag Coefficient for Two Cylinders in Tandem Arrangement.....	9-18
9.14	Steady Drag Coefficients for Two Cylinders in Tandem.....	9-19
9.15	Fluctuating Drag Coefficient for Two Cylinders in Tandem.....	9-20
9.16	Fluctuating Lift Coefficient for Two Cylinders in Tandem.....	9-21
9.17	Strouhal Number for Two Cylinders in Staggered Arrangement...	9-23
9.18	Steady Drag and Lift Coefficients for Two Cylinders in Staggered Arrangement.....	9-25
9.19	Vortex Shedding Excited Oscillations for Two Cylinders.....	9-27
9.20	Typical Oscillations at Maximum Amplitude for Vortex Shedding Oscillations.....	9-28
9.21	Tube Displacement Component for Two Tubes in Side-by-Side Arrangement.....	9-31
9.22	Tube Response Frequencies as a Function of Flow Velocity for Two Tubes in Side by Side Arrangement.....	9-32
9.23	Tube Displacement at Different Flow Velocities for Two Tubes in Side-by-Side Arrangements.....	9-33
9.24	Tube Orbital Paths for Two Tubes in Side-by-Side Arrangement	9-34
9.25	Flow Field for Two Cylinders Oscillating in the In-Line Direction with $P/D = 2.0$ for $U_r < 2.5$	9-36
9.26	Flow Field for Two Cylinders Oscillating in the In-Line Direction with $P/D = 4.0$ for $U_r < 2.5$	9-37
9.27	Tube Displacement Components for Two Tubes in Tandem.....	9-39
9.28	Tube Orbital Paths for Two Tubes in Tandem.....	9-40
9.29	Interference Regions.....	9-41
9.30	Schematic of Two Cylinders in Crossflow.....	9-45

9.31	Spatial Distribution of Steady Lift and Drag Coefficients in a Wake.....	9-47
9.32	Steady Drag and Lift Coefficients.....	9-48
9.33	Derivatives for Steady Lift and Drag Curves.....	9-49
9.34	Amplitude Response of Leeward Cylinder of Twin Cylinders.....	9-51
9.35	Flow Patterns for Two Cylinders in Tandem.....	9-53
9.36	Steady Drag Coefficient and Lift Coefficient for the Downstream Cylinder of Two Cylinders.....	9-54
10.1	Critical Flow Velocity.....	10-3
10.2	Cylinder Response PSDs for Various Flowrates	10-5
10.3	Fluid-Damping Coefficients for a Row of Cylinders.....	10-17
10.4	Fluid-Stiffness Coefficients for a Row of Cylinders.....	10-18
10.5	Fluid-Damping Coefficients for a Square Array.....	10-19
10.6	Fluid-Stiffness Coefficient for a Square Array.....	10-20
10.7	Critical Flow Velocity as a Function of Number of Cylinders..	10-30
10.8	Critical Flow Velocity for a Row of Five Cylinders.....	10-32
10.9	Critical Flow Velocity for a Row of Three Cylinders.....	10-33
10.10	Instability Modes for Rows of Cylinders with Two, Three, Four and Five Tubes.....	10-34
10.11	Effect of Detuning in Frequency of Different Cylinders on Critical Flow Velocity.....	10-35
10.12	Schematic of Tube Row in Crossflow.....	10-37
10.13	Tube Displacement as a Function of Flow Velocity.....	10-39
10.14	Stability Map.....	10-40
10.15	Effect of Tube Mass on Critical Flow Velocity.....	10-42
10.16	Stability Map for a Row of Cylinders.....	10-44
10.17	Stability Map for Square Arrays.....	10-45
10.18	Stability Map for Rotated Square Arrays.....	10-46
10.19	Stability Map for Triangular Arrays.....	10-47
10.20	Stability Map for Rotated Triangular Arrays.....	10-48
11.1	Flow-induced Vibration Evaluation Flow Chart.....	11-2
11.2	Fluid Dynamic Means for Interfering with Vortex Shedding.....	11-5

TABLES

<u>Table</u>		<u>Page</u>
1.1	U.S. Power Reactor Field Experience with Flow-induced Vibration	1-3
1.2	Parameters in Flow-induced Vibration.....	1-14
2.1	Added Mass Coefficient for Various Cylinder/Wall Diameter Ratios.....	2-11
3.1	Frequencies Obtained from Various Approximations.....	3-55
3.2	Dimensional Values of the Numerical Examples for Two Coaxial Tubes.....	3-62
5.1	Boundary Conditions and Elements a_{jk} 's.....	5-17
5.2	Experimental Studies of Pipes Conveying Fluid.....	5-41
5.3	Boundary Conditions and Elements a_{jk} 's.....	5-59
6.1	Mathematical Models and Forcing Functions Used by Various Investigators.....	6-8
6.2	Properties and Related Parameters of Test Elements (Circular Cylinders).....	6-23
7.1	Terminology According to Various Authors for Ranges Defined in Fig. 7.1.....	7-4
7.2	Visualization of Vortex Trails and Karman Vortex Streets.....	7-6
7.3	Collected Experimental Data from Various Sources--Fluctuating Force Coefficients and Reynolds Numbers.....	7-16
7.4	Correlation Lengths and Reynolds Numbers of Smooth Cylinders....	7-19
7.5	Characteristics of Lock-in Regions.....	7-45
7.6	Predictions of Resonant Vortex-induced Vibration Amplitude of Circular Cylindrical Structures as a Function of Mass-damping Parameter.....	7-51
8.1	Fluctuating Lift Coefficient of Cylinder Arrays	8-13
8.2	Fluctuating Lift Coefficient and Strouhal Numbers	8-14
8.3	Steady Lift and Drag Coefficients.....	8-20
9.1	Natural Frequencies in Air and Water of Two Tubes in Side-by-Side Arrangement.....	9-30
9.2	Classification of Interfering Flow-induced Oscillations.....	9-42

9.3	Comparison of Four Mathematical Models for the Fluid Dynamic Forces on Tandem Conductors in Motion.....	9-44
10.1	Effective Mass, Natural Frequency, and Modal Damping Ratio under Different Conditions.....	10-7
10.2	Values of α_1 and α_2 in Studies Where Critical Flow Velocity Is a Function of Mass Damping Parameter.....	10-8
10.3	Values of β_1 , β_2 , and β_3 in Studies Where Critical Flow Velocity Is a Function of Mass Ratio and Damping.....	10-9
10.4	Summary of Models for Stability of a Group of Circular Cylinders in Crossflow.....	10-11
10.5	Comparison of Two Instability Mechanisms.....	10-29
10.6	Experimental Data for a Tube Row in Crossflow.....	10-38
10.7	Lower Bounds on Critical Flow Velocities.....	10-52
C.1	Beams of Uniform Section.....	C-6

NOMENCLATURE 

NOMENCLATURE

a	Amplitude of harmonic oscillations
c	Velocity of sound
C_m	Added mass coefficient
c_p	Phase velocity
$[C]$	Damping matrix
$C_D (C_L)$	Steady drag (lift) coefficient
$C_{Dj} (C_{Lj})$	Steady drag (lift) coefficient for jth cylinder
$C_D' (C_L')$	Periodic fluctuating drag (lift) coefficient
$C_{Dj}' (C_{Lj}')$	Periodic fluctuating drag (lift) coefficient for jth cylinder
C_s, C_{sj}, C_{sp}	Viscous damping coefficient of a structure
C_v	Viscous damping coefficient
D	Diameter of a cylinder ($= 2R$)
D_h	Hydraulic diameter
D_o	Diameter of outer cylinder ($= 2R_o$)
E	Modulus of elasticity
E_j	Modulus of elasticity for shell j
E_p^I, EI	Flexural rigidity of cylinder
f	Oscillation frequency
f_f	Natural frequency in fluid
f_s	Frequency of vortex shedding
f_v	Natural frequency in vacuum
f_{fq}	Natural frequency of qth mode in fluid
f_{vj}	Natural frequency of jth cylinder in vacuum
F	Generalized force
g	Fluid force component
g_j	Fluid-force component in the x direction of jth cylinder
g_j'	Fluctuating fluid-force component in the x direction of jth cylinder

g_{sp}	Force per unit length
G	Generalized force or gap
h	Shell thickness
h_j	Fluid-force component in the y direction of jth cylinder or the wall thickness of the jth shell
h'_j	Fluctuating fluid-force component in the y direction of jth cylinder
i	$\sqrt{-1}$
I	Moment of inertia
k	Wave number ($= \omega/c$)
k_s	Spring constant
k_{sj}	Spring constant for cylinder j
k_f	Fluid stiffness
K	Bulk modulus of fluid
K_c	Keulegan-Carpenter parameter
$[K]$	Stiffness matrix
λ	Length or axial wave length
m	Cylinder mass per unit length
m'	$m + m_a$
m_j	Cylinder mass per unit length of cylinder j
m_p	$= m_j$ for $j = 1$ to N and m_{p-N} for $p = N + 1$ to $2N$
m_a	Added mass
$[M]$	Mass matrix
M_d	Displaced mass of fluid or mass of fluid inside a tube
M_c	Mach number
m_p	Displaced mass of fluid per unit length of cylinder j
M_k	Kinetic Mach number
N	Number of cylinders in an array
p	Fluid pressure
P	Pitch

$\{Q\}$	generalized coordinates
r, θ, z	Cylindrical coordinates
\vec{r}	Position vector
R	Radius of cylinder ($= D/2$) or radius of curved pipes
R_j	Radius of cylinder j or shell j
Re	Reynolds number
R_k	Kinetic Reynolds number
R_o	Radius of outer cylinder
St	Strouhal number
t	Time
T	Period, axial tension, transverse pitch
TI	Turbulence intensity
u	Cylinder displacement or shell displacement in the axial direction
\vec{u}	Velocity vector
u'	Fluctuating velocity component
u_j	Cylinder displacement of j th cylinder in the x direction or axial displacement of j th shell
u_p	$= u_j$ for $p = 1$ to N and v_j for $p = N + 1$ to $2N$
U	Flow speed
\bar{U}	Mean flow velocity
\vec{U}	Flow velocity ($= u_r \vec{e}_r, u_\theta \vec{e}_\theta, u_z \vec{e}_z$)
U_r	Reduced flow velocity
v	$= \left(\frac{M_d}{EI}\right)^{0.5} U \xi$ or $\left(\frac{M_d}{EI}\right)^{0.5} R U$, or shell displacement in the tangential direction
v_j	Cylinder displacement of j th cylinder in the y direction or circumferential displacement of the j th shell
V	Volume
x, y, z	Cartesian coordinates
w	Shell displacement in the radial direction

w_j	Radial displacement of the j th shell
α_e	Void fraction
$\alpha_{jk}, \beta_{jk}, \sigma_{jk}, \tau_{jk}$	Added mass coefficients
$\alpha'_{jk}, \beta'_{jk}, \sigma'_{jk}, \tau'_{jk}$	Fluid damping coefficients
$\alpha''_{jk}, \beta''_{jk}, \sigma''_{jk}, \tau''_{jk}$	Fluid stiffness coefficients
$\bar{\alpha}_{jk}, \bar{\beta}_{jk}, \bar{\sigma}_{jk}, \bar{\tau}_{jk}$	Added mass matrices
$\bar{\alpha}'_{jk}, \bar{\beta}'_{jk}, \bar{\sigma}'_{jk}, \bar{\tau}'_{jk}$	Fluid damping matrices
$\bar{\alpha}''_{jk}, \bar{\beta}''_{jk}, \bar{\sigma}''_{jk}, \bar{\tau}''_{jk}$	Fluid stiffness matrices
γ_{pq}	Added mass matrix
δ_s	Scruton's number (mass-damping parameter)
ζ	Damping ratio
ζ_n	Modal damping ratio of the n th mode
ζ_f	Damping ratio in fluid or fluid damping
ζ_v	Damping ratio in vacuum
ζ_{fq}	Damping ratio of q th mode in fluid
ζ_{vj}	Damping ratio of j th cylinder
μ	Viscosity
μ_p	Eigenvalue of added mass matrix
μ_s	Structural damping coefficient
ν	Kinematic viscosity or Poisson's ratio
ν_c	Dimensionless propagation constant
ν_j	Poisson's ratio of the j th shell
ρ	Fluid density
ρ_s	Structure density
ρ_j	Density of shell j
κ	Complex wave number
τ	Dimensionless axial tension
ϕ	Velocity potential function
ω	Circular frequency ($= 2\pi f$)

ω_f	Natural frequency in radian in fluid ($= 2\pi f_f$)
ω_v	Natural frequency in radian in vacuum ($= 2\pi f_v$)
ω_{vj}	Natural frequency in radian of jth cylinder in vacuum
ω_{vpn}	Natural frequency in radian of nth mode of pth cylinder in vacuum
ω_{fp}	Natural frequency in radian of pth mode in fluid
ω_{fpn}	Natural frequency in radian of coupled mode in fluid
$\bar{\omega}_{fj}$	Natural frequency in radian of uncoupled mode of j cylinder
$\Omega_D (\Omega_L)$	Circular frequency associated with the drag (lift) forces
$\Omega_{Dj} (\Omega_{Lj})$	Circular frequency associated with parameter in the drag (lift) direction
Ω_n	Dimensionless natural frequency of nth mode
ϕ	Flow velocity potential
$\phi_{Dj} (\phi_{Lj})$	Phase angle associated with parameter in the drag (lift) direction
$\phi_n(z)$	Orthonormal function of nth mode
ψ	Flow velocity distribution function

Subscripts

D (L)	Denote drag (lift) direction
f	Denote parameters related to fluid
j,k	Denote cylinder number j,k (j,k = 1 to N)21
m,n,l	0, 1, 2, ... ∞
N	Number of cylinders
p,q	1 to 2N
s	Denote parameters related to structure
v	Denote parameters measured in vacuum

ACKNOWLEDGMENTS

Argonne National Laboratory (ANL) has had a Flow Induced Vibration Program since 1967. The majority of the program activities have been funded by the U.S. Atomic Energy Commission (AEC), Energy Research and Development Administration (ERDA), and Department of Energy (DOE). Current DOE funding for this work is from the Office of Reactor Systems, Development and Technology within the Office of Nuclear Energy. A significant amount of material presented in this report is taken from the results of various program activities sponsored by AEC, ERDA, and DOE at ANL. The author is indebted to those who supported the program at ANL throughout the years, in particular, Messrs. Nicholas Grossman and Chet Bigelow for their interest and recognition of this important and challenging subject.

The author is grateful for the support received from his colleagues of the Vibration Analysis Section of the Components Technology Division of ANL, which provides the resources necessary to perform this work. The Section Manager, Dr. M. W. Wambsganss, with his unfaltering faith in me, gave me encouragement and confidence to complete this report.

Grateful appreciation is expressed to Miss Joyce Stephens for her superb typing and word-processing and to Mrs. S. K. Zussman for her expert editing of the manuscript.

CREDITS

The author and Argonne National Laboratory gratefully acknowledge the courtesy of the organizations and individuals who granted permission to use illustrations and other information in this report. The sources of this information are listed below.

- Fig. 2.12 "Damping and Hydrodynamic Mass of a Cylinder in Simulated Two-Phase Flow," L. N. Carlucci, ASME Journal of Mechanical Design, Vol. 102, No. 3, pp. 597-602, 1980, Fig. 10. Permission granted by the American Society of Mechanical Engineers.
- Fig. 2.13 "Experimental Studies of Damping and Hydrodynamic Mass of a Cylinder in Confined Two-Phase Flow," L. N. Carlucci and L. D. Brown, Journal of Vibration, Acoustics, Stress and Reliability in Design, Vol. 105, pp. 83-89, 1982, Fig. 8. Permission granted by the American Society of Mechanical Engineers.
- Figs. 5.6, 5.7 "Flutter of Conservative System of Pipes Conveying Incompressible Fluid," M. P. Paidoussis, J. of Mechanical Engineering Science, Vol. 17(1), pp. 19-25, 1975, Figs. 1 and 2. Reprinted by permission of the Council of the Mechanical Institution of Mechanical Engineers.
- Figs. 5.13, 5.14 "Unstable Oscillation of Tubular Cantilevers Conveying Fluid: I. Theory, II. Experiment," R. W. Gregory and M. P. Paidoussis, Proceedings of the Royal Society of London, 293 (Series A), pp. 512-542, 1966, Figs. 4 and 5. Permission granted by the Royal Society of London.
- Figs. 6.3, 6.4 "Dynamics of Cylindrical Structures Subjected to Axial Flow," M. P. Paidoussis, J. of Sound and Vibration, Vol. 29(3), pp. 365-385, 1973, Figs. 3 and 6. Permission granted by Academic Press, Inc.
- Fig. 6.5 "Dynamics of Flexible Slender Cylinders in Axial Flow, Part 1: Theory, Part 2: Experiment," M. P. Paidoussis, Journal of Fluid Mechanics, Vol. 26 (Pt. 4), pp. 717-751, 1966, Fig. 2. Permission granted by Cambridge University Press.
- Fig. 6.19 "The Dynamic Behavior of Cylindrical Structures in Axial Flow," M. P. Paidoussis, Annals of Nuclear Science and Engineering, Vol. 1, pp. 83-106, 1974, Fig. 7. Permission granted by Pergamon Press, Inc.
- Fig. 6.20 "The Dynamics of Clusters of Flexible Cylinders in Axial Flow: Theory and Experiments," M. P. Paidoussis, Journal of Sound and Vibration, Vol. 65(3), pp. 391-417, 1979, Fig. 11. Permission granted by Academic Press, Inc.

- Fig. 7.2,
Table 7.1 "Flow Around Fixed Circular Cylinders: Fluctuating Loads," C. Farell, Proc. of ASCE, EM3, Paper No. 16330, pp. 565-588, 1981, Fig. 3, Table 2. Permission granted by American Society of Civil Engineers.
- Fig. 7.3 "The Vortex-Shedding Process Behind Two-Dimensional Bluff Bodies," A. E. Perry et al., Journal of Fluid Mechanics, Vol. 116, pp. 77-90, 1982, Fig. 7. Permission granted by Cambridge University Press.
- Fig. 7.4,
Table 7.2 "Vortex Streets and Patterns," O. M. Griffin, Mechanical Engineering, pp. 56-61, March 1982, Fig. 1 and table, p. 56. Permission granted by the American Society of Mechanical Engineers.
- Figs. 7.7, 7.10,
7.27 "OTEC Cold Water Pipe Design for Problems Caused by Vortex-Excited Oscillations," O. M. Griffin, NRL Memorandum Report 4157, 1980, Figs. 4.3, 4.4, 4.11, and 4.18. Permission granted by the Naval Research Laboratory, U.S. Department of the Navy.
- Figs. 7.8, 7.9,
7.21, 7.24, 7.26;
Tables 7.3, 7.4 "A Review of Vortex Shedding Research and Its Application," R. King, Ocean Engineering, Vol. 4, pp. 141-171, 1977, Figs. 11, 12, 14.a, 14.b, and 14.c; Tables 1 and 2. Permission granted by Pergamon Press, Inc.
- Figs. 7.11, 7.12 "On the Force Fluctuations Acting on a Circular Cylinder in Crossflow from Subcritical up to Transcritical Reynolds Number," G. Schewe, Journal of Fluid Mechanics, Vol. 133, pp. 265-285, 1983, Figs. 2 and 3. Permission granted by Cambridge University Press.
- Figs. 7.13, 7.14,
7.15, 7.16 "Turbulence Effects on Some Aerodynamic Parameters of a Circular Cylinder at Supercritical Reynolds Numbers," J. C. K. Cheung and W. H. Melbourne, J. Wind Eng. and Industrial Aerodynamics, Vol. 14, pp. 399-410, 1983, Figs. 2, 4, 5, and 6. Permission granted by Elsevier Scientific Publishing Co.
- Fig. 7.20 "Vortex-Excited Oscillations of a Circular Cylinder in Steady Currents," R. King, Offshore Technology Conference, Preprint OTC 1948, 1974, Fig. 1. Permission granted by Offshore Technology Conference.
- Fig. 7.22 "Vortex Shedding from Oscillating Bluff Bodies," P. W. Bearman, Ann. Rev. Fluid Mech., Vol. 16, pp. 195-222, 1984, Fig. 6. Permission granted by Annual Reviews, Inc.

- Fig. 7.23 "Fluid Forces on Oscillating Cylinders," T. Sarpkaya, Journal of Waterway, Port, Coastal and Ocean Div. ASCE, Vol. 104, pp. 275-290, Fig. 10. Permission granted by the American Society of Civil Engineers.
- Fig. 7.28 "Universal Similarity in the Wakes of Stationary and Vibrating Bluff Structures," O. M. Griffin, Journal of Fluids Engineering, Vol. 103, pp. 52-58, 1981, Fig. 5. Permission granted by the American Society of Mechanical Engineers.
- Fig. 7.30 "The Effect of Seabottom Proximity of the Vortex-Induced Vibrations and Fatigue Life of Offshore Pipelines," D. T. Tsahalis, Journal of Energy Resources Technology, Vol. 105, pp. 464-468, 1983, Fig. 3. Permission granted by the American Society of Mechanical Engineers.
- Fig 7.31 "Ovalling Oscillations of Cantilevered and Clamped-Clamped Cylindrical Shells in Cross Flow: An Experimental Study," M. P. Paidoussis, S. J. Price, and H.-C. Suen, Journal of Sound and Vibration, Vol. 83, pp. 533-553, 1982, Fig. 2. Permission granted by Academic Press, Inc.
- Table 8.1 "Fluctuating Lift Forces of the Karman Vortex Streets on Single Circular Cylinders and in Tube Bundles, Part 3 - Lift Forces in Tube Bundles," Trans. ASME, J. Eng. for Industry 94, 603-628, 1972, Table 1. Permission granted by the American Society of Mechanical Engineers.
- Fig. 8.2 "Structure of Gas Flow and Vibration in Tube Banks with Tube Axes Normal to Flow," S. Ishigai, E. Nishikawa, and E. Yagi, Int. Sym. on Marine Engineering, Tokyo, pp. 1-5-23 to 1-5-33, Figs. 8, 9 and 10. Permission granted by The Marine Society of Japan.
- Table 8.2 "A Comprehensive Approach to Avoid Vibration on Fretting in Shell and Tube Heat Exchangers," Flow-Induced Vibration of Power Plant Components PVP-41, pp. 1-18, 1980, Table 1. Permission granted by the American Society of Mechanical Engineers.
- Figs. 8.3, 8.4 "Flow-induced Vibration in Heat Exchangers," J. S. Fitz-Hugh, Proceedings of the International Symposium on Vibration Problems in Industry, Paper No. 427, 1973, Figs. 3 and 4. Permission granted by U.K. Atomic Energy Authority.

- Figs. 8.5, 8.6, 8.7 "Structure of Interstitial Flow between Closely Spaced Tubes in Staggered Array," M. M. Zdravkovich and J. E. Namork, Flow Induced Vibrations, ASME Publication, pp. 41-46, 1979, Figs. 2, 3, and 5. Permission granted by the American Society of Mechanical Engineers.
- Table 8.3 "Flow Induced Vibrations in Staggered Tube Banks," M. M. Zdravkovich, J. A. Nuttall, and D. M. Causon, Sixth Thermodynamics and Fluid Mechanics Coinvention, Univ. of Durham, April 6-8, 1976, Table 1. Permission granted by the Institution of Mechanical Engineers, England.
- Fig. 8.8 "Turbulent Buffeting of Tube Arrays in Liquid Crossflow," J. B. Sandifer and R. T. Bailey, Sym. on Flow-Induced Vibration, Vol. 2, pp. 211-226, 1984, Fig. 5, ASME. Permission granted by the American Society of Mechanical Engineers.
- Fig. 8.12 "Skin Friction and Form Pressure Loss in Tube Bank Condensers," M. G. Morsy, Proc. Instn. Mech. Engr., Vol. 189, 49/75, 1975, Fig. 5. Permission granted by Institution of Mechanical Engineers.
- Figs. 8.13, 8.14 "Experiment on Vibration of Heat Exchanger Tube Arrays in Cross Flow," R. P. Blevins et al., Trans. 6th SMIRT, Paper No. B6/9, 1981, Figs. 2 and 3. Permission granted by North-Holland Publishing Co. and the Executive Committee of SMIRT-8.
- Figs. 8.15, 8.16, 8.17, 8.18, 8.19 "A Flow Visualization Study of a Square Array of Tubes in Water Crossflow," D. S. Weaver and A. Abd-Rabbo, Sym. on Flow Induced Vibration, ASME Publication, Vol. 2, pp. 165-177, 1984, Figs. 2, 4, 5, 6, and 19. Permission granted by the American Society of Mechanical Engineers.
- Figs. 9.2, 9.10, 9.19, 9.20 "Flow Induced Oscillations of Two Interfering Circular Cylinders," M. M. Zdravkovich, Int. Conf. on Flow Induced Vibrations in Fluid Engineering, Reading, England, Sept. 14-16, 1982, Paper No. D2, Figs. 1, 2, 3, and 4. Permission granted by BHRA Fluid Engineering.
- Figs. 9.3, 9.4, 9.5, 9.11, 9.12, 9.13 "Review of Flow Interference between Two Circular Cylinders in Various Arrangements," M. M. Zdravkovich, Journal of Fluids Engineering, Vol. 99, pp. 618-633, 1977, Figs. 2, 6, 11, 14, 15, and 19. Permission granted by the American Society of Mechanical Engineers.

- Fig. 9.17 "Vortex Shedding from Two Circular Cylinders in Staggered Arrangement," M. Kiya, et al., Journal of Fluids Engineering, Vol. 102, pp. 166-173, 1980, Fig. 13. Permission granted by the American Society of Mechanical Engineers.
- Fig. 9.18 "Interference between Two Circular Cylinders; Series of Unexpected Discontinuities," M. M. Zdravkovich and D. L. Pridden, Journal of Industrial Aerodynamics, Vol. 2, pp. 255-270, 1977, Figs. 8 and 9. Permission granted by Elsevier Scientific Publishing Co.
- Figs. 9.25, 9.26 "Wake Interaction Experiments with Two Flexible Circular Cylinders in Flowing Water," R. King and D. J. Johns, Journal of Sound and Vibration, Vol. 45(2), pp. 259-283, 1976, Figs. 15 and 16. Permission granted by Academic Press, Inc.
- Fig. 9.29 "Classification of Flow-Induced Oscillations of Two Parallel Circular Cylinders in Various Arrangements," M. M. Zdravkovich, Sym. on Flow Induced Vibration, ASME Publication, Vol. 2, pp. 1-18, 1984, Fig. 1 and Table 1. Permission granted by the American Society of Mechanical Engineers.
- Table 9.2
- Figs. 9.33, 9.32 "Wake Induced Flutter of Power Transmission Conductors," S. J. Price, Journal of Sound and Vibration, Vol. 38(1), pp. 125-147, 1975, Figs. 5 and 6. Permission granted by Academic Press, Inc.
- Table 9.3 "On Wake Induced Flutter of a Circular Conductor in the Wake of Another," Flow Induced Vibrations, ASME Publication, pp. 19-34, 1979, Table on p. 23. Permission granted by the American Society of Mechanical Engineers.
- Fig. 9.34 "Reduction of Flow-Induced Structural Vibrations," R. H. Scanlan and R. L. Wardlaw in Isolation of Mechanical Vibration, Impact and Noise, ASME 1973, page 35-63, Fig. 15. Permission granted by the American Society of Mechanical Engineers.
- Fig. 9.35, 9.36 "Aeroelastic Interference Effects between Slender Structures," H. P. Ruscheweyh, Journal of Wind Engineering and Industrial Aerodynamics, Vol. 14, pp. 129-140, 1983, Figs. 4 and 5. Permission granted by Elsevier Scientific Publishing Co.
- Fig. 11.2 "Review and Classification of Various Aerodynamic and Hydrodynamic Means for Suppressing Vortex Shedding," M. M. Zdravkovich, Journal of Wind Engineering and Industrial Aerodynamics, Vol. 7, pp. 145-189, 1981, Fig. 1. Permission granted by Elsevier Scientific Publishing Co.
- Table C.1 "Shock and Vibration Handbook," C. M. Harris, and C. E. Crede, Second Ed., 1976, Page 1-14. Permission granted by McGraw-Hill Book Co.

**FLOW-INDUCED VIBRATION OF
CIRCULAR CYLINDRICAL STRUCTURES**

by

Shoef-sheng Chen

ABSTRACT

Significant progress has been made in the understanding of vibration of circular cylinders subjected to flow, including development of analysis techniques and experiments on fluid forces, damping, stability boundary, and general structural response. This report summarizes the flow-induced vibration of circular cylinders in quiescent fluid, axial flow, and crossflow, and applications of the analytical methods and experimental data in design evaluation of various system components consisting of circular cylinders.

The information is organized into five general topic areas:

Introduction: Chapter 1 presents an overview of flow-induced vibration of circular cylinders. It includes examples of flow-induced vibration, various fluid force components, and nondimensional parameters as well as different excitation mechanisms. The general principles are applicable in different flow conditions.

Quiescent Fluid: Fluid inertia and fluid damping are discussed in Chapters 2, 3 and 4. Various flow theories are applied in different situations. The main results are the characterization of fluid effects on structural response. Emphasis is placed on isolated cylinders, multiple cylinders and circular cylindrical shells.

Axial Flow: Axial flow can cause subcritical vibration and instability. Chapter 5 summarizes the results for internal flow, while Chapter 6 considers the external flow. Both theoretical results and experimental data are examined.

Crossflow: Different excitation mechanisms can be dominant in different conditions for crossflow. Those include turbulent buffeting, acoustic resonance, vortex excitation, and dynamic instability. Appropriate excitation mechanisms are presented for a single cylinder, twin cylinders, and a group of cylinders.

Design Considerations: Applications of the general methods of analysis in the design evaluation of system components are described and various techniques to avoid detrimental vibration are presented. In addition, available design guides on this subject are discussed.

The results presented in this report are expected to be useful not only to designers but also researchers in this field.

1. INTRODUCTION

Flow-induced vibration is a term to denote those phenomena associated with the response of structures placed in or conveying fluid flow. More specifically, the term covers those cases in which an interaction develops between fluid-dynamic forces and the inertia, damping or elastic forces in the structures. The study of these phenomena draws on three disciplines: (1) structural mechanics, (2) mechanical vibration, and (3) fluid dynamics.

The vibration of circular cylinders subject to flow has been known to man since ancient times; the vibration of a wire at its natural frequency in response to vortex shedding was known in ancient Greece as aeolian tones. But systematic studies of the problem were not made until a century ago when Strouhal established the relationship between vortex shedding frequency and flow velocity for a given cylinder diameter. The early research in this area has been summarized by Zdravkovich (1985) and Goldstein (1965).

Flow-induced structural vibration has been experienced in numerous fields, including the aerospace industry, power generation/transmission (turbine blades, heat exchanger tubes, nuclear reactor components), civil engineering (bridges, building, smoke stacks), and undersea technology. The problems have usually been encountered or created accidentally through improper design. In most cases, a structural or mechanical component, designed to meet specific objectives, develops problems when the undesired effects of flow field have not been accounted for in the design. When a flow-induced vibration problem is noted in the design stage, the engineer has different options to eliminate the detrimental vibration. Unfortunately, in many situations, the problems occur after the components are already in operation; the "fix" usually is very costly.

Flow-induced vibration comprises complex and diverse phenomena; subcritical vibration of nuclear fuel assemblies, galloping of transmission lines, flutter of pipes conveying fluid, and whirling of heat exchanger tube banks are typical examples. Recently, flow-induced vibration has been studied extensively for several reasons. First, with the use of high-strength materials, structures become more slender and more susceptible to vibration. Second, the development of advanced nuclear power reactors requires high-velocity fluid flowing through components, which can cause detrimental vibrations. Third, the dynamic interaction of structure and fluid is one of the most fascinating problems in engineering mechanics. The increasing study is evidenced by many conferences directed to this subject and numerous publications, including reviews and books (see Additional References at the end of this section).

In a broad sense, flow-induced vibration encompasses all topics on the dynamic responses of structures submerged in fluid, containing fluid, or

subjected to external flow. In this report, discussions focus on circular cylindrical structures with emphasis on nuclear reactor system components.

1.1 EXAMPLES OF FLOW-INDUCED VIBRATION PROBLEMS

The power reactor industry has had a history of flow-induced vibration problems; Table 1.1 contains a list of field experiences. A large number of different reactor components have been identified. In all cases, the vibrations led to component failure, resulting in plant downtime and/or operation at reduced power.

It is important to note that flow-induced vibrations have persisted to the present. This can be attributed to two reasons:

- In the past, flow-induced vibration has not been considered an integral part of nuclear plant design as have reactor physics and thermohydraulics, which are considered the prime parameters. A deficiency in the prime parameters may mean that the plant will not work at all, while problems in the secondary parameters, such as flow-induced vibration problems, may simply mean that reliable operations will be short-lived.
- The state-of-the-art is such that, in many cases, it cannot predict flow-induced vibration problems with sufficient accuracy. Because of generally complicated geometries and high Reynolds numbers, it is extremely difficult to predict fluid-force components; therefore, it is difficult to predict the reliability of a particular component without extensive tests.

Let us consider two typical examples--the first and the last listed in Table 1.1. The first example is associated with a liquid-metal-cooled breeder reactor, the Enrico Fermi Atomic Power Plant (Smith et al. 1964; Shin and Wambsganss 1977). It has three parallel intermediate heat exchangers. The steam generators are vertical, single-wall-tube, once-through-type heat exchangers, with water and steam inside the tubes and sodium on the shell side. In preoperating testing, after 13 days of operation, six tubes had failed, all in front of the sodium inlet nozzle. As part of the investigation, system operation was continued for 42 days. Testing showed that 39 additional tubes were leaking. Figure 1.1 shows typical tube damage caused by wear due to vibration and the tubes impacting against each other and their supports. The vibration was induced by the sodium flow.

Most recently, leakage of a steam generator after only 3000 effective full-power hours of operation has attracted much attention (Reisch 1982; Christopher 1982). The leakage was caused by the so-called "shake and break" phenomenon. Dozens of the steam generator tubes at the Ringhals 3 reactor in Sweden were found to have worn down to only 10% of their original thickness. The leakage signaled the beginning of a troublesome period for a series of

Table i.1 U.S. Power Reactor Field Experience with Flow-induced Vibration*

Year	Reactor Type	Component/Structure
1962	LMFBR	Steam generator tubes
1962-63	BWR	Guide tube bolts
1964-65	BWR	Core thermal shield
Before 1965	PWR	Control rod blade
1968-72	PWR	Thermal shield
1969	BWR	Jet pump assembly
1970-77	PWR	Steam generator tubes/antivibration bars
1971-75	PWR	Fuel rod--corner fuel assemblies
1972	PWR	In-core instrument nozzles and guide tubes
1972	BWR	Jet pump holddown
1972-77	BWR	Feedwater spargers
1973	PWR	Core barrel support
1974	BWR	Jet pump restrainer
1974-75	BWR	In-core instrument tubes/fuel channels
1976	PWR	Steam generator tube
1980-82	PWR	Fuel pins
1981-84	PWR	Steam generator tubes--preheat section

* Provided by Dr. M. W. Wambsganss, Argonne National Laboratory.



Fig. 1.1. Steam Generator Tube Bank Damaged by Vibration
(Shin and Wambsganss 1977) (ANL Neg. Nos. 113-84-
88 and 113-84-89)

other reactor plants with similar design. The clear source of the problem is flow-induced vibration.

These two examples, as well as some other spectacular failures (Paidoussis 1980), show that flow-induced vibration can lead to economic, maintenance, safety, and operational problems. Therefore, reactor designers can no longer consider the flow-induced vibration problem as always being a secondary design parameter.

1.2 NONDIMENSIONAL PARAMETERS

Fluid-force components and system responses depend on different system parameters under different conditions. Frequently used parameters are discussed in this section.

Geometry: The geometry of a circular cylinder in an infinite fluid can be specified by its length-to-diameter ratio:

$$\frac{L}{D} = \frac{\text{length}}{\text{diameter}} .$$

In a confined region, such as a circular cylinder enclosed by a larger circular shell, a second nondimensional parameter, the diameter ratio, is needed:

$$\frac{D_o}{D} = \frac{\text{shell diameter}}{\text{cylinder diameter}} .$$

In a group of circular cylinders, the arrangement of the cylinders is important. For example, different cylinder arrays (see Fig. 1.2) are specified by the pitch-to-diameter ratio:

$$\frac{P}{D} = \frac{\text{pitch}}{\text{diameter}} .$$

In addition, cylinder surface conditions, such as for finned tubes, specified by the ratio of surface roughness to cylinder diameter, are also important.

Mass ratio: The ratio of cylinder mass to the displaced mass of fluid is proportional to:

$$\frac{m}{\rho D^2} = \frac{\text{mass per unit length of cylinder}}{\text{fluid density} \times \text{cylinder diameter}^2} .$$

The mass ratio provides a measure for different fluid-force components. For example, a small mass ratio indicates that the role of the fluid inertia is important.

Reynolds number (Re): It is a dimensionless number that is significant in the design of a model of any system in which the effect of viscosity is

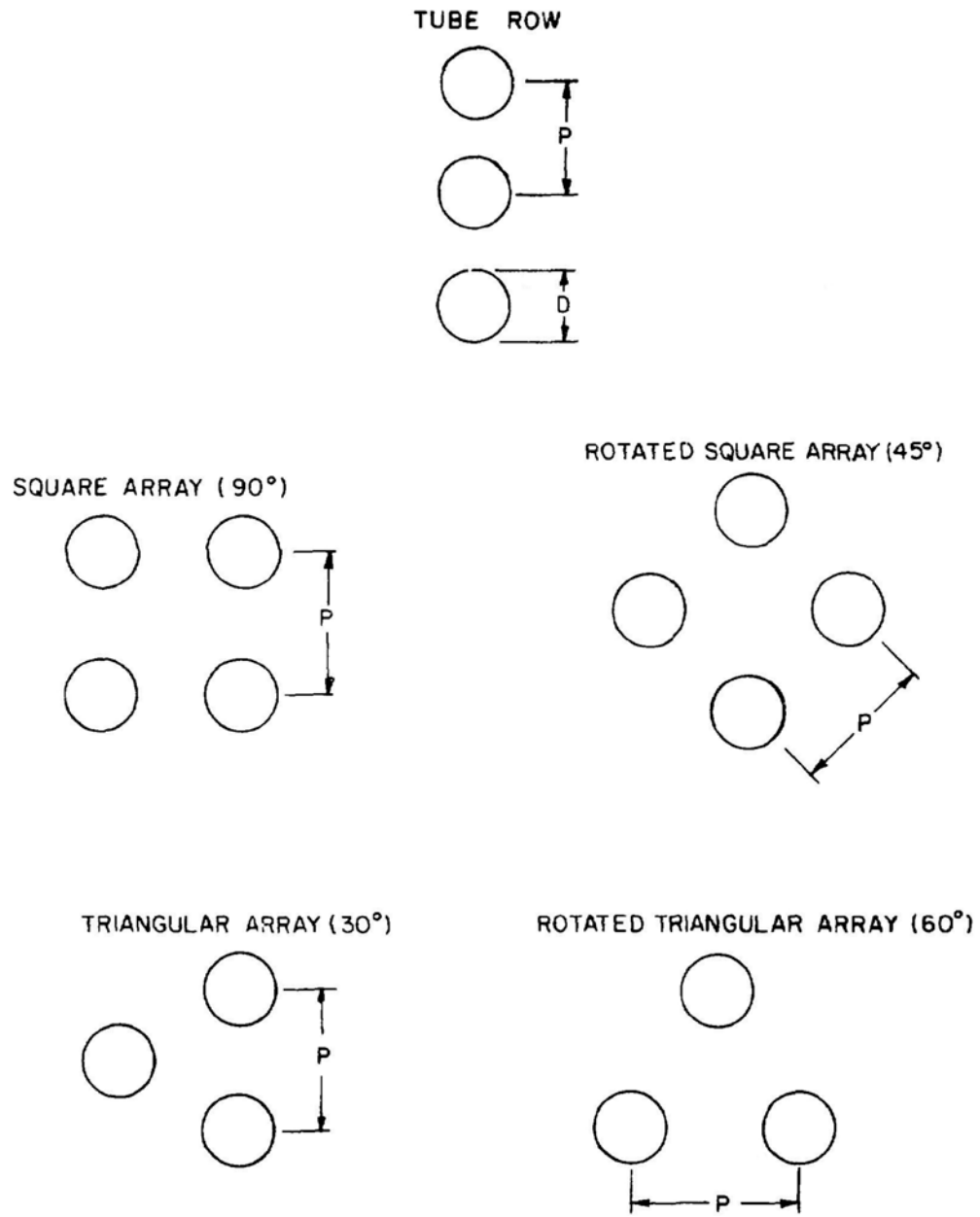


Fig. 1.2. Tube Arrangements

important in controlling the velocities or the flow pattern of a fluid; it is equal to the density of a fluid, times its velocity, times a characteristic length, divided by the fluid viscosity. It can be shown that the Reynolds number is also equal to the ratio of inertia force to viscous force in the fluid:

$$\frac{UD}{\nu} = \frac{\text{inertia force}}{\text{viscous force}},$$

where ν is the kinematic viscosity of the fluid, and is equal to the absolute viscosity (μ) divided by the fluid density. The Reynolds numbers give a measure of transition from laminar to turbulent flow, boundary layer thickness, and fluid field across the cylinder.

Kinetic Reynolds number (R_k): In a quiescent fluid or oscillating flow, the fluid force is a function of kinetic Reynolds number which is given by

$$R_k = \frac{\omega D^2}{\nu},$$

where ω is the circular frequency of oscillations. The role of the kinetic Reynolds number in quiescent fluid or oscillating flow is similar to the Reynolds number in a steady flow.

Mach number (M_c): The Mach number is equal to the ratio of flow velocity to the speed of sound:

$$M_c = \frac{U}{c}.$$

Mach number is a measure of the compressibility of the fluid. In the problems discussed in this report, the Mach number is generally small.

Kinetic Mach number (M_k): In a structure oscillating in a compressible quiescent fluid, the kinetic Mach number, given by

$$M_k = \frac{\omega D}{c},$$

is important. For small kinetic numbers, the fluid compressibility is insignificant.

Reduced flow velocity (U_r): The reduced flow velocity is given by

$$U_r = \frac{U}{fD},$$

where f is the frequency of oscillations. The fluid force is a function of the reduced flow velocity.

Strouhal number (St): The inverse of the reduced flow velocity is called the Strouhal number, provided that the frequency is the frequency associated with flow field, such as the vortex shedding. The Strouhal number is related to the oscillation frequency of periodic motion of a flow.

Keulegan-Carpenter parameter (K_c): In a harmonic flow, the Keulegan-Carpenter parameter is defined as follows:

$$K_c = \frac{UT}{D},$$

where U is the flow velocity amplitude and T is the period. In a harmonic flow, K_c is an important parameter.

For a cylinder oscillating in a quiescent fluid, $U = a\omega$ and $T = 2\pi/\omega$, where ω is the circular frequency of the cylinder oscillation and a is the cylinder displacement; i.e.,

$$K_c = \frac{2\pi a}{D}.$$

Therefore, the Keulegan-Carpenter parameter for a cylinder oscillating in a quiescent fluid corresponds to the amplitude ratio.

Damping ratio (ζ): Damping is the dissipation of energy with time or distance. When the viscous damping is equal to the minimum value that will allow a displaced system to return to its initial position without oscillation, it is called critical damping. Damping ratio for a system with viscous damping is the ratio of actual damping coefficient C_v to the critical damping coefficient.

For a linear, viscously damped structure, $2\pi\zeta$ (called the log decrement) is equal to the natural logarithm of the ratio of the amplitudes of any two successive cycles of a lightly damped structure in free decay. If the energy input to a structure is less than the energy dissipated in damping, the oscillation will diminish.

Mass-damping parameter (Scruton's number δ_s): The product of mass ratio $m/\rho D^2$ and log decrement $2\pi\zeta$ is called the mass-damping ratio:

$$\delta_s = \frac{2\pi m\zeta}{\rho D^2}.$$

This parameter appears frequently in flow-induced vibration problems.

1.3 FLUID-FORCE COMPONENTS

A structural component moving at a constant velocity in an infinite ideal fluid encounters no resistance. This phenomenon is commonly referred to as D'Alembert's paradox. In contrast, a body moving at a variable velocity, even

in a condition of potential flow, experiences resistance; the body behaves as though an added mass of fluid were rigidly attached to and moving with it. When the body is subjected to excitation, not only must the mass of the body be accelerated, but also that of the added fluid mass. The additional force required to accelerate the body is given by

$$g = -m_a \frac{\partial^2 u}{\partial t^2}, \quad (1.1)$$

where $\partial^2 u / \partial t^2$ is the acceleration of the body and m_a is referred to as added mass. Note that the force component $m_a(\partial^2 u / \partial t^2)$, in phase with the structural acceleration, arises because the fluid moves as the body oscillates. Every fluid element, even those far away from the cylinder, experiences acceleration when the cylinder oscillates; the added mass is the integrated effect of the fluid surrounding the cylinder. The added mass is proportional to the fluid density ρ and the body volume V , and is given by

$$m_a = \rho V C_m, \quad (1.2)$$

where C_m is the added mass coefficient.

Equation 1.1 is valid for an ideal incompressible fluid. In this case, the fluid responds instantaneously to the structural motion such that there is no phase difference between the structural acceleration and fluid acceleration. In contrast, when a structure oscillates in a viscous fluid or compressible fluid, in some conditions, the fluid at various locations does not necessarily respond instantaneously to the structural motion; i.e., there is a phase difference between structural motion and fluid motion. In this situation, there are two fluid force components:

- (1) $m_a(\partial^2 u / \partial t^2)$, in phase with the structural acceleration, arises because the fluid moves as the body oscillates.
- (2) $C_v(\partial u / \partial t)$, opposing the movement of the structure, results from the phase difference and is attributed to fluid viscosity and/or fluid compressibility.

Therefore, the resultant fluid force is

$$g = -m_a \frac{\partial^2 u}{\partial t^2} - C_v \frac{\partial u}{\partial t}, \quad (1.3)$$

where C_v is the fluid damping coefficient.

Equation 1.1 or 1.3 is applicable for a quiescent fluid. When the fluid is flowing with respect to a structure, in addition to the fluid inertial force $m_a(\partial^2 u / \partial t^2)$ and fluid damping force $C_v(\partial u / \partial t)$, there are two other fluid force components:

- (1) Fluid Excitation Force - When the structure is stationary in flow, it disturbs the flow field; therefore, different fluid

pressure and shear stress will act on the structure surface. The resultant effect of fluid pressure and shear stress is called fluid excitation force; these fluid forces are independent of structural motion.

- (2) Fluid Stiffness Force ($k_f u$) - Because of structural displacement, the structure will be subjected to fluid force that is proportional to the structural displacement. This fluid force component is called fluid stiffness force.

Fluid inertia force, fluid damping force, and fluid stiffness force are functions of structural motion. They do not exist if the structure is stationary; therefore, those force components are called motion-dependent fluid forces. On the other hand, fluid excitation forces are independent of structural motion. In many practical cases, fluid forces can be divided into these two groups.

So far we have discussed the case of a single structural component oscillating in a particular direction. For a structure that may oscillate in different directions or a group of structural elements in which each element may oscillate independently, the fluid surrounding the structure or inside the structure may introduce additional coupling. In these circumstances, the interaction of fluid and structural elements become much more complicated.

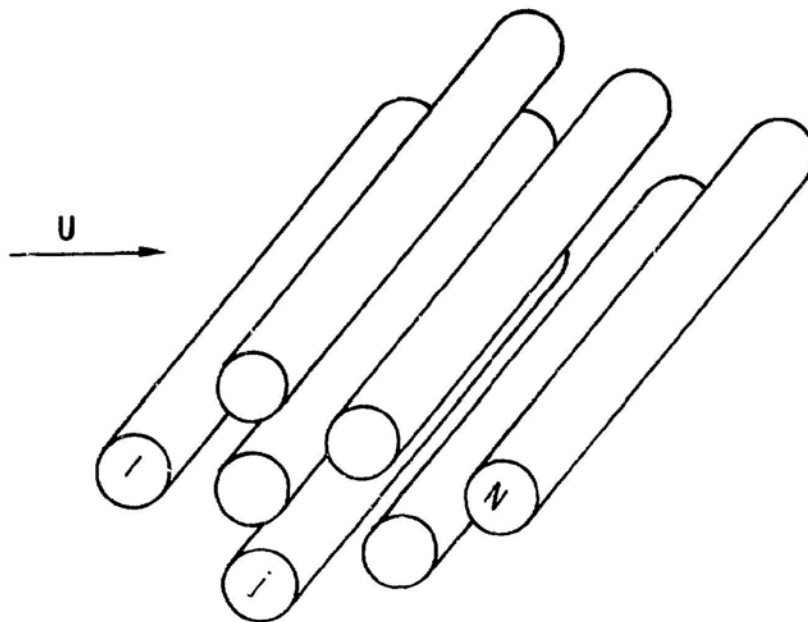
Without loss of generality, consider an array of N circular cylinders oscillating in a flow as shown in Fig. 1.3. The axes of the cylinders are parallel to the z axis. The subscript j is used to denote variables associated with cylinder j . The displacement components of cylinder j are u_j and v_j and the fluid force components are g_j and h_j . Mathematically, these fluid force components can be divided into two groups (Chen 1978): motion-dependent fluid forces and fluid excitation forces.

Motion-dependent Fluid Forces

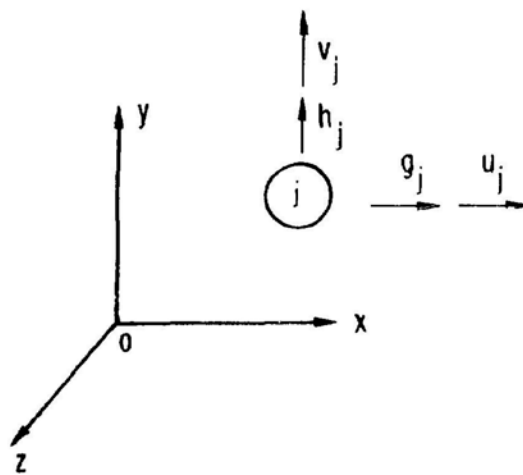
$$g_j = - \sum_{k=1}^N \left\{ \left[\bar{\alpha}_{jk} \frac{\partial^2 u_k}{\partial t^2} + \bar{\alpha}'_{jk} \frac{\partial u_k}{\partial t} + \bar{\alpha}''_{jk} u_k \right] + \left[\bar{\sigma}_{jk} \frac{\partial^2 v_k}{\partial t^2} + \bar{\sigma}'_{jk} \frac{\partial v_k}{\partial t} + \bar{\sigma}''_{jk} v_k \right] \right\}$$

and

$$h_j = - \sum_{k=1}^N \left\{ \left[\bar{\tau}_{jk} \frac{\partial^2 u_k}{\partial t^2} + \bar{\tau}'_{jk} \frac{\partial u_k}{\partial t} + \bar{\tau}''_{jk} u_k \right] + \left[\bar{\beta}_{jk} \frac{\partial^2 v_k}{\partial t^2} + \bar{\beta}'_{jk} \frac{\partial v_k}{\partial t} + \bar{\beta}''_{jk} v_k \right] \right\} . \quad (1.4)$$



(a) A GROUP OF CIRCULAR CYLINDERS



(b) FLUID FORCE AND CYLINDER DISPLACEMENT COMPONENTS

Fig. 1.3. A Group of Cylinders in Flow

Note that $\bar{\alpha}_{1j}$, $\bar{\sigma}_{1j}$, $\bar{\tau}_{1j}$, and $\bar{\beta}_{1j}$ are added mass matrices; $\bar{\alpha}'_{1j}$, $\bar{\sigma}'_{1j}$, $\bar{\tau}'_{1j}$, and $\bar{\beta}'_{1j}$ are damping matrices; and $\bar{\alpha}''_{1j}$, $\bar{\sigma}''_{1j}$, $\bar{\tau}''_{1j}$, and $\bar{\beta}''_{1j}$ are fluid stiffness matrices.

Fluid Excitation Forces

$$\begin{aligned} g_j &= \frac{1}{2} \rho U^2 C_{Dj} + \frac{1}{2} \rho U^2 C'_{Dj} \sin(\Omega_{Dj} t + \phi_{Dj}) + g'_j \\ h_j &= \frac{1}{2} \rho U^2 C_{Lj} + \frac{1}{2} \rho U^2 C'_{Lj} \sin(\Omega_{Lj} t + \phi_{Lj}) + h'_j, \end{aligned} \quad (1.5)$$

where C_{Dj} (C_{Lj}) is the steady drag (lift) coefficient, C'_{Dj} (C'_{Lj}) is the fluctuating drag (lift) coefficient, Ω_{Dj} (Ω_{Lj}) is the circular frequency of periodic flow excitation in the drag (lift) direction, ϕ_{Dj} (ϕ_{Lj}) is the corresponding phase angle, and g'_j (h'_j) is the other fluctuating drag (lift) force.

The various coefficients in Eqs. 1.1 to 1.5, in general, depend on structural displacement, velocity, and acceleration in addition to flow velocity. The characterizations of these force components are still incomplete. At present it is generally impossible to solve analytically those force components using the fundamental principles in fluid mechanics.

1.4 MECHANISMS OF FLOW-INDUCED VIBRATION

When an elastic structure is either immersed in a flowing fluid or conveying fluid, it experiences a distributed force that is exerted on it by the fluid. The structure responds to the flow in different manners; the structure may (1) deflect statically, (2) become unstable by divergence in flow, (3) resonate with periodic excitation of the flow, (4) respond to random fluid excitation, or (5) be subjected to dynamic instability by flutter. The types of response can be classified according to excitation mechanisms.

Different mathematical models have been developed to predict structural responses to different excitation sources. From a practical point of view, one is more interested in quantifying the system parameters at which large displacements (instability) occur or the structural response in subcritical flow velocity ranges. Let structural displacement components be defined as a column vector $\{Q\}$ consisting of u_j and v_j ($j = 1$ to N ; see Eqs. 1.4 and 1.5); $\{\dot{Q}\}$ and $\{\ddot{Q}\}$ are the generalized structural velocity and acceleration, respectively. The dynamic structural/fluid interaction is described by the following equations:

$$[M] \{\ddot{Q}\} + [C] \{\dot{Q}\} + [K] \{Q\} = \{G\} \quad (1.6)$$

or

$$[M_s + M_f]\ddot{\{Q\}} + [C_s + C_f]\dot{\{Q\}} + [K_s + K_f]\{Q\} = \{G\} , \quad (1.7)$$

where $[M]$ is the mass matrix, including structural mass $[M_s]$ and added mass $[M_f]$; $[C]$ is the damping matrix, including structural damping $[C_s]$ and fluid damping $[C_f]$; $[K]$ is the stiffness matrix, including structural stiffness $[K_s]$ and fluid stiffness $[K_f]$; and $\{G\}$ is the other excitation forces, including vortex shedding, turbulence, acoustic noises, etc. Note that the fluid matrices $[M_f]$, $[C_f]$, and $[K_f]$ are related to the matrices given in Eq. 1.4: $\bar{\alpha}_{ij}$, $\bar{\alpha}'_{ij}$, $\bar{\alpha}''_{ij}$, $\bar{\sigma}_{ij}$, $\bar{\sigma}'_{ij}$, $\bar{\sigma}''_{ij}$, $\bar{\beta}_{ij}$, $\bar{\beta}'_{ij}$, $\bar{\beta}''_{ij}$, $\bar{\tau}_{ij}$, $\bar{\tau}'_{ij}$, and $\bar{\tau}''_{ij}$.

In general, M , C , K , and G are functions of Q , \dot{Q} and \ddot{Q} ; therefore, a complete solution is rather difficult to obtain. Fortunately, in many practical situations, one can ignore all nonlinear terms such that M , C , K , and Q are independent of structural displacements.

By premultiplying $\{\dot{Q}\}^T$ and forming the symmetric and antisymmetric components of the matrices thus--

$$\begin{aligned} [M_1] &= \frac{1}{2} ([M] + [M]^T) , & [M_2] &= \frac{1}{2} ([M] - [M]^T) , \\ [C_1] &= \frac{1}{2} ([C] + [C]^T) & [C_2] &= \frac{1}{2} ([C] - [C]^T) , \\ \text{and} & & & \\ [K_1] &= \frac{1}{2} ([K] + [K]^T) , & [K_2] &= \frac{1}{2} ([K] - [K]^T) , \end{aligned} \quad (1.8)$$

we can separate terms, giving

$$\begin{aligned} &\{\dot{Q}\}^T [M_1] \ddot{\{Q\}} + \{\dot{Q}\}^T [C_2] \dot{\{Q\}} + \{\dot{Q}\}^T [K_1] \{Q\} \\ &= -(\{\dot{Q}\}^T [M_2] \ddot{\{Q\}} + \{\dot{Q}\}^T [C_1] \dot{\{Q\}} + \{\dot{Q}\}^T [K_2] \{Q\}) + \{\dot{Q}\}^T \{G\} . \end{aligned} \quad (1.9)$$

Equation 1.9 equates rates of work. Those terms on the right side produce a network resultant when integrated over a closed path through the space $\{Q\}$, the magnitude depending on the path taken. The forces corresponding to the matrices $[M_2]$, $[C_1]$, and $[K_2]$ appearing on the right side are thus by definition the nonconservative parts of the forces represented by $[M]$, $[C]$ and $[K]$. Similarly, the terms on the left side can be shown to give rise to a zero work resultant over any closed path, and therefore together are the sum of the rates of work from the potential forces and the rate of change of kinetic energy. Equation 1.9 is useful in discussing the different flow-induced vibration mechanisms.

In solving Eq. 1.6, either of two objectives will be sought: the instability threshold or the response of the structure. The solution procedures are straightforward. Based on Eq. 1.6, the parameters governing different phenomena are given in Table 1.2 and discussed below.

Table 1.2. Parameters in Flow-Induced Vibration

Structural Response	Fluid Excitation (G)	Dynamic Parameters: Mass (M_s, M_f), Damping (C_s, C_f)	Structural Stiffness (K_s)	Fluid Stiffness (K_f)	Structural Deformation (Q)
Static displacement	•		•	•	•
Static instability (divergence)			•	•	•
Dynamic response (forced vibration)	•	•	•	•	•
Dynamic instability		•	•	•	•
Combination of any of the above	•	•	•	•	•

Static Behavior

Static displacement: Static structural deformations can be induced by steady-state fluid forces, whose frequency is much lower than the structural natural frequency. Structural displacements are calculated by

$$\{Q\} = [K]^{-1}\{G\} . \quad (1.10)$$

Static instability (divergence): Static instability is caused by fluid stiffness force. The critical-flow-velocity boundaries that specify the regions of large structural displacements can be calculated from the following equation:

$$\text{Det}([K_s] + [K_f]) = 0. \quad (1.11)$$

Buckling of an elastic tube conveying steady fluid is a typical example of static instability.

Dynamic Behavior

Dynamic response: Structures are subjected to various excitations, either periodic, such as vortex shedding, or random, such as turbulence. Once the excitation is known, structural responses can be calculated in a straightforward manner.

Dynamic instability: Dynamic instability can be caused by high-velocity flow. Typical examples are whirling instability of tube arrays subjected to crossflow and flutter of pipes conveying fluid. Different types of dynamic instability can be classified according to the dominant terms in Eq. 1.9.

- **Fluid-damping-controlled instability (single mode flutter):** The dominant terms are associated with the symmetric damping matrix $[C_1]$. The flutter arises because the fluid dynamic forces create negative damping.

- **Fluid-stiffness-controlled instability (coupled-mode flutter):** The dominant terms are associated with the antisymmetric stiffness matrix $[K_2]$. It is called coupled mode flutter because a minimum of two modes are required to produce it.

Corresponding to the single-mode flutter and coupled-mode flutter, there may exist parametric resonance and combination resonance if the flow is a periodic function of time.

- **Parametric resonance:** When the period of the flow is a multiple of one of the natural frequencies of the cylinder, the cylinder may be dynamically unstable.

- **Combination resonance:** When the period of the flow is equal to the sum or difference divided by an integer of the natural frequency of the cylinder, the cylinder may also be subjected to dynamic instability.

In practical applications, two or more mechanisms may interact with one another and Eq. 1.7, in general, is applicable for most cases.

REFERENCES CITED--Sec. 1

- Chen, S. S. 1978. Crossflow-induced Vibrations of Heat Exchanger Tube Banks. Nucl. Eng. Des. 47(1), 67-86.
- Christopher, J. 1982. "Shake and Break" Plagues Pressurized-Water Reactor. New Scientist, May 27.
- Goldstein, S. 1965. Modern Developments in Fluid Dynamics. Dover Publications, New York.
- Paidoussis, M. P. 1980. Flow-Induced Vibrations in Nuclear Reactors and Heat Exchangers: Practical Experiences and State of Knowledge. pp. 1-81 in: E. Naudascher and D. Rockwell (Eds.), Practical Experiences with Flow-Induced Vibrations, Springer-Verlag, Berlin.
- Reisch, F. 1982. Technical Note: New Type of Steam Generator Fails in First Year of Operation. Nucl. Saf. 23(3), 355-358.
- Shin, Y. S., and Wambsganss, M. W. 1977. Flow-Induced Vibration in LMFBR Steam Generators: A State-of-the-Art Review. Nucl. Eng. Des. 40(2), 235-284.
- Smith, J. O., Boelter, W. A., McCarthy, J. H., and Brennan, J. H. 1964. Sodium Flow Induced Vibration in Steam Generator Tubes. Paper No. 64-WA/PWR-4, American Society of Mechanical Engineers.
- Zdravkovich, M. M. 1985. Complementary Comment on Review of Sound Induced by Vortex Shedding. J. Sound Vib. 99(2), 295-297.

ADDITIONAL REFERENCES--Sec. 1

Conference Proceedings

- Argonne National Laboratory. 1970. Flow-Induced Vibrations in Reactor System Components. ANL-7685, Argonne National Laboratory, Argonne, Ill., May 1970.
- Argonne National Laboratory (Sponsor). 1977. Summary Report - Specialists Meeting on LMFBR Flow Induced Vibrations. IAEA IWGFR/21, Argonne, Ill., Sept. 1977.
- Au-Yang, M. K., and Brown, S. J. (Eds.). 1977. Fluid Structure Interaction Phenomena in Pressure Vessel and Piping Systems. Winter Annual Meeting of the ASME, Nov. 1977.
- Au-Yang, M. K., and Brown, S. J. (Eds.). 1979. Dynamics of Fluid-Structure Systems in Energy Industry. ASME PVP-39.
- Au-Yang, M. K. (Ed.). 1980. Flow-Induced Vibration of Power Plant Components. ASME PVP-41.

- British Nuclear Energy Society and U.K. Atomic Energy Authority (Sponsors). 1978. Proceedings of the International Conference on Vibration in Nuclear Plants. Keswick, U.K., May 9-12, 1978.
- Chen, S. S., and Bernstein, M. D. (Eds.). 1979. Flow Induced Vibrations. The Third National Congress on Pressure and Piping Technology, San Francisco, Calif., June 1979.
- Chen, S. S., M. P. Paidoussis, and M. K. Au-Yang (Eds.). 1982. Flow-Induced Vibration of Circular Cylindrical Structures. ASME, PVP-Vol. 63.
- Chen, P. Y. (Ed.). 1981. Flow-Induced Vibration Design Guidelines. ASME PVP Vol. 52.
- Chenoweth, J. M. 1977. Flow-Induced Vibrations in Shell-and-Tube Heat Exchangers. SAN/1273-1, Heat Transfer Research, Inc., Feb. 1977.
- Chenoweth, J. M., and Stenner, J. R. (Eds.). 1980. Flow-Induced Heat Exchanger Tube Vibration - 1980. ASME HTD-Vol. 9.
- Greenspon, J. E. (Ed.). 1967. Fluid-Solid Interaction. ASME Publication.
- Ketsroni, G., and Steininger, D. A. 1978. Workshop Proceedings: Flow-Induced Vibrations, Aug. 21-22, 1978. Electric Power Research Institute, Palo Alto, Calif.
- International Association of Hydraulic Research (IAHR) and International Union of Theoretical and Applied Mechanics (IUTAM) (Sponsors). 1979. Symposium on Practical Experiences with Flow-Induced Vibrations. Karlsruhe, Germany.
- Naudascher, E. (Ed.). 1974. Flow-Induced Structural Vibrations. IUTAM-IAHR Symposium, Karlsruhe, 1972. Springer-Verlag.
- Paidoussis, M. P. (Ed.). 1984. Symposium on Flow-Induced Vibration. ASME Publication.
- Reiff, D. D. (Ed.). 1970. Flow-Induced Vibration in Heat Exchanger. ASME Publication.
- Sevik, M. M. (Ed.). 1983. Turbulence-Induced Vibrations and Noise of Structures. ASME Publication.
- U.K. Atomic Energy Authority and National Physical Laboratory (Sponsors). 1973. Vibration Problems in Industry. Keswick, U.K., April 10-12, 1973.

Books

- Bisplinghoff, R. L., and Ashley, H. 1962. Principles of Aeroelasticity. John Wiley and Sons, New York.
- Blevins, R. D. 1977. Flow-Induced Vibration. Van Nostrand Reinhold Co.

- Dowell, E. H. 1975. Aeroelasticity of Plates and Shells. Noordhoff International Publishing.
- Fung, Y. C. 1955. An Introduction to Theory of Aeroelasticity. John Wiley and Sons, New York.
- Goldstein, S. 1965. Modern Developments in Fluid Dynamics. Dover Pub., New York.
- Houghton, E. L., and Carruthers, N. B. 1976. Wind Forces on Buildings and Structures: An Introduction. John Wiley & Sons.
- Junger, M., and Feit, D. 1972. Sound, Structures and Their Interaction. MIT Press.
- Muga, M. J., and Wilson, J. F. 1970. Dynamic Analysis of Ocean Structures. Plenum Publishing.
- Sachs, P. 1978. Wind Forces in Engineering. Second Ed., Pergamon Press.
- Sarpkaya, T., and Isaacson, M. 1981. Mechanics of Wave Forces on Offshore Structures. Van Nostrand Reinhold Co.
- Scanlan, R. H., and Simiu, E. 1978. Wind Effects on Structures. John Wiley & Sons.

2. A SINGLE CYLINDER IN QUIESCENT FLUID

2.1 INTRODUCTION

When a structural component oscillates in a quiescent fluid, the fluid excitation force is zero and the motion-dependent fluid forces are the inertia and damping terms given in Eq. 1.3. Those force components depend on the following parameters: l/D , D_o/D , R_k , M_k and K_c .

A real fluid is viscous and compressible. In many cases, however, the effects of viscosity and the variation of density are so small that they can be neglected. A nonviscous and incompressible fluid is called a perfect fluid. In a perfect fluid, the damping term of the fluid is zero; therefore, for a structure oscillating in a quiescent perfect fluid, the only fluid-force component is associated with the fluid inertia, called the added mass.

In a compressible inviscid fluid, fluid damping may arise. In a confined region, enclosed by rigid walls, the energy cannot propagate out of the region; therefore, no damping will result from fluid oscillations. The only motion-dependent fluid force is attributed to fluid inertia. However, in an infinite region, energy can be carried away by the outgoing waves. The motion-dependent fluid forces will consist of inertia and damping.

In this section, added mass and fluid damping for a single circular cylinder are discussed based on different flow theories.

2.2 A SIMPLE EXAMPLE--A SINGLE CIRCULAR CYLINDER OSCILLATING IN AN INFINITE PERFECT FLUID

Consider an infinitely long circular cylinder supported by an elastic spring, as shown in Fig. 2.1. Its mass per unit length is m and the spring constant is k_s . When the cylinder oscillates in vacuum, the equation of motion is

$$m \frac{d^2 u}{dt^2} + k_s u = 0 . \quad (2.1)$$

The natural frequency in vacuum, f_v , is given by

$$f_v = \frac{1}{2\pi} \sqrt{\frac{k_s}{m}} . \quad (2.2)$$

When the cylinder is submerged in a perfect fluid, the motion of the cylinder disturbs the surrounding fluid. The two-dimensional equation of motion based on the perfect fluid is given by (see Appendix B)

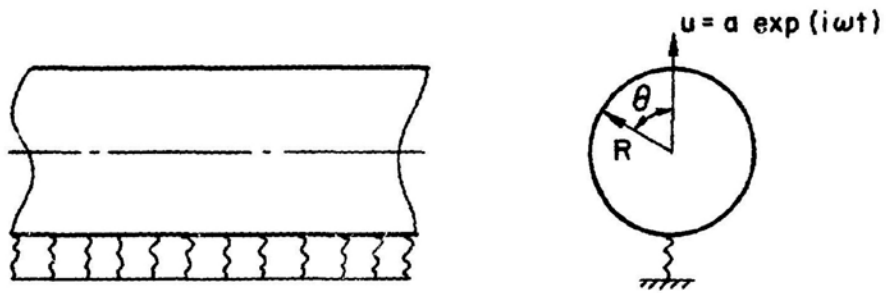


Fig. 2.1. A Circular Cylinder Oscillating in an Infinite Perfect Fluid

$$\nabla^2 \phi(r, \theta, t) = 0, \quad (2.3)$$

where ϕ is the flow velocity potential and ∇^2 is the Laplacian operator. The flow velocity and fluid pressure are given by

$$\vec{U} = \vec{\nabla} \phi$$

and (2.4)

$$p = -\rho \frac{\partial \phi}{\partial t}.$$

At infinity, the fluid is not disturbed and at the interface between the cylinder and fluid, the normal velocity of the fluid is equal to that of the cylinder:

$$\begin{aligned} u_r &= 0, & \text{at } r &= \infty, \\ u_r &= u \cos \theta, & \text{at } r &= R. \end{aligned} \quad (2.5)$$

Let

$$\begin{aligned} u &= a \exp(i\omega t), \\ \phi(r, \theta, t) &= F_r(r) F_\theta(\theta) \exp(i\omega t). \end{aligned} \quad (2.6)$$

Substituting Eq. 2.6 into Eq. 2.3 and separating the variables yields

$$\begin{aligned} \frac{d}{dr} \left[\frac{d}{dr} \left(r \frac{dF_r}{dr} \right) \right] - \frac{n^2}{r^2} F_r &= 0, \\ \frac{d^2 F_\theta}{d\theta^2} + n^2 F_\theta &= 0, \quad n = 0, 1, 2, \dots, \infty. \end{aligned} \quad (2.7)$$

The solutions of Eq. 2.7 are

$$F_r = A_1 r^{-n} + A_2 r^n$$

and (2.8)

$$F_\theta = \alpha_1 \sin n\theta + \alpha_2 \cos n\theta.$$

Based on the boundary condition, Eq. 2.5, n must be equal to 1; therefore

$$\phi(r, \theta, t) = \frac{C}{r} \cos \theta \exp(i\omega t) . \quad (2.9)$$

Using Eqs. 2.4-2.6 and 2.9 yields

$$C = -R^2 a$$

and (2.10)

$$\phi(r, \theta, t) = -\frac{R^2 a}{r^2} \cos \theta \exp(i\omega t) .$$

The fluid force acting on the cylinder is

$$g = -\int_0^{2\pi} p(r, \theta, t) \Big|_{r=R} R \cos \theta d\theta . \quad (2.11)$$

Using Eqs. 2.4, 2.10, and 2.11 yields

$$g = -m_a \frac{d^2 u}{dt^2} ; \quad m_a = \pi \rho R^2 . \quad (2.12)$$

This is the most simple case, in which the added mass of fluid is equal to the mass of the displaced fluid. m_a is called the added mass, hydrodynamic mass or apparent mass. In many cases, a coefficient C_m , called the added mass coefficient, is introduced such that the added mass is equal to the mass of the displaced fluid multiplied by the added mass coefficient. In this example, the added mass coefficient is equal to one.

Now, let us return to the vibration of the cylinder in a perfect fluid. Because of the added mass, the equation of motion for the cylinder in a fluid is given by

$$(m + m_a) \frac{d^2 u}{dt^2} + k_s u = 0 . \quad (2.13)$$

Therefore, the natural frequency of the cylinder oscillating in a fluid is

$$f_f = \frac{1}{2\pi} \sqrt{\frac{k_s}{m + m_a}} . \quad (2.14)$$

Comparing Eqs. 2.2 and 2.14 yields

$$\frac{f_f}{f_v} = \sqrt{\frac{m}{m + m_a}} . \quad (2.15)$$

The effect of the fluid is to reduce the natural frequency. In a perfect fluid, reducing the natural frequency is the only effect.

Based on this simple example, it is obvious that, for a single structural component oscillating in a perfect fluid, the key element is the added mass coefficient. As long as C_m is known, the natural frequency as well as the structural response can be calculated routinely.

2.3 A CIRCULAR CYLINDER NEAR A WALL

The added mass for a circular cylinder near a parallel wall is independent of the direction of motion in an ideal fluid; C_m is given (Mazur 1966) by

$$C_m = 1 + 4 \sinh^2 \alpha \sum_{j=1}^{\infty} j \frac{e^{-3j\alpha}}{\sinh(j\alpha)} ,$$

where (2.16)

$$\alpha = \ln \left(\frac{R + G + \sqrt{(R + G)^2 - R^2}}{R} \right) .$$

Values of C_m are presented in Fig. 2.2.

When the fluid surrounding the cylinder contains other structures or is confined by a pipe, the added mass increases, because the fluid elements in the region between the cylinder and the adjacent structures experience enhanced motion. Any additional confinement of the fluid results in an increase in the added mass.

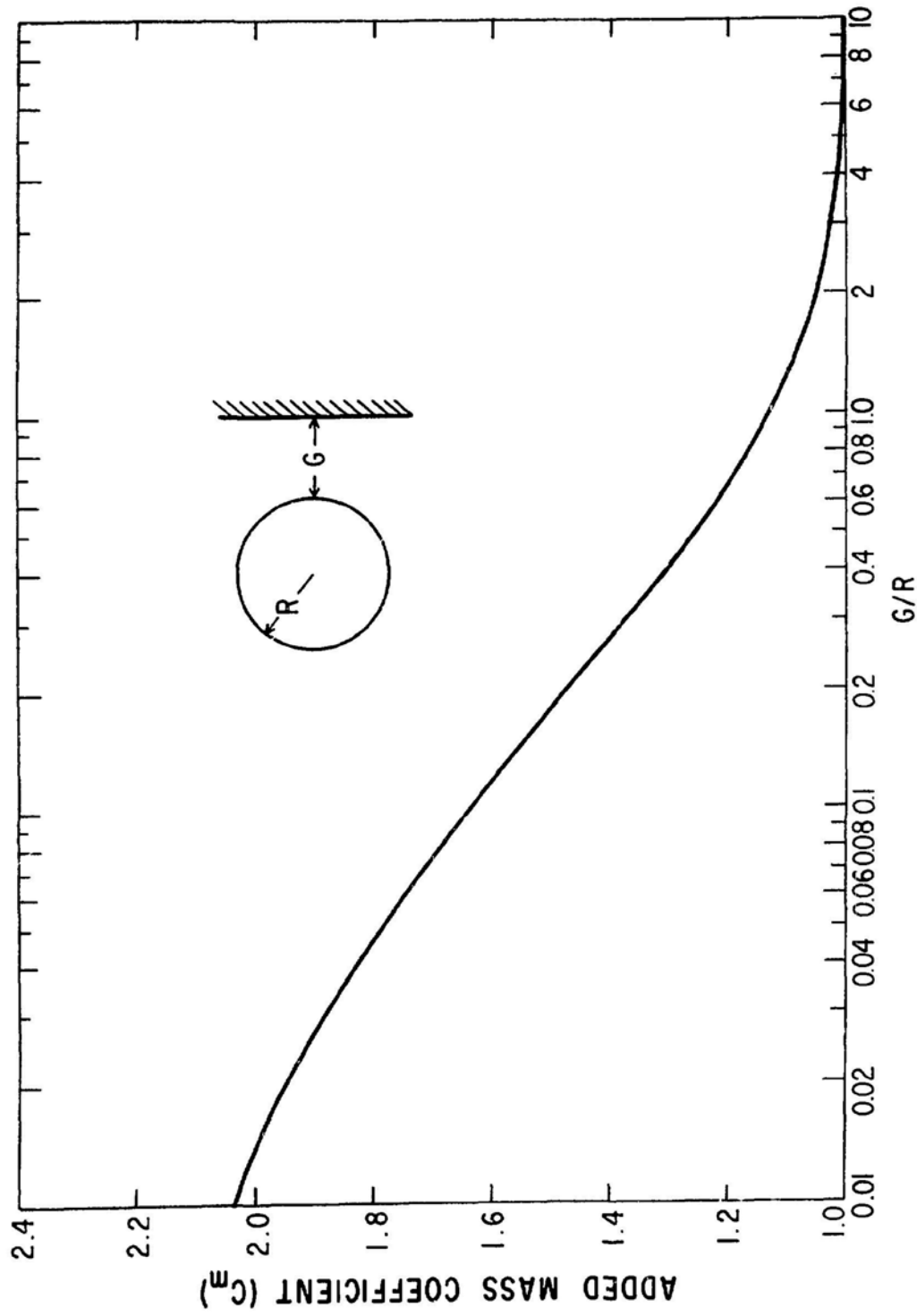


Fig. 2.2. Added Mass Coefficients for a Cylinder Vibrating Near a Wall (Chen and Chung 1976)

2.4 A CIRCULAR CYLINDER IN AN ANNULAR REGION OF COMPRESSIBLE INVISCID FLUID

Consider an infinitely long cylinder with diameter D , oscillating in a compressible inviscid fluid annular region with diameter D_0 , its displacement being u in the x direction shown in Fig. 2.3 (Chen and Wambsganss 1972). The fluid velocity and pressure based on the two-dimensional theory can be evaluated as follows (see Appendix B):

$$\vec{U} = \vec{\nabla}\phi$$

and (2.17)

$$p = -\rho \frac{\partial \phi}{\partial t} ,$$

where

$$\phi = \psi(r, \theta) \exp(i\omega t)$$

and (2.18)

$$\nabla^2 \psi + k^2 \psi = 0 , \quad k^2 = \omega/c .$$

The wall is not allowed to move; therefore, the boundary conditions are

$$u_r = 0 \quad \text{at } r = D_0/2$$

and (2.19)

$$u_r = \frac{\partial u}{\partial t} \cos \theta \quad \text{at } r = D/2 .$$

The solution of Eq. 2.18 is

$$\psi = F_r(r) F_\theta(\theta) , \quad (2.20)$$

where

$$F_r(r) = A_1 J_n(kr) + A_2 Y_n(kr)$$

and (2.21)

$$F_\theta(\theta) = \alpha_1 \sin n\theta + \alpha_2 \cos n\theta , \quad n = 0, 1, 2, 3, \dots .$$

J_n and Y_n are Bessel functions of the first and second kind, respectively, of

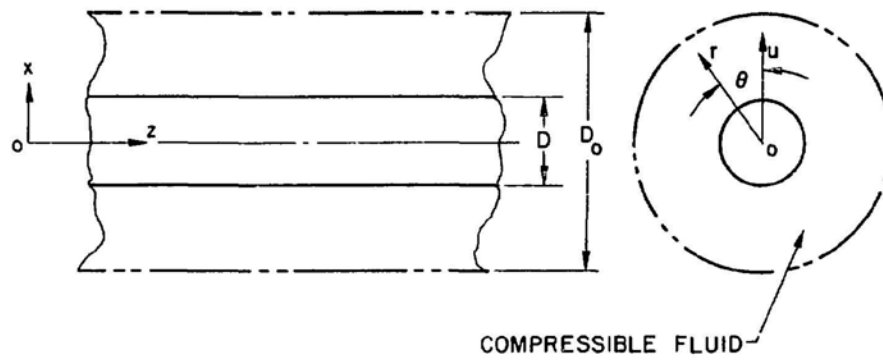


Fig. 2.3. A Circular Cylinder Vibrating in a Compressible Fluid Annulus

order n . Substituting Eq. 2.20 into Eqs. 2.18 and 2.17, we can determine the functions $F_r(r)$ and $F_\theta(\theta)$, using Eqs. 2.19. Finally, the resulting expressions for ϕ and p are

$$\phi = i\omega a \frac{Y_1'(\frac{\alpha}{2})J_1(kr) - J_1'(\frac{\alpha}{2})Y_1(kr)}{Y_1'(\frac{\alpha}{2})J_1'(\frac{\beta}{2}) - J_1'(\frac{\alpha}{2})Y_1'(\frac{\beta}{2})} \cos\theta \exp(i\omega t) \quad (2.22)$$

and

$$p = \omega^2 \rho a \frac{Y_1'(\frac{\alpha}{2})J_1(kr) - J_1'(\frac{\alpha}{2})Y_1(kr)}{Y_1'(\frac{\alpha}{2})J_1'(\frac{\beta}{2}) - J_1'(\frac{\alpha}{2})Y_1'(\frac{\beta}{2})} \cos\theta \exp(i\omega t), \quad (2.23)$$

where the prime denotes differentiation with respect to r , and $u = a \exp(i\omega t)$.

The net reaction force of the fluid on the cylinder in the direction of its motion is equal to the hydrodynamic force associated with the added mass; i.e.,

$$m_a \frac{\partial^2 u}{\partial t^2} = - \int_0^{2\pi} \frac{D}{2} p \cos\theta \, d\theta. \quad (2.24)$$

Let

$$m_a = \frac{\pi D^2}{4} \rho C_m, \quad (2.25)$$

where C_m is the added mass coefficient. From Eqs. 2.22, 2.23, 2.24, and 2.25,

$$C_m = \frac{[\beta J_0(\beta) - J_1(\beta)]Y_1(\alpha) - [\beta Y_0(\beta) - Y_1(\beta)]J_1(\alpha)}{[\beta Y_0(\beta) - Y_1(\beta)][\alpha J_0(\alpha) - J_1(\alpha)] - [\beta J_0(\beta) - J_1(\beta)][\alpha Y_0(\alpha) - Y_1(\alpha)]}, \quad (2.26)$$

where

$$\alpha = \frac{\omega D}{2c}$$

and

$$\beta = \frac{\omega D_0}{2c}.$$

(2.27)

Inspection of Eq. 2.26 shows that the added mass coefficient C_m depends on the oscillation frequency ω , velocity of sound c , and the diameters of the cylinder and the outer wall D and D_o . These parameters can be grouped into two parameters, kinetic Mach number $M_k (= \omega D/c)$ and diameter ratio D/D_o . The added mass coefficients depend on these two parameters.

In practical cases, kinetic Mach number is very small. Table 2.1 shows the values of C_m for several M_k as a function of diameter ratio D_o/D . It is noted that C_m is insensitive to M_k for small M_k ; therefore, in many practical applications, the fluid can be considered incompressible.

Note that the added mass coefficient given in Eq. 2.26 may vary from $-\infty$ to ∞ if it is not restricted to small values of M_k . For example, Fig. 2.4 shows the values of C_m as a function of M_k for a diameter ratio of 2.0. The physical explanation of different values of C_m is as follows:

- When C_m is a positive value, the surrounding fluid provides a resistance to structural oscillations. In this case, the dominant motion is associated with the structure.
- When the resultant fluid force acting on the structure is equal to zero, $C_m = 0$ and the fluid does not affect structural oscillations.
- When $C_m = \infty$, the structure corresponds to a rigid structure; i.e., it is associated with an acoustic mode.
- When C_m is a negative value, the motion is associated with an acoustoelastic mode; structural oscillations and fluid motion are coupled.

2.5 A CIRCULAR CYLINDER IN AN INFINITE COMPRESSIBLE INVISCID FLUID

Consider a uniform circular cylinder of radius R and mass per unit length m submerged in a compressible inviscid fluid (Lin and Chen 1977). The purpose is to find the response of the cylinder subjected to a plane wave traveling in the x direction, as shown in Fig. 2.5. The equation of motion of the rod is

$$m \partial^2 u / \partial t^2 + C_s \partial u / \partial t + k_s x = g(t), \quad (2.28)$$

where C_s is the structural damping coefficient, k_s is the spring constant, and g is the resultant force acting on the cylinder. g is obtained from

$$g(t) = - \int_0^{2\pi} p R \cos \theta \, d\theta, \quad (2.29)$$

where p is the fluid pressure on the cylinder surface. The incident plane wave is

Table 2.1. Added Mass Coefficient (C_m) for Various
Cylinder/Wall Diameter Ratios (D_o/D)

$D_o/D \backslash M_k$	0.00002	0.002	0.2
1.02	50.50873	50.50894	51.03145
1.04	25.51164	25.51169	25.77994
1.06	17.18247	17.18247	17.36652
1.08	13.02014	13.02013	13.16222
1.10	10.52454	10.52456	10.64147
1.2	5.54548	5.54549	5.54615
1.4	3.08334	3.08335	3.12611
1.6	2.28206	2.28206	2.28241
1.8	1.89287	1.89287	1.92497
2.0	1.66667	1.66667	1.69715
4.0	1.13333	1.13334	1.16431
6.0	1.05714	1.05715	1.09265
8.0	1.03175	1.03175	1.07267
10.0	1.02020	1.02021	1.06807

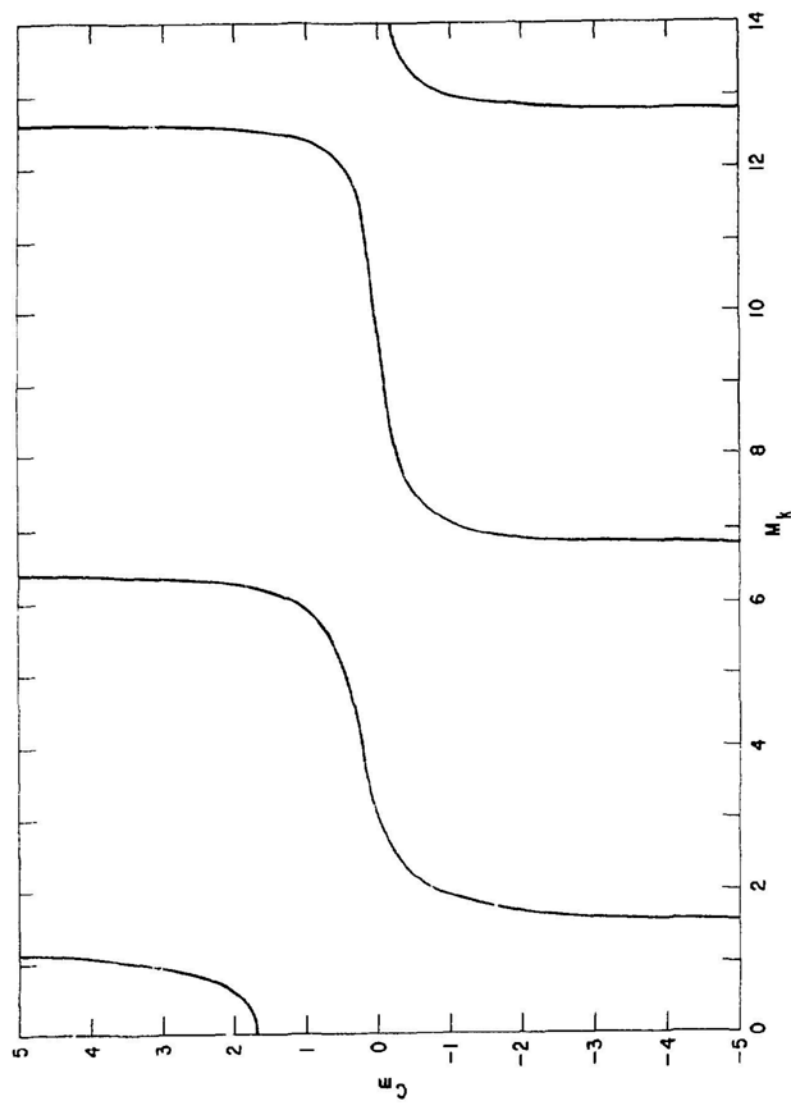


Fig. 2.4. Added Mass Coefficient for a Circular Cylinder Inside a Compressible Fluid Annulus

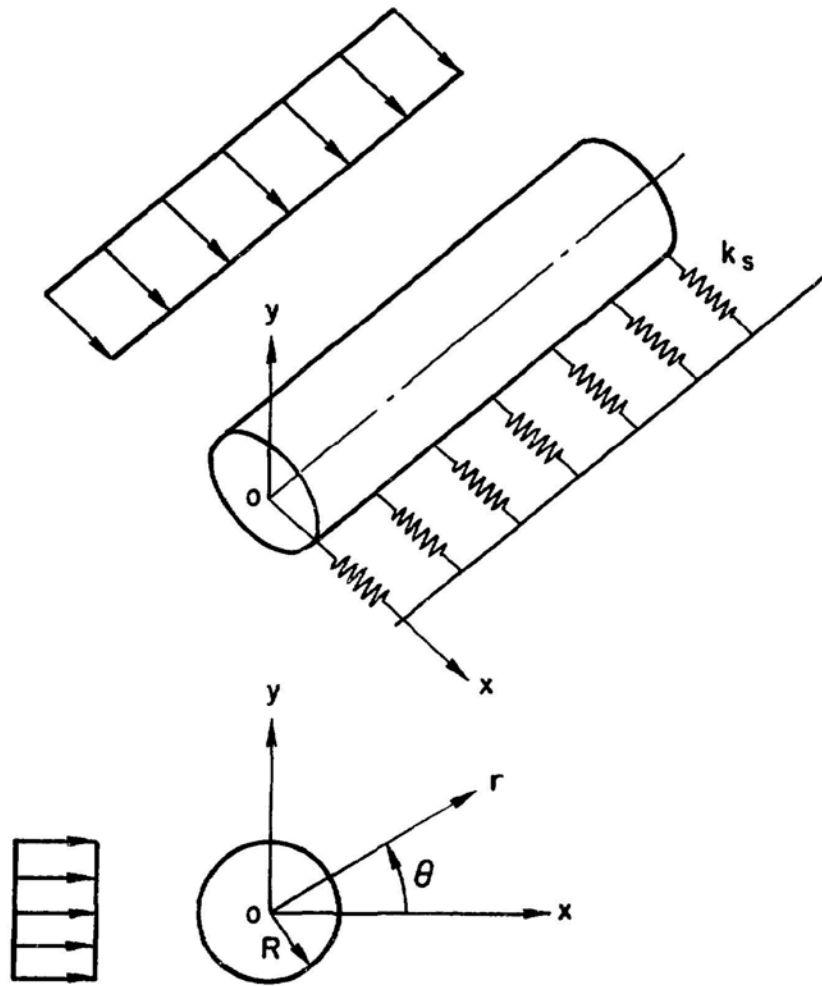


Fig. 2.5. Acoustically Induced Vibration of a Circular Cylinder

$$\bar{p}_r = p_0 e^{ik(r \cos \theta - ct)}, \quad (2.30)$$

where p_0 is the amplitude and k is the wave number, which is related to the circular frequency ω and the wave speed c by $k = \omega/c$. Equation 2.30 can be written in terms of cylindrical waves:

$$\bar{p}_r = p_0 \sum_{n=0}^{\infty} \epsilon_n (i)^n J_n(kr) \cos(n\theta) e^{-i\omega t}, \quad \epsilon_n = \begin{cases} 1, & n = 0 \\ 2, & n \neq 0 \end{cases} \quad (2.31)$$

Here $i = \sqrt{-1}$, and $J_n(kr)$ is the Bessel function of the first kind of order n . The radial velocity u_r corresponding to \bar{p}_r is

$$\bar{u}_r = \left(\frac{p_0}{\rho c}\right) \left\{ i J_1(kr) + \sum_{n=1}^{\infty} i^{n+1} [J_{n+1}(kr) - J_{n-1}(kr)] \cos(n\theta) \right\} e^{-i\omega t}. \quad (2.32)$$

Since the cylinder is submersed in an infinite medium, there exists an outgoing wave p_r :

$$p_r = \sum_{n=0}^{\infty} A_n H_n^{(1)}(kr) \cos(n\theta) e^{-i\omega t}, \quad (2.33)$$

where $H_n^{(1)}(kr)$ is the Hankel function of the first kind of order n , and A_n is a coefficient to be determined. The radial velocity u_r corresponding to p_r is

$$u_r = \left(\frac{i}{\rho c}\right) \left\{ A_0 H_1^{(1)}(kr) + \sum_{n=1}^{\infty} \frac{A_n}{2} [H_{n+1}^{(1)}(kr) - H_{n-1}^{(1)}(kr)] \cos(n\theta) \right\} e^{-i\omega t}. \quad (2.34)$$

The total field intensity is given by the sum of incident wave, Eq. 2.31, and the scattered and radiated wave, Eq. 2.33; i.e.,

$$p = \bar{p}_r + p_r = \left[p_0 \sum_{n=0}^{\infty} \epsilon_n i^n J_n(kr) + \sum_{n=0}^{\infty} A_n H_n^{(1)}(kr) \right] \cos(n\theta) e^{-i\omega t}. \quad (2.35)$$

Equation 2.35 must satisfy the boundary conditions imposed by the structure; i.e., the radial fluid velocity at the interface of fluid and solid must equal the normal velocity of the structure and $g(t)$ must be equal to the resultant fluid pressure. These boundary conditions can be stated mathematically as

$$(\bar{u}_r + u_r) \Big|_{r=R} = (\partial u / \partial t) \cos \theta \quad (2.36)$$

and

$$g(t) = - \int_0^{2\pi} (\bar{p}_r + p_r) \Big|_{r=R} R \cos \theta \, d\theta . \quad (2.37)$$

Substituting Eqs. 2.32 and 2.34 into Eq. 2.36 yields

$$\begin{aligned} & \{ i p_o J_1(kR) + p_o \sum_{m=1}^{\infty} i^{n+1} [J_{n+1}(kR) - J_{n-1}(kR)] \cos(n\theta) + i A_o H_1^{(1)}(kR) \\ & + i \sum_{n=1}^{\infty} \frac{A_n}{2} [H_{n+1}^{(1)}(kR) - H_{n-1}^{(1)}(kR)] \cos(n\theta) \} \left(\frac{1}{\rho c} \right) e^{-i\omega t} = \frac{\partial u}{\partial t} \cos \theta . \end{aligned} \quad (2.38)$$

The steady-state solution of the cylinder displacement can be expressed as

$$u = a \exp(-i\omega t) . \quad (2.39)$$

Substituting Eq. 2.39 into eq. 2.28 yields

$$(-\omega_m^2 - i\omega C_s + k_s) a e^{-i\omega t} = - \int_0^{2\pi} (\bar{p}_r + p_r) \Big|_{r=R} R \cos \theta \, d\theta . \quad (2.40)$$

Substituting Eq. 2.35 into Eq. 2.40 gives

$$a = [-12\pi R p_o J_1(kR) - A_1 \pi R H_1^{(1)}(kR)] / (k_s - i\omega C_s - \omega_m^2) . \quad (2.41)$$

The coefficient A_1 in Eq. 2.41 can be determined by multiplying both sides of Eq. 2.38 by $\cos \theta$ and then integrating from 0 to 2π , thus,

$$A_1 = -2\{ i p_o [J_2(kR) - J_0(kR)] + \rho c \omega a \} / [H_2^{(1)}(kR) - H_0^{(1)}(kR)] . \quad (2.42)$$

Note that Eq. 2.41 contains the coefficient A_1 only. This is due to the fact that a single cylinder subjected to a plane wave can excite only a one-

component scattered and radiated wave; therefore, all the coefficients except A_1 have vanished. From Eqs. 2.41 and 2.42 it follows that

$$\begin{aligned} & \{k_s - i\omega C_s - \omega_m^2 - 2\pi R \rho c \omega \left[\frac{H_1^{(1)}(kR)}{H_2^{(1)}(kR) - H_0^{(1)}(kR)} \right]\} a \\ &= i2\pi R p_0 \{-J_1(kR) + [J_2(kR) - J_0(kR)] \left[\frac{H_1^{(1)}(kR)}{H_2^{(1)}(kR) - H_0^{(1)}(kR)} \right]\} . \end{aligned} \quad (2.43)$$

Since

$$\frac{H_1^{(1)}(kR)}{H_2^{(1)}(kR) - H_0^{(1)}(kR)} = \frac{J_1(kR) + iY_1(kR)}{[J_2(kR) + iY_2(kR)] - [J_0(kR) + iY_0(kR)]} = \frac{\Delta_1 + i\Delta_2}{\Delta}, \quad (2.44)$$

where $Y_n(kR)$ is the Bessel function of the second kind of order n , and

$$\Delta = [J_2(\alpha) - J_0(\alpha)]^2 + [Y_2(\alpha) - Y_0(\alpha)]^2 ,$$

$$\Delta_1 = J_1(\alpha)[J_2(\alpha) - J_0(\alpha)] + Y_1(\alpha)[Y_2(\alpha) - Y_0(\alpha)] ,$$

(2.45)

$$\Delta_2 = Y_1(\alpha)[J_2(\alpha) - J_0(\alpha)] - J_1(\alpha)[Y_2(\alpha) - Y_0(\alpha)] ,$$

and

$$\alpha = kR = \frac{\omega R}{c} = M_c/2 ,$$

Eq. 2.41 becomes

$$a = \left(\frac{2\pi R p_0}{m' \omega_0^2} \right) \left[\frac{J_2(\alpha) - J_0(\alpha)(\Delta_2/\Delta) + i[J_1(\alpha) - \{J_2(\alpha) - J_0(\alpha)\}(\Delta_1/\Delta)]}{(\omega/\omega_0)^2 + i2(\omega/\omega_0)(\zeta_s + \zeta_f) - 1} \right] , \quad (2.46)$$

where

$$m' = m + C_m(\alpha)M_d = \text{virtual mass} ,$$

$$M_d = \rho \pi R^2 = \text{displaced mass of fluid} ,$$

$$C_m(\alpha) = (2/\alpha)(\Delta_1/\Delta) = \text{added mass coefficient} ,$$

$$C_v = M_d \omega \left(\frac{2\Delta_2}{\alpha\Delta} \right) = \text{fluid damping coefficient} , \quad (2.47)$$

$$\omega_o = \sqrt{k/m'} = \text{undamped natural frequency} ,$$

$$\zeta_s = C_s/2\omega_o m' = \text{structural damping} , \text{ and}$$

$$\zeta_f = (\omega/\omega_o) \left[\frac{M_d \Delta_2}{m\alpha\Delta + 2M_d \Delta_1} \right] = \text{fluid damping} .$$

Equations 2.39 and 2.46 provide the complete solution for the response of a circular cylinder subjected to a plane wave excitation in an acoustic medium.

The added mass coefficient C_m is a function of M_k only; i.e., for a given system, C_m is dependent on the wave number k only. Figure 2.6 shows the variation of C_m and C_v versus M_k . Note that for $M_k \rightarrow 0$, $C_m \rightarrow 1$ and $C_v \rightarrow 0$, and both C_m and C_v approach zero when $M_k \rightarrow \infty$. The maximum C_m occurs at $M_k \approx 0.9$ and the maximum C_v occurs at $M_k \approx 2.0$. For $M_k > 4$, the fluid inertia effect on structural vibration is almost negligible.

At resonance, the radiation damping is a function of kinetic Mach number and mass ratio M_d/m . Figure 2.7 shows the relationship between ζ_f and M_k for various values of M_d/m . It can be seen that $\zeta_f \rightarrow 0$ for $M_k \rightarrow 0$ and ∞ . The peak value of ζ_f occurs at M_k slightly greater than 2. The larger the values of M_d/m , the bigger the values of ζ_f . This is understandable because the radiation is more important in a dense medium than in a rarified medium. Therefore, in a lightly damped system, acoustic radiation can be important in removing the energy from a vibrating system; it is also responsible for the eventual decay of free vibration and is of primary importance in controlling steady-state responses.

2.6 A CIRCULAR CYLINDER IN A CONCENTRIC ANNULAR INCOMPRESSIBLE VISCOUS FLUID

Consider the same problem given in Fig. 2.3 except that the fluid is incompressible viscous fluid (Chen et al. 1976). For small amplitudes, the equation of state and motion can be linearized; the equations of motion for

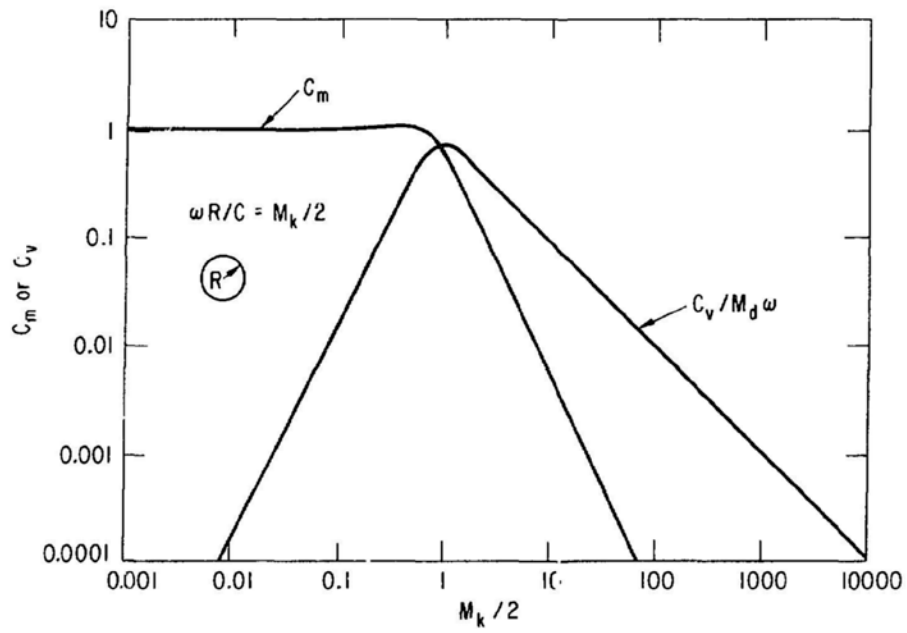


Fig. 2.6. Added Mass Coefficient and Fluid Damping Coefficient for a Circular Cylinder in a Compressible Inviscid Fluid (Lin and Chen 1977)

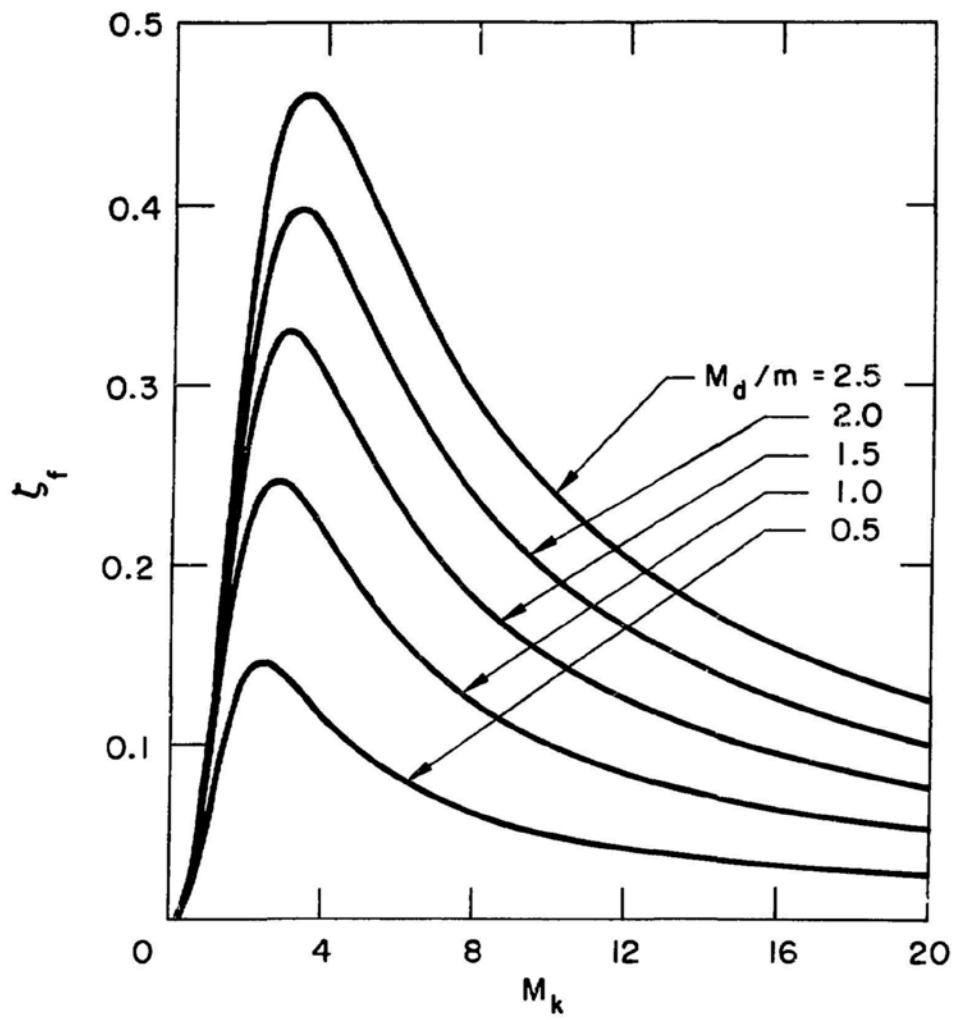


Fig. 2.7. Fluid Radiation Damping at Resonance (Lin and Chen 1977)

the fluid are (see Appendix B)

$$\nabla^4 \psi - \frac{1}{\nu} \frac{\partial}{\partial t} \nabla^2 \psi = 0 , \quad (2.48)$$

where ν is kinematic viscosity of the fluid. The velocity components of fluid in the r and θ directions are given by u_r and u_θ :

$$u_r = -\frac{\partial \psi}{r \partial \theta} ; \quad u_\theta = \frac{\partial \psi}{\partial r} . \quad (2.49)$$

The velocity of the fluid at the cylinder surface must be in the direction of oscillation, so that the conditions to be satisfied by u_r and u_θ on the cylinders are

$$u_r = a \cos \theta \exp(i\omega t)$$

and (2.50)

$$u_\theta = -a \sin \theta \exp(i\omega t) .$$

At $r = D_0/2$, the fluid velocity is zero; thus

$$u_r = u_\theta = 0 . \quad (2.51)$$

Equations 2.48-2.51 are the complete mathematical statement of the problem.

Equation 2.48 can easily be solved; the solution is

$$\psi = a \left[A_1 \left(\frac{D}{r} \right)^2 + A_2 r + A_3 D I_1(\lambda r) + A_4 D K_1(\lambda r) \right] \sin \theta \exp(i\omega t) , \quad (2.52)$$

where

$$\lambda = \sqrt{i \frac{\omega}{\nu}}$$

and A_1 , A_2 , A_3 , and A_4 are arbitrary constants. Using Eqs. 2.49-2.52, A_1 , A_2 , A_3 , and A_4 can be determined. The results are as follows:

$$\begin{aligned}
A_1 &= \{-\alpha^2[I_0(\alpha)K_0(\beta) - I_0(\beta)K_0(\alpha)] + 2\alpha[I_1(\alpha)K_0(\beta) + I_0(\beta)K_1(\alpha)] \\
&\quad - 2\alpha\gamma[I_0(\alpha)K_1(\beta) + I_1(\beta)K_0(\alpha)] + 4\gamma[I_1(\alpha)K_1(\beta) - I_1(\beta)K_1(\alpha)]\}/\Delta, \\
A_2 &= \{2\alpha\gamma[I_1(\beta)K_0(\beta) + I_0(\beta)K_1(\beta)] + \alpha^2\gamma^2[I_0(\alpha)K_0(\beta) - I_0(\beta)K_0(\alpha)] \\
&\quad - 2\alpha\gamma^2[I_1(\alpha)K_0(\beta) + I_0(\beta)K_1(\alpha)]\}/\Delta, \tag{2.53}
\end{aligned}$$

$$A_3 = \{-2\alpha K_0(\beta) - 4\gamma K_1(\beta) + \gamma^2[2\alpha K_0(\alpha) + 4K_1(\alpha)]\}/\Delta,$$

and

$$A_4 = \{-2\alpha I_0(\beta) + 4\gamma I_1(\beta) + \gamma^2[2\alpha I_0(\alpha) - 4I_1(\alpha)]\}/\Delta,$$

where

$$\alpha = \lambda D/2,$$

$$\beta = \lambda D_0/2,$$

$$\gamma = D_0/D,$$

and

$$\begin{aligned}
\Delta &= \alpha^2(1 - \gamma^2)[I_0(\alpha)K_0(\beta) - I_0(\beta)K_0(\alpha)] \\
&\quad + 2\alpha\gamma[I_0(\alpha)K_1(\beta) - I_1(\beta)K_0(\beta) + I_1(\beta)K_0(\alpha) - I_0(\beta)K_1(\beta)] \\
&\quad + 2\alpha\gamma^2[I_0(\beta)K_1(\alpha) - I_0(\alpha)K_1(\alpha) + I_1(\alpha)K_0(\beta) - I_1(\alpha)K_0(\alpha)]. \tag{2.54}
\end{aligned}$$

The resultant force per unit length of cylinder can be calculated in a straightforward fashion:

$$g = M_d a \omega [\operatorname{Re}(H) \sin \omega t + \operatorname{Im}(H) \cos \omega t]. \tag{2.55}$$

In the steady-state oscillations, Eq. 2.55 can be written

$$g = -C_m M_d \frac{d^2 u}{dt^2} - C_v \frac{du}{dt},$$

where

$$C_m = \text{Re}(H) ,$$

$$C_v = -M_d \omega \text{Im}(H) ,$$

$$M_d = \rho \pi R^2 ,$$

and

$$\begin{aligned} H = & \{ 2\alpha^2 [I_0(\alpha)K_0(\beta) - I_0(\beta)K_0(\alpha)] - 4\alpha [I_1(\alpha)K_0(\beta) + I_0(\beta)K_1(\alpha)] \\ & + 4\alpha\gamma [I_0(\alpha)K_1(\beta) + I_1(\beta)K_0(\alpha)] - 8\gamma [I_1(\alpha)K_1(\beta) - I_1(\beta)K_1(\alpha)] \} \\ & + \{ \alpha^2(1 - \gamma^2) [I_0(\alpha)K_0(\beta) - I_0(\beta)K_0(\alpha)] + 2\alpha\gamma [I_0(\alpha)K_1(\beta) \\ & - I_1(\beta)K_0(\beta) + I_1(\beta)K_0(\alpha) - I_0(\beta)K_1(\beta)] + 2\alpha\gamma^2 [I_0(\beta)K_1(\alpha) \\ & - I_0(\alpha)K_1(\alpha) - I_1(\alpha)K_0(\beta) - I_1(\alpha)K_0(\alpha)] \} - 1 . \end{aligned} \quad (2.56)$$

Two forces are associated with the fluid motion:

- (1) $M_d a \omega \text{Re}(H) \sin \omega t$, in phase with the acceleration, arises because the fluid is necessarily moved as the cylinder vibrates.
- (2) $M_d a \omega \text{Im}(H) \cos \omega t$, opposing the movement of the cylinder, is related to damping mechanism.

It is seen that H depends on α and β in a very complicated way. However, simplified results can be obtained in special cases:

$$(1) \quad D_0/D \sim \infty , \quad \nu = 0 ,$$

$$H = 1 ; \quad (2.57)$$

$$(2) \quad \nu = 0 ,$$

$$H = \frac{D_0^2 + D^2}{D_0^2 - D^2} ; \quad (2.58)$$

$$(3) \quad D_0/D \sim \infty ,$$

$$H = 1 + \frac{4K_1(\alpha)}{\alpha K_0(\alpha)} ; \quad (2.59)$$

(4) α and β are large,

$$\begin{aligned}
 H = & \{ [\alpha^2(1 + D_0^2/D^2) - 8D_0/D] \sinh(\beta - \alpha) \\
 & + 2\alpha(2 - D_0/D + D_0^2/D^2) \cosh(\beta - \alpha) - 2D_0^2/D^2 \sqrt{\alpha\beta} - 2\alpha(D_0/D)^{1.5} \} \\
 & + \{ \alpha^2(1 - D_0^2/D^2) \sinh(\beta - \alpha) - 2\alpha D_0/D(1 + D_0/D) \cosh(\beta - \alpha) \\
 & + 2D_0^2/D^2 \sqrt{\alpha\beta} + 2\alpha(D_0/D)^{1.5} \} .
 \end{aligned} \quad (2.60)$$

The values of C_m and C_v depend on H , which, in turn, is a function of the diameter ratio D_0/D and kinetic Reynolds number $R_k (= \omega D^2/\nu)$. The values of $\text{Re}(H)$ and $-\text{Im}(H)$ are given in Figs. 2.8 and 2.9, respectively. The corresponding values of H for a circular cylinder vibrating in an infinite viscous fluid is given in Fig. 2.10 (Chen 1983).

Based on the boundary-layer approximation, approximate expressions for C_m and C_v were developed (Sinyavaskii et al. 1980):

$$C_m = \frac{D_0^2 + D^2}{D_0^2 - D^2} + \frac{4}{D} \left(\frac{2\nu}{\omega} \right)^{1/2},$$

and

(2.61)

$$C_v = \frac{2\pi\mu D}{\sqrt{\frac{2\nu}{\omega}}} \left[\frac{D_0^4 + D^3 D_0}{(D_0^2 - D^2)^2} \right],$$

where $\sqrt{\omega/2\nu}$ is the viscous penetration depth. Note that Eq. 2.61 is similar to Eq. 2.60; it is applicable for $\omega D^2/4\nu \gg 1$. In many practical applications, Eq. 2.61 can be employed. Several additional approximate solutions for C_m and C_v also are given in Section 3.7.

The theoretical results and experimental data agree well for a cylinder oscillating in both an infinite fluid (Williams and Hussey 1972) and an annular region (Chen et al. 1976; Sinyavaskii et al. 1980). However, the linear theory is applicable only for small-amplitude oscillations (see Section 2.10 for discussion).

For a uniform cylinder with mass per unit length m , the modal damping ratio attributed to fluid viscosity can easily be obtained:

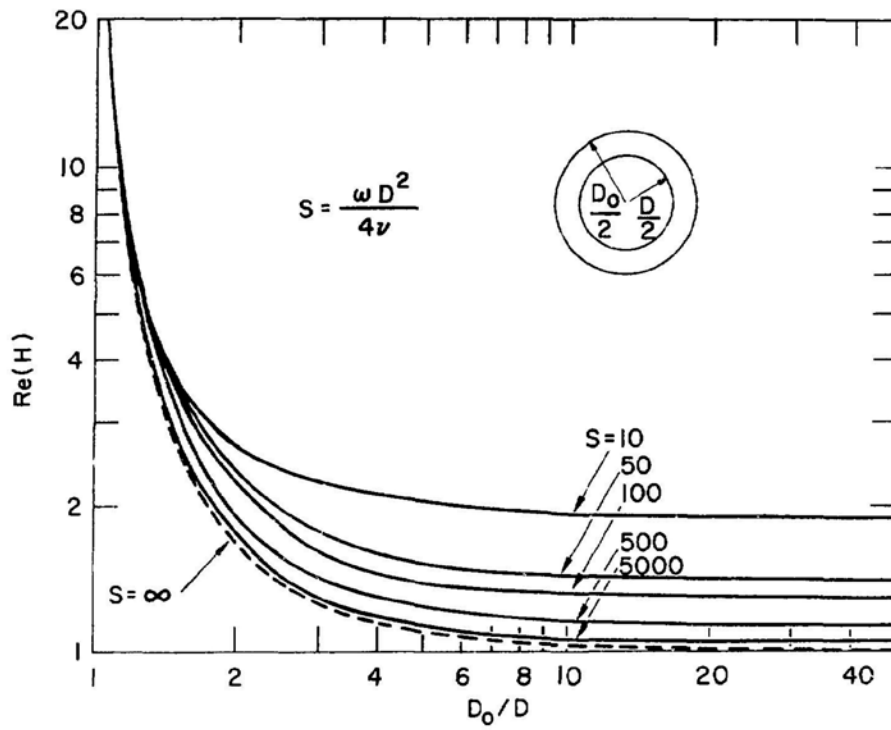


Fig. 2.8. Real Values of H as a Function of Diameter Ratio and Kinetic Reynolds Number (Chen et al. 1976)

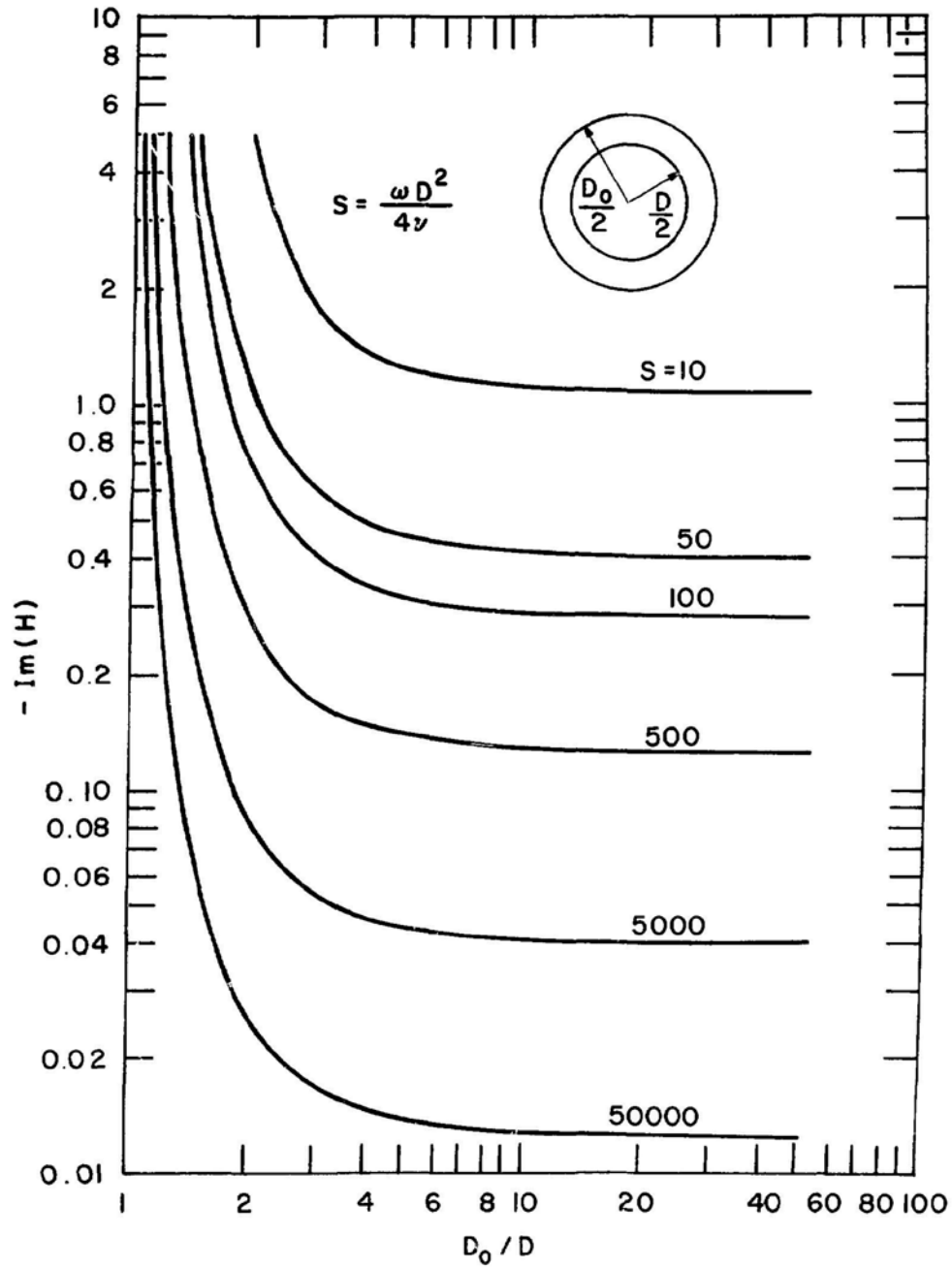


Fig. 2.9. Imaginary Values of H as a Function of Diameter Ratio and Kinetic Reynolds Number (Chen et al. 1976)

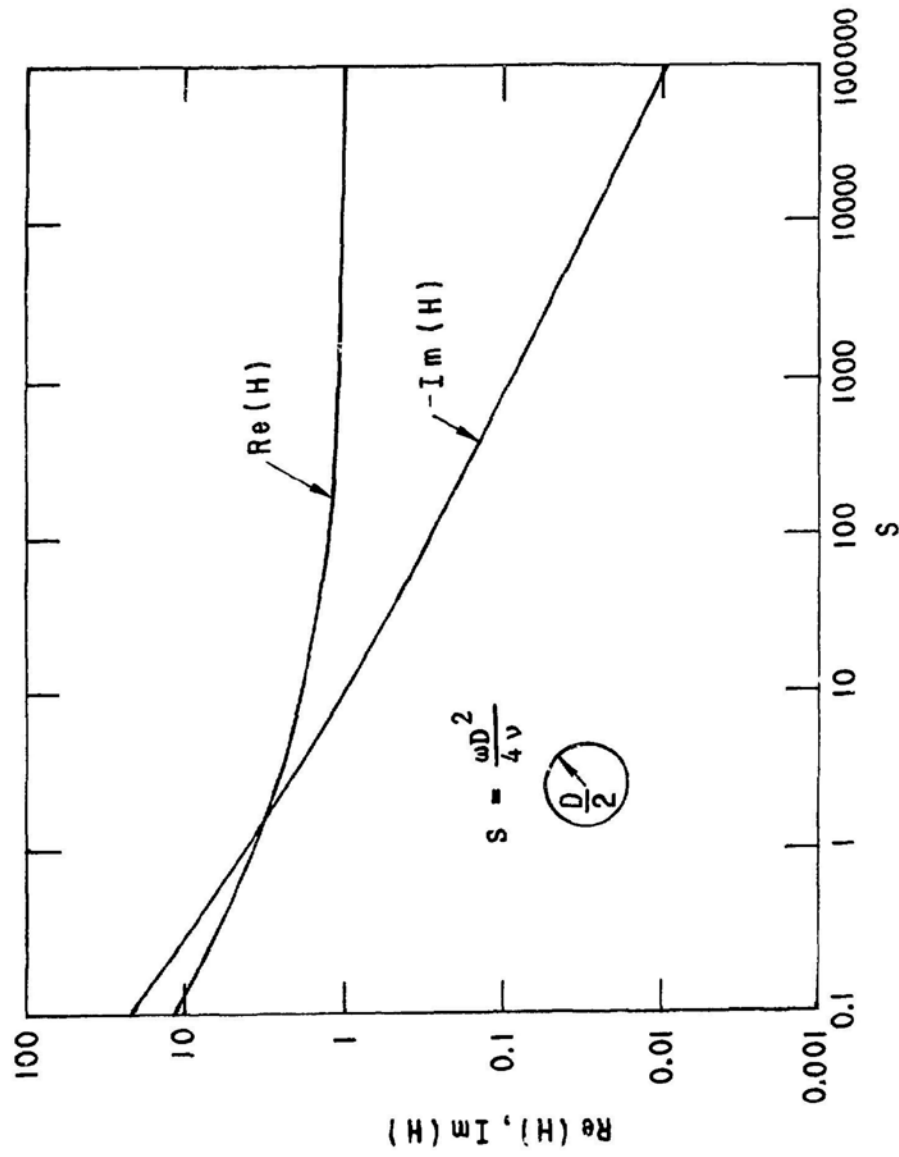


Fig. 2.10. Real and Imaginary Values of H for a Cylinder Vibrating in an Infinite Incompressible Viscous Fluid (Chien 1983)

$$\zeta_f = -\frac{1}{2} \left(\frac{M_d}{C_m M_d + m} \right) \text{Im}(H) . \quad (2.62)$$

The analytical results for ζ_f were verified using several viscous fluids (Chen et al. 1976); the agreement between theory and experiment is good.

2.7 A CIRCULAR CYLINDER IN AN ECCENTRIC ANNULAR INCOMPRESSIBLE VISCOUS FLUID

Closed form solution for this case is not available. However, added mass and viscous damping can be obtained using a finite-element method (Yang and Moran 1979). A system of discretized equations is obtained from the appropriate two-dimensional Navier-Stokes and continuity equations through Galerkin's process. The basic unknowns are velocity and pressure. The added mass and viscous damping coefficients are obtained through a line integration of stress and pressure around the circumference of the cylinder.

Typical results are given in Fig. 2.11. Both C_m and C_v increase with eccentricity.

2.8 A CIRCULAR CYLINDER IN A CONCENTRIC ANNULAR TWO-PHASE FLOW

There are varying flow regimes in two-phase flows, depending on the ratio of gas to liquid in the mixture. This ratio is generally called the void fraction α_e . $\alpha_e = 0$ and $\alpha_e = 1$ correspond to pure liquid and gas flows, respectively. The added mass and damping depend on α_e .

A circular cylinder vibrating in a confined two-phase flow was studied experimentally by several investigators (Carlucci 1980; Schumann 1981; Carlucci and Brown 1982; Hara and Kolgo 1982). The inertial and damping forces can be written

$$g = -C_m M_d \frac{d^2 u}{dt^2} - C_v \frac{du}{dt} . \quad (2.63)$$

$$C_v = C'_v + C_t .$$

The fluid viscous damping coefficient C_v consists of two parts: C'_v is attributed to fluid viscosity and C_t is called two-phase flow damping.

The added mass coefficient C_m and viscous damping coefficient C'_v are not the same as those for a single-phase flow. Based on the limited experimental data, and on analytical results, C_m can be calculated based on Eq. 2.56 except that the effective density should be used. The ratio of effective density ρ_e

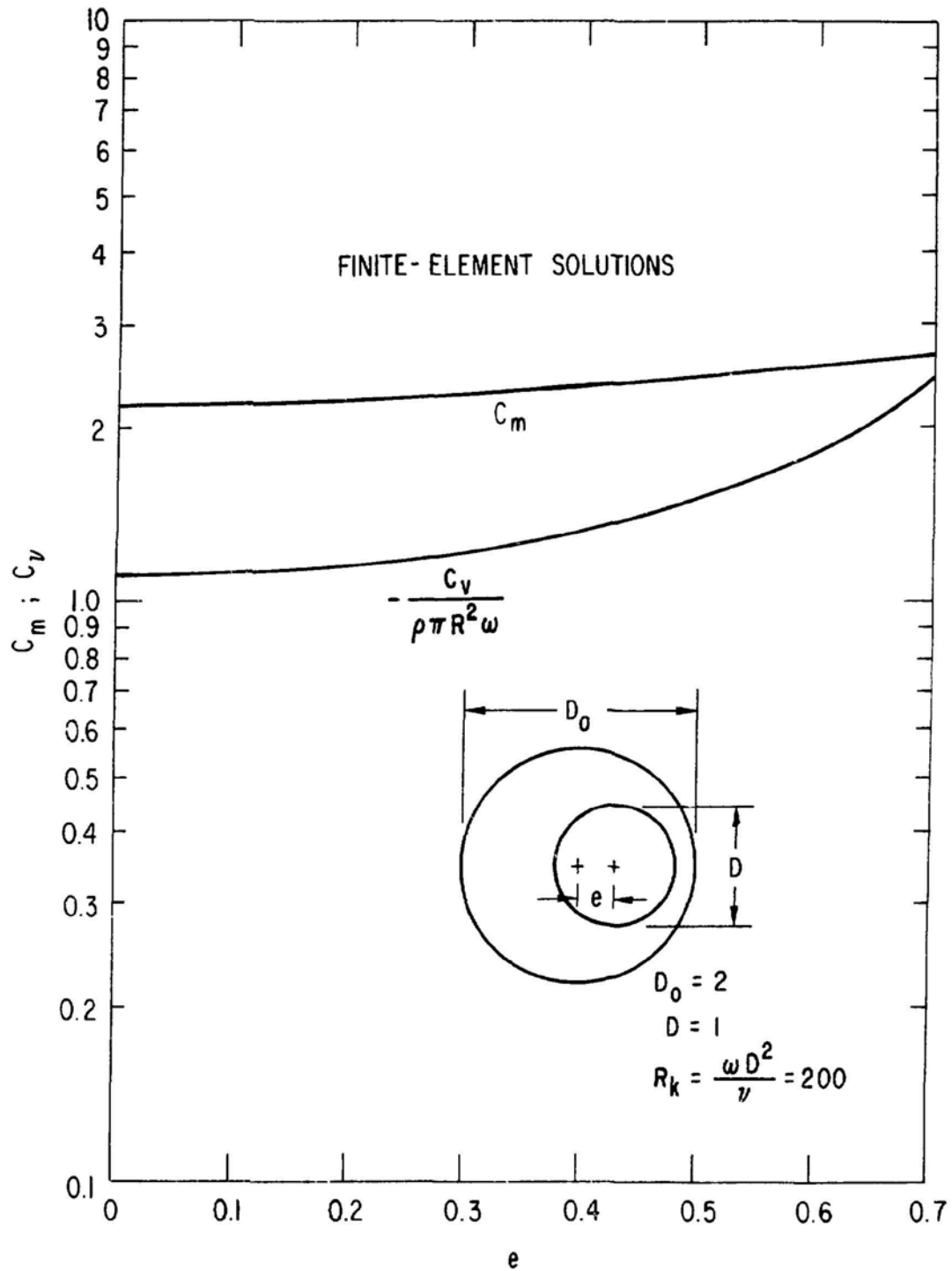


Fig. 2.11. Added Mass and Damping Coefficients as a Function of Eccentricity (Lang and Moran 1979)

to that of the single-phase flow ρ is given in Fig. 2.12, which includes experimental data and analytical results. The theoretical values ρ_e of the effective density are given by

$$\begin{aligned} (1) \quad \rho_e &= (1 - \alpha_e)\rho + \alpha_e\rho', \\ (2) \quad \rho_e &= \rho(1 - \alpha_e)/(2\alpha_e + 1), \\ (3) \quad \rho_e &= \rho(1 - \alpha_e)(1 + 2\alpha_e)/(1 + 4\alpha_e - 2\alpha_e^2), \end{aligned} \quad (2.64)$$

where ρ and ρ' are the densities of the two fluids. The first equation of Eq. 2.64 is applicable for small α_e ; at large α_e , it predicts much larger ρ_e than the experimental data. The last two equations in Eq. 2.64 correlate better with the experimental data at high values of α_e and are applicable in that range.

The coefficient C'_v in Eq. 2.63 for two-phase flow is calculated following the same method as C_v for a single-phase flow described in Section 2.6. However, the effective density ρ_e given in Eq. 2.64 and the mixture kinetic viscosity based on McAdams' definition (Collier 1972) should be used. The mixture viscosity according to McAdams is given by the following equation:

$$\frac{1}{\mu_{\text{mixture}}} = \frac{\alpha_e}{\mu_{\text{vapor}}} + \frac{(1 - \alpha_e)}{\mu_{\text{liquid}}}. \quad (2.65)$$

There is no analytical expression for C_t . The most complete experimental data are those by Carlucci and Brown (1982); these data are given in Fig. 2.13. With Fig. 2.13, the two-phase damping coefficient C_t can be calculated based on C'_v .

The added mass and damping of circular cylinders vibrating in a two-phase flow are still not well understood. More theoretical and experimental studies are needed.

2.9 FREE VIBRATION OF A CIRCULAR CYLINDER SUPPORTED AT BOTH ENDS IN A FLUID

Once the added mass and damping coefficients are obtained, the analysis of a cylinder in fluid is relatively simple. For example, consider a circular rod submerged in a fluid (Fig. 2.14). The equation of motion for free vibration is as follows:

$$EI \frac{\partial^4 u}{\partial z^4} + (C_s + C_v) \frac{\partial u}{\partial t} + (m + m_a) \frac{\partial^2 u}{\partial t^2} = 0, \quad (2.66)$$

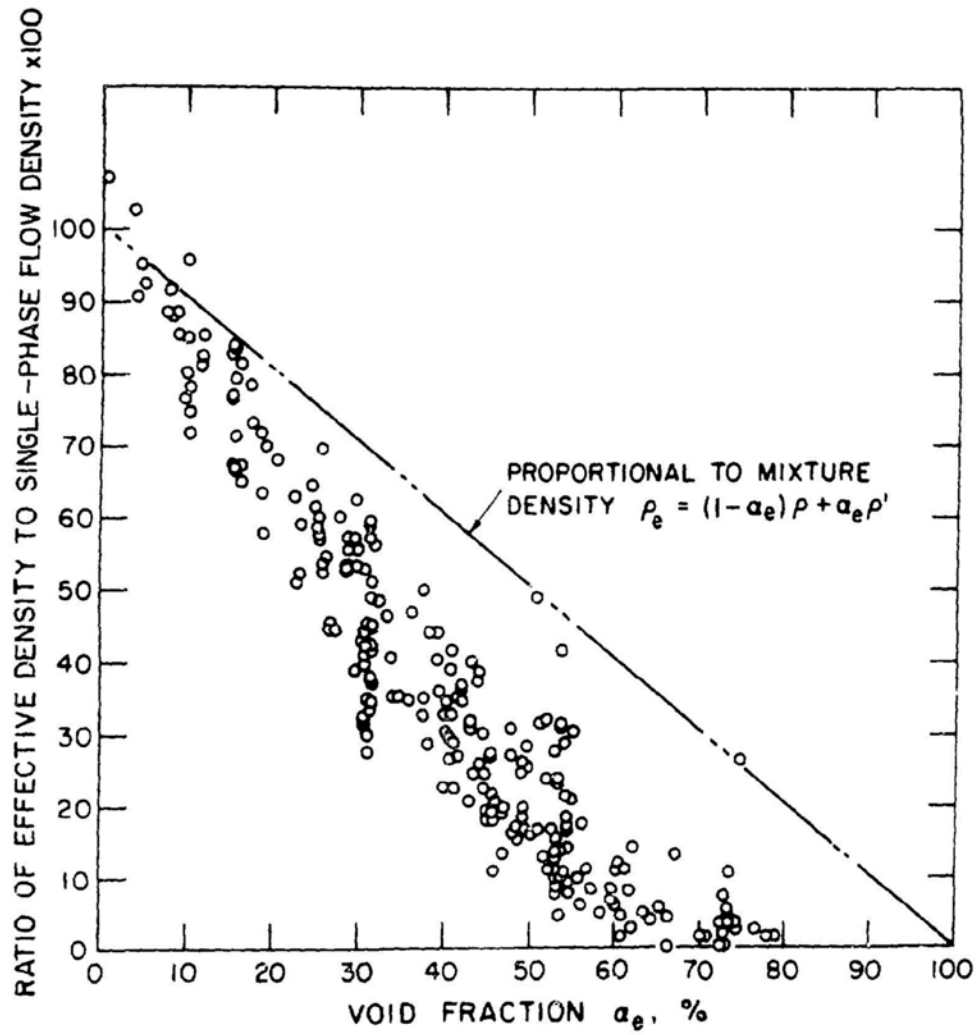


Fig. 2.12. Effective Density for Two-phase Flow as a Function of Void Fraction (from Carlucci 1980, with permission--see Credits)

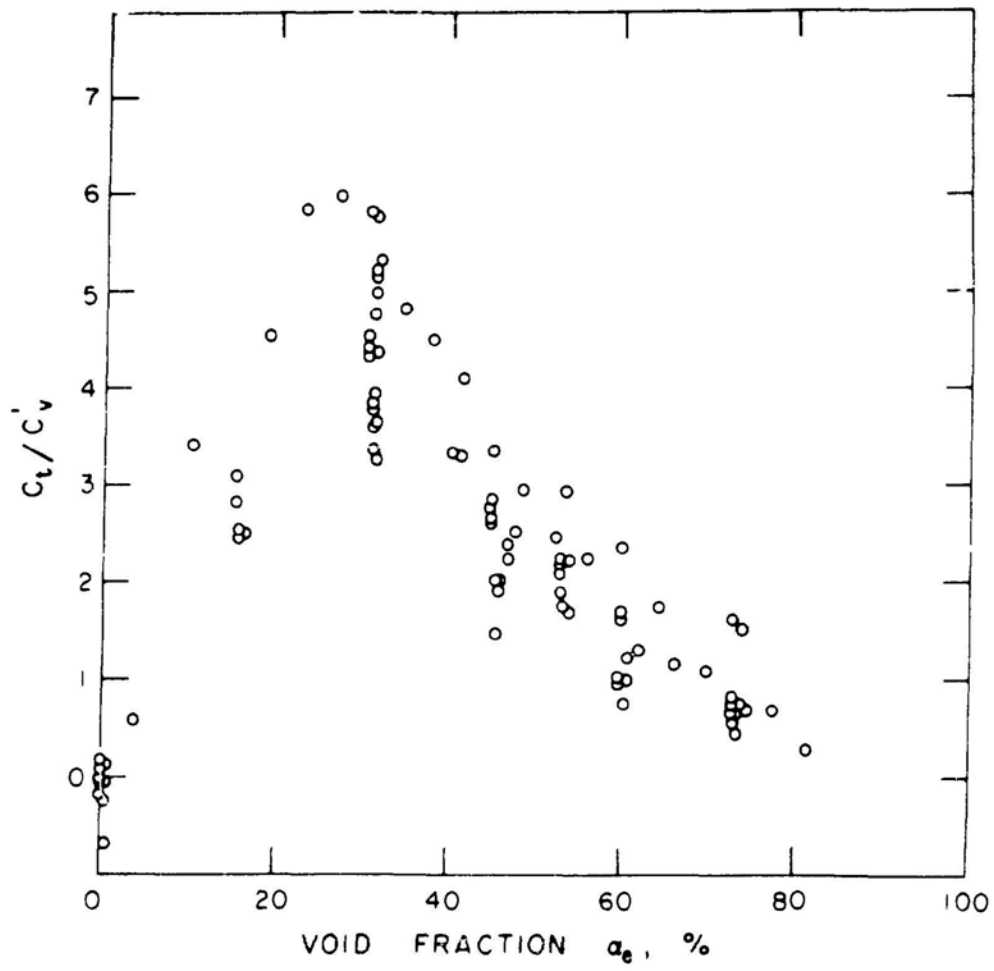


Fig. 2.13. Two-phase Flow Damping Coefficient (from Carlucci and Brown 1982, with permission---see Credits)

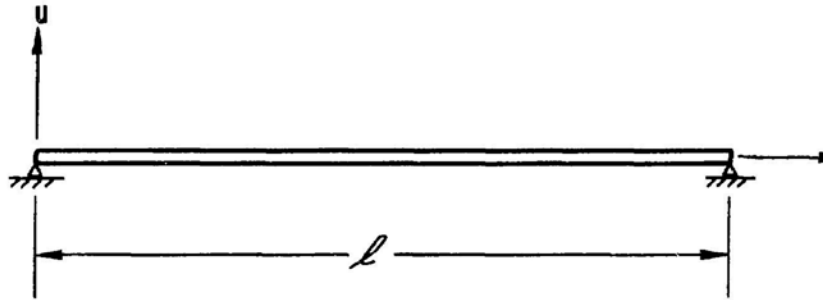


Fig. 2.14. A Circular Cylinder Vibrating in a Fluid

where EI is the flexural rigidity. The natural frequencies and modal damping ratios are

$$f_f = \frac{\lambda_n^2}{2\pi l^2} \left(\frac{EI}{m + m_a} \right)^{1/2}$$

and

$$\zeta_f = \frac{C_s + C_v}{4\pi(m + m_a)f_f} \quad (2.67)$$

where λ_n is a dimensionless parameter that is a function of the boundary conditions (see Appendix C).

When the rod is oscillating in a vacuum, $C_v = m_a = 0$. The corresponding natural frequencies and modal damping ratio are

$$f_v = \frac{\lambda_n^2}{2\pi l^2} \left(\frac{EI}{m} \right)^{1/2}$$

and

$$\zeta_v = \frac{C_s}{4\pi m f_v} \quad (2.68)$$

Using Eqs. 2.67 and 2.68 yields

$$\frac{f_f}{f_v} = \left(\frac{m}{m + m_a} \right)^{1/2} \quad (2.69)$$

and

$$\frac{\zeta_f}{\zeta_v} = \left(\frac{C_s + C_v}{C_s} \right) \left(\frac{m}{m + m_a} \right)^{1/2} \quad (2.70)$$

In most practical applications, m_a is positive; therefore, the added mass is to reduce the natural frequencies. From Eq. 2.69,

$$m_a = m \left(\frac{f_v^2}{f_f^2} - 1 \right) \quad (2.71)$$

By measuring the natural frequencies in vacuum and in a fluid, the added mass,

m_a , can be calculated. In fact, Eq. 2.71 has been used extensively in tests to determine the added mass.

The ratio of modal damping values in vacuum and in fluid given by Eq. 2.70 consists of two factors; the first ratio is always larger than 1, while the second factor is smaller than 1 in most cases. Theoretically, ζ_f can be smaller or larger than ζ_v . However, in most practical cases, ζ_f is slightly smaller than ζ_v . Equation 2.70 can also be employed to determine the fluid viscous damping coefficient C_v :

$$C_v = \left[\left(\frac{m + m_a}{m} \right)^{0.5} \frac{\zeta_f}{\zeta_v} - 1 \right] C_s \quad (2.72)$$

Measuring the damping values in vacuum and in fluid, the fluid viscous damping can be obtained from Eq. 2.72.

2.10 NONLINEAR EFFECTS OF A CIRCULAR CYLINDER OSCILLATING IN AN INFINITE FLUID

The results presented in Sections 2.2 through 2.9 are applicable to small-amplitude oscillations; i.e., the cylinder displacement must be much smaller than a characteristic length, such as cylinder diameter, or the clearance between the cylinder and its surrounding structures. When the displacement becomes large, nonlinear effects become important.

The added mass and damping of a circular cylinder were studied experimentally in detail by Skop et al. (1976). The added mass coefficient C_m is essentially equal to 1, as predicted by linear theory. For $K_c (= 2\pi a/D)$ larger than 2.51, the fluid damping contains both linear and velocity-squared components. The viscous damping coefficient C_v to account for the large amplitude oscillations is given as follows:

$$C_v = M_d \omega \left(\frac{1}{R_k} \right)^{0.5} \left[18 + 0.91 R_k^{0.5} \left(\frac{K_c}{2\pi} - 0.4 \right) H \left(\frac{K_c}{2\pi} - 0.4 \right) \right], \quad (2.73)$$

where H is the Heaviside unit step function. Equation 2.73 was determined from experimental data obtained for $920 < R_k < 2.1 \times 10^4$.

For large-amplitude vibrations, the results obtained from the linear theory are not strictly applicable, and there are very few data available for large-amplitude oscillations. Fortunately, in most practical applications, one is more interested in small-amplitude oscillations, since large-amplitude vibration is not acceptable in general. In addition, linear theory is also valid to determine the stability-instability boundary.

2.11 THREE-DIMENSIONAL EFFECT ON A CIRCULAR CYLINDER OSCILLATING IN FLUID

In the analysis presented in Sections 2.2 through 2.10, it has been assumed that the flow field can be considered as two-dimensional, although the motion of a cylinder may produce a three-dimensional flow field. To understand the three-dimensional effect of the flow field on C_m , let us consider the cylinder given in Fig. 2.3, in which the fluid is a perfect fluid.

Let the cylinder displacement be $u(z,t)$. The fluid in the annular region is governed by the Laplace equation

$$\begin{aligned}\nabla^2 \phi(r, \theta, z, t) &= 0, \\ \vec{U} &= \vec{\nabla} \phi, \\ p &= -\rho \frac{\partial \phi}{\partial t}.\end{aligned}\tag{2.74}$$

The boundary conditions are

$$u_r = 0 \quad \text{at } r = \frac{D}{2},$$

(2.75)

and

$$u_r = \frac{\partial u}{\partial t} \cos \theta \quad \text{at } r = \frac{D}{2}.$$

The transverse load acting on the cylinder is

$$g = -R \int_0^{2\pi} p(r, \theta, z, t) \Big|_{r=R} \cos \theta d\theta.\tag{2.76}$$

A traveling wave solution is sought for the cylinder

$$u = a \cos \theta \exp[i2\pi(c_p t - z)/\lambda],\tag{2.77}$$

where c_p is the phase velocity, λ is the axial wave length, and a is an arbitrary constant. Similarly, the potential ϕ may be defined by the following expression:

$$\phi = F_r(r) \cos \theta \exp[i2\pi(c_p t - z)/\lambda].\tag{2.78}$$

Substituting Eq. 2.78 into 2.74 gives the following form of Bessel's equation

$$\frac{d}{dr} \frac{d}{dr} \left(r \frac{dF}{dr} \right) - \left[\frac{1}{r^2} + \frac{4\pi^2}{\ell^2} \right] F_r = 0. \quad (2.79)$$

The solution of Eq. 2.79 is

$$F_r(r) = A_1 I_1 \left(\frac{2\pi}{\ell} r \right) + A_2 K_1 \left(\frac{2\pi}{\ell} r \right). \quad (2.80)$$

Using Eqs. 2.74-2.80, the added mass coefficient C_m can be easily obtained:

$$C_m = \frac{I_1' \left(\frac{\pi D}{\ell} \right) K_1 \left(\frac{\pi D}{\ell} \right) - I_1 \left(\frac{\pi D}{\ell} \right) K_1' \left(\frac{\pi D}{\ell} \right)}{I_1' \left(\frac{\pi D}{\ell} \right) K_1' \left(\frac{\pi D}{\ell} \right) - I_1 \left(\frac{\pi D}{\ell} \right) K_1 \left(\frac{\pi D}{\ell} \right)}. \quad (2.81)$$

When $D/\ell \rightarrow 0$, from Eq. 2.81, it can be shown that

$$C_m \Big|_{D/\ell \rightarrow 0} = \frac{D_o^2 + D^2}{D_o^2 - D^2}. \quad (2.82)$$

This is consistent with the results given in Eq. 2.58. The values of C_m are given in Fig. 2.15 for several values of $\pi D/\ell$. C_m decreases with increasing α . Therefore, the values of C_m calculated based on the two-dimensional theory is the upper bound for C_m based on the three-dimensional theory. In general, if ℓ is much larger than D , the two-dimensional theory is applicable. If D is of the same order as ℓ , three-dimensional effect should be considered.

2.12 A CIRCULAR CYLINDER IN A FINITE-LENGTH ANNULAR VISCOUS REGION

When the length of the annular region is small (see Fig. 2.16; L is the same order of magnitude as D), the three-dimensional effect becomes significant. An approximate solution for this case was obtained by Mulcahy (1980). It is based on the linearized Navier-Stokes equations and the assumption that the gap clearance is much less than the cylinder radius $D/2$. The fluid force acting on the cylinder is given by

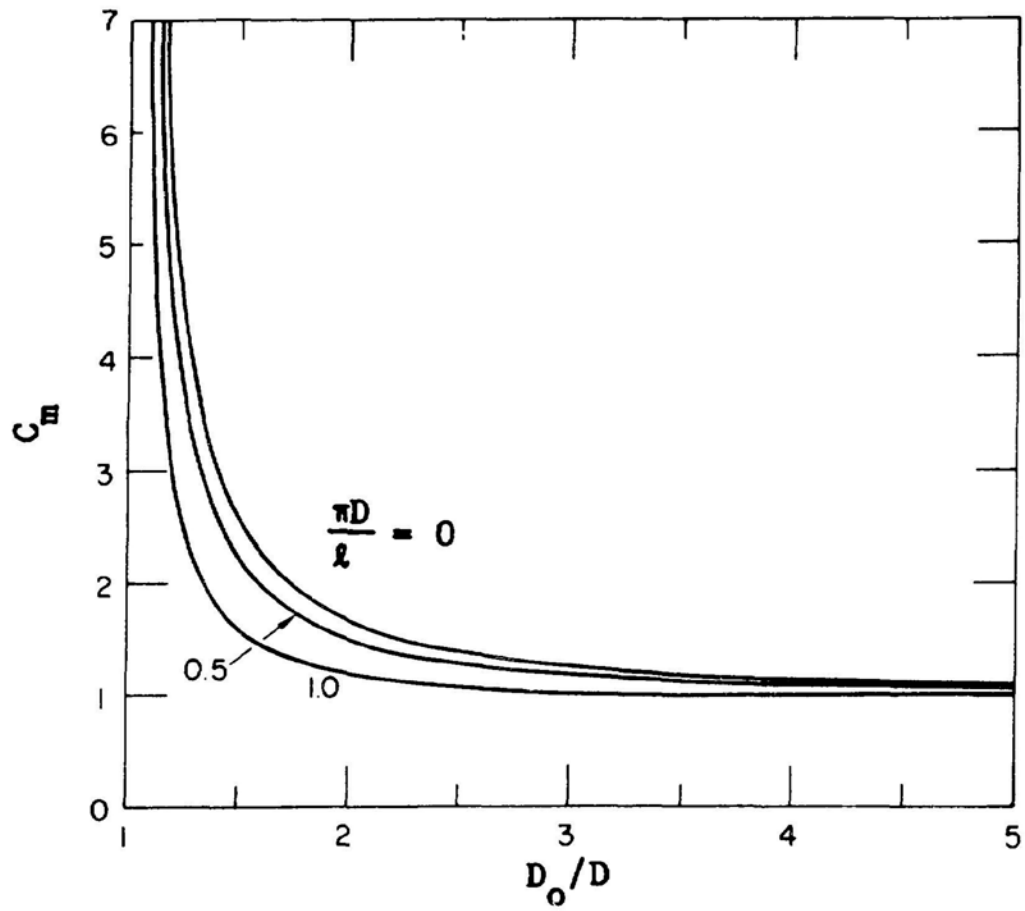


Fig. 2.15. Three-dimensional Effect on the Added Mass Coefficient
(Chen 1974)

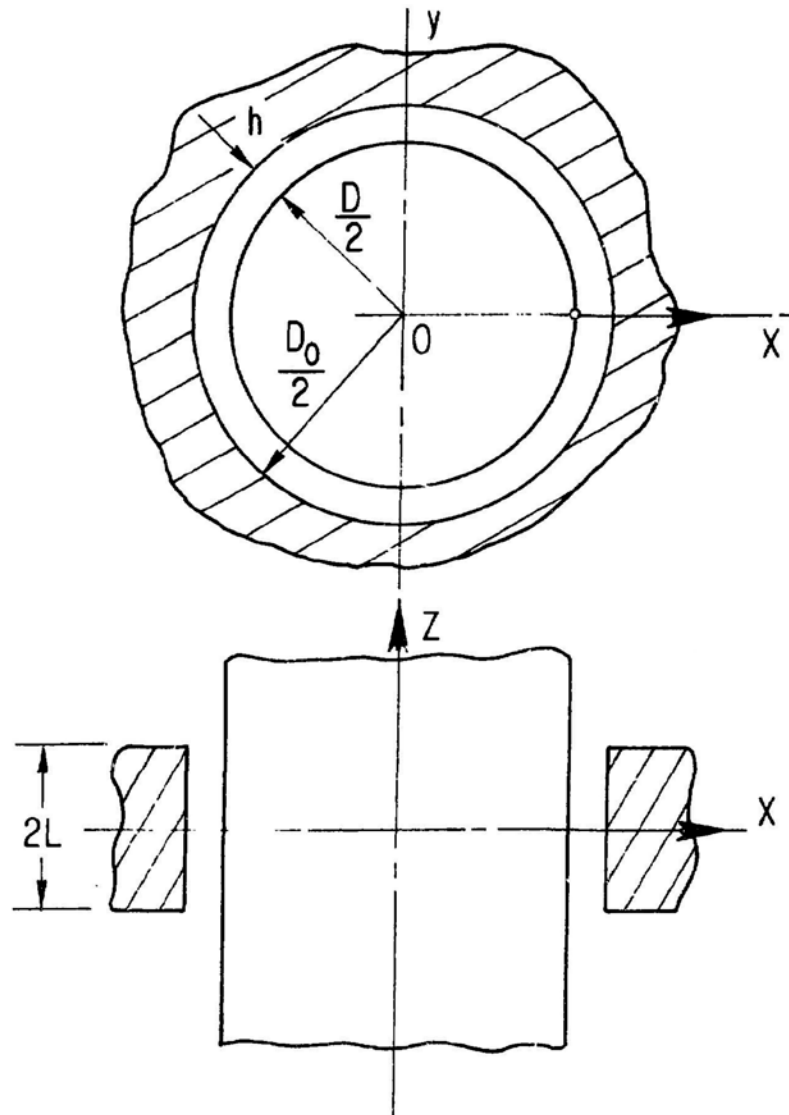


Fig. 2.16. A Circular Cylinder in a Fluid-filled Annular Region

$$g = -C_m M_d \frac{\partial^2 u}{\partial t^2} - C_v \frac{\partial u}{\partial t},$$

$$C_m = \left(\frac{D}{D_o - D} \right) \text{Re}(H) \left[1 - \frac{\cosh(2z/D_o)}{\cosh(2L/D_o)} \right],$$

$$C_v = -M_d \left(\frac{D}{D_o - D} \right) \omega \text{Im}(H) \left[1 - \frac{\cosh(2z/D_o)}{\cosh(2L/D_o)} \right] \quad (2.83)$$

$$H = \frac{\alpha \sinh \alpha}{(2 + \alpha \sinh \alpha - 2 \cosh \alpha)},$$

and

$$\alpha = \frac{(1+i)}{2} \sqrt{\frac{\omega(D_o - D)^2}{2\nu}}. \quad (2.84)$$

The theoretical values of $\text{Re}(H)$ and $-\text{Im}(H)$ are given in Fig. 2.17. Experimental data are shown to agree well with the theory. The solution is valid for $(D_o - D)/D \ll 1$ and the viscous penetration depth $\sqrt{\omega/2\nu}$ on the order of $\frac{1}{2}(D_o - D)$.

Note that Eq. 2.84 is applicable for transverse motion within the gap. The damping associated with the rotational motion is, in general, much smaller and can be ignored.

2.13 EXAMPLES OF APPLICATIONS

Consider a simply supported tube with a baffle plate at midspan (see Fig. 2.18). The tube is a stainless tube submerged in water (70°F). Tube properties are given as follows:

Tube OD (D) = 1 in.,

Tube wall thickness = 1/8 in.,

Tube length l = 48 in.,

Baffle-plate-hole diameter (D_o) = 1.02 in., and

Baffle plate thickness ($2L$) = 1.5 in.

We wish to calculate the fluid damping with and without the baffle plate.

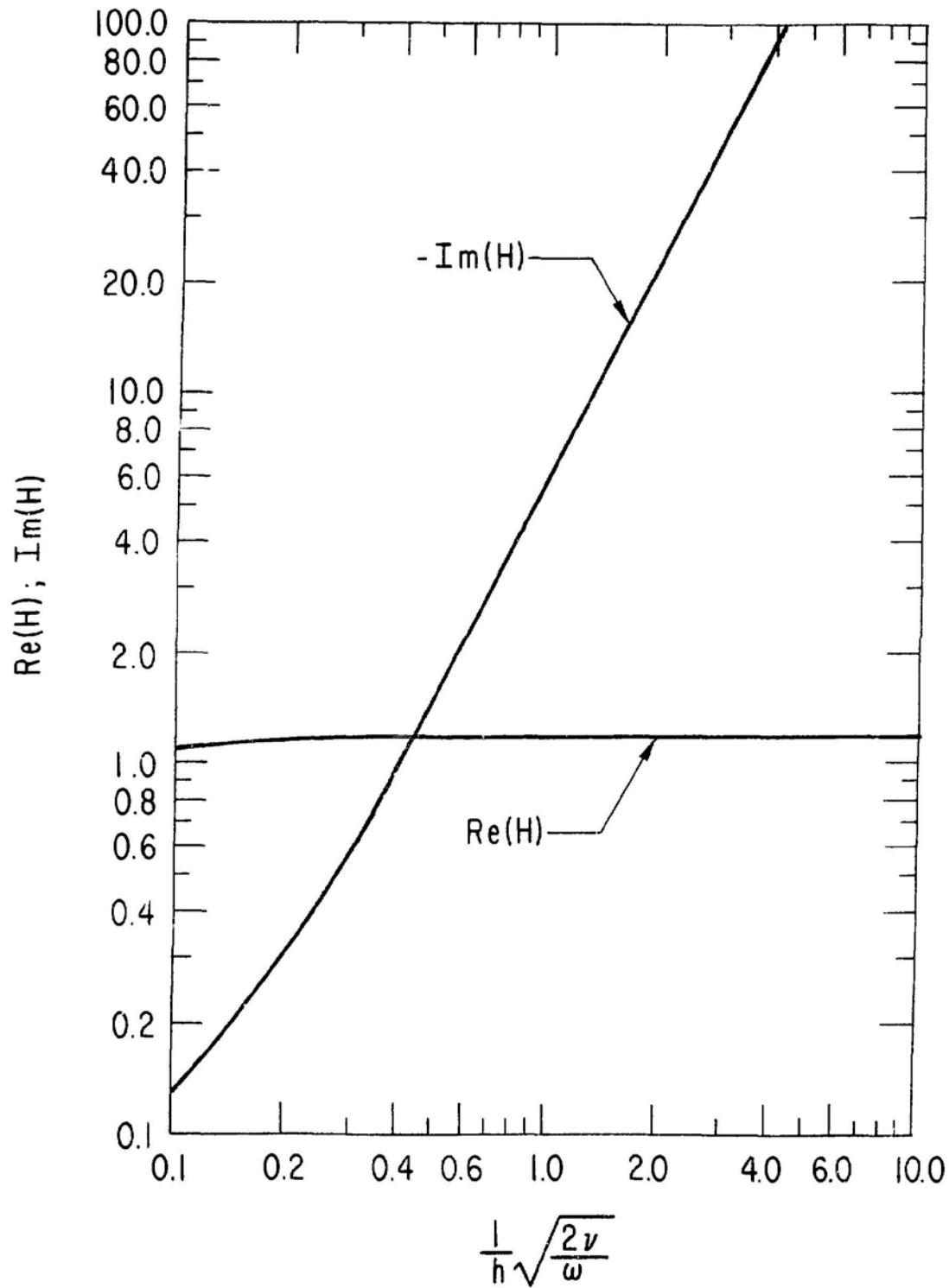


Fig. 2.17. Real and Imaginary Values of H for a Cylinder Vibrating in a Finite-length Annular Viscous Fluid (Mulcahy 1980)

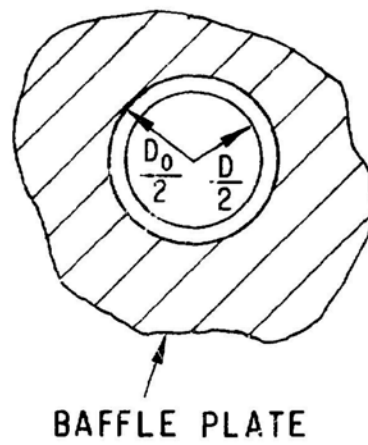
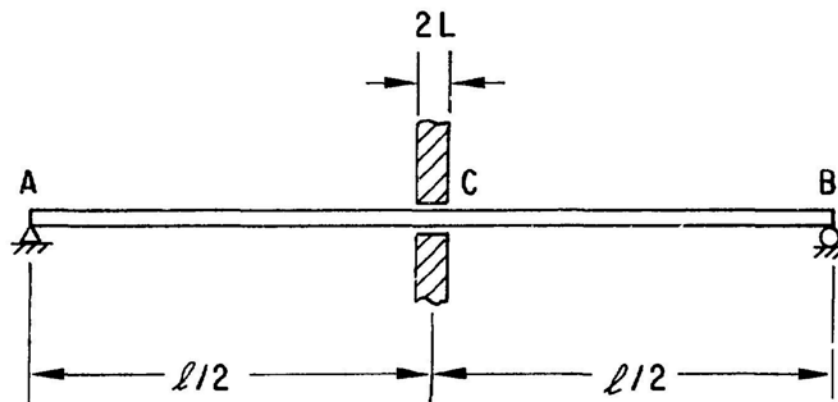


Fig. 2.18. A Simply Supported Tube with a Baffle Plate Support

No Baffle Plate

For the case of a tube vibrating in an infinite fluid, the modal damping ratio attributed to fluid can be calculated from Eq. 2.62:

$$\zeta_f = -\frac{1}{2} \left(\frac{M_d}{C_m M_d + m} \right) \text{Im}(H) . \quad (2.85)$$

Note that the natural frequency of the fundamental mode is given by

$$\omega_{f1} = \frac{\pi^2}{L^2} \left(\frac{EI}{C_m M_d + m} \right)^{0.5} , \quad (2.86)$$

and that

$$E = 30 \times 10^6 \text{ lb/in.} ,$$

$$I = \frac{\pi}{64} (1.0^4 - 0.75^4) \text{ in.}^4 = 0.0336 \text{ in.}^4 , \quad (2.87)$$

$$m = \frac{\pi}{4} (1^2 - 0.75^2) \cdot 7.5 \times 10^{-4} \text{ lb-sec}^2/\text{in.}^2 = 2.58 \times 10^{-4} \text{ lb-sec}^2/\text{in.}^2 ,$$

and

$$M_d = \frac{\pi}{4} \times 0.935 \times 10^{-4} \times 1.0^2 \text{ lb-sec}^2/\text{in.}^2 = 0.734 \times 10^{-4} \text{ lb-sec}^2/\text{in.}^2$$

The effect of fluid viscosity on C_m is small; C_m is assumed to be 1. Substituting these values into Eq. 2.86 yields

$$\omega_{f1} = 236.3 \text{ rad/sec}$$

and

$$S = \frac{\omega_{f1}^2 D^2}{4\nu} = \frac{236.3^2 \times 1^2}{4 \times 0.00157} \approx 3.76 \times 10^4 .$$

From Fig. 2.10, $\text{Re}(H) \approx 1$ and $-\text{Im}(H) = 0.0105$. Therefore,

$$\zeta_{f1} \approx \frac{1}{2} \left(\frac{0.734}{0.734 + 2.58} \right) \times 0.0105 = 0.116\% .$$

The modal damping attributed to fluid is small.

With Baffle Plate

The equation of motion of the tube is given as follows:

$$EI \frac{\partial^4 u}{\partial z^4} + C_g \delta \left(\frac{g}{2} \right) \frac{\partial u}{\partial t} + (m + C_m M_d) \frac{\partial^2 u}{\partial t^2} = 0 , \quad (2.88)$$

where EI = flexural rigidity, u = tube displacement, t = time, δ = delta function, m = tube mass per unit length, and $C_m M_d$ = added mass per unit length. The second term is the damping associated with the fluid in the annular region of the baffle plate; all other damping and excitation forces are neglected in Eq. 2.88. Since the tube is hinged at both ends, let

$$u = q(t) \sin \frac{n\pi x}{L} . \quad (2.89)$$

Using Eqs. 2.88 and 2.89 yields

$$\begin{aligned} \frac{d^2 q}{dt^2} + 2\zeta_{fn} \omega_{fn} \frac{dq}{dt} + \omega_{fn}^2 q &= 0 , \\ \omega_{fn} &= \frac{n^2 \pi^2}{L^2} \left(\frac{EI}{m + C_m M_d} \right)^{0.5} , \\ \zeta_{fn} &= \frac{C_g}{(m + C_m M_d) L_f \omega_{fn}} , \quad n = \text{odd} \\ &= 0 , \quad n = \text{even} . \end{aligned} \quad (2.90)$$

The damping coefficient C_g is given by

$$C_g = \int_{-L}^L C_v dz , \quad (2.91)$$

where C_v is given in Eq. 2.83,

$$C_v = -M_d \left(\frac{D}{D_o - D} \right) \omega_{fn} \text{Im}(H) \left[1 - \frac{\cosh(2z/D_o)}{\cosh(2L/D_o)} \right] . \quad (2.92)$$

Substituting Eq. 2.92 into 2.91 yields

$$C_g = 2L\lambda M \left(\frac{D}{D_o - D} \right) \omega_n [-\text{Im}(H)]$$

and

(2.93)

$$\lambda = 1 - \frac{D}{2L} \tanh \left(\frac{2L}{D} \right) .$$

Substituting Eq. 2.93 into 2.90 yields

$$\begin{aligned} \zeta_n &= \lambda M_d \left(\frac{D}{D_o - D} \right) [-\text{Im}(H)] \frac{2L}{(m + C M_d) \ell} , \quad n = \text{odd} \\ &= 0 , \quad n = \text{even} . \end{aligned} \quad (2.94)$$

When n is an odd number, the tube vibrates within the gap (see Fig. 2.19); the fluid in the annular contributes to damping. When n is even, the tube vibrates against the baffle plate, the midspan at the baffle plate is a nodal point, and the damping attributed to the fluid at the baffle plate is zero.

In Eq. 2.94, the function H depends on the oscillation frequency; therefore, the modal damping for different modes are different. Based on Eq. 2.94 and Fig. 2.17 the modal damping for the fundamental mode is calculated as follows:

$$\frac{2}{D_o - D} \sqrt{\frac{2\nu}{\omega_{f1}}} = \frac{1}{0.01} \left(\frac{2 \times 0.00157}{236.3} \right)^{0.5} = 0.365 .$$

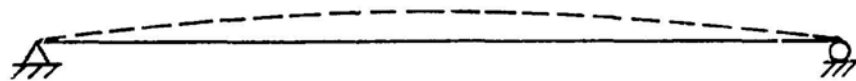
From Fig. 2.17, $-\text{Im}(H) = 0.82$,

$$\begin{aligned} \lambda &= 1 - \frac{D}{2L} \tanh \left(\frac{2L}{D} \right) \\ &= 1 - \frac{0.5}{0.75} \tanh \left(\frac{0.75}{0.5} \right) = 0.397 , \end{aligned}$$

$$\begin{aligned} \zeta_{f1} &= 0.397 \times 0.734 \times 10^{-4} \left(\frac{0.5}{0.01} \right) \times 0.82 \frac{1.5}{(2.58 + 0.734) \times 10^{-4} \times 48} \\ &= 11.27\% . \end{aligned}$$

Therefore, the total fluid damping is equal to

(1) TUBE VIBRATING WITHIN THE GAP



(2) TUBE VIBRATING AGAINST THE GAP



Fig. 2.19. Different Modes for a Tube with Motion-limiting Gap

$$\zeta_1 = 0.116\% + 11.27\% = 11.39\% .$$

Results of an experimental study of damping and natural frequency as functions of tube/tube-support-plate diametral clearance and plate thickness are reported by Jendrzejczyk (1985). The theoretical values and experimental data agree reasonably well.

2.14 CLOSING REMARKS

The effect of quiescent fluid on the oscillations of a single cylinder can be accounted for by using the motion-dependent fluid force given in Eq. 1.3. In this chapter, the values of added mass and fluid damping are presented for various cases. Most of these results are given for small motion; i.e., for small Keulegan-Carpenter parameter K_C , the linearized equation for the fluid force is applicable. When K_C is large, the linearized equation is no longer applicable, as illustrated in Section 2.10. In most applications for quiescent fluid, K_C is small; therefore, the results presented in this chapter are useful. However, when K_C is large, the nonlinear effect must be considered. The value of K_C separating the linear and nonlinear effect based on a single cylinder oscillating in a quiescent flow is about 2.5 (see Section 2.10). For additional discussions on the nonlinear effect, an extensive list of publications is available (e.g., Keulegan and Carpenter 1958; Sarpkaya and Isaacson 1981).

The effect of fluid on structural oscillation depends on structural geometries and fluid properties. For small K_C , added mass and fluid damping depend on fluid compressibility and viscosity.

- Incompressible Inviscid Fluid - The fluid damping is always zero and added mass is always a positive value.
- Compressible Inviscid Fluid - In a confined region, the energy cannot be carried away; therefore, there is no radiation damping. In an unconfined region, fluid damping attributed to radiation may be important. In a compressible fluid, there are acoustoelastic modes; thus, the added mass may be positive or negative.
- Viscous Fluid - Both added mass and fluid damping always exist. The damping is associated with fluid viscosity in addition to the radiation damping attributed to fluid compressibility.

In this chapter, only circular cylinders are considered. The fluid effects on other structural geometries are similar. In fact, the same method of solution can be applied to other geometries. In addition, there is an extensive amount of literature available for other geometries (Muga and Wilson 1970; Blevins 1977).

REFERENCES--Sec. 2

- Blevins, R. D. 1977. Flow-Induced Vibration. Van Nostrand Reinhold Co.
- Carlucci, L. N. 1980. Damping and Hydrodynamic Mass of a Cylinder in Simulated Two-Phase Flow. ASME J. Mech. Des. 102(3), 597-602.
- Carlucci, L. N., and Brown, L. D. 1982. Experimental Studies of Damping and Hydrodynamic Mass of a Cylinder in Confined Two-Phase Flow. J. Vibration, Acoustics, Stress and Reliability in Design 105, 83-89.
- Chen, S. S. 1974. Dynamics of a Rod-Shell System Conveying Fluid. Nucl. Eng. Des. 30, 223-233.
- Chen, S. S. 1983. Design Guide for Calculating Fluid Damping for Circular Cylindrical Structures. ANL-83-54, Argonne National Laboratory, Argonne, IL.
- Chen, S. S., and Chung, H. 1976. Design Guide for Calculating Hydrodynamic Mass, Part I: Circular Cylindrical Structures. ANL-CT-76-45, Argonne National Laboratory, Argonne, IL.
- Chen, S. S., and Wambsganss, M. W. 1972. Parallel-Flow-Induced Vibration of Fuel Rods. Nucl. Eng. Des. 18, 253-278.
- Chen, S. S., Wambsganss, M. W. and Jendrzejczyk, J. A. 1976. Added Mass and Damping of a Vibrating Rod in Confined Viscous Fluids. Trans. ASME, J. of Appl. Mech. 43(2), 325-329.
- Collier, J. G. 1972. Connective Boiling and Condensation. 1st Ed., McGraw Hill, London.
- Hara, F., and Kolgo, O. 1982. Added Mass and Damping of a Vibrating Rod in a Two-Phase Air-Water Mixed Fluid. In Flow-Induced Vibration of Circular Cylindrical Structures, 1982. ASME Publ. PVP Vol. 63, pp 1-8.
- Jendrzejczyk, J. A. 1985. Dynamic Characteristics of Heat Exchanger Tubes Vibrating in a Tube Support Plate Inactive Mode. Proc. 1985 ASME PVP Conf., Vol. 7, pp. 251-262.
- Keulegan, G., and Carpenter, L. H. 1958. Forces on Cylinders and Plates in an Oscillating Fluid. J. Res. Nat. Bur. Stand. 60, 423-460.
- Lin, H. C., and Chen, S. S. 1977. Acoustically Induced Vibrations of Circular Cylindrical Rods. J. Sound Vib. 51(1), 89-96.
- Mazur, V. Yu. 1966. Motion of a Circular Cylinder Near a Vertical Wall. Izv. Akad. Nauk SSSR, Mekhan. Zhidk. i Gaza, No. 3, pp. 75-79.
- Muga, M. J., and Wilson, J. F. 1970. Dynamic Analysis of Ocean Structures. Plenum Publishing.
- Mulcahy, T. M. 1980. Fluid Forces on Rods Vibrating in Finite Length Annular Regions. J. Appl. Mech. 47, 234-240.

- Sarpkaya, T., and Isaacson, M. 1981. Mechanics of Wave Forces on Offshore Structures. Van Nostrand Reinhold Co.
- Schumann, V. 1981. Virtual Density and Speed of Sound in a Fluid-Solid Mixture With Periodic Structures. Int. J. Multiphase Flow 7(6), 619-633.
- Sinyavskii, V. F., Fedotovskii, V. S., and Kukhtin, A. B. 1980. Oscillation of a Cylinder in a Viscous Liquid. Prikladnaya Mekhanika, 16(1), 62-27.
- Skop, R. A., Ramberg, S. E., and Ferer, K. M. 1976. Added Mass and Damping Forces on Circular Cylinders. ASME Paper No. 76-PET-3, Sept. 1976.
- Williams, R. E., and Hussey, R. G. 1972. Oscillating Cylinders and the Stokes' Paradox. The Physics of Fluids 15(12), 2083-2088.
- Yang, C. I., and Moran, T. J. 1979. Finite-Element Solution of Added Mass and Damping of Oscillation Rods in Viscous Fluids. J. Appl. Mech. 46, 519-523.

3. MULTIPLE CYLINDERS IN QUIESCENT FLUID

3.1 INTRODUCTION

For a single cylinder oscillating in a fluid, frequently a single added mass and a single viscous damping coefficient are sufficient in characterizing the effect of fluid on the structural response. However, for a multiple-cylinder component, the motion of a cylinder excites the surrounding cylinders through the fluid. Therefore all cylinders are coupled by the fluid. The fluid dynamic effects on multiple cylinders are much more complex. Lift forces may be generated that tend to act perpendicularly to the direction of motion; therefore, fluid inertia and damping forces are no longer necessarily in line with the direction of motion, and the added mass and fluid damping become matrices. The parameters affecting the added mass and damping matrices are the same as those for a single cylinder except that additional parameters are needed to characterize the cylinder arrangement, such as the pitch to diameter ratio, P/D .

In addition to nuclear fuel bundles, a range of other structural components consisting of a group of circular cylinders--such as heat exchanger tubes, piles, parallel pipelines, bundled transmission lines and rocket engines--frequently experience flow-induced vibrations. Since 1960, many investigators have studied the dynamics of various types of structural components consisting of multiple cylinders. These include two parallel cylinders (Livesey and Dye 1962; Wilson and Caldwell 1971; Chen 1975a), two cylinders located concentrically and separated by a fluid (Chen 1972; Cesari and Curioni 1973; Chen 1974; Chen and Rosenberg 1975), a row of cylinders (Livesey and Dye 1962; Roberts 1966; Connors 1970), and a group of cylinders (Laird and Warren 1963; Chen 1968; Shimogo and Inui 1971). Despite the progress being made on the dynamics of multiple cylinders in a liquid, a general method of analysis was not available until about 10 years ago. With the development of an analytical method to account for the inertia coupling (Chen 1975b), the dynamics characteristics of multiple cylinders oscillating in a fluid began to receive more attention. The same method has been used for a group of cylinders in different flow conditions (Paidoussis et al. 1977; Paidoussis and Besancon 1981; Chen 1983). In addition, other numerical methods have been developed for studying the dynamic response of a group of cylinders (Yang and Moran 1979; Loeber 1984).

In this chapter, the general characteristics of a group of cylinders oscillating in quiescent fluid are discussed, primarily based on the ideal fluid. The role of fluid viscosity and compressibility is also considered. Understanding of the dynamics of multiple cylinders in quiescent fluid is important for investigations of cylinders in flow.

3.2 A SIMPLE EXAMPLE--TWO PARALLEL CIRCULAR CYLINDERS OSCILLATING IN AN INFINITE PERFECT FLUID

3.2.1 Equations of Motion

Two infinitely long parallel circular cylinders with a pitch P , designated 1 and 2, are immersed in a perfect fluid, as illustrated in Fig. 3.1. Cylinder motions consist of out-of-plane displacements u_1 and u_2 along the x axis and in-plane displacements v_1 and v_2 along the y axis. The equations of motion can be written

$$m_j \frac{d^2 u_j}{dt^2} + k_{sj} u_j = g_j, \quad (3.1)$$

$$m_j \frac{d^2 u_j}{dt^2} + k_{sj} u_j = h_j, \quad j = 1, 2,$$

where m_j is the mass per unit length and k_{sj} is the spring constant of cylinder j in both directions.

The fluid forces associated with two vibrating cylinders were considered by Mazur (1966), using a two-dimensional theory (a general method of solution is given in Section 3.3):

$$g_1 = -M_1 \alpha_{11} \frac{\partial^2 u_1}{\partial t^2} - \rho \pi \left(\frac{R_1 + R_2}{2} \right)^2 \alpha_{12} \frac{\partial^2 u_2}{\partial t^2}$$

and

$$g_2 = -M_2 \alpha_{22} \frac{\partial^2 u_2}{\partial t^2} - \rho \pi \left(\frac{R_1 + R_2}{2} \right)^2 \alpha_{12} \frac{\partial^2 u_1}{\partial t^2} \quad (3.2)$$

for out-of-plane motion, and

$$h_1 = -M_1 \alpha_{11} \frac{\partial^2 v_1}{\partial t^2} + \rho \pi \left(\frac{R_1 + R_2}{2} \right)^2 \alpha_{12} \frac{\partial^2 v_2}{\partial t^2}$$

and

$$h_2 = -M_2 \alpha_{22} \frac{\partial^2 v_2}{\partial t^2} + \rho \pi \left(\frac{R_1 + R_2}{2} \right)^2 \alpha_{12} \frac{\partial^2 v_1}{\partial t^2} \quad (3.3)$$

for in-plane motion. M_1 and M_2 are the displaced masses of fluid by the two cylinders, and R_1 and R_2 are cylinder radii. The added mass coefficients α_{11} ,

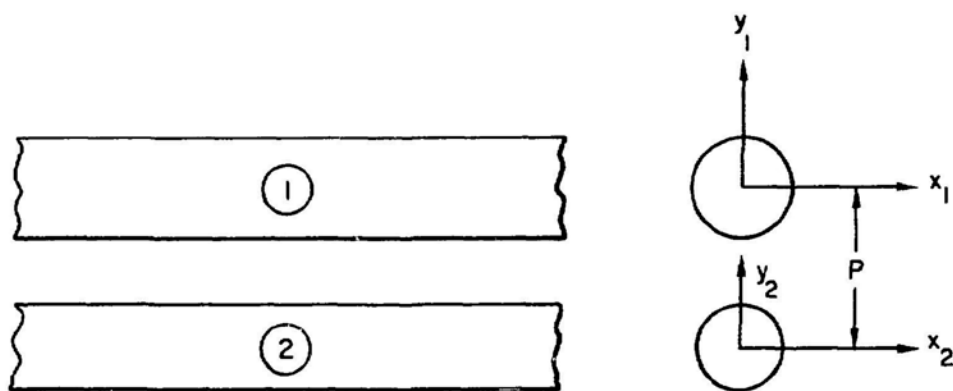


Fig. 3.1. Two Parallel Circular Cylinders Vibrating in a Fluid

α_{22} and α_{12} are given by (Mazur 1966):

$$\alpha_{11} = 1 + \frac{P^4 - 2P^2(R_1^2 + R_2^2) + (R_2^2 - R_1^2)^2}{P^2 R_1^2}$$

$$\sum_{n=1}^{\infty} n \frac{\exp[-n(\alpha + \alpha_1)]}{\sinh(n\alpha)},$$

$$\alpha_{22} = 1 + \frac{P^4 - 2P^2(R_1^2 + R_2^2) + (R_2^2 - R_1^2)^2}{P^2 R_2^2}$$

$$\sum_{n=1}^{\infty} n \frac{\exp[-n(\alpha + \alpha_2)]}{\sinh(n\alpha)}, \quad (3.4)$$

and

$$\alpha_{12} = \left[1 + \frac{P^4 - 2P^2(R_1^2 + R_2^2) + (R_2^2 - R_1^2)^2}{R_1^2 R_2^2} \right]$$

$$\sum_{n=1}^{\infty} \alpha \coth(n\alpha) \exp(-2n\alpha) \left[\frac{4R_1^2 R_2^2}{P^2 (R_1 + R_2)^2} \right],$$

where

$$\alpha = \ln \left\{ \frac{P^2 - R_1^2 - R_2^2}{2R_1 R_2} + \left[\left(\frac{P^2 - R_1^2 - R_2^2}{2R_1 R_2} \right)^2 - 1 \right]^{1/2} \right\},$$

$$\alpha_1 = 2 \ln \left\{ \frac{P^2 + R_1^2 - R_2^2}{2PR_1} + \left[\left(\frac{P^2 + R_1^2 - R_2^2}{2PR_1} \right)^2 - 1 \right]^{1/2} \right\},$$

and

$$\alpha_2 = 2 \ln \left\{ \frac{P^2 - R_1^2 + R_2^2}{2PR_2} + \left[\left(\frac{P^2 - R_1^2 + R_2^2}{2PR_2} \right)^2 - 1 \right]^{1/2} \right\}.$$

The values of α_{11} , α_{12} and α_{22} depend on the dimensionless parameters R_2/R_1 and P/R_1 .

Substituting Eqs. 3.2 and 3.3 into 3.1 yields

$$\begin{aligned} (m_1 + \alpha_{11}M_1) \frac{d^2 u_1}{dt^2} + \rho\pi \left(\frac{R_1 + R_2}{2} \right)^2 \alpha_{12} \frac{d^2 u_2}{dt^2} + k_{s1} u_1 &= 0 \\ (m_2 + \alpha_{22}M_2) \frac{d^2 u_2}{dt^2} + \rho\pi \left(\frac{R_1 + R_2}{2} \right)^2 \alpha_{12} \frac{d^2 u_1}{dt^2} + k_{s2} u_2 &= 0 \end{aligned} \quad (3.5)$$

for out-of-plane motion, and

$$\begin{aligned} (m_1 + \alpha_{11}M_1) \frac{d^2 v_1}{dt^2} - \rho\pi \left(\frac{R_1 + R_2}{2} \right)^2 \alpha_{12} \frac{d^2 v_2}{dt^2} + k_{s1} v_1 &= 0 \\ (m_2 + \alpha_{22}M_2) \frac{d^2 v_2}{dt^2} - \rho\pi \left(\frac{R_1 + R_2}{2} \right)^2 \alpha_{12} \frac{d^2 v_1}{dt^2} + k_{s2} v_2 &= 0 \end{aligned} \quad (3.6)$$

for in-plane motion.

3.2.2 Free Vibration

Equations 3.5 and 3.6 can be solved easily. Let

$$u_j = R_j \bar{u}_j \exp(i\omega t), \quad j = 1, 2. \quad (3.7)$$

Substituting Eq. 3.7 into Eq. 3.5 yields

$$\begin{bmatrix} (m_1 + \alpha_{11}M_1)\omega^2 - k_{s1} & \rho\pi \left(\frac{R_1 + R_2}{2} \right)^2 \alpha_{12} \omega^2 \\ \rho\pi \left(\frac{R_1 + R_2}{2} \right)^2 \alpha_{12} \omega^2 & (m_2 + \alpha_{22}M_2)\omega^2 - k_{s2} \end{bmatrix} \begin{Bmatrix} \bar{u}_1 \\ \bar{u}_2 \end{Bmatrix} = \begin{Bmatrix} 0 \\ 0 \end{Bmatrix} \quad (3.8)$$

From Eq. 3.8, the natural frequencies under different situations can be calculated.

Natural Frequencies in Vacuum

In this case, $\rho = 0$; therefore

$$\omega_{vj} = \left(\frac{k_{sj}}{m_j} \right)^{0.5}, \quad j = 1, 2. \quad (3.9)$$

Natural Frequencies of Uncoupled Vibration in Fluid

When only one of the cylinders is movable and all others are held rigid, the motion of the elastic cylinder is called uncoupled vibration. When Cylinder 2 is held rigid, the natural frequency of Cylinder 1 is given by

$$\bar{\omega}_{f1} = \left(\frac{k_{s1}}{m_1 + \alpha_{11}M_1} \right)^{0.5}. \quad (3.10)$$

Similarly, the natural frequency of uncoupled vibration for Cylinder 2 is

$$\bar{\omega}_{f2} = \left(\frac{k_{s2}}{m_2 + \alpha_{22}M_2} \right)^{0.5}. \quad (3.11)$$

Coupled Vibration in Fluid

For a coupled vibration in fluid (Chen 1975a), from Eq. 3.8, the frequency equation is

$$(1 - \beta_1\beta_2)\omega^4 - (\bar{\omega}_{f1}^2 + \bar{\omega}_{f2}^2)\omega^2 + \bar{\omega}_{f1}^2\bar{\omega}_{f2}^2 = 0, \quad (3.12)$$

$$\beta_1 = \rho\pi\left(\frac{R_1 + R_2}{2}\right)^2 \alpha_{12} / (m_1 + \alpha_{11}M_1),$$

and

$$\beta_2 = \rho\pi\left(\frac{R_1 + R_2}{2}\right)^2 \alpha_{12} / (m_2 + \alpha_{22}M_2).$$

Therefore, the coupled natural frequencies are given by

$$\omega_{f1}^2 = \frac{\bar{\omega}_{f1}^2 + \bar{\omega}_{f2}^2 - [(\bar{\omega}_{f1}^2 - \bar{\omega}_{f2}^2)^2 - 4\beta_1\beta_2\bar{\omega}_{f1}^2\bar{\omega}_{f2}^2]^{0.5}}{2(1 - \beta_1\beta_2)} \quad (3.13)$$

and

$$\omega_{f2}^2 = \frac{\bar{\omega}_{f1}^2 + \bar{\omega}_{f2}^2 + [(\bar{\omega}_{f1}^2 - \bar{\omega}_{f2}^2)^2 - 4\beta_1\beta_2\bar{\omega}_{f1}^2\bar{\omega}_{f2}^2]^{0.5}}{2(1 - \beta_1\beta_2)}.$$

The amplitude ratio \bar{u}_1/\bar{u}_2 is given by

$$\frac{\bar{u}_1}{\bar{u}_2} = \frac{\bar{\omega}_{f2} - \omega_{fq}}{\beta_2 \omega_{fq}}, \quad q = 1, 2. \quad (3.14)$$

From Eq. 3.12, it is easily shown that if

$$\beta_1 \beta_2 < 1 \quad (3.15)$$

the following relations are satisfied:

$$\begin{aligned} \omega_{f1} &< \bar{\omega}_{f1}, \bar{\omega}_{f2} \\ \text{and} \\ \omega_{f2} &> \bar{\omega}_{f1}, \bar{\omega}_{f2}. \end{aligned} \quad (3.16)$$

Equation 3.15 is found to be satisfied in all cases. Thus, the natural frequencies of the coupled modes may be lower or higher than those of the uncoupled modes.

When the two cylinders are identical, $\bar{\omega}_{f1} = \bar{\omega}_{f2}$ and $\beta_1 = \beta_2$; therefore Eqs. 3.13 and 3.14 are reduced to

$$\begin{aligned} \omega_{f1} &= \frac{\omega_{v1}}{\sqrt{1 + \beta_1}}, & \frac{\bar{u}_1}{\bar{u}_2} &= -1 \\ \text{and} \\ \omega_{f2} &= \frac{\omega_{v1}}{\sqrt{1 - \beta_1}}, & \frac{\bar{u}_1}{\bar{u}_2} &= 1. \end{aligned} \quad (3.17)$$

Equation 3.17 shows that the natural frequencies of the coupled vibration are proportional to the natural frequency in vacuum. Equation 3.17 can also be written

$$\begin{aligned} \omega_{f1} &= \left[\frac{\omega_{v1}}{m_1 + M_1(\alpha_{11} + \alpha_{12})} \right]^{0.5} \\ \text{and} \\ \omega_{f2} &= \left[\frac{\omega_{v1}}{m_1 + M_1(\alpha_{11} - \alpha_{12})} \right]^{0.5}. \end{aligned} \quad (3.18)$$

For coupled vibration, the added masses given in Eq. 3.18 are $M_1(\alpha_{11} + \alpha_{12})$ and $M_1(\alpha_{11} - \alpha_{12})$, respectively. These are called the effective added masses of coupled modes. They are the eigenvalues of added mass matrix (see Section 3.3 for details).

For two identical cylinders oscillating out of plane, the first mode is associated with the in-phase motion and the second mode is associated with the out-of-phase motion. It is straightforward to show that the natural frequencies of coupled modes for in-plane motion (Eqs. 3.6) are the same as those of out-of-plane motion. However, the first mode is associated with the out-of-phase motion and the second mode is associated with the in-phase motion. These four different modes are given in Fig. 3.2.

3.3 ADDED MASS MATRICES FOR A GROUP OF CYLINDERS OSCILLATING IN A FLUID BASED ON THE TWO-DIMENSIONAL POTENTIAL FLOW THEORY

3.3.1 Formulation and Solution

Consider a group of N circular cylinders vibrating in a perfect fluid as shown in Fig. 3.3. The axes of the cylinders are perpendicular to the x - y plane. Let R_j be the radius of cylinder j and (x_j, y_j) be the local coordinates associated with cylinder j .

The velocity potential associated with the motion of cylinder j , assuming all other cylinders are stationary, can be written (Chen 1975b)

$$\phi_j = \sum_{n=1}^{\infty} \left(\frac{R_j^{n+1}}{r_j^n} \right) (a_{jn} \cos n\theta_j + b_{jn} \sin n\theta_j), \quad (3.19)$$

where r_j and θ_j are cylindrical coordinates referred to as cylinder j , and a_{jn} and b_{jn} are arbitrary constants to be determined. The total field at a point in the fluid consists of the partial fields generated by all cylinders, i.e.,

$$\phi = \sum_{j=1}^N \phi_j. \quad (3.20)$$

All ϕ_j can be written in terms of the local coordinates associated with cylinder k using the following relationships (Chen 1975c):

$$\frac{\cos n\theta_j}{r_j^n} = (-1)^n \sum_{m=0}^{\infty} \frac{(n+m-1)! r_k^m}{m!(n-1)! R_{jk}^{n+m}} \cos[m\theta_k - (m+n)\psi_{jk}], \quad (3.21)$$

and

$$\frac{\sin n\theta_j}{r_j^n} = (-1)^{n+1} \sum_{m=0}^{\infty} \frac{(n+m-1)! r_k^m}{m!(n-1)! R_{jk}^{n+m}} \sin[m\theta_k - (m+n)\psi_{jk}], \quad (3.22)$$

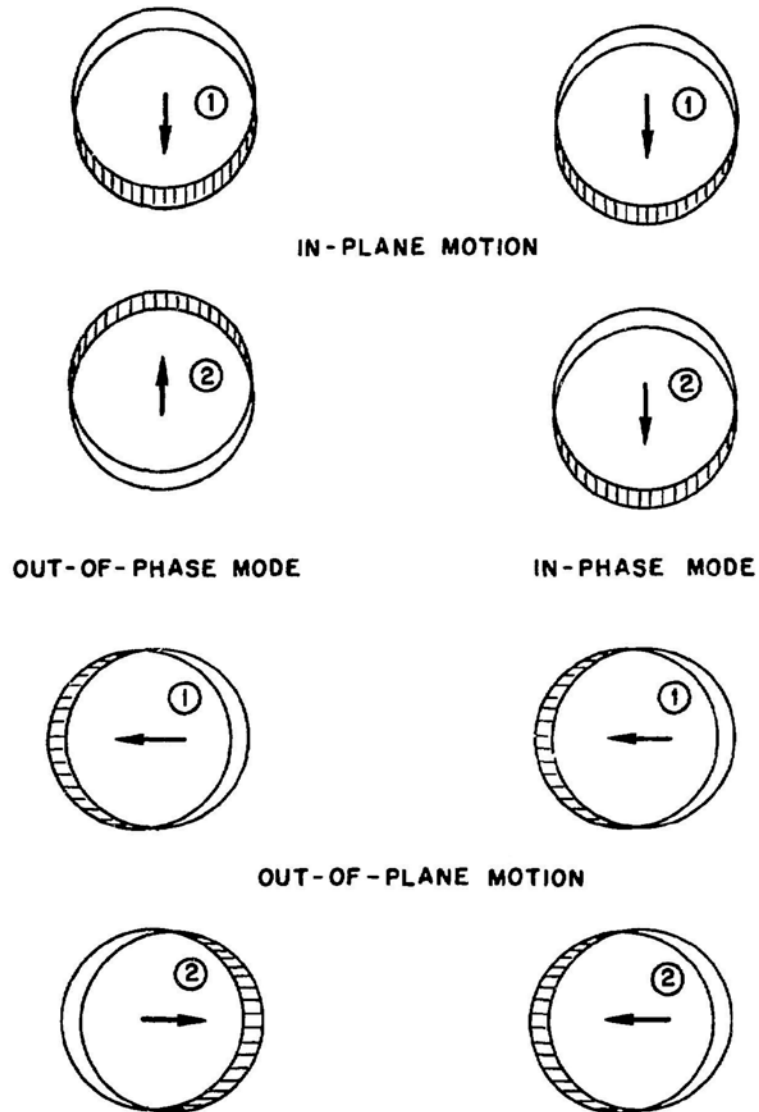


Fig. 3.2. Four Normal Modes of Two Identical Cylinders Vibrating in a Fluid (Chen 1975a)

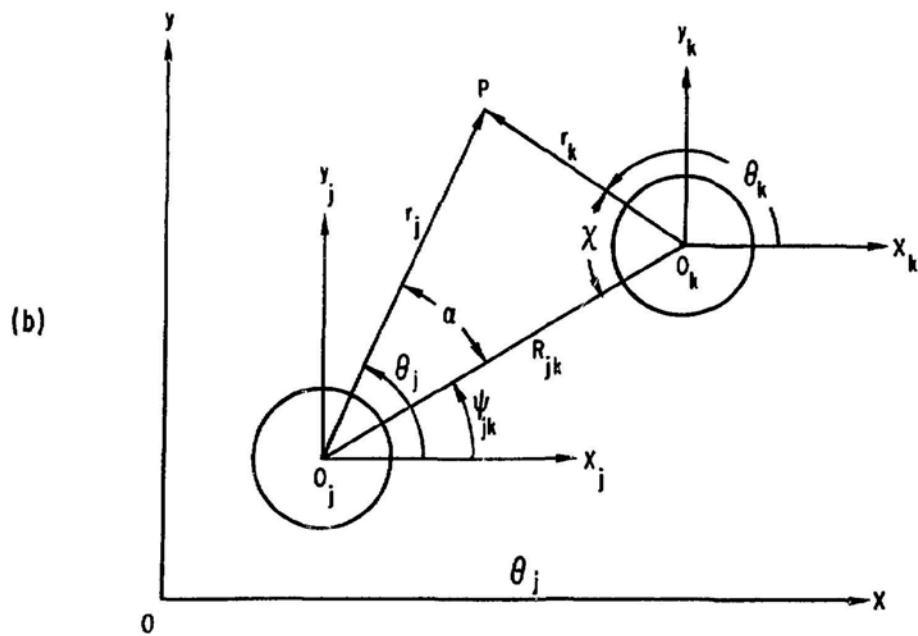
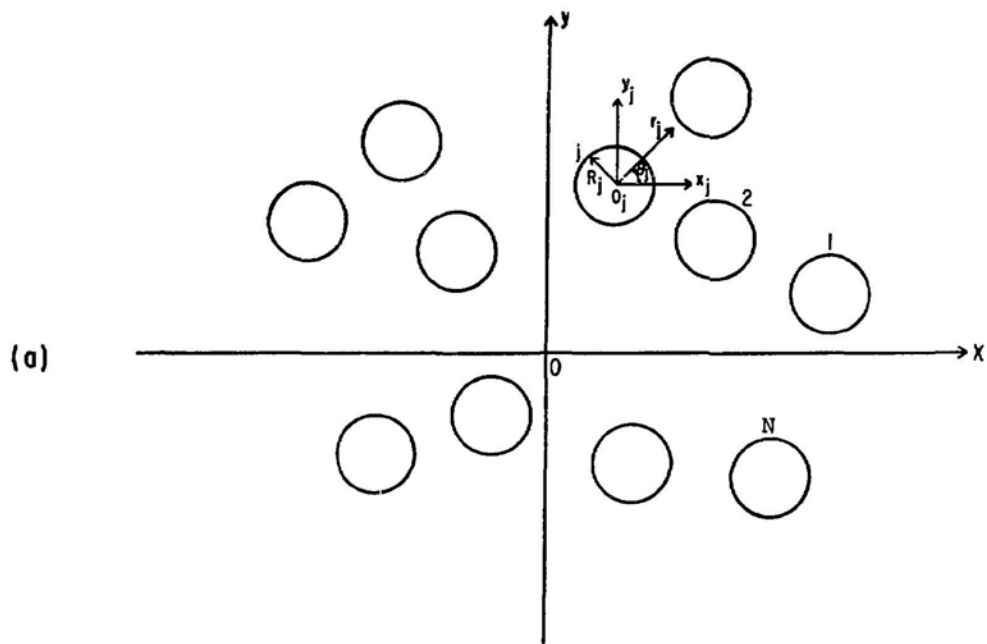


Fig. 3.3. A Group of N Circular Cylinders Vibrating in a Fluid

where R_{jk} is the distance between the centers of cylinders j and k , and ψ_{jk} is the angle between the x axis and the vector from the center of cylinder j to that of cylinder k . Let the superscript k denote the variable written in terms of the local coordinates associated with cylinder k . Therefore,

$$\phi^k = \phi_k + \sum_{j=1}^{N^*} \phi_j^k, \quad (3.23)$$

where \sum^* denotes the summation for j from 1 to N except $j = k$. Using Eqs. 3.19, 3.21, and 3.22 gives

$$\begin{aligned} \phi_j^k = \sum_{n=1}^{\infty} \sum_{m=0}^{\infty} \frac{(-1)^n (n+m-1)! R_j^{n+1} r_k^m}{m!(n-1)! R_{jk}^{n+m}} \{ a_{jn} \cos[m\theta_k - (m+n)\psi_{jk}] \\ - b_{jn} \sin[m\theta_k - (m+n)\psi_{jk}] \}. \end{aligned} \quad (3.24)$$

The velocity components of cylinder k in the x and y directions are $\partial u_k / \partial t$ and $\partial v_k / \partial t$, respectively. The fluid velocity component in the r direction is u_r . In terms of the local coordinates of cylinder k ,

$$u_r^k = \partial \phi^k / \partial r_k. \quad (3.25)$$

At the interface of the cylinders and fluid, the following conditions must be satisfied:

$$u_r^k \Big|_{r_k=R_k} = (\partial u_k / \partial t) \cos \theta_k + (\partial v_k / \partial t) \sin \theta_k, \quad (3.26)$$

$$k = 1, 2, 3, \dots, N.$$

Substituting Eq. 3.25 into 3.26 and using Eqs. 3.23 and 3.24, a_{kn} and b_{kn} are determined as follows:

$$a_{kn} = \sum_{\ell=1}^N \left(\alpha_{kn\ell} \frac{\partial u_{\ell}}{\partial t} + \gamma_{kn\ell} \frac{\partial v_{\ell}}{\partial t} \right), \quad (3.27)$$

and

$$b_{kn} = \sum_{\ell=1}^N \left(\delta_{kn\ell} \frac{\partial u_{\ell}}{\partial t} + \beta_{kn\ell} \frac{\partial v_{\ell}}{\partial t} \right),$$

where $\alpha_{kn\ell}$, $\beta_{kn\ell}$, $\gamma_{kn\ell}$, and $\delta_{kn\ell}$ are solutions of the following equations:

$$\begin{aligned}
 (-n)\alpha_{kn\ell} + \sum_{j=1}^{N_*} \sum_{m=1}^{\infty} \frac{(n+m-1)! R_k^{n-1} R_j^{m+1}}{(n-1)!(m-1)! R_{jk}^{n+m}} (-1)^m \\
 \cdot \{ \alpha_{jm\ell} \cos[(m+n)\psi_{jk}] + \delta_{jm\ell} \sin[(m+n)\psi_{jk}] \} = \delta_{n1} \delta_{k\ell} , \\
 (-n)\delta_{kn\ell} + \sum_{j=1}^{N_*} \sum_{m=1}^{\infty} \frac{(n+m-1)! R_k^{n-1} R_j^{m+1}}{(n-1)!(m-1)! R_{jk}^{n+m}} (-1)^m \\
 \cdot \{ \alpha_{jm\ell} \sin[(m+n)\psi_{jk}] - \delta_{jm\ell} \cos[(m+n)\psi_{jk}] \} = 0 , \\
 (-n)\gamma_{kn\ell} + \sum_{j=1}^{N_*} \sum_{m=1}^{\infty} \frac{(n+m-1)! R_k^{n-1} R_j^{m+1}}{(n-1)!(m-1)! R_{jk}^{n+m}} (-1)^m \\
 \cdot \{ \gamma_{jm\ell} \cos[(m+n)\psi_{jk}] + \beta_{jm\ell} \sin[(m+n)\psi_{jk}] \} = 0 , \\
 (-n)\beta_{kn\ell} + \sum_{j=1}^{N_*} \sum_{m=1}^{\infty} \frac{(n+m-1)! R_k^{n-1} R_j^{m+1}}{(n-1)!(m-1)! R_{jk}^{n+m}} (-1)^m \\
 \cdot \{ \gamma_{jm\ell} \sin[(m+n)\psi_{jk}] - \beta_{jm\ell} \cos[(m+n)\psi_{jk}] \} = \delta_{n1} \delta_{k\ell} ,
 \end{aligned} \tag{3.28}$$

$$k, \ell = 1, 2, 3, \dots, N, \quad n = 1, 2, 3, \dots, \infty.$$

The fluid forces acting on the cylinders can be calculated from fluid pressure p :

$$p = -\rho(\partial\phi/\partial t), \tag{3.29}$$

where ρ is the fluid density. The two components of fluid force acting on cylinder j in the x and y directions are g_j and h_j , respectively;

$$g_j = -\int_0^{2\pi} p_j^j \Big|_{r_j=R_j} R_j \cos\theta_j d\theta_j, \quad h_j = -\int_0^{2\pi} p_j^j \Big|_{r_j=R_j} R_j \sin\theta_j d\theta_j. \tag{3.30}$$

Using Eqs. 3.23, 3.24, 3.27, 3.29, and 3.30 gives

$$g_j = -\rho\pi \sum_{\ell=1}^N \left(\frac{R_j + R_\ell}{2}\right)^2 \left(\alpha_{j\ell} \frac{\partial^2 u_\ell}{\partial t^2} + \sigma_{j\ell} \frac{\partial^2 v_\ell}{\partial t^2}\right)$$

(3.31)

and

$$h_j = -\rho\pi \sum_{\ell=1}^N \left(\frac{R_j + R_\ell}{2}\right)^2 \left(\tau_{j\ell} \frac{\partial^2 u_\ell}{\partial t^2} + \beta_{j\ell} \frac{\partial^2 v_\ell}{\partial t^2}\right),$$

where

$$\begin{aligned} \alpha_{j\ell} &= \frac{4R_j^2}{(R_j + R_\ell)^2} \left\{ -\alpha_{j1\ell} - \sum_{k=1}^{N^*} \sum_{n=1}^{\infty} \left(\frac{R_k}{R_{jk}}\right)^{n+1} (-1)^n \right. \\ &\quad \cdot \left. n(\alpha_{kn\ell} \cos[(n+1)\psi_{jk}] + \delta_{kn\ell} \sin[(n+1)\psi_{jk}]) \right\}, \\ \beta_{j\ell} &= \frac{4R_j^2}{(R_j + R_\ell)^2} \left\{ -\beta_{j1\ell} - \sum_{k=1}^{N^*} \sum_{n=1}^{\infty} \left(\frac{R_k}{R_{jk}}\right)^{n+1} (-1)^n \right. \\ &\quad \cdot \left. n(\gamma_{kn\ell} \sin[(n+1)\psi_{jk}] - \beta_{kn\ell} \cos[(n+1)\psi_{jk}]) \right\}, \\ \sigma_{j\ell} &= \frac{4R_j^2}{(R_j + R_\ell)^2} \left\{ -\gamma_{j1\ell} - \sum_{k=1}^{N^*} \sum_{n=1}^{\infty} \left(\frac{R_k}{R_{jk}}\right)^{n+1} (-1)^n \right. \\ &\quad \cdot \left. n(\gamma_{kn\ell} \cos[(n+1)\psi_{jk}] + \beta_{kn\ell} \sin[(n+1)\psi_{jk}]) \right\}, \\ \tau_{j\ell} &= \frac{4R_j^2}{(R_j + R_\ell)^2} \left\{ -\delta_{j1\ell} - \sum_{k=1}^{N^*} \sum_{n=1}^{\infty} \left(\frac{R_k}{R_{jk}}\right)^{n+1} (-1)^n \right. \\ &\quad \cdot \left. n(\alpha_{kn\ell} \sin[(n+1)\psi_{jk}] - \delta_{kn\ell} \cos[(n+1)\psi_{jk}]) \right\} \end{aligned} \tag{3.32}$$

in which $\alpha_{j\ell}$, $\beta_{j\ell}$, $\sigma_{j\ell}$ and $\tau_{j\ell}$ are called added mass coefficients. α_{jj} , β_{jj} , σ_{jj} and τ_{jj} are self-added mass coefficients that are proportional to the hydrodynamic force acting on cylinder j due to its own acceleration, while the others are mutual-added mass coefficients that are proportional to the hydrodynamic force acting on a cylinder due to the acceleration of another cylinder.

3.3.2 Reciprocal Relations

Consider the case where, in a group of N cylinders, cylinder j is moving with a velocity $(\partial u_j / \partial t) \vec{e}_j$, where \vec{e}_j is a unit vector, and all other cylinders are stationary. The mathematical solution for the fluid velocity potential is given by

$$\phi = (\partial u_j / \partial t) \phi_j, \quad (3.33)$$

where ϕ_j is the solution to

$$\nabla^2 \phi_j = 0, \quad \nabla \phi_j \cdot \vec{n} = \partial \phi_j / \partial n = \vec{e}_j \cdot \vec{n} = n_j \quad \text{on } S_j, \quad (3.34)$$

$$\nabla \phi_j \cdot \vec{n} = 0 \quad \text{on all } S_\ell \quad (\ell \neq j),$$

and certain infinity conditions, where \vec{n} is a unit vector normal to the cylinder surface and S_j is the surface of cylinder j . The hydrodynamic force acting on cylinder ℓ in the direction of \vec{e}_ℓ is given by

$$F_{\ell j} = \left(\int_{S_\ell} \rho \phi_j n_\ell dS_\ell \right) (\partial^2 u_j / \partial t^2). \quad (3.35)$$

Similarly, consider the case where all cylinders are stationary except cylinder ℓ moving in the direction of \vec{e}_ℓ with a velocity $\partial u_\ell / \partial t$. The fluid velocity potential is

$$\phi = (\partial u_\ell / \partial t) \phi_\ell, \quad (3.36)$$

where ϕ_ℓ is the solution of the following problem:

$$\nabla^2 \phi_\ell = 0, \quad \nabla \phi_\ell \cdot \vec{n} = \partial \phi_\ell / \partial n = \vec{e}_\ell \cdot \vec{n} = n_\ell \quad \text{on } S_\ell, \quad (3.37)$$

$$\nabla \phi_\ell \cdot \vec{n} = 0 \quad \text{on all } S_j \quad (j \neq \ell).$$

The hydrodynamic force acting on cylinder j in the direction of \vec{e}_j is

$$F_{j\ell} = \left(\int_{S_j} \rho \phi_\ell n_j dS_j \right) (\partial^2 u_\ell / \partial t^2). \quad (3.38)$$

Using Eqs. 3.34, 3.35, 3.37, and 3.38 gives

$$F_{jl} = -\gamma_{jl}(\partial^2 u_l / \partial t^2), \quad F_{lj} = -\gamma_{lj}(\partial^2 u_j / \partial t^2), \quad (3.39)$$

where

$$\gamma_{jl} = -\rho \int \int_{S_j} \phi_l \frac{\partial \phi_j}{\partial n} dS_j, \quad \gamma_{lj} = -\rho \int \int_{S_l} \phi_j \frac{\partial \phi_l}{\partial n} dS_l. \quad (3.40)$$

Note that ϕ_j and ϕ_l are two harmonic functions. According to Green's theorem,

$$\int \int_{S_0} \phi_j \frac{\partial \phi_l}{\partial n} dS_0 = \int \int_{S_0} \phi_l \frac{\partial \phi_j}{\partial n} dS_0 \quad (3.41)$$

holds for any surface S_0 enclosing a region in which $\nabla^2 \phi_j$ and $\nabla^2 \phi_l$ are zero. Consider the region between the surface S_r enclosing $\sum_{j=1}^N S_j$ and apply Eq. 3.41 to the functions ϕ_j and ϕ_l .

$$\int \int_{S_l} \phi_j \frac{\partial \phi_l}{\partial n} dS_l - \int \int_{S_j} \phi_l \frac{\partial \phi_j}{\partial n} dS_j = \int \int_{S_r} (\phi_j \frac{\partial \phi_l}{\partial n} - \phi_l \frac{\partial \phi_j}{\partial n}) dS_r. \quad (3.42)$$

Let S_r go to infinity. The integral over S_r must vanish. Therefore,

$$\int \int_{S_l} \phi_j \frac{\partial \phi_l}{\partial n} dS_l = \int \int_{S_j} \phi_l \frac{\partial \phi_j}{\partial n} dS_j. \quad (3.43)$$

It follows from Eqs. 3.40 and 3.43 that

$$\gamma_{jl} = \gamma_{lj}. \quad (3.44)$$

Let

$$u_j \vec{e}_j = u_j \vec{e}_x \quad \text{and} \quad u_l \vec{e}_l = u_l \vec{e}_y, \quad (3.45)$$

then from Eqs. 3.31 and 3.39, Eq. 3.44 is reduced to

$$\sigma_{jl} = \tau_{lj}. \quad (3.46)$$

Similarly, let $u_j \vec{e}_j$ and $u_l \vec{e}_l$ be equal to other components of the cylinder displacements. It is shown that

$$\alpha_{jl} = \alpha_{lj} \quad \text{and} \quad \beta_{jl} = \beta_{lj} . \quad (3.47)$$

Eqs. 3.46 and 3.47 are the reciprocal relations. Physically, these mean that the hydrodynamic force acting on cylinder j in the \vec{e}_j direction due to a unit acceleration of cylinder l in the \vec{e}_l direction is equal to the hydrodynamic force acting on cylinder l in the \vec{e}_l direction due to a unit acceleration of cylinder j in the \vec{e}_j direction.

The added mass coefficients α_{jl} , β_{jl} , σ_{jl} , and τ_{jl} can be combined into a single added mass matrix γ_{pq} , where

$$\left[\gamma_{pq} \right]_{2N \times 2N} = \begin{bmatrix} \rho\pi \left(\frac{R_j + R_l}{2} \right)^2 \alpha_{jl} & \rho\pi \left(\frac{R_j + R_l}{2} \right)^2 \sigma_{jl} \\ \rho\pi \left(\frac{R_j + R_l}{2} \right)^2 \tau_{jl} & \rho\pi \left(\frac{R_j + R_l}{2} \right)^2 \beta_{jl} \end{bmatrix} \quad (3.48)$$

for cylinders with different radius, or

$$[\gamma_{pq}] = \rho\pi R^2 [\lambda_{pq}] = \rho\pi R^2 \begin{bmatrix} \sigma_{jl} & \sigma_{jl} \\ \tau_{jl} & \beta_{jl} \end{bmatrix} \quad (3.49)$$

for cylinders with the same radius.

Since γ_{pq} is symmetric, for a group of N cylinders, there are $N(2N + 1)$ independent added mass components. It is possible to find a group of $2N$ principal axes such that

$$\gamma_{pq} = 0 \quad \text{for } p \neq q . \quad (3.50)$$

Let the eigenvalues and eigenvectors of $[\gamma_{pq}]$ be μ_p and $\{\alpha_p\}$ ($p = 1, 2, 3, \dots, 2N$), respectively; one has the relation

$$[\gamma_{pq}]\{\alpha_p\} = \mu_p\{\alpha_p\} . \quad (3.51)$$

As an example, consider the case of two cylinders with the same radius R . Assume that the cylinders are located on the x axis. In this case, it is found that (Chen 1975a)

$$\begin{aligned}
\alpha_{j\ell} = \beta_{j\ell} = 0, \quad \alpha_{11} = \alpha_{22} = \beta_{11} = \beta_{22}, \\
\alpha_{12} = \alpha_{21} = -\beta_{12} = -\beta_{21}.
\end{aligned}
\tag{3.52}$$

Hence, the added mass matrix can be written

$$[\gamma_{pq}] = \rho\pi R^2 \begin{bmatrix} \alpha_{11} & -\alpha_{12} & 0 & 0 \\ -\alpha_{12} & \alpha_{11} & 0 & 0 \\ 0 & 0 & \alpha_{11} & \alpha_{12} \\ 0 & 0 & \alpha_{12} & \alpha_{11} \end{bmatrix}.
\tag{3.53}$$

It is found that the principal values of the added-mass matrix are

$$\begin{aligned}
\mu_1 = \rho\pi R^2(\alpha_{11} + \alpha_{12}), \quad \mu_2 = \rho\pi R^2(\alpha_{11} - \alpha_{12}), \\
\mu_3 = \rho\pi R^2(\alpha_{11} - \alpha_{12}), \quad \mu_4 = \rho\pi R^2(\alpha_{11} + \alpha_{12}),
\end{aligned}
\tag{3.54}$$

Those values can be considered as effective added masses for a group of cylinders; they agree with the results presented in Section 3.2.

3.3.3 Coordination Transformation

Equations 3.31 show the hydrodynamic forces in the x and y direction due to cylinder motion in these directions. The hydrodynamic forces in the other directions, x' and y' , can be calculated as follows (see Fig. 3.4):

$$\begin{aligned}
u_j &= u_j' \cos\psi - v_j' \sin\psi, \\
v_j &= u_j' \sin\psi + v_j' \cos\psi, \\
g_j &= g_j' \cos\psi - h_j' \sin\psi, \\
\text{and} \\
h_j &= g_j' \sin\psi + h_j' \cos\psi,
\end{aligned}
\tag{3.55}$$

where u_j' and v_j' are displacement components in the x' and y' directions for cylinder j . Substituting Eqs. 3.55 into 3.31, one can solve for g_j' and h_j' :

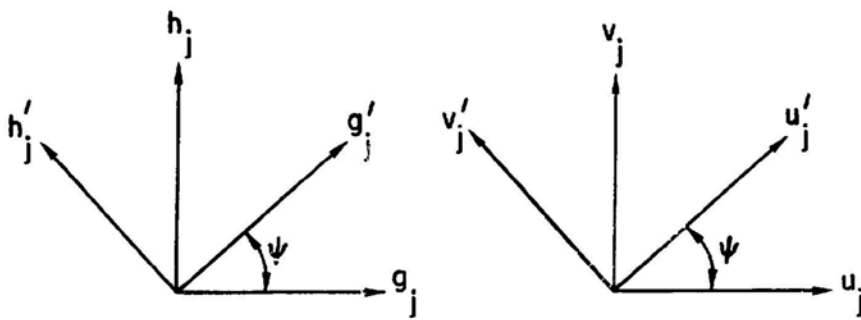


Fig. 3.4. Coordination Transformation

$$g'_j = -\rho\pi \sum_{\ell=1}^N \left(\frac{R_i + R_\ell}{2}\right)^2 \left(\alpha'_{j\ell} \frac{\partial^2 u'_\ell}{\partial t^2} + \sigma'_{j\ell} \frac{\partial^2 v'_\ell}{\partial t^2}\right)$$

and

$$h'_j = -\rho\pi \sum_{\ell=1}^N \left(\frac{R_i + R_\ell}{2}\right)^2 \left(\tau'_{j\ell} \frac{\partial^2 u'_\ell}{\partial t^2} + \beta'_{j\ell} \frac{\partial^2 v'_\ell}{\partial t^2}\right),$$

where

$$\begin{aligned}\alpha'_{j\ell} &= \alpha_{j\ell} \cos^2 \psi + \beta_{j\ell} \sin^2 \psi + (\sigma_{j\ell} + \tau_{j\ell}) \sin \psi \cos \psi, \\ \sigma'_{j\ell} &= \sigma_{j\ell} \cos^2 \psi - \tau_{j\ell} \sin^2 \psi + (\beta_{j\ell} - \alpha_{j\ell}) \sin \psi \cos \psi, \\ \tau'_{j\ell} &= -\sigma_{j\ell} \sin^2 \psi + \tau_{j\ell} \cos^2 \psi + (\beta_{j\ell} - \alpha_{j\ell}) \sin \psi \cos \psi,\end{aligned}$$

and

$$\beta'_{j\ell} = \alpha_{j\ell} \sin^2 \psi + \beta_{j\ell} \cos^2 \psi - (\sigma_{j\ell} + \tau_{j\ell}) \sin \psi \cos \psi.$$

Equations 3.57 define the transformation of the hydrodynamic mass coefficients. Once the hydrodynamic mass coefficients in a coordinate system are obtained, their values with respect to any other coordinate system can be calculated. Naturally, the symmetric properties are still preserved; i.e.,

$$\sigma'_{j\ell} = \sigma'_{\ell j}, \quad \beta'_{j\ell} = \beta'_{\ell j}, \quad \text{and} \quad \sigma'_{j\ell} = \tau'_{\ell j}.$$

Note that $\sigma'_{j\ell}$, $\beta'_{j\ell}$, $\sigma'_{j\ell}$, and $\tau'_{j\ell}$ vary with ψ . It is straightforward to find the ψ at which these coefficients are maximum or minimum. The axes corresponding to these are given by

$$\psi_1 = \frac{1}{2} \tan^{-1} \left(\frac{\sigma_{j\ell} + \tau_{j\ell}}{\alpha_{j\ell} - \beta_{j\ell}} \right)$$

for $\alpha_{j\ell}$ or $\beta_{j\ell}$, and

$$\psi_2 = \frac{1}{2} \tan^{-1} \left(\frac{\beta_{j\ell} - \alpha_{j\ell}}{\sigma_{j\ell} + \tau_{j\ell}} \right)$$

(3.59)

for $\sigma_{j\ell}$ or $\tau_{j\ell}$. Thus,

$$\tan(2\psi_1)\tan(2\psi_2) = 1. \quad (3.60)$$

3.3.4 Composite Motion of Cylinder Array

In addition to the individual cylinder motion, the whole array may respond as a rigid body. This involves translational motions in the x and y directions and torsional oscillations.

3.3.4.1 Translational Motion

Consider the translational motion in the x and y directions. For composite motion,

$$u_i = U_1$$

and

$$v_i = U_2 \quad (i = 1, 2, 3, \dots, N).$$

(3.61)

The resultant force acting on the whole cylinder array can be resolved into components G and H in the x and y directions:

$$G = \sum_{i=1}^N f_i$$

and

$$H = \sum_{i=1}^N g_i.$$

(3.62)

Substituting Eqs. 3.31 into 3.62 and using 3.61 yields

$$G = -\rho\pi R^2 \left(a_{11} \frac{\partial^2 U_1}{\partial t^2} + a_{12} \frac{\partial^2 U_2}{\partial t^2} \right)$$

and

$$H = -\rho\pi R^2 \left(a_{21} \frac{\partial^2 U_1}{\partial t^2} + a_{22} \frac{\partial^2 U_2}{\partial t^2} \right)$$

(3.63)

where

$$\begin{aligned}
a_{11} &= \sum_{j=1}^N \sum_{k=1}^N \left(\frac{R_j + R_k}{2R} \right)^2 \alpha_{jk} , \\
a_{12} &= \sum_{j=1}^N \sum_{k=1}^N \left(\frac{R_j + R_k}{2R} \right)^2 \sigma_{jk} , \\
a_{21} &= \sum_{j=1}^N \sum_{k=1}^N \left(\frac{R_j + R_k}{2R} \right)^2 \tau_{jk} , \\
a_{22} &= \sum_{j=1}^N \sum_{k=1}^N \left(\frac{R_j + R_k}{2R} \right)^2 \beta_{jk} ,
\end{aligned} \tag{3.64}$$

and

$$R = \frac{\sum_{i=1}^N R_i}{N} .$$

Since $\sigma_{jk} = \tau_{kj}$,

$$a_{12} = a_{21} . \tag{3.65}$$

The symmetry of the hydrodynamic mass coefficients for composite motion is similar to that of individual motion. The transformation of the hydrodynamic mass coefficients is also similar:

$$\begin{aligned}
a'_{11} &= a_{11} \cos^2 \psi + a_{22} \sin^2 \psi + (a_{12} + a_{21}) \sin \psi \cos \psi , \\
a'_{12} &= a_{21} \cos^2 \psi - a_{21} \sin^2 \psi + (a_{22} - a_{11}) \sin \psi \cos \psi , \\
a'_{21} &= -a_{12} \sin^2 \psi + a_{21} \cos^2 \psi + (a_{22} - a_{11}) \sin \psi \cos \psi ,
\end{aligned} \tag{3.66}$$

and

$$a'_{22} = a_{11} \sin^2 \psi + a_{22} \cos^2 \psi - (a_{12} + a_{21}) \sin \psi \cos \psi .$$

3.3.4.2 Rotational Motion

Assume that the cylinder array rotates around the z axis with an angular velocity $\frac{\partial \theta}{\partial t}$. The cylinder accelerations associated with the rotation are as follows:

$$\frac{\partial^2 u_j}{\partial t^2} = -\bar{r}_j \sin \theta_j \frac{\partial^2 \theta}{\partial t^2},$$

and

$$\frac{\partial^2 v_j}{\partial t^2} = \bar{r}_j \cos \theta_j \frac{\partial^2 \theta}{\partial t^2},$$

(3.67)

where \bar{r}_j is the distance from the center of the cylinder to the z axis, and θ_j is the angle between the x axis and the position vector \vec{r}_j . The torque is given by

$$\tau = \sum_{j=1}^N [-g_j \bar{r}_j \sin \theta_j + h_j \bar{r}_j \cos \theta_j]. \quad (3.68)$$

Substituting Eq. 3.31 into Eq. 3.68 and using Eq. 3.67 yields

$$\tau = -\rho \pi R^4 \gamma \frac{\partial^2 \theta}{\partial t^2}, \quad (3.69)$$

where

$$\gamma = \sum_{j=1}^N \sum_{\ell=1}^N \left(\frac{R_j + R_\ell}{2R^2} \right)^2 (\bar{r}_j \bar{r}_\ell) \cdot$$

$$(\alpha_{j\ell} \sin \theta_j \sin \theta_\ell - \sigma_{j\ell} \sin \theta_j \cos \theta_\ell - \tau_{j\ell} \cos \theta_j \sin \theta_\ell$$

$$+ \beta_{j\ell} \cos \theta_j \cos \theta_\ell). \quad (3.70)$$

Therefore, $\rho \pi R^4 \gamma$ is the added-mass moment of inertia.*

3.3.5 Numerical Examples

A computer program based on the analysis (AMASS; see Appendix D) is available for calculating added-mass coefficients. The program can be used to

*A generic phrase, "added mass," is used to refer to both hydrodynamic mass and hydrodynamic moment of inertia.

calculate all elements of added-mass matrix coefficients for a group of cylinders in which the cylinders may have different diameters and may be arranged in an arbitrary pattern.

Added-mass coefficients are in terms of series solutions. A finite number of undetermined coefficients is determined by inverting the matrix formed by truncating the infinite sets of Eqs. 3.28. In most practical applications, only a few terms (say, $n = 5$) are sufficient to obtain results with sufficient accuracy.

In many practical applications, cylinder arrays consisting of identical cylinders are arranged in rectangular or triangular patterns. The self-added-mass coefficient for the central element is of particular interest. Figure 3.5 shows the values of the coefficient as a function of the pitch-to-diameter ratio as well as the experimental mass obtained by Moretti and Lowery (1976). In both cases, $\alpha_{11} = \tau_{11} = 0$. β_{11} is always equal to α_{11} in a triangular array and β_{11} is equal to α_{11} for $P/D = T/D$ in a rectangular array. Analytical results and experimental data agree well over the range of parameters tested.

Figure 3.6 shows a tube array arranged in a hexagonal pattern. The added-mass coefficients α_{11} , β_{11} , α_{12} and β_{12} are computed for three arrays consisting of 7, 19, and 37 cylinders. Figure 3.7 shows the variation of these coefficients with P/D . α_{11} and β_{11} are equal and approach one as P/D becomes very large. β_{12} is not equal to α_{12} and they approach zero as P/D becomes infinite.

Figure 3.8 shows the upper and lower bounds of the added-mass matrix $[Y_{pq}]$, μ_p , as a function of P/D . For a group of N cylinders, there are $2N$ eigenvalues distributed between the upper and lower bounds. All μ_p 's approach one as P/D is increased, while the upper bound increases and lower bound decreases as P/D is reduced.

From Figs. 3.7 and 3.8, it is seen that as the number of cylinders increases, the absolute values of the added mass coefficients and their eigenvalues increase. The results for Cylinders 1 and 2 obtained from 19 cylinders and 37 cylinders do not differ significantly. The implication is that the coupling between a cylinder and other cylinders not immediately surrounding it can be neglected. For example, in the hexagonal arrangement, only the effects of the six cylinders surrounding the central cylinder must be considered if the motion of the central cylinder is of interest.

3.4 DYNAMICS OF A GROUP OF CYLINDERS IN A PERFECT FLUID

3.4.1 Equations of Motion

A cylinder array consisting of N cylinders whose axes are parallel to the z axis is shown in Fig. 3.9. Let u_j and u_{j+N} designate the displacement component of cylinder j in the x and y directions, respectively. The equation

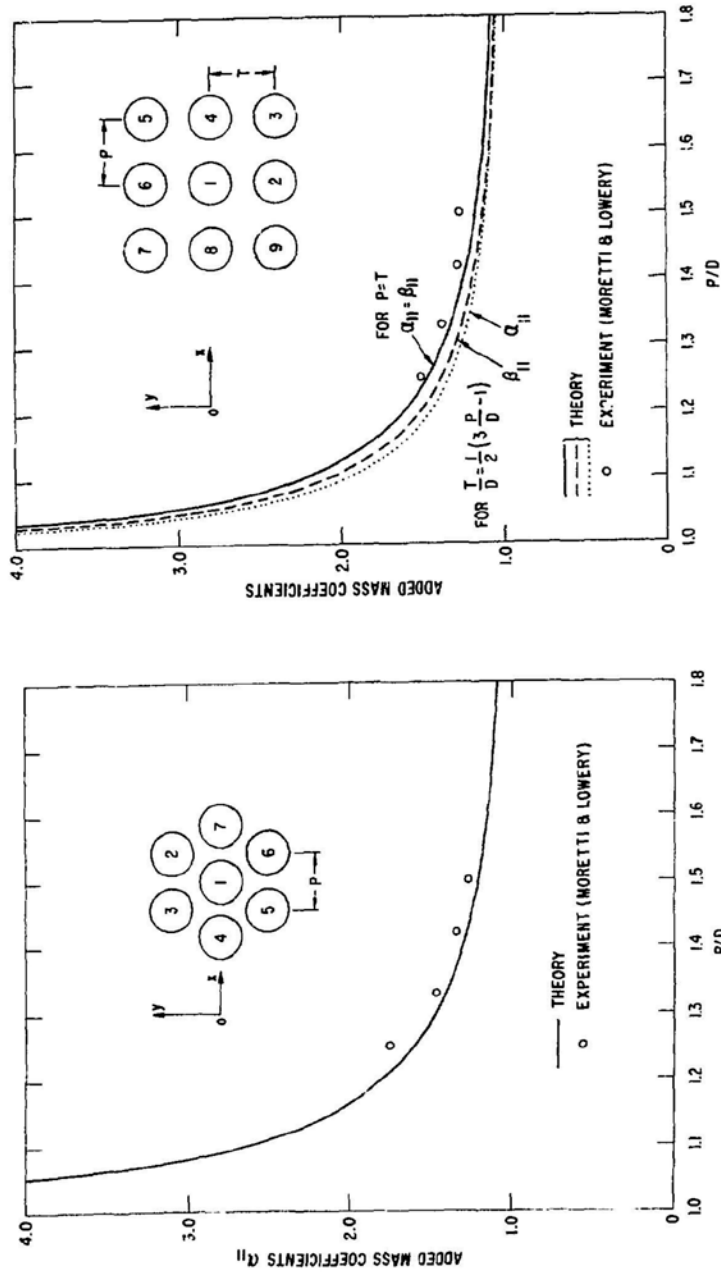


Fig. 3.5. Theoretical and Experimental Values of Added-mass Coefficients α_{11} and β_{11} for Seven and Nine Cylinders (Chen 1975b)

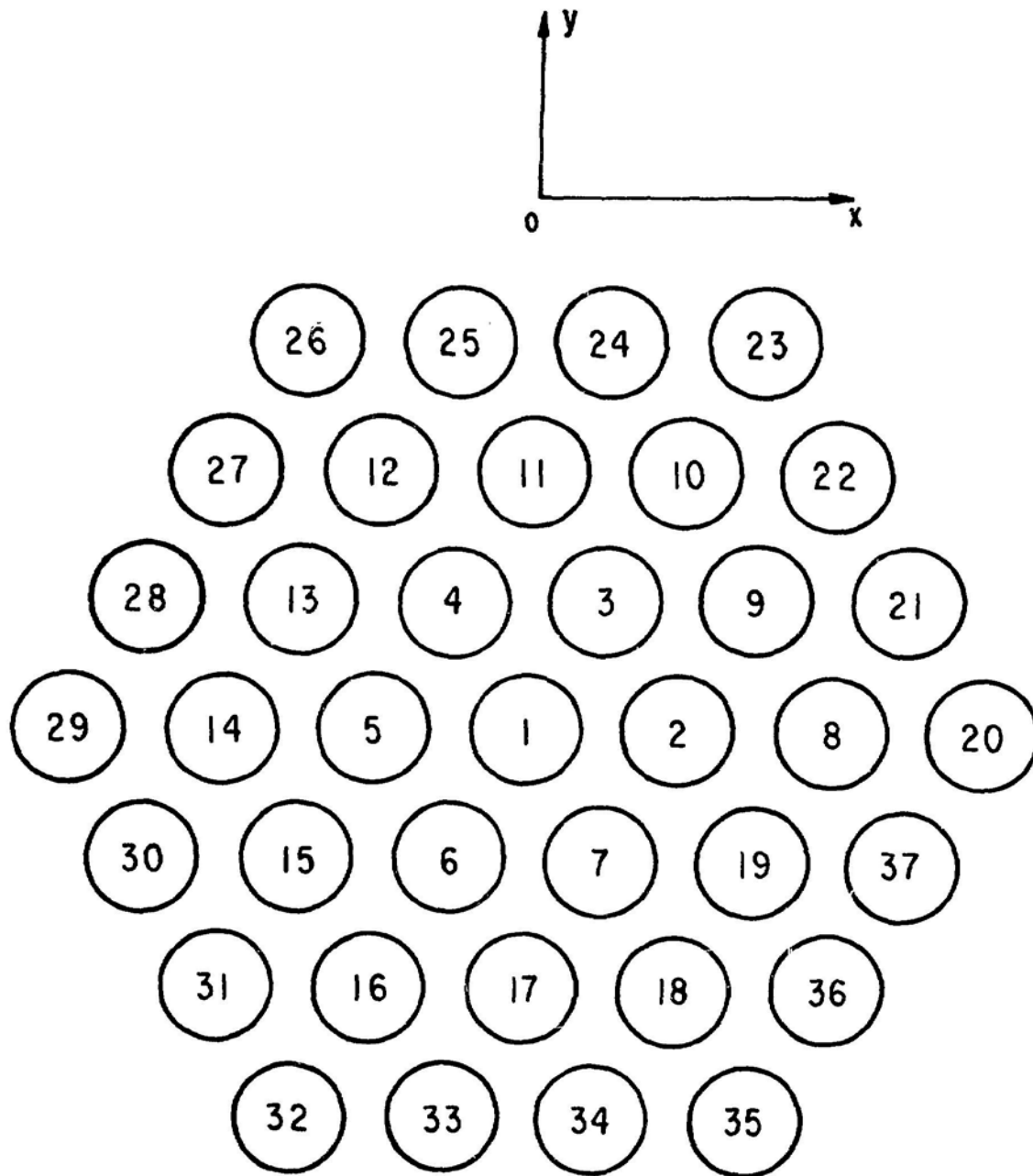


Fig. 3.6. Tube Bank Arranged in a Hexagonal Pattern

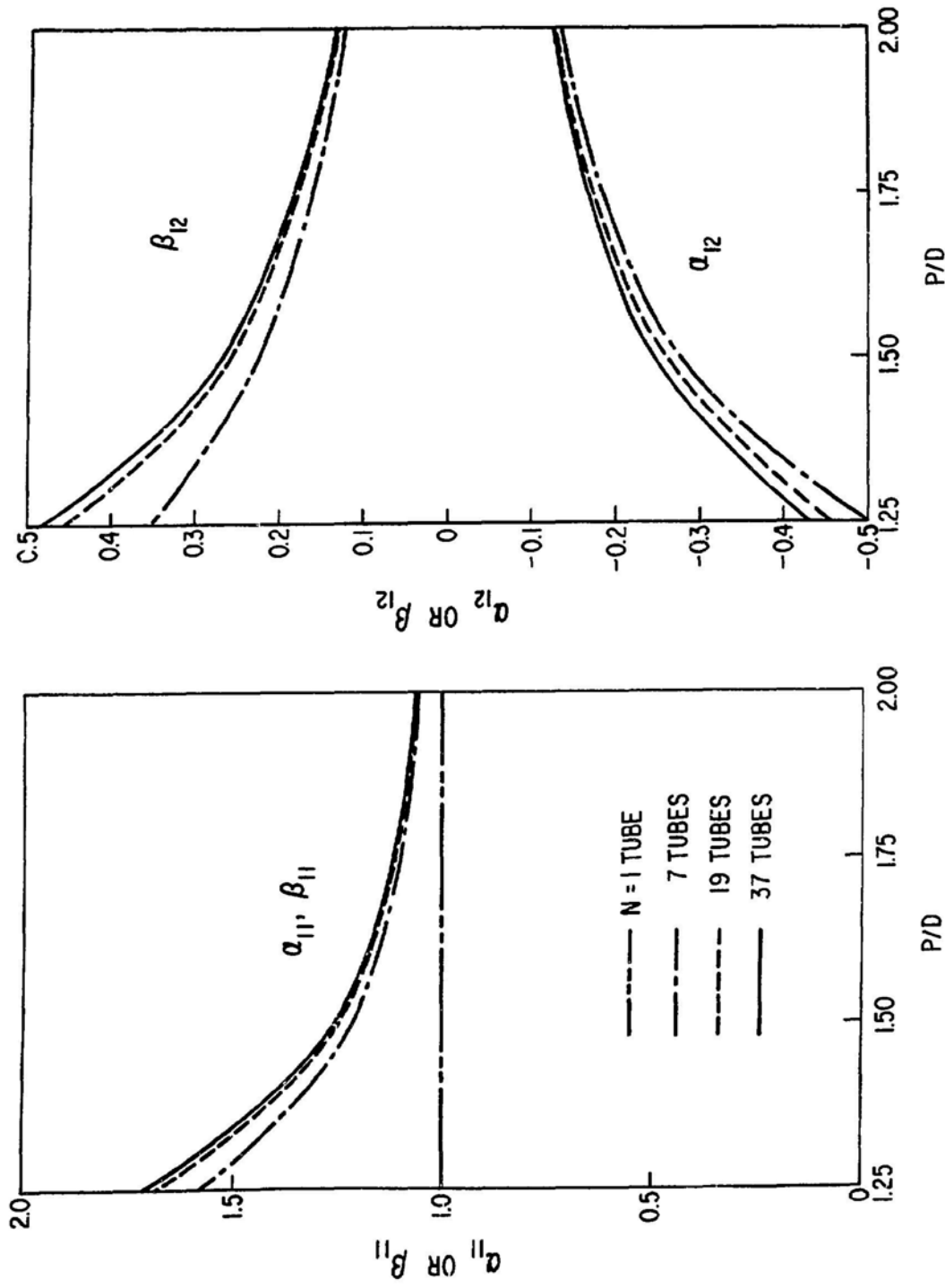


Fig. 3.7. Added-mass Coefficients as Functions of Pitch-to-diameter Ratio (Chen 1977)

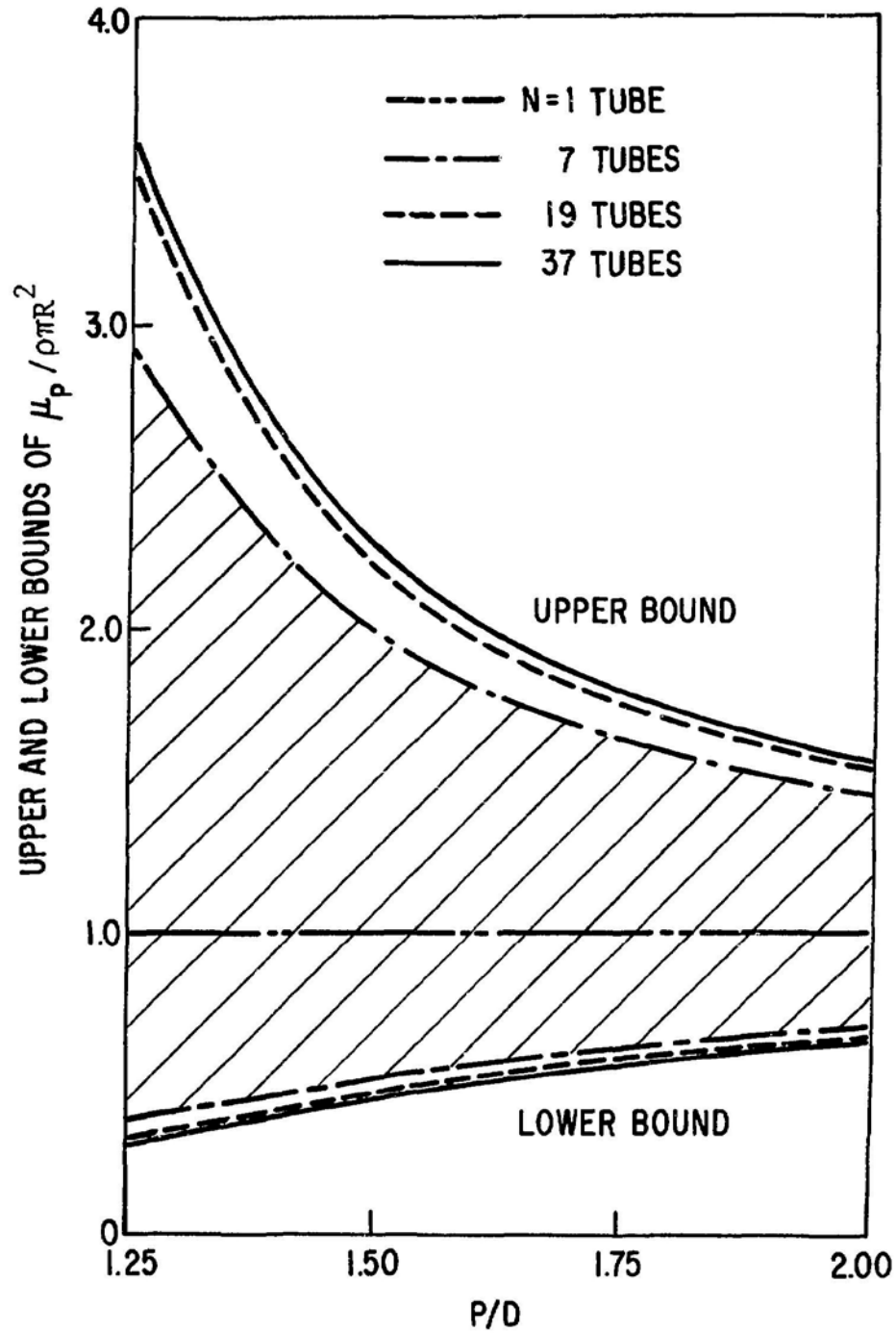


Fig. 3.8. Upper and Lower Bounds of Effective Added-mass Coefficients as Functions of Pitch-to-diameter Ratio (Chen 1977)

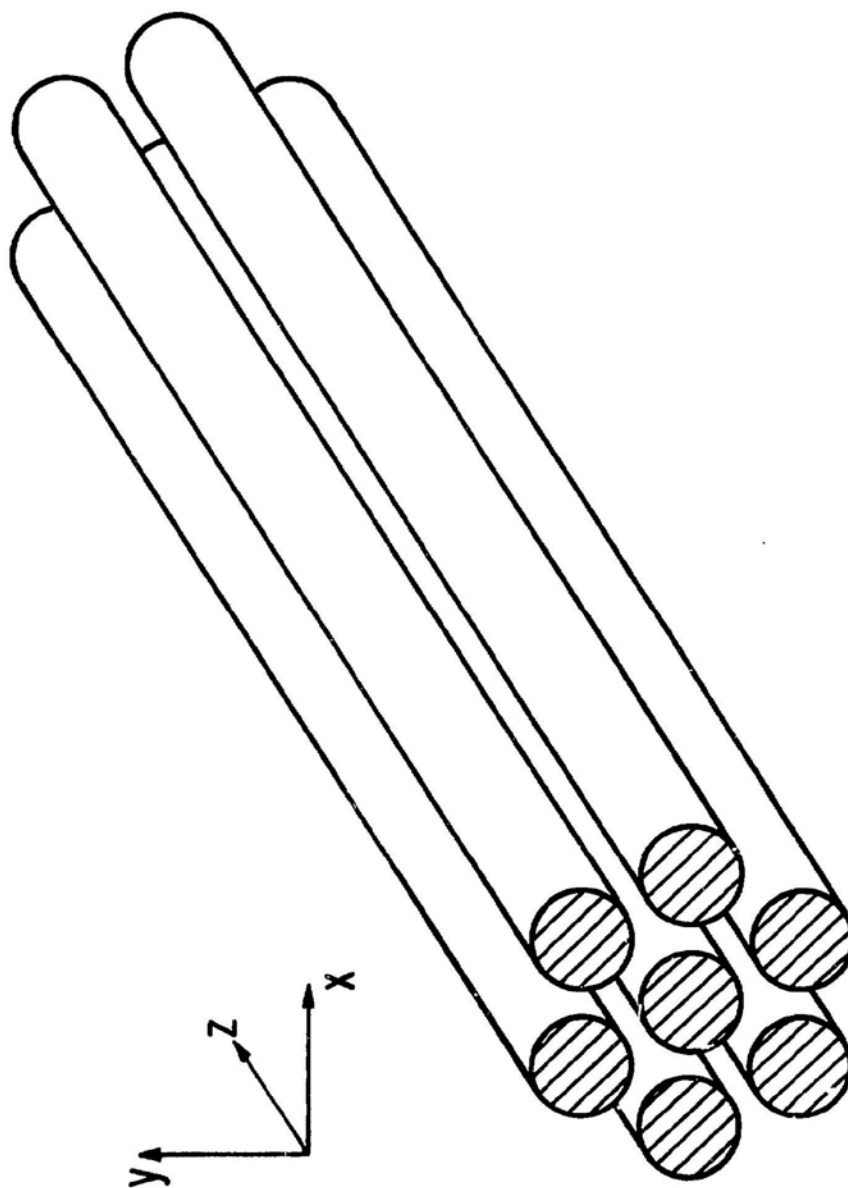


Fig. 3.9. A Group of Circular Cylinders Vibrating in a Fluid

of motion is

$$E_p I_p \frac{\partial^4 u_p}{\partial z^4} + C_{sp} \frac{\partial u_p}{\partial t} + m_p \frac{\partial^2 u_p}{\partial t^2} + \sum_{q=1}^{2N} \gamma_{pq} \frac{\partial^2 u_q}{\partial t^2} = g_{sp} . \quad (3.71)$$

The variables with subscript p (or q) from 1 to N are associated with motion in the x direction and from $N + 1$ to $2N$ in the y direction.

The added-mass matrix γ_{pq} developed in Section 3.3 is based on the two-dimensional flow theory. The vibration of a group of cylinders causes three-dimensional flow; however, for long cylinders, the two-dimensional theory for γ_{pq} will provide reasonable accuracy in many practical cases.

The boundary conditions at $z = 0$ and ℓ must be specified:

For simply-supported cylinders,

$$z = 0 \text{ and } \ell , \quad u_p = \frac{\partial^2 u_p}{\partial z^2} = 0 ,$$

for fixed-free cylinders,

$$z = 0 , \quad u_p = \frac{\partial u_p}{\partial z} = 0 , \text{ and}$$

(3.72)

$$z = \ell , \quad \frac{\partial^2 u_p}{\partial z^2} = \frac{\partial^3 u_p}{\partial z^3} = 0 ,$$

and for fixed-fixed cylinders,

$$z = 0 \text{ and } \ell , \quad u_p = \frac{\partial u_p}{\partial z} = 0 ,$$

where ℓ is the length of the cylinders. Without loss of generality, the initial state of the cylinders can be assumed as:

$$u_p(z, t) \Big|_{t=0} = u_{op}(z)$$

(3.73)

$$\frac{\partial u_p(z, t)}{\partial t} \Big|_{t=0} = v_{op}(z) .$$

Equations 3.71 through 3.73 are the complete mathematical statement of the problem.

3.4.2 Free Vibration

Let

$$u_p(z, t) = \sum_{n=1}^{\infty} q_{pn} \phi_n(z) , \quad (3.74)$$

where $\phi_n(z)$ is the n th orthonormal function of cylinders in vacuum, i.e.,

$$\frac{1}{L} \int_0^L \phi_m(z) \phi_n(z) dz = \delta_{mn} . \quad (3.75)$$

Using Eqs. 3.71 through 3.75 yields

$$[M]\{\ddot{Q}\} + [c]\{\dot{Q}\} + [K]\{Q\} = \{G\}$$

and

$$\{Q\}_{t=0} = \{A\} , \quad (3.76)$$

$$\{\dot{Q}\}_{t=0} = \{B\} ,$$

where $[M]$, $[C]$, and $[K]$ are symmetric matrices with elements m_{pq} , c_{pq} , and k_{npq} and $\{G\}$, $\{A\}$ and $\{B\}$ are generalized force, initial displacement, and initial velocity with elements q_{np} , a_{np} , b_{np} , in which

$$m_{pq} = m_p \delta_{pq} + \gamma_{pq} ,$$

$$c_{pq} = c_{sp} \delta_{pq} ,$$

$$k_{npq} = m_p \omega_{vpn}^2 \delta_{pq} ,$$

(3.77)

$$g_{np} = \frac{1}{L} \int_0^L g_{sp} \phi_n dz ,$$

$$a_{np} = \frac{1}{L} \int_0^L u_{op} \phi_n dz ,$$

and

$$b_{np} = \frac{1}{L} \int_0^L v_{op} \phi_n dz ,$$

where ω_{vpn} is the natural frequency of cylinder p of the n th mode in vacuum. Note that Eqs. 3.76 can be applied to all values of n . For each n there are $2N$ equations that are coupled. However, there is no coupling among the equations for different n . This is true for a group of cylinders with the same type of boundary conditions and of the same length.

For free vibration, neglect the damping and forcing terms and let

$$\{Q\} = \{\bar{Q}\} \exp(i\omega t) . \quad (3.78)$$

Natural frequencies and mode shapes can be calculated from the undamped homogeneous equations:

$$[K]\{\bar{Q}\} = \omega^2[M]\{\bar{Q}\} . \quad (3.79)$$

For a given value of n , $2N$ natural frequencies can be calculated from Eq. 3.79; these frequencies are denoted by ω_{fnp} ($n = 1, 2, \dots, \infty$; $p = 1, 2, \dots, 2N$). The mode shape can also be calculated from Eq. 3.79.

Let $[E]$ be the weighted modal matrix formed from the columns of eigenvectors. It is easily shown that

$$[E^TME] = [I] \quad \text{and} \quad [E^TKE] = [\Lambda] \quad (3.80)$$

where $[I]$ is an identity matrix and $[\Lambda]$ is a diagonal matrix formed from the eigenvalue ω_{fnp}^2 .

When all cylinders are identical, and have the same properties in the x and y directions,

$$\omega_{vpn} = \omega_{vn} \quad \text{and} \quad m_p = m . \quad (3.81)$$

In this case, Eq. 3.79 can be reduced to

$$[\gamma_{pq}]\{\bar{q}_q\} = \bar{\omega}^2\{\bar{q}_q\} ,$$

where (3.82)

$$\bar{\omega}^2 = m(\omega_{vn}^2 - \omega^2)/\omega^2 .$$

Equation 3.82 is identical to Eq. 3.51; i.e., the eigenvectors of the added mass matrix are the same as the mode shapes of the coupled modes and the eigenvalues of the added-mass matrix are related to the natural frequencies of coupled modes. Corresponding to each eigenvalue's μ_p , the natural frequency

of the coupled mode is

$$\omega_{fpn} = [m/(m + \mu_p)]^{0.5} \omega_v. \quad (3.83)$$

Equation 3.83 shows that the natural frequency of the coupled mode is reduced in proportion to $[m/(m + \mu_p)]^{0.5}$. This is similar to that for a single structure in a liquid; therefore, μ_p is the effective added mass. The role of μ_p for a group of cylinders is the same as m_a for an isolated cylinder.

In the case of a group of N identical cylinders, there are $2N$ natural frequencies corresponding to a single frequency for a solitary cylinder. These $2N$ frequencies are distributed near the frequency of a solitary cylinder. More precisely, the distribution of the natural frequencies of a group of cylinders in liquid can be presented in Fig. 3.10 for a group of simply supported cylinders. ω_{fn} ($n = 1, 2, \dots, \infty$) are the natural frequencies of a solitary cylinder in an infinite fluid. Note that

$$\omega_{fn} = \left(\frac{m}{m + M_d} \right)^{0.5} \omega_{vn}. \quad (3.84)$$

Corresponding to each ω_{fn} , there is a frequency band with the lower and upper bounding frequencies ω_{fn}^l and ω_{fn}^u , which are given by

$$\omega_{fn}^l = \left(\frac{m + M_d}{m + \mu_p|_{\max}} \right)^{0.5} \omega_{fn} \quad \text{and} \quad (3.85)$$

$$\omega_{fn}^u = \left(\frac{m + M_d}{m + \mu_p|_{\min}} \right)^{0.5} \omega_{fn}.$$

$\mu_p|_{\max}$ and $\mu_p|_{\min}$ denote the maximum and minimum values of the effective added masses. The $2N$ natural frequencies of the coupled modes are distributed in the frequency band from ω_{fn}^l to ω_{fn}^u .

The mode shapes associated with each natural frequency are, of course, different. For example, consider a group of cylinders simply supported at both ends. The axial variations of the motion are shown in Fig. 3.10. In the n th frequency band, the mode shapes associated with the axial variations are the same as the n th mode of a solitary cylinder.

Corresponding to each coupled mode, the cylinders are moving in different directions. For example, consider the following numerical examples: steel tubes whose outside radius is 1.27 cm, wall thickness 0.156 cm, and length

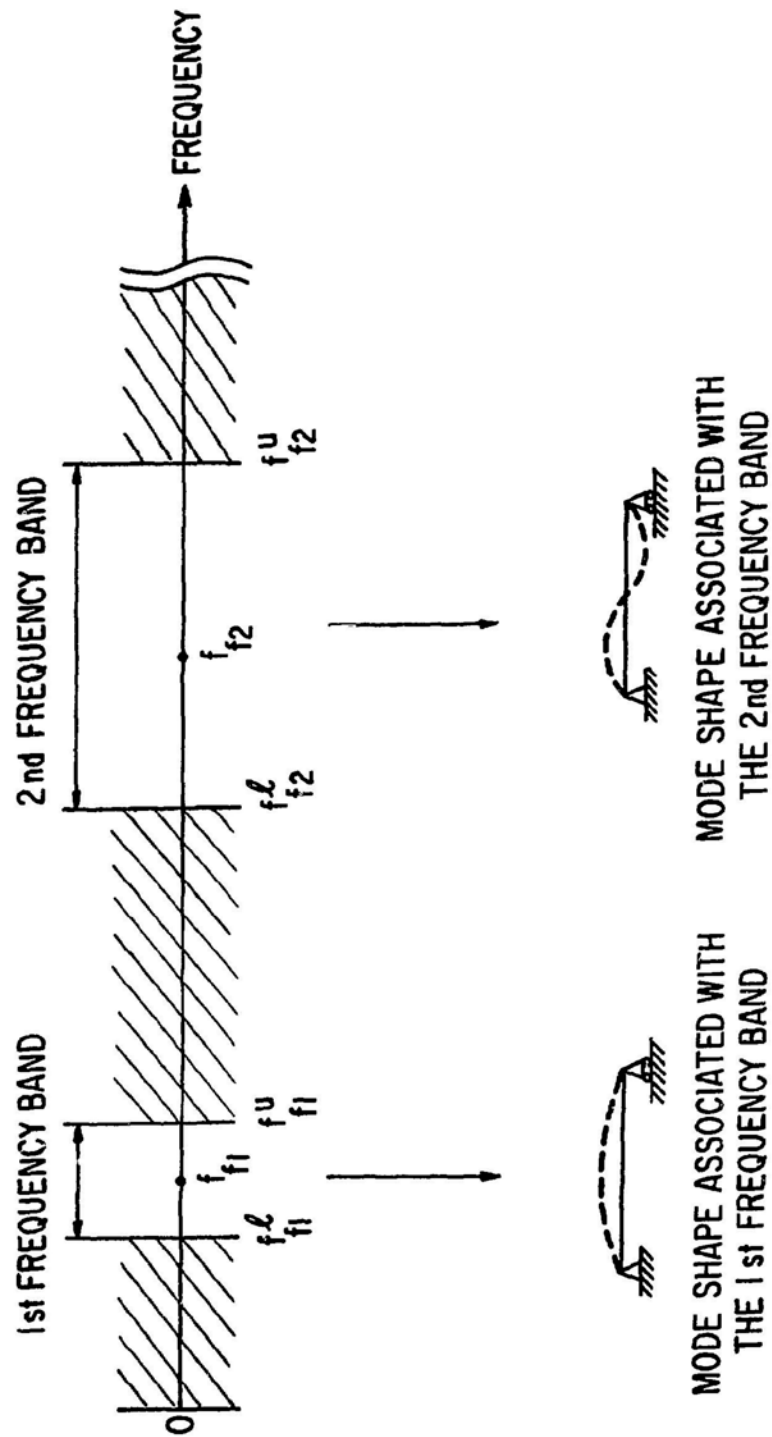


Fig. 3.10. Frequency Bands for an Array of Cylinders in Fluid

1.27 m and simply supported at both ends (Chen 1975b). In each group of tubes under consideration it is assumed that all tubes are identical. Figure 3.11 shows the normal modes in water of two groups of cylinders consisting of three and four cylinders for $n = 1$ when $P/D = 1.05$, and $T/D = 1.075$. For each n , there are $2N$ normal modes for a group of N cylinders. Figure 3.12 shows the frequencies of three tubes as a function of P/D . As the spacing decreases, the natural frequencies of lower modes decreases while those of the higher modes increase. When the spacing increases, all frequencies approach that of a solitary tube in an infinite fluid. Note that there are two repeated frequencies in Fig. 3.12. Corresponding to the second and third frequencies, there are two modes. The modes presented in the figure are orthogonal to each other. However, this set is not the only set of solutions for repeated frequencies; a linear combination of the two modes of the set also satisfies the conditions of orthogonality.

3.4.3 Forced Vibration

The response to an excitation can be calculated from Eqs. 3.76. For many practical situations, the damping matrix $[C]$ can be assumed to be proportional to the stiffness matrix $[K]$. In this case, Eq. 3.76 can be reduced to a set of $2N$ uncoupled modal equations by letting

$$\{Q\} = [E]\{W\} \quad (3.86)$$

and premultiplying Eq. 3.76 by the transpose $[E]^T$, the result being

$$[E]^T M E \{\ddot{W}\} + [E]^T C E \{\dot{W}\} + [E]^T K E \{W\} = [E]^T \{G\} \quad (3.87)$$

Based on the results given in Eq. 3.80, the square matrices on the left side are diagonal matrices. Thus, each equation reduces to that of a single oscillator and has the form

$$\ddot{w}_{pn} + 2\zeta_{fpn}\omega_{fpn}\dot{w}_{pn} + \omega_{fpn}^2 w_{pn} = \sum_{q=1}^{2N} e_{pqn}g_{qn}, \quad (3.88)$$

where ζ_{fpn} is the modal damping ratio of coupled modes in fluid. Equation 3.88 is easily solved and the displacement and other quantities of interest can be calculated from Eq. 3.74.

If $[C]$ is not proportional to the stiffness matrix, a damped vibration mode superposition method, as shown in Appendix A, can be used.

Figure 3.13 shows the response of seven tubes subjected to two step loads with the same magnitude—one applied to Tube 2 in the x direction and the

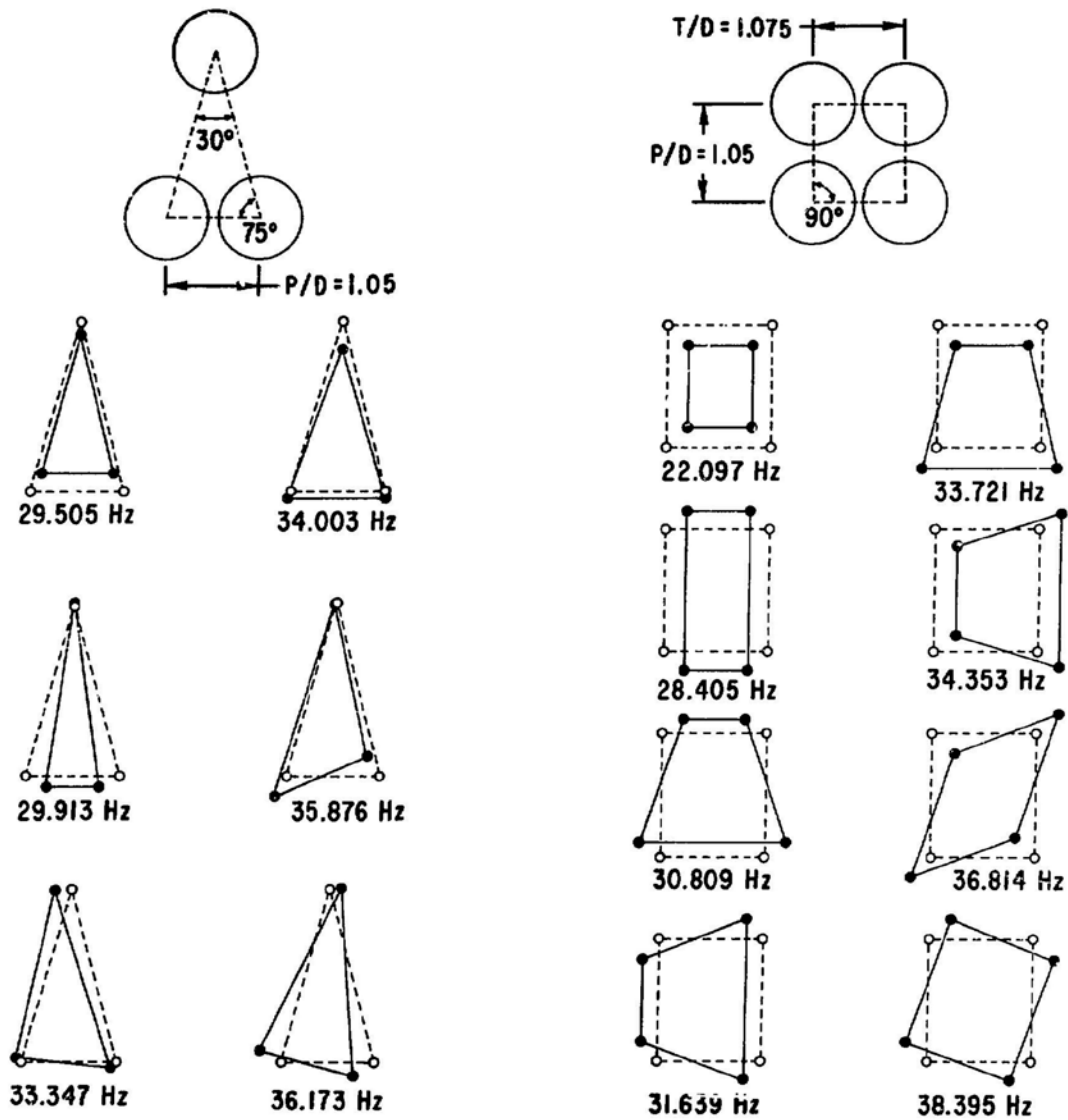


Fig. 3.11. Normal Modes of Three and Four Identical Cylinders Vibrating in a Fluid (Chen 1975b)

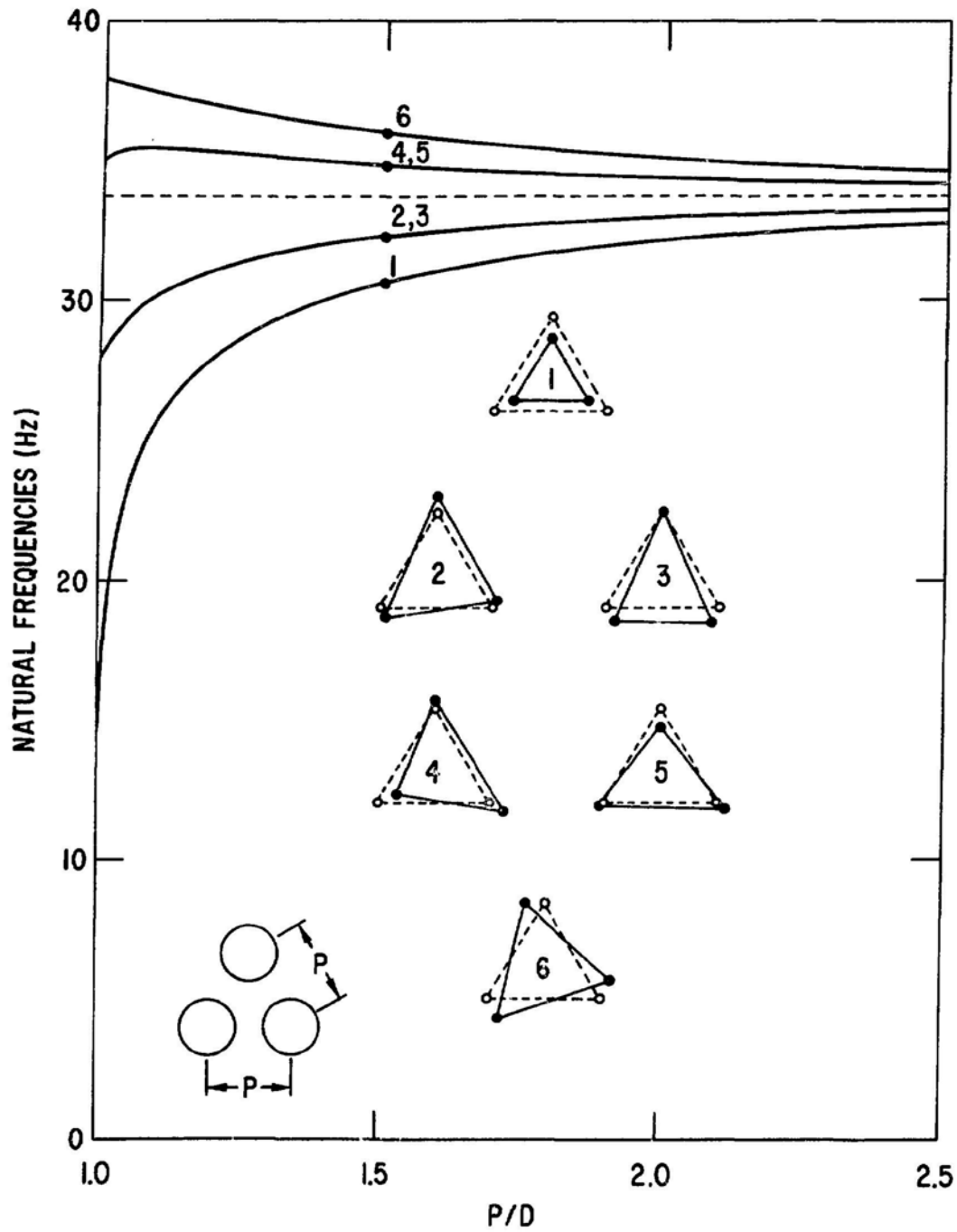


Fig. 3.12. Natural Frequencies of a Group of Three Cylinders as a Function of Pitch Ratio (Chen 1975b)

SIMPLY SUPPORTED TUBE SUBMERGED IN SODIUM AND CONTAINING SODIUM AT 516 °C

O.D. = 2.22 cm

WALL THICKNESS = 0.114 cm

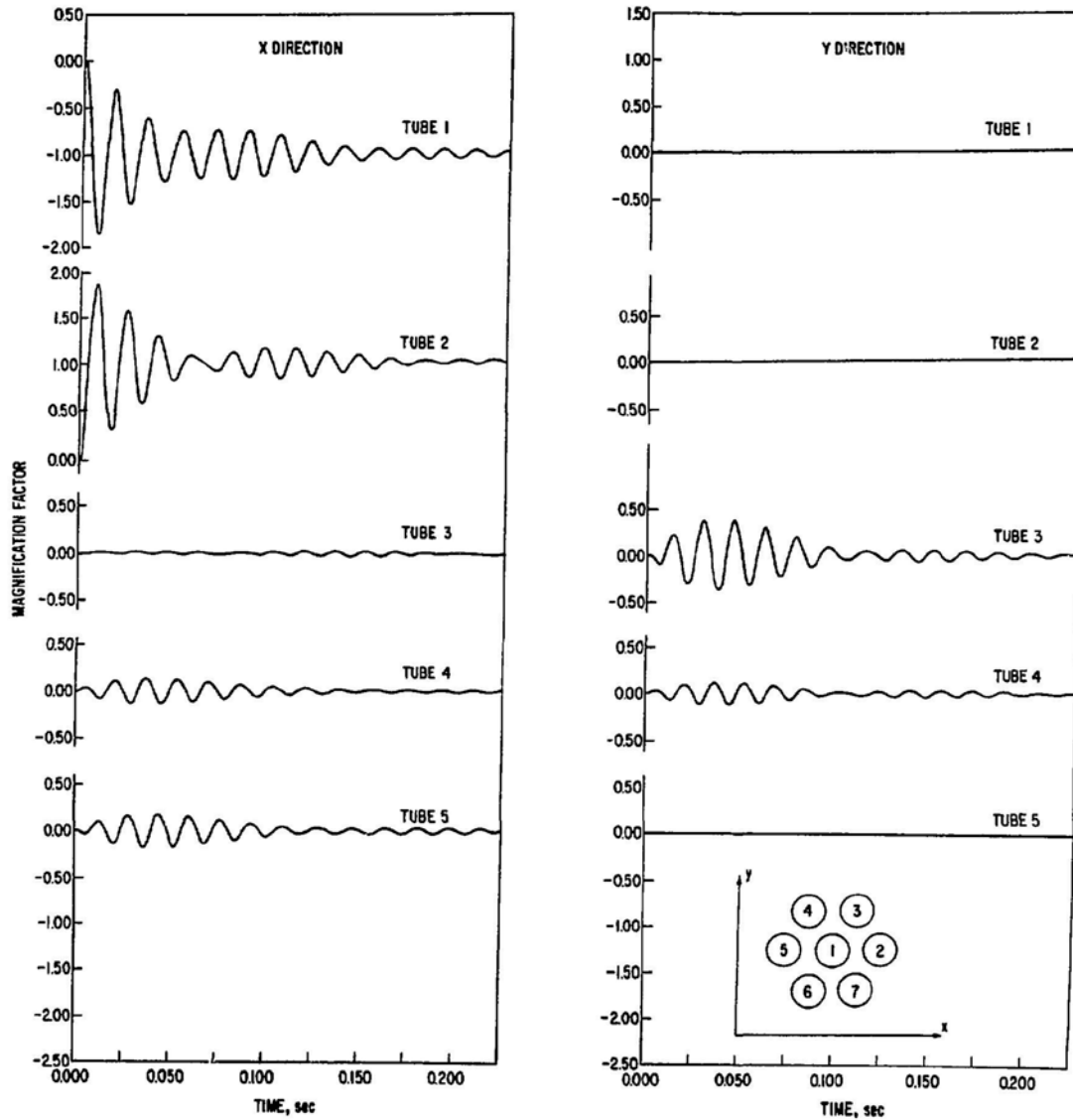
 $L = 76.2$ cm $P = 3.33$ cm $C_{sp} = 40.2$ N-s/m²

Fig. 3.13. Transient Response of a Tube Bank (Chen 1977)

other applied to Tube 1 in the opposite direction (Chen 1977). The magnification factor is defined as the ratio of the displacement at midspan to that of the deflection of Tube 2 in the x direction to a static load of the same magnitude. Because of symmetry, Tubes 1, 2, and 5 respond in the x direction only and the displacements of Tubes 6 and 7 are the same as those of Tubes 4 and 3 except that they are oscillating in the opposite direction.

Figure 3.14 shows the response of a row of five tubes to a sinusoidal excitation to Tube 5 in the y direction (Chen and Jendrzeczyk 1978). In this case, in the first frequency band there are 10 coupled modes. However, the x direction motion and y direction motion are uncoupled. When Tube 5 is subjected to an excitation in the y direction, all tubes respond in the y direction only. The tube accelerations given in Fig. 3.14 are in the y direction and there are five resonant peaks. The theoretical results and experimental data agree very well.

3.5 NATURAL FREQUENCIES OF A GROUP OF IDENTICAL CONTINUOUS CYLINDERS VIBRATING IN A FLUID

3.5.1 Natural Frequencies of a Cylinder on Multiple Supports with Equal Spans

Several methods of analysis can be used to study the frequency of continuous cylinders: the finite-element method, the transfer-matrix technique, the Rayleigh-Ritz procedure, the wave-propagation approach, the iterative procedure, and the conventional method of solving the equation of motion directly. In this section, the frequencies of multispan cylinders are obtained using the dynamic three-moment equation, which has several advantages over the other methods.

Consider a continuous cylinder, as shown in Fig. 3.15. The intermediate supports are assumed to prevent vertical deflection. The bending moment at the α support is denoted by M_α . The dynamic three-moment equation, which can be derived using the equation of motion and boundary conditions, relates the bending moments at three supports of any two consecutive spans. In an infinite periodically supported cylinder, the bending moment M_α at the α support is related to the moment at the preceding support $\alpha-1$ by

$$M_\alpha = M_{\alpha-1} \exp(i v_c), \quad (3.89)$$

where v_c is a dimensionless propagation constant (Gupta 1970). The real part $\text{Re}(v_c)$ represents the phase difference between moments at adjacent supports, and the imaginary part $\text{Im}(v_c)$ represents the exponential decay rate of the bending wave as it propagates from one support to the next. The propagation constant v_c depends on the frequency parameter λ and the dimensionless axial tension τ , which are related to natural frequency and axial tension of the cylinder by

BRASS TUBE SUBMERGED IN WATER, FIXED AT ONE END AND
EXCITED BY A SINUSOIDAL FORCE AT THE OTHER END

O.D. = 1.27 cm

WALL THICKNESS = 0.159 cm

$\ell = 40.48$ cm

$P/D = 1.5$

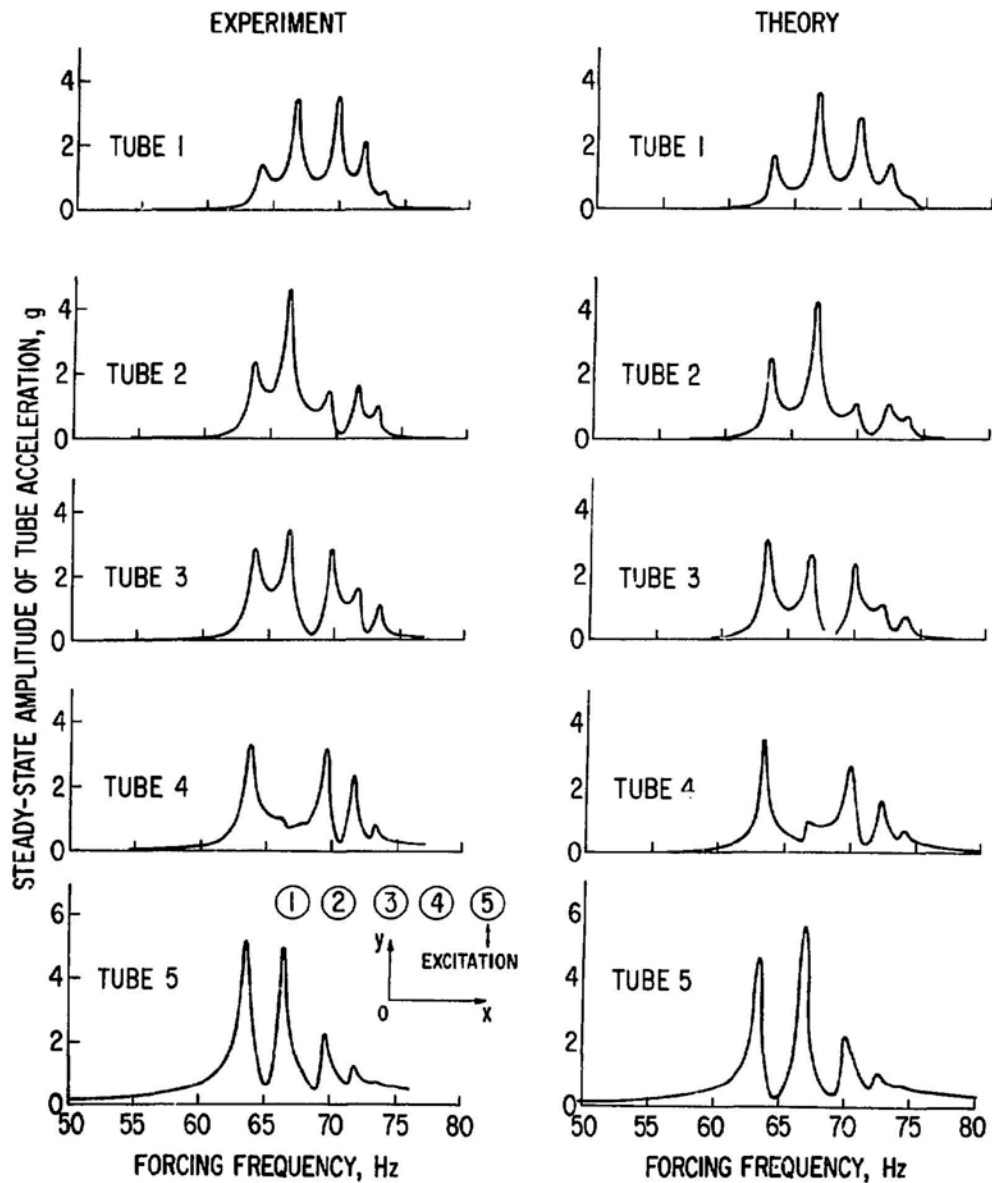


Fig. 3.14. Steady-state Response of a Row of Five Tubes to Excitation of Tube 5 in the y Direction (Chen and Jendrzejczyk 1978)

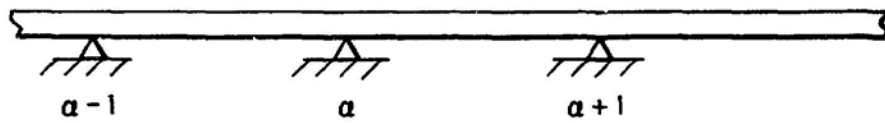


Fig. 3.15. A Continuous Cylinder with Intermediate Supports

$$f_v = \left(\frac{1}{2\pi}\right) \frac{\lambda}{l^2} \left(\frac{EI}{m}\right)^{1/2}$$

and

(3.90)

$$\tau = \frac{T l^2}{EI}.$$

Figure 3.16 shows values of v_c for $\tau = 0$ and 4. When $\text{Im}(v_c)$ is zero, bending waves can propagate without attenuation; these regions are called propagation bands. When $\text{Im}(v_c)$ is not zero, bending waves cannot propagate without attenuation; these regions are called stop bands. There exist alternate bands of free propagation and attenuation.

In a finite structure, natural frequencies are in the propagation bands. In calculating the frequency, only the real part of v_c is of interest; $\text{Re}(v_c)$ is zero or $\pm \pi$ in the stop band, and is between 0 and $\pm \pi$ in the propagation band. Values of p_c ($p_c = |\text{Re}(v_c)|/\pi$) are given in Fig. 3.17 for the first and second propagation bands and for various values of τ .

The p_c - λ curves are used to find the frequency of a finite structure. Consider a K span periodically supported beam. At the two extreme ends, the supports may be hinged/hinged, hinged/clamped or clamped/clamped. Use of the theory of determinants (Chen 1975d), or the concept of wave propagation (Gupta 1970), yields an extremely simple graphical method to calculate the frequency. The procedure is summarized as follows:

- For a continuous beam with K spans and hinged at two extreme ends, divide the ordinate over the range 0 to 1 into K equal parts, and draw horizontal lines separating the parts. The projections on the abscissa (λ axis) of the points of intersection of the p_c - λ curve and horizontal lines corresponding to $\alpha = 1, 2, \dots, K$ (odd-numbered propagation bands) or $\alpha = 0, 1, 2, \dots, K-1$ (even-numbered propagation bands) will give the frequency factors.

- For a continuous beam with K spans and hinged at one extreme end and clamped at the other, divide the ordinate over the range 0 to 1 into $2K$ equal parts, and draw horizontal lines separating the parts. The projections on the abscissa of the points of intersection of the p_c - λ curve and the horizontal lines corresponding to $\alpha = 1, 3, 5, \dots, 2K-1$ will give the frequency factors.

- For a continuous beam with K spans and clamped at two extreme ends, divide the ordinate over the range 0 to 1 into K equal parts, and draw horizontal lines separating the parts. The projections on the abscissa of the points of intersection of the p_c - λ curve and horizontal lines corresponding to

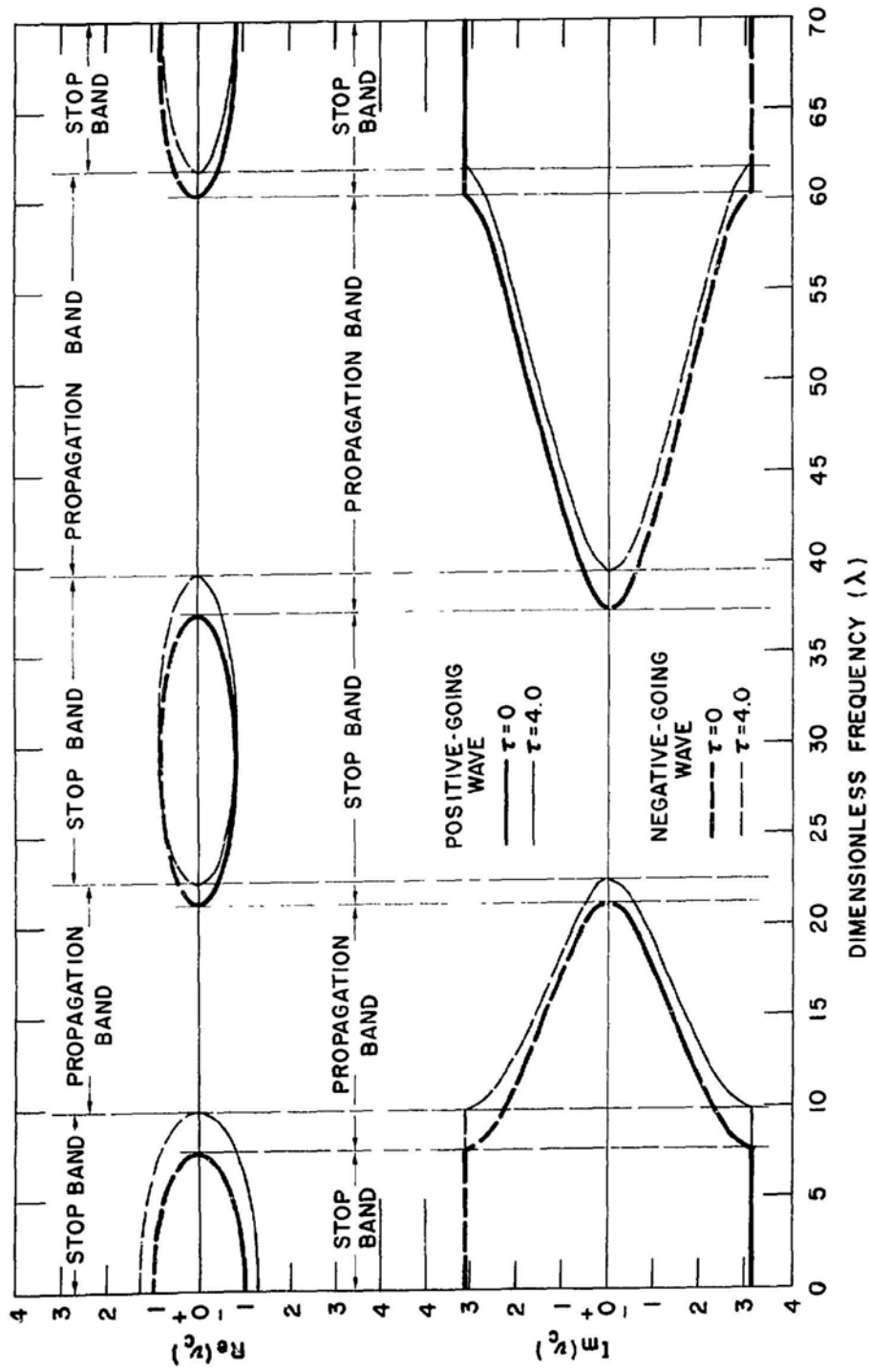


Fig. 3.16. Propagation Constant for a Periodically Supported Cylinder ($\Gamma = 0$)

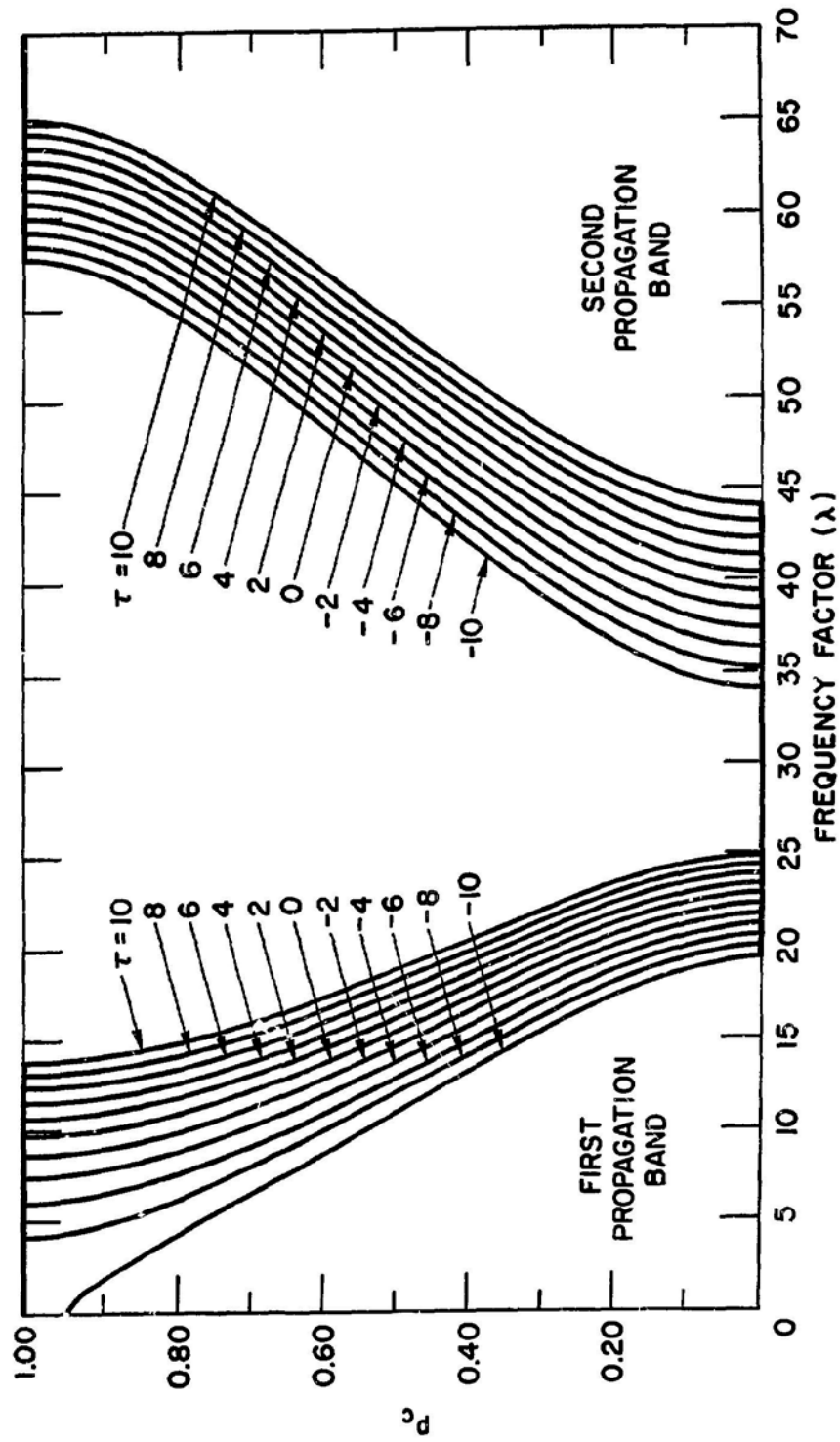


Fig. 3.17. Propagation Constant and Frequency ($p_c - \lambda$) Curves for a Cylinder, First and Second Propagation Bands

$\alpha = 0, 1, 2, \dots, K-1$ (odd-numbered bands) or $\alpha = 1, 2, 3, \dots, K$ (even-numbered propagation bands) give the frequency factors.

Figure 3.18 illustrates the graphical method used to find the frequency factors for a four-span beam hinged at the two extreme ends. Having the frequency factor $\lambda_{n\alpha}$, the frequency can be calculated by substituting $\lambda_{n\alpha}$ in Eq. 3.90 for λ .

Based on these results, we can summarize the natural frequencies of a cylinder as follows:

- For a single-span cylinder, the natural frequencies are

$$f_{vn} = \left(\frac{1}{2\pi}\right) \frac{\lambda_n}{L} \left(\frac{EI}{m}\right)^{1/2}, \quad n = 1, 2, 3, \dots, \infty, \quad (3.91)$$

where the λ_n 's are given in Appendix D.

- For a periodically supported single cylinder, the natural frequencies are

$$f_{vn\alpha} = \left(\frac{1}{2\pi}\right) \left(\frac{\lambda_{n\alpha}}{L}\right) \left(\frac{EI}{m}\right)^{1/2},$$

$$n = 1, 2, 3, \dots, \infty \quad (3.92)$$

and

$$\alpha = 1, 2, \dots, K.$$

3.5.2 Natural Frequencies of an Array of Cylinders on Multiple Supports in Fluid

The natural frequencies of coupled modes are presented in Section 3.4.2 for single-span cylinders. The same method can be applied to multispans cylinders. This can be demonstrated using Eq. 3.74. If $\phi_n(z)$ is taken to be the n th orthonormal function of the multispans cylinders, the results obtained for multispans cylinders will be similar to that for single-span cylinders. More specifically, if one follows through the same type of analysis for periodically supported cylinder arrays, it can be shown that the natural frequencies of coupled modes can be calculated as follows:

- Natural Frequencies of Periodically Supported Cylinder in Vacuum - Using the method given in Section 3.5.1 or other techniques, one can find the

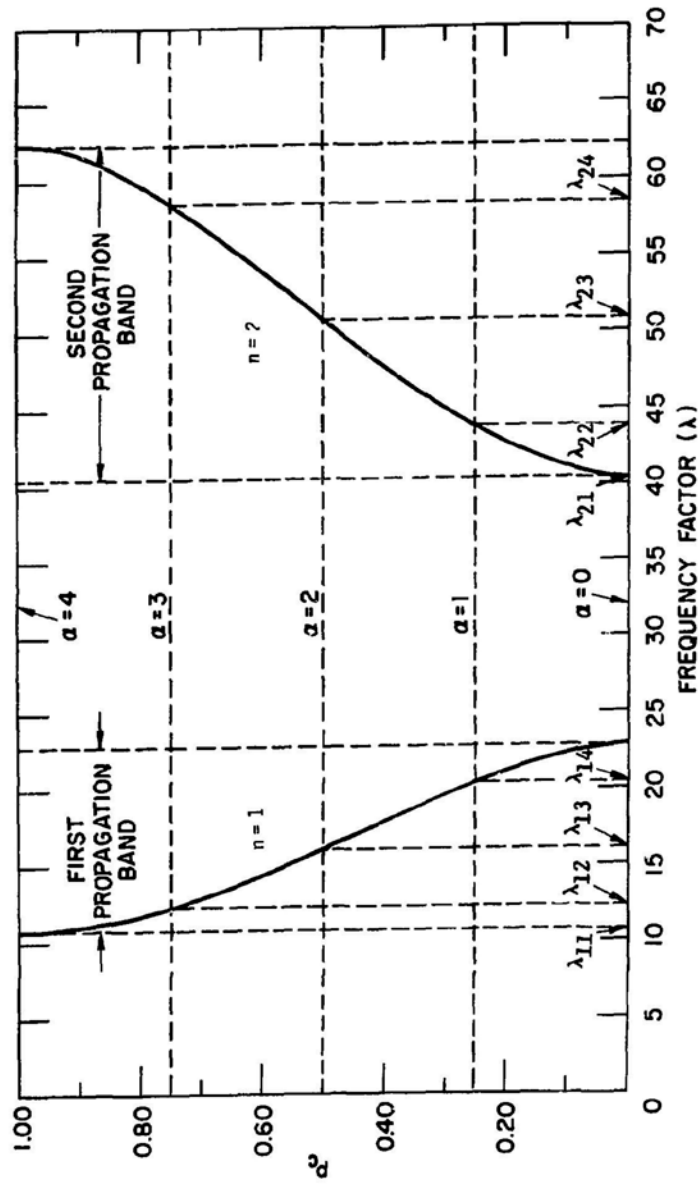


Fig. 3.18. Frequency Factor of a Four-span Cylinder Hinged at the Two Extreme Ends ($\tau = 2.0$)

natural frequency of a periodically supported cylinder in vacuum $\omega_{vn\alpha}$, where n ($= 1, 2, \dots, \infty$) denotes the n th propagation band and α ($= 1, 2, \dots, K$) denote the α th frequency in the n th band.

● **Eigenvalues of the Added Mass Matrix** - Since the added mass matrix is symmetric for a group of N cylinders, there are $2N$ eigenvalues which are denoted by μ_p , $p = 1, 2, \dots, 2N$.

● **Natural Frequencies of Periodically Supported Cylinder Arrays** - The natural frequencies of a continuous cylinder array are then given by $\omega_{fpn\alpha}$:

$$f_{fpn\alpha} = \frac{f_{vn\alpha}}{\left(1 + \frac{\mu_p}{m}\right)^{0.5}} ;$$

$$n = 1, 2, \dots, \infty \quad (3.93)$$

$$\alpha = 1, 2, \dots, K, \quad \text{and}$$

$$p = 1, 2, \dots, 2N .$$

It is seen that from Eq. 3.93 that corresponding to a single frequency for a solitary cylinder with a single span, there are $2KN$ natural frequencies of coupled modes for a group of N cylinders with K spans vibrating in a liquid. Then, it is not difficult to imagine that in many cases a multispan cylinder array will respond like anything but a narrow band filter.

3.6 TWO COAXIAL CYLINDERS COUPLED BY A PERFECT FLUID

The coupled vibration of multiple cylinders has been studied based on the two-dimensional flow theory. In this section, the three-dimensional effect is considered.

3.6.1 Statement of the Problem

Consider a fluid/structural system that consists of a cylindrical rod and a cylindrical shell located concentrically (Chen 1972). The annular region is filled with incompressible frictionless fluid (see Fig. 3.19). The rod radius is R_1 and the inside radius of the shell is R_2 . The rod and shell have the same length, l , which is much larger than R_2 . The beam-like vibration is studied: i.e., the rod and the outer shell are considered as Euler-Bernoulli beams.

The governing equations of motion are

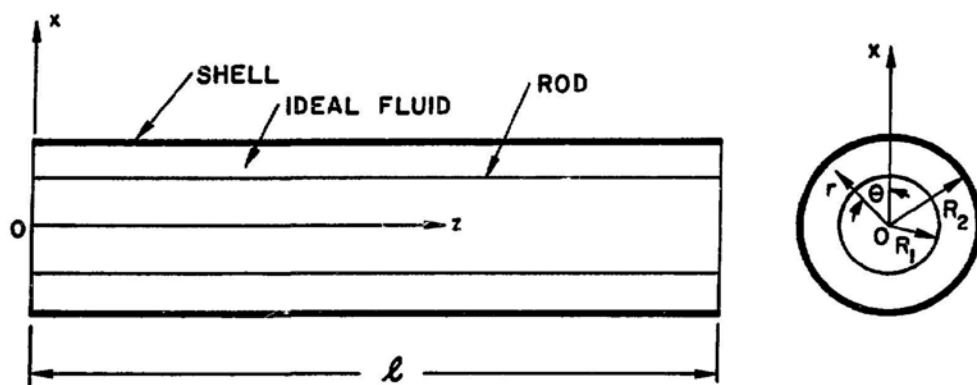


Fig. 3.19. A Cylindrical Rod Coupled to a Cylindrical Shell by a Perfect Fluid

$$E_j I_j \frac{\partial^4 u_j}{\partial z^4} + m_j \frac{\partial^2 u_j}{\partial t^2} = g_j \quad \text{and} \quad (3.94)$$

$$j = 1, 2,$$

where $E_j I_j$ is the flexural rigidity, u_j is the transverse displacement, z is the axial coordinate, t is the time, m_j is the mass per unit length, and g_j is the resultant force per unit length of fluid acting on the structures. As an example, simply supported conditions are considered; thus

$$u_j = \frac{\partial^2 u_j}{\partial z^2} = 0 \quad \text{at } x = 0, l, \quad j = 1, 2. \quad (3.95)$$

The force g_j is attributed to fluid motion; therefore, the motion of fluid in the annular region must be studied. The fluid motion is governed by Eq. 2.74. The fluid boundaries are the rod surface and shell inner surface; thus

$$u_r = \frac{\partial u_1}{\partial t} \cos \theta \quad \text{at } r = R_1, \quad \text{and} \quad (3.96)$$

$$u_r = \frac{\partial u_2}{\partial t} \cos \theta \quad \text{at } r = R_2.$$

At the two ends, either fluid pressure or fluid velocity has to be specified. As an example, the ends are taken to be stationary; thus

$$u_z = 0 \quad \text{at } x = 0 \text{ and } l. \quad (3.97)$$

Finally, the forces component g_1 and g_2 are given by

$$g_1(z, t) = -R_1 \int_0^{2\pi} p(z, r, \theta, t) \Big|_{r=R_1} \cos \theta \, d\theta$$

and

$$g_2(z, t) = R_2 \int_0^{2\pi} p(z, r, \theta, t) \Big|_{r=R_2} \cos \theta \, d\theta. \quad (3.98)$$

3.6.2 Frequency Equation

For free vibration, let

$$\begin{aligned} u_j(z,t) &= \phi_j(z)\exp(i\omega t) \quad \text{and} \\ g_1(z,t) &= \psi_j(z)\exp(i\omega t) . \end{aligned} \quad (3.99)$$

Substituting Eqs. 3.99 into Eqs. 3.94 and 3.95,

$$\begin{aligned} E_j I_j \frac{d^4 \phi_j}{dz^4} - m_j \omega^2 \phi_j &= \psi_j(z) \quad \text{and} \\ \phi_j = \frac{d^2 \phi_j}{dz^2} &= 0 \quad \text{at } z = 0 \text{ and } l \end{aligned} \quad (3.100)$$

$\phi_j(z)$ are modal functions of the rod and shell with fluid coupling. In general they are different from those without fluid coupling. In this analysis, $\phi_j(z)$ are represented in the series form as superposition of the uncoupled rod and shell modal function; i.e.,

$$\phi_j(z) = \sum_{n=1}^{\infty} a_{jn} \phi_{jn}(z) . \quad (3.101)$$

Here, $\phi_{jn}(z)$'s are orthonormal modal functions of the rod and shell in vacuum; i.e.,

$$\begin{aligned} E_j I_j \frac{d^2 \phi_{jn}}{dz^4} &= m_j \omega_{jn}^2 \phi_{jn} \quad \text{and} \\ \frac{1}{l} \int_0^l \phi_{jn} \phi_{jm} dz &= \delta_{nm} . \end{aligned} \quad (3.102)$$

Next, consider the fluid field. The solution of the Laplace equation is taken as

$$\phi = F_r(r) F_\theta(\theta) F_z(z) \exp(i\omega t) , \quad (3.103)$$

where $F_r(r)$, $F_\theta(\theta)$, and $F_z(z)$ are solutions of the following equations

$$\begin{aligned}
F_r(r) &= A_1 I_n(kr) + A_2 K_n(kr) , \\
F_\theta(\theta) &= B_1 \sin(n\theta) + B_2 \cos(n\theta) , \quad \text{and} \\
F_z(z) &= C_1 \sin(kz) + C_2 \cos(kz) ,
\end{aligned} \tag{3.104}$$

where n , k , A_1 , A_2 , B_1 , B_2 , C_1 and C_2 are to be determined.
To satisfy Eq. 3.97,

$$C_1 = 0 , \quad k = \frac{m\pi}{\ell} , \quad m = 0, 1, 3, \dots, \infty \tag{3.105}$$

Introducing the axial modal function for the fluid $\psi_m(z)$, such that

$$\frac{1}{\ell} \int_0^\ell \psi_m^2(z) dz = 1 , \quad m = 0, 1, \dots, \infty \tag{3.106}$$

for the present case, we have

$$\begin{aligned}
m = 0 , \quad \psi_m(z) &= 1 , \\
m > 1 , \quad \psi_m(z) &= \sqrt{2} \cos(k_m z) , \quad k_m = \frac{m\pi}{\ell} .
\end{aligned} \tag{3.107}$$

Therefore, Eq. 3.103 can be written as

$$\phi = \sum_{m=0}^{\infty} D_m \psi_m(z) F_r(r) F_\theta(\theta) \exp(i\omega t) . \tag{3.108}$$

To satisfy Eq. 3.96,

$$\begin{aligned}
B_1 &= 0 , \\
n &= 1 ,
\end{aligned} \tag{3.109}$$

$$\sum_{m=0}^{\infty} D_m \psi_m(z) F'_r(R_j) = i\omega \phi_j(z) , \quad j = 1, 2 .$$

The prime denotes differentiation with respect to r . From Eqs. 3.104, 3.108, and 3.109, ϕ can be written as

$$\phi = \sum_{m=0}^{\infty} [G_m I_1(k_m r) + H_m K_1(k_m r)] \psi_m(z) \cos \theta \exp(i\omega t), \quad (3.110)$$

where G_n and H_n are determined from the following equations:

$$G_m I_1'(k_m R_1) + H_m K_1'(k_m R_1) = i\omega \sum_{n=1}^{\infty} \gamma_{jmn} a_{jn} \quad (3.111)$$

and

$$\gamma_{jmn} = \frac{1}{\ell} \int_0^{\ell} \psi_m(z) \phi_{jn}(z) dz.$$

The fluid pressure is obtained from Eqs. 2.74 and 3.108:

$$p = -i\rho\omega \sum_{m=0}^{\infty} \{[G_m I_1(k_m r) + H_m K_1(k_m r)] \psi_m(z)\} \cos \theta \exp(i\omega t). \quad (3.112)$$

Substituting Eq. 3.112 into 3.98 yields

$$\psi_1(z) = \rho\pi R_1 \omega^2 \sum_{m=0}^{\infty} \{[\sigma_m \sum_{n=1}^{\infty} \gamma_{1mn} a_{1n} + \bar{\sigma}_m \sum_{n=1}^{\infty} \gamma_{2mn} a_{2n}] \psi_n(z)\} \quad (3.113)$$

and

$$\psi_2(z) = \rho\pi R_2 \omega^2 \sum_{m=0}^{\infty} \{[\tau_m \sum_{n=1}^{\infty} \gamma_{1mn} a_{2n} + \bar{\tau}_m \sum_{n=1}^{\infty} \gamma_{2mn} a_{2n}] \psi_n(z)\},$$

where

$$\begin{aligned} \sigma_m &= [-I_1(k_m R_1) K_1'(k_m R_2) + I_1'(k_m R_2) K_1(k_m R_1)] / \Delta_m, \\ \bar{\sigma}_m &= [-I_1'(k_m R_1) K_1(k_m R_1) + I_1(k_m R_1) K_1'(k_m R_1)] / \Delta_m, \\ \tau_m &= [-I_1'(k_m R_2) K_1(k_m R_2) + I_1(k_m R_2) K_1'(k_m R_2)] / \Delta_m, \\ \bar{\tau}_m &= [-I_1(k_m R_2) K_1'(k_m R_1) + I_1'(k_m R_1) K_1(k_m R_2)] / \Delta_m, \end{aligned} \quad (3.114)$$

and

$$\Delta_m = I_1'(k_m R_1) K_1(k_m R_2) - I_1'(k_m R_2) K_1(k_m R_1).$$

With Eqs. 3.102, substitution of Eqs. 3.113 into Eqs. 3.100 gives

$$\sum_{n=1}^{\infty} (\omega_{v1n}^2 - \omega^2) a_{1n} \phi_{1n}(z) = \frac{\rho \pi R_1^2}{m_1} \omega^2 \sum_{m=0}^{\infty} \left\{ \left[\sigma_m \sum_{n=1}^{\infty} \gamma_{1mn} a_{1n} + \bar{\sigma}_m \sum_{n=1}^{\infty} \gamma_{2mn} a_{2n} \right] \psi_{1n}(z) \right\}$$

(3.115)

and

$$\sum_{n=1}^{\infty} (\omega_{v2n}^2 - \omega^2) a_{2n} \phi_{2n}(z) = \frac{\rho \pi R_2^2}{m_2} \omega^2 \sum_{m=0}^{\infty} \left\{ \left[\tau_m \sum_{n=1}^{\infty} \gamma_{1mn} a_{1n} + \bar{\tau}_m \sum_{n=1}^{\infty} \gamma_{2mn} a_{2n} \right] \psi_{2n}(z) \right\}.$$

Multiplying the first equation by $\phi_{1m}(z)$ and the second equation by $\phi_{2m}(z)$ in Eq. 3.115 and integrating with respect to z from 0 to l yields

$$\sum_{n=1}^{\infty} \left\{ \left(\frac{\omega_{v1n}^2 - \omega^2}{\omega^2} \right) \delta_{nm} - \frac{\rho \pi R_1^2}{m_1} \sum_{\ell=0}^{\infty} \gamma_{1\ell n} \sigma_{\ell} \gamma_{1\ell n} \right\} a_{1n} - \frac{\rho \pi R_1^2}{m} \sum_{n=1}^{\infty} \frac{1}{R_2} \sum_{\ell=0}^{\infty} \gamma_{2\ell n} \tau_{\ell} \gamma_{1\ell n} a_{2n} = 0$$

(3.116)

and

$$- \frac{\rho \pi R_2^2}{m_2} \sum_{n=1}^{\infty} \frac{1}{R_2} \sum_{\ell=0}^{\infty} \bar{\gamma}_{2\ell n} \tau_{\ell} \gamma_{1\ell n} a_{1n} + \sum_{n=1}^{\infty} \left\{ \left(\frac{\omega_{v2n}^2 - \omega^2}{\omega^2} \right) \delta_{nm} - \frac{\rho \pi R_2^2}{m_2} \frac{1}{R_2} \sum_{\ell=0}^{\infty} \gamma_{1\ell n} \bar{\tau}_{\ell} \gamma_{2\ell n} \right\} a_{2n} = 0.$$

Equations 3.116 consist of an infinite number of ordinary equations. However, only a finite number of equations are taken in any particular case, according to the desired accuracy.

In this example, the boundary conditions of the two cylinders are identical and the two cylinders are of the same length. Therefore, the natural modes of uncoupled vibration are also identical. However, once the two cylinders are coupled by the fluid, the natural modes of coupled vibration are not the same as the natural modes of uncoupled vibration. In other words, the natural frequency and natural modes cannot be predicted using the simple

factor of added mass. Because the mode shapes depend on fluid coupling, the concept of added mass is not as useful as in the case where the natural modes do not change with fluid coupling.

For a general case in which the cylinders may be of different length, the natural modes of coupled vibration are not the same as the uncoupled vibration. Only under special conditions will the mode shapes of coupled and uncoupled vibration be identical. Two conditions must be satisfied:

- The natural modes of uncoupled vibration of the cylinders are identical.
- The modal function of the fluid $\psi_m(z)$ is the same as the modal function of the cylinders $\phi_{jm}(z)$.

If these two conditions are satisfied, Eq. 3.116 can be reduced to m sets of equations, each set containing two equations and no coupling among different sets of equations.

From Eqs. 3.116, the frequency equation can be written

$$F(\omega, \omega_{v1n}, \omega_{v2n}, m_1, m_2, R_1, R_2, l, \rho) = 0. \quad (3.117)$$

As an example, consider two simply supported cylinders:

$$\frac{\rho \pi R_1^2}{m_1} = 0.5,$$

$$\frac{\rho \pi R_2^2}{m_2} = 1.0,$$

$$R_2/R_1 = 2, \quad (3.118)$$

$$l/R_2 = 10, \quad \text{and}$$

$$\frac{E_2 I_2 m_1}{E_1 I_1 m_1} = 4.$$

With these nondimensional parameters, the dimensionless frequencies (λ) of coupled modes can be calculated:

$$\lambda = \left(\frac{m_1}{E_1 I_1} \right)^{0.5} \omega l^2. \quad (3.119)$$

The frequency equation is solved numerically. Table 3.1 shows the values of λ obtained from the frequency equation for various approximations in which n terms are included for an n -mode approximation. For an n mode approximation, the frequency equation is a polynomial equation of $2n$ order; therefore, $2n$ frequencies can be obtained. From Table 3.1, it is seen that the rate of convergence is fast. In general, if n frequencies are of interest, an $(n + 1)$ -mode approximation will yield results with sufficient accuracy. In particular, if only the fundamental frequency is needed, a two-mode approximation will be acceptable.

Figure 3.20 shows the first five frequencies as function of the uncoupled frequency ratio $E_2 I_{2m_1} / E_1 I_{1m_2}$. The mode shapes for five frequencies at $E_2 I_{2m_1} / E_1 I_{1m_2} = 2$, those circled on Fig. 3.20, are shown in Fig. 3.21. There exist in-phase and out-of-phase modes. When the motions of the two cylinders are out of phase, the fluid in between has to be displaced; thus, the fluid inertia's effect is very large. On the other hand, when the two structures are in phase, the coupling effect of the fluid inertia is reduced.

3.7 TWO COAXIAL CIRCULAR CYLINDERS SEPARATED BY VISCOUS FLUID

3.7.1 Added Mass and Fluid Damping Matrices

Consider the same problem as that given in Fig. 3.19 with the following two exceptions:

- The cylinder is infinitely long and the two-dimensional flow theory is applicable.
- The fluid is a viscous fluid.

For small amplitude oscillations, the equations of motion of the fluid are the same as those given in Section 2.6. The fluid forces acting on the two cylinders can be analyzed using the same techniques as those given in Section 2.6. The fluid forces acting on the two cylinders are obtained as follows (Yeh and Chen 1978):

$$g_j = \sum_{k=1}^2 \left(\bar{\alpha}_{jk} \frac{\partial^2 u_k}{\partial t^2} + \bar{\alpha}'_{jk} \frac{\partial u_k}{\partial t} \right),$$

$$\bar{\alpha}_{jk} = \rho \pi R_j R_k \operatorname{Re}(a_{jk}),$$

$$\bar{\alpha}'_{jk} = \rho \pi R_j R_k \omega \operatorname{Im}(-a_{jk}),$$

$$a_{11} = -(1 + 2b), \quad (3.120)$$

Table 3.1. Frequencies Obtained from Various Approximations

Frequencies	Approximations				
	One-mode	Two-mode	Three-mode	Four-mode	Five-mode
λ_1	7.364	7.052	7.052	7.044	7.044
λ_2	14.443	14.023	14.023	14.012	14.012
λ_3		30.581	28.933	28.933	28.872
λ_4		59.178	56.762	56.760	56.660
λ_5			71.194	67.345	67.345
λ_6			136.201	128.620	124.072
λ_7				130.684	129.962
λ_8				248.020	210.160
λ_9					236.188
λ_{10}					397.176

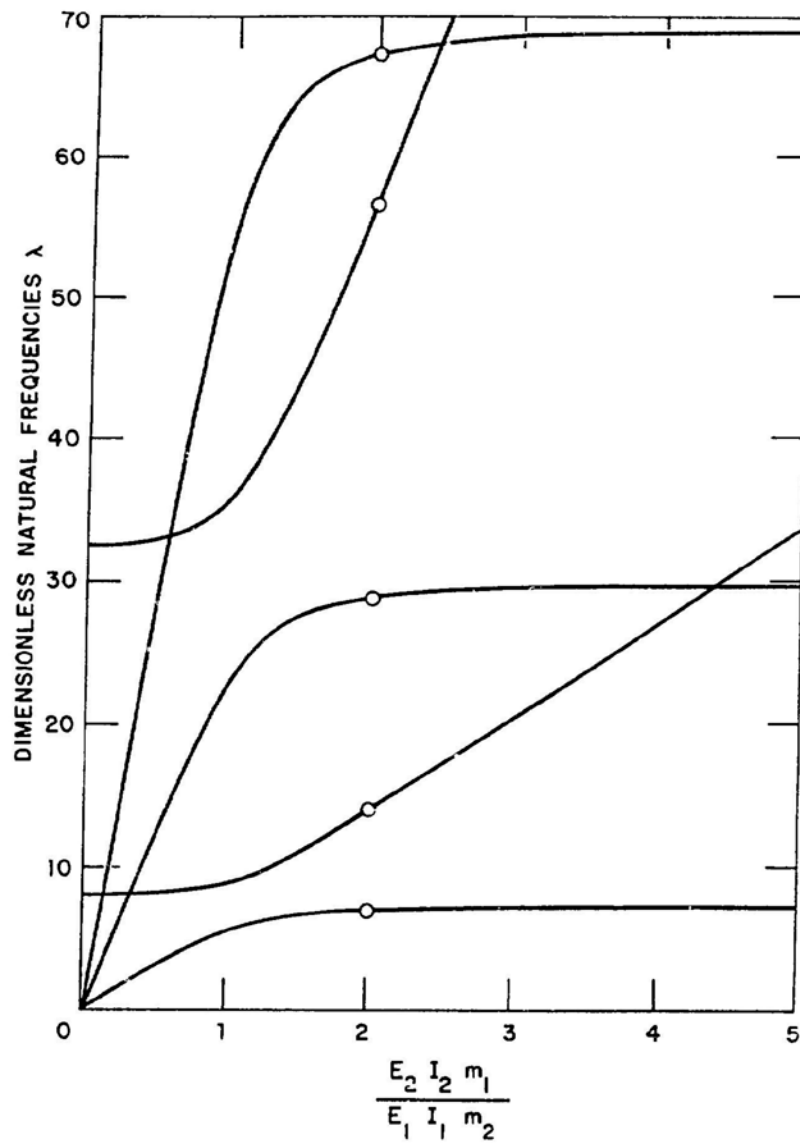


Fig. 3.20. Dimensionless Natural Frequency as a Function of the Uncoupled Frequency Ratio ($E_2 I_2 m_1 / E_1 I_1 m_2$) (Chen 1972)

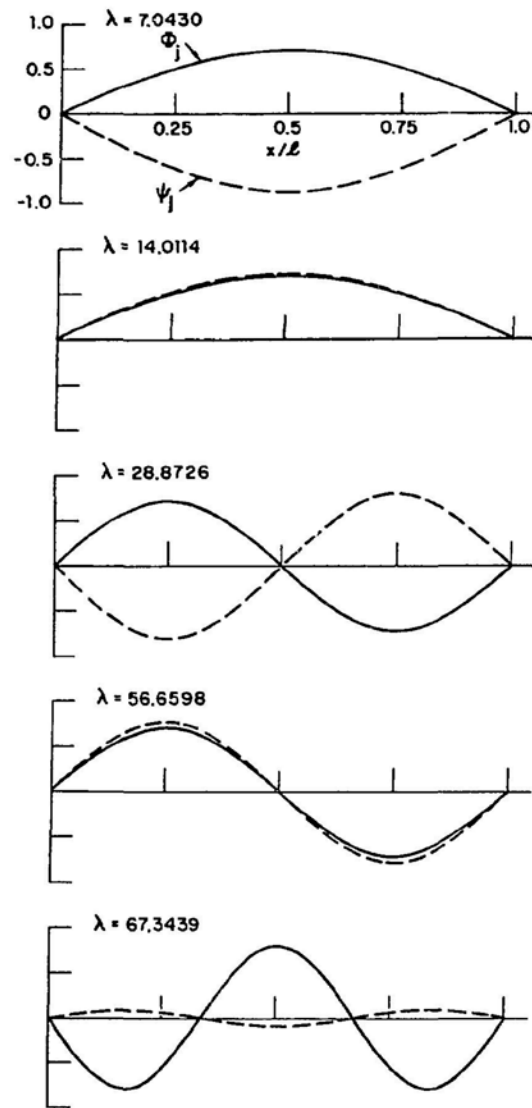


Fig. 3.21. Mode Shapes of Two Coupled Cylinders (Chen 1972)

$$a_{12} = a_{21} = 2\gamma b = -\gamma(1 + a_{11}) ,$$

$$a_{22} = 1 - 2\gamma^2 a = 1 + \gamma^2(1 + a_{11}) , \quad (3.120)$$

(Contd.)

$$b_j = (-i\omega/\nu)^{0.5} R_j ,$$

$$\gamma = R_1/R_2 ,$$

and

$$b = - \begin{vmatrix} 1 & 1 & F_1(b_1) & G_1(b_1) \\ 0 & 1 & \gamma F_1(b_2) & \gamma G_1(b_2) \\ 2 & 2 & b_1 F_o(b_1) & b_1 G_o(b_1) \\ 0 & 2 & b_1 F_o(b_2) & b_1 G_o(b_2) \end{vmatrix} + \begin{vmatrix} 1 & 1 & F_1(b_1) & G_1(b_1) \\ \gamma^2 & 1 & \gamma F_1(b_2) & \gamma G_1(b_2) \\ 0 & 2 & b_1 F_o(b_1) & b_1 G_o(b_1) \\ 0 & 2 & b_1 F_o(b_2) & b_1 G_o(b_2) \end{vmatrix} ,$$

where F_n and G_n are the n th-order Bessel functions. They can be either the first- and second-kind Bessel functions, J_n and Y_n , or the Hankel functions, $H_n^{(1)}$ and $H_n^{(2)}$. The selection of the functions mainly depends on computational considerations.

The coefficients $\bar{\alpha}_{1j}$ and $\bar{\alpha}_{2j}$ depend on the $R_k (= 4\omega r^2/\nu)$ and γ in a very complicated way. Approximate solutions can be obtained in special cases:

Viscous fluid and very large radius ratio (e.g., $\gamma < 0.1$, $R_k > 1$):

For $\gamma \rightarrow 0$ and $|b_2| \gg 1$,

$$a_{11} = 1 - 4H_1^{(2)}(b_1)/b_1 H_o^{(2)}(b_1) . \quad (3.121)$$

Furthermore, if $|b_1| \gg 1$,

$$a_{11} = 1 - \frac{4i}{b_1} . \quad (3.122)$$

Viscous fluid and large value of R_k (e.g., $R_k > 10^4$):

$$\begin{aligned}
 a_{11} = & -1 + \{[16b_1^2 - (73 - 578\gamma + 9\gamma^2)/8]\sin(\beta b_1) \\
 & - 2b_1(1 - \gamma)(16 + \sqrt{\gamma})\cos(\beta b_1)\} \\
 & + \{(1 - \gamma^2)[8b_1^2 - (9 + 30\gamma + 9\gamma^2)/16]\sin(\beta b_1) \\
 & + b_1(1 + \gamma)(1 + 14\gamma + \gamma^2)\cos(\beta b_1) - 32b_1\sqrt{\gamma}\} ,
 \end{aligned} \tag{3.123}$$

and

$$\beta = (1 - \gamma)/\gamma .$$

$R_k \gg 1$ and $\beta^2 R_k \ll 1$:

$$a_{11} = -31/\beta^3 R_k . \tag{3.124}$$

$R_k \gg 1$ and moderate gap (e.g., $\beta > 0.01$ and $R_k > 10^4$):

$$a_{11} = \frac{b_1(1 + \gamma^2)\sin(\beta b_1) - 2(2 - \gamma + \gamma^2)\cos(\beta b_1) + 4\gamma\sqrt{\gamma}}{b_1(1 - \gamma^2)\sin(\beta b_1) + 2\gamma(1 + \gamma)\cos(\beta b_1) - 4\gamma\sqrt{\gamma}} . \tag{3.125}$$

$R_k \gg 1$ and $\beta^2 R_k \gg 1$ (e.g., $R_k > 10^4$, and $\beta^2 R_k > 10^4$):

$$a_{11} = [b_1(1 + \gamma^2) - i2(2 - \gamma + \gamma^2)]/[b_1(1 - \gamma^2) + i2\gamma(1 + \gamma)] . \tag{3.126}$$

$R_k \gg 1$, $\beta^2 R_k \gg 1$ and $\beta \ll 1$ (e.g., $R_k > 10^7$, $\beta^2 R_k > 10^4$
and $\beta < 0.05$):

$$a_{11} = \frac{1 + \gamma^2}{1 - \gamma^2} + \frac{2\sqrt{2}}{\beta^2 R_k^{1/2}} \left[1 - i \left(1 - \frac{8\sqrt{2}}{R_k^{1/2}} \right) \right] . \tag{3.127}$$

$$\underline{v \rightarrow 0, R_k \rightarrow \infty:}$$

$$a_{11} = \frac{1 + \gamma^2}{1 - \gamma^2} \quad (3.128)$$

Although the general form of a_{jk} is very complicated, many practical applications belong to one of the special cases (Eqs. 3.121 through 3.128) discussed above. Because the typical value of R_k is usually larger than 10^4 , Eqs. 3.125 and 3.126 are often used.

It is noted that Eqs. 3.121 is the same as that in Eq. 2.59 and Eq. 3.123 is slightly different from Eq. 2.60; the latter is not accurate for $\beta \rightarrow 0$. However, for most applications, both equations given practically the same results.

Equation 3.120 shows that the added-mass matrix $\bar{\alpha}_{jk}$ and fluid-damping matrix $\bar{\alpha}'_{jk}$ are symmetric because $a_{12} = a_{21}$. This result is similar to those of an ideal fluid. Physically, these mean the hydrodynamic force acting on cylinder j in the \vec{e}_j direction due to a unit acceleration (velocity) of cylinder k in the \vec{e}_k direction is equal to the hydrodynamic force acting on the cylinder k in the \vec{e}_k direction due to a unit acceleration (velocity) of cylinder j in the \vec{e}_j direction. Thus, the reciprocal relations are valid for both perfect and viscous fluids.

3.7.2 Vibration of Two Coaxial Tubes

The equations of motion for two tubes coupled by viscous fluid are

$$E_j I_j \frac{\partial^4 u_j}{\partial z^4} + C_{sj} \frac{\partial u_j}{\partial t} + \sum_{k=1}^2 \bar{\alpha}'_{jk} \frac{\partial u_k}{\partial t} + \sum_{k=1}^2 \bar{\alpha}_{jk} \frac{\partial^2 u_k}{\partial t^2} + m_j \frac{\partial^2 u_j}{\partial t^2} = g_{sj}, \quad (3.129)$$

$$j = 1, 2.$$

The method of analysis presented in Section 3.4 can be used for this case. Equation 3.129 can be reduced to

$$[M]\{\ddot{Q}\} + [C]\{\dot{Q}\} + [K]\{Q\} = \{G\}, \quad (3.130)$$

where

$$m_{jk} = m_j \delta_{jk} + \bar{a}_{jk} ,$$

$$c_{jk} = c_{sj} \delta_{jk} + \bar{\alpha}_{jk} ,$$

$$k_{njk} = m_j \omega_{jn}^2 \delta_{jk} , \quad \text{and}$$

$$g_{np} = \frac{1}{l} \int_0^l g_{sp} \phi_n dz .$$

Note that the matrices [M], [C], and [K] are symmetric because \bar{a}_{jk} and $\bar{\alpha}_{jk}$ are symmetric.

For free vibration, the natural frequencies, modal damping ratio and mode shapes can be calculated in a straightforward manner based on Eq. 3.130. For forced vibration, depending on the damping matrix, different methods can be used.

If the damping matrix [C] is proportional to the stiffness matrix [K] or the mass matrix [M], the procedure given in Section 3.4.3 can be used. However, if the damping matrix [C] is proportional to neither [K] nor [M], the procedure given in Appendix A can be used.

For specific numerical examples, consider two concentric steel circular cylindrical tubes separated by water at room temperature. The dimensional values are shown in Table 3.2. The fluid gap, $\beta = (R_2 - R_1)/R_1$, is varied from 0.01 to 10. The tubes are assumed to be simply supported at both ends. Calculations are performed both with and without structural damping. The frequencies of the system depend on the axial mode number n . Unless specified, only the data associated with the lowest axial mode number (ie., $n = 1$) are given.

For comparison, calculations are included for several related cases: 1 - inner tube in vacuo; 2 - outer tube in vacuo; 3 - an uncoupled tube system with rigid outer tube; 4 - an uncoupled tube system with rigid inner tube; and 5 - a coupled cylindrical tube system.

Both the exact and approximate methods are used in calculations. It is found that the results obtained by these methods are practically identical except at the very small fluid gap region where the fluid viscosity effect and so the fluid damping are very large. For most practical applications, the approximate solution is as good as the exact one. Fig. 3.22 shows the system natural frequency as a function of fluid gap for $\zeta_{v1} = \zeta_{v2} = 0$.

The lower natural frequency is associated with the mode in which two tubes move out-of-phase, while the higher frequency is associated with the in-phase mode. The frequencies of the uncoupled modes (indicated by cases 3 and 4) are always in between those of the coupled modes (case 5). The out-of-

Table 3.2. Dimensional Values of the Numerical Examples for Two Coaxial Tubes

Parameter	Value
Inner interface radius	$R_1 = 5 \text{ cm}$
Wall thickness to tube radius ratios	
Inner tube	0.125
Outer tube	0.10
Steel mass density	$\rho_1 = \rho_2 = 7.47 \times 10^3 \text{ kg/m}^3$
Young's modulus	$E_1 = E_2 = 1.93 \times 10^{11} \text{ Pa}$
Rod length	$l = 150 \text{ cm}$
Structural modal damping ratio (ζ_s), two cases	$\zeta_{v1} = \zeta_{v2} = 0.01$ $\zeta_{v1} = \zeta_{v2} = 0$
Water density (ρ)	$1 \times 10^3 \text{ kg/m}^3$
Kinematic viscosity of water (ν)	$1 \times 10^{-6} \text{ m}^2/\text{s}$
Fluid gap, $\beta = (R_2 - R_1)/R_1$	$0.01 \leq \beta \leq 10$
End condition	Simple-simple

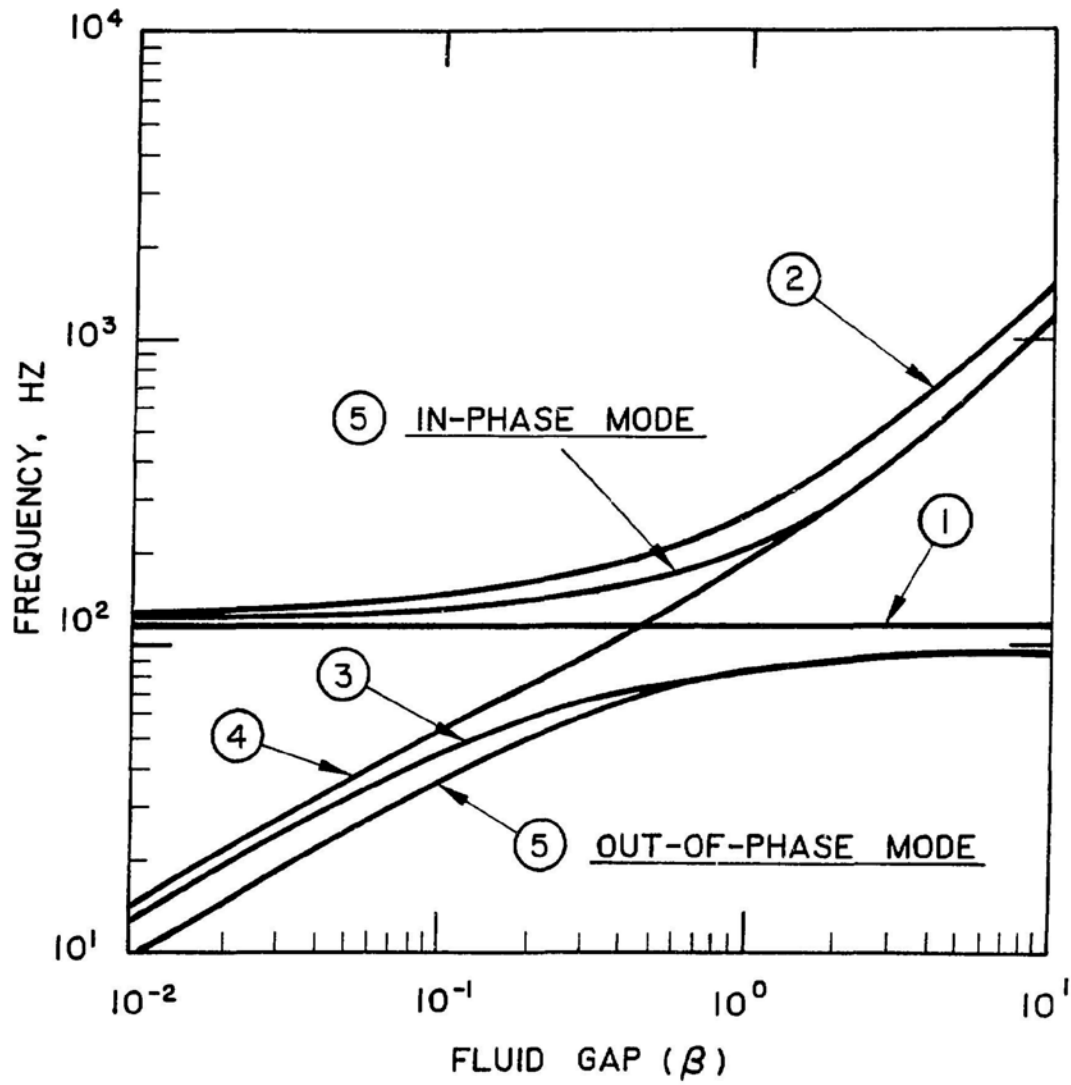


Fig. 3.22. Natural Frequencies of Two Coaxial Tubes as a Function of Fluid Gap β (Yeh and Chen 1978)

phase natural frequency is lower than either of the coupled modes; while the in-phase natural frequency is always higher than either of the uncoupled modes. This is similar to the results for two tubes in an ideal fluid (see Section 3.2).

As the fluid gap, β , increases, the effect of the existence of fluid decreases. Also the natural frequency of the out-of-phase mode approaches that of the uncoupled mode of a tube in an infinite fluid, and the frequency of the in-phase mode approaches that of the uncoupled mode of a tube containing a fluid.

As expected the fluid affects significantly both the out-of-phase modal frequency and the uncoupled modal frequencies as the fluid gap decreases. However, the in-phase modal frequency is practically unchanged as the fluid gap decreases.

Figures 3.23(a) and (b) show the system damping ratios as a function of fluid gap for $\zeta_{v1} = \zeta_{v2} = 0.01$ and $\zeta_{v1} = \zeta_{v2} = 0$ respectively. Except for the in-phase mode, the annulus fluid contributes significant damping to the system for all the cases especially at small fluid gaps. The in-phase modal damping ratio is not shown in Fig. 3.23 because it is too small. When $\zeta_{v1} = \zeta_{v2} = 0$, the modal damping ratios for coupled modes are higher (out-of-phase mode) or lower (in-phase mode) than either of the uncoupled modes. Usually the system damping ratio due to the fluid viscosity decreases as fluid gap increases as shown in Fig. 3.23(b). It is also interesting to point out that the total system damping ratio ζ_{f1} has a local minimum as Fig. 3.23 shows.

Figure 3.24 shows the effect of scale model on the system properties. For comparison, the data for a four-time scale and for potential flow solution are also included. The potential flow solution can be interpreted as that of an infinite-time scale model. Figure 3.24 shows that the natural frequency ratios (or added mass effect) are practically independent of the modal scale. However, the modal damping ratios are significantly different. This is because the fluid viscosity, ν or the kinetic Reynolds number, R_k , has a small effect on $\bar{\alpha}_{ij}$ and has a large effect on $\bar{\alpha}'_{ij}$. The change of natural frequency is due to fluid inertia effect while the increase in damping is mainly attributed to fluid drag. The total system damping ratio consists of structural and fluid damping. Usually structural damping will decrease and fluid damping will increase as fluid gap decreases. Therefore the value of ζ_{fj} could be an increasing function or a decreasing function of the gap depending on the values of structural damping and fluid damping.

Except for the potential flow solution in which the damping ratio always decreases as the gap decreases, all other cases in Fig. 3.24(b) show that there are local minimum values of damping ratio at some values of β . This behavior of minimum damping ratio seems to disappear as the modal scale decreases.

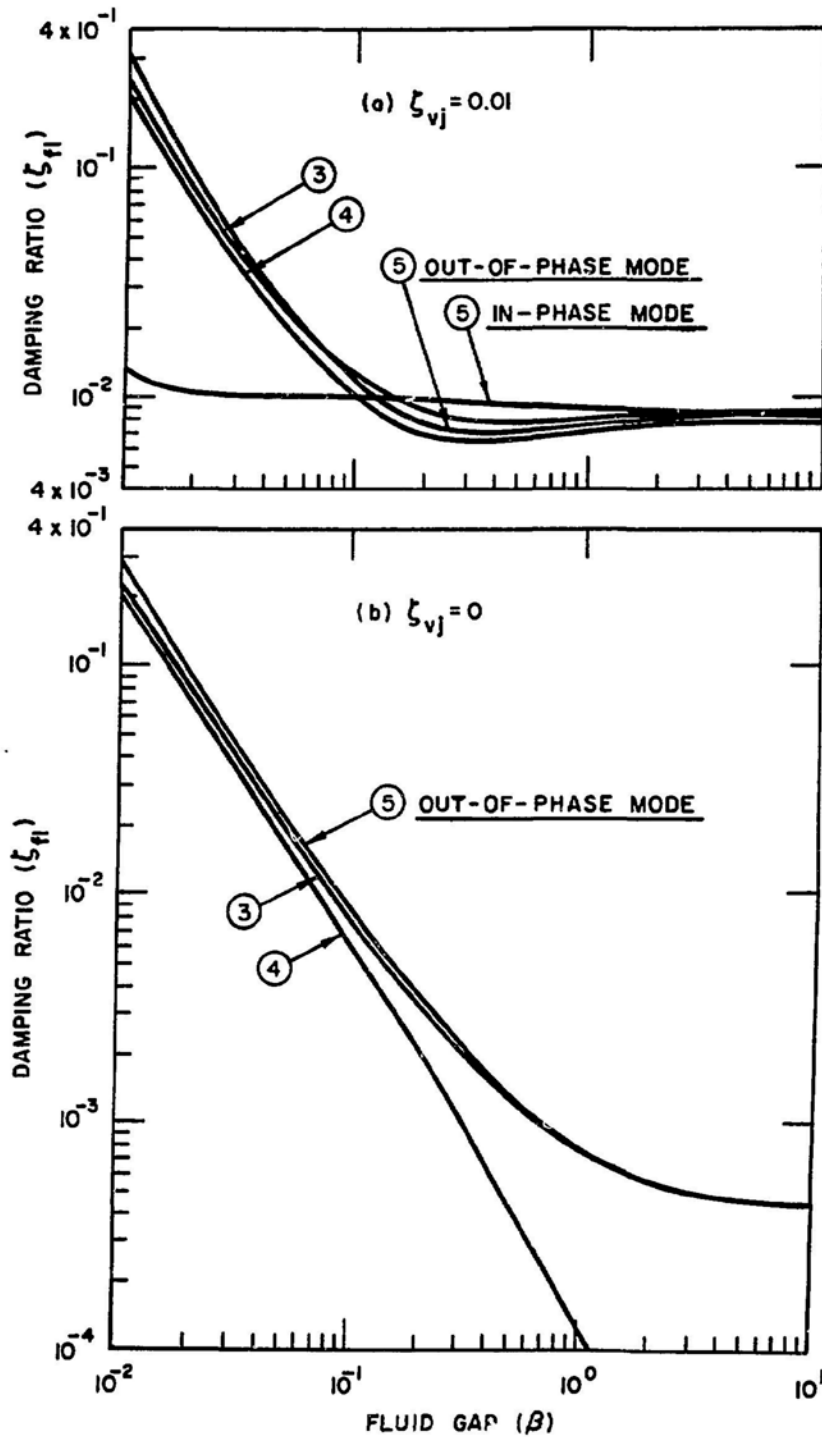


Fig. 3.23. Modal Damping Ratio ζ_{f1} of Two Coaxial Tubes as a Function of Fluid Gap β : (a) $\zeta_{vj} = 0.01$, (b) $\zeta_{vj} = 0$ (Yeh and Chen 1978)

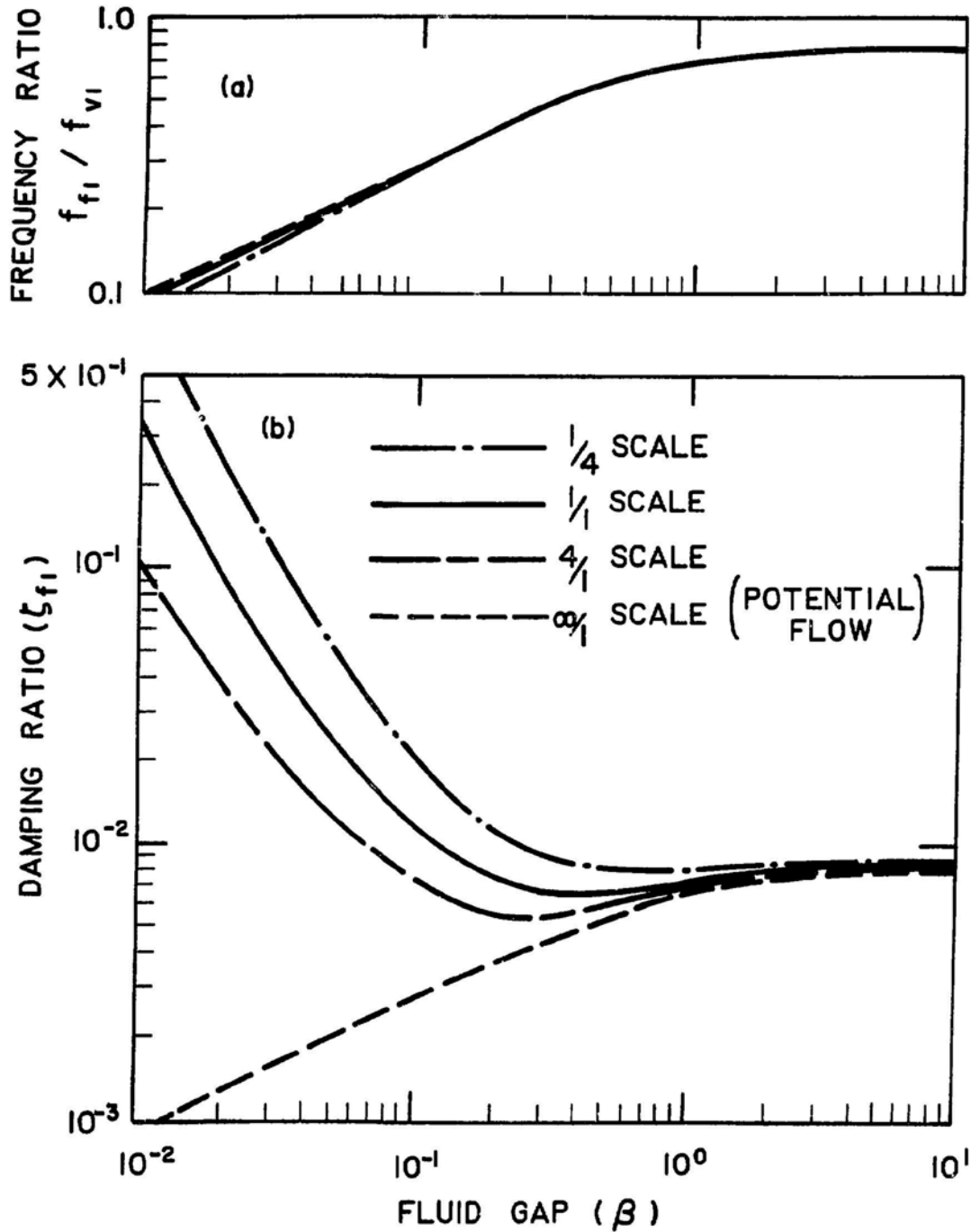


Fig. 3.24. Comparison of Natural Frequency and Modal Damping Ratio of Coupled Modes for Different Scale Models for $\zeta_{vj} = 0.01$ (Yeh and Chen 1978)

3.8 ADDED MASS AND DAMPING OF AN ARRAY OF CYLINDERS IN A COMPRESSIBLE INVISCID FLUID

Consider a group of N circular cylinders vibrating in a compressible inviscid fluid as shown in Fig. 3.3 (Lin and Chen 1981). The two-dimensional flow field associated with the motion of the cylinders can be solved using a similar procedure as given in Section 3.3.1.

The velocity potential of disturbances caused by the cylinders is composed of the partial fields due to the oscillation of each cylinder, namely

$$\begin{aligned}\phi &= \sum_{j=1}^N \phi_j, \\ \phi_j(r_j, \theta_j, t) &= \sum_{n=0}^{\infty} (a_{jn} \cos n\theta_j + b_{jn} \sin n\theta_j) H_n^{(1)}(\kappa r_j) \exp(-i\omega t),\end{aligned}\quad (3.131)$$

in which $H_n^{(1)}(\kappa r_j)$ is the Hankel function of the first kind of order n with argument κr_j ($\kappa = \omega/c$). This form of solution satisfies the radiation condition and includes all possible radiation and scattering of the acoustic fields generated by the oscillating cylinders.

With reference to Fig. 3.3, for a field point p the following relations between angles are established:

$$\alpha = \theta_j - \psi_{jk}; \quad \chi = \pi - \theta_k + \psi_{jk}. \quad (3.132)$$

If point p is at the circumference of cylinder j , then R_{jk} will be always greater than r_j and $0 \leq |\chi| \leq \pi/2$. According to Graf's formula (Watson 1944), the addition theorem for cylinder functions is

$$C_n(\kappa r_k) \exp(in\chi) = \sum_{m=-\infty}^{\infty} c_{n+m}(\kappa R_{jk}) J_m(\kappa r_j) \exp(im\alpha), \quad (3.133)$$

where C denotes J , Y , $H^{(1)}$ and $H^{(2)}$ and κ is any complex number. Substituting the expressions for α and χ into Eq. 1.133, we obtain

$$C_n(\kappa r_k) \begin{cases} \cos n\theta_k \\ \sin n\theta_k \end{cases} = \sum_{m=-\infty}^{\infty} c_{n+m}(\kappa R_{jk}) J_m(\kappa r_j) \begin{cases} \cos[m\theta_j - (m+n)\psi_{jk}] \\ \sin[m\theta_j - (m+n)\psi_{jk}] \end{cases} (-1)^n. \quad (3.134)$$

The velocity components of cylinder j in the x and y directions are $-\omega \bar{u}_j \exp(-i\omega t)$ and $-i\omega \bar{v}_j \exp(-i\omega t)$, respectively, where \bar{u}_j and \bar{v}_j are displacement amplitudes. The corresponding boundary conditions at cylinder j are

$$\left. \frac{\partial \phi}{\partial r_j} \right|_{r_j=R_j} = -i\omega(\bar{u}_j \cos \theta_j + \bar{v}_j \sin \theta_j) \exp(-i\omega t). \quad (3.135)$$

Note that the cylinder displacement is so small compared with the gaps between and the radii of cylinders that the boundary condition is applied on the rest position boundary of the cylinder.

Using Eqs. 3.131-3.135, one can determine the unknown coefficients a_{jm} and b_{jm} in terms of the cylinder displacements

$$\begin{aligned} a_{kn} &= -i\omega \sum_{\ell=1}^N (\alpha_{kn\ell} \bar{u}_\ell + \sigma_{kn\ell} \bar{v}_\ell) R_\ell, \quad \text{and} \\ b_{kn} &= -i\omega \sum_{\ell=1}^N (\tau_{kn\ell} \bar{u}_\ell + \beta_{kn\ell} \bar{v}_\ell) R_\ell, \end{aligned} \quad (3.136)$$

where the dimensionless coefficients $\alpha_{kn\ell}$, $\sigma_{kn\ell}$, $\tau_{kn\ell}$ and $\beta_{kn\ell}$ are solutions of the following equations:

$$\begin{aligned} \begin{bmatrix} \alpha_{kn\ell} \\ \sigma_{kn\ell} \\ \tau_{kn\ell} \\ \beta_{kn\ell} \end{bmatrix} & H_n^{(1)}(\kappa R_k) + \sum_{j=1}^{N^*} \sum_{m=0}^{\infty} \left\{ \begin{bmatrix} \alpha_{jml} \\ \sigma_{jml} \\ -\tau_{jml} \\ -\beta_{jml} \end{bmatrix} \cos(m+n)\psi_{kj} \right. \\ & + \left. \begin{bmatrix} \tau_{jml} \\ \beta_{jml} \\ \alpha_{jml} \\ \sigma_{jml} \end{bmatrix} \sin(m+n)\psi_{kj} \right\} (-1)^m H_{m+n}^{(1)}(\kappa R_{kj}) J_n'(\kappa R_k) \\ & + \sum_{j=1}^{N^*} \sum_{m=0}^{\infty} \left\{ \begin{bmatrix} \alpha_{jml} \\ \sigma_{jml} \\ \tau_{jml} \\ \beta_{jml} \end{bmatrix} \cos(m-n)\psi_{kj} + \begin{bmatrix} \tau_{jml} \\ \beta_{jml} \\ -\alpha_{jml} \\ -\sigma_{jml} \end{bmatrix} \sin(m-n)\psi_{kj} \right\}. \end{aligned} \quad (3.137)$$

$$(-1)^{m-n} H_{m-n}^{(1)}(\kappa R_{kj}) J'_{-n}(\kappa R_k) = \frac{1}{R_\ell} \begin{bmatrix} \delta_{k\ell} \delta_{1n} \\ 0 \\ 0 \\ \delta_{k\ell} \delta_{1n} \end{bmatrix} . \quad (3.137)$$

(Contd.)

The problem has been reduced to an infinite set of algebraic equations for the unknown coefficients of the expansions.

The fluid force components are obtained using (see Eqs. 3.30)

$$g_j = - \int_0^{2\pi} p^j \bigg|_{r_j=R_j} R_j \cos \theta_j d\theta_j , \quad \text{and} \quad (3.138)$$

$$h_j = - \int_0^{2\pi} p^j \bigg|_{r_j=R_j} R_j \sin \theta_j d\theta_j .$$

Using the equations for the fluid pressure

$$p^j = -\rho \frac{\partial \phi^j}{\partial t} , \quad (3.139)$$

we obtain

$$\begin{aligned} g_j = & -\rho\pi \sum_{\ell=1}^N \left(\frac{R_j + R_\ell}{2} \right)^2 \left(\alpha_{j\ell} \frac{\partial^2 u_\ell}{\partial t^2} + \sigma_{j\ell} \frac{\partial^2 v_\ell}{\partial t^2} \right) \\ & - \rho\pi \sum_{\ell=1}^N \left(\frac{R_j + R_\ell}{2} \right)^2 \left(\alpha'_{j\ell} \frac{\partial u_\ell}{\partial t} + \sigma'_{j\ell} \frac{\partial v_\ell}{\partial t} \right) , \\ h_j = & -\rho\pi \sum_{\ell=1}^N \left(\frac{R_j + R_\ell}{2} \right)^2 \left(\tau_{j\ell} \frac{\partial^2 u_\ell}{\partial t^2} + \beta_{j\ell} \frac{\partial^2 v_\ell}{\partial t^2} \right) \\ & - \rho\pi \sum_{\ell=1}^N \left(\frac{R_j + R_\ell}{2} \right)^2 \left(\tau'_{j\ell} \frac{\partial u_\ell}{\partial t} + \beta'_{j\ell} \frac{\partial v_\ell}{\partial t} \right) , \end{aligned} \quad (3.140)$$

where

$$\alpha_{jl} = \operatorname{Re}(\tilde{\alpha}_{jl}) , \quad \alpha'_{jl} = \operatorname{Im}(\tilde{\alpha}_{jl}) ,$$

$$\sigma_{jl} = \operatorname{Re}(\tilde{\sigma}_{jl}) , \quad \sigma'_{jl} = \operatorname{Im}(\tilde{\sigma}_{jl}) ,$$

$$\tau_{jl} = \operatorname{Re}(\tilde{\tau}_{jl}) , \quad \tau'_{jl} = \operatorname{Im}(\tilde{\tau}_{jl}) ,$$

$$\beta_{jl} = \operatorname{Re}(\tilde{\beta}_{jl}) , \quad \beta'_{jl} = \operatorname{Im}(\tilde{\beta}_{jl}) ,$$

and $\tilde{\alpha}_{jl}$, $\tilde{\sigma}_{jl}$, $\tilde{\tau}_{jl}$, and $\tilde{\beta}_{jl}$ are given by

$$\begin{aligned} \begin{bmatrix} \tilde{\alpha}_{jl} \\ \tilde{\sigma}_{jl} \\ \tilde{\tau}_{jl} \\ \tilde{\beta}_{jl} \end{bmatrix} &= \frac{-4R_j R_l}{(R_j + R_l)^2} \begin{Bmatrix} \begin{bmatrix} \alpha_{j1l} \\ \sigma_{j1l} \\ \tau_{j1l} \\ \beta_{j1l} \end{bmatrix} H_1^{(1)}(\kappa R_j) + \sum_{k=1}^{N_*} \sum_{n=0}^{\infty} \begin{bmatrix} \alpha_{knl} \\ \sigma_{knl} \\ -\tau_{knl} \\ -\beta_{knl} \end{bmatrix} \cos(n-1)\psi_{jk} \\ \\ \\ \end{Bmatrix} \\ &+ \begin{Bmatrix} \begin{bmatrix} \tau_{knl} \\ \beta_{knl} \\ \alpha_{knl} \\ \sigma_{knl} \end{bmatrix} \sin(n+1)\psi_{jk} \end{Bmatrix} \left. \begin{matrix} (-1)^{n_{H_{n+1}}(1)} (\kappa R_{jk}) J_1(\kappa R_j) \end{matrix} \right\} \\ &+ \sum_{k=1}^{N_*} \sum_{n=0}^{\infty} \begin{Bmatrix} \begin{bmatrix} \alpha_{knl} \\ \alpha_{knl} \\ \tau_{knl} \\ \beta_{knl} \end{bmatrix} \cos(n-1)\psi_{jk} + \begin{bmatrix} \tau_{knl} \\ \beta_{knl} \\ -\alpha_{knl} \\ -\alpha_{knl} \end{bmatrix} \sin(n-1)\psi_{kj} \\ \\ \\ \end{Bmatrix} \left. \begin{matrix} (-1)^{n_{H_{n-1}}(1)} (\kappa R_{kj}) J_{-1}(\kappa R_k) \end{matrix} \right\} . \end{aligned} \quad (3.141)$$

Equations 3.140 are similar to those of Eqs. 3.31 with the exception that there are fluid damping terms.

Following the same procedure given in Section 3.3.2, we can show that

$$\begin{aligned}\alpha_{jl} &= \alpha_{lj}, & \alpha'_{jl} &= \alpha'_{lj}, \\ \beta_{jl} &= \beta_{lj}, & \beta'_{jl} &= \beta'_{lj}, \\ \sigma_{jl} &= \tau_{lj}, & \sigma'_{jl} &= \tau'_{lj},\end{aligned}\tag{3.142}$$

These equations prove that the principle of reciprocity exists for the added mass and radiation damping.

Added mass and damping given in Eqs. 3.140 and 3.141 are obtained with respect to a particular coordinate system and are dependent on the location and orientation of the coordinate axis. Following the same procedure, we can derive the transformation formula for the added mass and damping; these transformation equations are exactly the same as Eqs. 3.57 for both added mass and damping.

Both added mass and damping depend on the arrangement of cylinders and wave numbers κR_j . For an array of cylinders with the same diameter, a single wave number κR ($R_j = R$, $j = 1$ to N) can be used to characterize the characteristics. For infinitesimal wavenumber κR (e.g., $\kappa R < 0.05$), the added mass coefficients are close to those obtained from incompressible flow theory, and the acoustic radiation damping coefficients are practically zero. This implies that if the radius of the cylinders is very small compared with the wave length, which is typical in many practical cases, the added mass is dominant and values of the added mass obtained from the incompressible potential flow theory can be used as a valid approximation. As the wavenumber increases, the absolute values of both added mass and damping coefficients increase, reach their maxima, and then decrease rapidly when the wavenumber is increased further. For $\kappa R > 1$, the values of these coefficients are generally small. The damping effect dominates over the added mass effect in the range of large wavenumbers.

The peculiar variation of the added mass and damping coefficient with wavenumber is due to the general characteristics of waves. When the wavelength is large compared with the size of the cylinders, the wave does not pay much attention to the existence of the cylinder and in effect travels "through" it. When the wavelength is small compared with the size of the cylinders, the wave behaves like a particle impacting on and reflecting off the cylinder. The acoustic wave radiated by the motion of one cylinder is reflected and diffracted by other cylinders; the reflecting and diffracting waves will, in turn, be reflected and diffracted again. The process of

reflecting and diffracting continues over and over to cause ultimately an appropriate shadow to be formed around each cylinder. The pressure amplitude inside the shadow is vanishingly small so that both the integrated pressure around the cylinder and hence the force coefficients are very small.

3.9 ADDED MASS AND DAMPING OF AN ARRAY OF CYLINDERS IN AN INCOMPRESSIBLE VISCOUS FLUID

The flow field \vec{U} is given by

$$\vec{U} = \nabla\phi + \nabla \times \vec{\psi} . \quad (3.143)$$

ϕ and ψ are solutions of Laplace and Helmholtz equations:

$$\begin{aligned} \nabla^2 \phi &= 0 , \\ \left(\nabla^2 - \frac{1}{\nu} \frac{\partial}{\partial t} \right) \vec{\psi} &= 0 . \end{aligned} \quad (3.144)$$

The solution for this problem can be obtained following the procedures given in Sections 3.3 and 3.8. The detailed development of the analysis has not been published.

The fluid force components obtained for this problem are the same as those for compressible inviscid fluid:

$$\begin{aligned} g_j &= -\rho\pi \sum_{k=1}^N \left(\frac{R_j + R_k}{2} \right)^2 \left(\alpha_{jk} \frac{\partial^2 u_k}{\partial t^2} + \sigma_{jk} \frac{\partial^2 v_k}{\partial t^2} \right) \\ &\quad - \rho\pi \sum_{k=1}^N \left(\frac{R_j + R_k}{2} \right)^2 \left(\alpha'_{jk} \frac{\partial u_k}{\partial t} + \sigma'_{jk} \frac{\partial v_k}{\partial t} \right) \\ h_j &= -\rho\pi \sum_{k=1}^N \left(\frac{R_j + R_k}{2} \right)^2 \left(\tau_{jk} \frac{\partial^2 u_k}{\partial t^2} + \beta_{jk} \frac{\partial^2 v_k}{\partial t^2} \right) \\ &\quad - \rho\pi \sum_{k=1}^N \left(\frac{R_j + R_k}{2} \right)^2 \left(\tau'_{jk} \frac{\partial u_k}{\partial t} + \beta'_{jk} \frac{\partial v_k}{\partial t} \right) \end{aligned} \quad (3.145)$$

The added mass and damping coefficient depend on P/D and R_k .

There are several experimental studies on the damping of multiple cylinders. Shimogo et al. (1975) present the results of two cylinders vibrating in a viscous fluid. The effects of fluid viscosity on tube motions are studied. A series of experiments to study the diagonal terms, α'_{ij} and β'_{ij} is reported by Chen et al. (1977).

The added mass coefficients of a cylinder array vibrating in a perfect fluid and the added mass coefficients and damping coefficients in a compressible inviscid fluid are symmetric. Such symmetric properties for linear incompressible viscous flow theory have not been proved theoretically for general cylinder arrays. However, numerical results based on a finite element calculation show that both coefficients are symmetric. It also has been shown in Section 3.7 for two coaxial cylinders, they are symmetric.

3.10 CLOSING REMARKS

The dynamics of a group of circular cylinders in a fluid is complex. Corresponding to a single natural frequency for an isolated single cylinder, there are $2N$ natural frequencies in a group of N cylinders. When an array of cylinders is subjected to an excitation, its response characteristics are different from those of a single cylinder. In the past, it was common to use a single cylinder as the model for a group of cylinders. Because of the difference between single and multiple cylinders, care has to be exercised in making such an assumption.

As in the case of a single cylinder, in most practical applications, the added mass matrix can be calculated based on the two-dimensional potential flow theory. When the motion is relatively large, the nonlinear effect becomes important. There is very limited data for multiple cylinders oscillating with large amplitudes. A systematic study to quantify the nonlinear effect of a group of cylinders is needed.

When the cylinders are relatively close to each other, fluid viscous effect is more important. The added mass and damping matrices can be solved in principle based on the linearized Navier-Stokes equation; however, no comprehensive theoretical results are available. To evaluate the added mass and damping given in Eqs. 3.145, an efficient technique for calculating Bessel's functions with complex argument is required. It is expected that continuing investigations on this subject will be conducted because of its practical applications for nuclear fuel bundles.

The general method of analysis presented in this Chapter is useful for studying the dynamic response of multiple cylinders. The same method is also applicable in different applications. For example, it can be applied to scattering and transmission of acoustic wave across an array of cylinders, vibration of perforated plates, and other engineering problems involving multiple circular cylindrical regions.

REFERENCES--Sec. 3

- Cesari, F., and Curioni, S. 1973. Velocity Influence on the Free Vibrations in a Coupled System Fluid Structure. 2nd Conf. on Structural Mechanics in Reactor Technology, Sept. 1973, Paper E5/3.
- Chen, S. S. 1972. Free Vibration of a Coupled Fluid/Structural System. J. Sound Vib. 21, 387-398.
- Chen, S. S. 1974. Dynamics of a Rod-Shell System Conveying Fluid. Nucl. Eng. Des. 30, 223-233.
- Chen, S. S. 1975a. Dynamic Responses of two Parallel Circular Cylinders in a Liquid. J. Pressure Vessel Technology 97, 77-83.
- Chen, S. S. 1975b. Vibration of Nuclear Fuel Bundles. Nucl. Eng. Des. 35, 399-422.
- Chen, S. S. 1975c. Vibrations of a Row of Circular Cylinders in a Liquid. J. Eng. for Industry 97, 1212-1218.
- Chen, S. S. 1975d. In-Plane Vibration of Continuous Curved Beams. Nucl. Eng. Des. 25, 413-431.
- Chen, S. S. 1977. Dynamics of Heat Exchanger Tube Banks. J. Fluids Eng. 99(3), 462-469.
- Chen, S. S. 1983. Instability Mechanisms and Stability Criteria of a Group of Circular Cylinders Subjected to Cross-Flow, Part I: Theory. J. Vibration, Acoustics, Stress and Reliability in Design 105, 51-58.
- Chen, S. S., and Jendrzejczyk, J. A. 1978. Experiments on Fluidelastic Vibration of Cantilevered Tube Bundles. J. Mechanical Design 100, 540-548.
- Chen, S. S., and Rosenberg, G. S. 1975. Dynamics of a Coupled Shell/Fluid System. Nucl. Eng. Des. 32, 302-310.
- Chen, S. S., Jendrzejczyk, J. A., and Wambsganss, M. W. 1977. An Experimental and Theoretical Investigation of Coupled Vibration of Tube Banks. In Fluid Structure Interaction Phenomena in Pressure Vessel and Piping Systems, ASME, 19-36.
- Chen, Y. N. 1968. Flow-Induced Vibration and Noise in Tube-Bank Heat Exchangers due to von Karman Streets. J. Eng. Ind. 90(Series B), 134-146.
- Connors, Jr., H. J. 1970. Fluidelastic Vibration of Tube Arrays Excited by Cross Flow. In Flow Induced Vibration in Heat Exchangers, ASME, pp. 42-56.
- Gupta, G. S. 1970. Natural Flexural Waves and the Normal Modes of Periodically-Supported Beams and Plates. J. Sound Vibration 13, 89-101.

- Laird, A. D. K., and Warren, R. P. 1963. Groups of Vertical Cylinders Oscillating in Water. J. Eng. Mech. Div., Proc. ASCE 89(EM 1), 25-35.
- Lin, W. H., and Chen, S. S. 1981. On the Added Mass and Radiation Damping of Rod Bundles Oscillating in Compressible Fluids. J. Sound and Vibration 76(3), 441-453.
- Livesey, J. L., and Dye, C. F. 1962. Vortex Excited Vibration of a Heat Exchanger Tube Row. J. Mech. Eng. Sci. 4, 349-352.
- Loeber, J. F. 1984. Consistent Hydrodynamic Mass for Parallel Prismatic Beams in a Fluid-Filled Container. J. Pressure Vessel Technology 106, 270-275.
- Mazur, V. Yu. 1966. Motion of a Circular Cylinder Close to a Vertical Wall. Izv. Akad. Nauk SSSR, Mekhan. Zhidk. i Gaza, No. 3.
- Moretti, P. M., and Lowery, R. L. 1976. Hydrodynamic Inertia Coefficients for a Tube Surrounded by Rigid Tubes. J. Pressure Vessel Technology 98, 190-193.
- Paidoussis, M. P., and Besancon, P. 1981. Dynamics of Arrays of Cylinders with Internal and External Axial Flow. J. Sound Vib. 76(3), 361-379.
- Paidoussis, M. P., Suss, S., and Pustejovsky, M. 1977. Free Vibration of Clusters of Cylinders in Liquid-Filled Channels. J. Sound Vib. 55, 443-459.
- Roberts, B. W. 1966. Low Frequency, Aeroelastic Vibrations in a Cascade of Circular Cylinders. Mechanical Engineering Science Monograph, No. 4.
- Shimogo, T., and Inui, T. 1971. Coupled Vibration of Many Elastic Circular Bars in Water. Proc. 21st Japan National Congress for Applied Mechanics, 495-505.
- Shimogo, T., Niino, T., and Setogawa, S. 1975. Coupled Vibration of Elastic Circular Bars in Viscous Fluid. ASME Paper No. 75-DET-76.
- Watson, G. N. 1944. Theory of Bessel Functions," Cambridge University Press.
- Wilson, J. F., and Caldwell, H. M. 1971. Force and Stability Measurements on Models of Submerged Pipelines. Trans. ASME, J. Eng. Ind. 93, 1290-1298.
- Yang, C. I., and Moran, T. J. 1979. Finite-Element Solution of Added Mass and Damping of Oscillation Rods in Viscous Fluids. J. Appl. Mech. 46, 519-523.
- Yeh, T. T., and Chen, S. S. 1978. The Effect of Fluid Viscosity on Coupled Tube/Fluid Vibrations. J. Sound and Vibration 59(3), 453-467.

4. CIRCULAR CYLINDRICAL SHELLS CONTAINING FLUID

4.1 INTRODUCTION

The dynamic characteristics of circular cylindrical shells containing fluid have been studied for a century. Earlier work was found on the response of rigid circular tanks to seismic loads. Subsequently, because of the interest in the dynamic behavior of rockets with liquid propellants, rapid advances were made in the analysis of elastic shells containing fluids (Abramson and Kana 1967). Most recently, the development of nuclear reactor system components has prompted further studies on this subject. In this chapter, general characteristics of shell/fluid systems are presented with the objective of illustrating the effect of fluid on shell response.

4.2 FREE VIBRATION OF CIRCULAR CYLINDRICAL SHELLS IN AIR

Let the displacement components of the mid-plane of the shell be u , v , and w in the axial, tangential, and radial directions. The motion of the shell is described by the following Flugge's shell equations (Flügge 1960):

$$\begin{aligned} & \left[\frac{\partial^2}{\partial z^2} + \left(\frac{1-\nu^2}{2r^2} \right) \left(1 + \frac{h^2}{12R^2} \right) \frac{\partial^2}{\partial \theta^2} \right] u + \frac{1+\nu}{2R} \frac{\partial^2 v}{\partial z \partial \theta} \\ & + \left[\frac{\nu}{R} \frac{\partial}{\partial z} - \frac{h^2}{12R} \frac{\partial^3}{\partial z^3} + \frac{(1-\nu)h^2}{24R^3} \frac{\partial^3}{\partial z \partial \theta^2} \right] w - \frac{\rho_s(1-\nu^2)}{E} \frac{\partial^2 u}{\partial t^2} = 0, \\ & \frac{1+\nu}{2R} \frac{\partial^2 u}{\partial z \partial \theta} + \left[\frac{1}{R^2} \frac{\partial^2}{\partial \theta^2} + \frac{1-\nu}{2} \left(1 + \frac{h^2}{4R^2} \right) \frac{\partial^2}{\partial z^2} \right] v \\ & + \left[\frac{1}{R^2} \frac{\partial}{\partial \theta} - \frac{(3-\nu)h^2}{24R^2} \frac{\partial^3}{\partial \theta \partial z^2} \right] w - \frac{\rho_s(1-\nu^2)}{E} \frac{\partial^2 v}{\partial t^2} = 0, \end{aligned} \quad (4.1)$$

and

$$\begin{aligned} & \left[-\frac{h^2}{12R} \frac{\partial^3}{\partial z^3} + \frac{\nu}{R} \frac{\partial}{\partial z} + \frac{(1-\nu)h^2}{24R^3} \frac{\partial^3}{\partial z \partial \theta^2} \right] u + \left[-\frac{(3-\nu)h^2}{24R^2} \frac{\partial^3}{\partial \theta \partial z^2} + \frac{1}{R^2} \frac{\partial}{\partial \theta} \right] v \\ & + \left(\frac{1}{R^2} + \frac{h^2}{12R^4} + \frac{h^2}{12} \frac{\partial^4}{\partial z^4} + \frac{h^2}{6R^2} \frac{\partial^4}{\partial z^2 \partial \theta^2} + \frac{h^2}{12R^4} \frac{\partial^4}{\partial \theta^4} + \frac{h^2}{6R^4} \frac{\partial^2}{\partial \theta^2} \right) w \\ & + \frac{\rho_s(1-\nu^2)}{E} \frac{\partial^2 w}{\partial t^2} = 0, \end{aligned}$$

where r , θ , and z are cylindrical coordinates, t is the time, and the physical characteristics of the shells are defined by the mean radius R , wall thickness h , density ρ_s , Young's modulus E , and Poisson's ratio ν .

A traveling wave solution is sought for the shell;

$$\begin{aligned} u &= \bar{u} \cos n\theta \exp[i2\pi(c_p t - z)/\lambda] , \\ v &= \bar{v} \sin n\theta \exp[i2\pi(c_p t - z)/\lambda] , \end{aligned} \quad (4.2)$$

and

$$w = \bar{w} \cos n\theta \exp[i2\pi(c_p t - z)/\lambda] ,$$

where \bar{u} , \bar{v} , and \bar{w} are arbitrary constants to be determined from the equations of motion. Substitution of Eqs. 4.2 into Eq. 4.1 gives three linear algebraic homogeneous equations for \bar{u} , \bar{v} , and \bar{w} :

$$\begin{bmatrix} a_{11} & a_{12} & a_{13} \\ a_{21} & a_{22} & a_{23} \\ a_{31} & a_{32} & a_{33} \end{bmatrix} \begin{Bmatrix} \bar{u} \\ \bar{v} \\ \bar{w} \end{Bmatrix} = \begin{Bmatrix} 0 \\ 0 \\ 0 \end{Bmatrix} , \quad (4.3)$$

where

$$\begin{aligned} a_{11} &= -\alpha^2 - \left(\frac{1-\nu}{2}\right)\left(1 + \frac{\delta^2}{12}\right)n^2 + \Omega^2 , \\ a_{12} = a_{21} &= -i\left(\frac{1+\nu}{2}\right)\alpha n , \\ a_{13} = a_{31} &= -i\left[\nu\alpha + \frac{\delta^2}{12}\alpha^3 - \frac{\delta^2}{24}(1-\nu)\alpha n^2\right] , \\ a_{22} &= n^2 + \left(\frac{1-\nu}{2}\right)\left(1 + \frac{\delta^2}{4}\right)\alpha^2 - \Omega^2 , \\ a_{23} &= n + \frac{\delta^2}{24}(3-\nu)n\alpha^2 , \\ a_{33} &= 1 + \frac{\delta^2}{12}\left[1 + (\alpha^2 + n^2)^2 - 2n^2\right] - \Omega^2 , \end{aligned} \quad (4.4)$$

and

$$\alpha = \frac{2\pi R}{l},$$

$$\delta = \frac{h}{R},$$

$$\Omega = R\omega \left[\frac{\rho_s(1 - \nu^2)}{E} \right]^{1/2}, \quad \text{and}$$

$$\omega = 2\pi c_p / l.$$

(4.4)
(Contd.)

For a nontrivial solution of these simultaneous equations, the determinant of the coefficients of the unknowns should vanish. The resulting determinantal equation is the frequency equation

$$|a_{ij}| = 0. \quad (4.5)$$

Alternatively, the frequency equation can be written in the functional form:

$$F(\Omega, \alpha, n, \delta, \nu) = 0. \quad (4.6)$$

The shell, undergoing free vibration, can be defined in a variety of ways, as shown in Fig. 4.1. The vibration of the shell can consist of a number of waves distributed around the circumference as shown in Fig. 4.1 for $n = 2, 3$, and 4. In the axial direction, the deformation of the shell consists of a number of waves distributed along the length of a generator, as shown in Fig. 4.1 for $1/2 l, l$, and $3/2 l$.

For a given shell, ν and δ are fixed. The natural frequency Ω depends on α and n only. Two special cases are considered:

• **Circumferential Modes:** Consider those modes of oscillations of the shell that are independent of the axial coordinate z ; i.e., those modes having frequencies corresponding to an infinite phase velocity. The equations for those modes are obtained by setting $\alpha = 0$ in Eq. 4.6; i.e.,

$$\Omega^2 = \left(1 + \frac{\delta^2}{12}\right) \left(\frac{1 - \nu^2}{2}\right) n^2 \quad \text{and}$$

$$\Omega^4 - \left[n^2 + 1 + \frac{\delta^2}{12} (n^2 - 1)^2\right] \Omega^2 + \frac{\delta^2}{12} n^2 (n^2 - 1)^2 = 0, \quad (4.7)$$

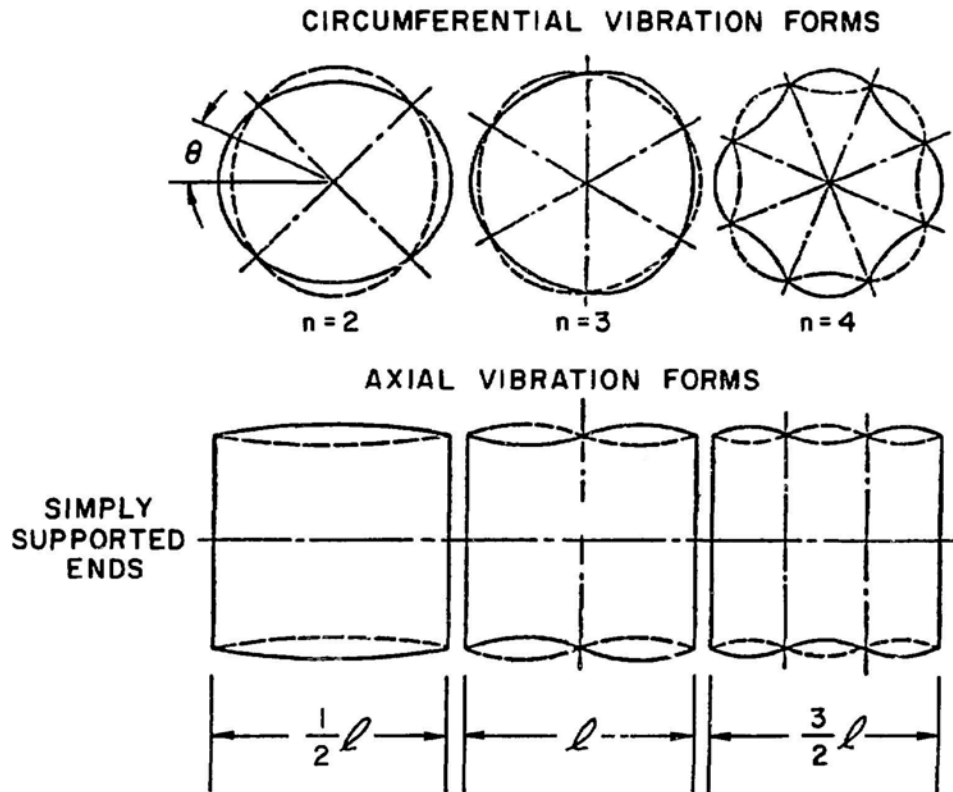


Fig. 4.1. Vibration Form for Circular Cylindrical Shells

• Symmetric Modes: For $n = 0$, Eq. 4.6 can be written

$$\Omega^2 - \left(1 + \frac{\delta^2}{4}\right)\left(\frac{1-\nu}{2}\right)\alpha^2 = 0 \quad \text{and} \quad (4.8)$$

$$(\Omega^2 - \alpha^2)\left[\Omega^2 - 1 - \frac{\delta^2}{12}(1 + n^4)\right] - \left(\nu\alpha + \frac{\delta^2}{12}\alpha^3\right)^2 = 0.$$

4.3 FREE VIBRATION OF CIRCULAR CYLINDRICAL SHELLS CONTAINING COMPRESSIBLE INVISCID FLUID

The equations of motion for a cylindrical shell containing compressible inviscid fluid are the same as those given in Eqs. 4.1 except that the additional fluid pressure is acting on the radial direction; therefore, the right side of the third equation zero is replaced by $(1 - \nu^2)p/Eh$. p is determined as follows:

$$p = -\rho \left. \frac{\partial \phi}{\partial t} \right|_{r=R},$$

$$\nabla^2 \phi - \frac{1}{c^2} \frac{\partial^2 \phi}{\partial t^2} = 0, \quad \text{and} \quad (4.9)$$

$$\left. \frac{\partial \phi}{\partial r} \right|_{r=R} = \frac{\partial w}{\partial t}.$$

The potential ϕ can be defined by

$$\phi = \bar{\phi}(r) \cos n\theta \exp[i2\pi(c_p t - z)/\lambda]. \quad (4.10)$$

Using Eqs. 4.9, 4.10, and 4.2 yields

$$\bar{\phi}(r) = i \frac{2\pi c_p}{\lambda} \frac{F_n(r)}{F'_n(r)} \bar{w}, \quad (4.11)$$

where

$$F_n(r) = I_n \left\{ \frac{2\pi}{\ell} \left(1 - \frac{c_p}{c} \right)^{2/2} \right\} \quad \text{if } c > c_p \quad \text{and} \quad (4.12)$$

$$F_n(r) = J_n \left\{ \frac{2\pi}{\ell} \left(\frac{c}{c_p} - 1 \right)^{1/2} \right\} \quad \text{if } a < c_p .$$

Therefore,

$$p = \frac{4\pi\rho}{\ell^2} c_p^2 \frac{F_n(R)}{F'_n(R)} \bar{w} . \quad (4.13)$$

The results for a cylindrical shell containing fluid are identical to those given in Eqs. 4.3 and 4.4 expect that the element a_{33} is given as follows:

$$a_{33} = 1 + \frac{\delta^2}{12} [1 + (\alpha^2 + n^2)^2 - 2n^2] - \Omega^2 \left(1 + \frac{\rho_s R}{\rho h} c_m \right)$$

and

$$c_m = \frac{I_n(\beta)}{I'_n(\beta)} \quad \text{for } \gamma\alpha > \Omega \quad \left(\gamma = c \left[\frac{\rho_s (1 - \nu^2)}{E} \right]^{1/2} \right) \quad (4.14)$$

$$= \frac{J_n(\beta)}{J'_n(\beta)} \quad \text{for } \gamma\alpha < \Omega .$$

The frequency spectra for $n = 0$ and 1 for empty and fluid-filled shell are given in Figs. 4.2 and 4.3 for $\delta = 0.01$ and $\gamma = 0.257$. We will use a system of suffixes, calling a mode M_{nm} . The first suffix indicates the circumferential wave number. The second number indicates the order of the mode. The first seven modes are given in each case. The torsional mode, denoted by T, is not affected by the fluid. For the purpose of understanding the shell motions, the amplitude ratios for the first three modes of the fluid-filled shell are given in Fig. 4.4.

In Fig. 4.2, M_{01} and M_{02} are the two modes of propagation that are not evanescent at low frequency ranges; all other coupled fluid/shell modes are evanescent. In M_{01} mode, the tangential displacement \bar{u} is much smaller than \bar{w} , especially for large α ; therefore, the displacement of this mode corresponds to predominantly radial vibration. When the shell is rigid, this mode becomes nondispersive. In M_{02} , the shell motion is predominantly axial vibration for $\alpha < 1.0$ and radial vibration for $\alpha > 1.0$. For α near 1.0, axial

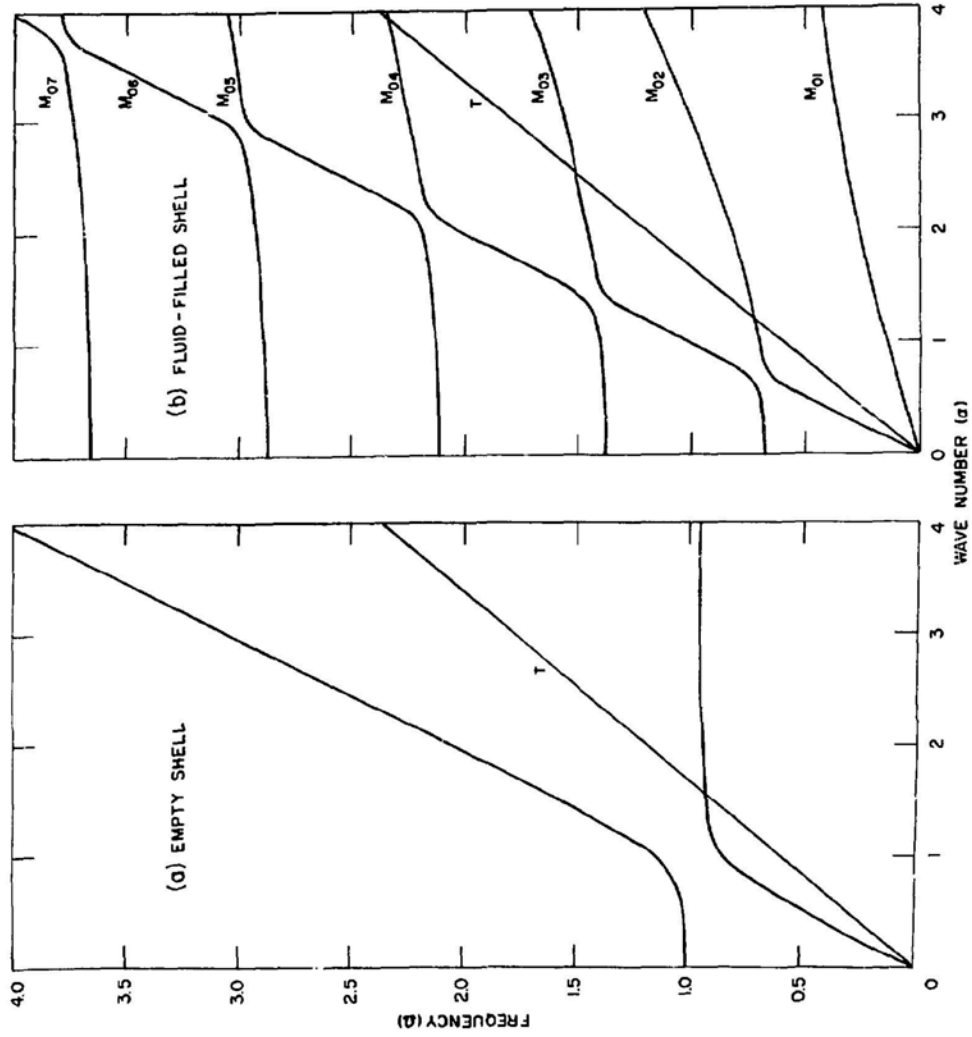


Fig. 4.2. Frequency Spectra of the Empty and Fluid-filled Shells for $n = 0$, $\delta = 0.01$, $\rho_s R / \rho h = 12.8$, and $\gamma = 0.257$ (Chen and Rosenberg 1974)

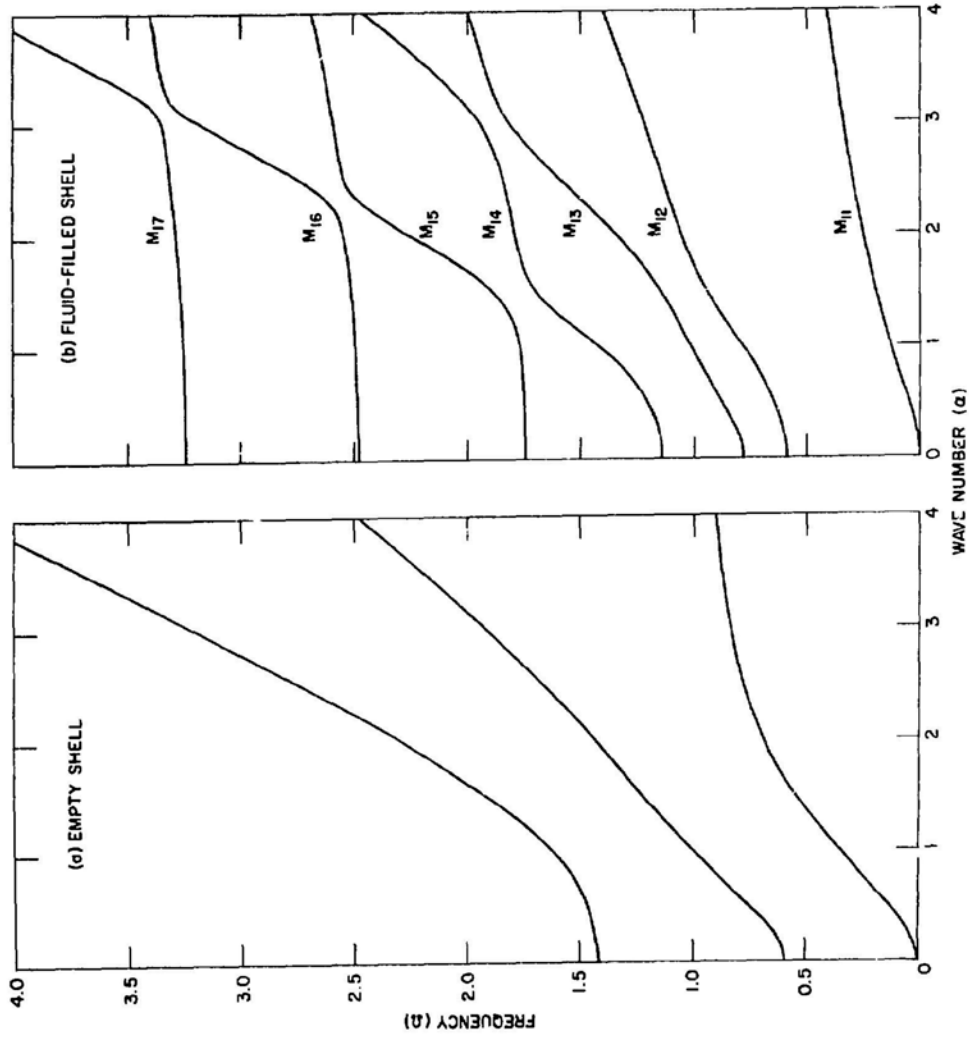


Fig. 4.3. Frequency Spectra of the Empty and Fluid-filled Shells for $n = 1$, $\delta = 0.01$, $\rho_g R / \rho h = 12.8$, and $\gamma = 0.257$ (Chen and Rosenberg 1974)

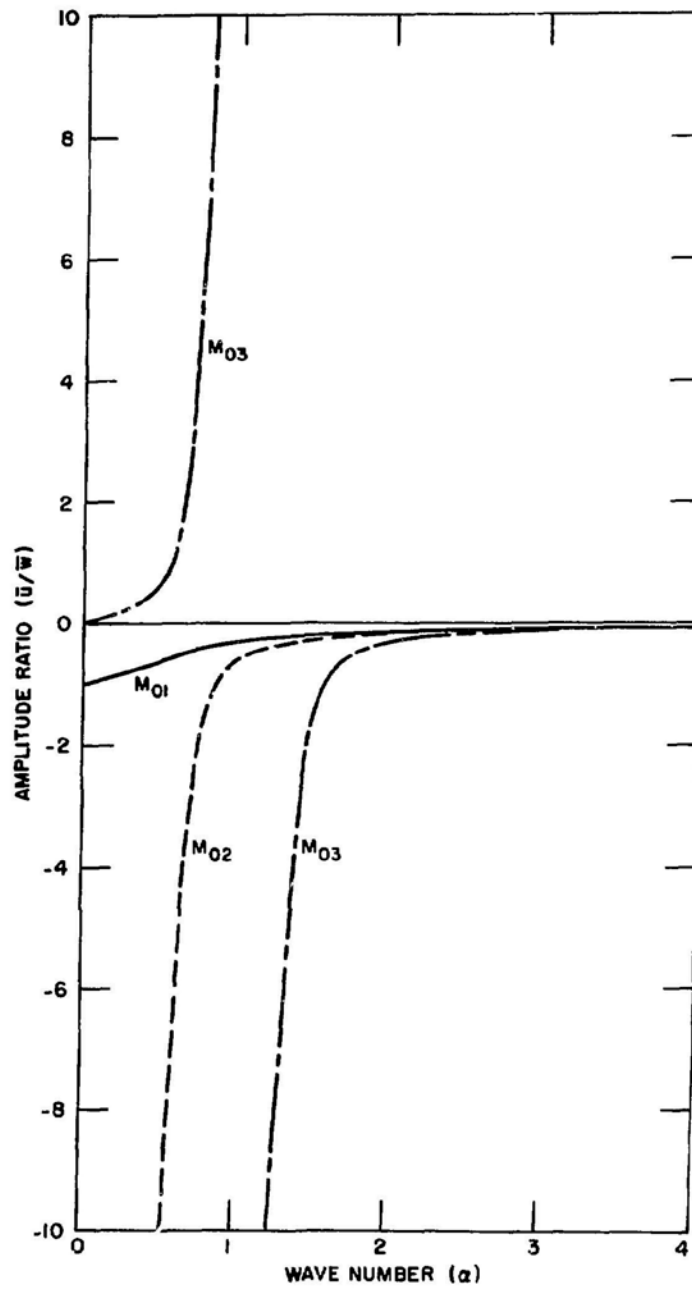


Fig. 4.4. Amplitude Ratios of a Fluid-filled Shell for $n = 0$, $\delta = 0.01$, $\rho_g R / \rho h = 12.8$ and $\gamma = 0.257$ (Chen and Rosenberg 1974)

and radial motions are strongly coupled. In M_{03} mode, the shell motion is predominantly axial vibration for $0.5 < \alpha < 1.6$ and radial vibration for other values of α . Comparing the spectra given in Figs. 4.2 (a and b), note that each mode of coupled fluid/shell system except M_{01} mode has a portion of the branch aligned in the vicinity of the corresponding empty shell mode. In these regions, the shell motion is predominantly axial vibration. All other portions of the branch correspond to predominantly radial vibration.

Figure 4.3 shows the frequency spectra for $n = 1$. Only M_{11} mode is not evanescent. The frequency of this mode is considerably reduced by the fluid loading. In other modes, the motion may be predominantly axial, radial, or torsional, depending on the wavelength.

In practical applications, vibrations in the low-frequency range are of interest. These correspond to waves whose length is great compared with the shell radius R . Two cases are considered--water hammer waves and approximate bending equations.

Water-Hammer Waves ($n = 0$)

For small Ω and α , from the frequency equation, it can be shown that

$$\begin{aligned} \left(1 + \frac{\delta^2}{12} + 2 \frac{\rho_s R}{\rho h} \gamma^2\right) c_p^4 - \left[\left(1 + \frac{\delta^2}{12}\right)(1 + \gamma^2) - v^2 + 2 \frac{\rho_s R}{\rho h} \gamma^2\right] c_p^2 \\ - \left(1 + \frac{\delta^2}{12} - v^2\right) \gamma^2 = 0. \end{aligned} \quad (4.15)$$

Equation 4.15 gives four values of c_p , accounted for as c_{p1} , $-c_{p1}$, c_{p2} , and $-c_{p2}$. These phase velocities are associated with two waves: one is the usual water hammer wave and the other is an extensional wave primarily in the shell wall.

When the phase velocities of the usual water hammer wave and extensional wave are not close to each other, simplified expressions for the phase velocity are obtainable. Neglecting the torsional motion and axial inertia of the shell, and using the frequency equation, we obtain

$$\pm c_{p1} = \left(\frac{1 + \frac{\delta^2}{12} - v^2}{1 + \frac{\delta^2}{12} - v^2 + \frac{2\rho_s R}{\rho h} \gamma^2} \right)^{1/2} \gamma. \quad (4.16)$$

Furthermore, for a thin shell (δ is small) the water hammer wave velocity reduced from Eq. 4.16 in terms of the real physical quantities is

$$\text{Water-hammer wave velocity} = \pm \frac{c}{\sqrt{1 + \frac{2KR}{Eh}}}, \quad (4.17)$$

where K is the bulk modulus of the fluid. This is the equation derived by Joukowsky in 1898 (Skalak 1956).

Similarly, neglecting the radial and torsional inertias of the shell, we obtain the extensional wave velocity

$$\pm c_{p2} = \left[\frac{1 - \frac{v^2}{1 + \frac{\delta^2}{12} + \frac{2 \frac{\rho_s R}{\rho h} \gamma^2}{1 - \gamma^2}}}{1} \right]^{0.5}. \quad (4.18)$$

Approximate Bending Equations ($n \neq 0$)

As suggested by Reissner (1955), if the axial and tangential inertias of the shell are disregarded, the coupled fluid/shell equations yield the following frequency equation:

$$\left(1 + \frac{\rho_s R}{\rho h} C_m\right) \Omega^2 = \frac{\delta^2}{12} (\alpha^2 + n^2)^2 + \frac{(1 - v^2) \alpha^4}{(\alpha^2 + n^2)^2}. \quad (4.19)$$

In many practical situations, the fluid can be considered as incompressible in the study of bending motion. In this case C_m is independent of Ω and Eq. 4.19 becomes

$$\Omega = \left(\frac{\frac{\delta^2}{12} (\alpha^2 + n^2)^2 + \frac{(1 - v^2) \alpha^4}{(\alpha^2 + n^2)^2}}{1 + \frac{\rho_s R}{\rho h} C_m} \right)^{1/2}. \quad (4.20)$$

The error of Eq. 4.20 is <5%. Moreover, the error decreases as $|\alpha|$ decreases, and is negligible for large wavelengths.

From Eq. 4.20, it is seen that due to the fluid loading, the frequency is lowered in proportion to $1 / \sqrt{1 + \rho_s R C_m / \rho h}$. The concept of the added

mass to the fluid/shell system is useful to us. In terms of real physical quantities, from Eq. 4.20 it is easily shown that the frequency of the fluid-filled shell is equal to that of the empty shell, whose density has been replaced by ρ' :

$$\rho' = \rho_s + \frac{\rho R}{h} C_m . \quad (4.21)$$

The values of the added mass coefficient for $n = 1-5$ are given in Fig. 4.5. For small n , C_m is highly dependent on the wave number. As n increases, C_m is almost independent of the wave number; the influence of the fluid on the reduction in the shell frequencies is more pronounced for those modes with lower circumferential wave numbers.

The effect of fluid on finite shells containing fluid is similar to that on an infinite shell. However, if there is a free surface, such as a liquid storage tank, in addition to the coupled shell/fluid mode, sloshing response of the liquid may be important. Extensive studies on the circular cylindrical tanks have been published (e.g., Clough et al. 1979; Fujita 1982; Haroun 1983).

4.4 DYNAMICS OF TWO SHELLS COUPLED BY A COMPRESSIBLE INVISCID FLUID

One set of problems including nominally circular cylindrical shells coupled to other shells through a fluid is of great concern in the development of some system components such as nuclear reactor system components. Consider two concentric circular cylindrical shells separated by an acoustic medium as shown in Fig. 4.6. The motion of the shells is described by the Flugge's shell equations (Flügge 1960):

$$\begin{aligned} & \left[\frac{\partial^2}{\partial z^2} + \left(\frac{1 - \nu_j}{2R_j^2} \right) \left(1 + \frac{h_j^2}{12R_j^2} \right) \frac{\partial^2}{\partial \theta^2} \right] u_j + \frac{1 + \nu_j}{2R_j} \frac{\partial^2 v_j}{\partial z \partial \theta} \\ & + \left[\frac{\nu_j}{R_j} \frac{\partial}{\partial z} - \frac{h_j^2}{12R_j} \frac{\partial^3}{\partial z^3} + \frac{(1 - \nu_j)h_j^2}{24R_j^3} \frac{\partial^3}{\partial z \partial \theta^2} \right] w_j - \frac{\rho_j(1 - \nu_j^2)}{E_j} \frac{\partial^2 u_j}{\partial t^2} = 0 , \\ & \frac{1 + \nu_j}{2R_j} \frac{\partial^2 u_j}{\partial z \partial \theta} + \left[\frac{1}{R_j^2} \frac{\partial}{\partial \theta^2} + \frac{1 - \nu_j}{2} \left(1 + \frac{h_j^2}{4R_j^2} \right) \frac{\partial^2}{\partial z^2} \right] v_j \\ & + \left[\frac{1}{R_j^2} \frac{\partial}{\partial \theta} - \frac{(3 - \nu_j)h_j^2}{24R_j^2} \frac{\partial^3}{\partial \theta \partial z^2} \right] w_j - \frac{\rho_j(1 - \nu_j^2)}{E_j} \frac{\partial^2 v_j}{\partial t^2} = 0 , \end{aligned} \quad (4.22)$$

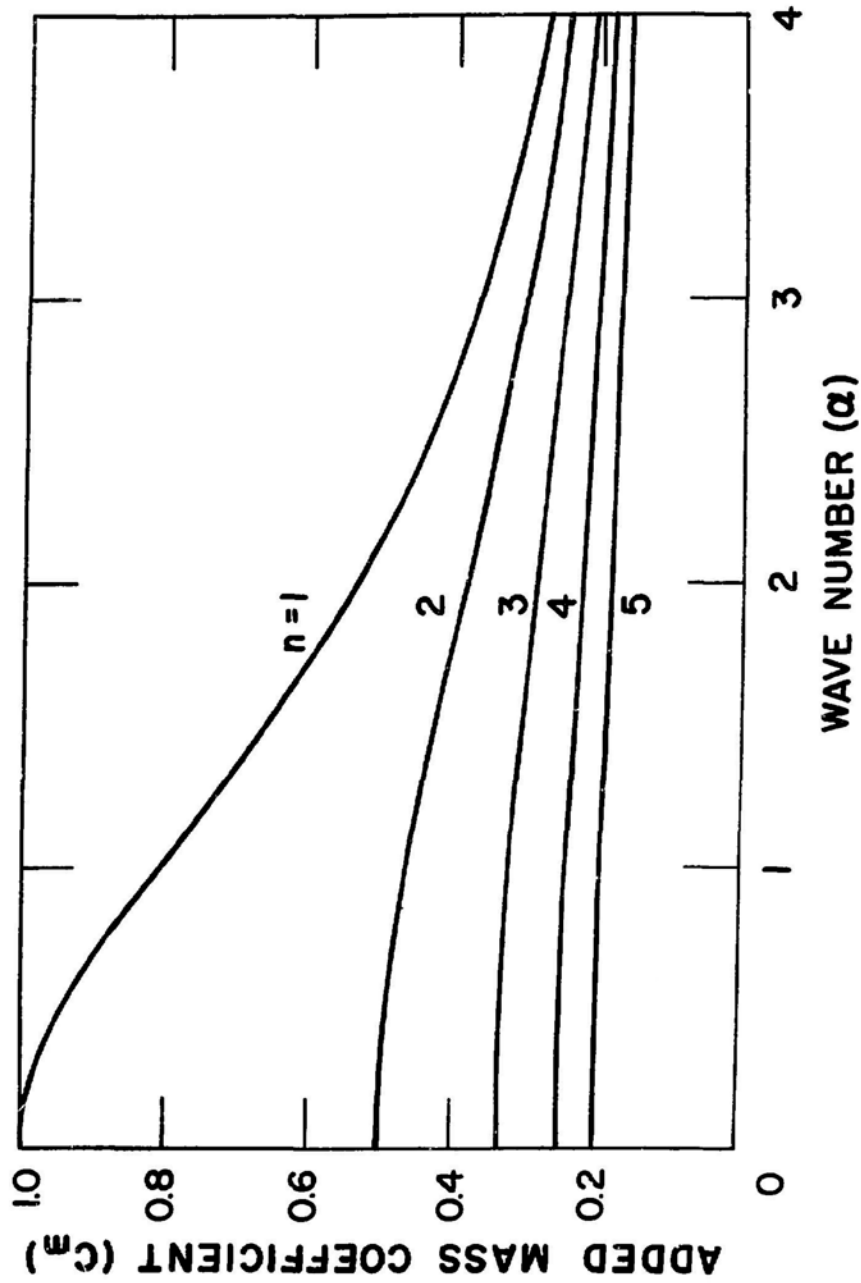


Fig. 4.5. Values of the Added Mass Coefficient for $n = 1$ to 5 (Chen and Rosenberg 1974)

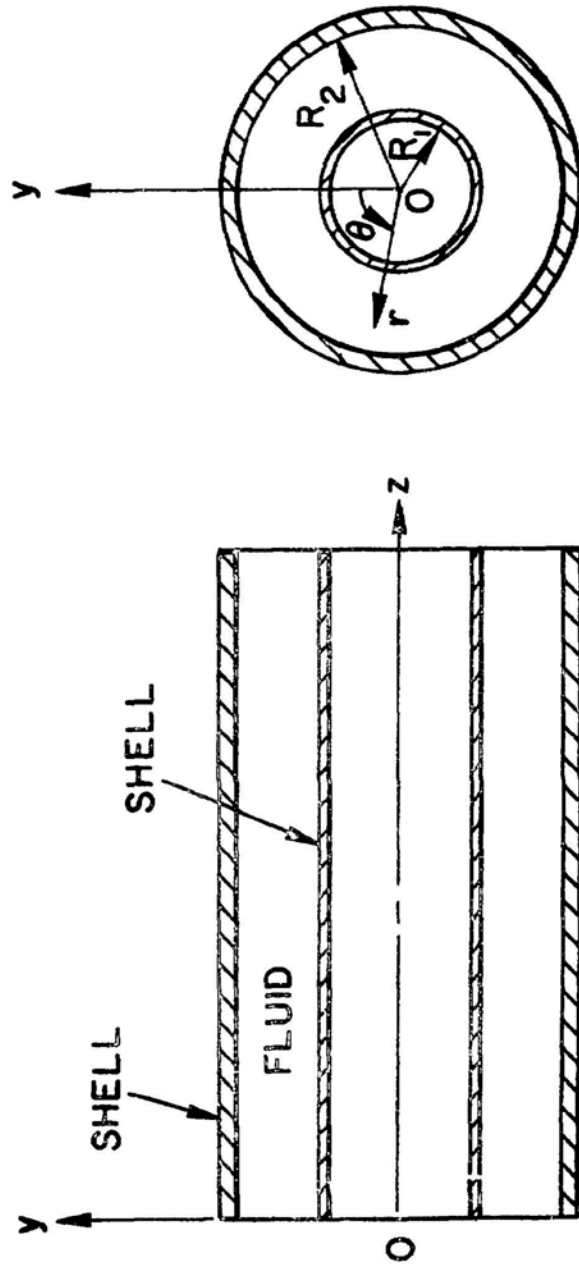


Fig. 4.6. Two Circular Cylindrical Shells Coupled by a Fluid

and

$$\begin{aligned}
 & \left[-\frac{h_j^2}{12R_j} \frac{\partial^3}{\partial z^3} + \frac{v_j}{R_j} \frac{\partial}{\partial z} + \frac{(1-v_j)h_j^2}{24R_j^3} \frac{\partial^3}{\partial z \partial \theta^2} \right] u_j + \left[-\frac{(3-v_j)h_j^2}{24R_j^2} \frac{\partial^3}{\partial \theta \partial z^2} \right. \\
 & \quad + \frac{1}{R_j} \frac{\partial}{\partial \theta} v_j + \left(\frac{1}{R_j} + \frac{h_j^2}{12R_j^4} + \frac{h_j^2}{12} \frac{\partial^4}{\partial z^4} + \frac{h_j^2}{6R_j^2} \frac{\partial^4}{\partial z^2 \partial \theta^2} + \frac{h_j^2}{12R_j^4} \frac{\partial^4}{\partial \theta^4} \right. \\
 & \quad \left. \left. + \frac{h_j^2}{6R_j^4} \frac{\partial^2}{\partial \theta^2} \right) w_j + \frac{\rho_j(1-v_j^2)}{E_j} \frac{\partial^2 w_j}{\partial t^2} = \frac{(1-v_j^2)}{E_j h_j} p_j, \quad (4.22)
 \end{aligned}$$

(Contd.)

where the index j denotes the variables associated with the inner shell ($j = 1$) and outer shell ($j = 2$); u_j , v_j and w_j are the displacement components of the shell middle surface and p_j is the radial surface loading component per unit area. The physical characteristics of the shells are defined by the mean radius R_j , wall thickness h_j , density ρ_j , Young's modulus E_j , and Poisson's ratio v_j .

The governing fluid field equation is

$$\begin{aligned}
 & \nabla^2 \phi - \frac{1}{c^2} \frac{\partial^2 \phi}{\partial t^2} = 0, \\
 & \vec{U} = \vec{\nabla} \phi, \quad \text{and} \\
 & p = -\rho \frac{\partial \phi}{\partial t}.
 \end{aligned} \quad (4.23)$$

The interference conditions are

$$\begin{aligned}
 & u_r \Big|_{r=R_1} = \frac{\partial w_1}{\partial t} \quad \text{and} \\
 & u_r \Big|_{r=R_2} = \frac{\partial w_2}{\partial t},
 \end{aligned} \quad (4.24)$$

and the surface loading p_j is given by

$$\begin{aligned} p_1 &= -p|_{r=R_1} \quad \text{and} \\ p_2 &= p|_{r=R_2} . \end{aligned} \quad (4.25)$$

Solutions of the following form are assumed:

$$\begin{aligned} u_j &= \bar{u}_j \cos n\theta \exp\{i2\pi(c_p t - z)/\ell\} , \\ v_j &= \bar{v}_j \sin n\theta \exp\{i2\pi(c_p t - z)/\ell\} , \\ w_j &= \bar{w}_j \cos n\theta \exp\{i2\pi(c_p t - z)/\ell\} , \quad \text{and} \\ \phi &= \bar{\phi}(r) \cos n\theta \exp\{i2\pi(c_p t - z)/\ell\} . \end{aligned} \quad (4.26)$$

Substituting Eq. 4.26 into 4.23 gives the following form of Bessel's equation

$$\frac{1}{r} \frac{d}{dr} \left(r \frac{d\bar{\phi}}{dr} \right) - \left\{ \frac{n^2}{r^2} + \frac{4\pi^2}{\ell^2} \left(1 - \frac{c_p^2}{c^2} \right) \right\} \bar{\phi} = 0 . \quad (4.27)$$

Integrating Eq. 4.27 and applying the interface conditions at $r = R_1$ and R_2 , Eq. 4.27 yields

$$\begin{aligned} \bar{\phi}(r) &= \frac{i2\pi(c_p/\ell)}{F'_{2n}(R_1)G'_{2n}(R_2) - F'_{2n}(R_2)G'_{2n}(R_1)} \left\{ [G'_{2n}(R_2)F_{2n}(r) \right. \\ &\quad \left. - F'_{2n}(R_2)G_{2n}(r)]\bar{w}_1 + [F'_{2n}(R_1)G_{2n}(r) - G'_{2n}(R_1)F_{2n}(r)]\bar{w}_2 \right\} , \end{aligned}$$

where

$$\begin{aligned} F_{jn}(r) &= I_n \left[\frac{2\pi}{\ell} \left(1 - \frac{c_p^2}{c^2} \right)^{1/2} r \right] \quad \text{for } c > c_p \\ &= J_n \left[\frac{2\pi}{\ell} \left(\frac{c_p^2}{c^2} - 1 \right)^{1/2} r \right] \quad \text{for } c < c_p \end{aligned} \quad (4.28)$$

and

$$\begin{aligned}
G_{jn}(r) &= K_n \left[\frac{2\pi}{\ell} \left(1 - \frac{c_p}{c} \right)^{1/2} r \right] \quad \text{for } c > c_p \\
&= J_n \left[\frac{2\pi}{\ell} \left(\frac{c_p}{c} - 1 \right)^{1/2} r \right] \quad \text{for } c < c_p .
\end{aligned}
\tag{4.28}$$

(Contd.)

Introduce the following dimensionless variables:

$$\begin{aligned}
\alpha_j &= \frac{2\pi R_j}{\ell} , \\
\gamma_j &= c \left[\frac{\rho_j (1 - v_j^2)}{E_j} \right]^{1/2} , \\
\delta_j &= \frac{h_j}{R_j} , \\
\mu_j &= \frac{\rho R_j}{\rho_j h_j} ,
\end{aligned}
\tag{4.29}$$

and the dimensionless frequency Ω_j which is related to the circular frequency of vibration ω by

$$\Omega_j = R_j \omega \left[\frac{\rho_j (1 - v_j^2)}{E_j} \right]^{1/2} .
\tag{4.30}$$

Substituting Eqs. 4.26 into 4.27 and using Eqs. 4.23, 4.25, 4.28, and 4.29 gives six linear algebraic homogeneous equations:

$$\begin{bmatrix}
a_{11} & a_{12} & a_{13} & 0 & 0 & 0 \\
a_{12} & a_{14} & a_{15} & 0 & 0 & 0 \\
a_{13} & a_{15} & a_{16} & 0 & 0 & a_{17} \\
0 & 0 & 0 & a_{21} & a_{22} & a_{23} \\
0 & 0 & 0 & a_{22} & a_{24} & a_{25} \\
0 & 0 & a_{27} & a_{23} & a_{25} & a_{26}
\end{bmatrix}
\begin{bmatrix}
\bar{u}_1 \\
\bar{v}_1 \\
\bar{w}_1 \\
\bar{u}_2 \\
\bar{v}_2 \\
\bar{w}_2
\end{bmatrix}
=
\begin{bmatrix}
0 \\
0 \\
0 \\
0 \\
0 \\
0
\end{bmatrix} ,
\tag{4.31}$$

where

$$\begin{aligned}
 a_{j1} &= -\alpha_j^2 - \left(\frac{1 - v_j}{2}\right)\left(1 + \frac{\delta_j^2}{12}\right)n^2 + \Omega_j^2, \\
 a_{j2} &= -\sqrt{-1} \left(\frac{1 + v_j}{2}\right)\alpha_{jn}, \\
 a_{j3} &= -\sqrt{-1} \left[v_j\alpha_j + \frac{\delta_j^2}{12}\alpha_j - \frac{\delta_j^2}{24}(1 - v_j)\alpha_j n^2\right], \\
 a_{j4} &= n^2 + \left(\frac{1 - v_j}{2}\right)\left(1 + \frac{\delta_j^2}{4}\right)\alpha_j^2 - \Omega_j^2, \\
 a_{j5} &= n^2 + \frac{\delta_j^2}{24}(3 - v_j)n\alpha_j^2, \\
 a_{16} &= 1 + \frac{\delta_1^2}{12}\{1 - 2n^2 + (\alpha_1^2 + n^2)^2\} - \Omega_1^2 - \mu_1 c_{m1}\Omega_1^2, \\
 a_{17} &= \mu_1 c_{m4}\Omega_1^2, \\
 a_{26} &= 1 + \frac{\delta_2^2}{12}\{1 - 2n^2 + (\alpha_2^2 + n^2)^2\} - \Omega_2^2 - \mu_2 c_{m2}\Omega_2^2, \quad \text{and} \\
 a_{27} &= \mu_2 c_{m3}\Omega_2^2,
 \end{aligned} \tag{4.32}$$

and

$$\begin{aligned}
 \Delta &= F_{2n}'(R_1)G_{2n}'(R_2) - F_{2n}'(R_2)G_{2n}'(R_1), \\
 c_{m1} &= (1/\Delta)\{G_{2n}'(R_2)F_{2n}'(R_1) - F_{2n}'(R_2)G_{2n}'(R_1)\}, \\
 c_{m2} &= (1/\Delta)\{F_{2n}'(R_1)G_{2n}'(R_2) - G_{2n}'(R_1)F_{2n}'(R_2)\} \\
 c_{m3} &= (1/\Delta)(R_1/R_2)\{G_{2n}'(R_2)F_{2n}'(R_2) - F_{2n}'(R_2)G_{2n}'(R_2)\}, \quad \text{and} \\
 c_{m4} &= (1/\Delta)(R_2/R_1)\{F_{2n}'(R_1)G_{2n}'(R_1) - G_{2n}'(R_1)F_{2n}'(R_1)\}.
 \end{aligned} \tag{4.33}$$

The frequency equation is obtained by setting the determinant of the coefficient matrix in Eq. 4.31 equal to zero; it can be written as

$$F(\Omega_j, \alpha_j, \delta_j, \mu_j, \nu_j, \gamma_j, \rho, n) = 0. \quad (4.34)$$

Several limiting cases can be deduced from Eq. 4.34:

- (a) For $\rho = 0$, the equation gives the frequency for two empty shells.
- (b) For $n = 0$, the equation gives the dispersion relation for axially symmetric modes.
- (c) $\alpha_j = 0$ yields the frequency equation of the circumferential motions.
- (d) When either one of the shells is rigid, the equation becomes the frequency equation of the other shell.

It is little trouble to obtain the roots of the exact frequency equation (4.34). However, it is still interesting to examine approximations to the low frequency for possible implications that may be reduced for the system.

Deleting the in-plane inertias of the shells, assuming that the fluids are incompressible, and using the Donell's shell equations (obtained by deleting all terms in Eq. 4.20 multiplied by δ_j^2 , except the term $(\delta_j^2/12)(\alpha_j^2 + n^2)^2$ in a_{16} and a_{26}), it can be shown that the radial displacements \bar{w}_1 and \bar{w}_2 are given by

$$\begin{bmatrix} \Omega_{v1}^2 - c_1 \Omega_1^2 & c_2 \Omega_1^2 \\ c_3 \Omega_1^2 & \Omega_{v2}^2 - c_4 \Omega_1^2 \end{bmatrix} \begin{Bmatrix} \bar{w}_1 \\ \bar{w}_2 \end{Bmatrix} = \begin{Bmatrix} 0 \\ 0 \end{Bmatrix}, \quad (4.35)$$

where

$$\begin{aligned} \Omega_{v1}^2 &= \frac{\delta_1^2}{12} (\alpha_1^2 + n^2)^2 + \frac{(1 - \nu_1^2) \alpha_1^4}{(\alpha_1^2 + n^2)^2}, \\ \Omega_{v2}^2 &= \frac{\delta_2^2}{12} (\alpha_2^2 + n^2)^2 + \frac{(1 - \nu_2^2) \alpha_2^4}{(\alpha_2^2 + n^2)^2}, \\ c_1 &= 1 + \mu_1 C_{m1}, \quad c_2 = \mu_1 C_{m4}, \quad c_3 = \mu_2 C_{m3} \beta^2, \\ c_4 &= (1 + \mu_2 C_{m2}) \beta^2. \quad \beta = \frac{R_2}{R_1} \left[\frac{\rho_2 E_1 (1 - \nu_2^2)^{1/2}}{\rho_1 E_2 (1 - \nu_1^2)} \right]. \end{aligned} \quad (4.36)$$

Consider two special cases:

1. The outer shell is rigid, which corresponds to a shell submerged in a fluid annulus, and
2. The inner shell is rigid, which corresponds to a shell containing fluid and a rigid cylinder.

The frequencies for these two cases are denoted by Ω_1 and Ω_2 , respectively. From Eqs. 4.35 and 4.36, it can be shown that

$$\Omega_1^2 = \frac{\Omega_{v1}^2}{1 + \mu_1 C_{m1}} \quad \text{and} \quad \Omega_2^2 = \frac{\Omega_{v2}^2}{(1 + \mu_2 C_{m2})\beta^2}. \quad (4.37)$$

It is obvious that both frequencies are reduced due to the fluid loading. In terms of dimensional quantities, from Eq. 4.37 it can be shown that the frequency of the shell with fluid is equal to that of the empty shell whose density has been replaced by the shell density and the added mass. The added masses are

$$\rho_{\text{added}} = \frac{\rho R_1}{\rho_1 h_1} C_{m1} \quad \text{for case 1;} \quad \rho_{\text{added}} = \frac{\rho R_2}{\rho_2 h_2} C_{m2} \quad \text{for case 2.} \quad (4.38)$$

C_{m1} and C_{m2} are the added mass coefficients, which are functions of n , α_j , and R_2/R_1 . For $\alpha_j = 0$, Eq. 4.33 gives

$$C_{m1} = C_{m2} = \frac{1}{n} \left[\frac{(R_2/R_1)^n + 1}{(R_2/R_1)^n - 1} \right]. \quad (4.39)$$

Next, return to Eq. 4.35 concerning the coupling system. In this case, the frequency equation is

$$(c_1 c_4 + c_2 c_4) \Omega_1^4 - (c_1 \Omega_{v2}^2 + c_4 \Omega_{v1}^2) \Omega_1^2 + \Omega_{v1}^2 \Omega_{v2}^2 = 0. \quad (4.40)$$

Equation 4.40 gives two frequencies: the smaller one Ω_0 is associated with the out-of-phase motion and the larger one Ω_1 is associated with the in-phase motion of the two shells. Mathematically, it can readily be shown that if

$$c_2 c_3 / c_1 c_4 < 1 , \quad (4.41)$$

then

$$\Omega_0 < \Omega_1, \Omega_2 \quad \text{and} \quad \Omega_i > \Omega_1, \Omega_2 . \quad (4.42)$$

Physically, this means that the frequency of the out-of-phase mode is always less than those of the uncoupled system, while the frequency of the in-phase mode is always larger than those of the uncoupled system provided that

$$(1 + \mu_2 C_{m2})[1 + \mu_1 C_{m1}] > \mu_1 \mu_2 C_{m3} C_{m4} . \quad (4.43)$$

Equation 4.43 can be replaced by

$$C_{m1} C_{m2} > C_{m3} C_{m4} . \quad (4.44)$$

Note that the coefficients C_{m1} and C_{m2} are proportional to the fluid pressure acting on the inner and outer shells due to the motion of the inner and outer shells, respectively, while the coefficients C_{m3} and C_{m4} are proportional to the fluid pressure acting on the outer and inner shells due to the motion of the inner and outer shells, respectively. Equation 4.44 is satisfied in all cases. This is similar to Eq. 3.15 in Section 3.2.

Consider a specific numerical example: $R_1 = 86.86$ cm, $R_2 = 87.95$ cm, $h_1 = 0.64$ cm, $h_2 = 1.59$ cm, $\nu_1 = \nu_2 = 0.27$, $E_1 = E_2 = 18.95 \times 10^{10}$ Pascals, $\rho_1 = \rho_2 = 0.008$ kg/cm³, $\rho = 0.000924$ kg/cm³, and $\ell = 104$ cm. The fluid is considered incompressible and the shell is assumed to be simply supported at both ends. The frequencies of this finite shell system can be obtained using the frequency equation (Eq. 4.34). The frequencies of the system depend on the axial wave and circumferential wave numbers; the lowest frequency is associated with the lowest axial wave number; i.e., the shell length is equal to the half wavelength. The frequencies of the out-of-phase and in-phase modes for this case have been computed and are presented in Fig. 4.7. For comparison, Fig. 4.7 also shows the frequencies for four related cases:

1. The inner shell in vacuo,
2. The outer shell in vacuo,
3. The shell system with rigid outer shell, and

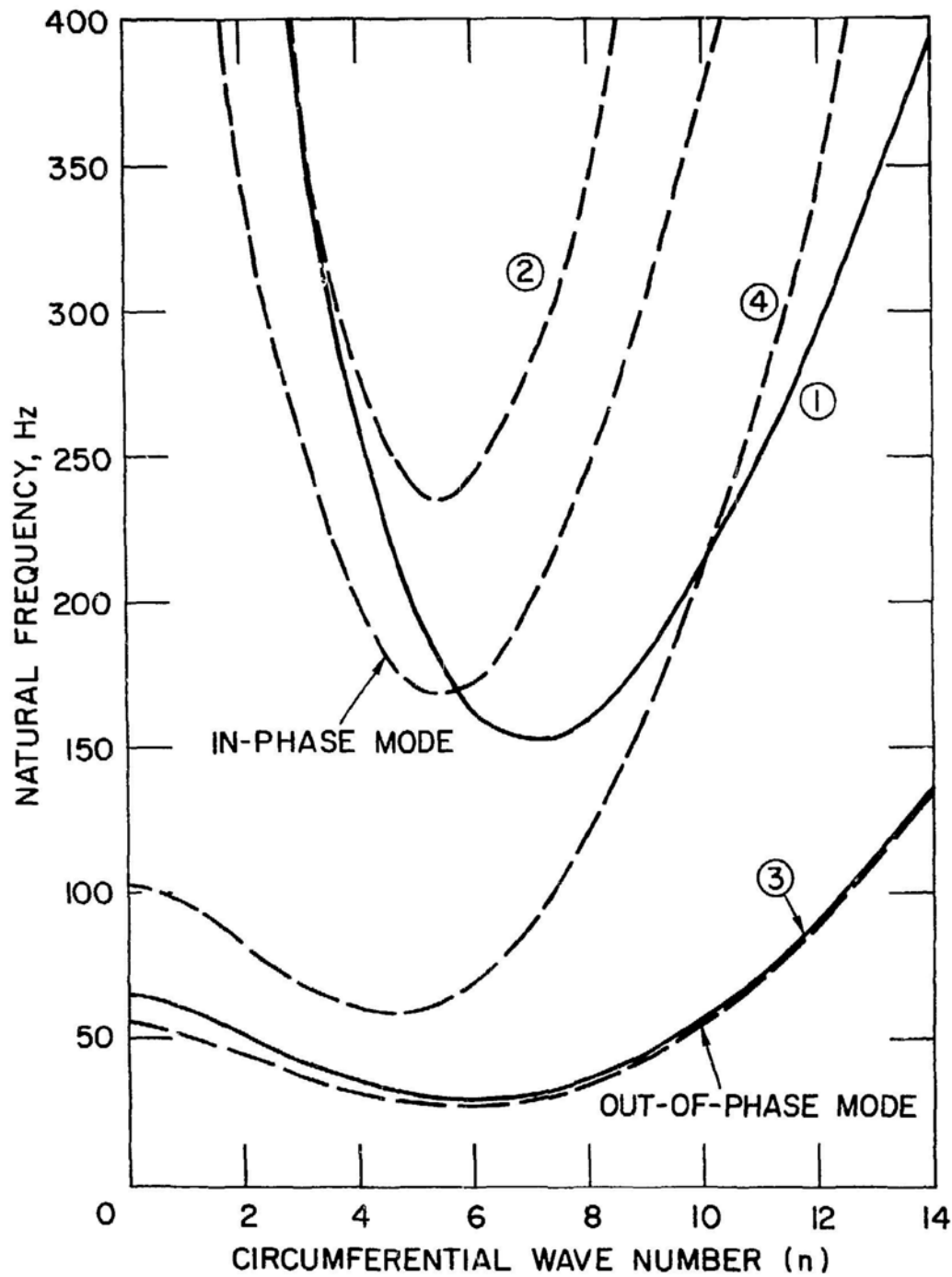


Fig. 4.7. Natural Frequencies of Out-of-phase and In-phase Modes of a Coupled Shell System and Related Cases: 1 - Inner Shell in Vacuum, 2 - Outer Shell in Vacuum, 3 - Shell System with Rigid Outer Shell, and 4 - Shell System with Rigid Inner Shell (Chen and Rosenberg 1975)

4. The shell system with rigid inner shell.

This example illustrates the dynamic characteristics of a coupled shell/fluid system as discussed previously. Another characteristic exhibited in this figure is that the circumferential wave number associated with the lowest frequency for a coupled shell/fluid system, in general, is different from that of an empty shell. As shown in the figure, this circumferential wave number of the inner shell changes from 7 to 6, while that of the outer shell does not change. In the case of the double shell system, the lowest frequency of the out-of-phase mode is associated with $n = 6$, while the in-phase mode is associated with $n = 5$. This behavior is attributed to the fact that the distribution of stretching energy and bending energy of the shell/fluid system is different from that of an empty shell.

Experimental studies on the coupled shell/fluid systems were reported by Chu and Brown (1981) and Chung et al. (1981). The analytical and experimental results agree reasonably well.

Shells of finite lengths and of different lengths are considered by Au-Yang (1976), Horvay and Bowers (1975) and Brown and Lieb (1980). In this case, then, because of the end conditions, the solution given in Eq. 4.26 generally cannot be applied. Instead, the similar procedure, as given in Section 3.6, can be employed to shell problems. The development of the analytical procedure was presented in detail by Au-Yang (1976).

4.5 TWO SHELLS COUPLED BY VISCOUS FLUID

Consider two concentric circular cylindrical shells separated by a viscous fluid as shown in Fig. 4.6 (Yeh and Chen 1977). The equations of motion for the shells are the same as those given in Eq. 4.22 with the following exceptions:

- The right side of the first equation is replaced by $-\frac{1 - \nu_j^2}{E_j h_j} p_{zj}$,
- The right side of the second equation is replaced by $-\frac{1 - \nu_j^2}{E_j h_j} p_{\theta j}$,
- The right side of the third equation is replaced by $\frac{1 - \nu_j^2}{E_j h_j} p_{rj}$.

p_{zj} , $p_{\theta j}$ and p_{rj} are the surface-loading components per unit area due to fluid.

For a nonsteady, small-amplitude oscillatory motion, the equation of motion for the viscous fluid can be expressed as follows (Landau and Lifshitz 1959):

$$\frac{\partial \rho}{\partial t} + \rho_0 \nabla \cdot \vec{U} = 0$$

$$\frac{\partial \vec{U}}{\partial t} = -\frac{1}{\rho} \nabla p + \left(\frac{4}{3} \nu_0 + \nu'_0\right) \nabla (\nabla \cdot \vec{U}) - \nu_0 \nabla \times \nabla \times \vec{U}, \quad \text{and} \quad (4.45)$$

$$\frac{\partial p}{\partial \rho} = c^2,$$

where ρ_0 and ρ are the mean and instantaneous fluid mass densities, ν_0 and ν'_0 are the kinetic and second viscosities of the fluid, c is the speed of sound in fluid, p is fluid pressure, and \vec{U} is fluid velocity vector.

At the interfaces between the shells and fluid, the following conditions must be satisfied:

$$\begin{aligned} u_z \Big|_{r=R_j} &= \frac{\partial u_j}{\partial t}, \\ u_\theta \Big|_{r=R_j} &= \frac{\partial v_j}{\partial t}, \quad \text{and} \\ u_r \Big|_{r=R_j} &= \frac{\partial w_j}{\partial t} \quad j = 1, 2. \end{aligned} \quad (4.46)$$

The surface loading acting on the shells is given by

$$\begin{aligned} p_{\ell 1} &= \tau_{r\ell} \Big|_{r=R_1}, \\ p_{\ell 2} &= -\tau_{r\ell} \Big|_{r=R_2} \quad \ell = z, \theta, r, \end{aligned} \quad (4.47)$$

where τ_{rr} , $\tau_{r\theta}$ and τ_{rz} are the fluid stresses.

$$\begin{aligned}
\tau_{rr} &= -p + 2\mu \frac{\partial u_r}{\partial r}, \\
\tau_{r\theta} &= \mu \left[r \frac{\partial}{\partial r} \left(\frac{u_\theta}{r} \right) + \frac{1}{r} \frac{\partial u_r}{\partial \theta} \right], \quad \text{and} \\
\tau_{rz} &= \mu \left(\frac{\partial u_r}{\partial z} + \frac{\partial u_z}{\partial r} \right).
\end{aligned} \tag{4.48}$$

Here μ is fluid viscosity.

Letting $\vec{U} = \nabla \times \vec{\psi} + \nabla \phi$ and inserting it into Eqs. 4.45 yields:

$$\left(\frac{\partial}{\partial t} - v_o \nabla^2 \right) \vec{\psi} = 0, \tag{4.49}$$

$$p = p_o - \rho_o \frac{\partial \phi}{\partial t} + \rho_o \left(\frac{4}{3} v_o + v_o' \right) \nabla^2 \phi, \quad \text{and} \tag{4.50}$$

$$\left[\left(1 + \frac{1}{\omega_o} \frac{\partial}{\partial t} \right) \nabla^2 - \frac{1}{c^2} \frac{\partial^2}{\partial t^2} \right] \phi = 0, \tag{4.51}$$

where

$$\omega_o = \frac{c^2}{\frac{4}{3} v_o + v_o'}. \tag{4.52}$$

Equation 4.50 shows that the fluid pressure is not affected by the waves produced from the vector potential $\vec{\psi}$, which is associated with the fluid viscosity.

In cylindrical coordinates, Eq. 4.49 yields

$$\begin{aligned}
\left(\frac{1}{v_o} \frac{\partial}{\partial t} - \nabla^2 \right) \psi_z &= 0, \\
\left(\frac{1}{v_o} \frac{\partial}{\partial t} - \nabla^2 \right) \psi_\theta + \frac{\psi_\theta}{r^2} - \frac{2}{r^2} \frac{\partial \psi_r}{\partial \theta} &= 0,
\end{aligned} \tag{4.53}$$

and

$$\left(\frac{1}{v_o} \frac{\partial}{\partial t} - \nabla^2 \right) \psi_r + \frac{\psi_r}{r^2} + \frac{2}{r^2} \frac{\partial \psi_\theta}{\partial \theta} = 0.$$

Solutions of the following form are assumed for the shells:

$$\begin{aligned}
 u_j &= i\bar{u}_j \cos(n\theta) \exp[i(\omega t - kz)] , \\
 v_j &= \bar{v}_j \sin(n\theta) \exp[i(\omega t - kz)] , \quad \text{and} \\
 w_j &= \bar{w}_j \cos(n\theta) \exp[i(\omega t - kz)] ,
 \end{aligned} \tag{4.54}$$

where $i = \sqrt{-1}$, n is the circumferential wave number, ω is the circular frequency, k is the axial wave number, and \bar{u}_j , \bar{v}_j , and \bar{w}_j are arbitrary constants to be determined.

Similarly, the fluid velocity potential can be assumed as follows:

$$\begin{aligned}
 \phi &= \bar{\phi}(r) \cos(n\theta) \exp[i(\omega t - kz)] , \\
 \psi_z &= \bar{\psi}_z(r) \sin(n\theta) \exp[i(\omega t - kz)] , \\
 \psi_\theta &= i\bar{\psi}_\theta(r) \cos(n\theta) \exp[i(\omega t - kz)] , \\
 \psi_r &= i\bar{\psi}_r(r) \sin(n\theta) \exp[i(\omega t - kz)] .
 \end{aligned} \tag{4.55}$$

Substituting Eqs. 4.55 into 4.51 and 4.53 gives the following forms of Bessel's equations:

$$\begin{aligned}
 \left[\frac{1}{r} \frac{\partial}{\partial r} \left(r \frac{\partial}{\partial r} \right) + \left(k_1^2 - \frac{n^2}{r^2} \right) \right] \bar{\phi} &= 0 , \\
 \left[\frac{1}{r} \frac{\partial}{\partial r} \left(r \frac{\partial}{\partial r} \right) + \left(k_2^2 - \frac{n^2}{r^2} \right) \right] \bar{\psi}_z &= 0 ,
 \end{aligned} \tag{4.56}$$

and

$$\begin{aligned}
 \frac{1}{r} \frac{\partial}{\partial r} \left(r \frac{\partial}{\partial r} \bar{\psi}_\theta \right) + \left(k_2^2 - \frac{n^2 + 1}{r^2} \right) \bar{\psi}_\theta + \frac{2n}{r^2} \bar{\psi}_r &= 0 , \\
 \frac{1}{r} \frac{\partial}{\partial r} \left(r \frac{\partial}{\partial r} \bar{\psi}_r \right) + \left(k_2^2 - \frac{n^2 + 1}{r^2} \right) \bar{\psi}_r + \frac{2n}{r^2} \bar{\psi}_\theta &= 0 ,
 \end{aligned}$$

where

$$k_1 = \left(-k^2 + \frac{\omega^2/c^2}{1 + i\omega/\omega_0} \right)^{1/2} \quad \text{and} \quad (4.57)$$

$$k_2 = (-k^2 - i\omega/\nu_0)^{1/2} .$$

The general solutions of Eqs. 4.56 are

$$\begin{aligned} \bar{\phi}(r) &= i\omega[A_1 F_n(k_1 r) + A_2 G_n(k_1 r)] , \\ \bar{\psi}_z(r) &= i\omega[A_3 F_n(k_2 r) + A_4 G_n(k_2 r)] , \quad \text{and} \quad (4.58) \\ \bar{\psi}_r(r) &= -\bar{\psi}_\theta(r) = i\omega[A_5 F_{n+1}(k_2 r) + A_6 G_{n+1}(k_2 r)] , \end{aligned}$$

where A_p are arbitrary constants and F_n and G_n are the n th-order Bessel functions. F_n and G_n can be either the first- and second-kind Bessel functions, J_n and Y_n , or the Hankel functions $H_n^{(1)}$ and $H_n^{(2)}$. The selection of the functions depends mainly on the computational consideration.

Substituting Eqs. 4.54, 4.55, and 4.58 into the interface conditions, Eq. 4.46, gives six linear algebraic equations

$$\sum_{q=1}^6 a_{pq} A_q = \hat{r}_p \hat{u}_p , \quad p = 1 - 6 , \quad (4.59)$$

where

$$\begin{aligned} \hat{r}_p &= R_1 \quad \text{for } p = 1 - 3 , \quad \hat{r}_p = R_2 \quad \text{for } p = 4 - 6 , \\ \hat{u}_1 &= \bar{u}_1 , \quad \hat{u}_2 = \bar{v}_1 , \quad \hat{u}_3 = \bar{w}_1 , \quad \hat{u}_4 = \bar{u}_2 , \quad \hat{u}_5 = \bar{v}_2 , \\ \text{and } \hat{u}_6 &= \bar{w}_2 , \end{aligned}$$

and the expression of a_{pq} is given as follows:

$$\begin{aligned}
a_{11} &= -\alpha_1 F_n(\gamma_1) , & a_{12} &= -\alpha_1 G_n(\gamma_1) , & a_{13} &= a_{14} = 0 , \\
a_{15} &= -\beta_1 F_n(\beta_1) , & a_{16} &= -\beta_1 G_n(\beta_1) , & a_{21} &= -nF(\gamma_1) , \\
a_{22} &= -nG_n(\gamma_1) , & a_{23} &= \beta_1 F_{n+1}(\beta_1) - nF_n(\beta_1) , \\
a_{24} &= \beta_1 G_{n+1}(\beta_1) - nG_n(\beta_1) , & a_{25} &= a_{35} = \alpha_1 F_{n+1}(\beta_1) , & (4.60) \\
a_{26} &= a_{36} = -\alpha_1 G_{n+1}(\beta_1) , & a_{31} &= nF_n(\gamma_1) - \gamma_1 F_{n+1}(\gamma_1) , \\
a_{32} &= nG_n(\gamma_1) - \gamma_1 G_{n+1}(\gamma_1) , & a_{33} &= nF_n(\beta_1) , \\
a_{34} &= nG_n(\beta_1) \quad \text{and} \quad \alpha_j = kR_j , & \beta_j &= k_2 R_j , & \gamma_j &= k_1 R_j .
\end{aligned}$$

The expressions of a_{pq} for $p = 4-6$ are similar to those for $p = 1-3$ and can be obtained by replacing α_1 , β_1 , and γ_1 by α_2 , β_2 , and γ_2 .

Now we are in a position to calculate the loading stresses on the shell surfaces. Here only the dynamic quantity is of interest, so the reference pressure p_0 will not be considered. Equation 4.48 is used to obtain the fluid stresses. Define the new variables \bar{p}_{zj} , $\bar{p}_{\theta j}$, and \bar{p}_{rj} as follows:

$$p_{zj} = i\rho_0\omega^2\bar{p}_{zj}\cos(n\theta)\exp[i(\omega t - kz)] , \quad (4.61)$$

$$p_{\theta j} = \rho_0\omega^2\bar{p}_{\theta j}\sin(n\theta)\exp[i(\omega t - kz)] ,$$

and

$$p_{rj} = \rho_0\omega^2\bar{p}_{rj}\cos(n\theta)\exp[i(\omega t - kz)] .$$

Substituting Eq. 4.61 into 4.47 and using 4.55 and 4.58 yields another six linear algebraic equations:

$$\sum_{q=1}^6 h_{pq} A_q = \hat{p}_p, \quad p = 1-6, \quad (4.62)$$

where

$$\hat{p}_1 = \bar{p}_{z1}, \quad \hat{p}_2 = \bar{p}_{\theta 1}, \quad \hat{p}_3 = \bar{p}_{r1}, \quad \hat{p}_4 = \bar{p}_{z2}, \quad \hat{p}_5 = \bar{p}_{\theta 1},$$

$$\hat{p}_6 = \bar{p}_{r2},$$

and the expression of h_{pq} is given as follows:

$$h_{11} = 2S_1 \sigma_1 [F_{n+1}(\gamma_1) - \frac{n}{\gamma_1} F_n(\gamma_1)],$$

$$h_{12} = 2S_1 \sigma_1 [G_{n+1}(\gamma_1) - \frac{n}{\gamma_1} G_n(\gamma_1)],$$

$$h_{13} = -\frac{S_2 \sigma_2^n}{\beta_1} F_n(\beta_1), \quad h_{14} = -\frac{S_2 \sigma_2^n}{\beta_1} G_n(\beta_1),$$

$$h_{15} = -S_2 [(\sigma_2^2 - 1)F_{n+1}(\beta_1) + \frac{n}{\beta_1} F_n(\beta_1)],$$

$$h_{16} = -S_2 [(\sigma_2^2 - 1)G_{n+1}(\beta_1) + \frac{n}{\beta_1} G_n(\beta_1)],$$

$$h_{21} = \frac{2S_1 n}{\gamma_1} [F_{n+1}(\gamma_1) - \frac{n-1}{\gamma_1} F_n(\gamma_1)],$$

$$h_{22} = \frac{2S_1 n}{\gamma_1} [G_{n+1}(\gamma_1) - \frac{n-1}{\gamma_1} G_n(\gamma_1)],$$

$$h_{23} = -S_2 \left\{ \left[\frac{2n(n-1)}{\beta_1^2} - 1 \right] F_n(\beta_1) + \frac{2}{\beta_1} F_{n+1}(\beta_1) \right\},$$

$$h_{24} = -S_2 \left\{ \left[\frac{2n(n-1)}{\beta_1^2} - 1 \right] G_n(\beta_1) + \frac{2}{\beta_1} G_{n+1}(\beta_1) \right\}, \quad (4.63)$$

$$h_{25} = S_2 \sigma_2 \left[F_n(\beta_1) - \frac{2(n+1)}{\beta_1} F_{n+1}(\beta_1) \right] ,$$

$$h_{26} = S_2 \sigma_2 \left[G_n(\beta_1) - \frac{2(n+1)}{\beta_1} G_{n+1}(\beta_1) \right] ,$$

$$h_{31} = \left[\frac{2S_1 n(n-1)}{\gamma_1^2} - \left(2S_1 + \frac{1}{1+i(\omega/\omega_0)} \right) \right] F_n(\gamma_1) + \frac{2S_1}{\gamma_1} F_{n+1}(\gamma_1) ,$$

$$h_{32} = \left[\frac{2S_1 n(n-1)}{\gamma_1^2} - \left(2S_1 + \frac{1}{1+i(\omega/\omega_0)} \right) \right] G_n(\gamma_1) + \frac{2S_1}{\gamma_1} G_{n+1}(\gamma_1) ,$$

$$h_{33} = \frac{2S_1 n}{\beta_1} \left[\frac{n-1}{\beta_1} F_n(\beta_1) - F_{n+1}(\beta_1) \right] ,$$

$$h_{34} = \frac{2S_1 n}{\beta_1} \left[\frac{n-1}{\beta_1} G_n(\beta_1) - G_{n+1}(\beta_1) \right] ,$$

(4.63)
(Contd.)

$$h_{35} = 2S_2 \sigma_2 \left[F_n(\beta_1) - \frac{n+1}{\beta_1} F_{n+1}(\beta_1) \right] ,$$

$$h_{36} = 2S_2 \sigma_2 \left[G_n(\beta_1) - \frac{n+1}{\beta_1} G_{n+1}(\beta_1) \right] ,$$

and

$$R_k = \frac{4\omega R_1^2}{v_2} , \quad M_k = \frac{2\omega R_1}{c} .$$

$$\sigma_1 = \alpha_1 / \gamma_1 , \quad \sigma_2 = \alpha_2 / \beta_1 ,$$

$$S_1 = 1 - \frac{4\gamma_1^2}{R_k} , \quad S_2 = 1 - \frac{4\beta_1^2}{R_k} , \quad \frac{\omega}{\omega_0} = \frac{M_k}{R_k} \left(\frac{4}{3} + \frac{v_0'}{v_0} \right)$$

Using Eqs. 4.59 and 4.62 gives the surface loading expressed in terms of the interface radii and the shell displacement as

$$\hat{p}_p = \sum_{q=1}^6 \alpha_{pq} \hat{r}_q \hat{u}_q , \quad p = 1-6 \quad (4.64)$$

where

$$\{\alpha_{pq}\} = \{h_{pq}\} \{a_{pq}\}^{-1} . \quad (4.65)$$

The coefficient α_{pp} is proportional to the dynamic fluid stress acting on a shell surface due to its own movement; while the others, α_{pq} for $p \neq q$, are proportional to the dynamic fluid stresses acting on a shell surface in one direction due to the movement in another direction.

The fluid stresses acting on the shells are linear functions of shell motions. In general, the coefficients α_{pq} are complex. The fluid stress can be separated into two components: one, proportional to $\text{Re}(\alpha_{pq})$, is in phase with the shell accelerations and is related to the added mass effect; the other, proportional to $\text{Im}(\alpha_{pq})$, is opposing to the movement of the shells and is related to damping mechanism. If the fluid is inviscid, the second component of the stress opposing shell motion will be zero.

The dynamic fluid-stress coefficient matrix α_{pq} is a function of the radius ratio R_2/R_1 , the circumferential wave number n , the axial wave number α_1 , the Mach number M_k , the Reynolds number R_k , and the ratio of the fluid viscosities ν'_0/ν_0 . It should be noted that the circular frequency ω and so Mach number M_k and Reynolds number R_k are in general complex numbers. The Mach number M_k is considered to include the compressibility effects of the fluid. However, the analysis is valid for a small compressible effect or a small Mach number M_k . The Reynolds number R_k and viscosity ratio ν'_0/ν_0 are the additional function parameters associated with fluid viscosity.

For the case of potential flow where $\nu_0 = 0$, and $\nu'_0 = 0$, the Reynolds number R_k and viscous ratio ν'_0/ν_0 are no longer defined and the coefficient is a function of R_2/R_1 , n , α_1 , and M_k only. Furthermore, all the elements of the coefficient matrix are zero except the real parts of the four elements: $\text{Re}\{\alpha_{33}\}$, $\text{Re}\{\alpha_{36}\}$, $\text{Re}\{\alpha_{63}\}$, and $\text{Re}\{\alpha_{66}\}$, and no damping is introduced to the system by the incompressible ideal fluid.

With respect to fluid shell interaction, substituting Eqs. 4.54, 4.61, and 4.64 into the shell equations gives six linear algebraic homogeneous equations:

$$\sum_{q=1}^6 b_{pq} \hat{u}_q = 0, \quad p = 1-6, \quad (4.66)$$

where

$$\begin{aligned} b_{pq} &= C_{pq} - \Omega_1^2(\delta_{pq} + \mu_1 \alpha_{pq}), & \text{for } p, q = 1-3 \\ &= -\Omega_1^2 \mu_1 (R_2/R_1) \alpha_{pq} & \text{for } p = 1-3 \text{ and } q = 4-6 \\ &= -\Omega_2^2 \mu_2 (R_1/R_2) \alpha_{pq} & \text{for } p = 4-6 \text{ and } q = 1-3 \\ &= C_{pq} - \Omega_2^2(\delta_{pq} + \mu_2 \alpha_{pq}), & \text{for } p, q = 4-6 \end{aligned} \quad (4.67)$$

$$\Omega_j = R_j \omega \left[\frac{\rho_j (1 - \nu_j^2)}{E_j} \right]^{1/2} \quad \mu_j = \frac{\rho_o R_j}{\rho_j h_j}, \quad (4.67)$$

$$\delta_{pq} = 1 \quad \text{for } p = q, \quad \text{otherwise } \delta_{pq} = 0, \quad (\text{Contd.})$$

and the expression C_{pq} is given as follows:

$$C_{11} = \alpha_1^2 + \frac{1}{2} (1 - \nu_1) n^2 \left(1 + \frac{1}{12} \delta_1^2 \right),$$

$$C_{12} = C_{21} = \frac{1}{2} (1 + \nu_1) \alpha_1 n,$$

$$C_{22} = n^2 + \frac{1}{2} (1 - \nu_1) \left(1 + \frac{1}{4} \delta_1^2 \right) \alpha_1^2,$$

$$C_{13} = C_{31} = \alpha_1 \nu_1 + \frac{1}{12} \alpha_1^3 \delta_1^2 - \frac{1}{24} \alpha_1 (1 - \nu_1) \delta_1^2 n^2, \quad (4.68)$$

$$C_{23} = C_{32} = n + \frac{1}{24} \alpha_1^2 (3 - \nu_1) \delta_1^2 n,$$

$$C_{33} = 1 + \frac{1}{12} \delta_1^2 [1 - 2n^2 + (\alpha_1^2 + n^2)^2],$$

$$\delta_j = h_j / R_j.$$

The frequency equation of the coupled fluid/shell system is obtained by setting the determinant of the coefficient matrix b_{pq} in Eq. 4.66 equal to zero; it can be written as $|b_{pq}| = 0$ or in the function form as

$$F(\alpha_1, R_2/R_1, M_k, R_k, \nu_o'/\nu_o, n, R_j, \delta_j, \mu_j) = 0. \quad (4.69)$$

In contrast with the incompressible potential flow theory, the stress coefficient for a given physical condition is a function of the frequency parameter ω , which in general is a complex number. Therefore, in order to determine the natural frequency and the damping ratio of the coupled system, an iteration procedure generally is required.

It should be noted that, for the case of an incompressible viscous fluid, the dynamic fluid stress is not only a function of n , R_2/R_1 , and α_1 but also a function of the kinetic Reynolds number R_k . This additional parameter R_k makes the simulation of a scaled model test for a coupled viscous fluid/shell system very difficult when fluid viscosity effect is important. In a reduced-scale model test, the geometrical simulation commonly employed tends to overestimate the fluid damping; thus the test result may not be conservative.

4.6 CLOSING REMARKS

The general characteristics of coupled shell/fluid systems are discussed in this chapter for infinite shells. A closed-form solution is obtainable based on the linear theory. For a finite shell, either an approximate analytical solution (Au-Yang 1977) or a numerical solution can be obtained: These are not considered here; however, the role of fluid on shell response is similar.

One important problem is the storage tanks, which are basically a finite circular cylindrical shell containing fluid with free surface. The response of the tanks due to seismic excitation is of particular interest. A summary of this problem is available (ASCE 1984).

The effect of fluid on shell vibration is much more complicated than that on a circular cylinder. In general, the fluid added mass and damping depend on mode shapes; therefore, it is necessary to solve the coupled problem. The concept of added mass is not as useful as for a circular cylinder.

REFERENCES--Sec. 4

- Abramson, H. N., and Kana, D. D. 1967. Some Recent Research on Vibrations of Elastic Shells Containing Liquid. Proc. Sym. on Theory of Shells, Houston Univ., Houston, Texas.
- ASCE (American Society of Civil Engineers). 1984. Fluid/Structure Interaction During Seismic Excitation. ASCE Committee on Seismic Analysis.
- Au-Yang, M. K. 1976. Free Vibration of Fluid-Coupled Coaxial Cylindrical Shells of Different Lengths. J. of Appl. Mech. 98, 480-484.
- Au-Yang, M. K. 1977. Response of Fluid-Elastically Coupled Coaxial Cylindrical Shells to External Flow. J. Fluids Eng. 99, 319-324.
- Brown, S. J., Jr., and Lieb, B. W. 1980. A Comparison of Experimental and Theoretical Vibration Results for Narrow Gap, Fluid-Coupled, Coaxial Flexible Cylinders. ASME Paper No. 80-C2/PVP-104.
- Chen, S. S., and Rosenberg, G. S. 1974. Free Vibrations of Fluid-Conveying Cylindrical Shells. J. Eng. for Industry 96(2), 420-426.
- Chen, S. S., and Rosenberg, G. S. 1975. Dynamics of a Coupled Shell-Fluid System. Nucl. Eng. Des. 32, 302-310.
- Chu, M. L., and Brown, S. 1981. Experiments on the Dynamic Behavior of Fluid-Coupled Concentric Cylinders. Experimental Mechanics 5, 129-136.
- Chung, H., Turula, P., Mulcahy, T. M., and Jendrzejczyk, J. A. 1981. Analysis of a Cylindrical Shell Vibrating in a Cylindrical Fluid Region. Nucl. Eng. Des. 63, 109-120.
- Clough, R. W., Niwa, A., and Clough, D. P. 1979. Experimental Seismic Study of Cylindrical Tanks. ASCE J. of the Structural Division 105(ST12), 2565-2589.
- Flügge, W. 1960. Stresses in Shells. Springer-Verlag, Berlin.
- Fujita, K. 1982. A Seismic Response Analysis of a Cylindrical Liquid Storage Tank on an Elastic Foundation. Bulletin of the JSME 25, 1977-1984.
- Haroun, M. A. 1983. Vibration Studies and Tests of Liquid Storage Tanks. Earthquake Eng. and Str. Dynamics 11, 179-206.
- Horvay, G., and Bowers, G. 1975. Influence of Entrained Water Mass on the Vibration Modes of a Shell. J. Fluids Eng. 97, 211-216.
- Landau, L. D., and Lifshitz, E. M. 1959. Fluid Mechanics. Addison-Wesley, Reading, MA.
- Reissner, E. 1955. On Transverse Vibrations of Thin, Shallow Elastic Shells. Quarterly of Applied Mathematics 8, 169-176.
- Skalak, R. 1956. An Extension of the Theory of Water Hammer. Trans. ASME 78, 105-116.
- Yeh, T. T., and Chen, S. S. 1977. Dynamics of a Cylindrical Shell System Coupled by Viscous Fluid. J. Acoust. Soc. Am. 62(2), 262-270.

5. PIPES CONVEYING FLUID

5.1 INTRODUCTION

In the last three decades, we have witnessed a great surge of interest in the dynamic behavior of pipes conveying fluid, largely for two reasons:

- The dynamic behavior of pipes conveying fluid is of considerable importance; oscillations have been observed in oil pipelines, various elements of high-performance launch vehicles, missiles, moving wire and belts, nuclear reactor system components, etc.
- Pipes conveying fluid is one of the few physically realizable cases of nonconservative systems; the problem is of great academic interest.

According to a historical search by Paidoussis and Issid (1974), the first publication on this subject was by Bourrieres (1939). Bourrieres derived the equation of motion and examined theoretically and experimentally the dynamic instability of a cantilevered pipe conveying fluid.

In the 1950s, interest in the subject was motivated by vibration problems encountered in the transport of crude oil in pipes (Ashley and Haviland 1950; Feodos'ev 1951; Housner 1952; Niordson 1953). Since then no fewer than a hundred papers and reports have been published on this subject; see reviews by Chen (1974) and Paidoussis and Issid (1974).

5.2 HAMILTON'S PRINCIPLE FOR PIPES CONVEYING FLUID

Hamilton's principle usually is formulated for a system composed of the same particles or a system with material moving through it but maintaining constant mass and with no net energy transfer between the moving medium and the system. In a pipe conveying fluid, because of pipe deformation the constituent particles change with time and there may be net energy transfer between the pipe and fluid. Therefore, a more general form of Hamilton's principle is needed for this problem.

There have been several attempts to extend the Hamilton's principle for systems of changing mass with the specific objective of dealing with pipes conveying fluid (Housner 1952; Benjamin 1961; McIver 1973). The following discussion is based on the work of McIver, who presented the extended Hamilton Principle, which is applicable to a wide range of problems.

Consider a continuous material system of particles of fixed identity contained within a moving region of space $R_c(t)$ bounded by the surface $B_c(t)$ across which there is no mass transport at any point. At position \vec{r} at time t , the particle density is ρ and the velocity \vec{u} , where the system is subjected to a virtual displacement $\delta\vec{r} = \delta\vec{r}(\vec{r}, t)$. The principle of virtual work for the system is

$$\delta \mathcal{L} + \delta W - \frac{D}{Dt} \iiint_{R_c(t)} \rho(\vec{u} \cdot \delta \vec{r}) dV = 0, \quad (5.1)$$

where \mathcal{L} is the Lagrangian of the system in the closed region $R_c(t)$, δW is the virtual work performed by the generalized forces undergoing the generalized virtual displacements, and D/Dt is the material derivative following a particle or a specific collection of particles; then $\vec{u} = D\vec{r}/Dt$.

Hamilton's principle for a "closed" system, in which the constituent elements of the system are the same for all time, is obtained by integrating Eq. 5.1 with respect to time between two instants t_1 and t_2 , when the system configuration is prescribed ($\delta \vec{r} = 0$); i.e.,

$$\delta \int_{t_1}^{t_2} \mathcal{L} dt + \int_{t_1}^{t_2} \delta W dt = 0. \quad (5.2)$$

A general statement of Hamilton's principle that is appropriate for "open" systems of changing mass can be obtained based on the open control volume (see Fig. 5.1), which is partly open across the surface $B_o(t)$ and partly closed over the surface $B_c(t)$. $B_c(t)$, across which mass is transported, is moving with an arbitrary normal velocity $\vec{U} \cdot \vec{n}$; \vec{n} is the unit outward normal vector to the open part of the system. At all instants t the system is defined as the collection of particles inhabiting the open control volume $R_o(t)$. Note that the system does not possess a constant mass or, if it does, the mass need not consist always of the same set of particles. The region $R_c(t)$ is a closed system bounded by $B_c(t)$ if $\vec{U} \cdot \vec{n} = \vec{u} \cdot \vec{n}$.

If at the instant it is considered the open control volume $R_o(t)$ coincides with the closed control volume $R_c(t)$, the general transport theorem is

$$\begin{aligned} \frac{d}{dt} \iiint_{R_o(t)} (\) dt &= \frac{D}{Dt} \iiint_{R_c(t)} (\) dV \\ &+ \iint_{B_o(t)} (\) (\vec{U} - \vec{u}) \cdot \vec{n} dS. \end{aligned} \quad (5.3)$$

Since the notation $D(\)/Dt$ is employed for a closed control volume, it is permissible to write

$$\frac{D}{Dt} \iiint_{R_c(t)} (\) dV = \frac{D}{Dt} \iiint_{R_o(t)} (\) dV. \quad (5.4)$$

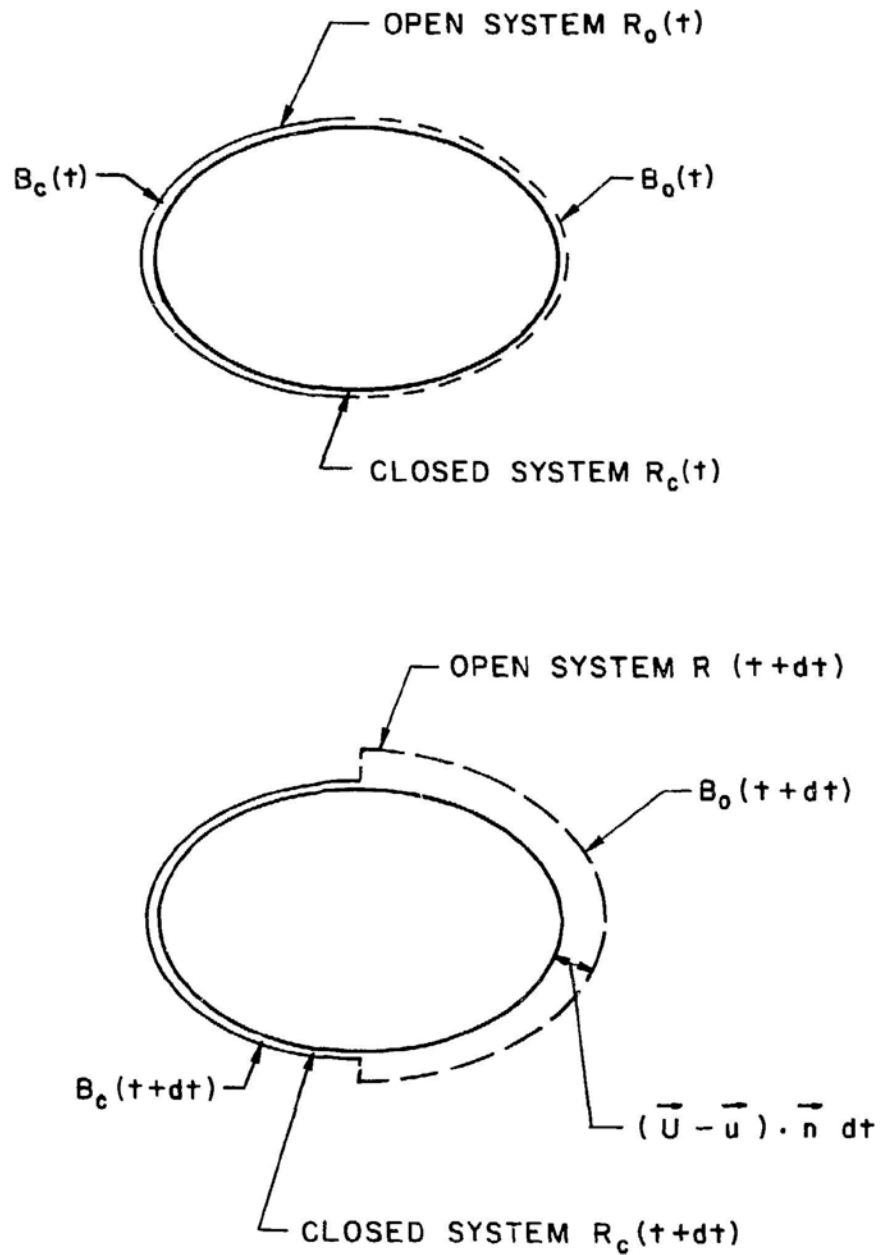


Fig. 5.1. Definition of Control Volume R under Specified Conditions. At time t the open system coincides with a fictitious closed system and at time $t + dt$, there is momentum transport across the surface $B_o(t)$.

Employing Eqs. 5.1 and 5.4 yields

$$\begin{aligned} \delta \mathcal{L} + \delta W + \iint_{B_o(t)} \rho(\vec{u} \cdot \delta \vec{r})(\vec{U} - \vec{u}) \cdot \vec{n} dS \\ - \frac{d}{dt} \iiint_{R_o(t)} \rho(\vec{u} \cdot \delta \vec{r}) dV = 0 . \end{aligned} \quad (5.5)$$

Integrating Eq. 5.5 with respect to time from t_1 to t_2 , when the system configuration is prescribed, yields the Hamilton's principle for a system of changing mass:

$$\delta \int_{t_1}^{t_2} \mathcal{L} dt + \int_{t_1}^{t_2} \delta W dt + \iint_{B_o(t)} \rho(\vec{u} \cdot \delta \vec{r})(\vec{U} - \vec{u}) \cdot \vec{n} dS = 0 \quad (5.6)$$

The last integral is the virtual momentum transport across the surface $B_o(t)$. The statement given in Eq. 5.6 is very general and is applicable for a system with changing mass.

Now the general principle given in Eq. 5.6 can be applied to pipes conveying fluid. The system is open with the control volume surface coinciding with the exterior surface of the pipe and the pipe inlet and exit (Fig. 5.2). $S_i(t)$ and $S_e(t)$ are the open control surfaces at the pipe inlet and exit respectively. The pipe is fixed so there can be no virtual work contribution from the force and moment of reaction. The fluid velocity at the pipe exit is $\vec{u} = \dot{\vec{R}} + U\vec{\tau}$ and the normal velocity relative to the control surface $S_o(t)$ is $(\vec{u} - \vec{U}) \cdot \vec{n} = U$. Thus, the last term in Eq. 5.6 becomes

$$\begin{aligned} \delta H &= \iint_{S_e(t)} \rho(\vec{u} \cdot \delta \vec{r})(\vec{U} - \vec{u}) \cdot \vec{n} dS \\ &= -M_d U(\dot{\vec{R}} + U\vec{\tau}) \cdot \delta \vec{R} \end{aligned} \quad (5.7)$$

when M_d is the mass of fluid per unit length. Therefore

$$\delta \int_{t_1}^{t_2} \mathcal{L} dt + \int_{t_1}^{t_2} \delta W dt - \int_{t_1}^{t_2} M_d U(\dot{\vec{R}} + U\vec{\tau}) \cdot \delta \vec{R} dt = 0 . \quad (5.8)$$

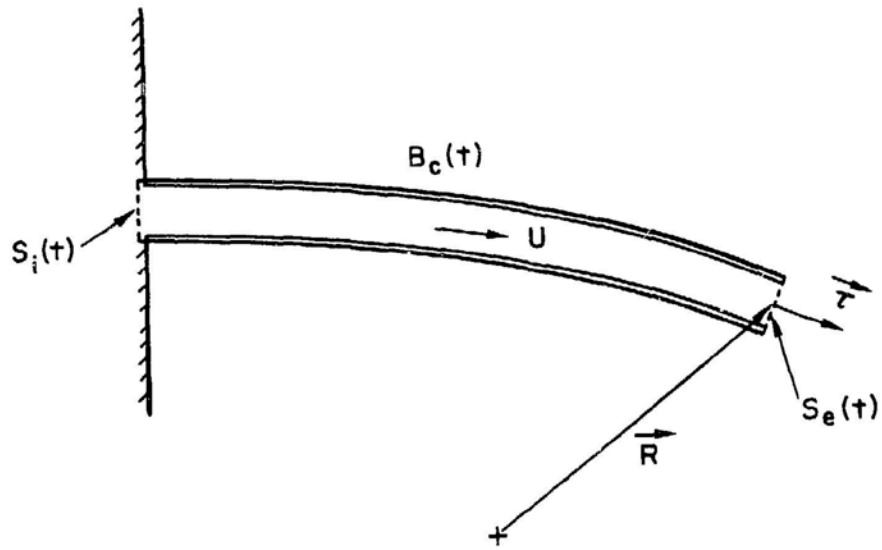


Fig. 5.2. A Cantilevered Pipe Conveying Fluid

Equation 5.8 is useful in deriving the equation of motion and boundary conditions for pipes conveying fluid and characterization of different systems and their stability characteristics.

Equation 5.8 is the same as that developed by Benjamin (1961) for a cantilevered pipe conveying fluid. However, it is different from the one applied by Housner (1952), who studied a pipe hinged at both ends, using Eq. 5.2. For a pipe not allowed to move at both ends, such as a hinged-hinged pipe, the last term in Eq. 5.8 is zero. Therefore, the conventional Hamilton's principle, Eq. 5.2, can be successfully applied.

5.3 STRAIGHT PIPES CONVEYING FLUID

5.3.1 Equations of Motion

The equation of motion is derived based on the following assumptions:

- Fluid is inviscid and incompressible.
- All motions are small.
- Rotary inertia and shear deformation of the pipe are neglected.
- The gravity and material damping are neglected.

Consider a pipe of length l , mass per unit length m , and flexural rigidity EI , conveying fluid of mass per unit length M_d and flowing axially at velocity U . The pipe axis is in the z direction and its displacement is u . The equation of motion can be derived based on the Hamilton's principle (Eq. 5.8) or equilibrium method.

The Lagrangian is given by

$$\mathcal{L} = T_s + T_f - V_s - V_f . \quad (5.9)$$

here T_s and V_s are the kinetic and potential energies associated with the pipe, and T_f and V_f are the corresponding quantities for the fluid. The potential and kinetic energies for the pipes are

$$V_s = \frac{1}{2} EI \int_0^l (u'')^2 dz \quad \text{and} \quad (5.10)$$

$$T_s = \frac{1}{2} m \int_0^l (\dot{u})^2 dz ,$$

where the prime denotes differentiation with respect to z and the dot denotes

differentiation with respect to time. Since the fluid is assumed to be incompressible, the potential energy of the fluid is zero; i.e.,

$$V_f = 0 . \quad (5.11)$$

Next, consider fluid flow kinetics. An element dz of the pipe in the deformed condition is shown in Fig. 5.3. The pipe is assumed to be inextensible. Let \vec{e}_y and \vec{e}_z be the unit vectors in the y and z direction. The flow velocity \vec{U} is

$$\begin{aligned} \vec{U} &= \vec{e}_z \left[U \left(1 - \frac{1}{2} u'^2 \right) - \dot{C} \right] + \vec{e}_y (\dot{u} + Uu') \quad \text{and} \\ C &= \int_0^z \frac{1}{2} (u')^2 dz . \end{aligned} \quad (5.12)$$

Therefore,

$$T_f = \frac{1}{2} M_d \int_0^L (\dot{u}^2 + 2U\dot{u}u' + U^2 - 2\dot{C}U) dz . \quad (5.13)$$

The motion of the pipe at the downstream end depends on the support. Consider the case of a cantilevered pipe, in which the downstream end is free (see Fig. 5.2). The position vector \vec{R} and the unit vector \vec{t} tangential to the pipe are

$$\begin{aligned} \vec{R} &= -\vec{e}_z C_L + \vec{e}_y u_L , \\ \vec{t} &= \vec{e}_z + \vec{e}_y u'_L , \end{aligned} \quad (5.14)$$

where

$$C_L = C \Big|_{j=L} , \quad u_L = u \Big|_{z=L} , \quad u'_L = \frac{\partial u}{\partial z} \Big|_{z=L} .$$

Substituting Eqs. 5.9-5.14 into Eq. 5.8 yields

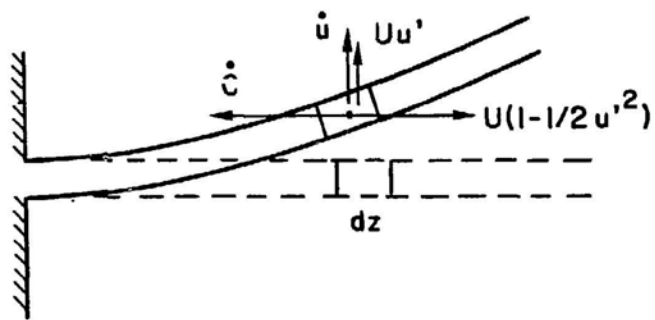


Fig. 5.3. A Pipe Conveying Fluid

$$\delta \int_{t_1}^{t_2} \int_0^l \left\{ \frac{1}{2} (M_d + m) \dot{u}^2 + M_d U (\dot{u} u' + \frac{1}{2} U u'^2 - \dot{C}) - \frac{1}{2} E I u''^2 \right\} dz dt - \int_{t_1}^{t_2} M_d U (\dot{u}_l + U u'_l) \delta u_l dt = 0 . \quad (5.15)$$

From Eq. 5.15, we obtain

$$\begin{aligned} E I \frac{\partial^4 u}{\partial z^4} + M_d U^2 \frac{\partial^2 u}{\partial z^2} + 2 M_d U \frac{\partial^2 u}{\partial z \partial t} + (M_d + m) \frac{\partial^2 u}{\partial t^2} &= 0 , \\ E I \frac{\partial^3 u}{\partial z^3} \delta u \Big|_0^l &= 0 , \quad \text{and} \\ E I \frac{\partial^2 u}{\partial z^2} \delta u' \Big|_0^l &= 0 . \end{aligned} \quad (5.16)$$

Therefore, the equations of motion and boundary conditions for cantilevered pipes are

$$\begin{aligned} E I \frac{\partial^4 u}{\partial z^4} + M_d U^2 \frac{\partial^2 u}{\partial z^2} + 2 M_d U \frac{\partial^2 u}{\partial z \partial t} + (M_d + m) \frac{\partial^2 u}{\partial t^2} &= 0 , \\ z = 0 , \quad u = 0 , \quad u' = 0 , \\ z = l , \quad u'' = 0 , \quad u''' = 0 . \end{aligned} \quad (5.17)$$

Similarly, consider the case of a pipe, in which the downstream end is allowed to move only in the z direction:

$$\begin{aligned} \vec{R} &= -\vec{e}_z C_l \quad \text{and} \\ \vec{r} &= \vec{e}_z + \vec{e}_y u'_l \end{aligned} \quad (5.18)$$

Substituting Eqs. 5.9-5.13, and 5.18 into 5.8 gives

$$EI \frac{\partial^4 u}{\partial z^4} + M_d U^2 \frac{\partial^2 u}{\partial z^2} + 2M_d U \frac{\partial^2 u}{\partial z \partial t} + (M_d + m) \frac{\partial^2 u}{\partial t^2} = 0 ,$$

$$\left\{ M_d U (\dot{u} + Uu') + EIu'''' \right\} \delta y \Big|_0^{\ell} = 0 , \quad \text{and} \quad (5.19)$$

$$EIu'' \delta u' \Big|_0^{\ell} = 0 .$$

Therefore the boundary conditions are as follows:

Hinged-hinged pipes:

$$z = 0 \text{ and } \ell , \quad u = 0 , \quad u'' = 0 . \quad (5.20)$$

Fixed-fixed pipes:

$$z = 0 \text{ and } \ell , \quad u = 0 , \quad u' = 0 . \quad (5.21)$$

Fixed-hinged pipes:

$$\begin{aligned} z = 0 , \quad u = 0 , \quad u' = 0 , \\ z = \ell , \quad u = 0 , \quad u'' = 0 . \end{aligned} \quad (5.22)$$

If the downstream end is not allowed to move axially, the cross-sectional area is reduced by a factor of $(1 - \frac{1}{2} u'^2)$ to maintain the fluid volume and the fluid velocity relative to the pipe increases to $U(1 + \frac{1}{2} u'^2)$ to maintain locally the rate of mass flow. The fluid kinetic energy in this case is

$$T_f = \frac{1}{2} M_d \int_0^{\ell} [(\dot{u} + Uu')^2 + U^2] dz . \quad (5.23)$$

Based on Eq. 5.23 and \dot{R} being zero at the downstream end, the same set of equations of motion and boundary conditions are obtained for fixed-fixed, fixed-hinged, and hinged-hinged pipes.

The equation of motion can also be derived using the equilibrium method (Gregory and Paidoussis 1966; Paidoussis 1970; Paidoussis and Issid 1974). Consider the specific case of a pipe hanging vertically, so that the z axis is in the direction of the gravity (Fig. 5.4). Without loss of generality, the motion of the pipe is assumed to take place in the x - z plane. The cross-sectional flow area is A and the fluid pressure is p . The flow velocity is a function of time.

Consider elements δz of the pipe and the enclosed fluid, subjected to a small lateral motion $u(z,t)$, as shown in Fig. 5.4. The acceleration of a fluid particle in the x and z directions are $M_d \frac{\partial u}{\partial t}$ and $[(\frac{\partial}{\partial t} + U \frac{\partial}{\partial z})^2]u$ to the first order in the small displacement u and its derivatives. For the fluid element, force balances in the x and z direction yield

$$A \frac{\partial p}{\partial z} + qS - M_d g - F \frac{\partial u}{\partial z} = 0 \quad \text{and} \quad (5.24)$$

$$F + M_d \left(\frac{\partial}{\partial t} + U \frac{\partial}{\partial z} \right)^2 u + A \frac{\partial}{\partial z} \left(p \frac{\partial u}{\partial z} \right) + qS \frac{\partial u}{\partial z} = 0 , \quad (5.25)$$

where q is the shear stress on the internal surface of the pipe and F is the transverse force per unit length between pipe wall and fluid.

Similarly, for the pipe element,

$$\frac{\partial T}{\partial z} + qS - mg - F \frac{\partial u}{\partial z} = 0 , \quad (5.26)$$

$$\frac{\partial Q}{\partial z} + F - m \frac{\partial^2 u}{\partial t^2} + \frac{\partial}{\partial z} \left(T \frac{\partial u}{\partial z} \right) + qS \frac{\partial u}{\partial z} = 0 , \quad \text{and} \quad (5.27)$$

$$Q = - \frac{\partial M}{\partial z} = -EI \frac{\partial^3 u}{\partial z^3} , \quad (5.28)$$

where T is the longitudinal tension, Q is the transverse shear force in the pipe and M is the bending moment. Using Eqs. 5.25, 5.27, and 5.28 yields

$$EI \frac{\partial^4 u}{\partial z^4} + \frac{\partial}{\partial z} \left[(pA - T) \frac{\partial u}{\partial z} \right] + M \left(\frac{\partial}{\partial t} + U \frac{\partial}{\partial z} \right)^2 u + m \frac{\partial^2 u}{\partial t^2} = 0 . \quad (5.29)$$

Using Eqs. 5.24 and 5.26 gives

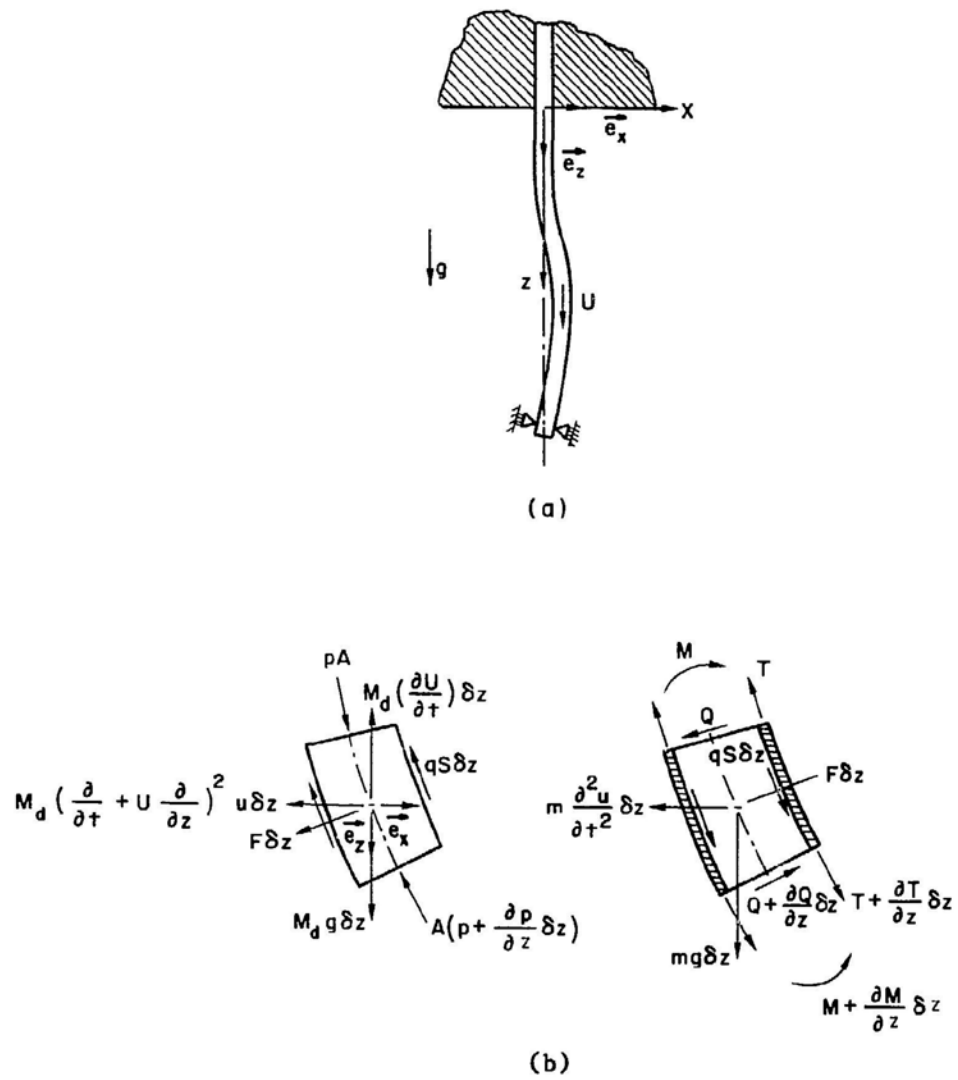


Fig. 5.4. (a) A Vertical Pipe Conveying Fluid and (b) Forces and Moments Acting on Elements of the Fluid and Pipe

$$\frac{\partial}{\partial z} (T - pA) + (M_d + m)g = M_d \frac{\partial U}{\partial t} . \quad (5.30)$$

Integrating Eq. 5.30 from z to l gives

$$(T - pA) = (T - pA) \Big|_{z=l} + [(M_d + m)g - M \frac{\partial u}{\partial t}](l - z) . \quad (5.31)$$

If the pipe is horizontal, and flow velocity is a constant, $(T - pA)$ will be equal to that at the downstream end. Furthermore, if the fluid pressure and axial tension are zero at the downstream end, Eq. 5.29 will be reduced to Eq. 5.17.

The system response characteristics depend on the support condition. Without loss of generality, it is assumed that the upstream end is not allowed to move axially or transversely. Physically, this means that the flow getting into the pipe does not vary with the pipe motion; i.e., the fluid energy supply to the pipe is at a constant rate. Depending on the downstream end condition, all pipes can be divided into two groups.

- Nonconservative Systems - If the energy loss at the exit is not equal to the energy gain at the inlet, the system is a nonconservative system.
- Gyroscopic Conservative Systems - If the energy loss at the exit is equal to the energy gain at the inlet, it is a gyroscopic conservative system. (It is called gyroscopic because of the existence of the Coriolis force, which is discussed in Sec. 5.3.3.3).

Figure 5.5 shows typical examples of the two groups. In the nonconservative systems, the free end is allowed to move and rotate; therefore, the flow velocity at the outlet is not necessarily the same as U . However, in the gyroscopic conservative systems, the downstream end is constrained in the transverse direction. Therefore, the flow velocity at the exit is always equal to U .

5.3.2 Free Vibration and Stability Analysis

It is more convenient to use dimensionless terms by introducing the following quantities:

$$w = u/l ,$$

$$\xi = z/l , \quad (5.32)$$

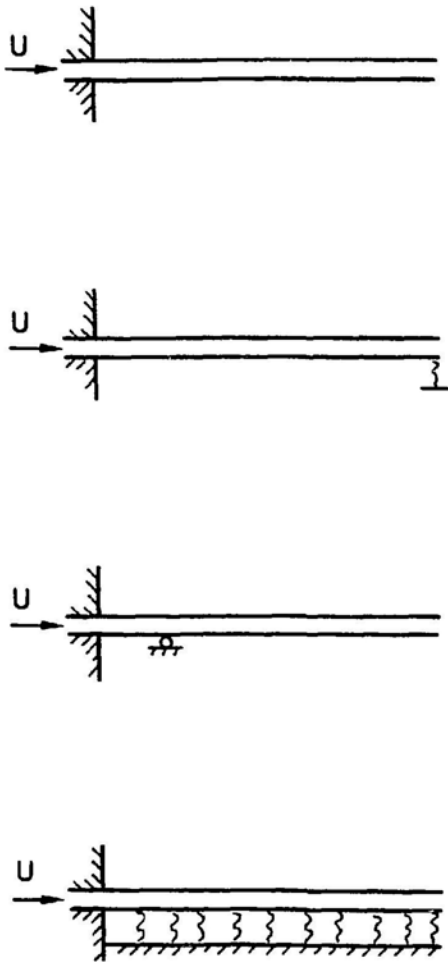
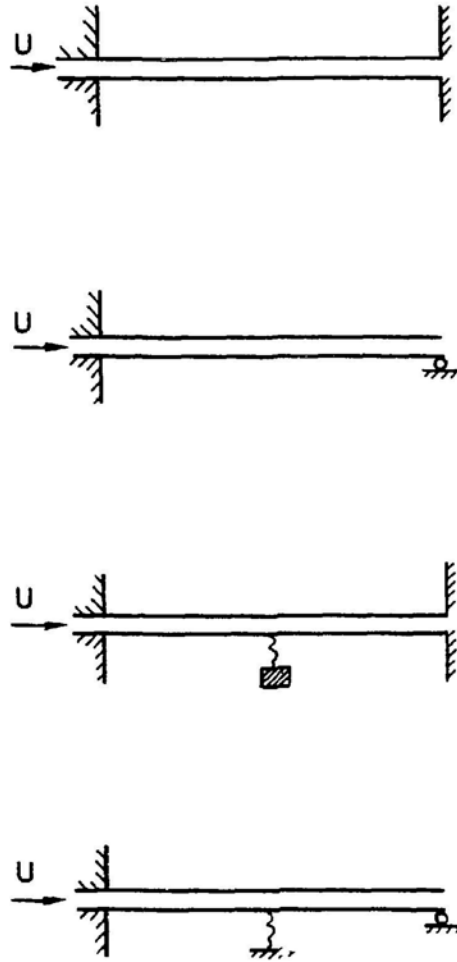
(a) NONCONSERVATIVE
SYSTEMS(b) GYROSCOPIC CONSERVATIVE
SYSTEMS

Fig. 5.5. Nonconservative and Gyroscopic Conservative Systems

$$\beta = \frac{M_d}{m + M_d} ,$$

$$v = \left(\frac{M_d}{EI} \right)^{0.5} U l , \quad \text{and} \quad (5.32)$$

$$\tau = \left(\frac{EI}{m + M_d} \right)^{0.5} \frac{t}{l^2} . \quad (\text{Contd.})$$

Using Eq. 5.32, Eqs. 5.17 become

$$\frac{\partial^4 w}{\partial \xi^4} + v^2 \frac{\partial^2 w}{\partial \xi^2} + 2\beta^{0.5} v \frac{\partial^2 w}{\partial \xi \partial \tau} + \frac{\partial^2 w}{\partial \tau^2} = 0 ,$$

$$\xi = 0 , \quad w = 0 , \quad w' = 0 , \quad (5.33)$$

$$\xi = 1 , \quad w'' = 0 , \quad w''' = 0 .$$

Equations 5.33 describe the motion for a cantilevered pipe. Pipes with other end conditions can be similarly nondimensionalized.

Many different techniques have been used to analyze the pipe system. Those different technique can be divided into two groups: exact solution and approximate solution. Either can be applied to a nonconservative or gyroscopic system.

First, consider the exact solution. Let

$$w(\xi, \tau) = \phi(\xi) \exp(i\Omega\tau) . \quad (5.34)$$

Ω is the dimensionless frequency of oscillation of the pipe. Substituting Eq. 5.34 into 5.33 yields

$$\frac{d^4 \phi}{d\xi^4} + v^2 \frac{d^2 \phi}{d\xi^2} + i2\beta^{0.5} v \Omega \frac{d\phi}{d\xi} - \Omega^2 \phi = 0 . \quad (5.35)$$

Let

$$\phi(\xi) = \sum_{j=1}^4 C_j \exp(i\lambda_j \xi) , \quad (5.36)$$

where λ_j 's are solution of the following equation:

$$\lambda^4 - v^2 \lambda^2 - 2\beta^{0.5} v \Omega \lambda - \Omega^2 = 0 . \quad (5.37)$$

Substituting Eq. 5.36 into the boundary conditions in 5.33 yields a set of simultaneous equations to determine the constants C_j ($j = 1$ to 4). These equations can be written

$$[a_{jk}] \{C_k\} = \{0\} , \quad j, k = 1 \text{ to } 4 . \quad (5.38)$$

The element a_{jk} 's are given in Table 5.1 for four boundary conditions.

Setting the determinant of coefficients in Eq. 5.38 equal to zero gives the frequency equation. The frequency depends on the system parameters, β , and v ; therefore, the frequency equation can be written

$$F(\Omega, \beta, v) = 0 . \quad (5.39)$$

Natural frequencies and mode shapes can be calculated numerically using Eq. 5.38, Table 5.1, and Eq. 5.39 for various boundary conditions.

Alternatively, an approximate solution can be obtained. Let

$$w(\xi, \tau) = \sum_{n=1}^{\infty} q_n(\tau) \phi_n(\xi) , \quad (5.40)$$

where the $q_n(\tau)$ are unknown time-dependent functions and $\phi_n(\xi)$ are space-dependent functions forming a complete set. The $\phi_n(\xi)$ are chosen as mode-shape functions of the free vibrations at zero flow velocity; more precisely, they are the eigenfunctions of the system of Eq. 5.33, neglecting the flow-velocity dependent terms,

$$\frac{\partial^4 w}{\partial \xi^4} + \frac{\partial^2 w}{\partial \tau^2} = 0 . \quad (5.41)$$

Table 5.1. Boundary Conditions and Elements a_{jk} 's

		End Conditions			
		Fixed-Fixed	Fixed-Hinged	Hinged-Hinged	Fixed-Free
Boundary Conditions	$\xi = 0$	$w = 0$	$w = 0$	$w = 0$	$w = 0$
		$\frac{\partial w}{\partial \xi} = 0$	$\frac{\partial w}{\partial \xi} = 0$	$\frac{\partial^2 w}{\partial \xi^2} = 0$	$\frac{\partial w}{\partial \xi} = 0$
	$\xi = 1$	$w = 0$	$w = 0$	$w = 0$	$\frac{\partial^2 w}{\partial \xi^2} = 0$
		$\frac{\partial w}{\partial \xi} = 0$	$\frac{\partial^2 w}{\partial \xi^2} = 0$	$\frac{\partial^2 w}{\partial \xi^2} = 0$	$\frac{\partial^3 w}{\partial \xi^3} = 0$
Elements a_{jk}	a_{1k}	1	1	1	1
	a_{2k}	λ_k	λ_k	λ_k	λ_k
	a_{3k}	$\exp(i\lambda_k)$	$\exp(i\lambda_k)$	$\exp(i\lambda_k)$	$\lambda_k^2 \exp(i\lambda_k)$
	a_{4k}	$\lambda_k \exp(i\lambda_k)$	$\lambda_k^2 \exp(i\lambda_k)$	$\lambda_k^2 \exp(i\lambda_k)$	$\lambda_k^3 \exp(i\lambda_k)$

It can be shown that Eq. 5.41 and any sets of boundary conditions given in Table 5.1 are self-adjoint. Such a system has a complete set of real orthogonal eigenfunctions. The eigenfunctions and natural frequencies can be obtained by conventional methods.

Having an orthonormal set of functions, the orthogonality condition is used to obtain the function q_n . On substituting Eq. 5.40 into 5.33, multiplying through by ϕ_n , and integrating over $0 \leq \xi \leq 1$, we find that

$$\ddot{q}_n + \varepsilon \sum_m a_{nm} \dot{q}_m + v^2 \sum_m b_{nm} q_m + \Omega_n^2 q_n = 0 ,$$

$$\varepsilon = 2\beta^{0.5} v ,$$
(5.42)

$$a_{nm} = \int_0^1 \phi_n \frac{d\phi_m}{d\xi} d\xi , \quad \text{and}$$

$$b_{nm} = \int_0^1 \phi_n \frac{d^2\phi_m}{d\xi^2} d\xi .$$

Let

$$q_n = \bar{q}_n \exp(i\Omega\tau) .$$
(5.43)

Substitution of Eq. 5.43 into Eq. 5.42 leads to the algebraic equations

$$(\Omega_n^2 - \Omega^2) \bar{q}_n + i\varepsilon\Omega \sum_m a_{nm} \bar{q}_m + v^2 \sum_m b_{nm} \bar{q}_m = 0 ,$$

$$m, n = 1, 2, \dots, \infty .$$
(5.44)

Natural frequencies can be calculated from the following equation:

$$|(\Omega_n^2 - \Omega^2) \delta_{nm} + i\varepsilon\Omega a_{nm} + v^2 b_{nm}| = 0 .$$
(5.45)

Calculations of the frequency from Eq. 5.39 or 5.45 are relatively easy.

Because of the existence of the mixed derivative term, the system possesses several interesting characteristics. Other techniques have also been used to analyze the problem; see Li and DiMaggio (1964), Jones and Goodwin (1971), Mote (1971), Kornecki (1971).

5.3.3 Frequency Characteristics

The frequency characteristics of the pipes vary with support conditions, mass ratio β , and flow velocity v . However, it is the support condition that determines the major characteristics.

5.3.3.1 Gyroscopic Conservative System

Figure 5.6 shows the real and imaginary parts of the dimensionless frequency Ω_n of the lowest three modes of a fixed-fixed pipe ($\beta = 0.1$) as functions of v (Paidoussis 1975). For $v = 0$, the Ω are real and equal to the dimensionless natural frequencies of a fixed-fixed beam, namely $\Omega = 22.373, 61.673, 120.903, \dots$. As the flow velocity increases, the real part of Ω decreases with v and the imaginary part is zero. As the flow increases to 2π , the first-mode frequency vanishes altogether; this corresponds to the divergence of the pipe. Beyond the critical point of $v = 2\pi$, the first-mode frequency becomes wholly imaginary. If the flow velocity is increased further, divergence in the second mode occurs at $v \sim 8.99$. However, at a slightly higher flow velocity, the frequencies of the first and second modes coalesce and the frequencies become complex conjugates. This indicates the onset of coupled-mode flutter.

In Fig. 5.6 the threshold of coupled mode flutter is associated with $\text{Re}(\Omega) = 0$. For higher β , however, this is not the case, as shown in Fig. 5.7, where the onset of coupled-mode flutter is preceded by a region of stability ($8.99 < v < 9.61$). In this case the critical flow velocity, $v = 8.99$, no longer corresponds to divergence associated with the second mode, but rather to the point where the system regains stability in its first mode. As the flow velocity is increased further, the system is briefly restabilized, and is subsequently subject to divergence once again, at $v = 4\pi$, followed by coupled-mode flutter involving the third mode at $v = 13.1$.

The results given in Figs. 5.6 and 5.7 are for a pipe fixed at both ends, but similar results are obtained for other gyroscopic conservative systems. The general characteristics can be summarized as follows:

- For flow velocity less than the first divergence flow velocity, the imaginary part of Ω is zero; i.e., the fluid flow does not contribute to damping. As the flow velocity increases, the real part of Ω_n decreases with flow.
- The pipe loses stability first by divergence. It is the same as that of a pipe subjected to an axial compression of magnitude v^2 . Because the

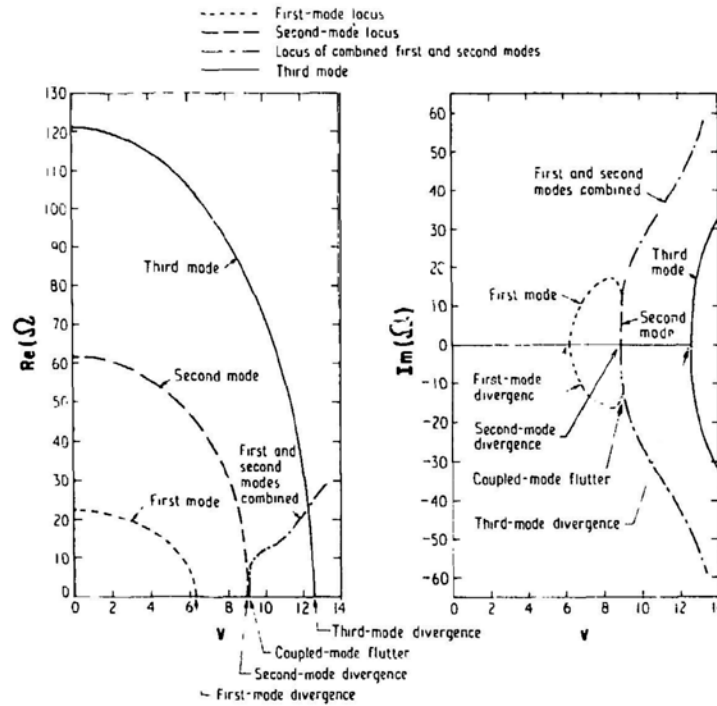


Fig. 5.6. Real and Imaginary Components of Dimensionless Frequency Ω as Functions of Dimensionless Flow Velocity v for the Lowest Three Modes of a Pipe with $\beta = 0.1$ (from Paidoussis 1975, with permission--see Credits)

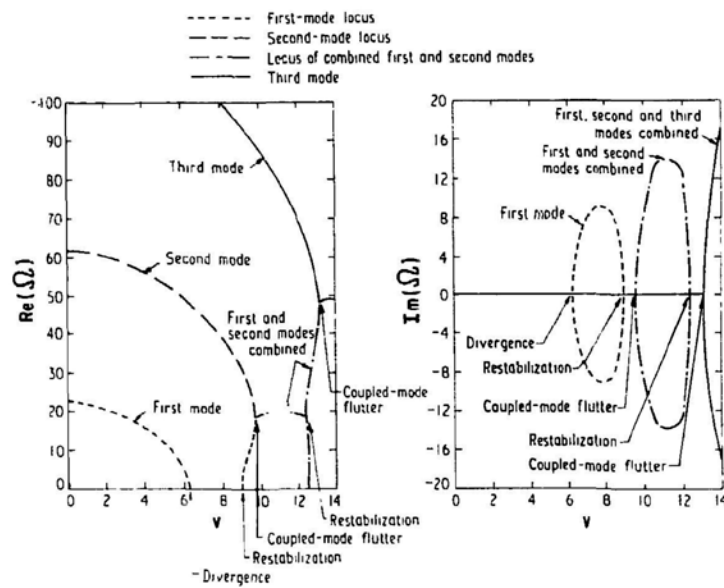


Fig. 5.7. Real and Imaginary Components of Dimensionless Frequency Ω as Functions of the Dimensionless Flow Velocity v for the Lowest Three Modes of a Pipe with $\beta = 0.8$ (from Paidoussis 1975, with permission--see Credits)

divergence is a static phenomenon, the critical flow velocity for divergence is independent of β .

- For small values of β , the system buckles in both the first and second modes before the onset of flutter. For large values of β , the system does not buckle in the second mode prior to the onset of flutter.

Based on the linear theory, a gyroscopic conservative system may be subjected to coupled-mode flutter for flow velocity higher than the lowest divergence flow velocity. This is probably of academic interest only. Once the pipe buckles, relatively large deformations occur and the nonlinear terms become more important. In fact, the nonlinear theory shows that a pipe supported at both ends cannot flutter (Holmes 1978).

5.3.3.2 Nonconservative System

Figures 5.8 and 5.9 show the dimensionless complex frequency of a pipe fixed at the upstream end and at the other supported by a spring whose constant is k_s ($\bar{\alpha} = k_s l^3/EI$) (Chen 1971a). All roots of the frequency equation are located in the upper half of the complex plane when v is small, and the system performs damped oscillation in all modes. The effects of the flowing fluid are to reduce the natural frequencies and to contribute to damping. As the flow velocity increases, the imaginary part of Ω becomes negative, and the system loses stability by buckling for $\text{Re}(\Omega) = 0$ and by flutter for $\text{Re}(\Omega) \neq 0$.

In the case of $\bar{\alpha} = 10$ and $\beta = 0.2$ (Fig. 5.8), for increasing v , the locus of the first mode bifurcates on the $\text{Im}(\Omega)$ -axis. It approaches the origin on the $\text{Im}(\Omega)$ -axis, but then moves away from it without crossing to the unstable region; accordingly, buckling-type instability does not occur in this case. The second-mode locus crosses to the lower half of the complex plane at $v \approx 6.27$; it corresponds to the flutter-type instability.

Consider Fig. 5.9, where $\bar{\alpha} = 100$ and $\beta = 0.6$. One branch of the first-mode locus crosses the origin at $v \approx 4.7$, which is the threshold for the buckling-type instability. With increasing flow velocity, the negative branch of the first-mode locus eventually becomes positive at $v \approx 7.2$; thus, the pipe regains stability. But at still higher flow velocity, the pipe stability is lost again, the instability this time being a flutter mode. The locus of the second mode is very similar to that of the first mode, but its locus on the imaginary axis does not cross the origin. The buckling-type instability is impossible in the second mode. Although there is no buckling instability, the second mode also loses stability by flutter as the flow velocity increases. The third and fourth modes are always stable for the low-velocity ranges investigated. Although they might lose stability at higher velocities, those velocities will be higher than those associated with the lower modes and therefore do not have practical significance.

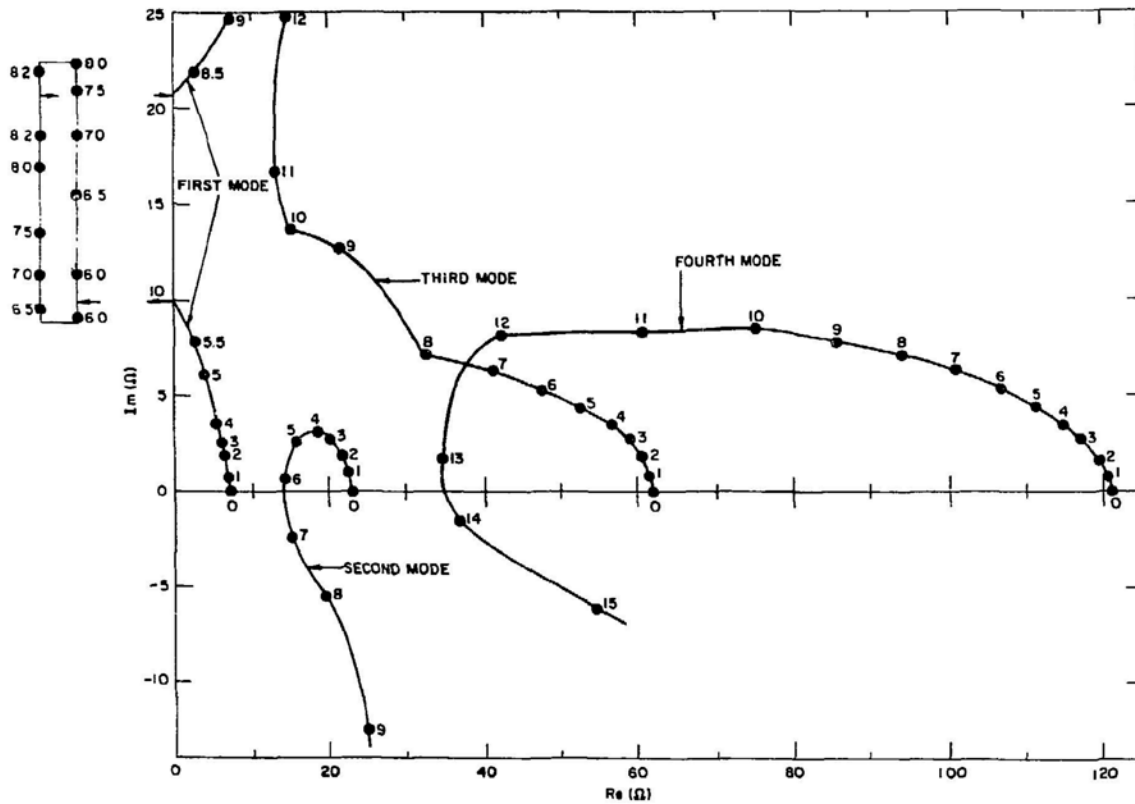


Fig. 5.8. Dimensionless Complex Frequency of a Pipe Fixed at the Upstream End and Supported by a Spring at the Downstream End for $\alpha = 10$, $\beta = 0.2$ (the dots represent dimensionless flow velocity) (Chen 1971a)

In contrast to gyroscopic conservative system, the pipe may lose stability by divergence or single-mode flutter, depending on the system parameters. The frequency is normally a complex number; at low flow velocity, the motion is damped.

5.3.3.3 The Role of the Coriolis Force

The two force components that dominate the response characteristics are the centrifugal force $M_d U^2 (\partial^2 u / \partial z^2)$ or $v^2 (\partial^2 w / \partial \xi^2)$ and the Coriolis force $2M_d U (\partial^2 u / \partial z \partial t)$ or $2\beta^{0.5} v (\partial^2 w / \partial \xi \partial \tau)$. The centrifugal force is the same as an axial compression for a gyroscopic conservative system and a compressive follower force for a nonconservative system. The centrifugal force can cause buckling-type instability in a conservative system, but can cause buckling and flutter types of instability in a nonconservative system. The role of the Coriolis force also depends on the support conditions. Consider the coefficient a_{nm} in Eq. 5.42:

$$\begin{aligned} a_{nm} + a_{mn} &= \int_0^1 \left(\phi_n \frac{d\phi_m}{d\xi} + \phi_m \frac{d\phi_n}{d\xi} \right) d\xi \\ &= \phi_n(1)\phi_m(1) + \phi_n(0)\phi_m(0). \end{aligned} \quad (5.46)$$

For any gyroscopic conservative system in which the pipe is not allowed to move transversely at the end, the right side of Eq. 5.46 vanishes; therefore

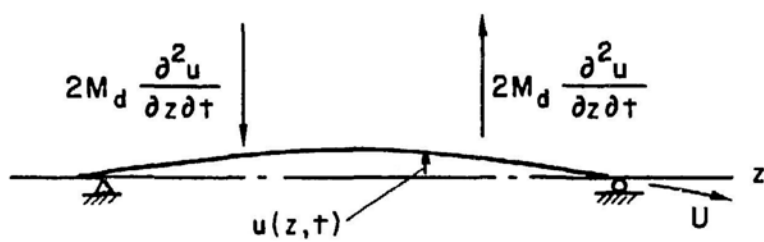
$$a_{nm} = -a_{mn}. \quad (5.47)$$

For a conservative system, the Coriolis force does not dissipate or supply any energy; i.e., it is not a resistant force or an energy source. However, for a nonconservative system,

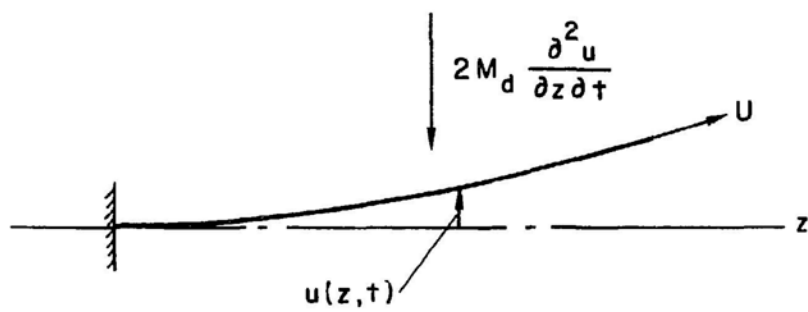
$$a_{nn} = \frac{1}{2} \phi_n^2(1), \quad (5.48)$$

a_{nn} is always positive. From Eq. 5.42, it is seen that the Coriolis force is a damping mechanism for a nonconservative system.

The role of the Coriolis force can also be understood by considering the two typical examples shown in Fig. 5.10--a conservative pipe and a non-conservative pipe. Figure 5.10a shows a pipe hinged at both ends conveying a fluid with a constant flow velocity U . At a particular instant, assume that its deflected shape $u(z, t)$ is symmetric with respect to the midspan. The Coriolis force acting on the pipe is antisymmetric with respect to the



(a)



(b)

Fig. 5.10. Coriolis Force for Gyroscopic Conservative and Nonconservative Systems

midspan. Therefore, the symmetric displacement $u(z,t)$ will result in antisymmetric Coriolis force. The total work done by the Coriolis force on the pipe from $z = 0$ to l is zero; the Coriolis force does not supply or dissipate any energy. However, the motions associated with the symmetric modes will produce the Coriolis force, which will induce the motion of antisymmetric modes. This is the reason that in pipes conveying fluid, there are no classical normal modes.

The role of the Coriolis force in a nonconservative system, such as a cantilevered pipe, is quite different. The pipe in Fig. 5.10b is assumed to deflect in the first mode. The Coriolis force is in the direction against the motion along the whole pipe. This tends to decay the oscillations. Therefore, the Coriolis force is a damping mechanism. This is the reason that at low flow velocity, all modes of a nonconservative pipe are damped.

Because of the Coriolis force, no simple harmonic free vibrations (classical normal modes) can occur. The natural vibration of a finite pipe can be regarded as standing waves produced by traveling waves of equal wavelength and amplitude, proceeding in opposite directions. Only when waves of equal length travel in opposite directions at the same velocity can such standing waves occur. The flowing fluid tends to accelerate the positive waves along the flow and retard the negative ones. Mathematically, this can be seen from Eq. 5.42, which can be written in matrix form:

$$[M]\{\ddot{Q}\} + [C]\{\dot{Q}\} + [K]\{Q\} = \{0\} . \quad (5.49)$$

The necessary and sufficient condition for the existence of a classical normal mode is that given in Eq. A.5. For pipes conveying fluid, this condition is not satisfied for $U \neq 0$. Therefore, no classical normal modes exist in pipes conveying fluid.

Figure 5.11 shows the variation of amplitudes of the fundamental mode and second mode for a pipe hinged at both ends at different flow velocities during a period of oscillation (Chen and Rosenberg 1971). At $v = 0$, various parts of the pipe pass through the equilibrium at the same instant of time; therefore, they belong to the classical normal modes. However, when $v \neq 0$, the Coriolis force causes distortion of the different modes.

5.3.4 Stability Boundaries

The frequencies calculated from Eq. 5.39 can be used to establish the stability boundaries. The critical flow velocity at which the pipe loses stability is designated by v_{cr} , and the corresponding frequency by Ω_{cr} .

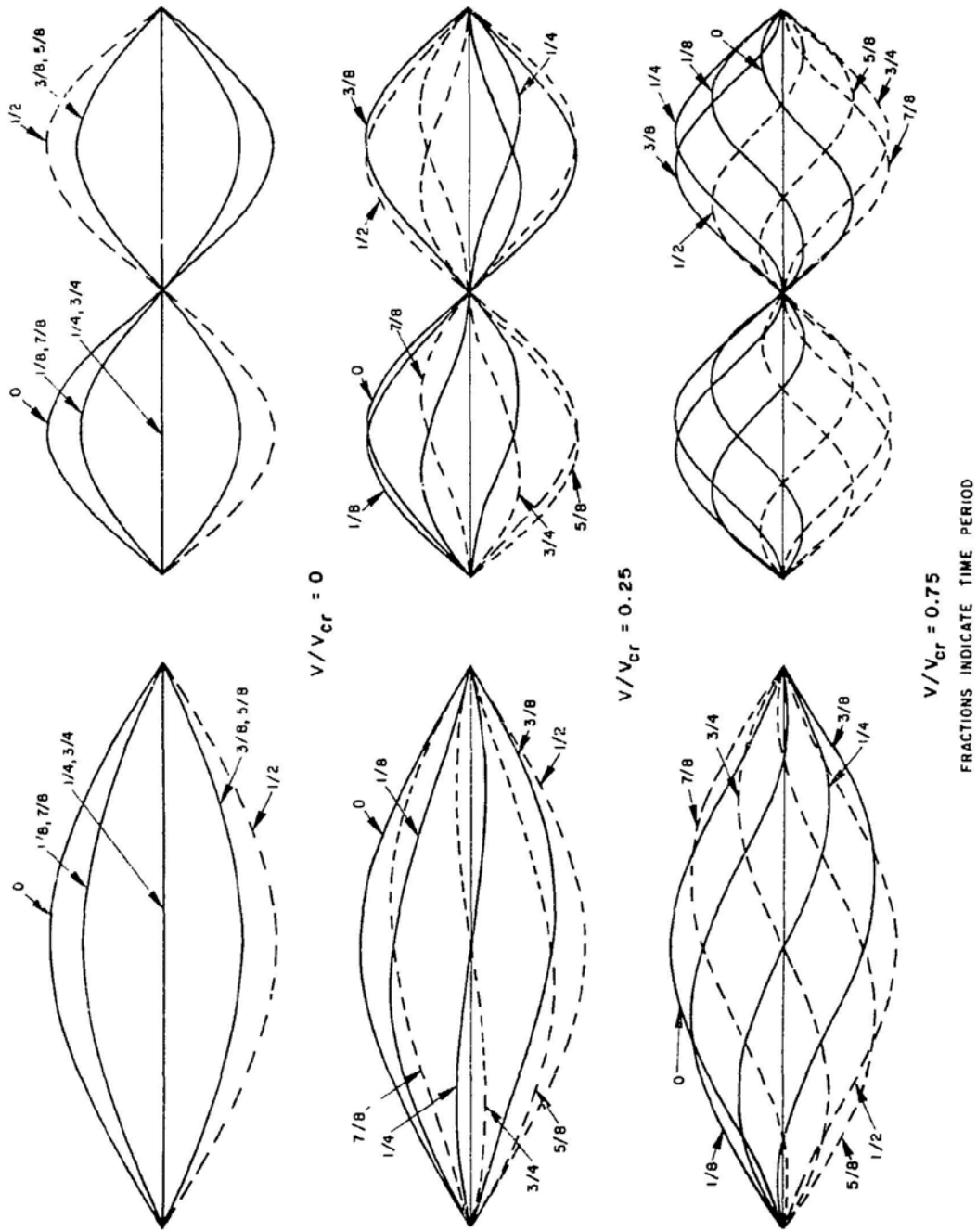


Fig. 5.11. Variation of Amplitudes of Fundamental and Second Modes during a Period of Oscillation
(Chen and Rosenberg 1971)

In a gyroscopic conservative system, the pipe loses stability by divergence; i.e., at the critical flow velocity $\Omega_{cr} = 0$. Divergence is a static phenomenon; therefore, the time-dependent terms do not affect the critical flow velocity. For example, Fig. 5.12 shows the frequency ratio Ω/Ω_0 (Ω_0 is Ω at zero flow velocity) as a function of v for a simply supported pipe for different β . The fundamental natural frequency varies with β , as do the frequencies of the higher modes. However, these frequencies for different β vanish at the same flow velocity; i.e., the critical flow velocity is independent of β . In this case the dimensionless critical flow velocity is equal to π , which corresponds to a pipe subjected to an axial compressive force of $\pi^2 EI/l^2$.

As long as the system is a gyroscopic conservative system, the critical flow velocity for divergence can be calculated rather easily. The method to determine the critical flow velocity is the same as that for divergence subjected to axial compressive force. The dimensionless critical flow velocities for different support conditions are:

Fixed-fixed pipes: 2π

Hinged-hinged pipes: π

Fixed-hinged pipes: $\frac{3}{2}\pi$

When the pipes have become unstable by divergence, the nonlinear effects associated with relatively large tube displacement become important. The linear theory is not expected to be applicable beyond the critical flow velocity associated with the divergence. Based on the nonlinear theory, it has been shown that a pipe in a gyroscopic conservative configuration cannot flutter. Although flutter can occur in other structures, such as plates and shells submerged in flow, the gyroscopic conservative system consisting of a pipe conveying fluid apparently does not lose stability by flutter.

In contrast to a gyroscopic conservative system, a nonconservative system may be subjected to flutter and/or divergence types of instability. Figures 5.13 and 5.14 show the critical flow velocities and the corresponding oscillation frequencies for a cantilevered pipe conveying fluid, a system in which stability is lost only by flutter. Rather irregular behavior of the v_{cr} and Ω_{cr} curves is noted in the vicinity of $\beta = 0.3, 0.6$, and 0.9 . Further increases in flow velocity cause the pipe to regain stability and to become stable again. The real component of frequency is shown in Fig. 5.14 for parameters that produce neutral stability. The real part of the frequency does not go to zero at the onset of instability, as for divergence of a gyroscopic conservative pipe. The cantilevered pipe does not buckle if the flow velocity exceeds a critical value, as in the case of the hinged-hinged pipe. Instead, the pipe oscillates violently, as shown in Fig. 5.15 for one cycle of oscillation. Note that the pipe becomes unstable in the second mode and the free end of the pipe slopes backward to the direction of motion for

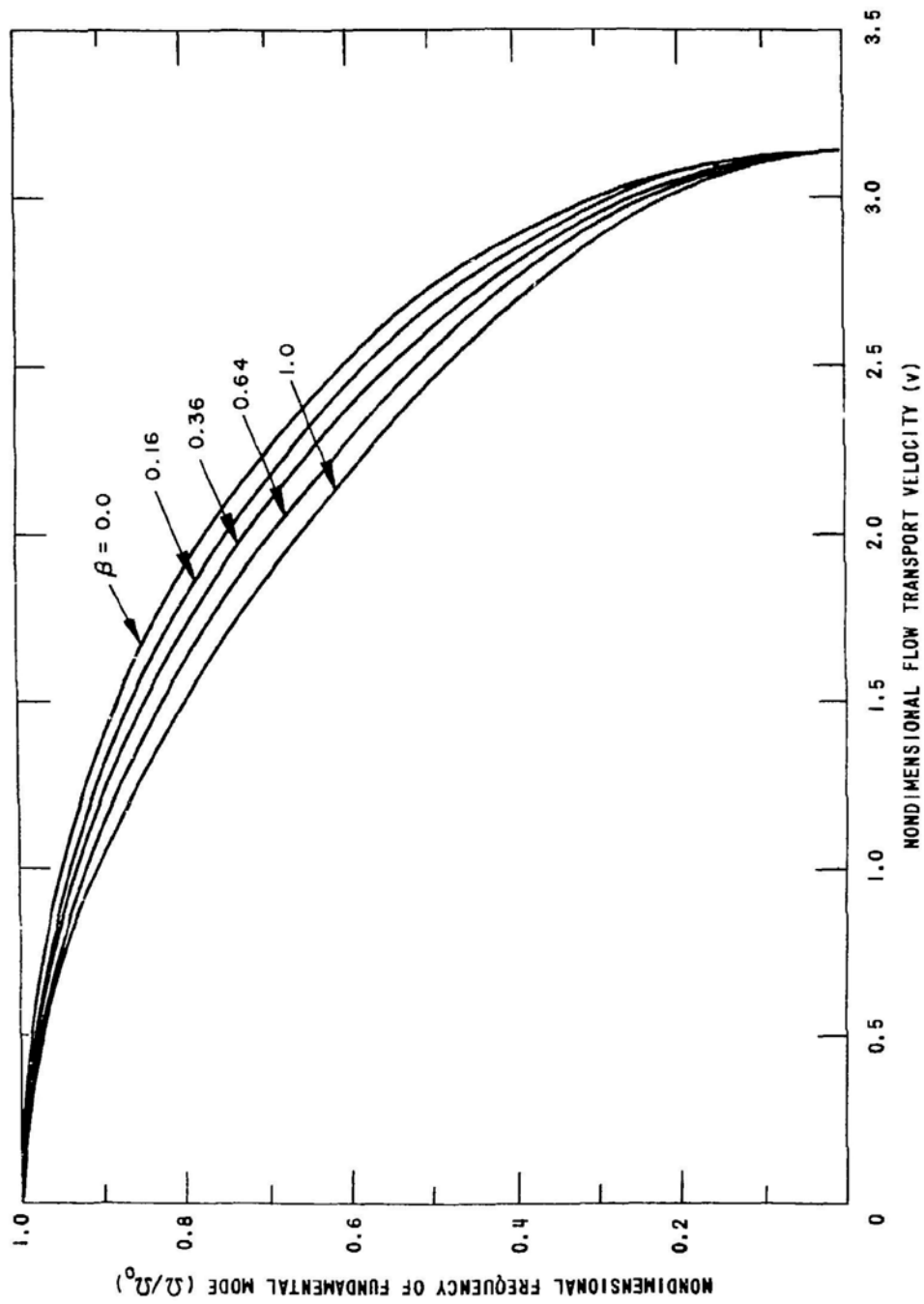


Fig. 5.12. Fundamental Natural Frequency vs. Nondimensional Flow Velocity (Chen and Rosenberg 1971)

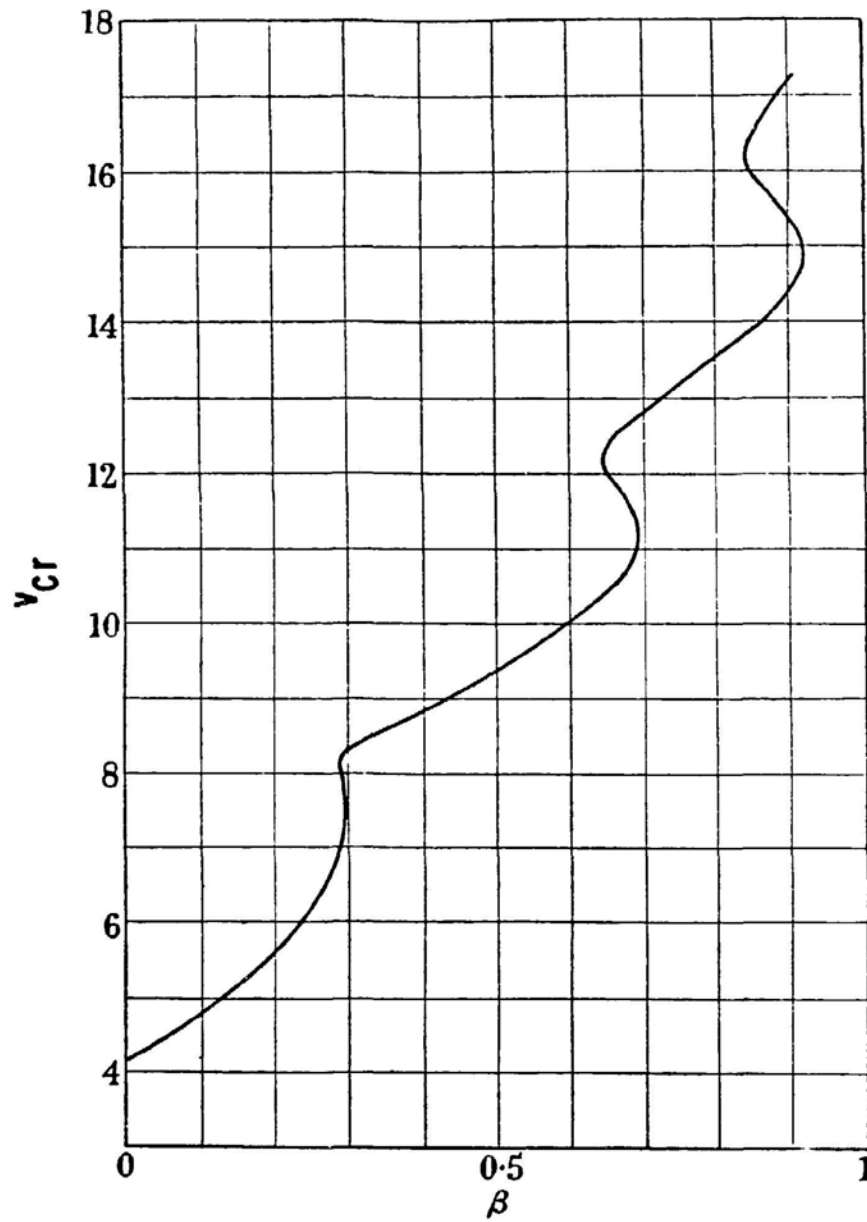


Fig. 5.13. Dimensionless Critical Flow Velocity as a Function of β for a Cantilevered Pipe (from Gregory and Paidoussis 1966, with permission--see Credits)

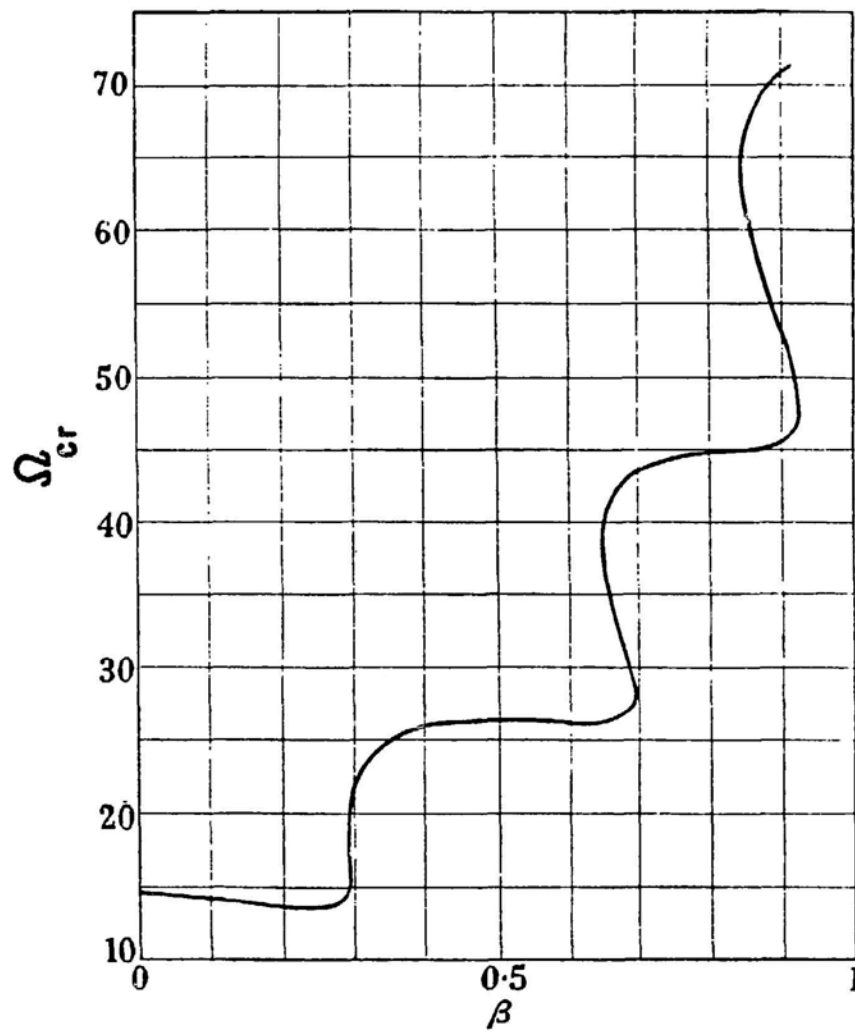


Fig. 5.14. Dimensionless Critical Frequency as a Function of β for a Cantilevered Pipe (from Gregory and Paidoussis 1966, with permission--see Credits)

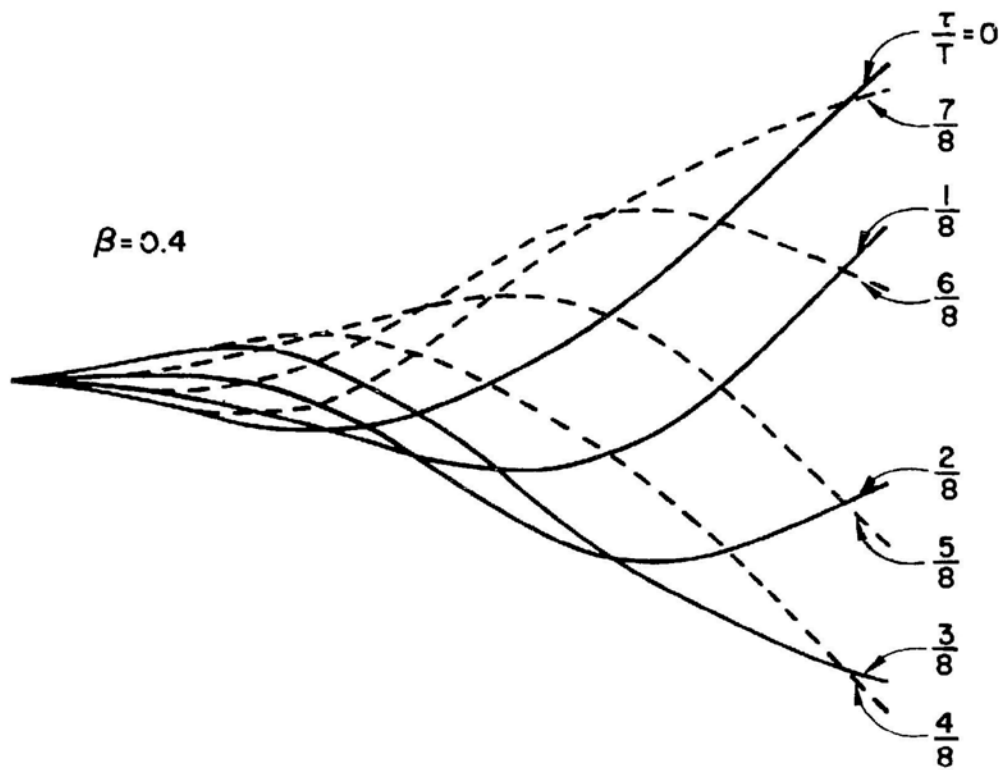


Fig. 5.15. Mode Shape for Flutter of a Cantilevered Pipe for $\beta = 0.4$
(fractions indicate time period) (Chen 1971a)

the greater part of the cycle. This "dragging" motion can be interpreted using the energy transfer between the pipe and flow. Based on Eq. 5.8, the energy gained by the pipe is

$$\Delta W = \int_{t_1}^{t_2} -M_d U (\dot{\vec{R}}^2 + \dot{\vec{U}}_T \cdot \dot{\vec{R}}) dt . \quad (5.50)$$

If the system is to excite vibrations of constant amplitude about equilibrium, the average energy transfer to the pipes must be zero, so the quantity given by Eq. 5.50 must vanish when the integration extends over one cycle. When U is small, Eq. 5.50 shows that vibrations about stable equilibrium are always damped, since the first term in the integrand predominates and therefore makes ΔW negative. The first term is always negative, but amplified vibrations ($\Delta W > 0$) are possible when U is large, provided $\dot{\vec{U}}_T$ and $\dot{\vec{R}}$ are sufficiently out of phase that $\dot{\vec{U}}_T \cdot \dot{\vec{R}}$ has a negative value. This is why the pipe must slope backward.

5.3.5 Effects of Various Parameters

5.3.5.1 Fluid Pressure

The pressure term $\frac{\partial}{\partial z} (pA \frac{\partial u}{\partial z})$ in Eq. 5.29 arises because the radial component of the pressure is acting over a larger area on the tensile side of the neutral axis than on the compressive side (Naguleswaran and Williams 1968; Stein and Tobriner 1970). If the pipe ends are closed, and the hydrostatic pressure is thereby transmitted to the pipe, then the two pressure terms would exactly cancel one another and there would be no net effect of internal pressure. However, in the case of pipes conveying fluid, the ends are open; the action of the pressure term on the pipe is equivalent to an axial compressive load of magnitude pA . The presence of the pressure term affects appreciably the natural frequency of a pipe and its effect is the same order of magnitude as that due to flow.

5.3.5.2 Gravity

The effect of fluid gravity on pipe vibration can be analyzed using Eqs. 5.29 and 5.31. The combined effects of gravity and flow are different for different support conditions. Its effect on the cantilevered pipe is of particular interest (Paidoussis 1970).

- Hanging cantilevers - Gravity does not affect the fundamental instability mechanism of flutter. Divergence-type instability is not possible even with the effect of gravity.

- Standing cantilevers - A standing cantilever, if it is long enough, can become unstable by buckling under its own weight. Therefore, a standing

cantilevered pipe conveying fluid may be subjected to buckling in addition to flutter-type instability. The lowest critical flow velocity may be associated with flutter or divergence, depending on the system parameters.

In the gyroscopic conservative system, the gravity force is not expected to change the fundamental stability characteristics. Therefore, flutter-type instability is not expected to be associated with the lowest critical flow velocity.

5.3.5.3 Damping Forces

In the course of pipe motion, energy will be dissipated by friction between the pipe and the surrounding fluid medium, by internal friction within the material of the tube and by the friction at the supports. In general, these dissipation effects can be accounted for adding the viscous damping term $C_s \frac{\partial u}{\partial t}$ or structural damping term $\mu_s EI (\partial^5 u / \partial t \partial z^4)$ added to the equation of motion. The analysis of the equation of motion including these additional terms remained the same.

The effects of those dissipation forces on nonconservative systems are complex; they may stabilize the pipe or destabilize it (Paidoussis 1970; Gregory and Paidoussis 1966). The destabilizing effect of dissipative forces on nonconservative systems, which was discovered by Ziegler (Herrmann 1967), is a feature of a nonconservative system (Herrmann and Jong 1965; Nemat-Nasser et al. 1966). In contrast to flutter instability, the dissipative forces do not affect the divergence boundary.

5.3.5.4 Elastic Springs

A pipe, fixed at the upstream end and supported by a rotational spring and a displacement spring with spring constants k_r and k_s , respectively, is of particular interest in demonstrating the transition of instability mechanisms (see Fig. 5.16) (Lin and Chen 1976; Noah and Hopkins 1980). Two dimensionless constants, $\bar{\alpha} = k_s l^3 / EI$ and $\bar{\beta} = k_r l / EI$, are introduced. The analysis of this problem is similar to those described in Sec. 5.3.2.

The pipe may lose its stability by divergence, flutter, or both, depending on the magnitudes of the springs $\bar{\alpha}$ and $\bar{\beta}$. Figure 5.17 shows the stability map in the $v^2 - \bar{\alpha}$ plane for $\bar{\beta} = 0$ and three values of $\bar{\beta}$. In Fig. 5.17(a), a buckling-type instability will not occur for $\bar{\alpha} < \alpha_2$. At $\bar{\alpha} = \alpha_1$, the critical flow velocities for the first flutter instability and second buckling instability coincide. For $\alpha_2 < \bar{\alpha} < \alpha_1$, there are multiple stable and unstable ranges of flow velocity. For $\bar{\alpha} > \alpha_1$, the system may lose stability by buckling and flutter, but the lowest critical flow velocity is associated with buckling. In Fig. 5.17(b), no buckling instability exists for $\alpha_3 < \bar{\alpha} < \alpha_2$, multiple stable and unstable regions exist for $\bar{\alpha} < \alpha_3$ and $\alpha_2 < \bar{\alpha} < \alpha_1$, and for $\bar{\alpha} > \alpha_1$, the lowest critical flow velocity is attributed to buckling. Figure 5.17(c) has the same implication except that at $\bar{\alpha} = \alpha_1$

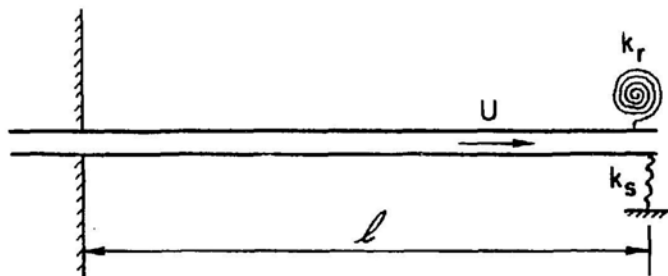


Fig. 5.16. Pipe Fixed at Upstream End and Supported by Rotational Spring and Displacement Spring at Downstream End

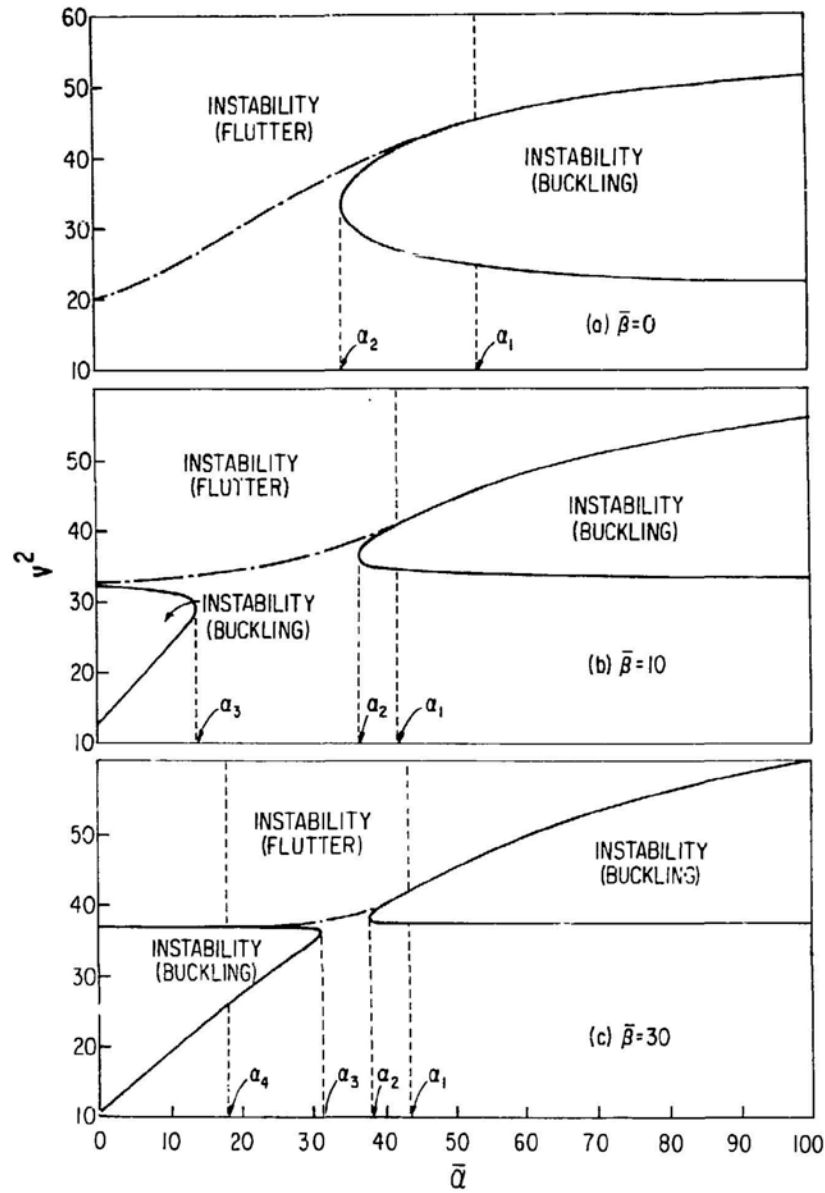


Fig. 5.17. Stability Maps in $\bar{\alpha} - v^2$ plane (Lin and Chen 1976)

and α_4 , the flutter-type instabilities coincide with the values of buckling type. We have not extended the investigation beyond α_1 for flutter-type instability because the system is unlikely to survive to that region after the two lowest buckling loads. Based on the results presented in Fig. 5.17 and similar results for other values of $\bar{\beta}$, Fig. 5.18 is the stability map in the $\bar{\alpha} - \bar{\beta}$ plane. The numbers in the figure indicate the square of the lowest critical flow velocity; solid lines are for buckling type and dashed lines are for flutter type. The region bounded by the two dotted lines does not have buckling-type instabilities; therefore only flutter-type instability exists there. Outside the region bounded by the dotted lines, the lowest critical flow velocity of flutter type is always higher than those of buckling type; thus only buckling-type critical flow velocities are shown there. Note that on the left side of the flutter region, for a given $\bar{\beta}$, increasing $\bar{\alpha}$ tends to increase the buckling flow velocity, while on the right side, increasing $\bar{\alpha}$ tends to reduce the critical flow velocity. On the other hand, for a given $\bar{\alpha}$, increasing $\bar{\beta}$ tends to destabilize the system on the left side and stabilize the system on the right side of the flutter region. For large values of $\bar{\alpha}$ or $\bar{\beta}$, the lowest critical flow velocities are associated with buckling.

5.3.5.5 Pulsating Flow

When the flow is a periodic function of time, e.g.,

$$U(z,t) = U_0(1 + \mu \cos \omega t), \quad (5.51)$$

two additional types of dynamic instability can occur--parametric resonance and combination resonance.

- Parametric resonance occurs over specific ranges of the oscillating frequency of the flow ω in the vicinity of $2\omega_n/m$, $n, m = 1, 2, 3, \dots, \infty$, where ω_n 's are the characteristic frequency of the pipe. The ranges of ω vary with μ . For a conservative system, the Coriolis force is not a damping mechanism; as $\mu \rightarrow 0$, parametric resonance occurs at $\omega \rightarrow 2\omega_n/m$. For nonconservative systems, generally there is a minimum μ below which parametric resonance is impossible.
- Combination resonance occurs in the neighborhood of $\omega = (\omega_m \pm \omega_n)/q$, $m \neq n$, and $m, n, q = 1, 2, 3, \dots$. The frequency ranges of combination resonance depend on the steady flow component U_0 , excitation parameter μ , and pipe support condition.

These two types of instability have been discussed extensively by several investigators, e.g., Hopkins (1969), Chen (1971b), Ginsberg (1973), Bohn and Herrmann (1974a), Paidoussis and Sundararajan (1975), Singh and Mallik (1978),

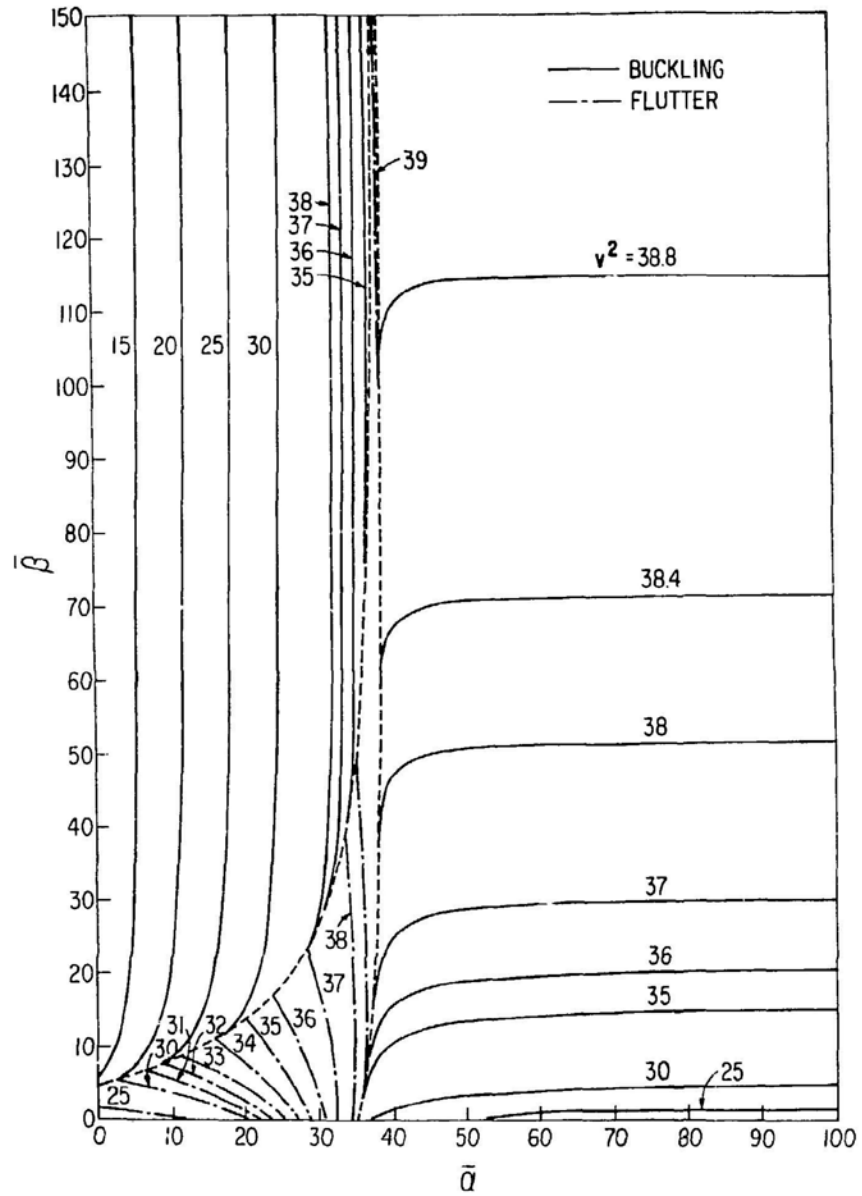


Fig. 5.18. Stability Map in $\bar{\alpha}$ - $\bar{\beta}$ Plane (Lin and Chen 1976)

Ahmadi and Satter (1978), Singh and Mallik (1979), and Noah and Hopkins (1980).

5.3.5.6 Two-Phase Flow

When the fluid passing through the pipe is in two-phase flow, the time-varying density of the two-phase flow may cause parametric resonance and combination resonance. Therefore, the effects of two-phase flow are characteristically similar to those of pulsating flow. A series of studies was published by Hara (1973, 1977) and by Hara et al. (1972). He found a significant relation between piping system fundamental natural frequency and dominant frequency of water slug arrival in the two-phase flow, their ratios being $1/2$, $1/1$, $3/2$, and so on, where strong vibration occurred. The theoretical characteristics of two-phase flow in a pipe are very complex, even without pipe oscillations. Further study of this problem is needed.

5.3.5.7 Nonlinear Effect

Nonlinear analyses of pipes conveying fluid have been done by Thurman and Mote (1969), Holmes (1978), Lundgren, Sethna, and Bajaj (1979), Bajaj, Sethna, and Lundgren (1980), Rousselet and Herrmann (1981), and Edelstein, Chen, and Jendrzejczyk (1986). These studies were performed to evaluate the applicable range of the linear theory, and response in the postcritical flow velocity range. Based on the nonlinear theory and experimental data, the linear theory is generally applicable at subcritical flow velocities if the nonlinear effect is not important. For example, for a cantilevered pipe, the linear theory predicts that the natural frequency and mode shape very well up to the critical flow velocity. Even at the critical flow velocity, the linear theory predicts correct flutter mode shape except for magnitude. However, for those cases in which the nonlinear effect caused by the flow is important (e.g., for the tension induced in a fixed-fixed pipe), the linear theory is not applicable for flow velocity larger than about 60% of the lowest critical flow velocity.

5.3.6 Experimental Studies

Table 5.2 lists experimental investigations of pipes conveying fluid. Most experiments focus on instability. A successful test of the instability of pipes conveying fluid is by no means trivial. Such testing generally requires a high-pressure loop for metal pipes with high flexural rigidity, while for a low-pressure loop, pipes of rubber, plastic, or other materials with very low flexural rigidity are required. In some experiments, no instability is observed because of the limitations of the available equipment. A high-pressure loop may be more expensive, but for a low-pressure loop, the material properties are much more difficult to control and the initial imperfection may affect the instability boundaries. One way to

Table 5.2. Experimental Studies of Pipes Conveying Fluid

Authors	Tube Material	Fluid	Support Condition	Tube Orientation	Instrumentation	Measured Parameters	Instability Type	Comment
Long (1955)	Steel tubes	Water	Hinged-hinged, Fixed-free, Fixed-fixed	Horizontal	Strain gauges	Damping, frequency		Flow velocity low; no instability.
Dodds and Ruyten (1965)	Aluminum alloy	Water (high-pressure)	Hinged-hinged	Horizontal	Strain gauges	Tube displacement, critical flow velocity, tube frequency, and damping.	Divergence	
Gregory and Paidoussis (1966)	Rubber tubes Metal tubes	Water and air, oil (high-pressure)	Fixed-free	Horizontal	Camera	Critical flow velocity, frequency and mode at instability.	Flutter	Nozzle attached to free end in some cases.
Greenwald and Dugundji (1967)	Elastomeric and polyethylene tubes	Water	Fixed-free Fixed-hinged	Hanging vertically	Strain gauges	Critical flow velocity, frequency and mode at instability.	Flutter Divergence	
Magulavaran and Williams (1968)	Neoprene tube	Water	Fixed-fixed	Horizontal	Capacitance pickups	Frequency		No buckling observed because of nonlinear effects.
Feldousis (1970)	Rubber tubes	Air or water	Fixed-free	Standing and hanging vertically	Fiber optics	Critical flow velocity, frequency and mode at instability.	Divergence and flutter	
Hill and Shennan (1970)	Latex surgical tubes	Water	Fixed-free			Critical flow velocity, frequency at instability.		Lumped masses attached to tubes.
Lin and Mace (1971)	Aluminum	Oil (high-pressure)	Fixed-free, Fixed-fixed, Fixed-hinged	Hanging vertically	Strain gauges and accelerometers	Natural frequency, static displacement.		No instability observed because of nonlinear effects.
Paidoussis and Isid (1974)	Silicon rubber tubes	Water	Fixed-free, Fixed-fixed	Hanging vertically		Boundaries of parametric resonance.	Parametric resonance	Tubes conveying pulsating flow.
Becker and Bauger (1978)	Plastic drinking straws	Air	Fixed-free		Stroboscope	Critical flow velocity, frequency and mode at instability.	Flutter	
Hannoyer and Paidoussis (1979)	Silicon rubber tubes	Water	Fixed-free	Hanging vertically		Flow velocity and oscillation frequency at instability.	Flutter	Tapered tubes.
Shilling and Lou (1980)	PVC pipes	Water	Fixed-free	Hanging vertically	Accelerometers	Frequency and tube response spectra to forced excitation.		No instability observed because of limitations of equipment availability; lumped masses attached to tubes.
Jandrasecnyk and Chen (1983)	Polyethylene and acrylic	Water	Six different supports	Vertically	Optical tracker	Frequency, static deformation, and RMS displacement.	Divergence, Flutter	Techniques for control stability are studied.

alleviate the problem is to use articulated pipes (Benjamin 1961; Bohn and Herrmann 1974b; Rousselet and Herrmann 1978). However, the characteristics of an articulated pipe are not necessarily the same as those of a continuous pipe (Paidoussis and Deksnis 1970).

Figure 5.19 shows a series of static deformation shapes for a pipe fixed at the upstream end and a spring at the downstream end. The static deformation increases with flow velocity; it is caused by fluid centrifugal force. As the flow velocity is increased to a value close to the critical one, static deformation increases more rapidly. The dominant oscillation frequency is associated with the fundamental mode. Based on the linear theory, the pipe fundamental frequency will become zero and the pipe will lose stability by divergence. However, the theoretical results of the divergence behavior based on a linear analysis are physically unrealistic since nonlinear effects dominate the behavior under these conditions. Difficulty was experienced experimentally in obtaining values of frequency at flow speeds greater than about 60% of the theoretically predicted divergence speeds. A condition of zero frequency was never achieved (Liu and Mote 1974; Jendrzejczyk and Chen 1983).

Based on the linear theory, the critical flow velocity is independent of initial disturbance. In experiment, the flutter can be initiated by transient excitation. If the tube is not excited with a mechanical excitation other than the flow in the pipe, the pipe loses stability by flutter spontaneously when the flow velocity is increased to a critical value. This flow velocity is called the critical flow velocity for intrinsic flutter. If the tube is excited by mechanical excitation, the pipe may lose stability at a different flow velocity; this flow velocity is called the critical flow velocity for excited flutter. The critical flow velocity for excited flutter due to transient excitation is smaller than that for intrinsic flutter. Typical responses of a cantilevered pipe for the two different types of flutter are given in Figs. 5.20 and 5.21, in which the pipe displacement and dominant frequency are given as functions of flow velocity for increasing and decreasing flow velocity (Chen and Jendrzejczyk 1984).

Excited Flutter: The pipe in Fig. 5.20 is excited at different flow velocities. Once the flow velocity is increased to the excited flutter velocity, large pipe oscillations occur. With the increase of flow velocity, pipe displacement and dominant response frequency continue to increase with the flow velocity. When the flow velocity is reduced, pipe displacement and dominant response frequency follow the same trends as those for increasing flow velocity.

Intrinsic Flutter: In Fig. 5.21, no excitation is given to the pipe. The pipe becomes unstable by intrinsic flutter at about 23.8 m/s. There is a significant jump in response amplitude at the intrinsic flutter velocity.

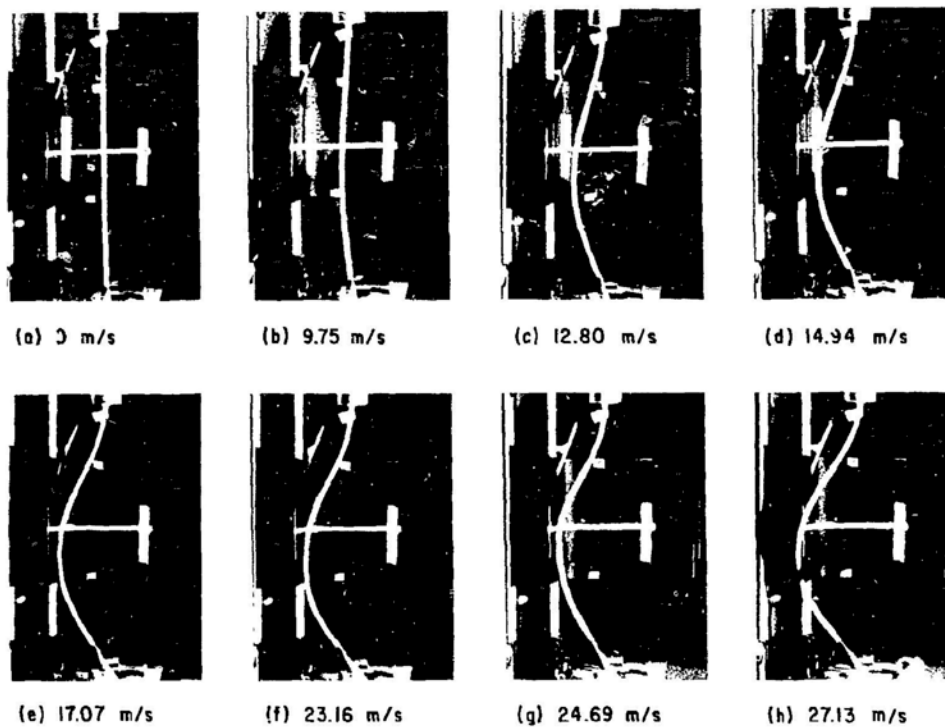


Fig. 5.19. Static Deformation Shapes for a Polyethylene Tube 60.96 cm long with 1.27 cm OD and 0.16 cm Wall Thickness, and a Spring Support at the End with Spring Constant 0.876 N/cm (Jendrzejczyk and Chen 1983) (AN, Neg. No. 113-83-4)

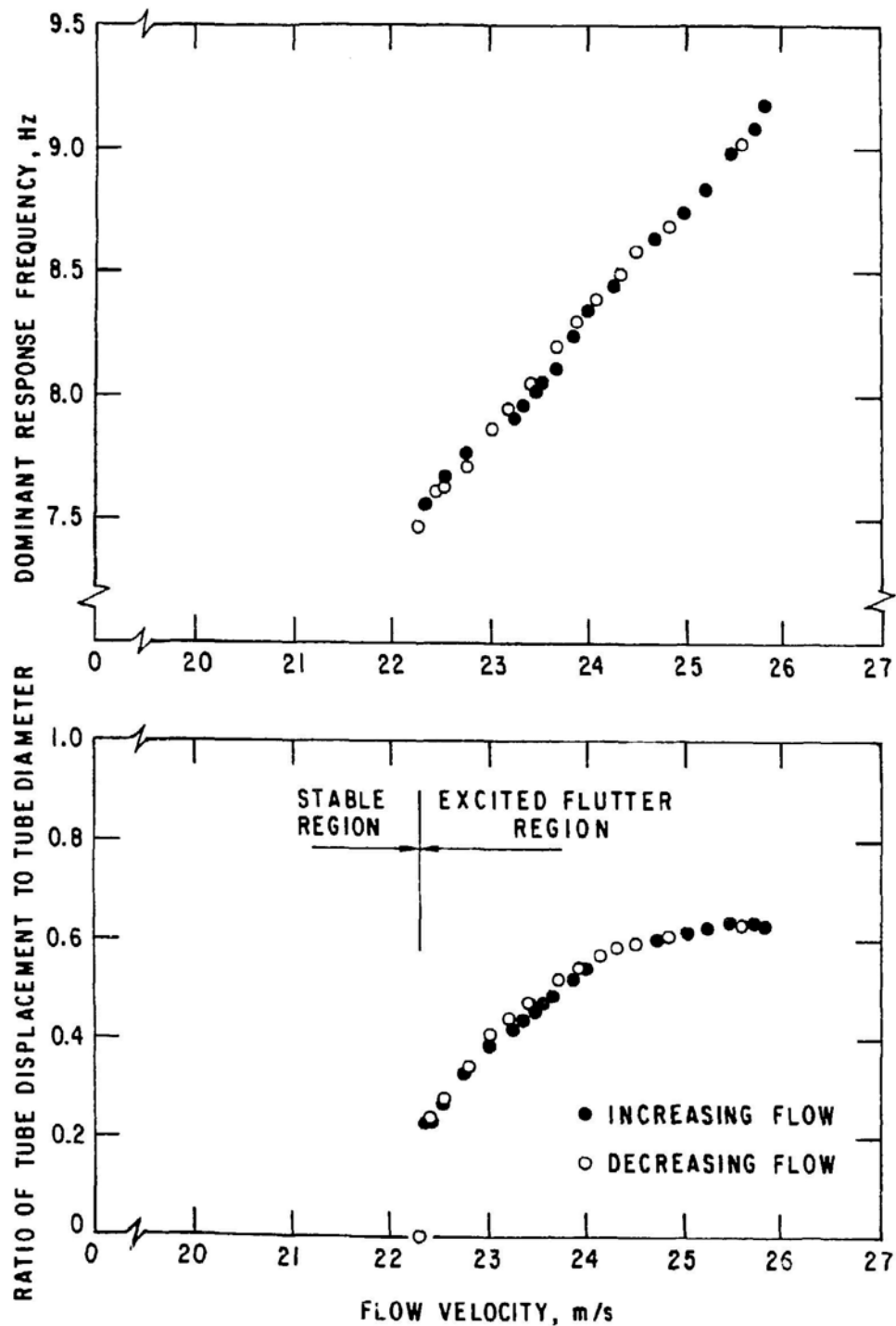


Fig. 5.20. Displacement and Dominant Response Frequency of an Excited Polyethylene Tube (60.96 cm long, 0.95 cm OD, 0.16 cm Wall Thickness) as a Function of Water Flow Velocity (Chen and Jendrzejczyk 1984)

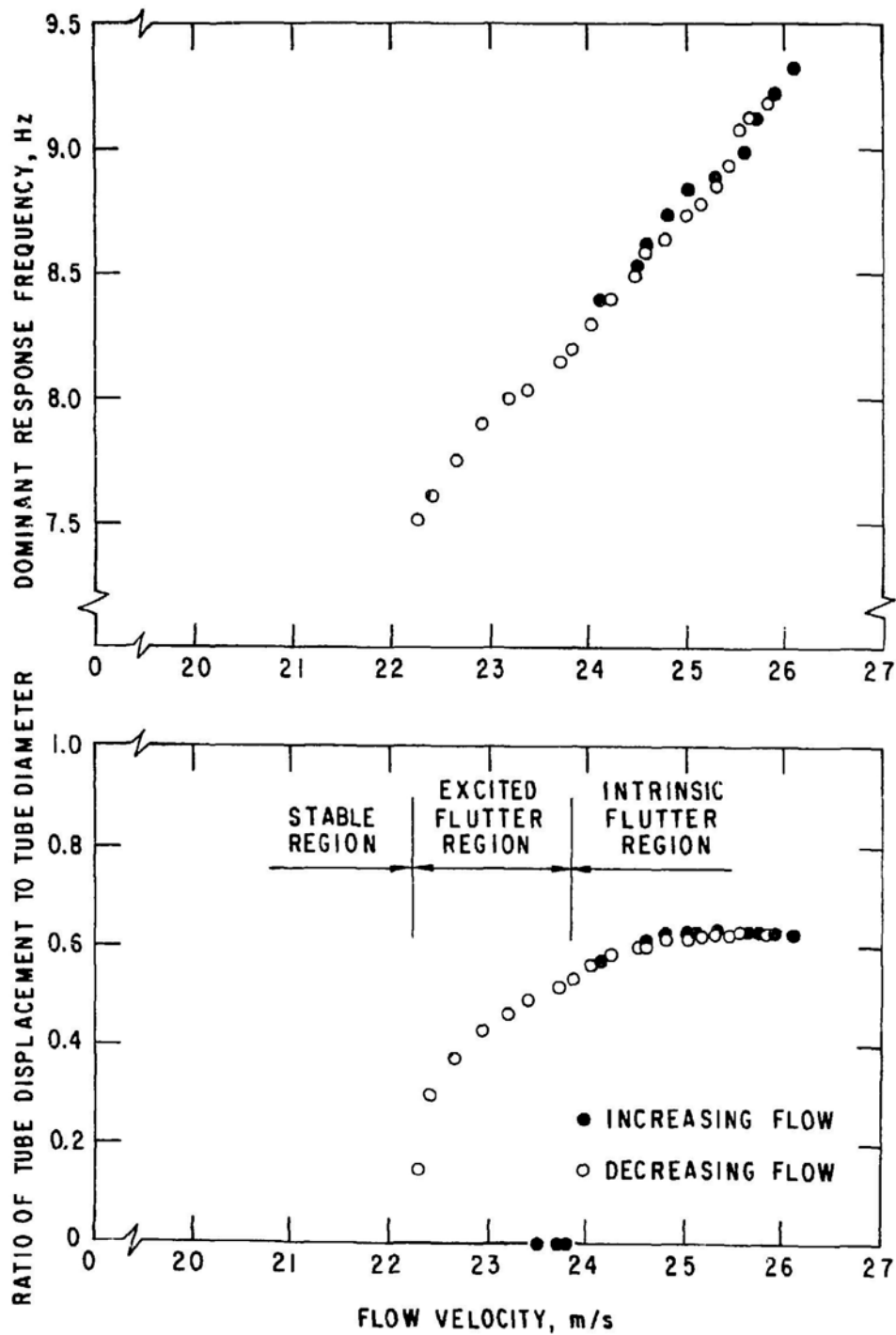


Fig. 5.21. Displacement and Dominant Response Frequency of an Unexcited Polyethylene Tube (60.96 cm long, 0.95 cm OD, 0.16 cm Wall Thickness) as a Function of Water Flow Velocity (Chen and Jendrzejczyk 1984)

With the increase in flow velocity in the intrinsic flutter region, pipe displacement and response frequency increase with the flow velocity. When the flow velocity is decreased, large oscillations continue in the excited flutter region. Finally, the pipe regains stability at about 22.2 m/s, which is the excited flutter velocity.

A series of tubes fixed at the upstream end and a knife-edge support movable along the tube were tested by Chen and Jendrzeczyk (1984) to study the transition of two types of instability. The tubes were polyethylene, 68.58 cm long with 0.16 cm wall thickness. The critical flow velocities for the tube with 1.27 cm OD as a function of the knife-edge support location are given in Fig. 5.22. The stability of the tube can be divided into two regions, $l_1/l > R_t$ and $l_1/l < R_t$.

$l_1/l > R_t$: At low flow velocities, the natural frequencies can be measured. At high flow velocities, the tube natural frequencies are not easily obtained. When the flow velocity is increased to the critical flow velocity, the tube buckles. Figure 5.23 shows the tube deformation at various flow velocities for $l_1/l = 0.82$. Note that when the flow velocity is increased to the critical value, the overhung portion is straight. This is consistent with the results obtained from the linear theory.

$l_1/l < R_t$: At low flow velocities, the tube displacement is small; tube displacement is caused by the turbulent flow. As the flow velocity increases, the modal damping value increases because of the Coriolis force. In the higher flow velocity region, the tube is overdamped. As the flow velocity is increased to the critical value, the tube loses stability by flutter. Figure 5.24 shows the flutter modes for $l_1/l = 0$ and 0.24. These pictures are taken for flow velocity a little higher than the intrinsic flutter flow velocity. The instability is associated with the second mode.

Figure 5.25 shows time histories of tube oscillations at various flow velocities with $l_1/l = 0.25$. The response characteristics are noted below:

- At 0 low, the tube is damped; its natural frequency is less than 3 Hz.
- As the flow velocity is increased, the tube is overdamped (see Figs. 5.25b and c). Any disturbance to the tube does not cause the tube to oscillate.
- With further increase in flow velocity, the tube damping becomes smaller again (see Figs. 5.25d and e).
- At 25.2 m/s (see Fig. 5.25), the flow velocity is about equal to the critical value.
- For the flow velocity above the critical value (see Figs. 5.25g-i), the tube loses stability by flutter. It takes only a few cycles of oscillations for it to reach the limit cycle.

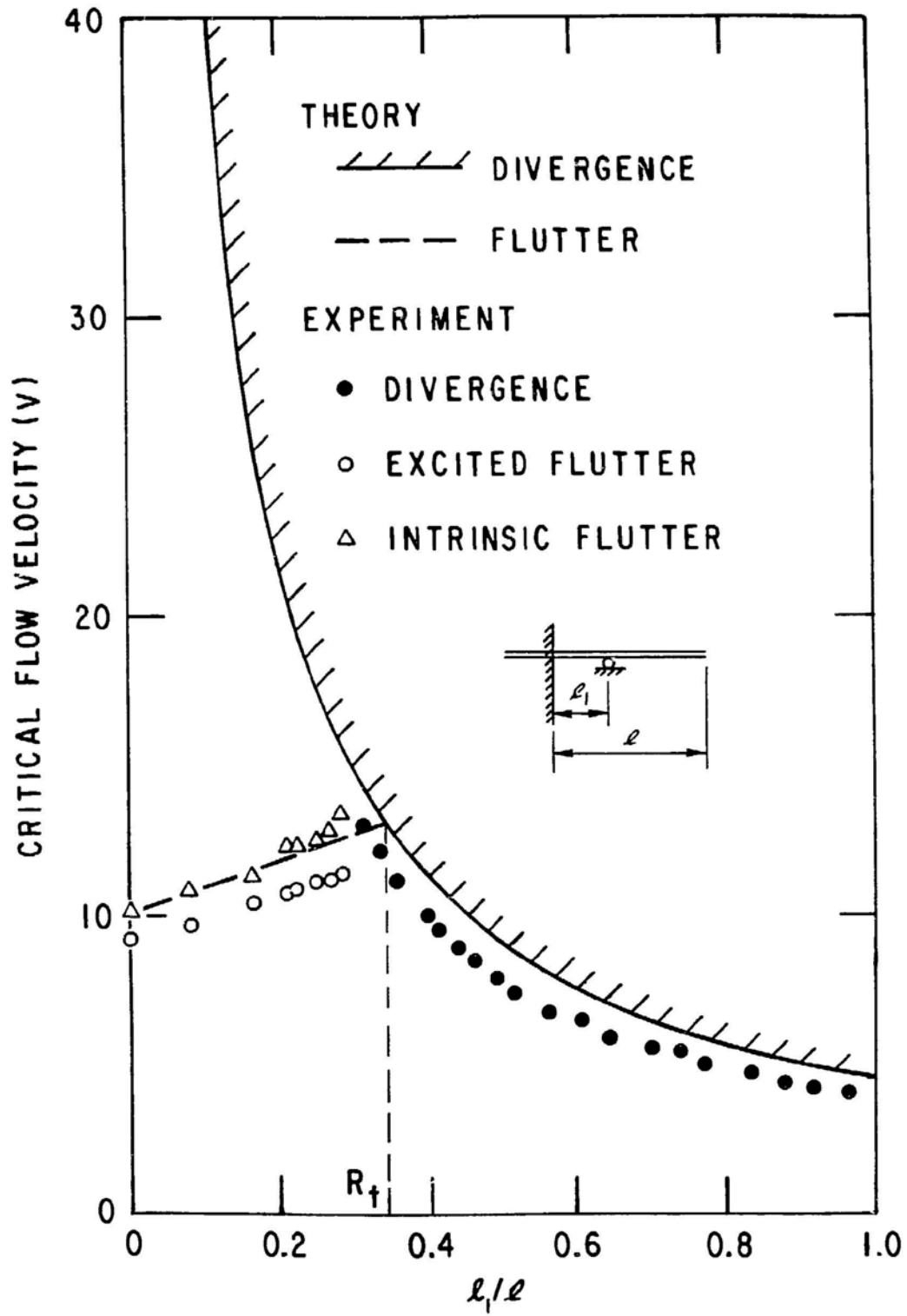


Fig. 5.22. Critical Flow Velocities for a Pipe Fixed at the Upstream End and a Knife-Edge Support Movable along the Pipe (Chen and Jendrzejczyk 1984)

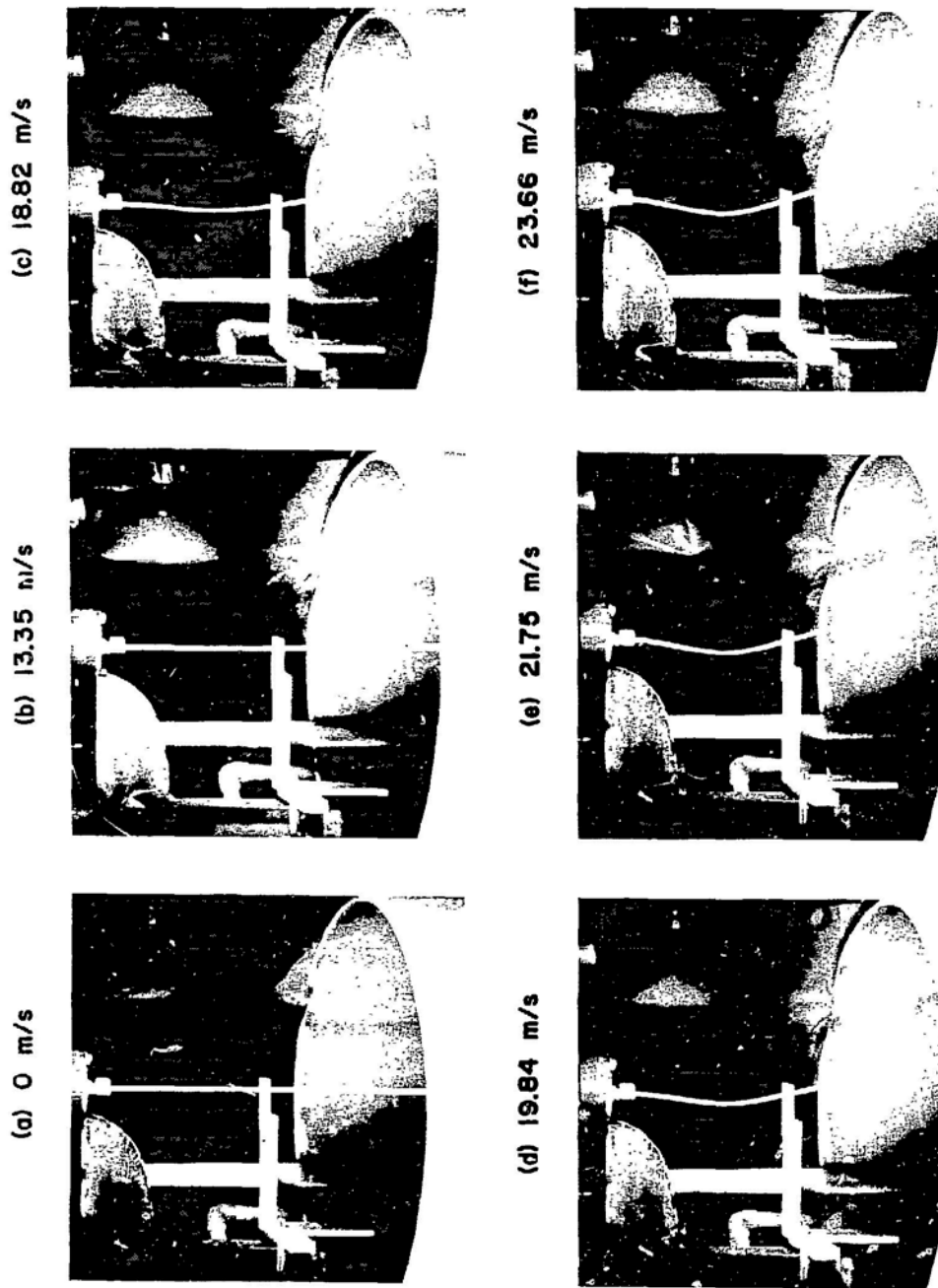


Fig. 5.23. Static Deformation Shapes for a Polyethylene Tube 68.58 cm long with 0.95 cm OD and 0.16 cm Wall Thickness for $k_1/k_2 = 0.82$ (Chen and Jendrzejczyk 1984) (ANL Neg. No. 113-83-220)

(a) $I/L = 0$



(b) $I/L = 0.24$

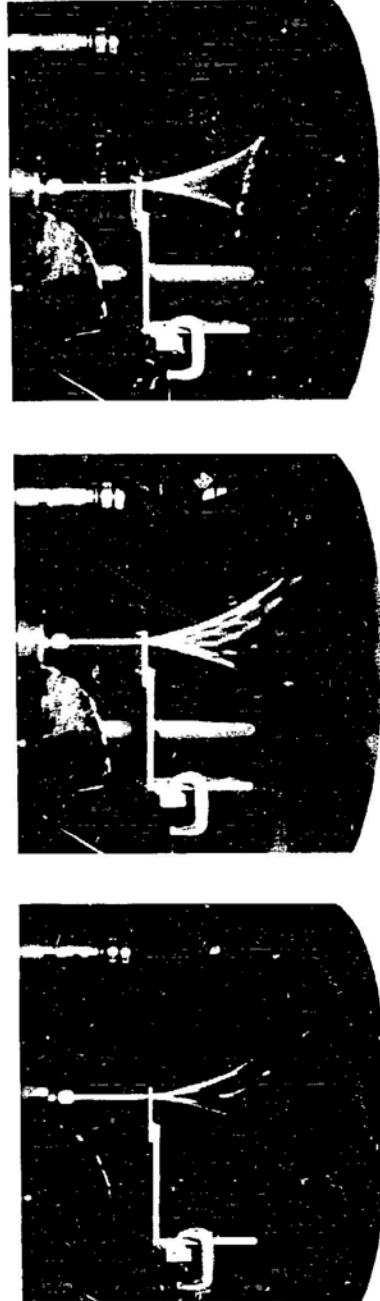


Fig. 5.24. Flutter Modes of a Polyethylene Tube 68.58 cm long with 0.95 cm OD and 0.16 cm Wall Thickness (Chen and Jendrzejczyk 1984) (ANL Neg. No. 113-83-222)

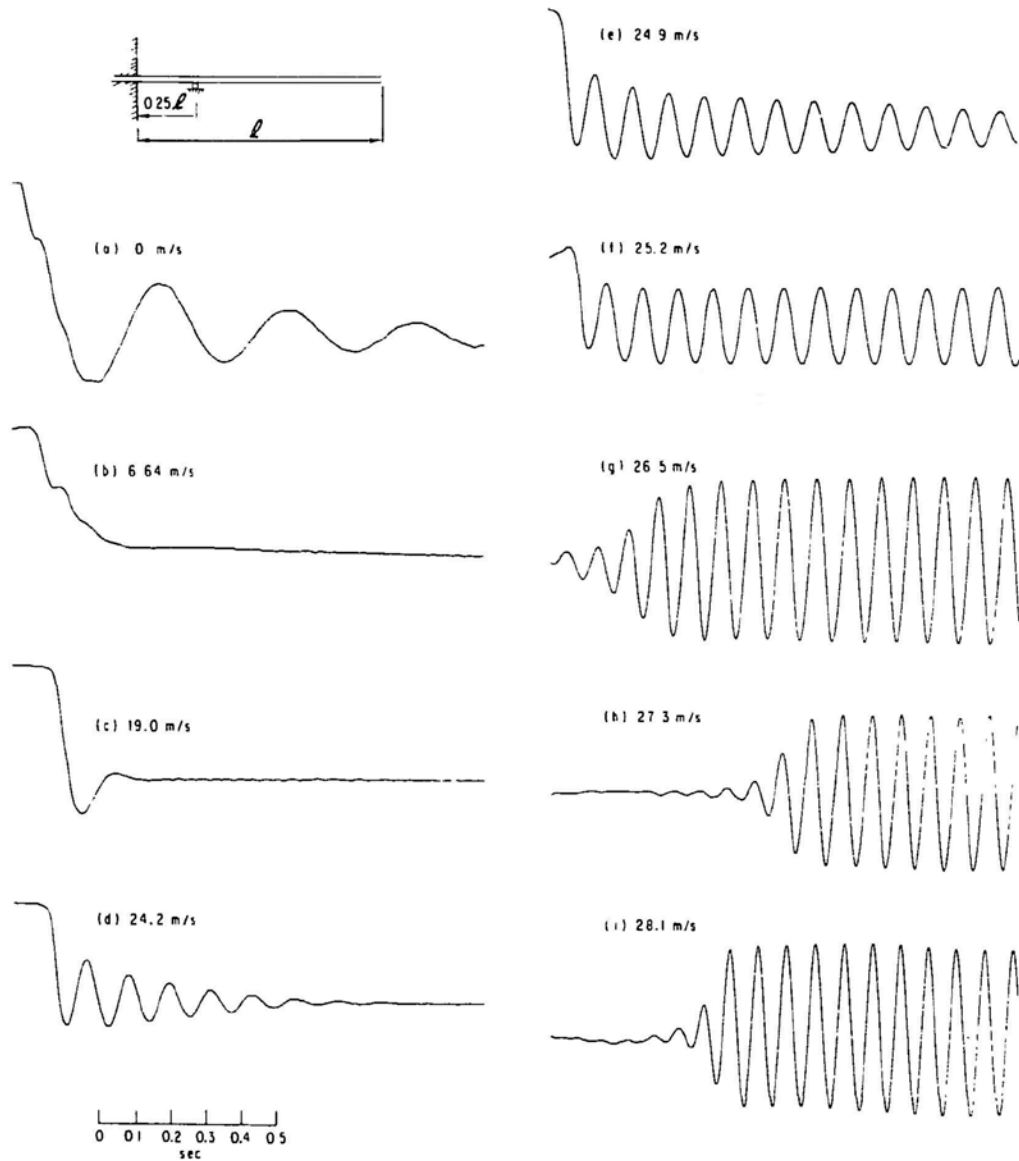


Fig. 5.25. Time History of Tube Oscillations at Various Velocities for a Polyethylene Tube 68.58 cm long with 0.95 cm OD and 0.16 cm Wall Thickness (Chen and Jendrzejczyk 1984)

At $\lambda_1/\lambda = R_c$, the critical flow velocities for divergence and flutter are identical. Theoretically, the tube can buckle and flutter simultaneously. However, in experiment, this phenomenon is difficult to demonstrate. There is a suggestion that the interaction of different types of instability mechanisms may be one of the mechanisms to cause "chaotic motions" (Dowell 1982).

5.4 CURVED PIPES

The dynamics of curved pipes conveying fluid has been studied theoretically by several investigators (Springfield 1970; Unny et al. 1970; Chen 1972a and b; Chen 1973; Hill and Davis 1974; Doll and Mote 1976; Chen and Bert 1977). Apparently, no experimental work has been published on this subject. In this section, analysis will be presented based on the linear theory.

5.4.1 Equations of Motion

The system under consideration consists of a uniformly curved pipe conveying fluid (Fig. 5.26). The pipe has a radius of curvature R , internal cross-sectional area A , mass per unit length m , flexural rigidity EI , torsional rigidity GJ , and subtended angle α . The fluid density is ρ and the fluid is flowing with a constant velocity U ; thus the mass flowrate is ρAU . The following assumptions are made in deriving the equations of motion:

- The effects of gravity and material damping are negligible.
- The pipe is inextensible.
- The rotatory inertia and shear deformation are negligible.
- The small-scale details of fluid motions--for example, turbulence and secondary flow--are neglected.
- All motions are small.

The equations of motion can be derived from the equilibrium of a pipe/fluid element or from Hamilton's principle (Eq. 5.8). The initially unstressed state of the pipe is in the x - y plane (Fig. 5.26). In the stressed state, pipe deformations consist of radial displacement u along the N axis, transverse displacement v along the z axis, axial displacement w along the T axis, and the twist angle ϕ . The potential and kinetic energies of the pipe are

$$V_S = \int_0^\alpha \left\{ \frac{M_N^2}{2EI} + \frac{M_z^2}{2EI} + \frac{M_T^2}{2GJ} \right\} R \, d\theta$$

and

$$T_S = \int_0^\alpha \frac{m}{2} \left[\left(\frac{\partial u}{\partial t} \right)^2 + \left(\frac{\partial v}{\partial t} \right)^2 + \left(\frac{\partial w}{\partial t} \right)^2 \right] R \, d\theta ,$$

(5.52)

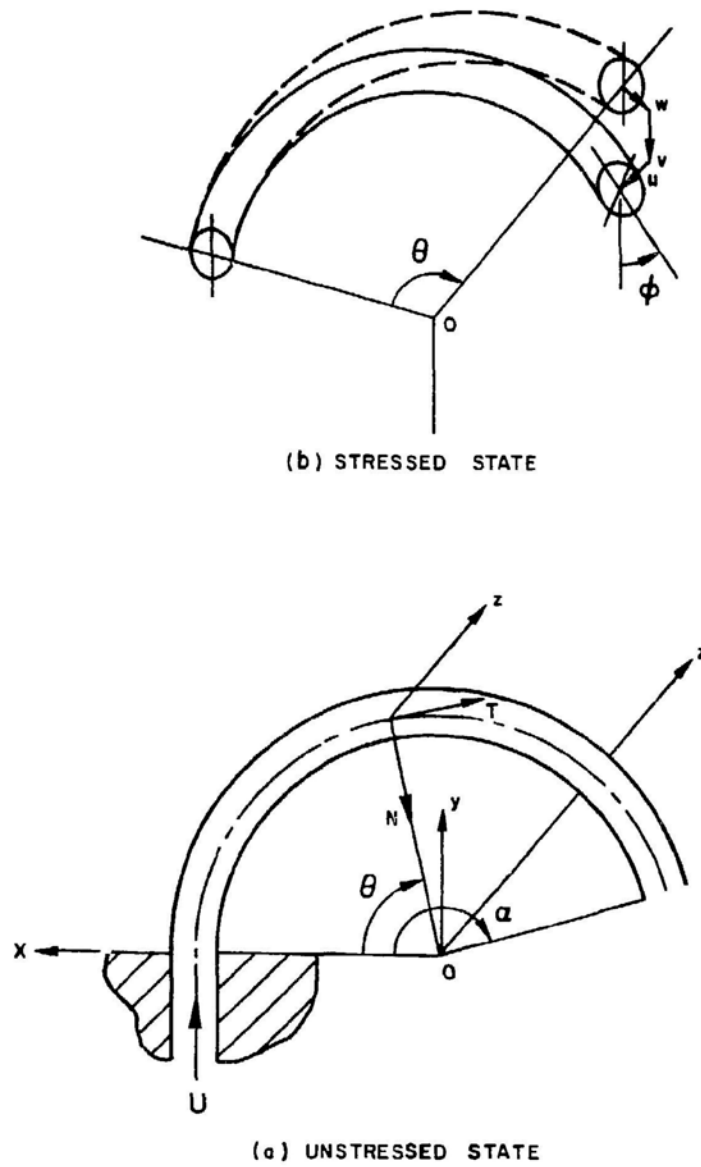


Fig. 5.26. Definition of Coordinates and Displacements of a Uniformly Curved Pipe Conveying Fluid

where

$$\begin{aligned} M_N &= \frac{EI}{R^2} \left(R\phi - \frac{\partial^2 v}{\partial \theta^2} \right), \\ M_z &= \frac{EI}{R^2} \left(\frac{\partial^2 u}{\partial \theta^2} + \frac{\partial w}{\partial \theta} \right), \end{aligned} \quad (5.53)$$

and

$$M_T = \frac{GJ}{R^2} \left(R \frac{\partial \phi}{\partial \theta} + \frac{\partial v}{\partial \theta} \right).$$

Because the pipe is taken to be inextensible, it is required that

$$u = \frac{\partial w}{\partial \theta}. \quad (5.54)$$

Next, consider fluid flow kinematics. The position vector of a point on the center line of the deformed pipe is

$$\begin{aligned} \vec{R} &= [(R - u)\cos\theta - w \sin\theta]\vec{e}_x \\ &\quad + [(R - u)\sin\theta + w \cos\theta]\vec{e}_y + v\vec{e}_z, \end{aligned} \quad (5.55)$$

where \vec{e}_x , \vec{e}_y , and \vec{e}_z are unit vectors along the x, y, and z axes. The unit vector \vec{t} tangential to the tube center line can be obtained from Eq. 5.55; i.e.,

$$\begin{aligned} \vec{t} &= \left[-\sin\theta - \frac{1}{R} \left(\frac{\partial u}{\partial \theta} + w \right) \cos\theta \right] \vec{e}_x \\ &\quad + \left[\cos\theta - \frac{1}{R} \left(\frac{\partial u}{\partial \theta} + w \right) \sin\theta \right] \vec{e}_y + \frac{1}{R} \frac{\partial v}{\partial \theta} \vec{e}_z. \end{aligned} \quad (5.56)$$

Because the pipe is assumed inextensible and the fluid incompressible, the enclosed volume of the fluid is constant and the relative velocity of the fluid with respect to the tube is always equal to $U\vec{t}$. For neglecting the effect of the twisting motion on the fluid, the absolute flow velocity is

$$\vec{U} = \frac{\partial \vec{R}}{\partial t} + U\vec{t}. \quad (5.57)$$

Substitution of Eqs. 5.55 and 5.56 into Eq. 5.57 yields

$$\begin{aligned}\vec{U} = & \left\{ \left[-\frac{\partial u}{\partial t} - \frac{U}{R} \left(\frac{\partial u}{\partial \theta} + w \right) \right] \cos \theta - \left(U + \frac{\partial w}{\partial t} \right) \sin \theta \right\} \vec{e}_x \\ & + \left\{ \left(U + \frac{\partial w}{\partial t} \right) \cos \theta - \left[\frac{\partial u}{\partial t} + \frac{U}{R} \left(\frac{\partial u}{\partial \theta} + w \right) \right] \sin \theta \right\} \vec{e}_y \\ & + \left(\frac{\partial v}{\partial t} + \frac{U}{R} \frac{\partial v}{\partial \theta} \right) \vec{e}_z .\end{aligned}\quad (5.58)$$

Therefore, the kinetic energy of the enclosed volume of fluid is

$$\begin{aligned}T_f = & \frac{M_d}{2} \int_0^\alpha \left[U^2 + \left(\frac{\partial u}{\partial t} \right)^2 + \left(\frac{\partial w}{\partial t} \right)^2 + \left(\frac{\partial v}{\partial t} \right)^2 + 2U \frac{\partial w}{\partial t} \right. \\ & + 2 \frac{U}{R} \left(\frac{\partial u}{\partial \theta} + w \right) \frac{\partial u}{\partial t} + \frac{2U}{R} \frac{\partial v}{\partial \theta} \frac{\partial v}{\partial t} + \frac{U^2}{R^2} \left(\frac{\partial u}{\partial \theta} + w \right)^2 \\ & \left. + \frac{U^2}{R^2} \left(\frac{\partial v}{\partial \theta} \right)^2 \right] R \, d\theta .\end{aligned}\quad (5.59)$$

Because the fluid is assumed incompressible, the potential energy of the fluid is zero; i.e.,

$$V_f = 0 . \quad (5.60)$$

Substituting for \mathcal{L} ($= V_s + T_s + V_f + T_f$), \vec{R} , and \vec{r} into Eq. 5.8, we obtain the resulting Euler-Lagrange equations

$$\begin{aligned}\frac{EI}{R^3} \left(\frac{\partial^6 w}{\partial \theta^6} + 2 \frac{\partial^4 w}{\partial \theta^4} + \frac{\partial^2 w}{\partial \theta^2} \right) + \frac{M_d U^2}{R} \left(\frac{\partial^4 w}{\partial \theta^4} + 2 \frac{\partial^2 w}{\partial \theta^2} + w \right) \\ + 2M_d U \left(\frac{\partial^4 w}{\partial \theta^3 \partial t} + \frac{\partial^2 w}{\partial \theta \partial t} \right) + R(m + M_d) \left(\frac{\partial^4 w}{\partial \theta^2 \partial t^2} - \frac{\partial^2 w}{\partial t^2} \right) = 0 ,\end{aligned}\quad (5.61)$$

$$\begin{aligned} \frac{EI}{R^3} \left(\frac{\partial^4 v}{\partial \theta^4} - R \frac{\partial^2 \phi}{\partial \theta^2} \right) - \frac{GJ}{R^3} \left(\frac{\partial^2 v}{\partial \theta^2} + R \frac{\partial^2 \phi}{\partial \theta^2} \right) + \frac{M_d U^2}{R} \frac{\partial^2 v}{\partial \theta^2} \\ + 2M_d U \frac{\partial^2 v}{\partial \theta \partial t} + R(m + M_d) \frac{\partial^2 v}{\partial t^2} = 0, \end{aligned} \quad (5.62)$$

and

$$\frac{EI}{R^2} \left(R\phi - \frac{\partial^2 v}{\partial \theta^2} \right) - \frac{GJ}{R^2} \left(R \frac{\partial^2 \phi}{\partial \theta^2} + \frac{\partial^2 v}{\partial \theta^2} \right) = 0. \quad (5.63)$$

The associated boundary conditions are

$$\begin{aligned} \left[\frac{EI}{R^3} \left(\frac{\partial^5 w}{\partial \theta^5} + 2 \frac{\partial^3 w}{\partial \theta^3} + \frac{\partial w}{\partial \theta} \right) + \frac{M_d U^2}{\partial \theta} \left(\frac{\partial^3 w}{\partial \theta^3} + \frac{\partial w}{\partial \theta} \right) \right. \\ \left. + 2MU \frac{\partial^3 w}{\partial \theta^2 \partial t} + M_d U \frac{\partial w}{\partial t} + R(m + M_d) \frac{\partial^3 w}{\partial \theta \partial t^2} \right] \delta w \Big|_0^\alpha \\ + (M_d U \frac{\partial w}{\partial t} + M_d U^2) \delta w \Big|_{\theta=\alpha} = 0, \\ - \left[\frac{EI}{R^3} \left(\frac{\partial^4 w}{\partial \theta^4} + \frac{\partial^2 w}{\partial \theta^2} \right) + \frac{M_d U^2}{R} \left(\frac{\partial^2 w}{\partial \theta^2} + w \right) \right. \\ \left. + M_d U \frac{\partial^2 w}{\partial \theta \partial t} \right] \delta \left(\frac{\partial w}{\partial \theta} \right) \Big|_0^\alpha + \left[M_d U \frac{\partial^2 w}{\partial \theta \partial t} \right. \\ \left. + \frac{M_d U^2}{R} \left(\frac{\partial^2 w}{\partial \theta^2} + w \right) \right] \delta \left(\frac{\partial w}{\partial \theta} \right) \Big|_{\theta=\alpha} = 0, \\ \frac{EI}{R^3} \left(\frac{\partial^3 w}{\partial \theta^3} + \frac{\partial w}{\partial \theta} \right) \delta \left(\frac{\partial^2 w}{\partial \theta^2} \right) \Big|_0^\alpha = 0, \end{aligned} \quad (5.64)$$

$$\begin{aligned}
& \left[\frac{EI}{R^3} \left(R \frac{\partial \phi}{\partial \theta} - \frac{\partial^3 v}{\partial \theta^3} \right) + \frac{GJ}{R^3} \left(R \frac{\partial \phi}{\partial \theta} + \frac{\partial v}{\partial \theta} \right) - \frac{M_d U^2}{R} \frac{\partial v}{\partial \theta} \right. \\
& \quad \left. - M_d U \frac{\partial v}{\partial t} \right] \delta v \Big|_0^\alpha + \left(M_d U \frac{\partial v}{\partial t} + \frac{M_d U^2}{R} \frac{\partial v}{\partial \theta} \right) \delta v \Big|_{\theta=\alpha} = 0 \\
& \frac{EI}{R^3} \left(R \phi - \frac{\partial^2 v}{\partial \theta^2} \right) \delta \left(\frac{\partial v}{\partial \theta} \right) \Big|_0^\alpha = 0 , \tag{5.65}
\end{aligned}$$

and

$$\frac{GJ}{R^2} \left(R \frac{\partial \phi}{\partial \theta} + \frac{\partial v}{\partial \theta} \right) \delta \phi \Big|_0^\alpha = 0 .$$

Equations 5.61 and 5.64 pertain to the in-plane displacements, while Eqs. 5.62, 5.63, and 5.65 are associated with the out-of-plane displacements and twist. There is no coupling between in-plane motion and out-of-plane motion; therefore, in-plane motion and out-of-plane motion can be studied independently. Equations 5.64 and 5.65 display all admissible end conditions for the system under consideration; the most-often-assumed end conditions are free, pinned, and clamped.

5.4.2 Out-of-Plane Vibration and Stability Analysis

Out-of-plane flexural-twist motions are governed by Eqs. 5.62, 5.63, and 5.65. With the following nondimensional parameters,

$$\begin{aligned}
\xi &= v/R , \quad \beta = \frac{M_d}{m + M_d} \\
v &= \left(\frac{M_d}{EI} \right)^{1/2} R U , \quad \tau = \left(\frac{EI}{m + M_d} \right)^{1/2} t/R^2 \\
\kappa &= \frac{GJ}{EI} ,
\end{aligned} \tag{5.66}$$

Equations 5.62 and 5.63 become

$$\begin{aligned}
& \frac{\partial^4 \xi}{\partial \theta^4} - \frac{\partial^2 \xi}{\partial \theta^2} - \kappa \left(\frac{\partial^2 \xi}{\partial \theta^2} + \frac{\partial^2 \phi}{\partial \theta^2} \right) + v^2 \frac{\partial^2 \xi}{\partial \theta^2} \\
& \quad + 2\beta^{0.5} v \frac{\partial^2 \xi}{\partial \theta \partial \tau} + \frac{\partial^2 \xi}{\partial \tau^2} = 0 \tag{5.67}
\end{aligned}$$

and

$$\frac{\partial^2 \xi}{\partial \theta^2} - \phi + \kappa \left(\frac{\partial^2 \phi}{\partial \theta^2} + \frac{\partial^2 \xi}{\partial \theta^2} \right) . \quad (5.68)$$

Let

$$\xi(\theta, \tau) = \eta(\theta) e^{i\Omega\tau}$$

and

$$\phi(\theta, \tau) = \psi(\theta) e^{i\Omega\tau} .$$

(5.69)

Substitution of Eqs. 5.69 into 5.67 and 5.68 yields

$$\begin{aligned} \frac{d^4 \eta}{d\theta^4} - \frac{d^2 \psi}{d\theta^2} - \kappa \left(\frac{d^2 \eta}{d\theta^2} + \frac{d^2 \psi}{d\theta^2} \right) + v^2 \frac{d^2 \xi}{d\theta^2} \\ + i2\beta^{0.5} v^2 \Omega \frac{d\xi}{d\theta} - \Omega^2 \xi = 0 \end{aligned} \quad (5.70)$$

and

$$\frac{d^2 \eta}{d\theta^2} - \psi + \kappa \left(\frac{d^2 \psi}{d\theta^2} + \frac{d^2 \eta}{d\theta^2} \right) = 0 . \quad (5.71)$$

Elimination of η from Eqs. 5.70 and 5.71 gives

$$\begin{aligned} \frac{d^6 \psi}{d\theta^6} + (2 + v^2) \frac{d^4 \psi}{d\theta^4} + i2\beta^{0.5} v \Omega \frac{d^3 \psi}{d\theta^3} + \left(1 - \frac{v^2}{\kappa} - \Omega^2 \right) \frac{d^2 \psi}{d\theta^2} \\ - i2\beta^{0.5} v \Omega \frac{d\psi}{d\theta} + \frac{\Omega^2}{\kappa} \psi = 0 . \end{aligned} \quad (5.72)$$

The solution of Eq. 5.72 is

$$\psi = \sum_{j=1}^6 C_j e^{i\lambda_j \theta} , \quad (5.73)$$

where C_n 's are some constants to be evaluated by using the boundary conditions and λ_n 's are the six roots of the equation

$$\begin{aligned} \lambda^6 - (2 + v^2)\lambda^4 - 2\beta^{0.5}v\Omega\lambda^3 + \left(1 - \frac{v^2}{\kappa} - \Omega^2\right)\lambda^2 \\ - 2\beta^{0.5}v\Omega\lambda - \frac{\Omega^2}{\kappa} = 0 . \end{aligned} \quad (5.74)$$

Integrating Eq. 5.71 twice, we have

$$\eta = \frac{1}{1 + \kappa} \left(\int \int \psi d\theta d\theta - \kappa \psi \right) , \quad (5.75)$$

in which the two integration constants, in general, are zero. Substitution of Eq. 5.73 into 5.75 yields

$$\eta = - \frac{1}{1 + \kappa} \sum_{j=1}^6 C_j \left(\frac{1}{\lambda_j^2} + \kappa \right) e^{i\lambda_j \theta} . \quad (5.76)$$

The coefficient C_j 's are determined from the equations obtained by substituting Eqs. 5.73 and 5.76 into the boundary conditions at $\theta = 0$ and $\theta = \alpha$. The equations to determine C_j can be written

$$[a_{jk}] \{C_k\} = \{0\} ; \quad j, k = 1, 2, 3, 4, 5, 6 . \quad (5.77)$$

The element a_{jk} 's are given in Table 5.3 for four boundary conditions. Setting the determinant of coefficients in Eq. 5.77 equal to zero gives the frequency equation. The frequency depends on the system parameters v , κ , α , and β ; therefore, the frequency equation can be written

$$F(\Omega, v, \kappa, \alpha, \beta) = 0 . \quad (5.78)$$

Table 5.3. Boundary Conditions and Elements a_{jk} 's

End Conditions	Clamped-Clamped	Clamped-Pinned	Pinned-Pinned	Clamped-Free
Boundary conditions	$\xi = 0$	$\xi = 0$	$\xi = 0$	$\xi = 0$
	$\theta = 0$ $\frac{\partial \xi}{\partial \theta} = 0$	$\frac{\partial \xi}{\partial \theta} = 0$	$\frac{\partial \xi}{\partial \theta} + \frac{\partial \phi}{\partial \theta} = 0$	$\frac{\partial \xi}{\partial \theta} = 0$
	$\phi = 0$	$\phi = 0$	$\frac{\partial^2 \xi}{\partial \theta^2} - \phi = 0$	$\phi = 0$
	$\xi = 0$	$\xi = 0$	$\xi = 0$	$\frac{\partial \xi}{\partial \theta} + \frac{\partial \phi}{\partial \theta} = 0$
	$\theta = \alpha$ $\frac{\partial \xi}{\partial \theta} = 0$	$\frac{\partial \xi}{\partial \theta} + \frac{\partial \phi}{\partial \theta} = 0$	$\frac{\partial \xi}{\partial \theta} + \frac{\partial \phi}{\partial \theta} = 0$	$\frac{\partial^2 \xi}{\partial \theta^2} - \phi = 0$
	$\phi = 0$	$\frac{\partial^2 \xi}{\partial \theta^2} - \phi = 0$	$\frac{\partial^2 \xi}{\partial \theta^2} - \phi = 0$	$\frac{\partial^3 \xi}{\partial \theta^3} - \frac{\partial \phi}{\partial \theta} = 0$
Elements a_{jk}	a_{1k} $\frac{1}{\lambda_k^2} + k$	$\frac{1}{\lambda_k^2} + k$	$\frac{1}{\lambda_k^2} + k$	$\frac{1}{\lambda_k^2} + k$
	a_{2k} $\lambda_k \left(\frac{1}{\lambda_k^2} + k \right)$	$\lambda_k \left(\frac{1}{\lambda_k^2} + k \right)$	$\frac{\lambda_k^2 - 1}{\lambda_k}$	$\lambda_k \left(\frac{1}{\lambda_k^2} + k \right)$
	a_{3k} 1	1	$\lambda_k^2 - 1$	1
	a_{4k} $\left(\frac{1}{\lambda_k^2} + k \right) e^{i\lambda_k \alpha}$	$\left(\frac{1}{\lambda_k^2} + k \right) e^{i\lambda_k \alpha}$	$\left(\frac{1}{\lambda_k^2} \right) e^{i\lambda_k \alpha}$	$\left(\frac{\lambda_k^2 - 1}{\lambda_k} \right) e^{i\lambda_k \alpha}$
	a_{5k} $\lambda_k \left(\frac{1}{\lambda_k^2} + k \right) e^{i\lambda_k \alpha}$	$\left(\frac{\lambda_k^2 - 1}{\lambda_k} \right) e^{i\lambda_k \alpha}$	$\left(\frac{\lambda_k^2 - 1}{\lambda_k} \right) e^{i\lambda_k \alpha}$	$(\lambda_k^2 - 1) e^{i\lambda_k \alpha}$
	a_{6k} $e^{i\lambda_k \alpha}$	$(\lambda_k^2 - 1) e^{i\lambda_k \alpha}$	$(\lambda_k^2 - 1) e^{i\lambda_k \alpha}$	$\lambda_k (\lambda_k^2 - 1) e^{i\lambda_k \alpha}$

With these qualitative results, we can evaluate the frequency numerically from Eq. 5.78. The frequency depends on the stiffness ratio κ ; for a circular pipe,

$$\kappa = \frac{1}{1 + \nu}, \quad (5.79)$$

where ν is Poisson's ratio of the pipe. The natural frequencies of a conservative system and a nonconservative system for $\nu = 0.3$ and $\alpha = \pi$ are shown in Figs. 5.27 and 5.28 (Chen 1973).

Figure 5.27 shows the frequencies of a clamped-clamped pipe as functions of the flow velocity v . With no flow, the pipe behaves as an incomplete ring. As the flow velocity increases, the frequency becomes smaller. With further increase in flow velocity, some frequencies become zero and the system loses stability by buckling. We observe that for increasing β the first frequency decreases while the others increase for conservative systems. This characteristic is the same as that of straight pipes.

Figure 5.28 shows the complex frequencies of the first four modes of a cantilevered pipe. The numbers in the figure indicate the values of flow velocity v . When v is small, all roots of Eq. 5.78 for the cantilevered tube are located in the upper half of the complex Ω plane and system oscillations are damped in all modes. The effects of the flowing fluid are to reduce the natural frequencies and to contribute to the damping; the damping effect is due to the Coriolis acceleration. As the flow velocity increases, some roots cross the $\text{Re}(\Omega)$ axis, and the system loses stability by flutter. For the example shown in Fig. 5.28, the first, third, and fourth modes are always stable in the ranges of flow velocity considered. The frequency of the second mode crosses the $\text{Re}(\Omega)$ axis at $v = 1.5$, 1.85 , and 2.2 ; thus the system loses stability at $v = 1.5$, regains stability at $v = 1.85$, and loses stability again at $v = 2.2$. The other modes may also become unstable if the flow velocity is increased further; however, these flow velocities will be higher than that of the second mode and have no practical significance.

The stability of gyroscopic nonconservative systems can be studied only by the dynamic method. Therefore, the critical flow velocity of a clamped-free pipe is obtained from Eq. 5.78. The critical flow velocity for conservative systems is a function of the subtended angle α and Poisson's ratio ν . The results for $\nu = 0.3$ are given in Figs. 5.29-5.31. For nonconservative systems, the critical flow velocity depends on the mass ratio β in addition to α and ν . The instability boundaries are obtained from Eq. 5.78; the results are shown in Fig. 5.32 for $\nu = 0.3$ and $\alpha = \pi/2$, $3\pi/4$, and π as functions of β .

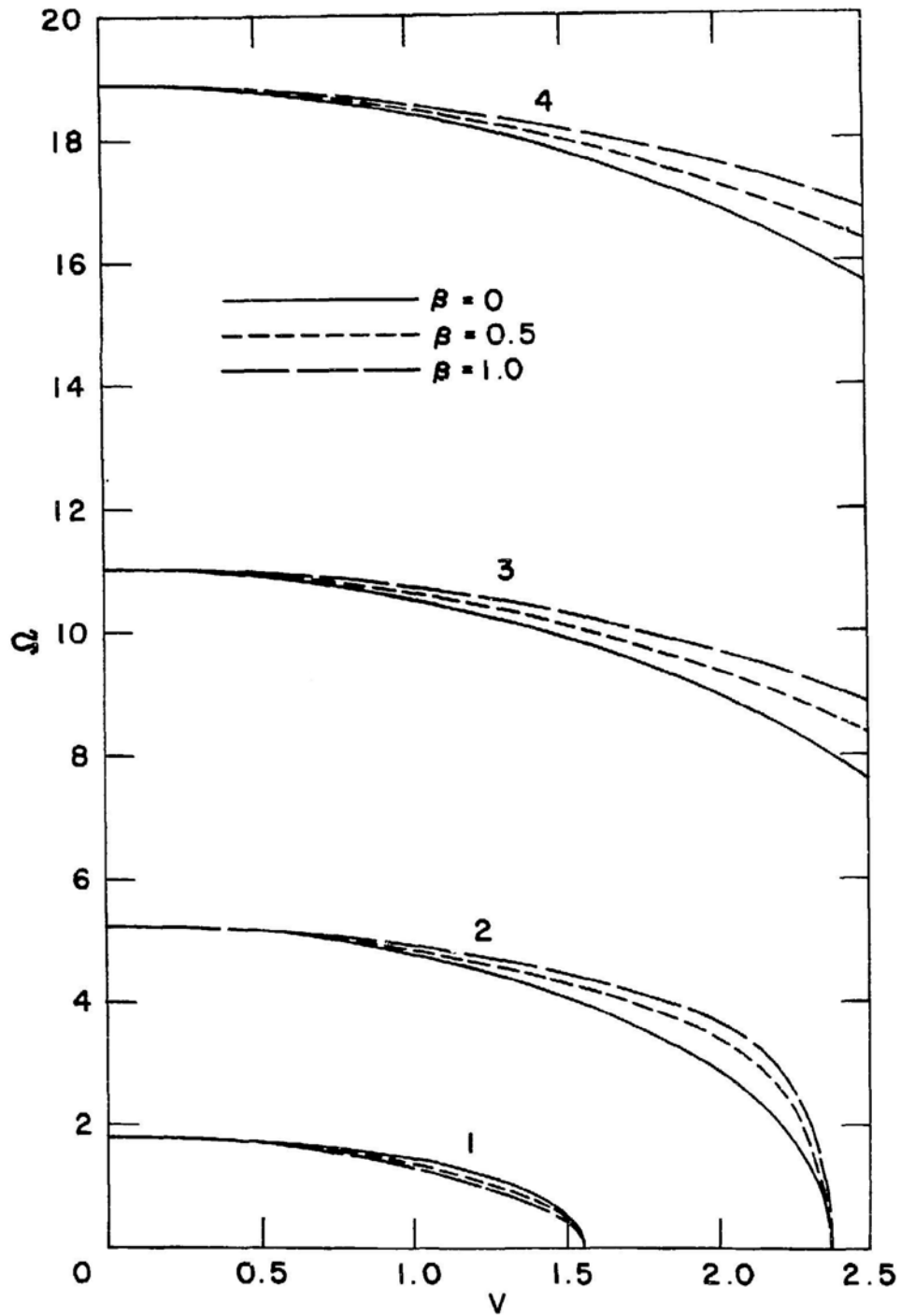


Fig. 5.27. Natural Frequency of a Fixed-Fixed Pipe as a Function of Flow Velocity for $\alpha = \pi$ (Chen 1973)

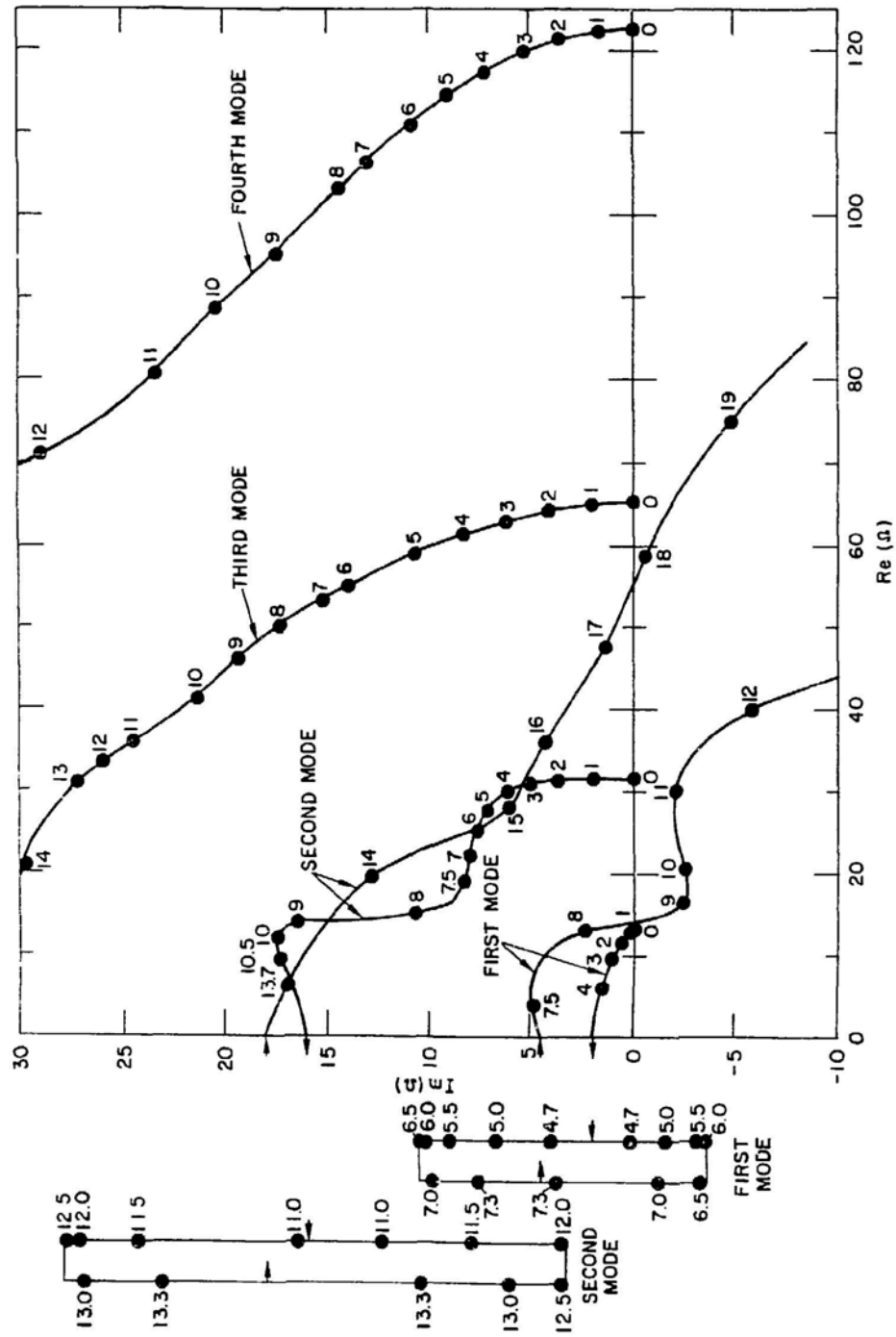


Fig. 5.28. Complex Frequencies of a Fixed-Free Pipe for $\alpha = \pi$ and $\beta = 0.75$ (the dots represent dimensionless flow velocity and the numbers are values of flow velocity) (Chen 1973)

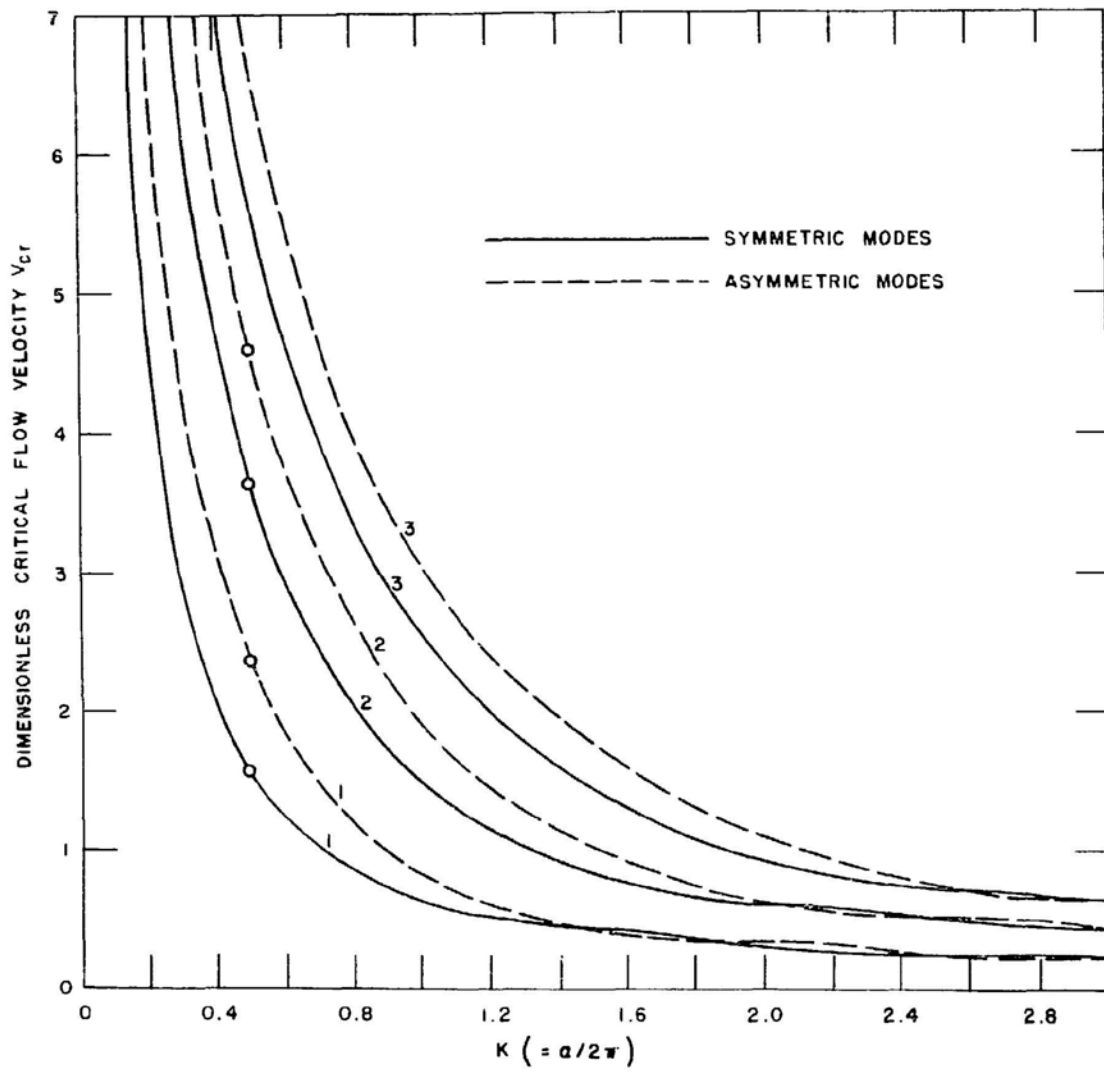


Fig. 5.29. Dimensionless Critical Flow Velocities Under Fixed-Fixed Conditions (Chen 1973)

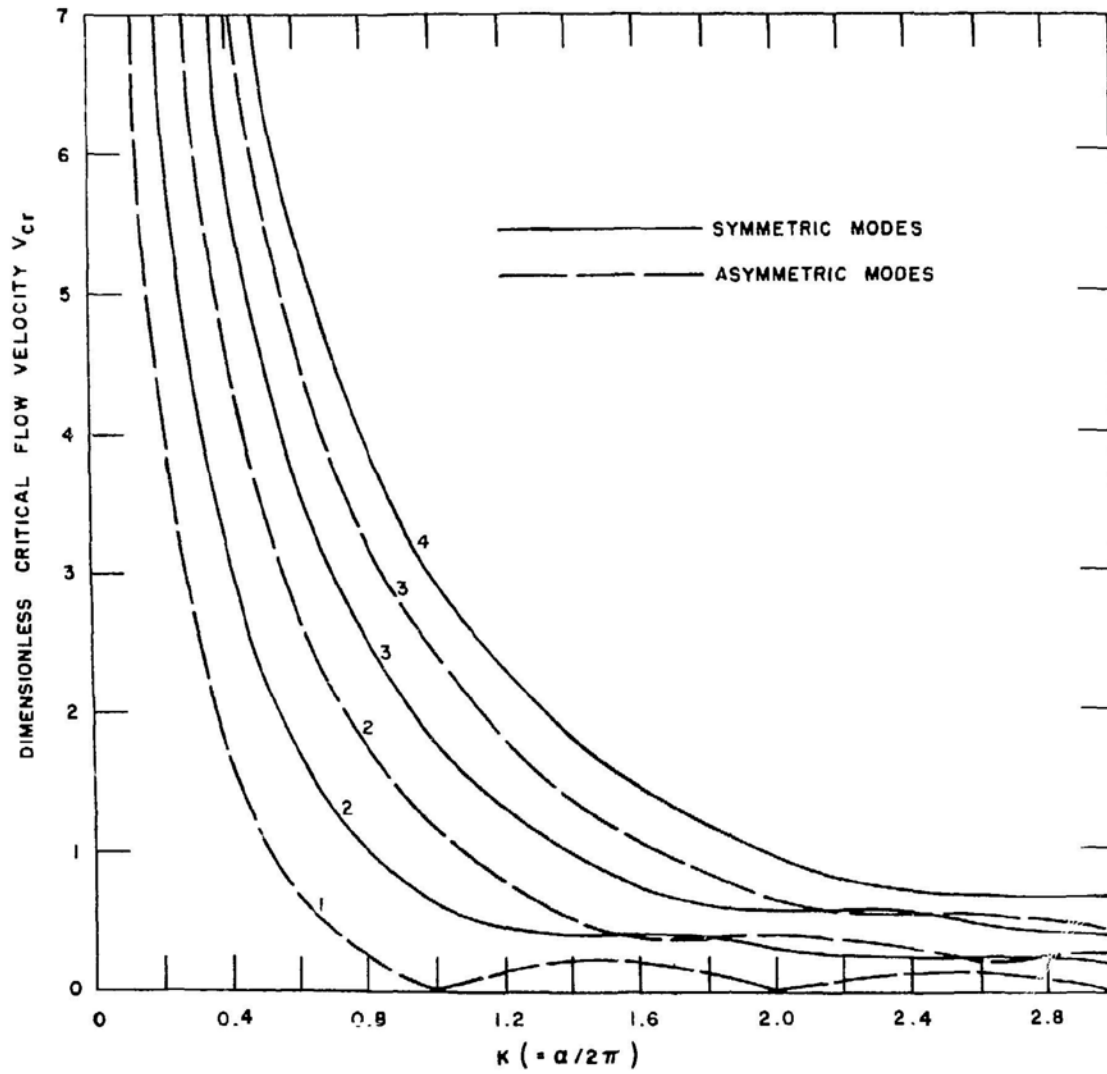


Fig. 5.30. Dimensionless Critical Flow Velocities Under Hinged-Hinged Conditions (Chen 1973)

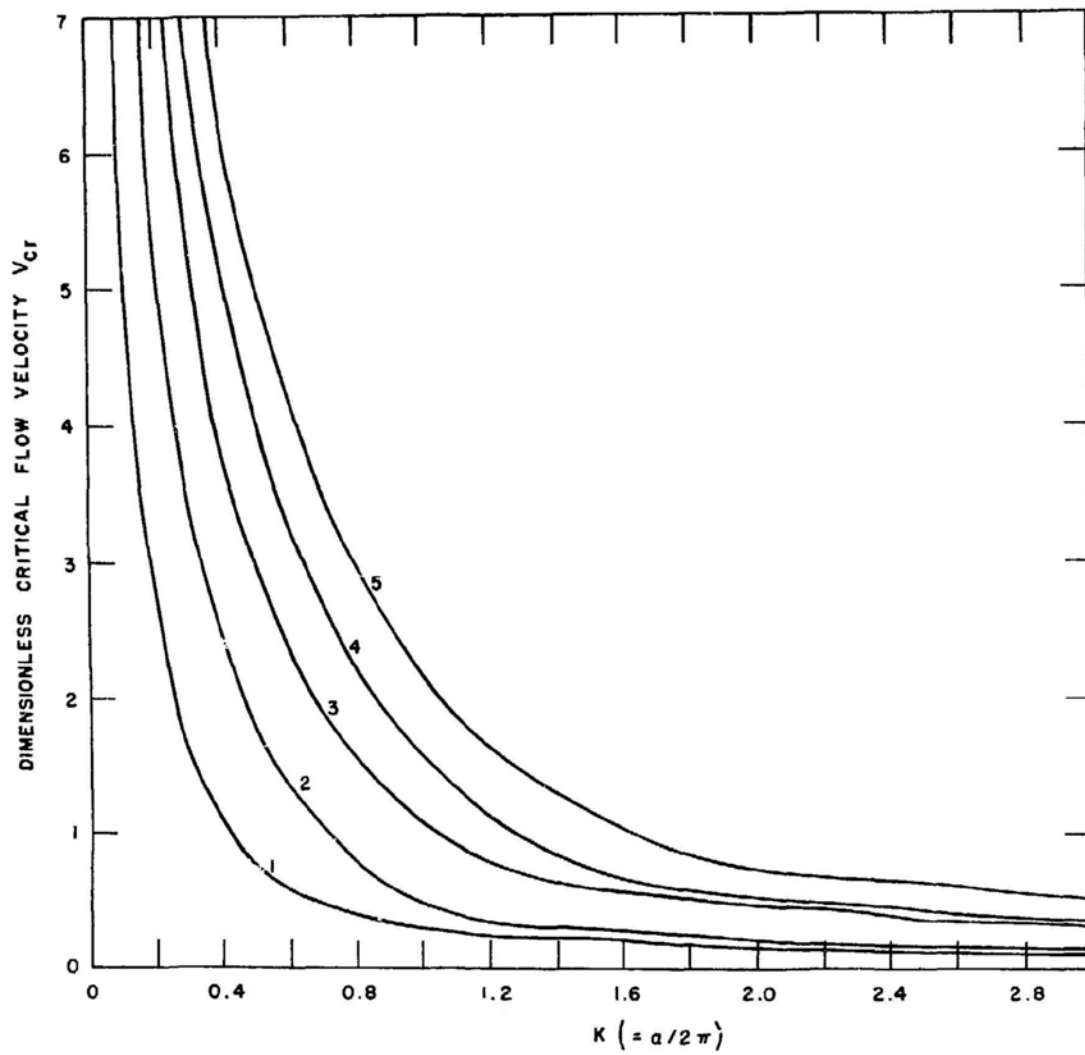


Fig. 5.31. Dimensionless Critical Flow Velocities Under Fixed-Hinged Conditions (Chen 1973)

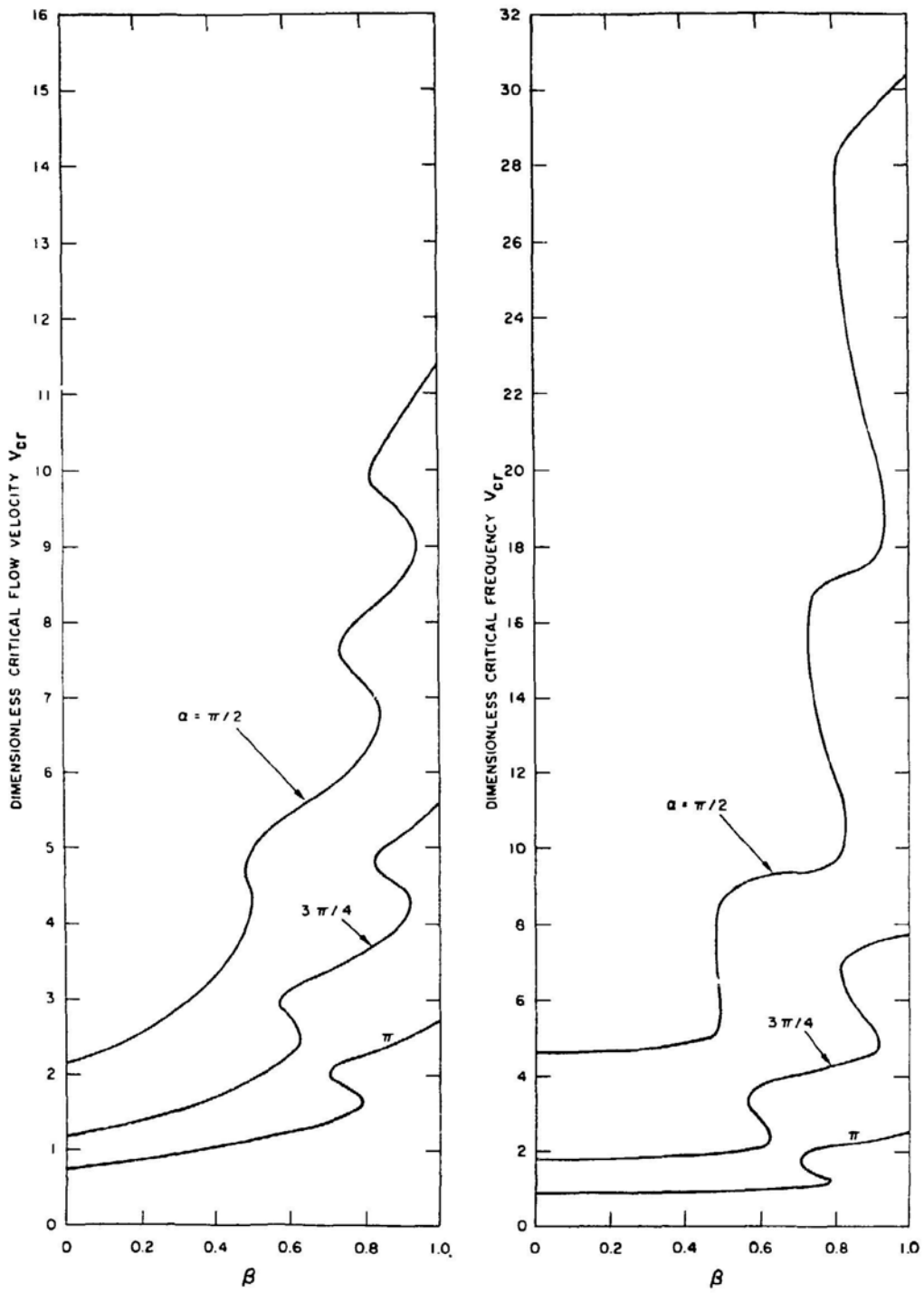


Fig. 5.32. Dimensionless Critical Flow Velocities and Associated Frequencies as Functions of Mass Ratio β for a Cantilevered Pipe (Chen 1973)

As can be seen from Figs. 5.29 and 5.30, the clamped-clamped and pinned-pinned pipes can lose stability in the symmetric and asymmetric modes. The lowest critical flow velocity of the clamped-clamped pipe is associated with the first symmetric mode for $K (= \alpha/2\pi)$ smaller than 1.46. But for K larger than 1.46, the lowest critical flow velocity is alternatively associated with the first asymmetric and first symmetric modes. For the pinned-pinned pipe, the first symmetric mode is a pendulum motion with zero strain energy and is always unstable; therefore, the lowest critical flow velocity is zero. The first critical flow velocity shown in Fig. 5.30 is in the first asymmetric mode. When K is an integer, the first asymmetric mode is also unstable for any small flow velocity.

The stability map for a nonconservative system is shown in Fig. 5.32; the system is stable for values of v lying below the curve with the appropriate value of α , and unstable above it. The instability of nonconservative systems is of the fluttering type and depends strongly on the mass ratio β . Increasing the value of β tends to stabilize the system. For certain ranges of β , the system possesses multiple stable and unstable ranges of flow velocity. For example, consider the case for $\alpha = \pi$ and $\beta = 0.75$. The tube loses stability at $v = 1.50$, regains stability at $v = 1.85$, and loses stability again at $v = 2.20$. This phenomenon is easily understood from Fig. 5.29 and is similar to that of a straight tube.

5.4.3 In-Plane Vibration and Stability

In-plane motion is governed by Eqs. 5.54, 5.61, and 5.64. Upon introducing the dimensionless parameters given in Eq. 5.66 and

$$\eta = u/R, \quad \xi = w/R, \quad (5.80)$$

the equation of motion becomes

$$\begin{aligned} \frac{\partial^6 \xi}{\partial \theta^6} + (2 + v^2) \frac{\partial^4 \xi}{\partial \theta^4} + (1 + 2v^2) \frac{\partial^2 \xi}{\partial \theta^2} + v^2 \xi \\ + 2\beta^{1/2} v \frac{\partial^4 \xi}{\partial \tau \partial \theta^3} + 2\beta^{1/2} v \frac{\partial^2 \xi}{\partial \tau \partial \theta} + \frac{\partial^4 \xi}{\partial \tau^2 \partial \theta^2} - \frac{\partial^2 \xi}{\partial \tau^2} = 0. \end{aligned} \quad (5.81)$$

The boundary conditions to be satisfied are as follows:

- For fixed-fixed tubes,

$$\left. \begin{aligned} \xi(\theta, \tau) &= 0 \\ \eta(\theta, \tau) &= 0 \\ \frac{\partial \eta(\theta, \tau)}{\partial \theta} &= 0 \end{aligned} \right\} \text{ at } \theta = 0 \text{ and at } \theta = \alpha. \quad (5.82)$$

- For fixed-hinged tubes,

$$\left. \begin{aligned} \xi(\theta, \tau) &= 0 \\ \eta(\theta, \tau) &= 0 \\ \frac{\partial \eta(\theta, \tau)}{\partial \theta} &= 0 \end{aligned} \right\} \text{ at } \theta = 0 ; \quad \left. \begin{aligned} \xi(\theta, \tau) &= 0 \\ \eta(\theta, \tau) &= 0 \\ \frac{\partial^3 \xi(\theta, \tau)}{\partial \theta^3} &= 0 \end{aligned} \right\} \text{ at } \theta = \alpha. \quad (5.83)$$

- For hinged-hinged tubes,

$$\left. \begin{aligned} \xi(\theta, \tau) &= 0 \\ \eta(\theta, \tau) &= 0 \\ \frac{\partial^3 \xi(\theta, \tau)}{\partial \theta^3} &= 0 \end{aligned} \right\} \text{ at } \theta = 0 \text{ and } \theta = \alpha. \quad (5.84)$$

- For clamped-free pipes,

$$\left. \begin{aligned} \xi(\theta, \tau) &= 0 \\ \eta(\xi, \tau) &= 0 \\ \frac{\partial \eta(\theta, \tau)}{\partial \theta} &= 0 \end{aligned} \right\} \text{ at } \theta = 0 ; \quad (5.85)$$

$$\left. \begin{aligned}
 \frac{\partial^3 \xi(\theta, \tau)}{\partial \theta^3} + \frac{\partial \xi(\theta, \tau)}{\partial \theta} &= 0 \\
 \frac{\partial^4 \xi(\theta, \tau)}{\partial \theta^4} + \frac{\partial^2 \xi(\theta, \tau)}{\partial \theta^2} &= 0 \\
 \frac{\partial^5 \xi(\theta, \tau)}{\partial \theta^5} + \frac{\partial^3 \xi(\theta, \tau)}{\partial \theta^3} + 2\beta^{1/2} v \left[\frac{\partial^3 \xi(\theta, \tau)}{\partial \theta^2 \partial \tau} + \frac{\partial \xi(\theta, \tau)}{\partial \tau} \right] \\
 + \frac{\partial^3 \xi(\theta, \tau)}{\partial \theta \partial \tau^2} + v^2 &= 0 .
 \end{aligned} \right\} \text{ at } \theta = \alpha , \quad (5.85) \text{ (Contd.)}$$

where α is the total angle of the curved tube.

The solution can be obtained following the same procedure as that for the out-of-plane motion:

$$\begin{aligned}
 \xi(\theta, \tau) &= \text{Re} \left[\left(\sum_{j=1}^6 C_j e^{i\lambda_j \theta} \right) e^{i\Omega \tau} \right] \quad \text{and} \\
 \eta(\theta, \tau) &= \text{Re} \left[\left(\sum_{j=1}^6 i\lambda_j C_j e^{i\lambda_j \theta} \right) e^{i\Omega \tau} \right]
 \end{aligned} \quad (5.86)$$

where λ_j 's are the solution of the equation

$$\begin{aligned}
 \lambda^6 - (2 + v^2)\lambda^4 - 2\beta^{0.5} v \Omega \lambda^3 + (1 + 2v^2 - \Omega^2)\lambda^2 \\
 + 2\beta^{0.5} v \Omega \lambda - \Omega^2 - v^2 = 0 .
 \end{aligned} \quad (5.87)$$

The constants C_j 's are determined by

$$\begin{bmatrix} a_{11} & a_{12} & a_{13} & a_{14} & a_{15} & a_{16} \\ a_{21} & a_{22} & a_{23} & a_{24} & a_{25} & a_{26} \\ a_{31} & a_{32} & a_{33} & a_{34} & a_{35} & a_{36} \\ a_{41} & a_{42} & a_{43} & a_{44} & a_{45} & a_{46} \\ a_{51} & a_{52} & a_{53} & a_{54} & a_{55} & a_{56} \\ a_{61} & a_{62} & a_{63} & a_{64} & a_{65} & a_{66} \end{bmatrix} \begin{Bmatrix} C_1 \\ C_2 \\ C_3 \\ C_4 \\ C_5 \\ C_6 \end{Bmatrix} = \begin{Bmatrix} 0 \\ 0 \\ 0 \\ 0 \\ 0 \\ \mu \end{Bmatrix} , \quad (5.88)$$

where

$$a_{1k} = 1 ,$$

$$a_{2k} = \lambda_k ,$$

$$a_{3k} = -\lambda_k^2 , \text{ for fixed-fixed and fixed-hinged tubes,}$$

$$= -i\lambda_k^3 , \text{ for hinged-hinged tubes,}$$

$$a_{4k} = e^{i\lambda_k \alpha} ,$$

$$a_{5k} = i\lambda_k e^{i\lambda_k \alpha} , \quad (5.89)$$

$$a_{6k} = -\lambda_k^2 e^{i\lambda_k \alpha} , \text{ for fixed-fixed tubes,}$$

$$= -i\lambda_k^3 e^{i\lambda_k \alpha} , \text{ for fixed-hinged and hinged-hinged tubes,}$$

$$k = 1, 2, 3, 4, 5, 6.$$

and

$$\mu = 0 , \text{ for fixed-fixed, fixed-hinged and hinged-hinged pipes ,}$$

$$= v^2 , \text{ for fixed-free pipe.}$$

The frequency equation is obtained by setting the determinant of coefficients in Eqs. 5.88 equal to zero. It is a functional relation between the frequency Ω and system parameters, such as the total angle α , mass ratio β , and flow velocity v . Therefore, the frequency equation can be written as

$$F(\Omega, \alpha, \beta, v) = 0 . \quad (5.90)$$

The critical flow velocity depends on the subtended angle α . The stability map for fixed-fixed pipe is given in Fig. 5.33; the mode shapes at instability for four modes, identified as A, B, C, and D in Fig. 5.33, are shown in Fig. 5.34.

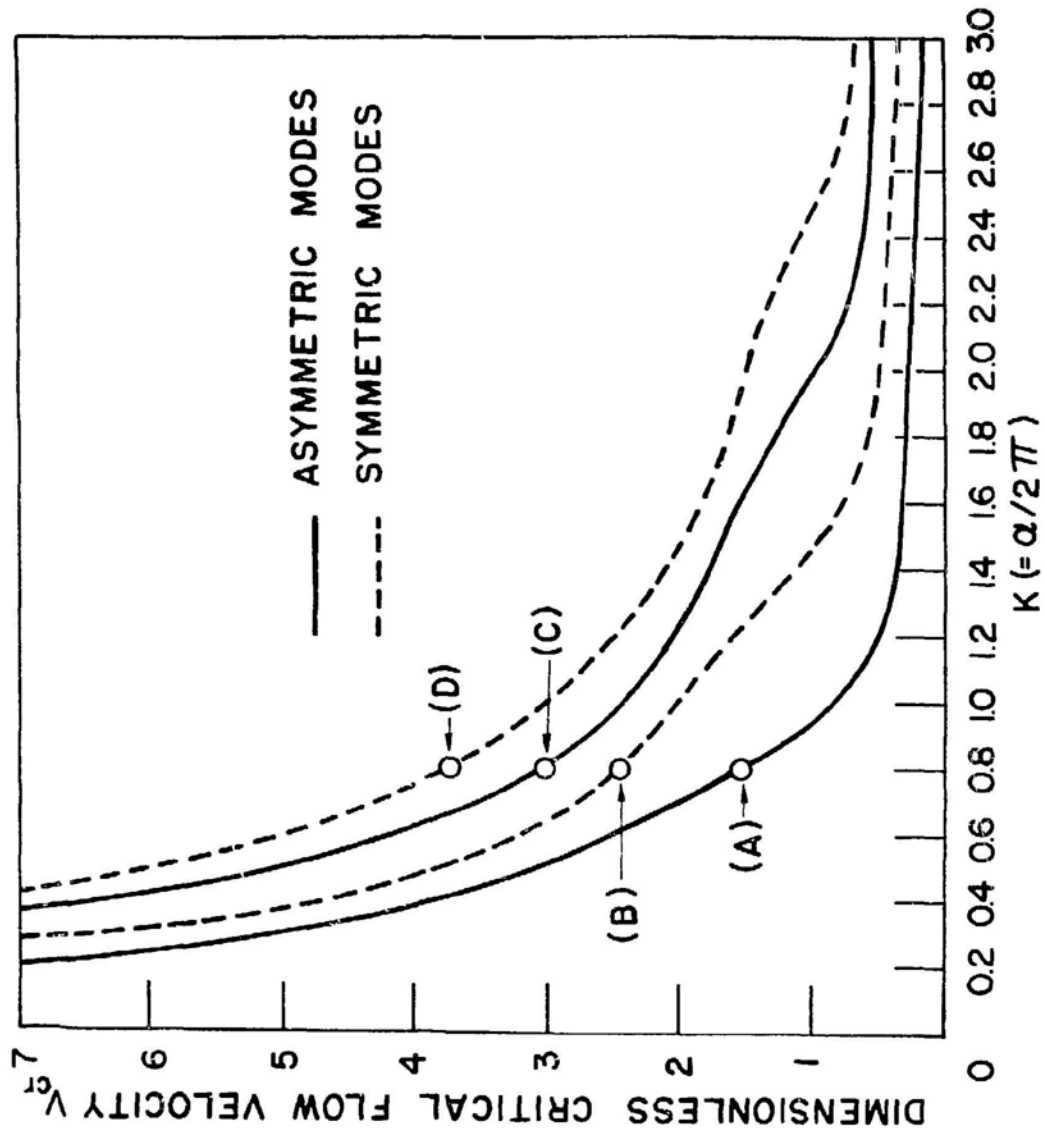


Fig. 5.33. Dimensionless Critical Flow Velocities for Fixed-Fixed Pipes (Chen 1972a)

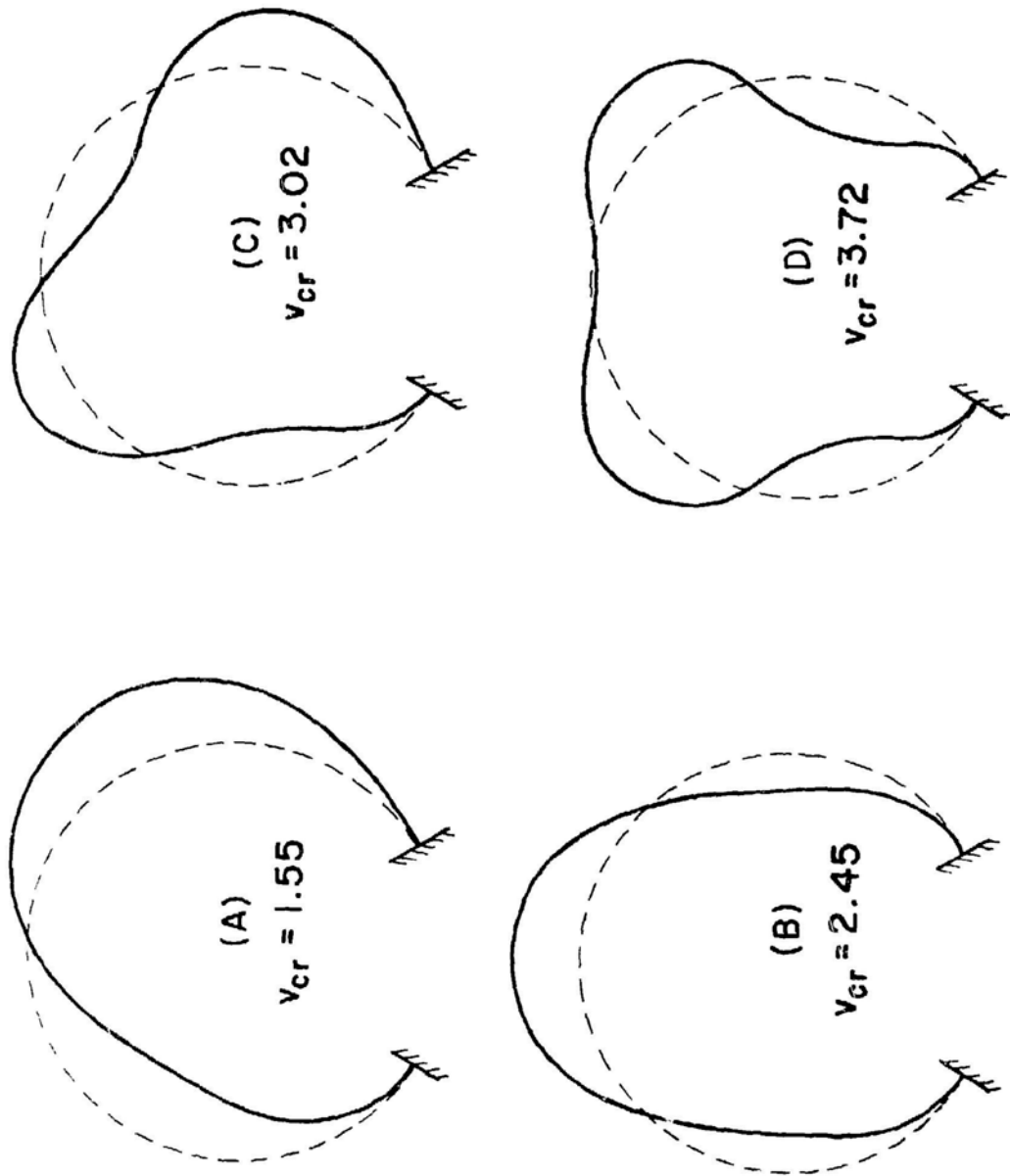


Fig. 5.34. Asymmetric and Symmetric Mode Shapes for $\alpha/2\pi = 0.8$ for Fixed-Fixed Pipes (Chen 1972a)

The static deformation caused by the fluid centrifugal force on the pipe has not been included in the analysis. If these initial forces are included, they stabilize the pipe and the pipe does not buckle (Hill and Davis 1974). Apparently, there are no experimental results available to confirm these predictions.

5.5 CIRCULAR CYLINDRICAL SHELLS CONVEYING FLUID

In Sections 5.3 and 5.4, the pipes were analyzed by using beam theory and slug flow. If the pipe wall is thin and its length-to-radius ratio is not large, the pipe can be considered a beam. Analyses according to the cylindrical shell theory have been made by Niordson (1953), Clinch (1970), Paidoussis and Denise (1972), Weaver and Myklatun (1973), Chen and Rosenberg (1974), and Weaver and Paidoussis (1977).

The dynamic characteristics can be predicted using the thin shell and potential flow theories. The equations of motion for a circular cylindrical shell conveying an ideal fluid are the same as those given in Eqs. 4.1 except that there is an additional fluid pressure acting on the shell in the radial direction; i.e., the right side of the third equation zero is replaced by $(1 - \nu^2)p/Eh$. p is internal fluid pressure, which is given by

$$p = -\rho \left(\frac{\partial \phi}{\partial r} + U \frac{\partial \phi}{\partial z} \right) \bigg|_{r=R}. \quad (5.91)$$

Here U is the flow velocity and ϕ is the velocity potential. ϕ satisfies the Laplace equation

$$\nabla^2 \phi = 0,$$

and

(5.92)

$$\frac{\partial \phi}{\partial r} \bigg|_{r=R} = \frac{\partial w}{\partial t} + U \frac{\partial w}{\partial z}.$$

Using Eqs. 4.1, 5.91, and 5.92, and following the procedure given in Section 4.3, we can analyze the shell response in a straightforward manner [see Niordson (1953), Paidoussis and Denise (1972), and Chen and Rosenberg (1974), for details].

The general behavior of circular cylindrical shell conveying fluid is not much different from that of a pipe conveying fluid. Its instability characteristics also depend on the boundary conditions. For a cantilevered shell, the lower modes are damped by low flow velocities; with increasing flow velocity, the system eventually loses stability by flutter. The lowest

critical flow velocity may be associated with different circumferential wave number n , depending on the physical and geometrical characteristics of the system.

The behavior with increasing flow of cylindrical shells with both ends clamped or hinged is also similar to a gyroscopically conservative pipe using a beam theory. Increasing the flow velocity reduces the natural frequencies. At sufficiently high flow velocity, each frequency vanishes, which corresponds to the onset of divergence-type instability in that mode. However, coupled-mode flutter usually follows at a flow velocity a little higher than the divergence critical flow velocity. Thus, the system is subject to divergence instabilities followed by flutter. In experiments, flutter was observed but divergence was not (Paidoussis and Denise 1972), probably due to the difficulty in determining the divergence. Because flutter-type instability is a more violent oscillation, it is much easier to demonstrate.

The subcritical vibration of circular cylindrical shell has also been studied theoretically and experimentally. The complete analysis is complicated, but the general theory is simple. Details are given by Clinch (1970), Lakis and Paidoussis (1972), and Au-Yang (1975).

5.6 CLOSING REMARKS

More than 100 publications on the dynamic response of pipes conveying fluid have been published in the last three decades. Most of these discuss pipe response based on linear theories; only a few studies are based on nonlinear theory in an effort to understand nonlinear behavior at postcritical flow velocities. A more systematic study of nonlinear behavior is needed for understanding of the nonlinear characteristics of a typical nonconservative system.

For practical system components, the critical flow velocity is usually very high. Thus, instability is unlikely except for structural components with very low rigidity and high velocity flow. To the contrary, subcritical vibration always exists and may be important. To predict subcritical response, we can use the general theory presented in this chapter. For response to turbulent pressure fluctuations, the technique to be discussed in Chapter 6 can be applied.

Another important aspect of pipes conveying fluid is the transient response of pipe and fluid, which is generally called fluid transients in pipes or waterhammer. This is not covered in this report; see Streeter and Wylie (1967) and Chaudhry (1979) for details.

REFERENCES--Sec. 5

- Ahmadi, G., and Satter, M. A. 1978. Stability of a Pipe Carrying Time-Dependent Flowing Fluid. *J. of the Franklin Institute* 305(1), 1-9.
- Ashley, H., and Haviland, G. 1950. Bending Vibrations of a Pipe Line Containing Flowing Fluid. *J. Appl. Mech., Trans. ASME* 17(3), 229-232.
- Au-Yang, M. K. 1975. Response of Reactor Internals to Fluctuating Pressure Forces. *Nucl. Eng. Des.* 35, 361-375.
- Bajaj, A. K., Sethna, P. R., and Lundgren, T. S. 1980. Hopf Bifurcation Phenomena in Tubes Carrying a Fluid. *SIAM J. Appl. Math.* 39, 213-230.
- Becker, M., and Hauger, W. 1978. Exact Stability Analysis of Uniform Cantilevered Pipes Conveying Fluid or Gas. *Archives of Mechanics* 30(6), 757-768.
- Benjamin, T. B. 1961. Dynamics of a System of Articulated Pipes Conveying Fluid: I. Theory, II. Experiment. *Proc. Royal Soc. London* 261(Series A), 457-499.
- Bohn, M. P., and Herrmann, G. 1974a. The Dynamic Behavior of Articulated Pipes Conveying Fluid with Periodic Flow Rate. *J. Appl. Mech., Trans. ASME* 41(1), 55-62.
- Bohn, M. P., and Herrmann, G. 1974b. Instabilities of a Spatial System of Articulated Pipes Conveying Fluid. *J. Fluids Eng.* 41, 289-295.
- Bourrieres, F.-J. 1939. Sur un Phénomène d'Oscillation Auto-Entretenu en Mécanique des Fluides Réels. *Publications Scientifiques et Techniques du Ministère de l'Air*, No. 147.
- Chaudhry, M. H. 1979. *Applied Hydraulic Transients*. Van Nostrand Reinhold Co.
- Chen, S. S. 1971a. Flow-Induced Instability of an Elastic Tube. *ASME Vib. Conf.*, ASME Paper 71-Vibr-39, Toronto, Canada.
- Chen, S. S. 1971b. Dynamic Stability of Tubes Conveying Fluid. *J. Engr. Mech. Div., ASCE* 97(EM5), 1469-1485.
- Chen, S. S. 1972a. Vibration and Stability of a Uniformly Curved Tube Conveying Fluid. *J. Acoust. Soc. Am.* 51(1), 223-232.
- Chen, S. S. 1972b. Flow-Induced In-Plane Instabilities of Curved Pipes. *Nucl. Eng. Des.* 23, 29-38.
- Chen, S. S. 1973. Out-of-Plane Vibration and Stability of Curved Tubes Conveying Fluid. *J. Appl. Mech., Trans. ASME* 40(2), 362-368.
- Chen, S. S. 1974. Parallel-Flow-Induced Vibrations and Instabilities of Cylindrical Structures. *Shock and Vibration Digest* 6(10), 2-12.
- Chen, S. S., and Rosenberg, G. S. 1971. Vibration and Stability of a Tube Conveying Fluid. *USAE Rept.*, ANL-7762.

- Chen, S. S., and Rosenberg, G. S. 1974. Free Vibrations of Fluid-Conveying Cylindrical Shells. *Trans. ASME, J. Eng. for Indus.* 96, 420-426.
- Chen, S. S., and Jendrzejczyk, J. A. 1984. Stability of Tubes Conveying Fluid. Argonne National Lab. ANL-84-5.
- Chen, T. L. C., and Bert, C. W. 1977. Dynamic Stability of Isotropic or Composite-Material Cylindrical Shells Containing Swirling Fluid Flow. *J. Appl. Mech.* 99(1), 112-116.
- Clinch, J. M. 1970. Prediction and Measurement of the Vibrations Induced in the Thin-Walled Pipes by the Passage of Internal Turbulent Water Flow. *J. Sound Vib.* 12(4), 429-451.
- Dodds, H. L., and Runyan, H. L. 1965. Effect of High-Velocity Fluid Flow on the Bending Vibrations and Static Divergence of a Simply Supported Pipe. NASA-TN-D-2870.
- Doll, R. W., and Mote, C. D., Jr. 1976. On the Dynamic Analysis of Curved and Twisted Cylinders Transporting Fluids. *J. Pres. Vessel Tech., Trans. ASME*, 98(2), 143-150.
- Dowell, E. H. 1982. Flutter of a Buckled Plate as an Example of Chaotic Motion of a Deterministic Autonomous System. *J. Sound Vib.* 85(3), 333-344.
- Edelstein, W. S., Chen, S. S., and Jendrzejczyk, J. A. 1986. A Finite Element Computation of the Flow-Induced Oscillations in a Cantilevered Tube. *J. Sound Vib.* (In press).
- Feodos'ev, V. P. 1951. Vibrations and Stability of a Pipe When Liquid Flows Through It. *Inzhenernyi Sbornik* 10, 169-170.
- Ginsberg, J. H. 1973. The Dynamic Stability of a Pipe Conveying a Pulsatile Flow. *Int. J. Eng. Sci.* 11, 1013-1024.
- Greenwald, A. S., and Dugundji, J. 1967. Static and Dynamic Instabilities of a Propellant Line. AFOSR Sci. Rept., AFOSR 67-1395.
- Gregory, R. W., and Paidoussis, M. P. 1966. Unstable Oscillation of Tubular Cantilevers Conveying Fluid: I. Theory, II. Experiment. *Proc. Royal Soc. London* 293(Series A), 512-542.
- Hannoyer, M. J., and Paidoussis, M. P. 1979. Dynamics of Slender Tapered Beam with Internal or External Axial Flow; Part 2: Experiments. *J. Appl. Mech.* 46, 52-57.
- Hara, F. 1973. A Theory on the Two-Phase Flow-Induced Vibrations in Piping Systems. *Proc. 2nd Int. Conf. Struc. Mech. in Reactor Tech.*, Paper No. F5/1, Berlin, Germany.
- Hara, F. 1977. Two-Phase-Flow-Induced Vibrations in a Horizontal Piping System. *Bulletin of the JSME* 20(142), 419-427.
- Hara, F., Shigeta, T., and Shibata, H. 1972. Two-Phase Flow-Induced Random Vibrations. *Proc. Symp. on Flow-Induced Struc. Vib.*, Paper No. G5, Karlsruhe, Germany (Aug. 14-16, 1972).

- Herrmann, G. 1967. Stability of Equilibrium of Elastic Systems Subjected to Nonconservative Forces. *Appl. Mech. Reviews* 20(2), 103-108.
- Herrmann, G., and Jong, I. C. 1965. On the Destabilizing Effect of Damping in Non-Conservative Elastic Systems. *J. Appl. Mech.* 32, 592-597.
- Hill, J. L., and Swanson, C. P. 1970. Effects of Lumped Masses on the Stability of Fluid Conveying Tubes. *J. Appl. Mech., Trans. ASME* 37(2), 494-497.
- Hill, J. L., and Davis, C. G. 1974. The Effect of Initial Forces on the Hydroelastic Vibration and Stability of Planar Curved Tubes. *J. Appl. Mech., Trans. ASME* 41(2), 355-359.
- Holmes, P. J. 1978. Pipes Supported at Both Ends Cannot Flutter. *J. Appl. Mech.* 45, 619-622.
- Hopkins, G. R. 1969. Stability of Fluid Conveying Tubes with Periodic Perturbations. PhD Thesis, Univ. Ala.
- Housner, G. W. 1952. Bending Vibrations of a Pipe Line Containing Flowing Fluid. *J. Appl. Mech., Trans. ASME* 19(2), 205-208.
- Jendrzeczyk, J. A., and Chen, S. S. 1983. Experiments on Tubes Conveying Fluid. Argonne National Lab. ANL-83-18.
- Jones, L. H., and Goodwin, B. E. 1971. The Transverse Vibrations of a Pipe Containing Flowing Fluid: Methods of Integral Equations. *Quart. Appl. Math.* 29, 363-374.
- Kornecki, A. 1971. On Application of Galerkin's Method to Non-Self-Adjoint Equations. *Israel Journal of Technology* 9(1-2), 189-194.
- Lakis, A. A., and Paidoussis, M. P. 1972. Prediction of the Response of a Cylindrical Shell to Arbitrary or Boundary Layer Induced Random Pressure Fields. *J. Sound Vib.* 25(1), 1-27.
- Li, T., and DiMaggio, O. D. 1964. Vibration of a Propellant Line Containing Flowing Fluid. *AIAA 5th Annual Struc. and Matl. Conf.* CP-8, 194-199.
- Lin, H. C., and Chen, S. S. 1976. Vibration and Stability of Fluid-Conveying Pipes. *Shock Vib. Bull.* 46(Part 2), 267-283.
- Liu, H. S., and Mote, C. D. 1974. Dynamic Response of Pipes Transporting Fluids. *J. Eng. for Indus.* 96, 591-596.
- Long, R. H., Jr. 1955. Experimental and Theoretical Study of Transverse Vibration of a Tube Containing Flowing Fluid. *J. Appl. Mech., Trans. ASME* 22(1), 65-68.
- Lundgren, T. S., Sethna, P. R., and Bajaj, A. K. 1979. Stability Boundaries for Flow Induced Motions of Tubes with an Inclined Terminal Nozzle. *J. Sound Vib.* 64, 553-571.
- McIver, D. B. 1973. Hamilton's Principle for Systems of Changing Mass. *J. of Eng. Mathematics* 7(3), 249-261.

- Mote, C. D. 1971. Nonconservative Stability by Finite Element. J. Engr. Mech. Div., ASCE 97(EM3), 645-657.
- Naguleswaran, S., and Williams, C. J. H. 1968. Lateral Vibration of a Pipe Conveying a Fluid. J. Mech. Eng. Sci. 10(3), 228-238.
- Nemat-Nasser, S., Prasad, S. N., and Herrmann, G. 1966. Destabilizing Effect of Velocity-Dependent Forces in Nonconservative Continuous Systems. AIAA J. 4(7), 1276-1280.
- Niordson, F. I. N. 1953. Vibrations of a Cylindrical Tube Containing Flowing Fluid. Trans. Royal Inst. Tech. (Stockholm), No. 73.
- Noah, S. T., and Hopkins, G. R. 1980. Dynamic Stability of Elastically Supported Pipes Conveying Fluid. J. Sound Vib. 71(1), 103-116.
- Paidoussis, M. P. 1970. Dynamics of Tubular Cantilevers Conveying Fluid. J. Mech. Engr. Sci. 12(2), 85-103.
- Paidoussis, M. P., and Deksnis, E. B. 1970. Articulated Models of Cantilevers Conveying Fluid: The Study of a Paradox. J. Mech. Eng. Sci. 12(4), 288-300.
- Paidoussis, M. P., and Denise, J. P. 1972. Flutter of Thin Cylindrical Shells Conveying Fluid. J. Sound Vib. 20(1), 9-26.
- Paidoussis, M. P., and Issid, N. T. 1974. Dynamic Stability of Pipes Conveying Fluid. J. Sound Vib. 33(3), 267-294.
- Paidoussis, M. P. 1975. Flutter of Conservative System of Pipes Conveying Incompressible Fluid. J. Mech. Eng. Sci. 17(1), 19-25.
- Paidoussis, M. P., and Sundararajan, C. 1975. Parametric and Combination Resonances of a Pipe Conveying Pulsating Fluid. J. Appl. Mech., Trans. ASME 42(4), 780-784.
- Paidoussis, M. P., and Issid, N. T. 1976. Experiments on Parametric Resonance of Pipes Containing Pulsatile Flow. J. Appl. Mech. 43, 198- 02.
- Roussellet, J., and Herrmann, G. 1978. Influence of Nonlinearities on the Behavior of Parametrically Excited Articulated Pipes Conveying Fluid. Trans. de la SCGM 5(1), 31-38.
- Roussellet, J., and Herrmann, G. 1981. Dynamic Behavior of Continuous Cantilevered Pipes Conveying Fluid Near Critical Velocities. J. Appl. Mech. 48, 943-947.
- Shilling, R., and Lou, Y. K. 1980. An Experimental Study on the Dynamic Response of a Vertical Cantilever Pipe Conveying Fluid. J. Energy Resources Technol. 102, 129-139.
- Singh, K., and Mallik, A. K. 1978. Use of Dynamic Absorbers to Control Parametric Instabilities of a Pipe. J. Appl. Mech. 45, 949-951.
- Singh, K., and Mallik, A. K. 1979. Parametric Instabilities of a Periodically Supported Pipe Conveying Fluid. J. Sound Vib. 62(3), 379-397.

- Springfield, T. H. 1970. Stability and Vibration of Fluid Conveying Incomplete Circular Tubes. PhD Thesis, Univ. Ala.
- Stein, R. A., and Tobriner, M. W. 1970. Vibration of Pipes Containing Flowing Fluids. J. Appl. Mech., Trans. ASME 37(4), 906-916.
- Streeter, V. L., and Wylie, E. B. 1967. Hydraulic Transients. McGraw-Hill Book Co., New York.
- Thurman, A. L., and Mote, C. D. 1969. Nonlinear Oscillation of a Cylinder Containing a Flowing Fluid. J. Eng for Indus., Trans. ASME 91, 1147-1155.
- Unny, T. E., Martin, E. L., and Dubey, R. N. 1970. Hydroelastic Instability of Uniformly Curved Pipe-Fluid Systems. J. Appl. Mech., Trans. ASME 37(3), 817-822.
- Weaver, D. S., and Myklatun, B. 1973. On the Stability of Thin Pipes with an Internal Flow. J. Sound Vib. 31(4), 399-410.
- Weaver, D. S., and Paidoussis, M. P. 1977. On Collapse and Flutter Phenomena in the Tubes Conveying Fluid. J. Sound Vib. 50(1), 117-132.

6. CIRCULAR CYLINDERS IN AXIAL FLOW

6.1 INTRODUCTION

The study of the dynamics of circular cylinders in axial flow is relatively new. The original focus of fluidelastic studies on circular cylinders was the stability problem--in particular, flutter of a flexible rod. Generally, the instability flow velocity for practical system components occurs at relatively high flow, which is unlikely to be encountered. The recent development of the subject is in connection with the design and development of nuclear reactor cores because the vibration of fuel rods can promote anomalous behavior, as exhibited in neutron flux oscillations (Williams 1970; Pazsit et al. 1984) and fretting and wear (Wambsganss 1967; Kinsel 1975; Pickman 1975; Schmugar 1975).

Starting in the late 1950s, each of the earlier studies had one or more of the following objectives:

- Assessing the significance of fluidelastic instability of fuel rods,
- Measuring the amplitude of vibration in a simulated model,
- Mathematical modeling of flow-induced vibration,
- Identifying the damping mechanism, and
- Identifying the forcing function.

The studies have yielded several expressions that offer guidance to reactor designers on the order of magnitude of vibration.

6.2 EQUATION OF MOTION OF A CIRCULAR CYLINDER IN AXIAL FLOW

Consider a circular cylinder immersed in a fluid flowing at velocity U parallel to the z axis (Fig. 6.1). The cylinder has linear density (mass per unit length) m , flexural rigidity EI , and total length L . All motions of the cylinder are to be confined in the y - z plane. Conventionally, the equation of motion is derived by "slender body" theory, which is based on studies of flow about ships in the early 1920s (Hawthorne 1961).

Consider a small element δz of the cylinder, as shown in Fig. 6.2, where T is the tension, Q is the shear force, M is the bending moment, $m(\partial^2 u / \partial t^2) \delta z$ is the inertial force of the rod, $g \delta z$ is the external force acting on the cylinder surface, $F_D \delta z$ is the viscous damping force, and F_N and F_L are the drag forces per unit length in the transverse and longitudinal directions. F_I , which represents the lateral force per unit length acting on the rod, is given by the change in momentum of the lateral flow about the cylinder (Lighthill 1960):

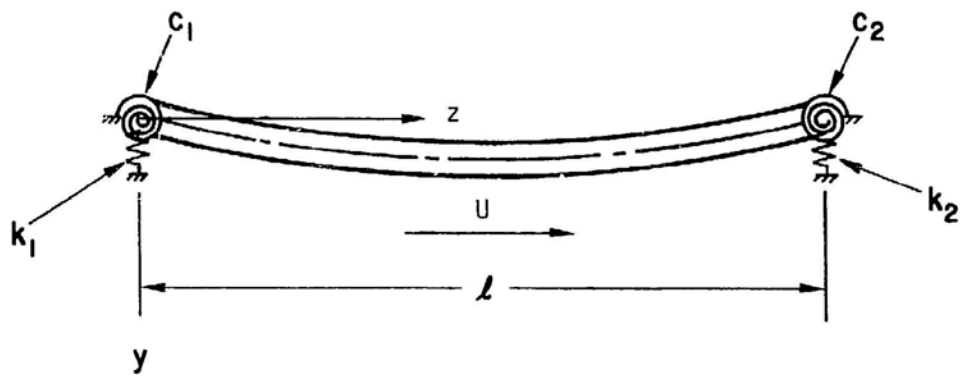


Fig. 6.1. Circular Cylinder in Axial Flow

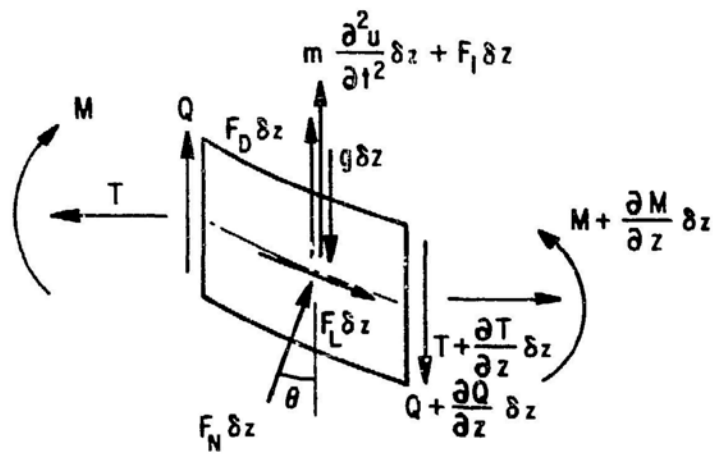


Fig. 6.2. Forces and Moments Acting on an Element of the Cylinder

$$F_I = m_a \left(\frac{\partial}{\partial t} + U \frac{\partial}{\partial x} \right)^2 u . \quad (6.1)$$

Here, m_a is the added mass of the cylinder, which is given by (see Chapter 2)

$$m_a = \frac{\pi D^2}{4} \rho C_m . \quad (6.2)$$

The differential equations for translatory motions in z and y directions of the element are

$$\frac{\partial T}{\partial z} + F_L = 0 \quad (6.3)$$

and

$$\frac{\partial Q}{\partial z} - m \frac{\partial^2 u}{\partial t^2} - F_I - F_N - F_D + F_L \frac{\partial y}{\partial z} + q = 0 . \quad (6.4)$$

If rotatory inertia is neglected, the equation of rotational equilibrium in the y - z plane is

$$\frac{\partial M}{\partial z} - Q + T \frac{\partial y}{\partial z} = 0 . \quad (6.5)$$

The cylinder material is postulated to obey a stress-strain relationship of the Kelvin type, i.e.,

$$\sigma = Ee + \mu \dot{e} , \quad (6.6)$$

where E is Young's modulus of elasticity, μ is the internal damping coefficient, σ and e are the stress and strain, and the dot denotes differentiation with respect to time. Classical beam theory is employed, and the stress and strain are

$$\sigma = \frac{Mx}{I} \quad (6.7)$$

and

$$e = -x \frac{\partial^2 y}{\partial z^2}, \quad (6.8)$$

where x is the distance of each fiber to the neutral axis. Substituting Eqs. 6.7 and 6.8 into 6.6 gives

$$M = -E(I \frac{\partial^2 y}{\partial z^2} + \mu \frac{\partial^3 y}{\partial t \partial z^2}). \quad (6.9)$$

From Eqs. 6.1, 6.3, 6.4, 6.5, and 6.9, we obtain a single partial differential equation of motion for the transverse displacement:

$$\begin{aligned} EI \frac{\partial^4 u}{\partial z^4} + \mu I \frac{\partial^5 u}{\partial z^4 \partial t} + m_a \left(\frac{\partial}{\partial t} + U \frac{\partial}{\partial z} \right)^2 u + F_N + F_D \\ - T \frac{\partial^2 u}{\partial z^2} + m \frac{\partial^2 u}{\partial t^2} = g. \end{aligned} \quad (6.10)$$

Next, consider the drag forces F_N and F_L , damping force F_D , and tensile force T . The forces acting on a rod set obliquely to a stream of fluid are discussed by Taylor (1952). For rough cylinders,

$$F_N = \frac{1}{2} \rho D U^2 (C_D \sin^2 \theta + C_f \sin \theta) \quad (6.11)$$

and

$$F_L = \frac{1}{2} \rho D U^2 C_f \cos \theta, \quad (6.12)$$

where C_D and C_f are the drag coefficients due to pressure and shear forces, and θ is the angle of incidence, which is related to the normal and axial components of flow velocity by

$$\theta = \sin^{-1} \left[\frac{1}{U} \left(\frac{\partial u}{\partial t} + U \frac{\partial u}{\partial z} \right) \right]. \quad (6.13)$$

For small cylinder motion, θ is small; therefore, Eqs. 6.11 and 6.12 are approximated by

$$F_N = \frac{1}{2} \frac{m_a}{D} U C_N \left(\frac{\partial u}{\partial t} + U \frac{\partial u}{\partial z} \right) \quad (6.14)$$

and

$$F_L = \frac{1}{2} \frac{m_a}{D} U^2 C_T, \quad (6.15)$$

where

$$C_N = C_T = \frac{4C_f}{\pi C_m}. \quad (6.16)$$

Here, C_N and C_T will be considered not necessarily equal. Typically, $C_f = 0.01$ to 0.03 for $Re > 10^4$.

The longitudinal tension consists of externally applied tension and tension arising from fluid friction. For a cylinder supported at both ends, the initial axial tension is taken as T_0 when $U = 0$; and as U increases, no further motion of the supports is allowed. For a cylinder with one end free, the initial axial tension is zero for $U = 0$, but as U increases, the free end is subjected to a tensile force

$$T(l, t) = \frac{1}{2} C_T^* m_a U^2, \quad (6.17)$$

where C_T^* is the form drag coefficient at the free end. Thus, on substituting Eq. 6.15 into Eq. 6.3, integrating the resulting equation and then using the assumption stated above, we find that the axial tension is

$$T(z, t) = \gamma T_0 + \frac{1}{2} C_T \frac{m_a U^2}{D} \left[\left(1 - \frac{1}{2} \gamma\right) l - z \right] + \frac{1}{2} (1 - \gamma) C_T^* m_a U^2, \quad (6.18)$$

where $\gamma = 1$ if the downstream end is supported such that the displacement is zero, and $\gamma = 0$ if it is unsupported or elastically supported.

The force representing the viscous damping effect can be expressed as

$$F_D = C_v \frac{\partial u}{\partial t}, \quad (6.19)$$

where C_v is an effective viscous damping coefficient.

Finally, on substituting Eqs. 6.14, 6.15, 6.18, and 6.19 into Eq. 6.10, we obtain*

$$\begin{aligned}
 & EI \frac{\partial^4 u}{\partial z^4} + \mu I \frac{\partial^5 u}{\partial t \partial z^4} + m_a U^2 \frac{\partial^2 u}{\partial z^2} - \gamma T_o \frac{\partial^2 u}{\partial z^2} \\
 & - \frac{1}{2} C_T \frac{m_a U^2}{D} \left[\left(1 - \frac{1}{2} \gamma\right) l - z \right] \frac{\partial^2 u}{\partial z^2} - \frac{1}{2} (1 - \gamma) C_T' m_a U^2 \frac{\partial^2 u}{\partial z^2} \\
 & + 2m_a U \frac{\partial^2 u}{\partial z \partial t} + \frac{1}{2} C_N \frac{m_a U^2}{D} \frac{\partial u}{\partial z} + \frac{1}{2} C_N \frac{m_a U}{D} \frac{\partial u}{\partial t} \\
 & + C_v \frac{\partial u}{\partial t} + (m + m_a) \frac{\partial^2 u}{\partial t^2} = g(x, t) .
 \end{aligned} \tag{6.20}$$

Equation 6.20 is the equation of motion for a flexible, cylindrical rod in nominally axial flow and can be used for studies of both stability and response problems. The equation is complicated and an exact solution is difficult to obtain; however, it can be simplified in many cases.

Table 6.1 is a summary of equations of motion and forcing functions employed in earlier studies. Most of the studies were based on the classical Bernoulli-Euler beam equations, and the equations of motion contain parts of the terms given in Eq. 6.20.

The appropriate boundary conditions associated with the equation of motion are:

For $z = 0$,

$$k_1 u + EI \frac{\partial^3 u}{\partial z^3} = 0$$

and

$$c_1 \frac{\partial u}{\partial z} - EI \frac{\partial^2 u}{\partial z^2} = 0 ; \tag{6.21}$$

*The capital letters identify terms in equations of motion employed by investigators listed in Table 6.1.

Table 6.1 Mathematical Models and Forcing Functions Used by Various Investigators

Investigator	Mathematical Model	Forcing Function (g)	Comments
Burgreen et al. (1958)	A, J, K	$C_F \rho d_h U^2$	d_h is the hydraulic diameter and C_F is a proportional constant.
Quinn (1962)	A, C, J, K	No forcing function (the system motion is considered as self-excited vibration)	The sign of C was minus, which is believed to be wrong.
Paidoussis (1966a, 1966b)	A, C, D, E, F, G, H, I, K	$\frac{1}{2} \rho D U^2 [C_D (\frac{V}{U})^2 + C_F (\frac{V}{U})]$	V = cross-flow component of U . No solution was given for the suggested forcing function.
Reavis (1969)	A, J, K	Turbulent-boundary-layer pressure fluctuation	
Gorman (1969, 1970)	A, J, K	Turbulent-boundary-layer pressure fluctuation	
Basile et al. (1968)	A, K	Turbulence of the coolant flow	
Kanazawa (1969)	A, C, J, K	Turbulent-boundary-layer pressure fluctuation	The coefficient C was evaluated from drag force and Coriolis force. (Note: It is incorrect to consider Coriolis force as a damping mechanism for a simply supported rod.)
Addae and Fenech (1970)	A, C, G, K	Turbulent-boundary-layer pressure fluctuation	
Namatame (1969)	A, C, K	Turbulent-boundary-layer pressure fluctuation	
Knudson and Smith (1970a, 1970b)	A, J, K	Support excitation	
Chen and Weber (1970)	A, C, E, I, K	None (the motion is considered as parametric resonance)	
Chen and Wambeganss (1970, 1972)	A, B, C, E, F, G, H, I, J, K	Turbulent-boundary-layer pressure fluctuation	

and for $z = \ell$,

$$k_2 u - EI \frac{\partial^3 u}{\partial z^3} = 0 ,$$

and

$$c_2 \frac{\partial u}{\partial z} + EI \frac{\partial^2 u}{\partial z^2} = 0 ,$$

(6.21)

(Contd.)

where c_1 and c_2 are torsional spring constants, and k_1 and k_2 are displacement spring constants (see Fig. 6.1). If the downstream end is free, depending on the end geometries, the boundary conditions at $z = \ell$ are (Paidoussis 1966b).

$$EI \frac{\partial^3 u}{\partial z^3} + \kappa M_a U \left(\frac{\partial u}{\partial t} + U \frac{\partial u}{\partial z} \right) - (m + \kappa M_a) z_\ell \frac{\partial^2 u}{\partial t^2} = 0$$

and

(6.22)

$$\frac{\partial^2 u}{\partial z^2} = 0 .$$

It is assumed that the downstream end tapers smoothly from a cross-sectional area S to zero in a distance L ($L \ll \ell$), where $z_\ell = \left(\int_{\ell-L}^{\ell} S(z) dz \right) / S$. The parameter κ is a measure of departures from the ideal slender case ($0 < \kappa < 1$). For a blunt free end, $\kappa = 0$ and $z_\ell = 0$.

In this section, the dynamic response of a single cylinder is presented. The interaction of multiple cylinders is given in Section 6.9. The general method of analysis can be applied to both single and multiple cylinders.

6.3 ANALYSIS FOR A SINGLE CYLINDER IN AXIAL FLOW

For the purpose of analysis, it is more convenient to use dimensionless parameters; accordingly, we let

$$\xi = z/\ell ,$$

$$\epsilon = \frac{\ell}{D} ,$$

$$w = u/\ell ,$$

$$\alpha = \left[\frac{1}{E(m + m_a)} \right]^{1/2} \mu / \ell^2 ,$$

$$v = \left(\frac{m_a}{EI} \right)^{1/2} U \ell ,$$

$$\beta = \frac{m_a}{m + m_a} ,$$

(6.23)

$$\begin{aligned}
G &= \frac{g \ell^3}{EI}, & \delta &= \frac{C_v \ell}{[EI(m_r + m_f)]^{1/2}}, \\
\tau &= \left(\frac{EI}{m + m_a} \right)^{1/2} t / \ell^2, & \Gamma &= T_o \ell^2 / EI, \\
a_1 &= \frac{EI}{k_1 \ell^3}, & \Omega &= \left(\frac{m + m_a}{EI} \right) \omega \ell^2, \\
a_2 &= \frac{EI}{k_2 \ell^3}, & b_1 &= \frac{EI}{c_1 \ell},
\end{aligned} \tag{6.23}$$

(Contd.)

and

$$b_2 = \frac{EI}{c_2 \ell}.$$

On substituting Eqs. 6.23 into Eqs. 6.20, 6.21, and 6.22, we obtain

$$\begin{aligned}
\frac{\partial^4 w}{\partial \xi^4} + \alpha \frac{\partial^5 w}{\partial \xi^4 \partial \tau} - \gamma \Gamma \frac{\partial^2 w}{\partial \xi^2} + v^2 \left\{ \left[1 - \frac{1}{2} \epsilon C_T \left(1 - \frac{1}{2} \gamma - \xi \right) - \frac{1}{2} (1 - \gamma) C_T' \right] \frac{\partial^2 w}{\partial \xi^2} \right. \\
\left. + \frac{1}{2} \epsilon C_N \frac{\partial w}{\partial \xi} \right\} + 2\beta^{0.5} u \frac{\partial^2 w}{\partial \xi \partial \tau} + \frac{1}{2} \epsilon C_N \beta^{0.5} u \frac{\partial w}{\partial \tau} + \delta \frac{\partial w}{\partial \tau} \\
+ \frac{\partial^2 w}{\partial \tau^2} = G(\xi, \tau).
\end{aligned} \tag{6.24}$$

The boundary conditions are

$$w + a_1 \frac{\partial^3 w}{\partial \xi^3} = \frac{\partial w}{\partial \xi} - b_1 \frac{\partial^2 w}{\partial \xi^2} = 0 \quad \text{at } \xi = 0,$$

and

$$w - a_2 \frac{\partial^3 w}{\partial \xi^3} = \frac{\partial w}{\partial \xi} + b_2 \frac{\partial^2 w}{\partial \xi^2} = 0 \tag{6.25}$$

or

$$\frac{\partial^3 w}{\partial \xi^3} + \kappa v^2 \frac{\partial w}{\partial \xi} + \kappa \beta^{1/2} v \frac{\partial w}{\partial \tau} - \{1 + (\kappa - 1)\beta\} z \frac{\partial^2 w}{\partial \tau^2} = \frac{\partial^2 w}{\partial \xi^2} = 0 \quad (6.25)$$

(Contd.)

at $\xi = 1$.

An exact solution to the mathematical problem specified by Eqs. 6.24 and 6.25 is difficult to obtain because

- The system does not possess classical normal modes,
- The problem is of a non-self-adjoint type,
- The equation of motion has a term with a variable coefficient.

In the text following, an approximate solution is presented.

We shall use a modal expansion technique with Galerkin's method to solve the system shown in Fig. 6.1; i.e, the displacement is taken in the form

$$w(\xi, \tau) = \sum_{n=1}^{\infty} q_n(\tau) \phi_n(\xi), \quad (6.26)$$

where $\phi_n(\xi)$ is the n th normal mode, and $q_n(\tau)$ is the time coordinate. Generally, $\phi_n(\xi)$ is chosen as the undamped n th classical normal mode. Since classical normal modes do not exist in the present case, we employ the modal functions, which satisfy the following system:

$$\frac{d^4 \phi}{d\xi^4} + \chi \frac{d^2 \phi}{d\xi^2} - \lambda \phi = 0,$$

$$\phi + a_1 \frac{d^3 \phi}{d\xi^3} = \frac{d\phi}{d\xi} - b_1 \frac{d^2 \phi}{d\xi^2} = 0 \quad \text{at } \xi = 0,$$

and

$$\phi - a_2 \frac{d^3 \phi}{d\xi^3} = \frac{d\phi}{d\xi} + b_2 \frac{d^2 \phi}{d\xi^2} = 0 \quad \text{at } \xi = 1,$$

where

(6.27)

$$\chi = v^2 \left[1 - \frac{1}{2} \epsilon C_T (1 - \frac{1}{2} \gamma) - \frac{1}{2} (1 - \gamma) C_T' \right] - \gamma r$$

and λ is the eigenvalue to be determined. Equations 6.27 are obtained by neglecting the Coriolis force term, the variable coefficient term, the damping terms, and the terms associated with $\partial w / \partial \xi$ in Eq. 6.24, and then applying a separation-of-variables technique to the resulting equation and Eqs. 6.25. As shown in Appendix C, the adjoint system to Eqs. 6.27 is

$$\begin{aligned} \frac{d^4 \psi}{d\xi^4} + \chi \frac{d^2 \psi}{d\xi^2} - \lambda \psi &= 0, \\ \psi + a_1 \alpha \frac{d\psi}{d\xi} + a_1 \frac{d^3 \psi}{d\xi^3} &= b_1 \alpha \psi - \frac{d\psi}{d\xi} + b_1 \frac{d^2 \psi}{d\xi^2} = 0 \quad \text{at } \xi = 0, \end{aligned} \quad (6.28)$$

and

$$\psi - a_2 \alpha \frac{d\psi}{d\xi} - a_2 \frac{d^3 \psi}{d\xi^3} = b_2 \alpha \psi + \frac{d\psi}{d\xi} + b_2 \frac{d^2 \psi}{d\xi^2} = 0 \quad \text{at } \xi = 1.$$

The eigenvalue problem is non-self-adjoint because the boundary conditions for the two systems are different.

It is well known that if λ_n is an eigenvalue of Eqs. 6.27, it is also an eigenvalue of its adjoint system, Eqs. 6.28. Moreover, the sets of eigenfunctions $\{\phi_n\}$ and $\{\psi_n\}$ are biorthogonal; that is, each function of either set is orthogonal to every member of the other set except the one belonging to the same eigenvalue, i.e.,

$$\langle \phi_n, \psi_m \rangle = \int_0^1 \phi_n \psi_m d\xi = \begin{matrix} M_n, & n = m \\ 0, & n \neq m \end{matrix}, \quad (6.29)$$

where $\langle \rangle$ is used to denote the scalar product.

The eigenvalues and eigenfunctions of Eqs. 6.27 and Eqs. 6.28 are analyzed by conventional methods (see Appendix C). Having two complete sets of biorthogonal eigenfunctions, we substitute Eq. 6.26 into Eq. 6.24, multiply the resulting equation by ψ_m , and then integrate with respect to ξ from 0 to 1; these operations yield the following equation:

$$\ddot{q}_n + \alpha \sum_m a_{nm} \dot{q}_m + \epsilon_1 \sum_m b_{nm} \dot{q}_m + (\epsilon_2 + \delta) \dot{q}_n + \epsilon_3 \sum_m c_{nm} q_m + \epsilon_3 \sum_m b_{nm} q_m + \lambda_n q_n = g_n ,$$

where

$$\epsilon_1 = 2\beta v ,$$

$$\epsilon_2 = \frac{1}{2} \epsilon C_N \beta v ,$$

$$\epsilon_3 = \frac{1}{2} \epsilon C_N v^2 , \quad (6.30)$$

$$a_{nm} = \left\langle \frac{d^4 \phi_m}{d\xi^4} , \psi_n \right\rangle / M_n ,$$

$$b_{nm} = \left\langle \frac{d\phi_m}{d\xi} , \psi_n \right\rangle / M_n ,$$

$$c_{nm} = \left\langle \xi \frac{d^2 \phi_m}{d\xi^2} , \psi_n \right\rangle / M_n ,$$

and

$$Q_n = \langle Q, \psi_n \rangle / M_n .$$

Therefore, Eq. 6.30 can be written in the matrix form

$$[M]\{\ddot{Q}\} + [C]\{\dot{Q}\} + [K]\{Q\} = \{G\} . \quad (6.31)$$

In this case $[M]$ is an identity matrix and $[C]$ and $[K]$ are usually not symmetric.

Alternatively, in Eq. 6.26, $\phi_n(\xi)$ can be taken as the orthonormal functions for $\chi = 0$; i.e., ϕ_n 's are the solution of Eq. 6.27 for $\chi = 0$. In

this case, Eq. 6.27 are self-adjoint; therefore, ϕ_n 's are an orthogonal set of function. Using the same procedure, we also obtain Eq. 6.31.

Based on Eq. 6.31, the natural frequencies of the cylinder can be calculated as functions of flow velocity. In addition, the critical flow velocity associated with flutter or divergence can be calculated routinely.

For forced vibration, the technique outlined in Appendix A can be employed. In practical applications, the dimensionless flow velocity v usually is very small. The following approximate method can be used. We can make the following simplifications:

- Internal damping of the structures such as nuclear fuel rods is small; therefore, damping coupling is neglected.
- The terms generated by the Coriolis force, $\epsilon_1 \sum_m b_{nm} \dot{q}_m$, contribute to damping and mode coupling. When the flow velocity is relatively small with respect to the critical flow velocity, the effects of the off-diagonal terms are very small and are neglected.
- The parameters ϵ_3 and ϵ_2 are small; therefore, the off-diagonal terms associated with these two parameters are neglected.

With these simplifications, the equations decouple and we obtain

$$\ddot{q}_n + 2\zeta_n \Omega_n \dot{q}_n + \Omega_n^2 q_n = g_n, \quad (6.32)$$

where

$$\Omega_n^2 = \lambda_n + \epsilon_3 c_{nn} + b_{nn}$$

and

$$\zeta_n = \frac{1}{2\Omega_n} (\chi_{nn}^a + \epsilon_1 b_{nn} + \epsilon_2 + \delta).$$

Recall that the dimensionless generalized force $g_n(\tau)$ is random with time. From Eqs. 6.30,

$$g_n(\tau) = \frac{1}{M_n} \int_0^1 G(\xi, \tau) \psi_n(\xi) d\xi$$

and

$$g_m(\tau + \tau_o) = \frac{1}{M_m} \int_0^1 G(\eta, \tau + \tau_o) \psi_m(\eta) d\eta.$$

(6.34)

The correlation of the generalized force is defined by

$$R_{g_n g_m}(\tau_0) = \lim_{\tau \rightarrow \infty} \frac{1}{2\tau} \int_{-\tau}^{\tau} g_n(\tau) g_m(\tau + \tau_0) d\tau. \quad (6.35)$$

Using Eqs. 6.34 and interchanging the order of integration, we have

$$R_{g_n g_m}(\tau_0) = \frac{1}{M_n M_m} \int_0^1 \int_0^1 \psi_n(\xi) \psi_m(\eta) R_{GG}(\xi, \eta, \tau_0) d\xi d\eta. \quad (6.36)$$

where R_{GG} is the correlation of the random pressure; i.e.,

$$R_{GG} = \lim_{\tau \rightarrow \infty} \frac{1}{2\tau} \int_{-\tau}^{\tau} G(\xi, \tau) G(\eta, \tau + \tau_0) d\tau. \quad (6.37)$$

Further define the power spectra

$$\Phi_{GG}(\Omega) = \frac{1}{\pi} \int_{-\infty}^{\infty} R_{GG} e^{i\Omega\tau_0} d\tau_0$$

and

$$(6.38)$$

$$\Phi_{g_n g_m}(\Omega) = \frac{1}{\pi} \int_{-\infty}^{\infty} R_{g_n g_m} e^{i\Omega\tau_0} d\tau_0.$$

Taking the Fourier transform of Eq. 6.36 yields

$$\Phi_{g_n g_m}(\Omega) = \frac{1}{M_n M_m} \int_0^1 \int_0^1 \psi_n(\xi) \psi_m(\eta) \Phi_{GG}(\xi, \eta, \Omega) d\xi d\eta. \quad (6.39)$$

Similarly, we can obtain the correlation and power spectrum of displacement from Eq. 6.26. These are

$$R_{ww}(\xi, \eta, \tau_0) = \sum_n \sum_m R_{q_n q_m}(\tau_0) \phi_n(\xi) \phi_m(\eta)$$

and

$$(6.40)$$

$$\Phi_{ww}(\xi, \eta, \tau) = \sum_n \sum_m \Phi_{q_n q_m}(\Omega) \phi_n(\xi) \phi_m(\eta).$$

From Eq. 6.32 it is known that

$$\phi_{q_n q_m}(\Omega) = |H_n(\Omega)H_m(\Omega)| \phi_{g_n g_m}(\Omega) , \quad (6.41)$$

where

$$H_n(\Omega) = [(\Omega_n^2 - \Omega^2) + i2\zeta_n \Omega_n \Omega]^{-1} . \quad (6.42)$$

Finally, substituting Eq. 6.39 into Eq. 6.41 and then into Eq. 6.40, we obtain as the power spectral density of displacement

$$\phi_{ww}(\xi, \eta, \Omega) = \phi_{GG}(\Omega) \sum_n \sum_m |H_n(\Omega)H_m(\Omega)| \phi_n(\xi) \phi_m(\eta) J_{nm}^2(\Omega) , \quad (6.43)$$

where

$$J_{nm}^2 = \frac{1}{M_n M_m} \int_0^1 R_{GG}(\xi, \eta, \Omega) \psi_n(\xi) \psi_m(\eta) d\xi d\eta . \quad (6.44)$$

J_{nm}^2 is called the cross acceptance if $n \neq m$, and the joint acceptance if $n = m$. The mean-square displacement \bar{w}^2 is given by

$$\bar{w}^2(\xi) = \int_0^\infty \phi_{ww}(\xi, \xi, \Omega) d\Omega . \quad (6.45)$$

These results are similar to those obtained by Powell (1958) for a beam. The difference is the acceptances, which, in the present case, are in terms of adjoint eigenfunctions. If the system possesses orthogonal eigenfunctions, Eq. 6.64 is reduced to the classical results. The problems remaining are to characterize the acceptances and power spectral density of the pressure field and to compute the acceptances.

6.4 DYNAMIC BEHAVIOR

In addition to the fluid centrifugal force, Coriolis force, and inertia force, as in the case of pipes conveying fluid, there are several frictional force components for a cylinder in axial flow. However, the overall behavior is not very much different from that of a pipe conveying fluid.

The frequency Ω , which can be calculated based on Eq. 6.31, depends on the end conditions. For cylinders not allowed to move at the ends, the

dominant fluid force component is the fluid centrifugal force; therefore, as the flow velocity increases, the natural frequencies decrease with flow velocity. The damping at small flow velocity increases with flow because of the fluid frictional force components. As the flow velocity is increased to a certain value, the cylinder loses stability by divergence. The effect of fluid frictional force on the divergence flow velocity usually is small. Therefore, the critical flow velocity can be estimated based on the buckling load of the corresponding beam subjected to axial compression. With further increase in flow velocity, the cylinder may be subjected to flutter.

Figure 6.3 shows the complex frequencies associated with the first three modes of a hinged-hinged cylinder as a function of flow velocity for $\alpha = \delta = 0$ (Paidoussis 1973). This is a typical case, illustrating the behavior of such a system. At zero flow, the frequencies are real and correspond to $\text{Re}(\Omega) = \pi^2, 4\pi^2$ and $9\pi^2$. As the flow velocity increases, $\text{Re}(\Omega)$ decreases while $\text{Im}(\Omega)$ increases. As the flow velocity increases further, the first mode ceases being oscillatory at v about 3.1 and is subject to divergence at $v \sim 3.14$. At higher flow velocities the second mode becomes unstable by divergence at $v \sim 6.3$. At a slightly larger flow velocity of 6.5, the cylinder becomes unstable by the coupled-mode flutter.

For cylinders allowed to move at the ends, at low flow velocities, the free motions are damped. The damping is associated with the Coriolis force and frictional force. As the flow velocity increases, the cylinder may become unstable by divergence and flutter. Figure 6.4 shows the complex frequency for a cantilevered cylinder with a streamlined end. With the increase in flow velocity, the cylinder loses stability by divergence at $v \sim 2.0$ and is followed by flutter associated with the second and third modes at $v \approx 5.2$ and 8.2.

The dynamic behavior in cylinders subjected to axial flow is not the same for all cases. There are many parameters, such as $\varepsilon, \beta, \delta, \Gamma, a_1, a_2, b, b_2, C_N$, and C_T , that can affect response characteristics. It is imperative to analyze each case separately.

The dynamic behavior of the cylinder at high and low flow velocities predicted by the linear theory agrees reasonably well with experimental data. Using a rubber cylinder, either clamped or pinned at the upstream end and free at the other, or pinned at both ends, Paidoussis (1966a) has shown that both buckling and flutter instability are possible (see Fig. 6.5).

In practical system components the critical flow velocities for divergence and flutter usually are very large. The high flow velocity is not likely to be encountered in practice. Therefore, the stability of a cylinder in axial flow is more of academic interest.

For small flow velocities, the modal damping ratio can be obtained from Eq. 6.33:

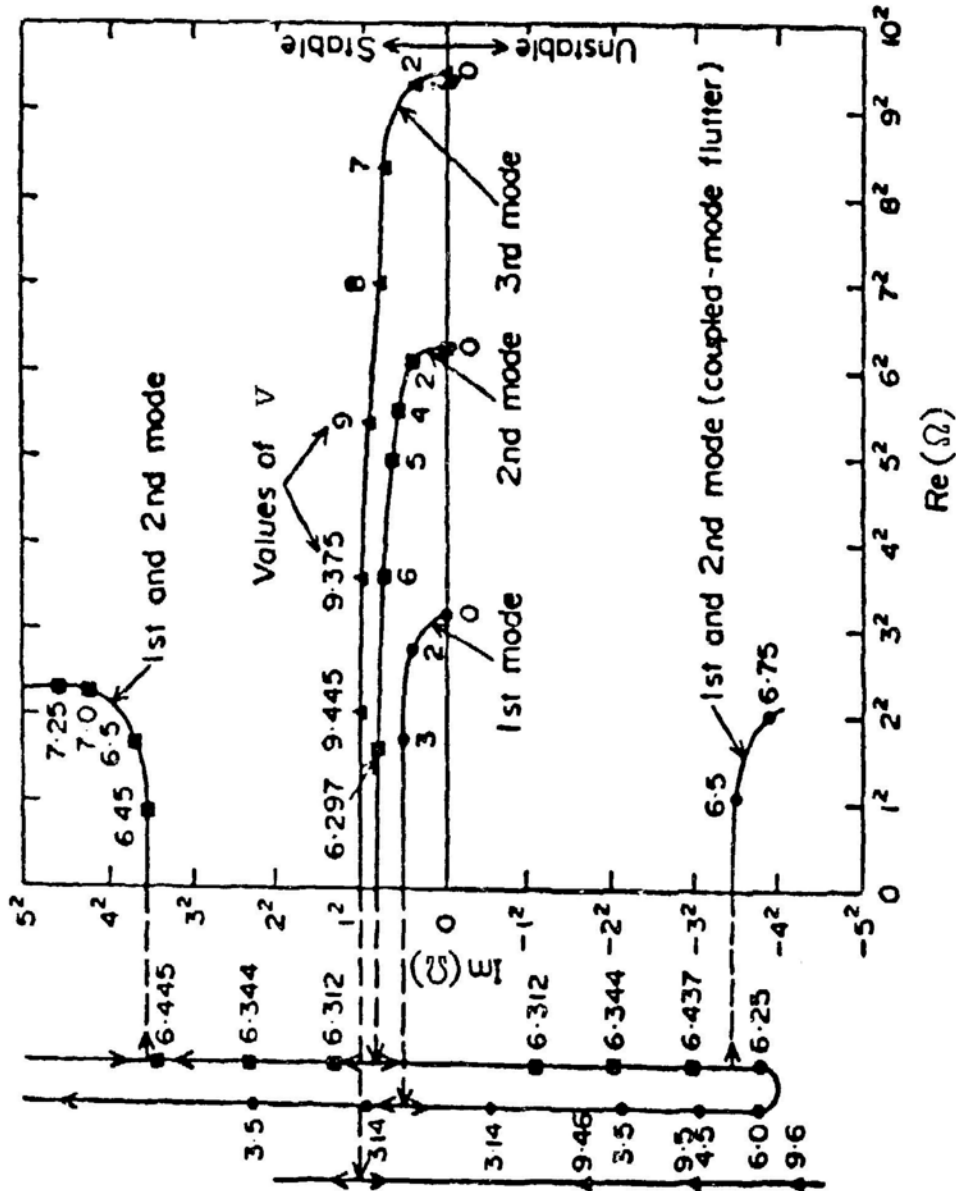


Fig. 6.3. Complex Frequencies Ω of the First Three Modes of a Hinged-Hinged Cylinder in Axial Flow, as a Function of v , for $\beta = 0.1$, $eC_N = eC_T = 1$, and $r = 0$ (from Paidoussis 1973, with permission--see Credits)

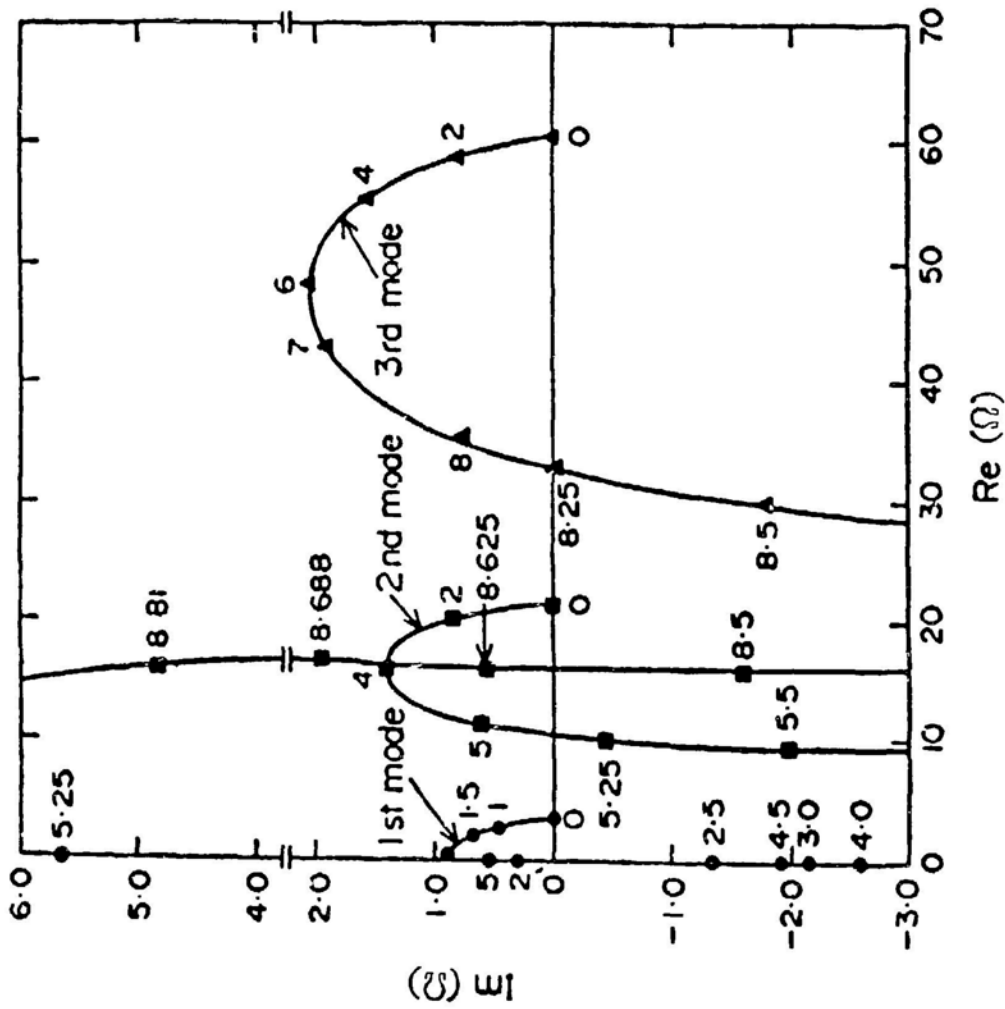
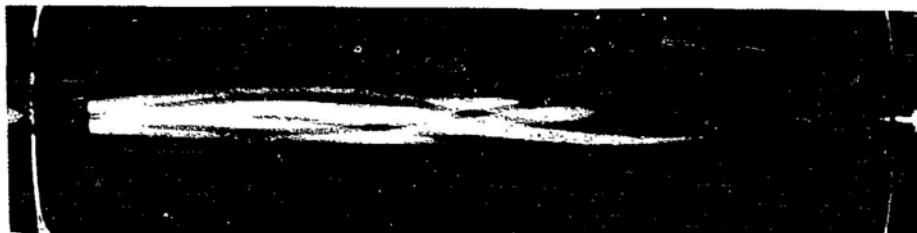


Fig. 6.4. Complex Frequencies Ω of the First Three Modes of a Cantilevered Cylinder in Axial Flow, as a Function of v , for $\beta = 0.5$, $\epsilon_N = \epsilon_T = 1$ (from Paidoussis 1973, with permission-- see Credits)



(a)



(b)

Fig. 6.5. Second-mode Flutter of (a) Fixed-Free Cylinder and (b) Pinned-Pinned Cylinder in Axial Flow (flow is from left to right) (from Paidoussis 1966b, with permission--see Credits)

$$\zeta_n = \zeta_n^e + \zeta_n^d + \zeta_n^c, \quad (6.46)$$

where

$$\begin{aligned} \zeta_n^e &= \frac{1}{2\Omega_n} (\alpha a_{nn} + \delta), \\ \zeta_n^d &= \frac{\varepsilon C_N \beta u}{4\Omega_n}, \end{aligned} \quad (6.47)$$

and

$$\zeta_n^c = \frac{b_{nn} \beta u}{\Omega_n}.$$

In Eqs. 6.47, ζ_n^e is the damping associated with external viscous effects and the internal viscoelastic effect; ζ_n^d is the damping induced by the normal drag force, and increases with increasing flow velocity; and ζ_n^c is attributed to the Coriolis force and also increases with increasing flow velocity.

The values of ζ_n^c is highly dependent on end conditions. For a rod that is not allowed to move at the ends, i.e., $k_1 = k_2 = \infty$, or $a_1 = a_2 = 0$, the eigenvalue problem specified by Eqs. 6.27 is self-adjoint. In this case, $\phi_n = \psi_n$, and the value of ζ_n^c is zero, since, from Eqs. 6.30,

$$b_{nn} = \frac{1}{M_n} \int_0^1 \frac{d\phi_n}{d\xi} \phi_n d\xi = 0. \quad (6.48)$$

For a rod elastically supported at both ends or unsupported at one end, the value of ζ_n^c can be quite large. The physical reason for the difference is that the energy dissipated by the Coriolis force from time t_0 to t_1 is

$$\Delta W = - \int_{t_0}^{t_1} m_a U \left[\frac{\partial u(0,t)}{\partial t} \right]^2 dt + \int_{t_0}^{t_1} m_a U \left[\frac{\partial u(l,t)}{\partial t} \right]^2 dt. \quad (6.49)$$

Thus if there is no displacement at the ends, the Coriolis force is gyroscopic and does not dissipate any energy.

From Eq. 6.46, we can conclude the following:

- Modal damping increases with increasing flow velocity.

• For cylinders that are not allowed to move at the ends, the Coriolis force does not contribute damping. Therefore, any increase in damping with flow velocity is attributed to the normal drag force.

• For cylinders that are allowed to move at the ends (e.g., cantilever cylinders), the Coriolis force acts as a strong damping mechanism. Thus, damping of elastically supported rods generally is larger than that of rods without end displacement.

The effect of small flow velocities on the dynamics of cylinders in axial flow was tested by Chen and Wambsganss (1972). The related parameters of two cylinders with fixed-fixed and fixed-free conditions are given in Table 6.2.

Theoretical values of the fundamental natural frequency were computed from Eqs. 6.33; the results are compared with experimental values in Figs. 6.6 and 6.7. For fixed-fixed cylinders, the frequency decreases with increasing flow velocity; this is because the centrifugal fluid force acts as a compressive axial force on the cylinder. For cantilevered cylinders, the fundamental frequency increases with increasing flow velocity; this is due to the centrifugal fluid force and the normal drag force. In this case, the centrifugal fluid force acts as a follower force on the free end; thus, the fundamental frequency increases while the others decrease with increasing flow velocity.

The corresponding modal damping ratios for fixed-fixed and cantilevered rods are plotted in Figs. 6.8 and 6.9. In both instances, the calculated values agree well with the experimental results, attesting to the adequacy of the mathematical model, Eq. 6.46.

6.5 NEARFIELD FLOW NOISE

A cylinder located in a closed-loop flow circuit is exposed to flow noise, consisting of far-field and near-field components, and to structural-borne excitation. The near-field components are pressure fluctuations incurred by the adjacent fluid; boundary-layer turbulence is the most important near-field noise. The far-field components comprise all system-dependent noises that propagate at the speed of sound. Sources of far-field noise include flow pulsations, vortex shedding over the submerged objects, turbulence generated by bends, cavitation, and the like.

Boundary layer noise is always present if the flow is turbulent; however, the strength of far-field noise depends on system design. In the following, only the excitation due to near-field noise is considered.

Corcos (1963) proposed a phenomenological model to describe the cross-spectral-density of the wall pressure field (see Fig. 6.10)

$$\psi_{pp}(\omega, z_1, z_2, \theta_1, \theta_2) = \phi_{pp}(\omega) A\left(\frac{\omega z}{U_c}\right) B\left(\frac{\omega x}{U_c}\right) \exp(i\omega z/U_c), \quad (6.50)$$

Table 6.2. Properties and Related Parameters of Test Elements (Circular Cylinders)

Test No.	m , $\frac{\text{lb-sec}^2}{\text{ft}^2}$	m_a , $\frac{\text{lb-sec}^2}{\text{ft}^2}$	D , in.	l , in.	EI , lb-ft^2	d_h , in.	β	δ	ϵ	r	C_T	C_N	a_1	a_2	b_1	b_2
1-A*	0.0224	0.00264	0.5	46.875	330	1.5	0.3249	0.146	93.750	7.25	0.011	0.101	0	0	0	0
1-B*	0.0224	0.00330	0.5	46.875	330	1.0	0.3582	0.267	93.750	8.0	0.011	0.103	0	0	0	0
1-C*	0.0224	0.00436	0.5	46.875	330	0.5	0.4034	0.267	93.750	6.75	0.011	0.044	0	0	0	0
2-A ⁺	0.0224	0.00264	0.5	26.50	330	1.5	0.3249	0.025	53.0	0	0.019	0.10	0	∞	0.266	∞
2-B ⁺	0.0224	0.00330	0.5	26.50	330	1.0	0.3582	0.025	53.0	0	0.019	0.056	0	∞	0.236	∞
2-C ⁺	0.0224	0.00436	0.5	26.50	330	0.5	0.4034	0.025	53.0	0	0.019	0	0	∞	0.240	∞
3 [#]	0.00553	0.00264	0.5	40.875	270	1.5	0.5685	0.145	81.75	0	0.012	0.025	0	0	0	0

Rod material

End conditions

* Brass

Fixed-fixed

+ Brass

Fixed-free

Steel (hollow)

Fixed-fixed

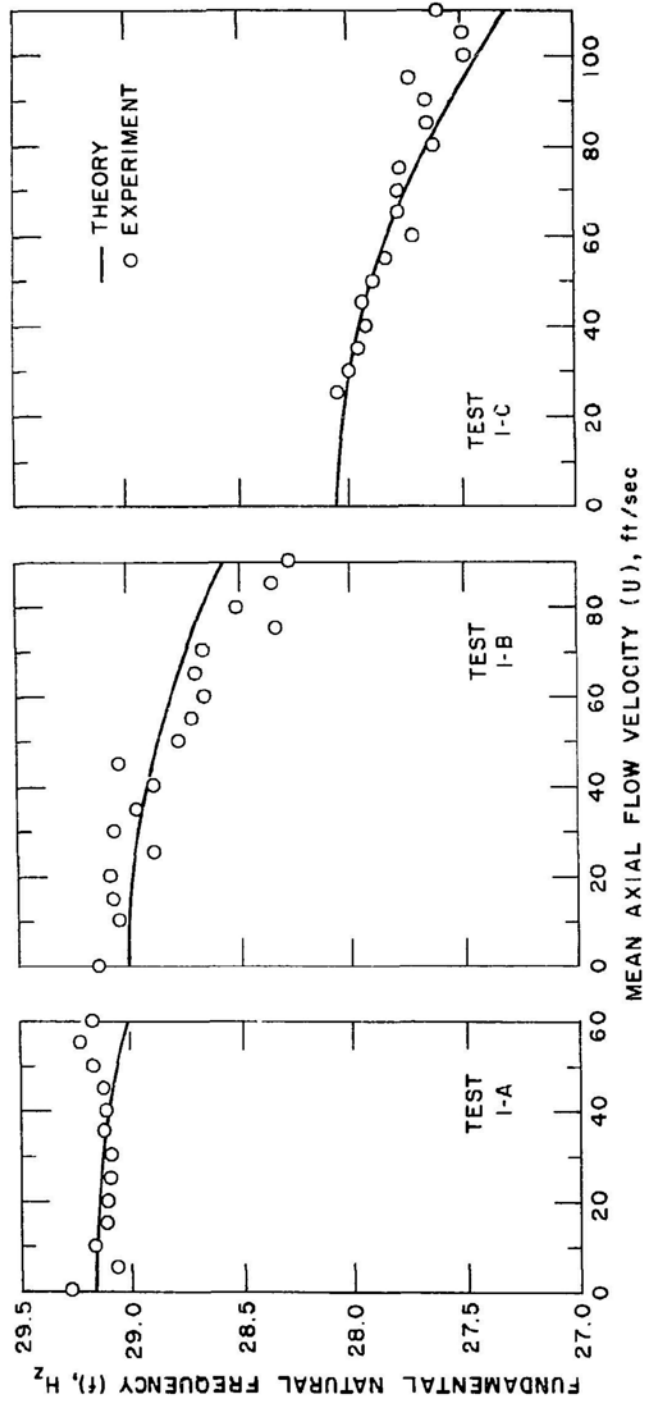


Fig. 6.6. Fundamental Natural Frequency of Fixed-Fixed Rods (Chen and Wambsganss 1972)

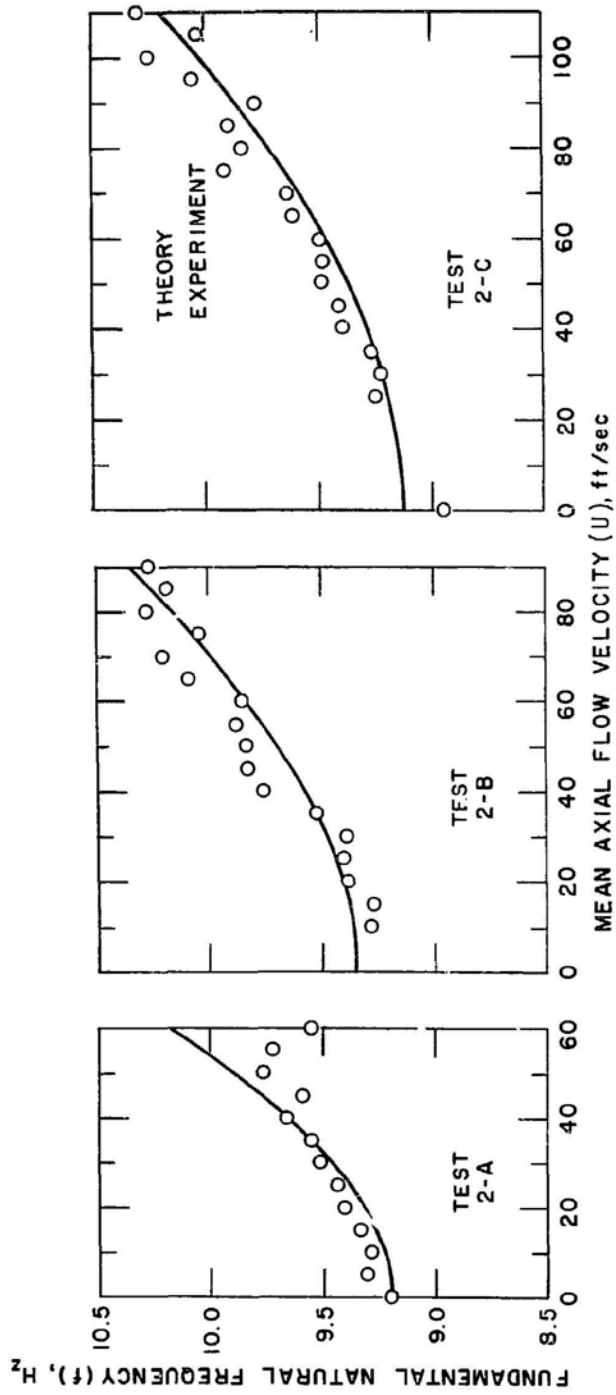


Fig. 6.7. Fundamental Natural Frequency of Fixed-Free Cylinders (Chen and Wambsganss 1972)

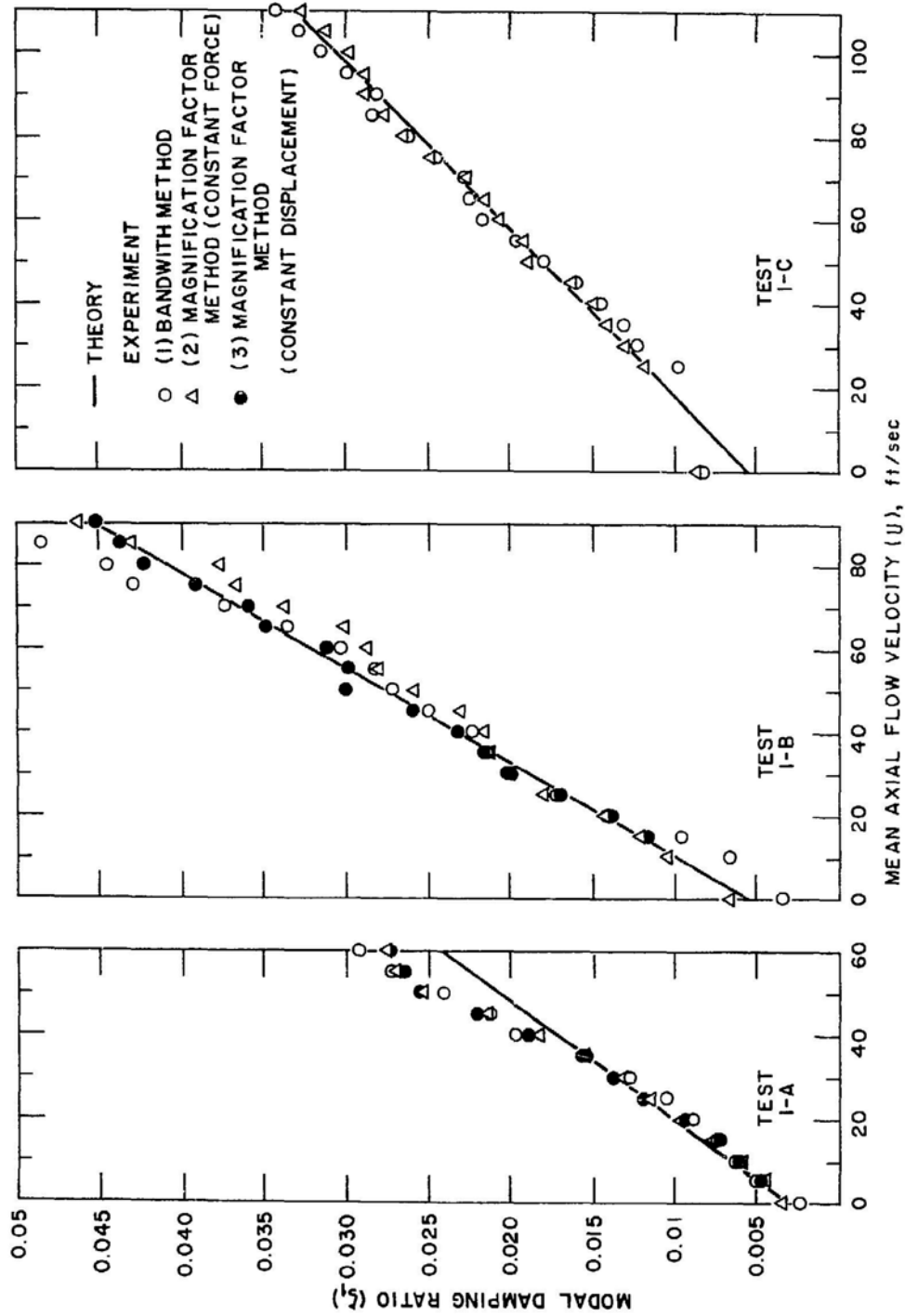


Fig. 6.8. Modal Damping Ratio of Fixed-Fixed Cylinders (Chen and Wambsgans 1972)

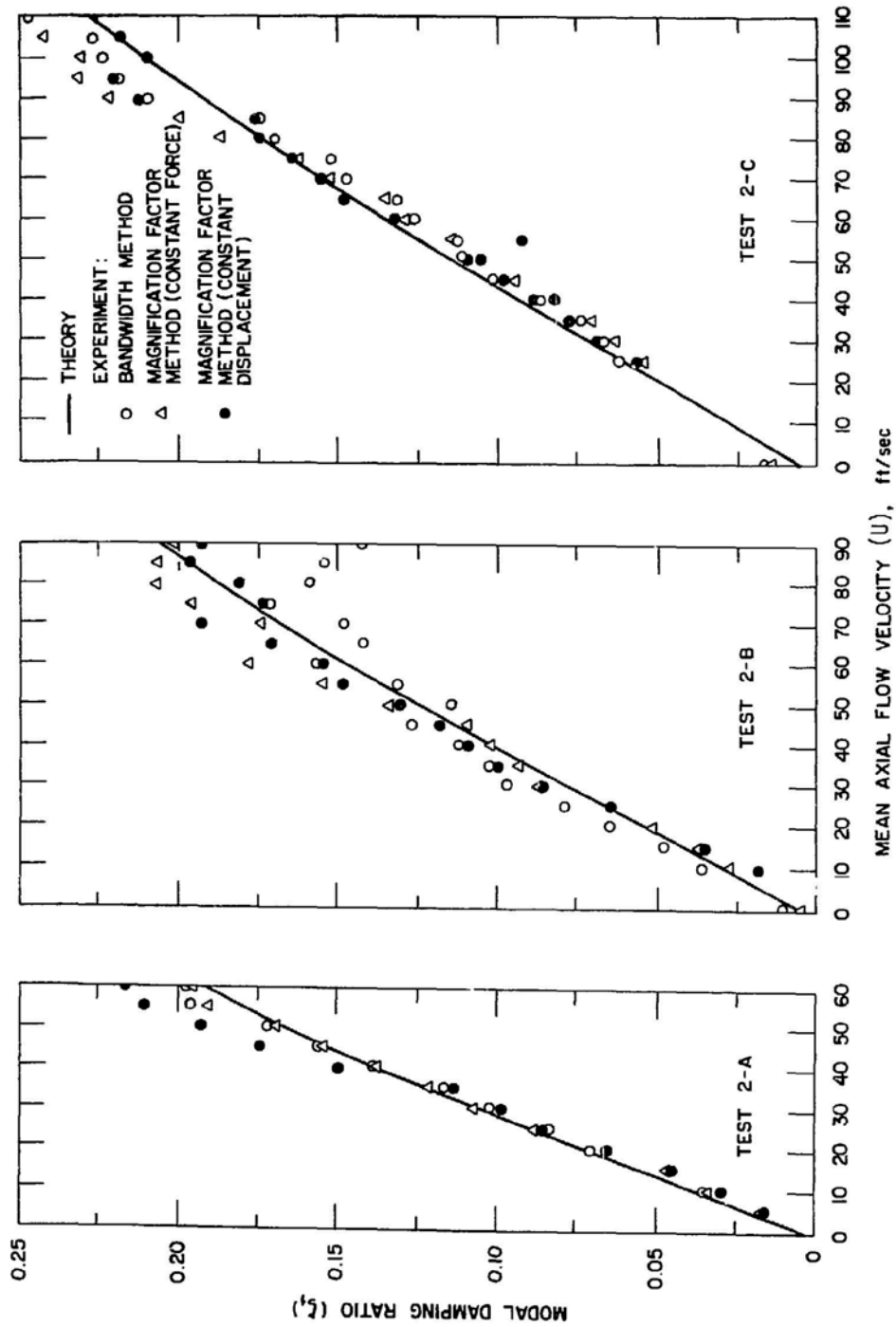


Fig. 6.9. Modal Damping Ratio of Fixed-Free Cylinders (Chen and Wambsganss 1972)

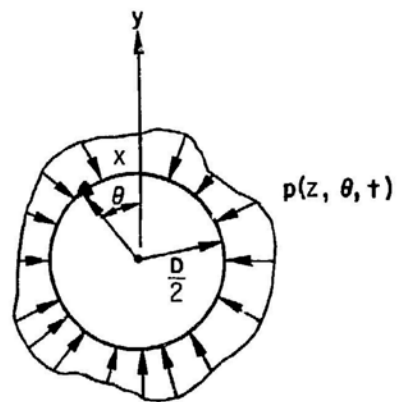
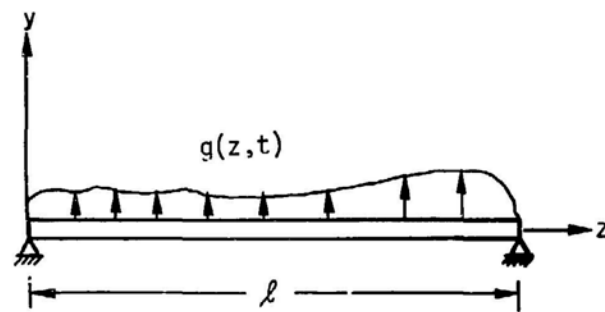


Fig. 6.10. Circular Cylinder Subject to Turbulent Pressure Fluctuations

where $\psi_{pp}(\omega)$ is the wall pressure power spectral density at a point; $\bar{z} = |z_2 - z_1|$ and $\bar{x} = |\theta_1 - \theta_2| \frac{D}{2}$ are separation distances in the longitudinal and circumferential directions, respectively; A and B are spatial functions describing the axial and circumferential decay of the correlation; and U_c is the convection velocity. Corcos' model, as given in Eq. 6.50, assumes a spatially homogeneous field; the model is a function of the separation distances \bar{z} and $\bar{\theta}$, and the wall pressure PSD $\psi_{pp}(\omega)$ is the same at every point on the surface.

Although many investigators have published experimental data for U_c , $A(\omega\bar{z}/U_c)$, $B(\omega\bar{x}/U_c)$, and $\phi_{pp}(\omega)$, most of the data pertain to turbulent pipe flows (Corcos 1964; Clinch 1969) or turbulent boundary layers on flat plates (Skudrzyk and Haddle 1960; Willmarth and Wooldridge 1962). Only a few experiments have been performed in water tunnels and for bodies of revolution (Gorman 1969; Wambsganss and Zaleski 1970; Bakewell 1968). The experimental results for U_c , $A(\cdot)$, $B(\cdot)$, and $\phi_{pp}(\omega)$ obtained by Bakewell (1968) and other investigators (Schloemer 1967; Clinch 1969; Skudrzyk and Haddle 1960; Willmarth and Wooldridge 1962) are replotted in Figs. 6.11-6.14, where δ^* is the boundary-layer displacement thickness and $\phi_{pp}(\omega)$ has been plotted logarithmically.

The convection velocity U_c is a weak function of frequency. It is higher for low frequencies and lower for high frequencies. In the calculations, it will be taken as

$$\frac{U_c}{U} = 0.6 + 0.4 \exp[-2.2(\omega\delta^*/U)] \quad (6.51)$$

This expression correlates the data of Bakewell (1968) and Schloemer (1967) quite well. The expressions selected to represent the A and B functions are

$$\begin{aligned} A(\omega\bar{z}/U_c) &= \exp(-0.10|\omega\bar{z}/U_c|) \quad \text{and} \\ B(\omega\bar{x}/U_c) &= \exp(-0.55|\omega\bar{x}/U_c|) \end{aligned} \quad (6.52)$$

which are shown in Figs. 6.12 and 6.13. In these two figures, Willmarth and Wooldridge's data (1962) are also included for comparison.

Plots of ϕ_{pp} are shown in Fig. 6.12; these were obtained by Clinch (1969), Skudrzyk and Haddle (1960), Willmarth and Wooldridge (1962), and Bakewell (1968). The values agree well at the higher frequencies, but the

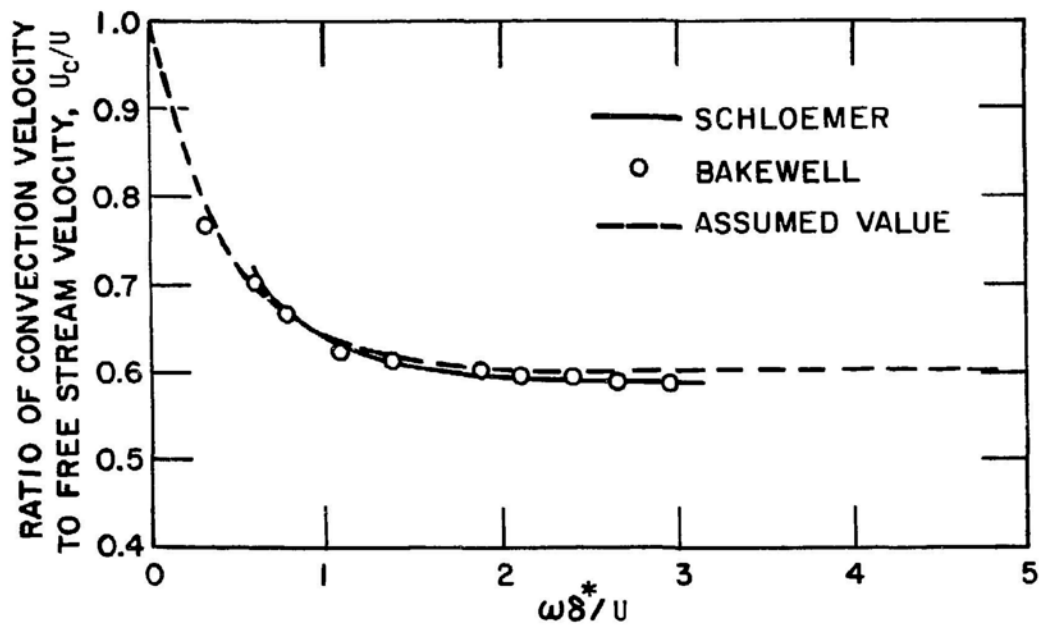


Fig. 6.11. Dependence of Convection Velocity on Dimensionless Frequency
(Chen and Wambsganss 1970)

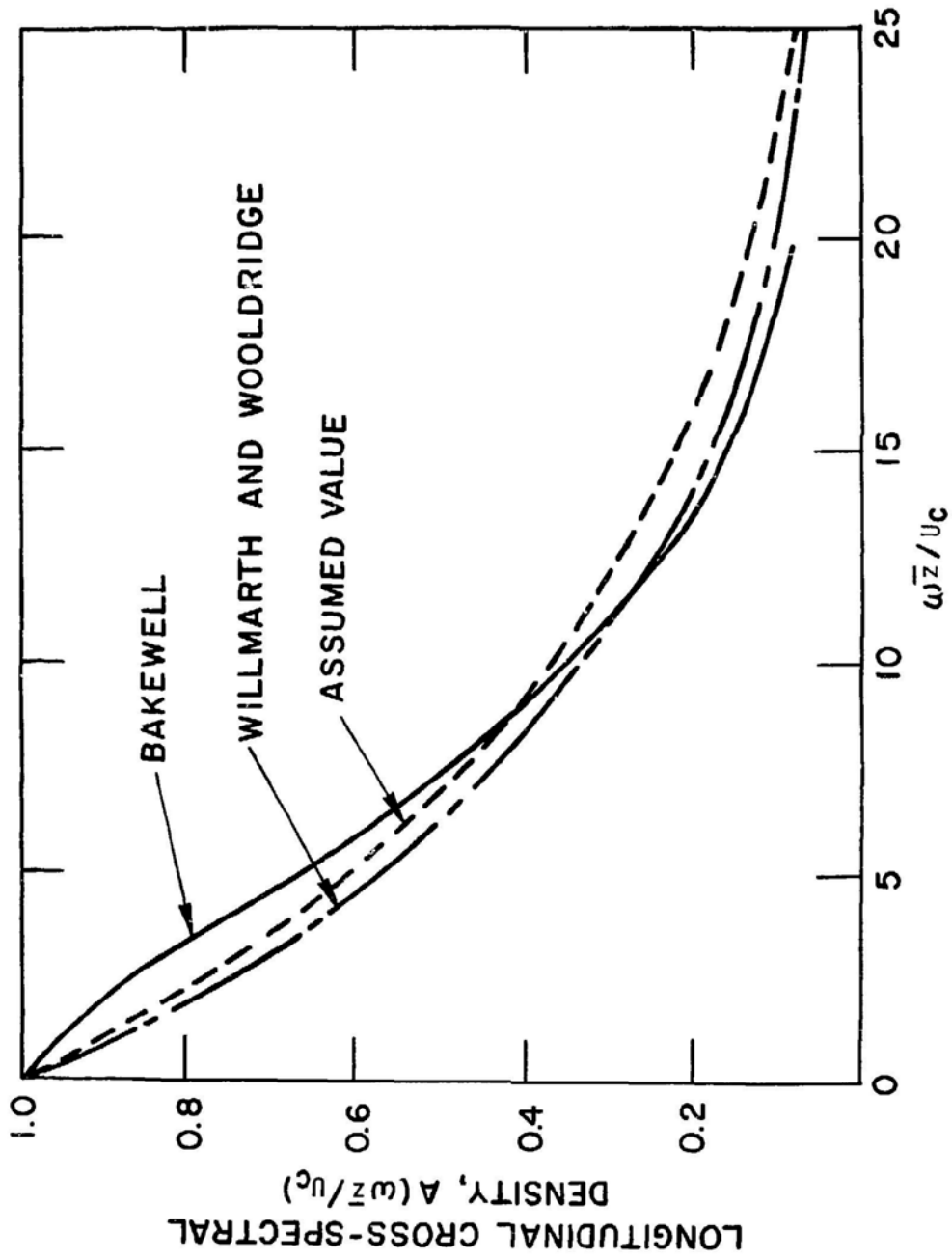


Fig. 6.12. Magnitude of Longitudinal Cross-spectral Density of Turbulent Wall Pressure (Chen and Wambsganss 1970)

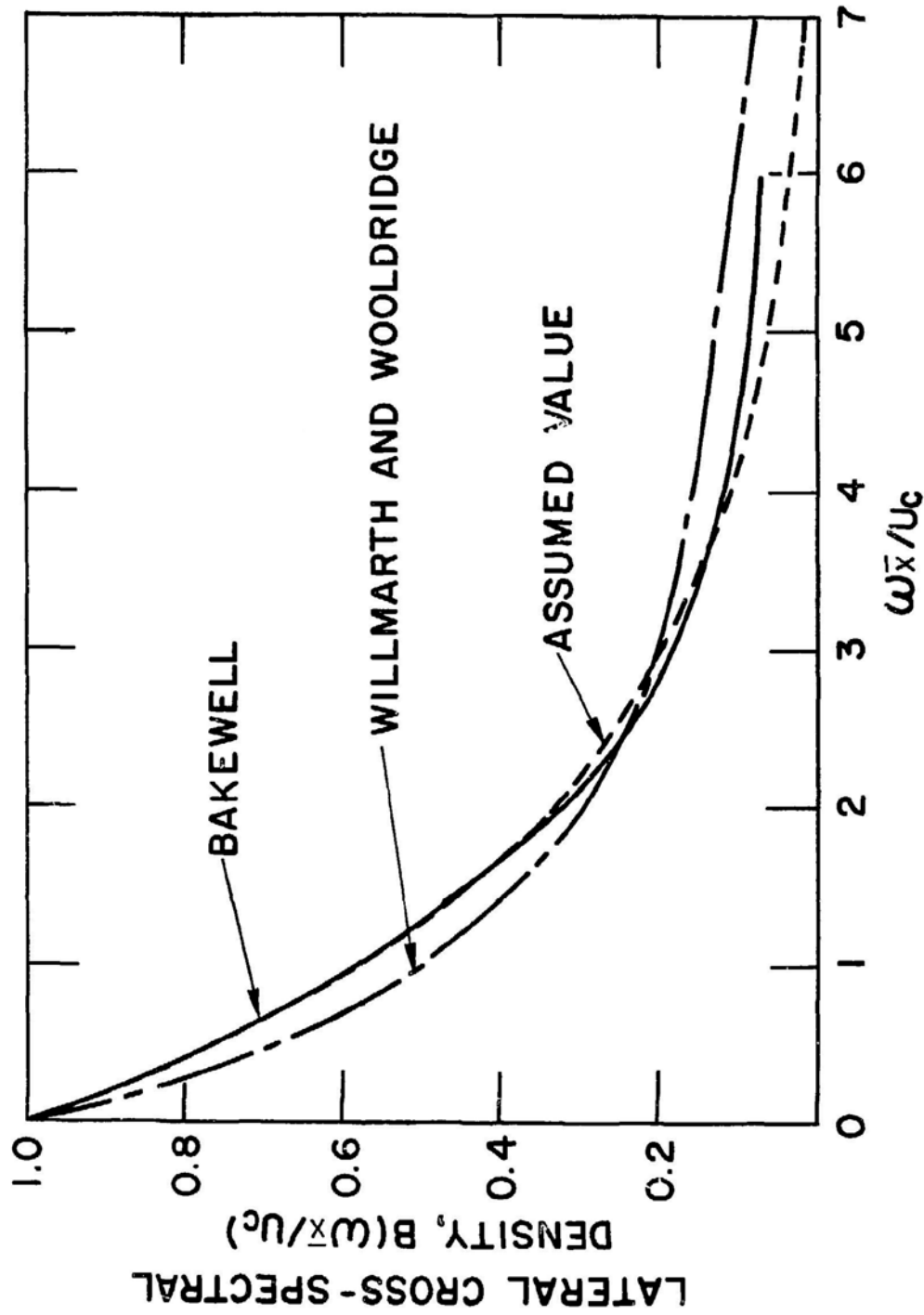


Fig. 6.13. Magnitude of Lateral Cross-spectral Density of Turbulent Wall Pressure (Chen and Wambsganss 1970)

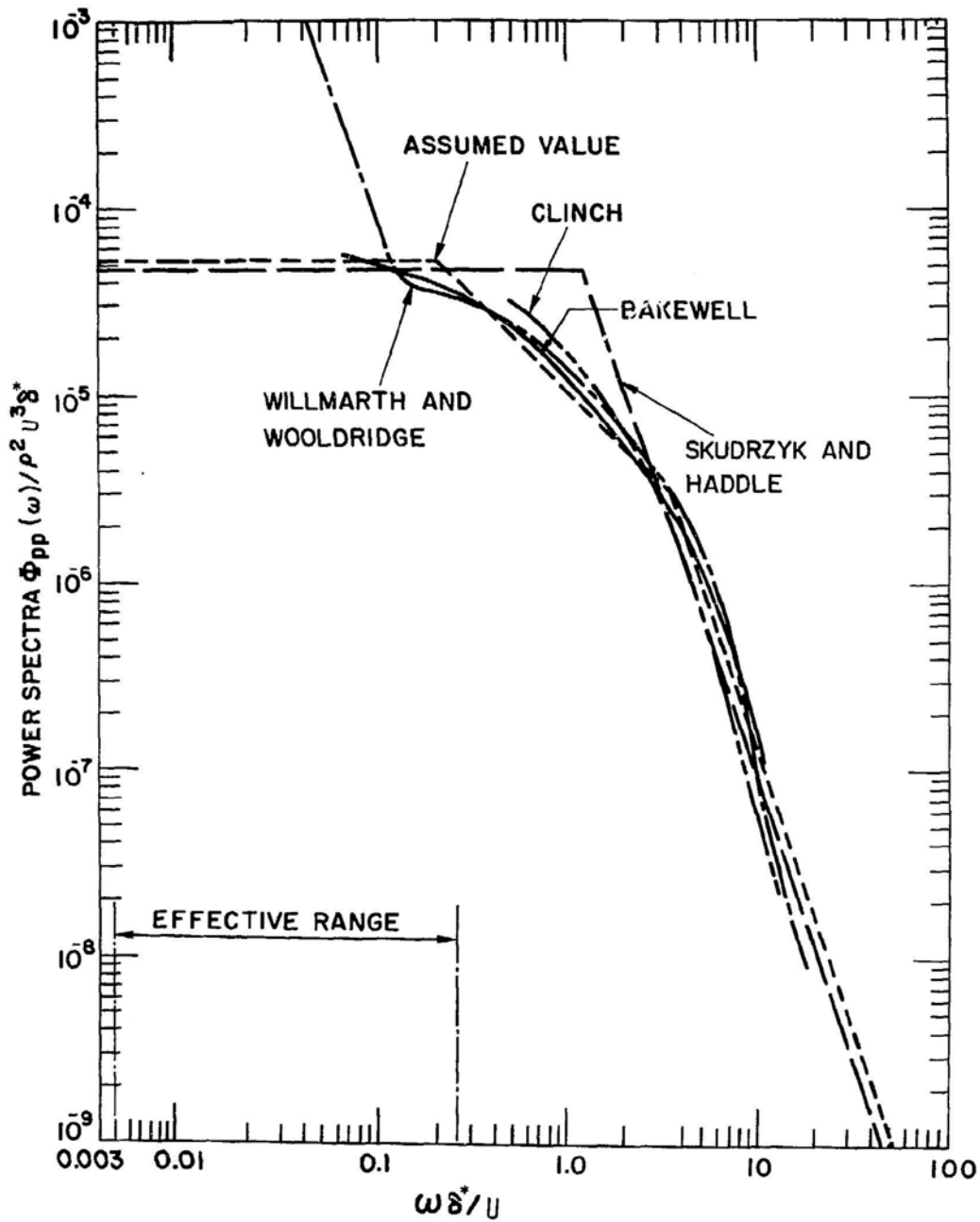


Fig. 6.14. Turbulent Wall Pressure Power Spectra (Chen and Wambsganss 1972)

low-frequency spectra vary widely. Yet this is precisely the range of interest in the study of flow-induced vibration of fuel rods, as indicated by "effective range."

The power spectral density based on the assumed value given in Fig. 6.14 has been used in the prediction of cylinder response (Chen and Wambsganss 1972). Because the data in the low-frequency range are not reliable, experimental data (Wambsganss and Zaleski 1970) specifically measured for tests given in Table 6.2 are used here. The spectral density is given in Fig. 6.15, where d_h is hydraulic diameter. For computational convenience, the normalized power spectra of the pressure field are represented by

$$\Phi_{PP}(f) = \begin{cases} 0.272/S^{0.25} & S < 5, \\ 22.75/S^3 & S > 5, \end{cases} \quad (6.53)$$

where

$$\Phi_{PP}(f) = \Phi_{pp}(f)/\rho^2 U^3 d_h,$$

$$S = \omega d_h / U,$$

(6.54)

and

$$f = \omega / 2\pi.$$

Having the cross-spectral density $\Psi_{pp}(\omega, z, \bar{\theta})$, we can compute the nondimensional spectrum $\Phi_{GG}(\Omega)$ and dimensionless longitudinal correlation $R_{GG}(\xi, \eta, \Omega)$. Both are required to perform the integration in Eq. 6.45, and are given by Chen and Wambsganss (1972).

$$\Phi_{GG}(\Omega) = \frac{16}{\pi} \beta \bar{\delta} \epsilon^2 v^3 \chi^2 \Phi_{PP}(\Omega)$$

and

(6.55)

$$R_{GG}(\xi, \eta, \Omega) = \exp(-0.1 \bar{\sigma} |\xi - \eta|) \cos(|\xi - \eta|),$$

where

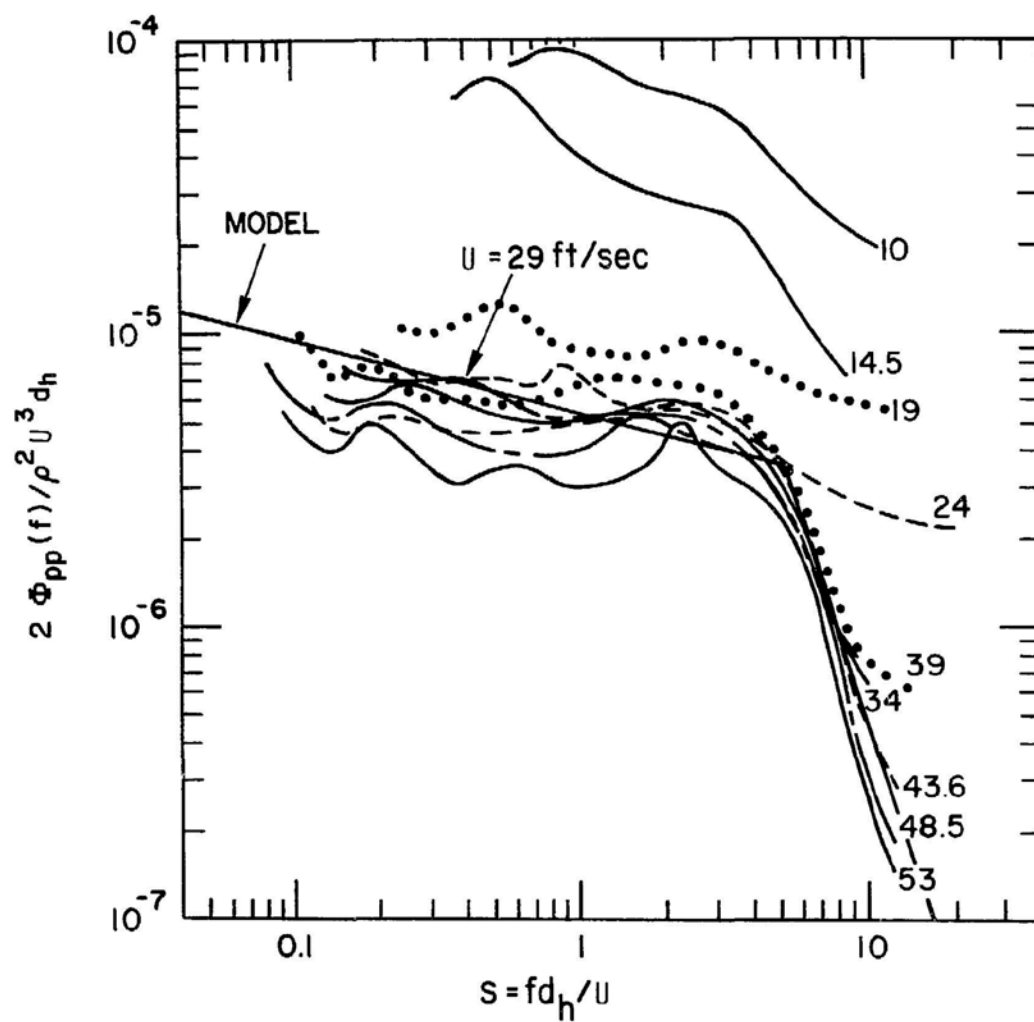


Fig. 6.15. Nondimensional Nearfield Turbulent Wall Pressure Power Spectra (Chen and Wambsganss 1972)

$$\bar{x}^2 = \frac{v}{2(1+v^2)} \left[\pi - \frac{v(1-e^{-2\pi v})}{1+v^2} \right]$$

$$v = 0.275 \left(\frac{\omega D}{U_c} \right) = 0.275 \left(\frac{\beta \Omega}{\epsilon s v} \right),$$

$$\sigma = \frac{\ell \omega}{U_c} = \frac{\beta \Omega}{s v}, \quad (6.56)$$

$$\bar{\delta} = \frac{d_h}{\ell}.$$

The analytical model for estimating rms response to axial flow excitation assumes the wall pressure field to be spatially homogeneous and use Corcos' (1963) phenomenological model to describe the convecting random pressure field. Application of the analytical models requires knowledge of the statistics of the wall pressure fluctuations. Analytical prediction of the wall pressure fluctuations is presently not feasible; consequently, experiments and tests are needed for a description of the pressure field.

6.6 CYLINDER RESPONSE TO NEARFIELD FLOW NOISE

The mean-square value of the cylinder can be calculated from Eq. 6.45. From the mathematical model and pressure field, the following conclusions can be drawn:

- The response of the first mode dominates; the contribution from higher modes is small at low flow velocities. A one-mode approximation will give sufficient accuracy in many practical situations.

- With the magnitude of the power spectral density of the pressure field proportional to the axial flow cubed, as indicated by available experimental results (Figs. 6.14 and 6.15), the rms cylinder displacement is proportional to flow velocity to the 1.5 to 3.0 power. The lower value is for a system with a low fundamental natural frequency; hence low $S (= f d_h / U)$, while the higher value is associated with higher S . As an approximation, we can write

$$\begin{aligned} \bar{\omega} &\propto v^{1.5}, & S < 0.2, \\ \bar{\omega} &\propto v^{2.0}, & 0.2 < S < 3.5, \\ \bar{\omega} &\propto v^{3.0}, & 3.5 < S. \end{aligned} \quad (6.57)$$

This is based on the assumption that $\bar{\chi}^2$ (Eq. 6.56) and the joint acceptance (Eq. 6.44) are constants. These two parameters are actually functions of the frequency; therefore, the exact power will depend on the parameter involved.

The important aspect of the problem is that the power spectra of the pressure at lower values of S are not known accurately. The power spectra measured by various workers differ widely at low S (Fig. 6.14). This is due to the spurious disturbances arising in the test channels as acoustic waves. It is precisely this lower range of S that is important in practical applications. This suggests the pressing necessity of making power-spectra measurements in this range of S .

We turn now to specific numerical examples. Figures 6.16 and 6.17 show the rms displacements at the midpoint for fixed-fixed rods, and at $x = 2$ ft for cantilevered rods (see Table 6.2 for details). At low flow velocity, the predicted displacements are much smaller than the experimental values. This may be due to the far-field noises, which are not accounted for in the theory; or the larger experimental values may be the result of structural-borne vibration. As the flow velocity increases, the turbulent-boundary-layer pressure fluctuations become more important and the theory successfully predicts the essential trends of rms response.

As can be seen from Figs. 6.16 and 6.17, the effect of hydraulic diameter is significant. Experimental rms values for Tests 1-C and 2-C are much lower than corresponding values from the other tests. The theoretical values, in turn, are much larger than the experimental results. The reason for this discrepancy is that the power spectral density of pressure used in the model is based on measurements on a cylindrical rod with a hydraulic diameter of 1.0 in. (Wambsganss and Zaleski 1970). In Tests 1-C and 2-C, the hydraulic diameter is 0.5 in. As the hydraulic diameter decreases, the intensity of turbulence also decreases and rms response is less. It also follows that using PSD data from tests with a larger hydraulic diameter to compute rms displacement would give results that are larger than experimental measurements.

Absolute values of amplitude are meaningless because we are dealing with a random vibration phenomenon. Therefore, we have developed a relationship to predict the rms displacement response. Although this information is useful, a complete description of the random signal requires knowledge of the probability law describing the amplitude distribution. Based on the displacement-time histories from a number of different flow tests, the shapes of the curves obtained suggest a normal or Gaussian distribution. As shown in Fig. 6.18, which is a typical probability density representation of vibration amplitude, the normal probability law approximates the data quite well.

Based on this agreement, we can assume a normal distribution for the distribution of vibration amplitude in a given direction, and write the

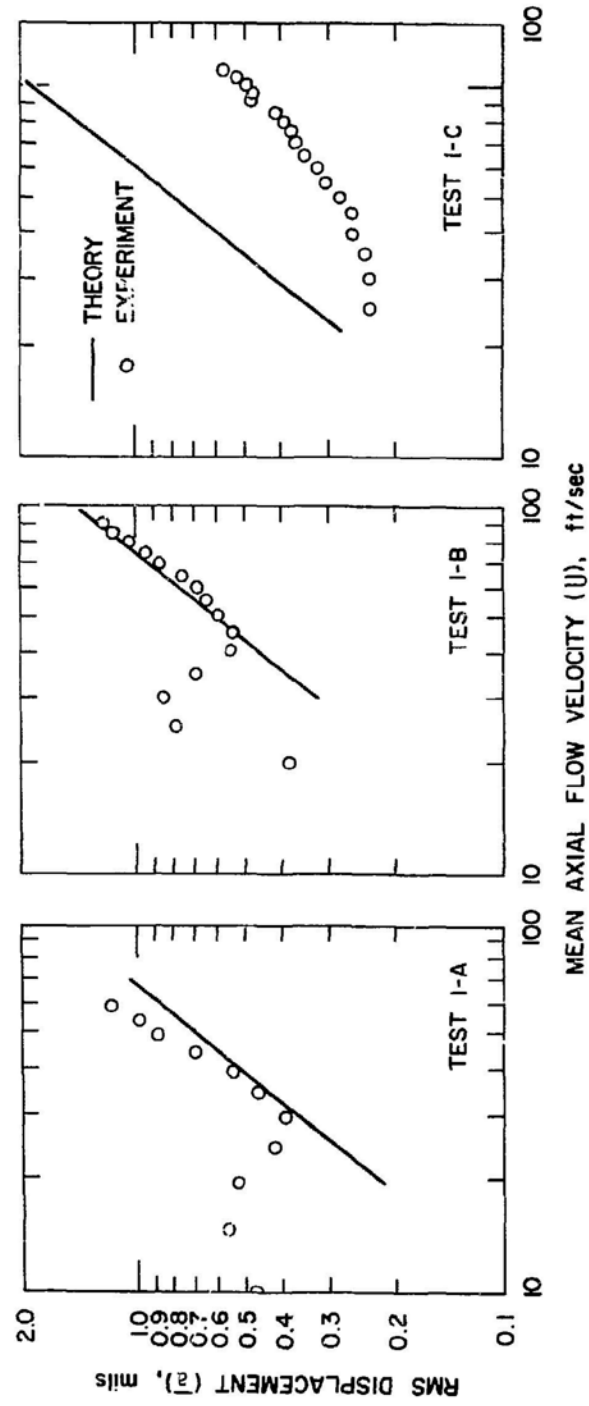


Fig. 6.16. RMS Displacement of Fixed-Fixed Cylinders at Midspan (Chen and Wambeganss 1972)

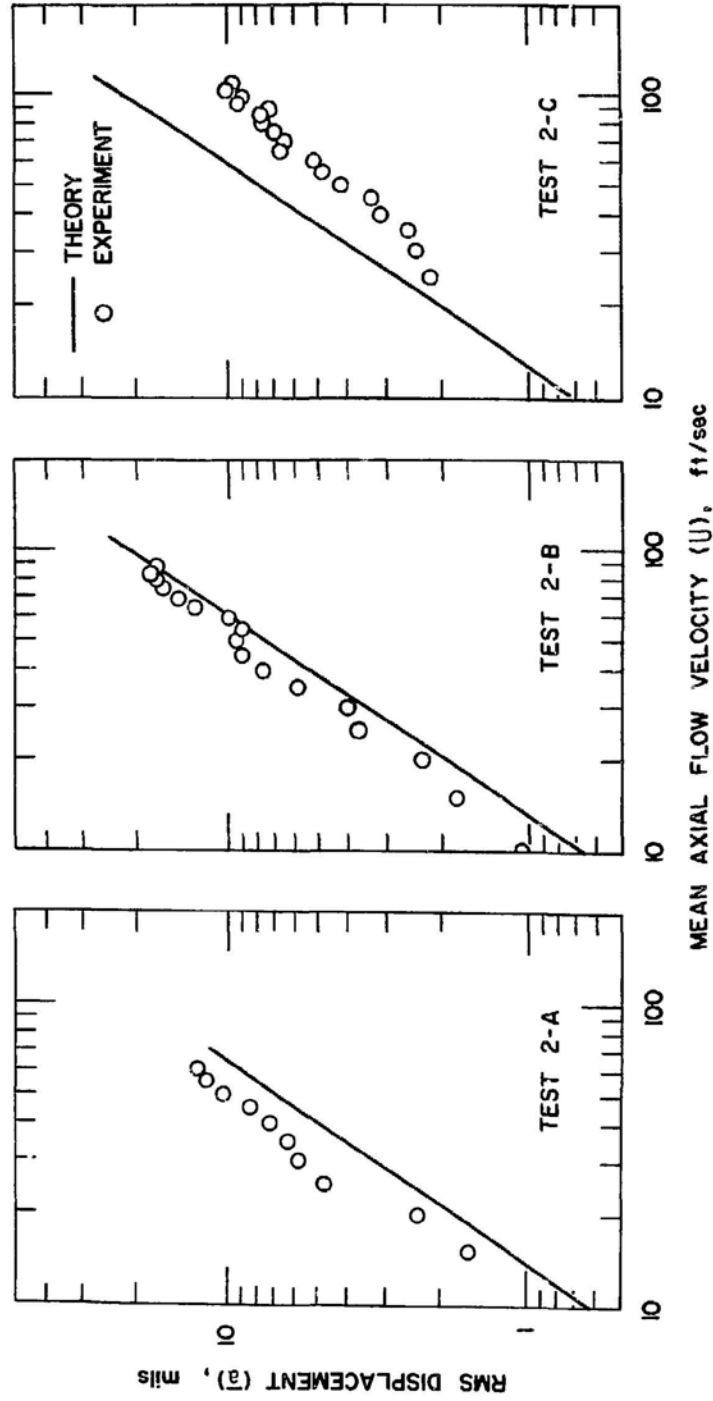


Fig. 6.17. RMS Displacement of Cantilevered Rods 2 ft from Fixed End (Chen and Wambsganss 1972)

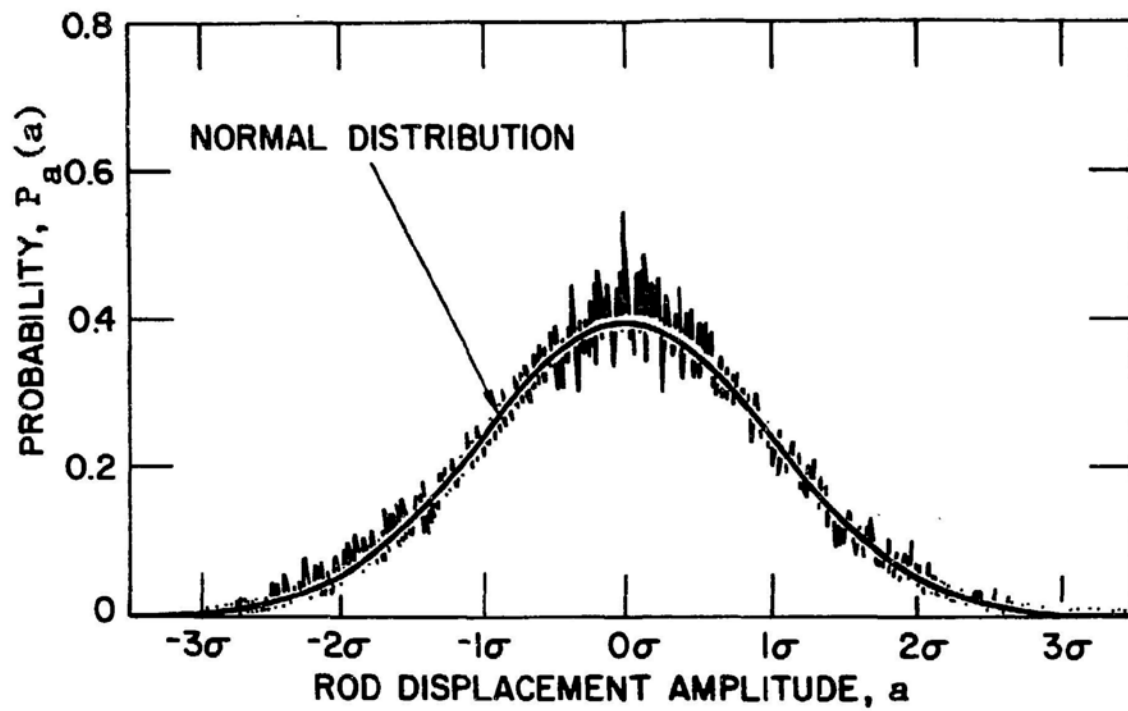


Fig. 6.18. Typical Probability Density Representation of Displacement of Flexible Cylinder Vibrating in Parallel-flowing Fluid (σ = rms value = 2.34 mils; U = 16 ft/s) (Wambsganss and Chen 1971)

probability law as

$$p_a(a) = \frac{1}{\sqrt{2\pi} \sigma} \exp\left[-\frac{1}{2} \left(\frac{a}{\sigma}\right)^2\right], \quad (6.58)$$

which implies a mean value of zero (σ is the standard deviation, and for a zero mean value is equal to the rms value). The probability that an observed value of displacement will range between $-a_0$ and a_0 is determined by the integration

$$P[-a_0 \leq a \leq a_0] = \int_{-a_0}^{a_0} p_a(a) da = \frac{1}{\sqrt{2\pi} \sigma} \int_{-a_0}^{a_0} \exp\left[-\frac{1}{2} \left(\frac{a}{\sigma}\right)^2\right] da. \quad (6.59)$$

The normal probability integral has been evaluated and is tabulated in various sources. Several of these values are listed below:

<u>n</u>	<u>P[-n ≤ a ≤ n]</u>
0.5	0.383
1.0	0.683
1.5	0.866
2.0	0.954
2.5	0.988
3.0	0.997

Observe the probability of 0.997 that the absolute vibration amplitude will be less than 3σ , that is, 99.7% of the time the amplitude can be expected to be less than 3σ , or $3a_{\text{rms}}$. Such information is useful in fatigue and wear studies and in determining if impact with adjacent components or support members may occur.

6.7 EMPIRICAL CORRELATIONS FOR SUBCRITICAL VIBRATION

A number of nuclear reactor system components are beam-like members exposed to fluid flows that are nominally parallel to their long axis. These components include the fuel rod, control rods, control rod guide tubes, instrumentation guide tubes, shroud tubes, heat exchanger tubes, etc. With exposure to highly turbulent flow fields, these components are prone to subcritical vibration, and, in some cases, fluidelastic instability.

Empirical correlations have been proposed to predict component response to subcritical flow excitations. A brief discussion of the various correlations is given here. Further information can be obtained from the references cited.

Burgreen's Correlation

The equation derived by Burgreen et al. (1958) was the first attempt to correlate test data of subcritical vibration and it is the simplest correlation. From a dimensional analysis, the vibration amplitude is found to be a function of three dimensionless parameters: $\rho U^2 l^4 / EI$, $\rho U^2 / \mu \omega$, and Re (see Nomenclature):

$$\left(\frac{a}{D_h}\right)^{1.3} = 0.83 \times 10^{-10} \kappa \left(\frac{\rho U^2 l^4}{EI}\right) \left(\frac{\rho U^2}{\mu \omega}\right), \quad (6.60)$$

where κ is the end fixity factor ($\kappa = 5$ for simply supported rods) and a is the peak-to-peak amplitude.

When this correlation was developed, the excitation mechanism was still not well understood. In comparison with test data, the discrepancies can be up to two orders of magnitude (Paidoussis 1965; Pavlica and Marshall 1966).

Reavis' Correlation

Reavis (1969) develops the correlation for the response amplitude based on the random vibration theory for turbulent excitation:

$$a = C_d \eta_D \eta_h \eta_l \frac{D}{m_f^{1.5} \zeta^{0.5}} U \rho v^{0.5}. \quad (6.61)$$

η_D , η_h , and η_l are scale factors and are functions of fD/U , fD_h/U , and fl/U ; the other symbols are listed in the Nomenclature. The forcing function is based on that by Bakewell's measurements (Bakewell 1964) for turbulent wall pressure fluctuations in pipe flow. When compared with available experimental data, the purely theoretical prediction is found to underestimate measured maximum displacements by a factor ranging from 3.5 to 240. Therefore, a disparity ratio C_d is introduced in the correlation.

Paidoussis' Correlation

Paidoussis (1969) postulates that vibration arises from departures from purely axial steady uniform flow:

$$\frac{a_{\max}}{D} = \alpha_1^{-4} \left[\frac{v^{1.6} \epsilon^{1.8} Re^{0.25}}{1 + v} \right] \left[\left(\frac{D_h}{D} \right)^{0.4} \left[\frac{\beta^{2/3}}{1 + 4\beta} \right] [5 \times 10^{-4} \kappa] \right], \quad (6.62)$$

where v , ϵ , β , and D are defined in Section 6.3. a_{\max} is the maximum amplitude, α_1 is the dimensionless first-mode eigenvalue of the cylinder, Re is the Reynolds number based on the hydraulic diameter, D_h is the hydraulic diameter, and κ represents a measure of departures from axial, steady and uniform flow conditions and of mechanically transmitted vibration. $\kappa = 1$ corresponds to conditions for low upstream disturbance and low mechanically transmitted vibration level. On the other hand, for realistic industrial environments $\kappa = 5$.

The "maximum" amplitude in this correlation is not precisely defined. For practical purposes, it is the maximum displacement from equilibrium to be expected if one were to scan an oscillograph record of cylinder vibration about 5 ft long. A more precise definition would be the probability of a_{\max} , because the vibration is random.

Figure 6.19 compares the empirical expression with the experimental data. The agreement is reasonable. A large discrepancy exists at low flow velocities. This is due to the mechanically transmitted vibration and to other system characteristics, which are overshadowed at higher flow velocities. A similar discrepancy occurs at a low flow velocity in other tests (Fig. 6.16).

Chen and Weber Correlations

Chen and Weber (1970) consider that the excitation of the cylinder is attributable to parametric excitation. Introducing a sinusoidally varying velocity fluctuation into the equation of motion, they determine the critical buckling velocity U_{cr} , the velocity at which the cylinder buckles:

$$U_{cr} = \left[\frac{(\pi^2/l^2)EI}{\frac{\pi}{4} C_f \rho l D + m_a} \right]^{0.5}, \quad (6.63)$$

where C_f is the surface drag coefficient. Chen and Weber propose an empirical correlation:

$$\frac{a}{D_h} = \left[1 - \left(\frac{U}{U_{cr}} \right)^2 \right]^{-1} \left(\frac{\kappa U}{U_{cr}} \right)^2 \quad (6.64)$$

where κ is an initial turbulence factor ranging from 0.5 for ideally quiet flow to 2 for poor flow condition.

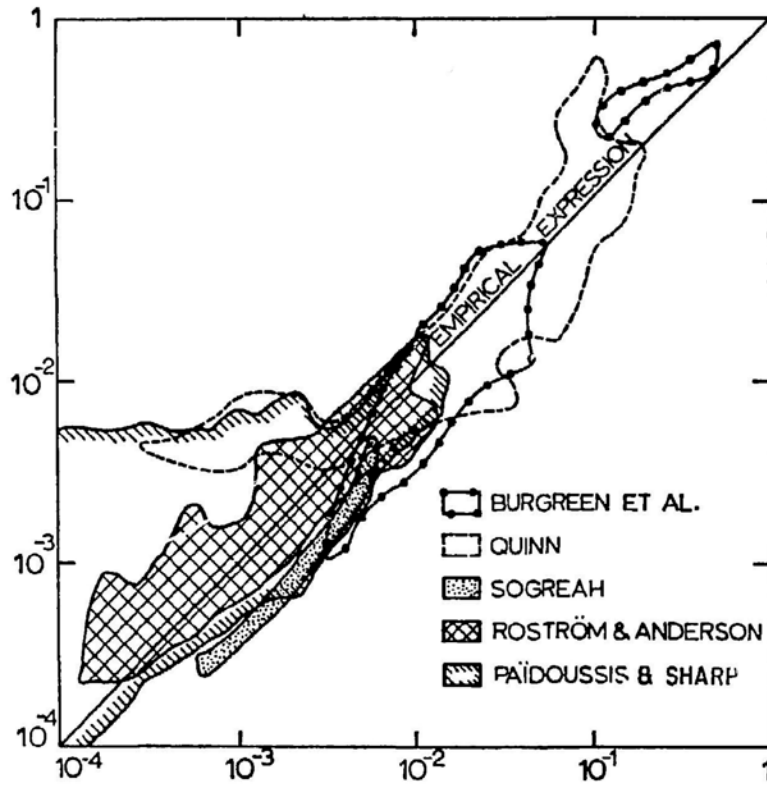


Fig. 6.19. Agreement Between Measured and Predicted Amplitudes of Vibration According to Paidoussis' Empirical Expression (from Paidoussis 1974, with permission--see Credits)

Wambsganss and Chen Correlation

Wambsganss and Chen (1971) derive a theoretical relationship for calculating the rms displacement of a rod in nominally axial flow as follows:

$$a_{rms}(z,U) = \frac{0.018 \kappa D^{1.5} D_h^{1.5} U^2 \phi(z)}{\lambda^{0.5} f^{1.5} (m + m_a) \zeta}, \quad (6.65)$$

where $\kappa = 2.56 \times 10^{-3} \text{ (lb)(sec)}^{2.5} / \text{ft}^{5.5}$, $\phi(z)$ is the modal function and other symbols are given in the Nomenclature. Equation 6.65 gives rms displacement. It is recommended that this correlation be used to obtain a lower bound on the actual displacement, the lowest rms response to be expected.

Summary

The empirical models have generally been developed using dimensional analysis and test results. The empirical correlations have the advantage of correlating actual test data. However, the scatter in reported data may be large, so that often a correlation factor is introduced into the models. In application, there is uncertainty as to what value of correction factor to assume. Additionally, an empirical correlation is valid only for the ranges of parameters that are included in the test area used in developing the correlation. Extrapolation of the correlation to predict response of components with flow and structural characterizing parameters outside the ranges for which test data are available is fraught with uncertainty.

6.8 EFFECTS OF DIFFERENT FLOW CONDITIONS**6.8.1 Fluid Compressibility**

The effect of fluid compressibility on the dynamic behavior of the cylinder and, especially, on its stability is studied theoretically by Paidoussis and Ostoja-Starzewski (1981). The effect of compressibility is shown to be rather weak. This can be predicted on physical grounds. The dominant effect is associated with the fluid centrifugal force and Coriolis force, which do not depend on the fluid compressibility significantly.

6.8.2 Towed Cylinders

A towed slender flexible cylinder is related to a towed ship, and yawing of airships moored to a mast. The theory presented in Section 6.2 is applicable to this case, but the boundary conditions at the two ends are different. Proper boundary conditions can be developed for different end shapes (Paidoussis 1968). In this case, the body may be subject to divergence

and flutter. At small U , the instability may be associated with the rigid-body motion. At higher U , the system may be subject to the instabilities of a cylinder in axial flow.

6.8.3 Pulsating Flow

Since the basic characteristics of a cylinder in axial flow are similar to those of a pipe conveying fluid (see Chapter 5), parametric and combination resonances are possible. Because of the complexity of the fluid forces acting on the system, its dynamic behavior is considerably more intricate than that of a conventional dynamic system, such as a column subjected to an oscillating axial load.

The equation of motion for pulsating flow can be derived using the techniques given in Section 6.2 (Paidoussis 1975; Paidoussis et al. 1980). In the published literature, only parametric resonance has been studied theoretically and experimentally; combination resonance apparently has not been considered experimentally.

6.8.4 Combined Internal and External Flows

When a tubular cylinder is subjected simultaneously to internal and external flow, both the fluid inside and the fluid outside affect the dynamic characteristics (Hannoyer and Paidoussis 1978). The analysis of this case can be done by combining Eqs. 5.29 and 6.20; therefore, the characteristics of the system can be inferred from knowledge of its state when subjected separately to internal and external flows. The stability characteristics of the cylinder supported at both ends are similar to those of a cylinder subjected to an external flow. Increasing the internal or external flow velocity or both results in the system eventually losing stability by divergence; its subsequent behavior with increasing flows involves a succession of flutter and buckling instabilities. In the case of cantilevered tubes, the system behavior is much more complex; it depends on the values of internal and external flow velocities and the flow conditions at the downstream end.

6.8.5 Confined Region

The effect of lateral confinement of the flow is to increase the added mass m_a ; therefore, the cylinder may lose stability at a lower flow velocity than if it were in effectively unbounded flow. The general characteristics are not much different from those for infinite fluid. One of the interesting results (Paidoussis and Pettigrew 1979) is the demonstration of succession of instabilities. As flow velocity is increased, there is an essentially continuous succession of instabilities of increasingly complex modal shape. In an unbounded fluid, at the first instability flow velocity, the cylinder displacement increases drastically. In the confined region, the instability

of a particular mode may be eliminated because of the change of boundary conditions; therefore, it is possible to induce higher-mode instability.

6.8.6 Two-Phase Flow

The analytical and experimental techniques for single-phase flow can be used for two-phase flow. An analytical and experimental investigation of cylinders in two-phase flow has been done by Gorman (1971). Good agreement is found between measured and predicted vibration amplitudes. For a given mass flow, the rms amplitude depends on quality factor. With the increase in quality factor, rms displacement rises rapidly and peaks at a quality factor of ~ 12 before falling off fairly rapidly. The main cause for the higher amplitude of vibration in two-phase flow lies in the much higher peripheral spatial correlation of the pressure fluctuations on the surface of the cylinder. Other response characteristics in two-phase flow are that:

- The modal damping attributed to two-phase flow is larger than that for a liquid flow,
- The analytical model for single phase flow is applicable for a two-phase flow but with different empirical constants, and
- The excitation is the time-varying random pressure fluctuations on the surface of the cylinder.

In contrast to Gorman's conclusion regarding the excitation mechanism, Hara (1975a, 1975b) shows that there are two excitation sources--an external force due to two-phase pressure fluctuations, and a periodic change of fluid mass in the vibration system coming from periodic water-slug conveyance in the two-phase flow. The former excitation is a forced vibration, while the latter is a parametric or combination resonance.

There is no systematic characterization of the pressure field for two-phase flow. Theories developed for two-phase flow face difficulties. The two-phase flow data are considered preliminary in nature; much more integrated theoretical and experimental investigations are needed.

6.9 MULTIPLE CYLINDERS IN AXIAL FLOW

In addition to nuclear fuel bundles, other structural components consisting of a group of circular cylinders--such as heat exchanger tubes, piles, parallel pipelines, and bundled transmission lines--may be subjected to axial flow. Many investigators have studied the dynamics of various types of structural components consisting of multiple cylinders. Those include two parallel cylinders, two cylinders located concentrically and separated by a fluid, a row of cylinders and a group of cylinders. These studies have revealed some complex fluid/structure interaction characteristics. Despite the progress being made on the dynamics of multiple cylinders, the prediction of cylinder response in axial flow remains a difficult task.

6.9.1 Equations of Motion of a Group of Circular Cylinders in Axial Flow

The equations of motion for a group of cylinders can be derived following the same method as that for a single cylinder, as given in Section 6.2. The details are not presented here; see Chen (1975).

A cylinder array consisting of N cylinders whose axes are parallel to the z axis is shown in Fig. 3.9. The cylinders are immersed in a fluid flowing at a constant velocity U parallel to the z axis. For convenience, a subscript p is used to denote variables associated with cylinder p in the x - z plane, while $p + N$ denotes the y - z plane. For example, $u_p(z, t)$, $E_p I_p$, C_{vp} , and g'_p are the displacement, flexural rigidity, damping coefficient, and excitation in the x direction, and corresponding quantities in the y direction are u_{N+p} , $E_{N+p} I_{N+p}$, $C_{v, N+p}$, and g'_{N+p} . The equations of motion for a group of N cylinders are as follows:

$$\begin{aligned}
 E_p I_p \frac{\partial^4 u_p}{\partial z^4} + \mu_p I_p \frac{\partial^5 u_p}{\partial t \partial z^4} + \sum_{q=1}^{2N} \gamma_{pq} \left(\frac{\partial}{\partial t} + U \frac{\partial}{\partial z} \right)^2 u_q \\
 - [T_p(l) - (m_p g - \rho R_p U^2 C_{fp})(l - z) + p A_p] \frac{\partial^2 u_p}{\partial z^2} \\
 - (m_p g + \frac{\partial p}{\partial z} A_p) \frac{\partial u_p}{\partial z} + \rho R_p U C_{fp} \left(\frac{\partial u_p}{\partial t} + U \frac{\partial u_p}{\partial z} \right) \\
 + C_{vp} \frac{\partial u_p}{\partial t} + m_p \frac{\partial^2 u_p}{\partial t^2} = g'_p,
 \end{aligned}$$

$$p, q = 1, 2, 3, \dots, 2k, \quad (6.66)$$

where μ_p is the structural damping, γ_{pq} is the added mass matrix, $T_p(l)$ is the tension at the downstream end, g the gravity, p is the fluid pressure, m_p is cylinder mass per unit length, C_{fp} is the drag coefficient, and C_{vp} is the viscous damping coefficient. Equations 6.66 are derived based on several important assumptions:

- The added mass matrix is based on the two-dimensional potential flow theory presented in Section 3.3.
- The fluid pressure p is constant along the cylinders.
- The flow velocity is constant.
- The fluid damping attributed to viscous coupling (see Eq. 3.145) is not included.

The essential characteristics of cylinder arrays in axial flow can be studied using Eqs. 6.66.

6.9.2 Dynamic Characteristics of an Array of Cylinders in Axial Flow

The analysis of a group of cylinders in axial flow is the same as that for cylinders in quiescent fluid (see Sec. 3.4). With the equations of motion and boundary conditions, the dynamics of an array of cylinders can be reduced to the standard form:

$$[M]\{\ddot{Q}\} + [C]\{\dot{Q}\} + [K]\{Q\} = \{G\} \quad (6.67)$$

If the potential flow theory is used for the added mass γ_{pq} , M is symmetric. However, C and K are generally not symmetric.

The general characteristics of cylinder arrays in axial flow can also be inferred from those of a group of cylinders in quiescent fluid, as discussed in Chapter 3, and a single cylinder in axial flow (Sections 6.4 and 6.6).

One of the most notable characteristics is the coupling of all cylinders so that the different modes of the system are characterized not only by the axial modal shapes of each cylinder, but also the cross-sectional patterns of motion involving all cylinders in an array corresponding to a single frequency for a single cylinder. There are $2N$ frequencies for $2N$ different cross-sectional patterns; i.e., there are $2N$ frequencies located in a frequency band close to that for a single cylinder. These characteristics are the same as those for quiescent fluid.

At subcritical flow velocities, the random vibration of the cylinders occurs in a frequency band, in contrast to a single frequency for a single cylinder. As the flow velocity increases, the rms amplitude increases. At the same time, the frequency band broadens. This is attributed to the fact that the fluid centrifugal force tends to lower the frequencies of coupled modes and its effect is more significant for lower frequency modes (Paidoussis et al. 1982).

As the flow velocity is further increased, the cylinders are subject to divergence and flutter. The precise mechanism or sequence of instabilities depends on boundary conditions and flow conditions. For example, Fig. 6.20 shows some buckling modes of three and four cylinders; Figs. 6.20a to e are for a hinged-hinged end, while 6.20f to j show cylinders clamped at both ends (Paidoussis 1979). With increasing flow, the instability modes may change and a different instability mechanism such as flutter may become dominant.

The basic characteristics of cylinder response can be characterized. Analytical and experimental data show reasonable agreement (Paidoussis 1979; Paidoussis et al. 1982). However, a more detailed prediction of cylinder

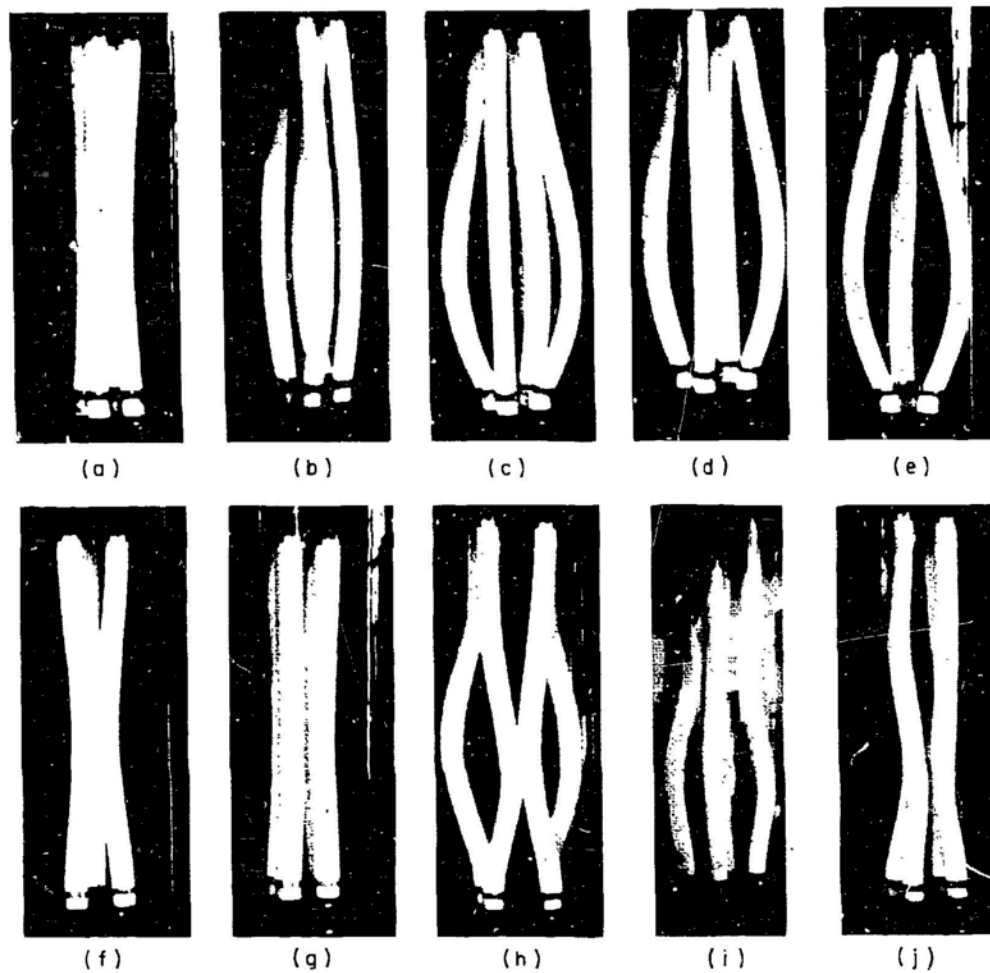


Fig. 6.20. Buckling Modes of Four- and Three-cylinder Systems: a-e Hinged at Both Ends, f-j Fixed at Both Ends but Free to Slide Axially (from Paidoussis 1979, with permission--see Credits)

response in axial flow will require a more refined representation of the fluid forces. These are the subjects of current research. Efforts have been made to measure the wall pressure fluctuations within a cylinder array (Lin et al. 1981) and to characterize cylinder responses in fuel bundles (Hayes 1981).

6.10 LEAKAGE FLOW-INDUCED VIBRATION

Self-excited vibrations of components employing slip joints and seals have been encountered on various system components (Miller 1970; Thomann 1976; Denton and Hutton 1978; Torres 1980). The cause of these vibrations has been the fluidelastic mechanism, involving a leakage flow across a restrictor with a large pressure drop. Because of the complexity of the flow field and the geometry involved, attempts to study these phenomena experimentally and analytically have faced difficulty. A recent survey on this subject is presented by Mulcahy (1983).

One of the instability mechanisms can be demonstrated using a two-dimensional model, as shown in Fig. 6.21 (Miller 1970). Assume that

- The flow restrictor is a rigid blade with a flow restricting enlargement at one end,
- The blade is constrained to have translation across the flow channel only (no rotation),
- The effect of blade motion on pressure loss is neglected, and
- The pressure drop across the flow restrictor is very large compared with the pressure difference from the right end of a channel to the flow restrictor.

If the blade has a small upward velocity $\partial u/\partial t$ while the fluid flow is from left to right, the flow velocity between the flow restrictor and the channel walls remains essentially the same above and below the flow restrictor. Because of the reduction of the clearance between the blade and the upper channel wall, the total flow past the upper side decreases with time. The opposite situation exists with respect to the flow between the blade and lower channel wall. Because of the flow velocity redistribution, the resulting distribution of static pressure acts on the blade, as shown in Fig. 6.21. The net fluid forces on the blade are upward; i.e., the movement of the blade induces a fluid force acting on the blade in the same direction as the motion. Under this condition, the flow restrictor and blade interact with the fluid to produce a damping-controlled type of instability. A similar reasoning shows that, if the flow is from right to left, the flow will provide a damping mechanism.

Figure 6.21 illustrates the instability mechanism for translational motion only. In most practical situations of typical flow paths, as shown in Fig. 6.22, the central body can be excited into a rotational motion as well as

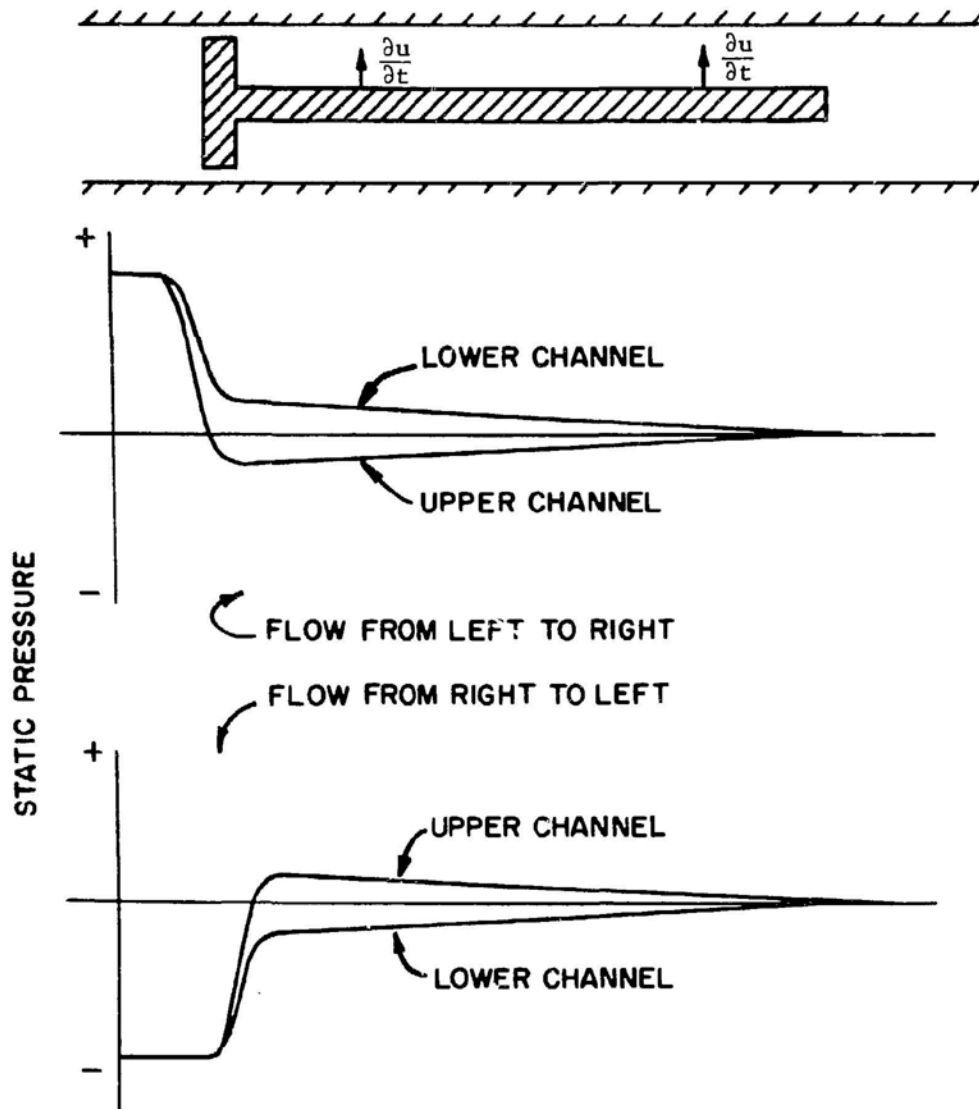


Fig. 6.21. Generation of Positive and Negative Damping in Leakage Flow (Miller 1970)

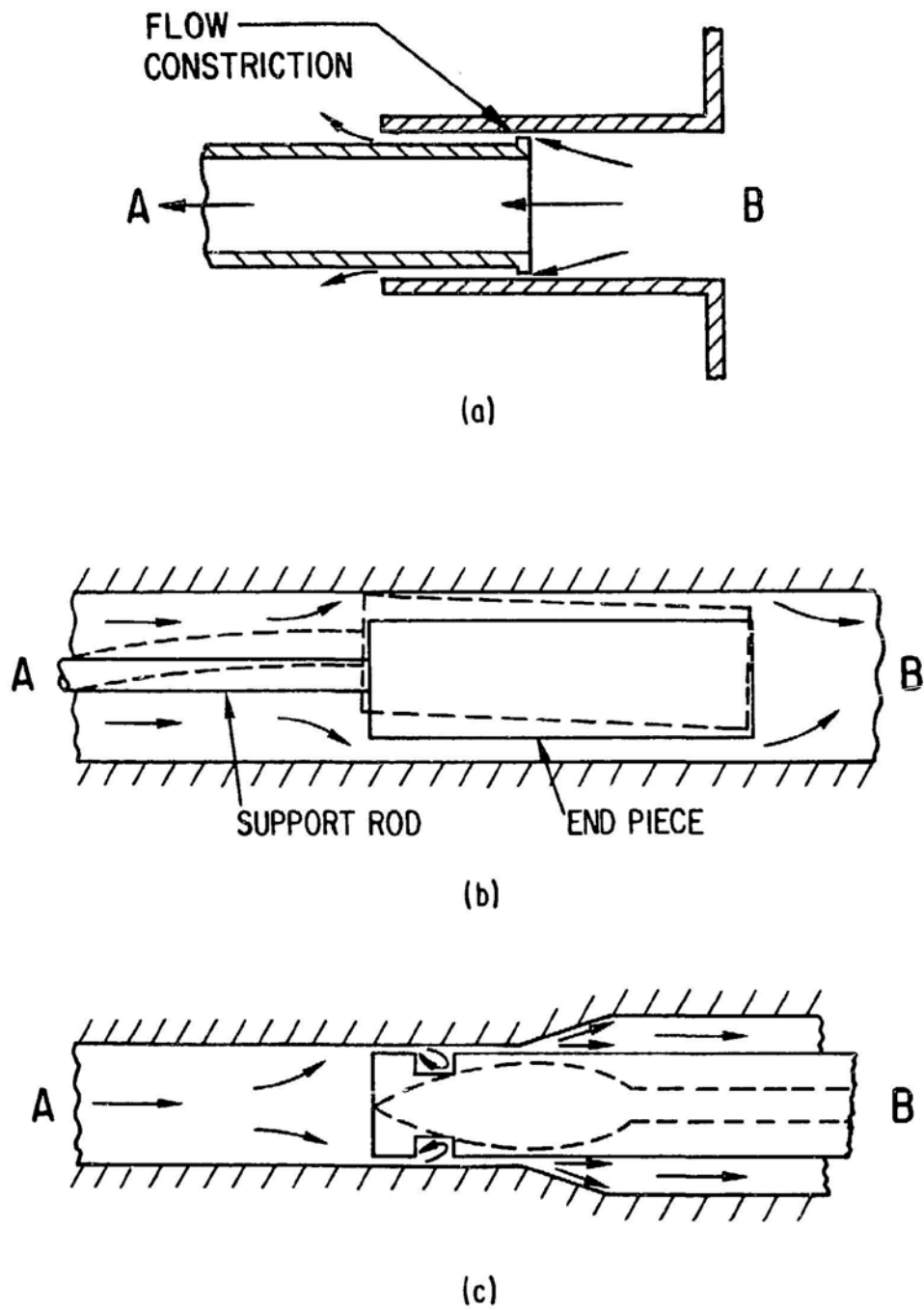


Fig. 6.22. Leakage Flow Geometries (Mulcahy 1983)

translational motion. In this case, both the fluid-damping-controlled and fluid-stiffness-controlled types of instability are possible.

Another fluid-damping-controlled instability can be created in a diverging leakage flow path (Fig. 6.22c). If the flow efficiency of the diverging section increases as the central body motion increases the throat size, a fluid-damping controlled instability is possible. This is specifically associated with diffuser efficiency variations.

An interesting experiment was conducted by Mulcahy (1984) using a cantilevered tube conveying water with leakage flow through a slip joint, which was formed by inserting a smaller rigid tube into the free end of the cantilevered tube. The three lower modes are shown in Fig. 6.23. The orbital paths of the tube at various flowrates are shown in Fig. 6.24. The unstable motion of the end of the upper tube occurs at a very small flowrate in a nearly one-dimensional translation, which is the dominant motion of the fundamental mode. As the flow velocity is increased, the tube begins to orbit in an elliptic path. With further increase in flow velocity, the orbit is nearly circular at 4 GPM. At 7 GPM the tube impacts the inner tube once during each cycle, but at 8 GPM, there are two contact points, resulting in precision of oscillations. At higher flowrates, more points of contact result in chaotic motion. The unstable motion in the fundamental mode is nonlinear in that a limit cycle of oscillations occurs at a constant flow, even before tube-to-tube impact. The fundamental frequency increases with flowrate. When the flowrate is increased to 15-25 GPM, where the second hinged mode frequency (see Fig. 6.23b) becomes a superharmonic of the fundamental frequency, the response switches intermittently between the first two modes. At 25 GPM, the second mode becomes dominant. The switch to the second mode indicates the significance of rotation.

The development of analytical methods to predict leakage-flow-induced vibration is still in its infancy. Efforts have been made to predict the stability-instability boundary using the unsteady flow theory (Hobson 1982; Mateescu and Paidoussis 1984). However, the stability associated with the leakage flow mechanism depends on the detailed geometries of the restrictor and its response is nonlinear. Significant research remains to be done in this area.

6.11 CLOSING REMARKS

Circular cylinders, either isolated one or in an array, that are subject to axial flow may become unstable by divergence or flutter. When the instability occurs, relatively large displacement develops until nonlinear effects become important. In practice, instability is generally unacceptable and therefore should be avoided. Based on existing analytical techniques, the critical flow velocity can be calculated with reasonable accuracy. An

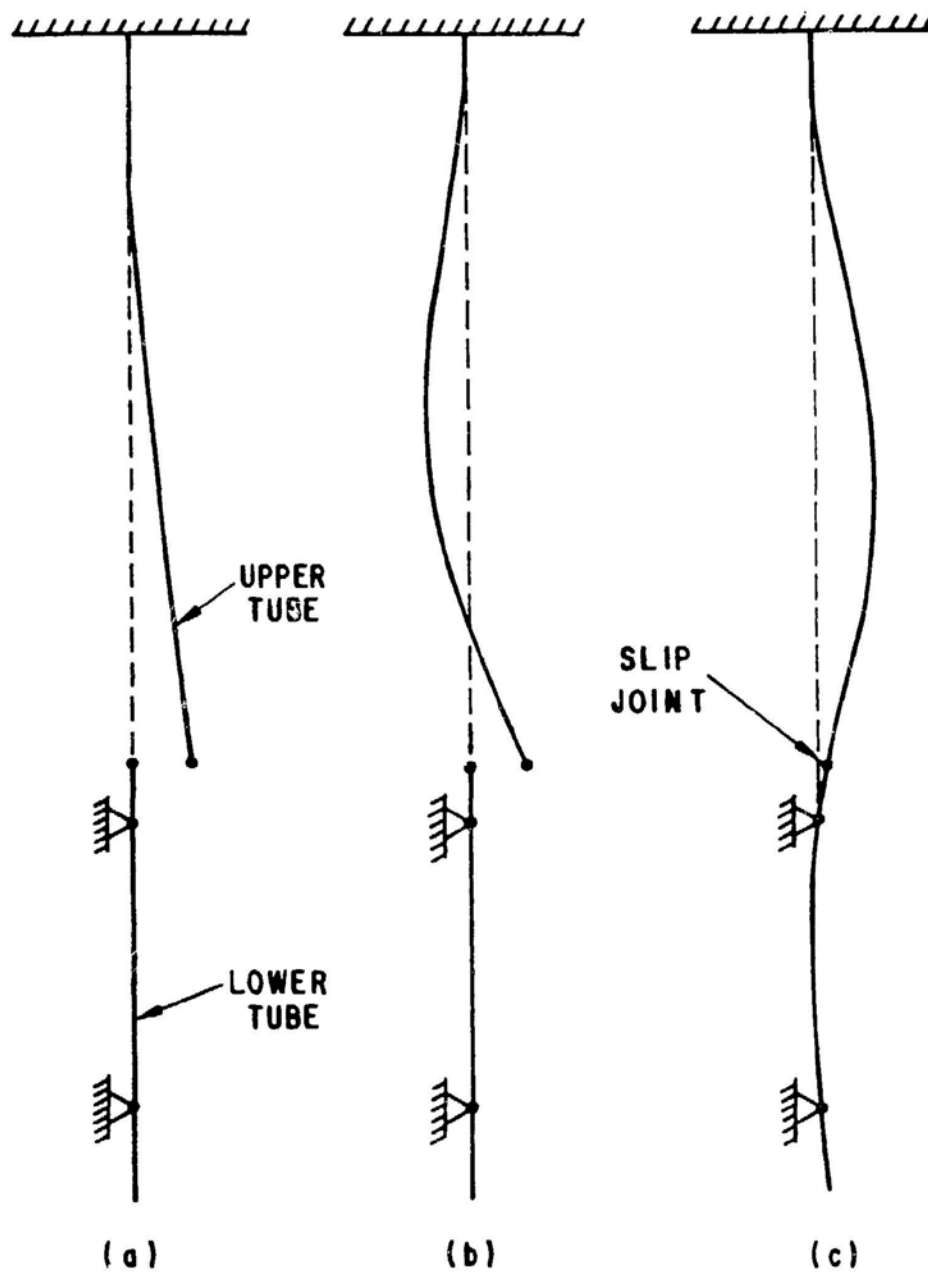


Fig. 6.23. Vibration Modes: (a) Unhinged First Mode (3.4 Hz), (b) Unhinged Second Mode (23 Hz), and (c) Hinged First Mode (13 Hz) (Mulcahy 1984)

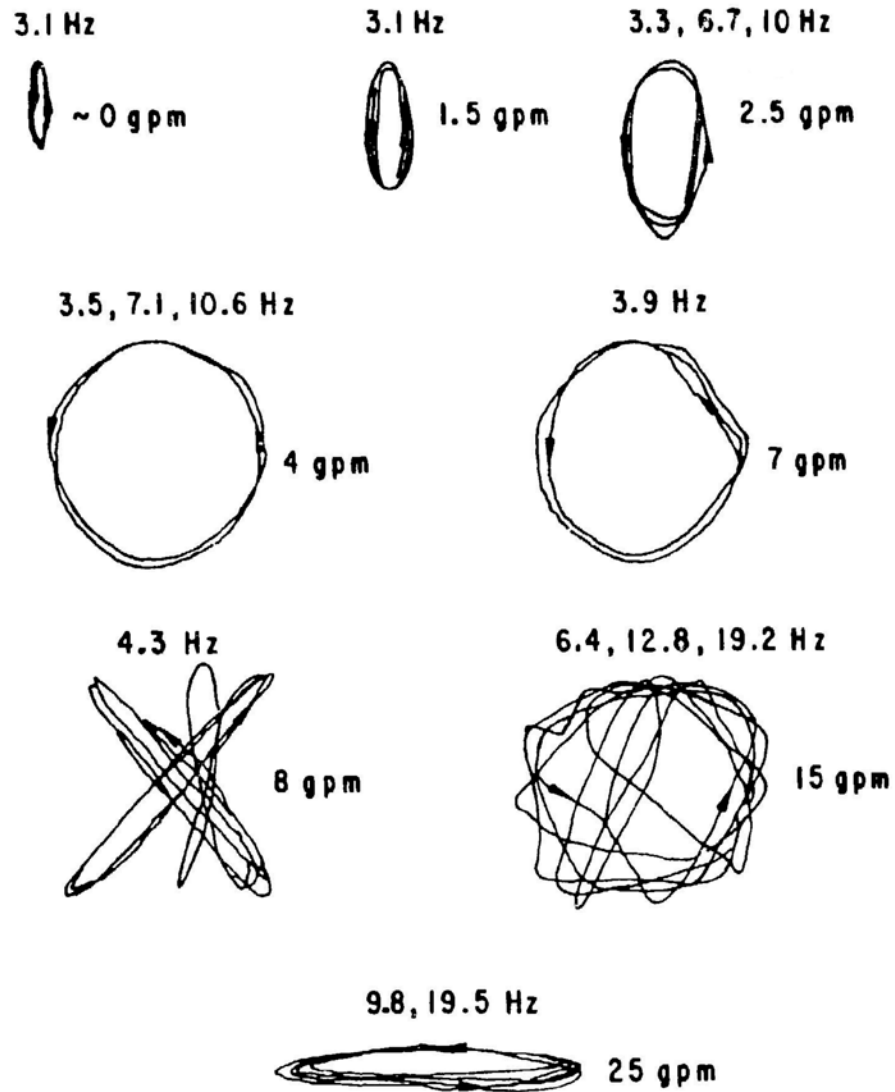


Fig. 6.24. Limit Cycle of Unstable Motion (Mulcahy 1984)

exception is leakage flow. Because this problem depends critically on the detailed geometries, no analytical methods are currently available to model the details of the restrictor in a leakage flow problem.

Instability can be avoided; however, subcritical vibration always exists. At any flow velocity, a cylinder in axial flow vibrates because of flow excitation. Determining the effect of subcritical vibration is difficult. A 10 mil displacement may be acceptable for one component but totally unacceptable in another. Thus, subcritical vibration is difficult to predict precisely, and its effect is difficult to evaluate, as well. To solve this problem, two critical areas remain to be studied:

- Systematic measurements as well as theoretical work are needed to quantify flow excitations in the subcritical flow velocity region, and
- The effects of small vibrations on the cylinder, such as wear and fatigue due to flow, are not well known.

Because of the complicated geometries in most practical system components, it is difficult to predict dynamic behavior precisely. In design evaluation, model tests are frequently used. It is expected that the new designs will continue to rely on model tests for detailed evaluation.

REFERENCES--Sec. 6

- Addae, A. K., and Fenech H. 1970. Experimental Determination and Analysis of Vibrations Induced by the Near-Field Flow Noise in Tubes. Proc. Conference on Flow-Induced Vibrations in Reactor System Components, ANL-7685, Argonne National Laboratory, Argonne, Ill., May 14-15, 1970, pp. 32-46.
- Bakewell, P. 1964. Narrow-Band Investigations of the Longitudinal Space-Time Correlation Function in Turbulent Airflow. J. Acoust. Soc. Am. 36, 146-148.
- Bakewell, Jr., H. P. 1968. Turbulent Wall-Pressure Fluctuations on a Body of Revolution. J. Acoust. Soc. Am. 43(6), 1358-1363.
- Basile, D., Fauré, J., and Ohlmer, E. 1968. Experimental Study on the Vibrations of Various Fuel Rod Models in Parallel Flow. Nucl. Eng. Des. 7, 517-534.
- Burgreen, D., Byrnes, J. J., and Benforado, D. M. 1958. Vibration of Rods Induced by Water in Parallel Flow. Trans. ASME 80(5), 991-1003.
- Chen, S. S. 1975. Vibration of Nuclear Fuel Bundles. Nucl. Eng. Des. 35, 399-422.
- Chen, S. S., and Wambsganss, Jr., M. W. 1970. Response of a Flexible Rod to Near-Field Flow Noise. Proc. Conference on Flow-Induced Vibrations in Reactor System Components, ANL-7685, Argonne National Laboratory, Argonne, Illinois, May 14-15, 1970, pp. 5-31.
- Chen, S. S., and Wambsganss, M. W. 1972. Parallel-Flow-Induced Vibration of Fuel Rods. Nucl. Eng. Des. 18, 253-278.
- Chen, Y. N., and Weber, M. 1970. Flow-Induced Vibrations in Tube Bundle Heat Exchangers with Cross and Parallel Flow. ASME Symp. on Flow-Induced Vibration in Heat Exchangers, New York, December 1970, pp. 57-77.
- Clinch, J. M. 1969. Measurements of the Wall Pressure Field at the Surface of a Smooth-Walled Pipe Containing Turbulent Water Flow. J. Sound Vib. 9(3), 398-419.
- Corcos, G. M. 1963. Resolution of Pressure in Turbulence. J. Acoust. Soc. Am., 35(2), 192-199.
- Corcos, G. M. 1964. The Structure of the Turbulent Pressure Field in Boundary-Layer Flows. J. Fluid Mech. 18(Pt. 3), 353-378.
- Denton, J. D., and Hutton, M. F. 1978. Vibration Mechanisms Associated with Annular Flow through a Flow Control Device. Proc. International Conf. on Vibration in Nuclear Plant, Keswick, U.K., May 9-12, 1978, Paper No. 5.5.
- Gorman, D. J. 1969. The Role of Turbulence in the Vibration of Reactor Fuel Elements in Liquid Flow. AECL-3371, Atomic Energy of Canada Limited, Chalk River, Ontario, Canada.
- Gorman, D. J. 1970. An Experimental and Analytical Investigation of Fuel Element Vibration in Two-Phase Parallel Flow. Trans. Am. Nucl. Soc. 13(1), 333.

- Gorman, D. J. 1971. An Analytical and Experimental Investigation of the Vibration of Cylindrical Reactor Fuel Elements in Two-Phase Parallel Flow. Nucl. Sci. and Eng. 44, 277-290.
- Hannoyer, M. J., and Paidoussis, M. P. 1978. Instabilities of Tubular Beams Simultaneously Subjected to Internal and External Axial Flows. J. Appl. Mech 100, 328-336.
- Hara, F. 1975a. A Theory on the Vibration of a Fuel Pin Model in Parallel Two-Phase Flow. Trans. 3rd Int. Conf. on Structural Mechanics in Reactor Technology, London, Paper No. D2/4.
- Hara, F. 1975b. Experimental Study of the Vibrations of a Fuel Pin Model in Parallel Two-Phase Flow. Trans. 3rd Int. Conf. on Structural Mechanics in Reactor Technology, London, Paper No. D2/3.
- Hawthorne, W. R. 1961. The Early Development of the Dracone Flexible Barge. Proc. Inst. Mech. Eng. 175, 52-83.
- Hayes, C. G. 1981. Fuel Rod Vibration with Reduced Spacer Spring Preload. GEAP-24381, General Electric Co.
- Hobson, D. E. 1982. Fluid-Elastic Instabilities Caused by Flow in an Annulus. Third Int. Conf. on Vibration in Nuclear Plant, Keswick, U.K., 1982.
- Kanazawa, R. M. 1969. Hydroelastic Vibration of Rods in Parallel Flows. Ph.D. dissertation, University of Illinois.
- Kinsel, W. C. 1975. Flow-Induced Vibrations of Spiral Wire-Wrapped Fuel Assemblies. ASME Paper No. 75-WA/HT-76.
- Knudson, S. A., and Smith, G. M. 1970a. Dynamic Response of Slender Tubes in Parallel Flow When Subjected to Time-Varying Boundary Conditions. Proc. Conference on Flow-Induced Vibrations in Reactor System Components, ANL-7685, Argonne, Illinois, May 14-15, 1970, pp. 64-90.
- Knudson, S. A., and Smith, G. M. 1970b. Vibration of Support Excited Tubes in Coaxial Flow. J. Eng. Mech. Div., Am. Soc. Civil Eng. 97(FM6), 1039-1060.
- Lighthill, M. J. 1960. Note on Swimming of Slender Fish. J. Fluid Mech. 9(2), 305-317.
- Lin, W. H., Wambsganss, M. W., and Jendrzejczyk, J. A. 1981. Wall Pressure Fluctuations within a Seven-Rod Array. GEAP-24375, General Electric Co.
- Mateescu, D., and Paidoussis, M. P. 1984. Annular-Flow-Induced Vibrations of an Axially Variable Body of Revolution in a Duct of Variable Cross-Section. Sym. on Flow-Induced Vibrations, Vol. 4, ASME Publication.
- Miller, D. R. 1970. Generation of Positive and Negative Damping with a Flow Restrictor in Axial Flow. Proc. Conference on Flow-Induced Vibrations in Reactor System Components, ANL-7685, Argonne, Illinois, May 14-15, 1970, pp. 304-307.

- Mulcahy, T. M. 1983. Leakage Flow-Induced Vibrations of Reactor Components. The Shock and Vibration Digest 15(9), 11-18.
- Mulcahy, T. M. 1984. Leakage-Flow-Induced Vibration of a Tube-In-Tube Slip Joint. Sym. on Flow-Induced Vibrations, Vol. 4, ASME Publication.
- Namatame, K. 1969. Theoretical Analysis of Fuel Rod Vibration Induced by Parallel Coolant Flow. J. Atomic Energy Soc. (Japan) 11, 398-405.
- Paidoussis, M. P. 1965. The Amplitude of Fluid-Induced Vibration of Cylinders in Axial Flow. AECL-2225, Atomic Energy of Canada Limited, Chalk River, Ontario, Canada.
- Paidoussis, M. P. 1966a. Vibration of Flexible Cylinders with Supported Ends, Induced by Axial Flow. Proc. Inst. Mech. Eng. 180(Pt. 3J), 268-279.
- Paidoussis, M. P. 1966b. Dynamics of Flexible Slender Cylinders in Axial Flow; Part 1: Theory; Part 2: Experiment. J. Fluid Mech. 26(Pt. 4), 717-751.
- Paidoussis, M. P. 1968. Stability of Towed, Totally Submerged Flexible Cylinders. J. Fluid Mech. 34(Pt. 2), 273-297.
- Paidoussis, M. P. 1969. An Experimental Study of Vibration of Flexible Cylinders Induced by Nominally Axially Flow. Nucl. Science and Engineering 35(1), 127-138.
- Paidoussis, M. P. 1973. Dynamics of Cylindrical Structures Subjected to Axial Flow. J. Sound Vib. 29(3), 365-385.
- Paidoussis, M. P. 1974. The Dynamical Behavior of Cylindrical Structures in Axial Flow. Annals of Nuclear Science and Engineering 1, 83-106.
- Paidoussis, M. P. 1975. Stability of Flexible Slender Cylinders in Pulsatile Axial Flow. J. Sound Vib. 42(1), 1-11.
- Paidoussis, M. P. 1979. The Dynamics of Clusters of Flexible Cylinders in Axial Flow: Theory and Experiments. J. Sound Vib. 65(3), 391-417.
- Paidoussis, M. P., and Ostojic-Starzewski, M. 1981. Dynamics of a Flexible Cylinder in Subsonic Axial Flow. AIAA Journal 19(11), 1467-1475.
- Paidoussis, M. P., and Pettigrew, M. J. 1979. Dynamics of Flexible Cylinders in Axisymmetrically Confined Axial Flow. J. Appl. Mech. 46, 37-44.
- Paidoussis, M. P., Curling, L. R., and Gagnon, J. O. 1982. Experiments on Fluidelastic Instability of Cylinder Clusters in Axial Flow. J. Fluid Eng. 104, 342-347.
- Paidoussis, M. P., Issid, N. T., and Tsui, M. 1980. Parametric Resonance Oscillations of Flexible Slender in Harmonically Perturbed Axial Flow; Part I: Theory and Part II: Experiments. J. Appl. Mech. 47, 709-419.
- Pavlica, R. T., and Marshall, R. C. 1966. An Experimental Study of Fuel Assembly Vibrations Induced by Coolant Flow. Nucl. Eng. Des. 4, 54-60.

- Pazsit, Z., Antonopoulos-Domis, M., and Glockler, O. 1984. Stochastic Aspects of Two-Dimensional Vibration Diagnostics. Progress in Nuclear Energy 14(2), 165-196.
- Pickman, D. O. 1975. Interactions between Fuel Pins and Assembly Components. Nucl. Eng. Des. 33, 125-140.
- Powell, A. 1958. On the Response of Structure to Random Pressures and Jet Noise in Particular. pp. 187-229 in: S. H. Crandall (Ed.), Random Vibration, Vol. 1, The MIT Press, Cambridge, Mass.
- Quinn, E. P. 1962. Vibration of Fuel Rods in Parallel Flow. GEAP-4059, General Electric Co.
- Quinn, E. P. 1965. Vibration of SEFOR Fuel Rods in Parallel Flow. GEAP-4966, General Electric Co.
- Reavis, J. R. 1969. Vibration Correlation for Maximum Fuel-Element Displacement in Parallel Turbulent Flow. Nucl. Sci. Eng. 38(1), 63-69.
- Schloemer, H. H. 1967. Effects of Pressure Gradients on Turbulent-Boundary-Layers Wall-Pressure Fluctuations. J. Acoust. Soc. Am. 42, 93-113.
- Schmugar, K. L. 1975. Vibratory Wear of Fuel Rods. ASME Paper 75-WA/HT-79.
- Skudrzyk, E. J., and Haddle, G. P. 1960. Noise Production in a Turbulent Boundary Layer by Smooth and Rough Surfaces. J. Acoust. Soc. Am. 32(1), 19-34.
- Taylor, G. 1952. Analysis of the Swimming of Long and Narrow Animals. Proc. Royal Soc. London A 214, 158-183.
- Thomann, H. 1976. Oscillations of a Simple Valve Connected to a Pipe. J. Appl. Mech. and Physics 27, 23-40.
- Torres, M. R. 1980. Flow-Induced Vibration Testing of BWR Feedwater Spargers. Flow-Induced Vibration of Power Plant Components, ASME Publ. PVP 41, pp. 159-176.
- Wambsganss, Jr., M. W. 1967. Vibration of Reactor Core Components. Reactor-Fuel Process. Technol. 10(1), 208-219.
- Wambsganss, M. W., and Chen, S. S. 1971. Tentative Design Guide for Calculating the Vibration Response of Flexible Cylindrical Elements in Axial Flow. ANL-ETD-71-07, Argonne National Laboratory, Argonne, Ill.
- Wambsganss, Jr., M. W., and Zaleski, P. L. 1970. Measurement, Interpretation, and Characterization of Near-field Flow Noise. Proc. Conference on Flow-Induced Vibrations in Reactor System Components, ANL-7685, Argonne, Illinois, May 14-15, 1970, pp. 112-140.
- Williams, M. M. R. 1970. Reactivity Changes due to the Random Vibration of Control Rods and Fuel Elements. Nucl. Sci. Eng. 40(1), 144-150.
- Willmarth, W. W., and Wooldridge, C. E. 1962. Measurements of the Fluctuating Pressure at the Wall beneath a Thick Turbulent Boundary Layer. J. Fluid Mech. 14(Pt. 2), 187-210.

7. A SINGLE CYLINDER IN CROSSFLOW

7.1 INTRODUCTION

Flow past a circular cylinder and its effect on cylinder response have been the subject of research for more than a century. Many hundreds of papers have been published and recently several reviews have been written, e.g., Marris (1964), Morkovin (1964), Mair and Maull (1971), Berger and Wille (1972), Parkinson (1974), King (1977a), Sarpkaya (1979a), and Bearman (1984).

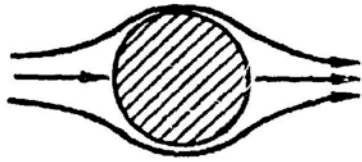
The interest in this subject is attributed to two reasons:

- It is relevant to various problem areas, such as dynamics of stacks, piles, trashracks, wires, periscopes, cables, etc. For example, oscillations excited by vortex shedding can lead to amplitudes as large as two cylinder diameters, which is not acceptable in most engineering applications.
- There are many fascinating phenomena in the interaction of the flow and cylinder.

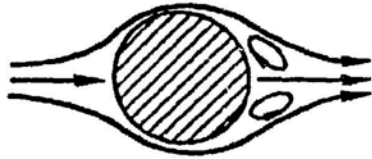
Flow past a circular cylinder is probably one of the most extensively studied subjects, but its effects still are not fully understood.

7.2 FLOW REGIMES

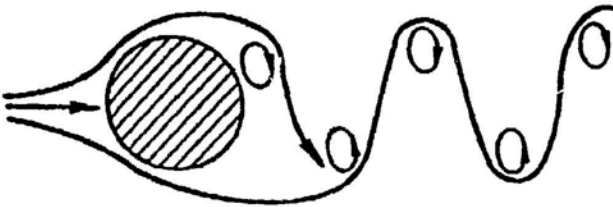
The flow characteristics depend on Reynolds number (Re). Figure 7.1 shows the major identifiable regions presented by Lienhard (1966). (A comparison of the many terminologies proposed by investigators, as summarized by Farell (1981), is presented in Fig. 7.2 and Table 7.1.) At low Reynolds numbers, the flow does not separate. As Re is increased, the flow separates to form a pair of recirculating eddies on each side of the cylinder. As Re is further increased, the shedding eddies become elongated in the flow direction; their length increases linearly with Reynolds number until the flow becomes unstable at $Re \sim 4.0$. The vortices then break away; consequently, a periodic, staggered-vortex street is formed. At Reynolds up to ~ 150 , the vortex street grows in width downstream for some diameters. The initially spreading wake develops into two parallel rows of staggered vortices. Von Karman's inviscid theory shows the street to be stable when the ratio of width to streamwise spacing is 0.28. In this region, the vortex street is laminar. At a Re of 300, the boundary layer is laminar over the front part of the cylinder; the layer separates and breaks up into a turbulent wake. The separate points move forward as the Reynolds number is increased. At a Re of about 3×10^5 , depending on free stream turbulence and surface roughness, the flow separation point moves backward, the drag drops sharply, and the vortex shedding is disorganized. At higher Re , the vortex streets are reestablished. Reviews of the fluid dynamics of this problem can be found in Morkovin (1964), Marris (1964), Mair and Maull (1971), and Berger and Wille (1972).



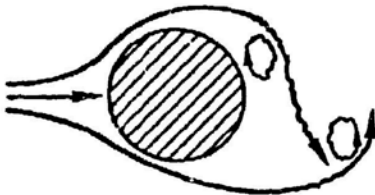
$Re < 5$ REGIME OF UNSEPARATED FLOW



$5 \text{ TO } 15 \leq Re < 40$ A FIXED PAIR OF FÖPPL
VORTICES IN WAKE

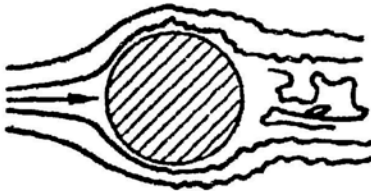


$40 \leq Re < 90$ AND $90 \leq Re < 150$
TWO REGIMES IN WHICH VORTEX
STREET IS LAMINAR



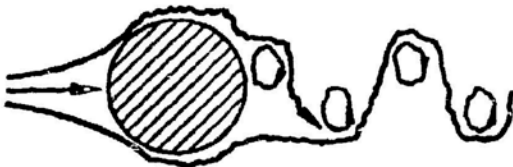
$150 \leq Re < 300$ TRANSITION RANGE TO TURBU-
LENCE IN VORTEX

$300 \leq Re \lesssim 3 \times 10^5$ VORTEX STREET IS FULLY
TURBULENT



$3 \times 10^5 \lesssim Re < 3.5 \times 10^6$

LAMINAR BOUNDARY LAYER HAS UNDERGONE
TURBULENT TRANSITION AND WAKE IS
NARROWER AND DISORGANIZED



$3.5 \times 10^6 \leq Re$

RE-ESTABLISHMENT OF TURBU-
LENT VORTEX STREET

Fig. 7.1. Regimes of Flow Across a Circular Cylinder (from Shin and Wambsganss; original source from Lienhard 1966)

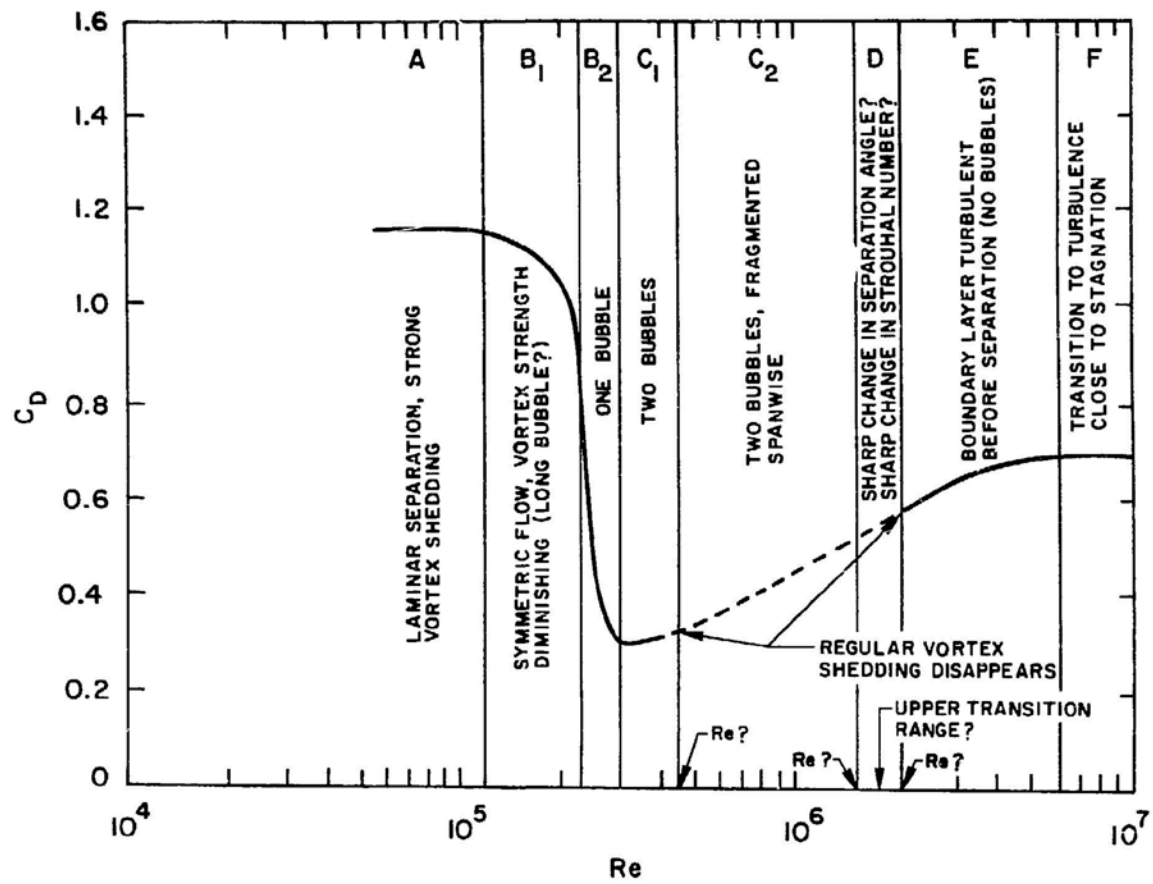


Fig. 7.2. Flow Regimes (from Farell 1981, with permission--see Credits)

Table 7.1. Terminology According to Various Authors for Ranges Defined in Fig. 7.1*

AUTHOR	RANGE						
	A	B ₁	B ₂	C ₁	C ₂	D	E
ROSHKO (1961)	SUBCRITICAL	TRANSITION RANGE (LOWER TRANSITION)			SUPERCRITICAL		TRANSCRITICAL
ACHENBACH (1968)					CRITICAL		SUPERCRITICAL
ACHENBACH (1975)	SUBCRITICAL	CRITICAL			SUPERCRITICAL		TRANSCRITICAL
GUVEN et al (1980)	SUBCRITICAL			CRITICAL		SUPERCRITICAL	TRANSCRIT
BEARMAN (1969)	SUBCRITICAL	CRITICAL			SUPERCRITICAL		TRANSCRITICAL
SZECHENYI (1975)	SUBCRITICAL				TRANSCRITICAL		SUPERCRITICAL
SACHS (1978)	SUBCRITICAL			SUPERCRITICAL			ULTRACRITICAL
FARELL (1981)	SUBCRITICAL	TRANSITION RANGE (LOWER TRANSITION)		SUPERCRITICAL		UPPER TRANSITION RANGE	POSTCRITICAL (ULTRACRITICAL)
							ULTIMATE

* From Farell (1981), with permission--see Credits.

The many experimental measurements of vortex shedding at subcritical Reynolds numbers are in fairly good agreement, but at higher Reynolds numbers, there is little agreement. One reason is the sensitivity of the flow to small perturbations. The flow characteristics at high Reynolds numbers are discussed in Section 7.11.

As pointed out by Farell (1981), defining different flow-regime terminology can be very confusing. Most investigators appear to prefer their own versions of the terminology for two major reasons:

- Different people have different interpretations of the flow phenomena, and
- Existing measurements are still not unambiguous.

Under these circumstances it is probably best to leave existing nomenclature alone as much as possible. In this report, the terminology proposed by Farell will be used.

7.3 STROUHAL NUMBER

The Karman vortex street and other vortex patterns have been observed and studied for centuries. The earliest recorded observation of the phenomenon of vortex shedding can be traced back to the sixteenth century when Leonardo da Vinci made drawings of the surface pattern of the flow past an obstacle. Remarkable similarities have been found in these complex fluid dynamic flow patterns over many orders of magnitude in the nondimensional Reynolds numbers that characterize them, as illustrated by Griffin (1982) in Table 7.2. Figure 7.3 shows the typical traces and a close-up view of a Karman vortex street behind a cylinder at $Re = 80$; Fig. 7.4 shows the vortex pattern in the clouds downstream from the Island of Guadalupe for Re at 10^{10} . Distinctive flow patterns are observed in laboratory tests at small Re and in naturally occurring phenomena.

The frequency of vortex shedding (f_s) from a single cylinder in a uniform flow is related to the cylinder diameter D and flow velocity U through the nondimensional Strouhal number St :

$$St = \frac{f_s D}{U} . \quad (7.1)$$

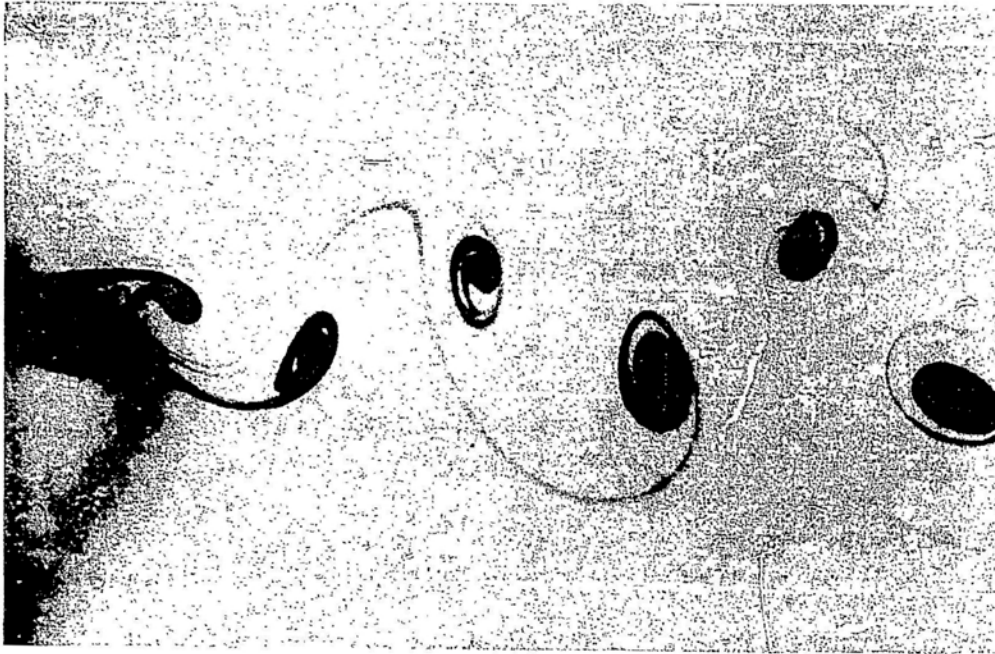
St is known as the Strouhal number after the Czech physicist Vincenz Strouhal (1850-1922), who, in 1878, first investigated the "singing" of wire. The Strouhal number for a circular cylinder is a function of Reynolds number.

Figure 7.5 shows a reasonable envelope within $\pm 10\%$ accuracy over a large Reynolds number range (Lienhard 1966). The Strouhal number remains nearly constant with a value of 0.2 within the range of Reynolds numbers from 300 to

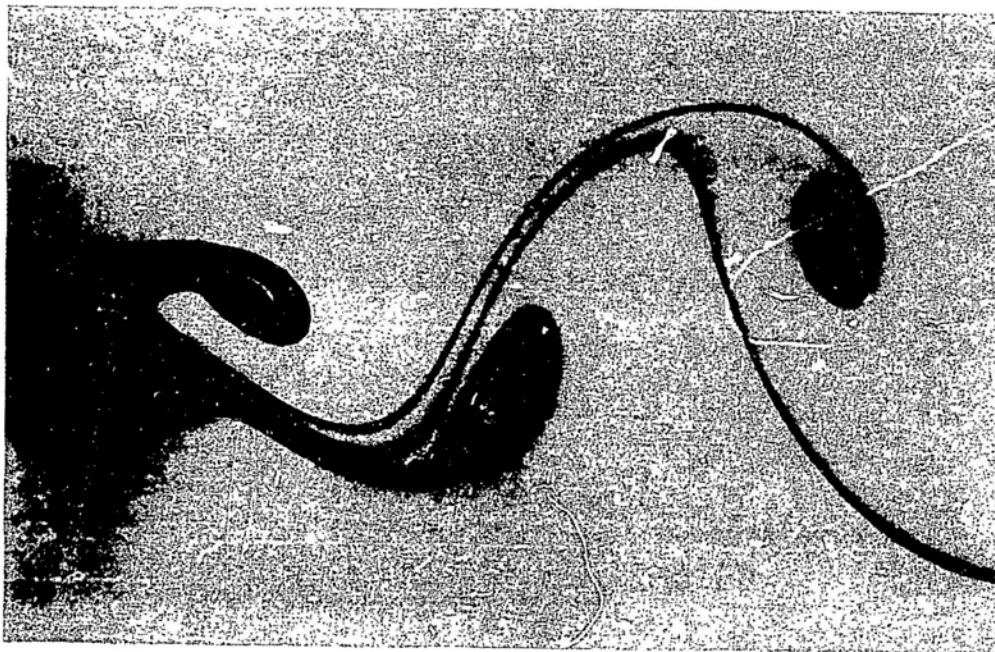
Table 7.2. Visualization of Vortex Trails and Karman Vortex Streets*

Type of Flow	Location	Reynolds Number	Tracer
Wind, past an ocean island	Jan Mayen Guadalupe	10^{11} 10^{10}	Clouds Clouds
Water, past a ship aground	Nantucket Island	10^7 - 10^8	Oil
Water, past a marine pile	English Coast	10^8	None
Water, past a drill casing pipe	North Sea	10^5	None
Water, past a model pile	Laboratory channel	10^4	Dye
Late wake of a sphere towed in water	Towing channel	$3(10^3)$	Dye
Wake of an inclined flat plate	Water channel	10^3	Aluminum particles
Air, past a circular cylinder	Wind tunnel	$2(10^2)$	Aerosol

*From Griffin (1982), with permission--see Credits.



(a)



(b)

Fig. 7.3. Typical Traces in a Karman Vortex Street Behind a Circular Cylinder (from Perry et al. 1982, with permission--see Credits)

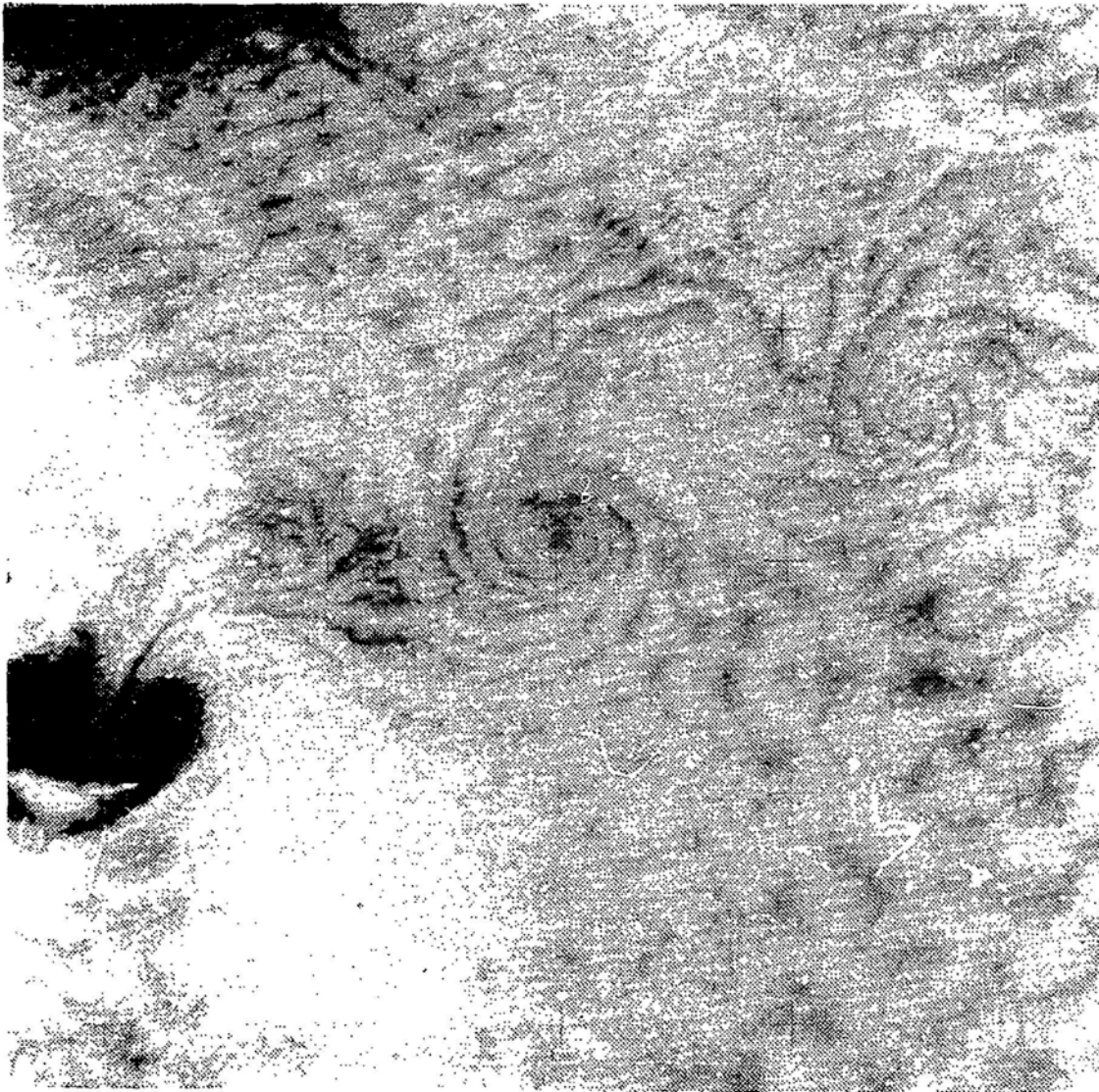


Fig. 7.4. A Pattern of Vortices in the Clouds Downstream from the Island of Guadalupe, West of Baja California (from Griffin 1982, with permission--see Credits)

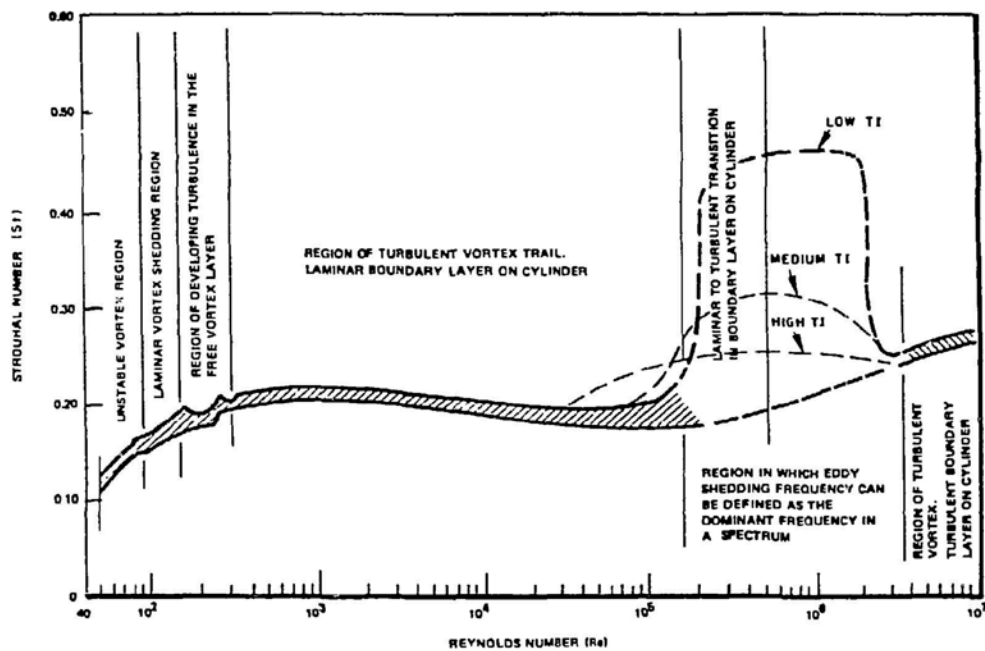


Fig. 7.5. Envelope of Strouhal/Reynolds Number Relationship for Circular Cylinders (Jendrzejczyk and Chen 1985)

2×10^5 , defined as the subcritical range. As the Reynolds number is further increased to about 3.5×10^5 , the Strouhal number seems to increase. However, the vortex shedding in this region is much weaker and defining an accurate shedding frequency is sometimes difficult. Beyond a Reynolds number of about 3.5×10^6 , the Strouhal number again seems to remain constant with $S \approx 0.27$, with a strengthening of vortex shedding. The limits of the regions and the figures quoted are modified by cylinder roughness, turbulence in the incoming flow, cylinder aspect ratio, and influence of wall or adjacent cylinders. Some of these effects are discussed in Section 7.11.

7.4 STEADY FLUID-FORCE COEFFICIENTS

When a circular cylinder is submerged in a uniform crossflow, the steady lift force acting on it generally is zero. However, the fluid exerts a drag force on the surface as a result of viscous effect. The resultant frictional force in the downstream direction is usually called the skin friction drag. But when the flow occurs past a surface that is not everywhere parallel to the main stream, there is an additional drag force resulting from differences of pressure over the surface. This force is called the pressure drag, or form drag. The skin friction drag is the resultant of the forces tangential to the surface and the pressure drag is the resultant of the forces normal to the surface.

In a flow around a circular cylinder, the boundary layers separate from the surface at some point. Downstream of the separation point, the flow contains relatively large-scale eddies, known as the wake. Since the flow is separated over much of the cylinder surface in practical applications, the wake is large and the pressure drag is much greater than the skin friction. The total drag is expressed in terms of a dimensionless drag coefficient C_D as the total drag force per unit length divided by $\frac{1}{2} \rho U^2 D$.

Figure 7.6 shows the variation of C_D with Re for an infinitely long, smooth, circular cylinder with its axis perpendicular to the flow. Various coefficients are used by different investigators, including: C_D , the time-averaging value of total drag force; $C_{D_{rms}}$, the root-mean-square variation of the drag force; C_{Dp} , the pressure drag; and $C_{D'}$, the oscillation drag force. At small Re (say < 0.5), inertia forces are negligible compared with viscous forces and the drag is almost directly proportional to U . In this region, friction drag accounts for a large part of the total drag and in the limit, as $Re \rightarrow 0$, friction drag is two-thirds of the total. When separation of the boundary layer occurs, pressure drag becomes a larger contribution, and the slope of the C_D curve becomes less steep. By $Re = 200$, the von Karman vortex street is well established, and the pressure drag then accounts for nearly 90% of the total. The drag coefficient reaches a minimum value of about 0.9 at $Re \sim 2000$ and then there is a slight rise to 1.2 for $Re \sim 3 \times 10^4$.

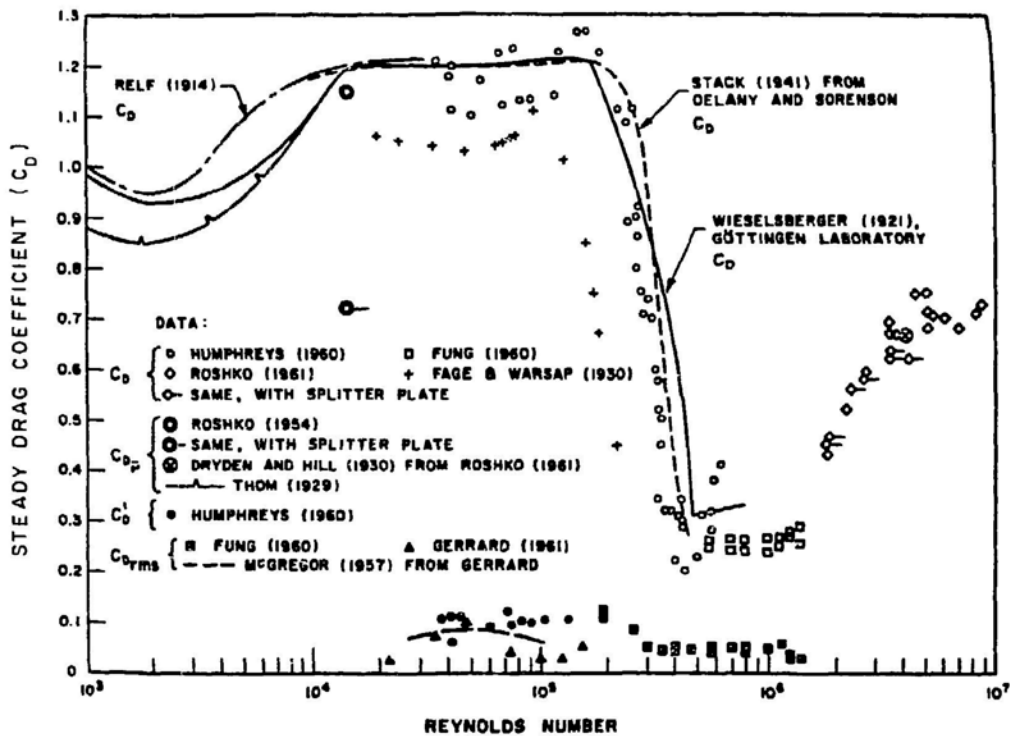
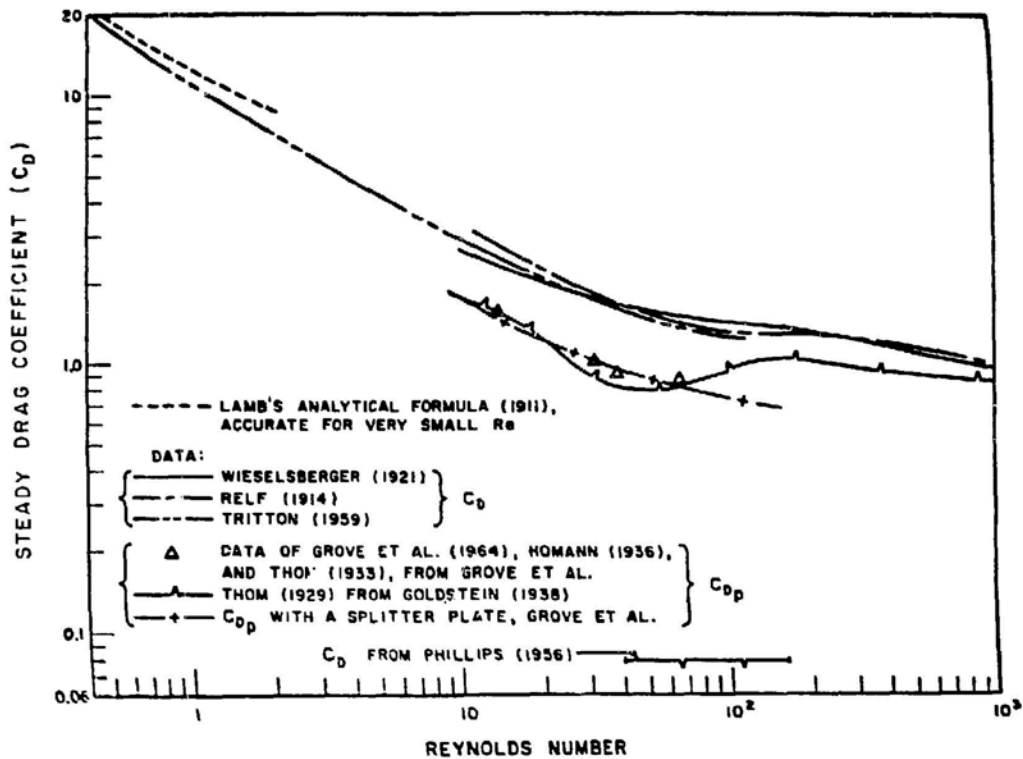


Fig. 7.6. Drag Coefficient for a Circular Cylinder in Crossflow (from Shin and Wambsganss; original source from Lienhard 1966)

At $Re \sim 2 \times 10^5$ the boundary layer becomes turbulent before separation, the separation position moves farther downstream, and the wake narrows. Consequently, the drag falls drastically. Over the approximate range $5 \times 10^5 < Re < 4 \times 10^6$, C_D drops to about 0.3 and then rises to about 0.7.

The curve $1/St$ versus Re is markedly similar to the C_D versus Re curve. In the range $10^3 < Re < 10^5$, the value of $1/St$ is about 5.

Free-stream turbulence and cylinder surface characteristics affect C_D . Therefore, the standard curve of C_D versus Re for smooth cylinders alone cannot be used to determine the drag coefficient in turbulent flow or for rough cylinders. To determine the effect of turbulence on the drag coefficient, one should consider turbulence intensity, turbulence scale, and surface characteristics in addition to Reynolds number; i.e.,

$$C_D = C_D(Re, \text{turbulence intensity, turbulence scale, surface characteristics}) . \quad (7.2)$$

The detailed variations of C_D with turbulence characteristics at different Re are still not well understood. For example, for $1350 < Re < 8000$, Ko and Graf (1972) found that at low turbulence intensity, C_D decreases. The lowest C_D is obtained at a turbulence intensity of 4%. Further increase in turbulence intensity causes the drag coefficient to continue to increase. The highest drag coefficient was $C_D = 1.25$ at a turbulence intensity of 21%.

The critical value of Re at which the large drop of C_D occurs is smaller both for a greater degree of turbulence in the main flow and for greater roughness of the surface upstream of the separation point. If a small roughness element such as a wire is placed on the surface of the cylinder upstream of the separation position, the transition from a laminar to a turbulent boundary layer occurs at a smaller Reynolds number. Therefore, the drag can be significantly reduced by increasing the surface roughness if the Reynolds number is such that a wholly laminar layer can by this means be made turbulent.

When the cylinder is oscillating, C_D increases substantially as a result of vortex-excited oscillations. The steady drag coefficient for a vibrating cylinder can be several times that for a stationary cylinder. The steady amplification on a circular cylinder due to vortex-excited oscillations is illustrated in Fig. 7.7, in which the ratio of drag coefficients is plotted against the wake response parameter W_r . W_r is defined as follows (Griffin 1980):

$$W_r = \left(1 + \frac{2a}{D}\right) \left(\frac{U}{fD} St\right)^{-1} . \quad (7.3)$$

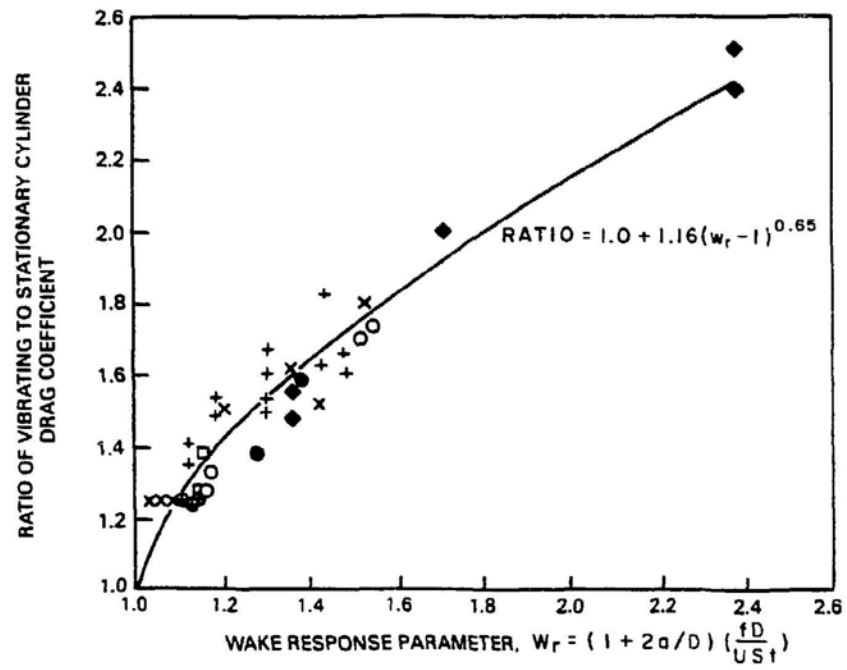


Fig. 7.7. Ratio of Vibrating to Stationary Cylinder Drag Coefficient
(from Griffin 1980, with permission--see Credits)

7.5 FLUCTUATING FLUID-FORCE COEFFICIENTS

Each time a vortex is shed from the cylinder it experiences a time-varying force at the frequency of vortex shedding. The periodic fluctuating force components are

$$g = \frac{1}{2} \rho U^2 D C'_D \sin(\Omega_D t) \quad \text{and} \quad (7.4)$$

$$h = \frac{1}{2} \rho U^2 D C'_L \sin(\Omega_L t) .$$

Ω_L is equal to the Strouhal frequency and Ω_D is equal to twice the Strouhal frequency. The drag and lift coefficients, obtained from Eq. 7.4, are referred to as fluctuating drag and lift coefficients. When the excitation is not at a discrete frequency, the coefficients of fluctuating drag and lift are defined by the root mean square value of the drag and lift fluctuations as obtained from an integration of the corresponding frequency spectra, viz.,

$$C'_D = \frac{\text{RMS value of fluctuating drag force per unit length}}{\frac{1}{2} \rho U^2 D}$$

and

$$C'_L = \frac{\text{RMS value of fluctuating lift force per unit length}}{\frac{1}{2} \rho U^2 D} .$$

The coefficients obtained in this manner are referred to as RMS fluctuating drag and lift coefficients.

The fluctuating force coefficients C'_D and C'_L depend on different parameters:

$$C'_D = C'_D(\text{Re, turbulence characteristics, surface characteristics,} \\ \text{oscillation amplitude})$$

and

$$C'_L = C'_L(\text{Re, turbulence characteristics, surface characteristics,} \\ \text{oscillation amplitude}) .$$

(7.5)

Stationary Cylinders

The fluctuating lift and drag coefficients are obtained from measurements of the fluctuating forces. Table 7.3 lists the RMS fluctuating force coefficients and the corresponding Reynolds numbers (King 1977a). There is considerable scatter between the values obtained by different investigators; values may vary from about 0.1 to 1.4. The use of 1.2 for C_L' and 0.2 for C_D' is considered conservative for all Re.

The scatter of the data could be due to the dependence of the force coefficients on Reynolds number, aspect ratio, surface roughness, turbulence, and boundary effects. A significant variation of forces can be measured on almost identical cylinders in different test loops.

Oscillating Cylinder

The drag and lift coefficients obtained from experimental force measurements on oscillating cylinders are compared with results from mathematical models of the fluid/cylinder system. Figs. 7.8 and 7.9 present the fluctuating lift and drag coefficients against amplitudes of oscillation for the crossflow and in-line directions. At low amplitudes, the lift coefficient increases with increasing amplitude. As the amplitude rises above 0.5 diameter, the lift coefficient begins to decrease, and approaches zero as the amplitude exceeds about 1.5 to 2.0 diameter. Thus the vortex strength appears to be self-limiting.

The fluctuating drag coefficients C_D' for cylinders oscillating in the two instability regions (see Section 7.9) given in Figs. 7.9 show that C_D' increases linearly with oscillation amplitude. Contrary to the crossflow results, the amplitude does not have a maximum for the amplitude up to the order of 0.2 diameter. These force coefficients were measured in tests conducted with smooth flexible cylinders vibrating in the fundamental and second normal modes; the Reynolds numbers of the experiments are small ($Re \sim 5 \times 10^3$) (King et al. 1973).

Correlation Length

Vortices are shed in cells from stationary cylinders. The length of each cell is called the correlation length. The correlation length varies with Reynolds number, turbulence, length/diameter ratio, and surface roughness. Typical results are summarized in Table 7.4 (King 1977a).

An important consequence of cylinder oscillation and vortex shedding is the greatly increased coherence or correlation of the vortex shedding along the length of the cylinder, when the cylinder amplitude is greater than the threshold value--typically $a/D \approx 10\%$ for crossflow oscillations and 1-2% for in-line oscillations. This implies that the cylinder oscillations must reorganize the vortex shedding process.

Table 7.3. Collected Experimental Data from Various Sources--Fluctuating Force Coefficients and Reynolds Numbers

Source	RMS		Reynolds Number Range
	Fluctuating Lift Coefficient (C_L')	Ratio (C_L'/C_D')	
Jones (1968)	0.08		$0.4 \times 10^6 - 1.9 \times 10^7$
McGregor (1957)	0.60	10	$4.3 \times 10^4 - 1.3 \times 10^5$
Surry (1969)	0.60	2.5-10	4.4×10^4
Bishop and Hassan (1964)	0.60	10	$3.6 \times 10^3 - 1.1 \times 10^4$
Ruedy (1935)	0.93		Approx. 10^5
Woodruff and Kozak (1958)	0.65		0.2×10^6
Vickery and Watkins (1962)	0.78		10^4
King (1974)	0.78	5.7-10	4×10^4
Fung (1958)	0.20-0.30	10	0.2×10^6
Glenny (1966)		3	0.2×10^6
Keefe (1961)	0.43	10	$4 \times 10^4 - 10^5$
Humphreys (1960)	0.30-1.35		$3 \times 10^5 - 5 \times 10^5$
Phillips (1956)	0.75		200
Schwabe (1935)	0.45		Approx. 700
Protos et al. (1968)	0.30		4.5×10^4

* From King (1977a), with permission--see Credits.

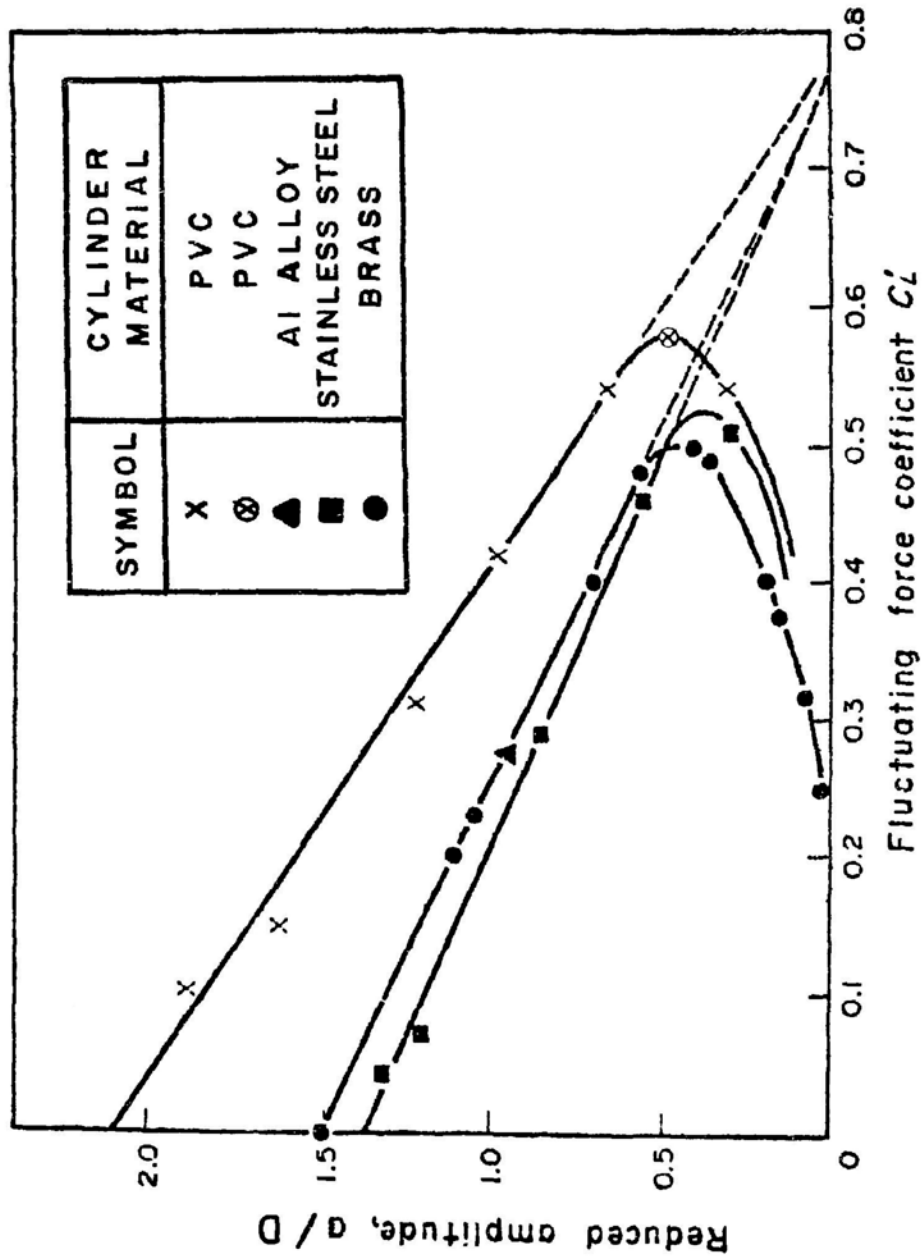


Fig. 7.8. Fluctuating Lift Coefficients versus Amplitudes of Oscillation (from King 1977a, with permission--see Credits)

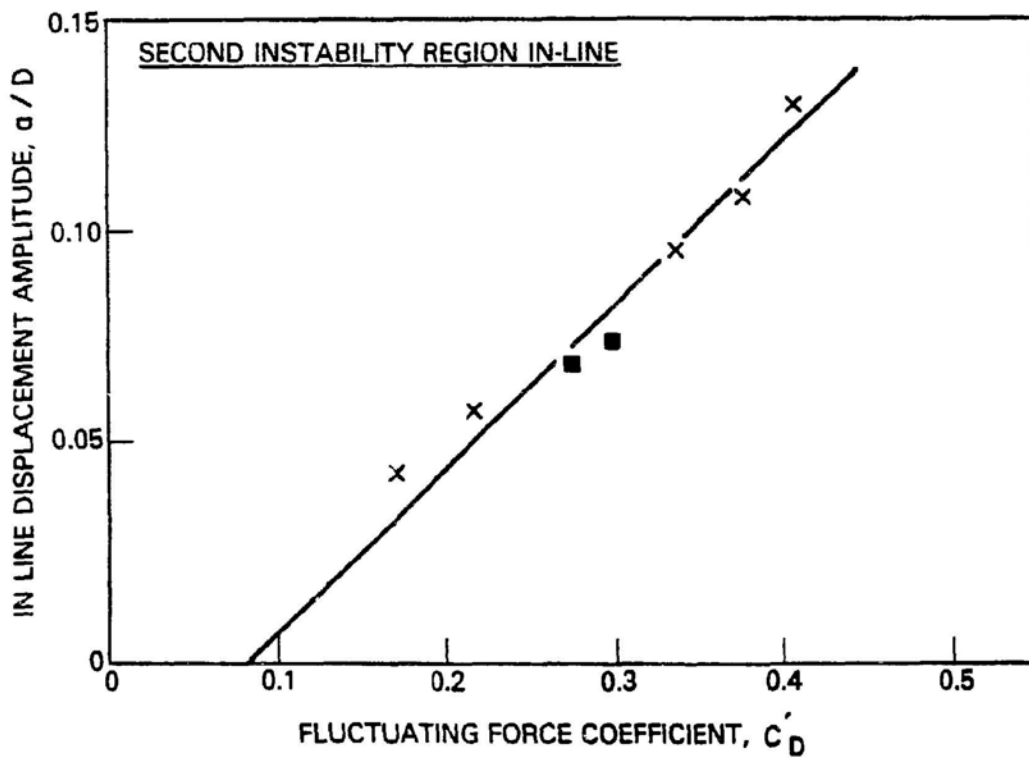
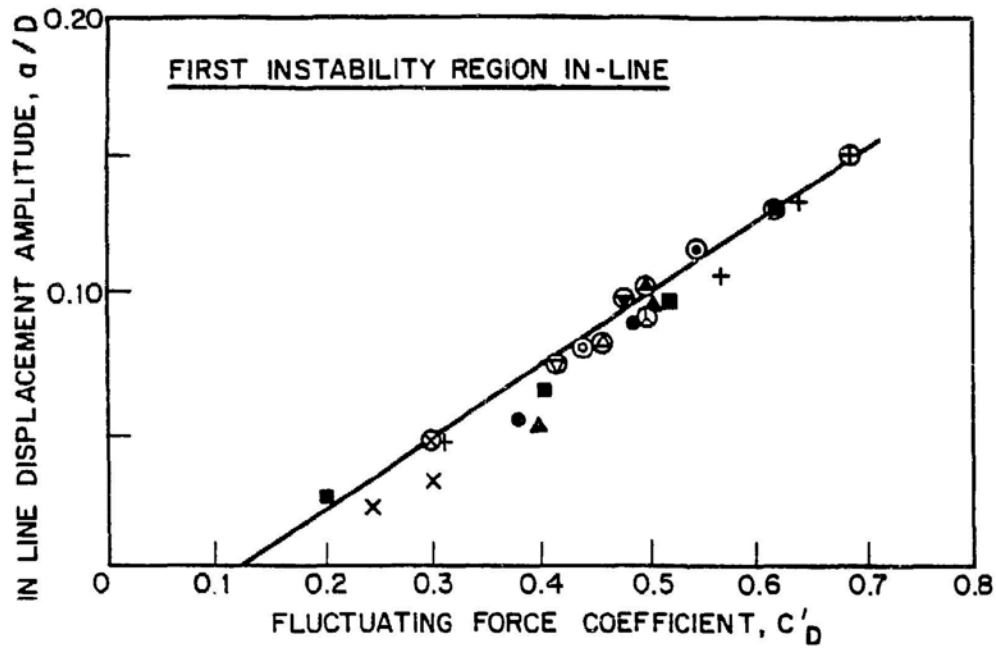


Fig. 7.9. Fluctuating Drag Coefficients vs. Amplitudes of Oscillation
(from King 1977a, with permission--see Credits)

Table 7.4. Correlation Lengths and Reynolds Numbers of Smooth Cylinders*

Reynolds number	Correlation length	Source
$40 < Re < 150$	15D-20D	Gerlach and Dodge (1970)
$150 < Re < 10^5$	2D-3D	Gerlach and Dodge (1970)
$1.1 \times 10^4 < Re < 4.5 \times 10^4$	3D-6D	El-Baroudi (1960)
$> 10^5$	0.5D	Gerlach and Dodge (1970)
2×10^5	1.56D	Humphreys (1960)

*From King (1977a), with permission--see Credits.

Detailed investigations of the spanwise coherence that accompanies lock-in are made by Ramberg and Griffin (1976) for $Re = 7.5 \times 10^3$. The spanwise correlation coefficient between the fluctuating pressures measured on a vibrating cylinder is given in Fig. 7.10. It is apparent that when the displacement amplitude increases to about 0.1 diameter, the correlation increases significantly. Similar results were noted by Koopmann (1967) for Re below 300 and Toebe's (1969) for $Re \sim 68,000$.

7.6 HIGH REYNOLDS NUMBERS

The detailed flow field from the transition region up to the postcritical region is still not well understood. An excellent experiment was reported by Schewe (1983) recently. It shed some additional light on fluid forces. Force measurements were conducted in a pressurized wind tunnel in regions ranging from subcritical to postcritical. Figure 7.11 shows the steady drag coefficient C_D , Strouhal number St , and RMS lift coefficient C'_L as functions of Reynolds number, and Fig. 7.12 shows the frequency spectra of the lift fluctuations.

Figure 7.11 shows that in the transition region there are two discontinuous drops of C_D (A and B) in the supercritical state, which begins at $Re \approx 3.5 \times 10^5$. The value of C_D is nearly constant up to about $Re \approx 10^6$ with $C_D = 0.22$. Behind the upper transition range ($10^6 < Re \approx 5 \times 10^6$), in which C_D is increasing again, there is a further plateau where C_D is nearly constant, with $C_D = 0.52$.

In the subcritical range, the Strouhal number is about 0.2. The transition range exhibits two discontinuous transitions, A and B, where the Strouhal number jumps to 0.3 and then to 0.48, which is in agreement with Bearman's data (Bearman 1969). These two jumps are directly associated with the two drops of C_D . At the supercritical Reynolds numbers, the Strouhal number remains constant until the upper transition region. Finally, the Strouhal number reaches 0.29 for $Re \approx 7.1 \times 10^6$.

In the subcritical Reynolds number, C'_L contains a narrow band spectrum. At the supercritical and postcritical regions, the frequency spectra also exhibit a narrow peak. However, in the upper transition region, there is no typical spectrum. The dotted lines in Figs. 7.12b-d are caused by mechanical vibration.

Flow characteristics at high Reynolds numbers remain not very well understood. This is a subject of current research (e.g., see Roshko 1961, Bearman 1969, James et al. 1980, and Farell and Blessmann 1983).

7.7 TURBULENT EXCITATION

In an ideal crossflow, the periodic drag and lift forces are the two excitation force components. In a turbulent crossflow, the frequency spectra

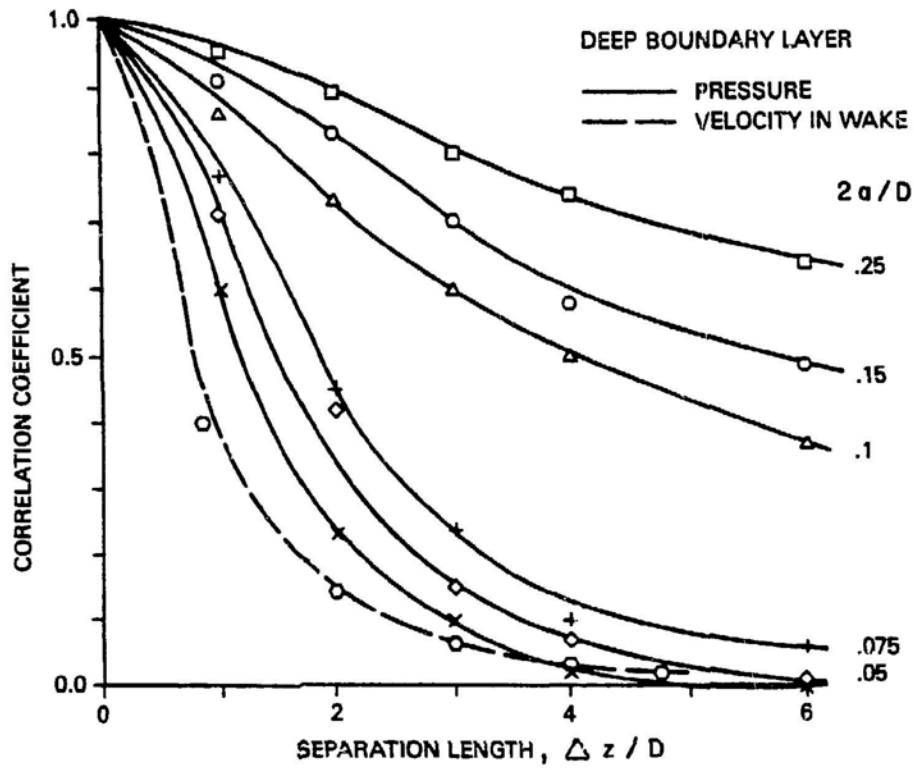


Fig. 7.10. Correlation Coefficient for Fluctuating Pressures Measured on a Cylinder (from Griffin 1980, with permission--see Credits)

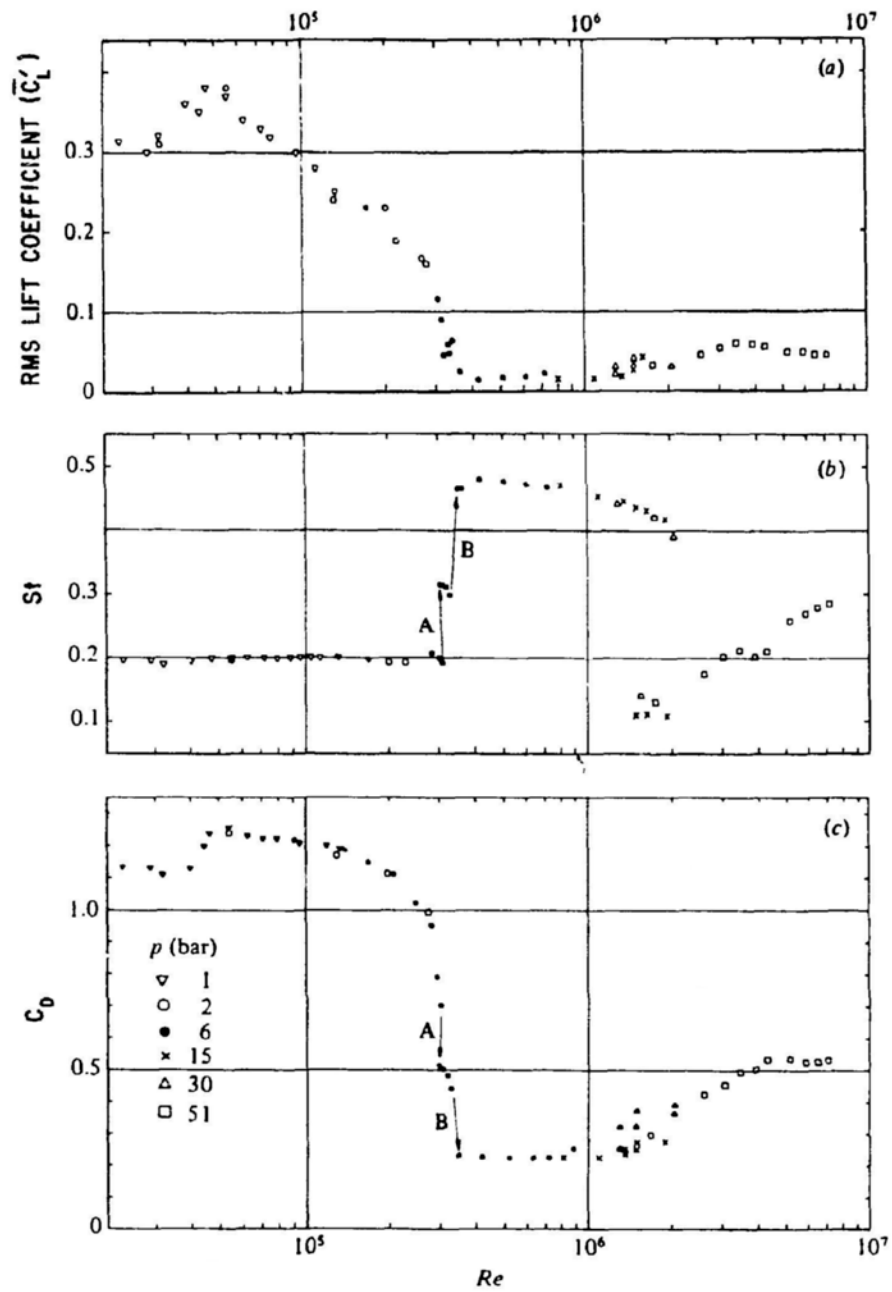


Fig. 7.11. RMS Lift Coefficient, Strouhal Number and Steady Drag Coefficient at High Reynolds Numbers (from Schewe 1983, with permission--see Credits)

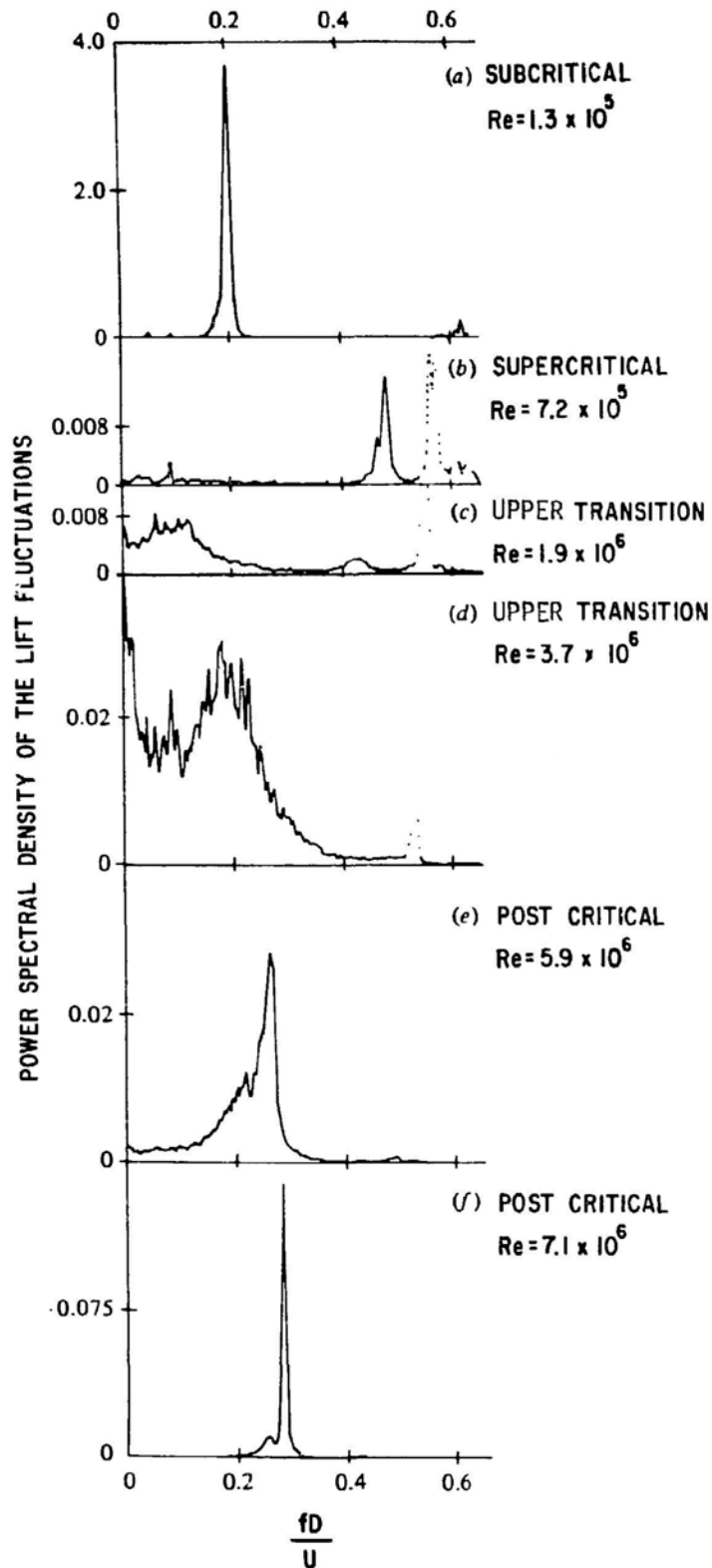


Fig. 7.12. Power Spectra of the Lift Fluctuations at Various Reynolds Numbers (from Schewe 1983, with permission--see Credits)

of the lift and drag force components consist of a component in a narrow band of frequencies due to organized vortex shedding and a component covering a wide band of frequencies predominantly below the vortex shedding frequency due to flow turbulence in the incoming flow stream and in the wake. The roles of these two components depend on Re and turbulence of the flow stream.

The turbulence in the flow stream may have significant effects on the fluid force characteristics acting on a cylinder. It is generally known that the effect of introducing turbulence into the flow is to produce a change in effective Reynolds number in the measurement of drag. This corresponds to the shift in the transitional region to a lower Reynolds number range.

The effect of turbulence on drag, lift, and Strouhal number in the Reynolds number range of 10^5 to 10^6 was investigated systematically in a study by Cheung and Melbourne (1983). Figure 7.13 shows the steady drag force coefficient as a function of Re . It decreases with turbulence intensities at subcritical Reynolds numbers. The drop in drag coefficient occurs at a lower Reynolds number in turbulent flow than in smooth flow, indicating that there is a shift in the effective transitional Reynolds number due to turbulence.

Figures 7.14 and 7.15 show the fluctuating drag and lift coefficients. In the presence of turbulence, the decrease in fluctuating lift in the critical flow regime occurs at a lower Reynolds number, which is consistent with the idea that the effect of turbulence is in part a change in the effective transitional Reynolds number. The fluctuating lift also decreases significantly in the subcritical regime. The turbulence introduced may reduce both the coherence and the strength of the shed vortices in this high subcritical regime. In the supercritical flow regime, the increased entrainment due to turbulence could reduce the vorticity in the free shear layers and cause the wake to fluctuate more, effectively broadening the wake. The swinging of the wake, in effect, induces a slight increase in the fluctuating lift. A similar trend is noted for fluctuating drag.

The Strouhal numbers are plotted against Reynolds numbers in Fig. 7.16. The rise in Strouhal number occurs earlier at a lower Reynolds number as the turbulence intensity increases.

The effect of turbulence in flow on fluid forces can be summarized as follows (Mulcahy 1982):

- The Reynolds number at which the boundary layer undergoes transition from laminar to turbulent flow is reduced. This can be observed from the relatively sharp declines in C_D as well as the increase in St . Thus the critical region appears to occur over a larger Reynolds number range, and the associated wake forces are random at Re , where they were periodic in ideal flow: the more turbulent the flow, the smaller the subcritical range of Reynolds numbers.

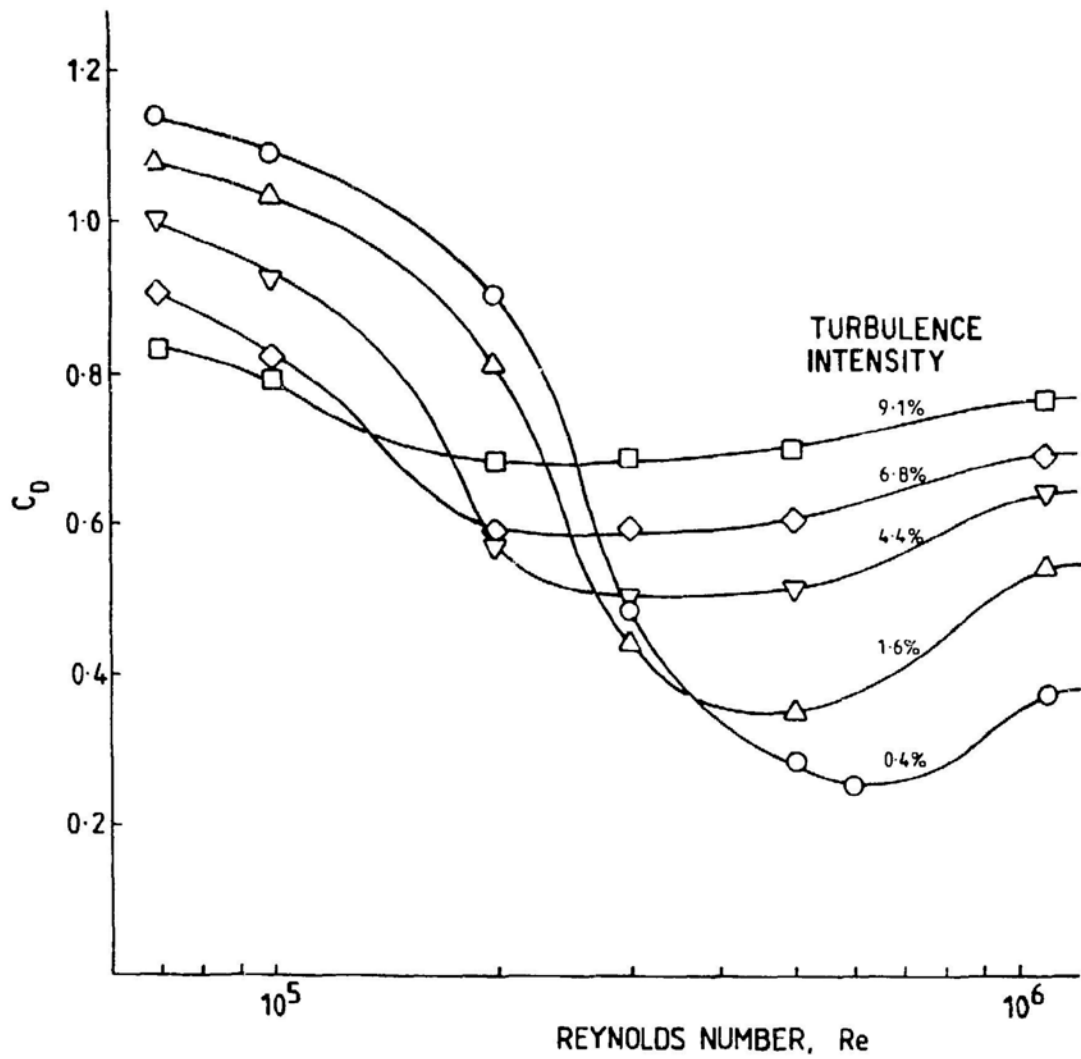


Fig. 7.13. Steady Drag Force Coefficient as a Function of Reynolds Number for Various Turbulence Intensities (from Cheung and Melbourne 1983, with permission--see Credits)

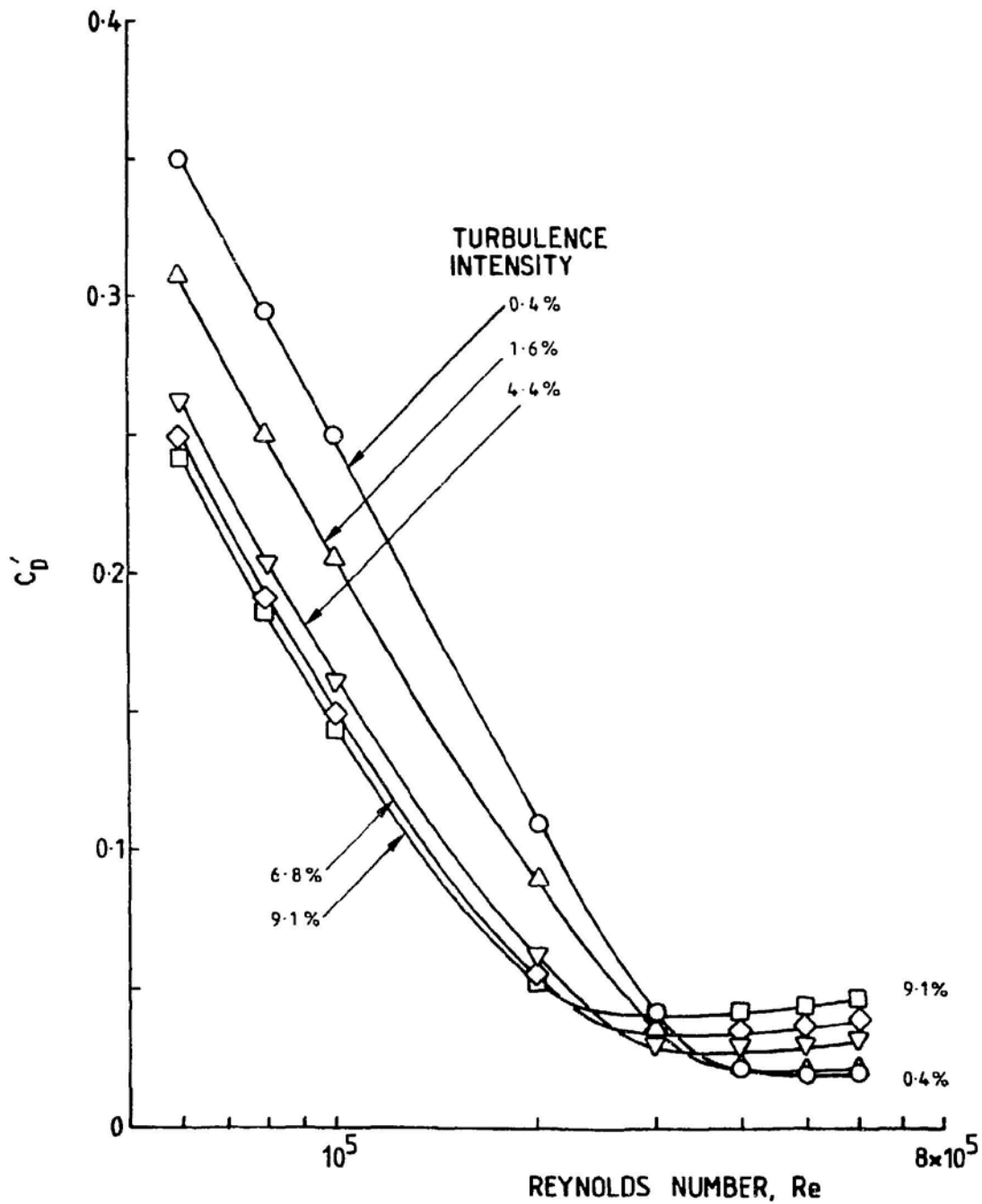


Fig. 7.14. Fluctuating Drag Coefficient as a Function of Reynolds Number for Various Turbulence Intensities (from Cheung and Melbourne 1983, with permission--see Credits)

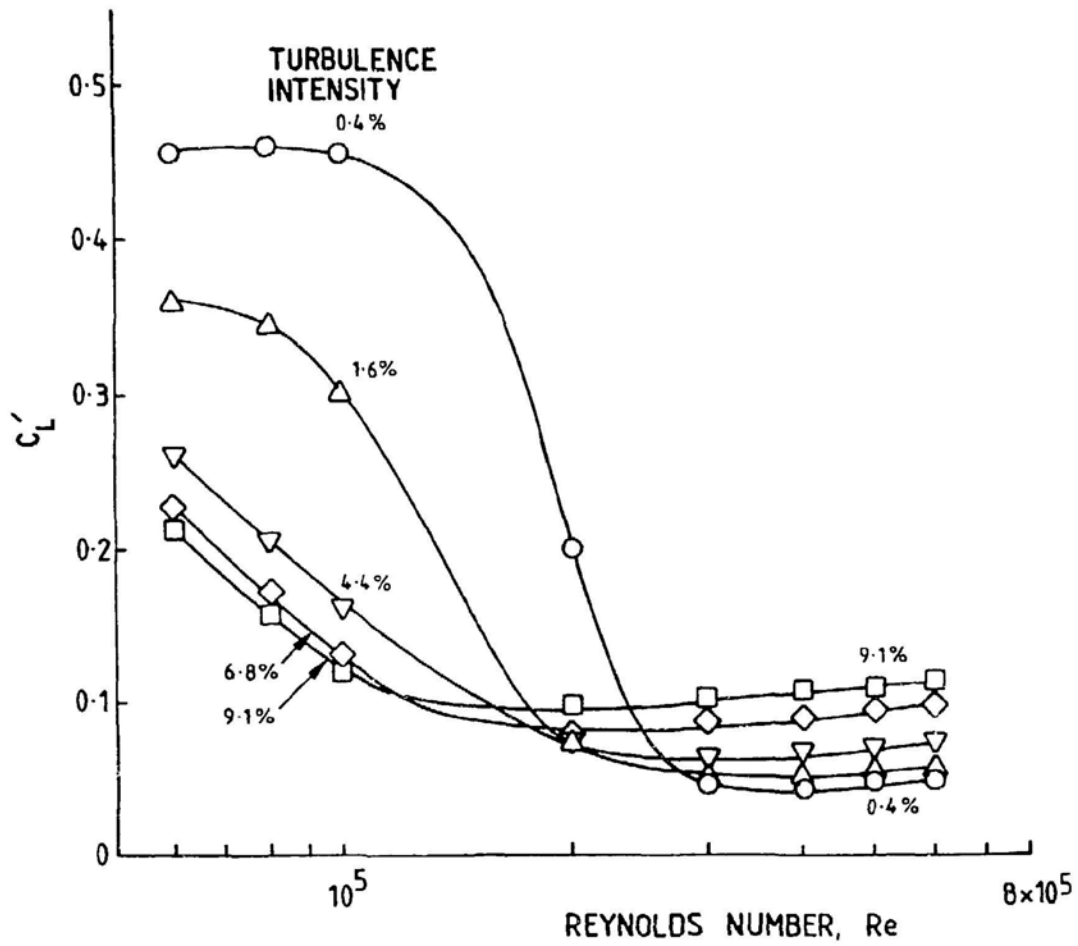


Fig. 7.15. Fluctuating Lift Coefficient as a Function of Reynolds Number for Various Turbulence Intensities (from Cheung and Melbourne 1983, with permission--see Credits)

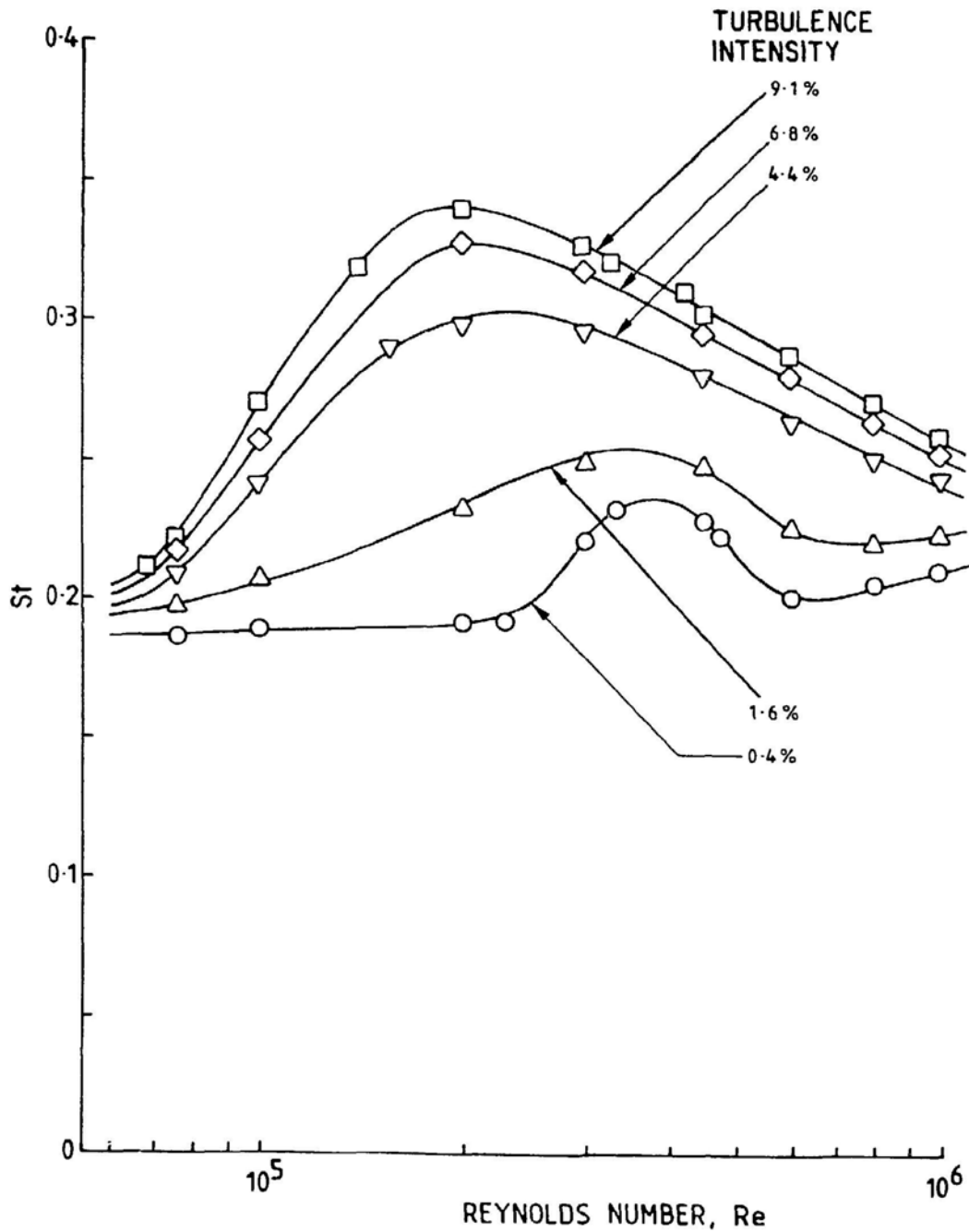


Fig. 7.16. Strouhal Number as a Function of Reynolds Number for Various Turbulence Intensities (from Cheung and Melbourne 1983, with permission--see Credits)

- The second effect of turbulence in the flow is the degradation of the two-dimensional vortex shedding process for subcritical Reynolds numbers, as measured by the broadening and reduction in amplitude of the vortex shedding peak in the lift force spectral density.
- The third effect is the pressure fluctuations created by the impinging turbulence. The associated random excitation forces are difficult to separate from those created by the wake.

7.8 EQUATIONS OF MOTION IN CROSSFLOW

Let the cylinder displacement components be u and v along and normal to the flow, respectively, and the relative velocity between the fluid and cylinder be V (Fig. 7.17). The drag and lift forces acting on the cylinder based on the steady flow are as follows:

$$\bar{g} = \frac{1}{2} \rho V^2 D C_D \quad \text{and} \quad (7.6)$$

$$\bar{h} = \frac{1}{2} \rho V^2 D C_L .$$

C_D and C_L are the steady drag and lift coefficients. Note from Fig. 7.17 that

$$\theta = \tan^{-1} \left[\frac{\frac{\partial v}{\partial t}}{U - \frac{\partial u}{\partial t}} \right] . \quad (7.7)$$

The fluid force components acting on the cylinder in the x and y direction are obtained from Eqs. 7.6 and Fig. 7.17:

$$g = \frac{1}{2} \rho V^2 D (C_D \cos \theta + C_L \sin \theta) \quad \text{and} \quad (7.8)$$

$$h = \frac{1}{2} \rho V^2 D (-C_D \sin \theta + C_L \cos \theta) .$$

Using Eqs. 7.7 and 7.8 gives

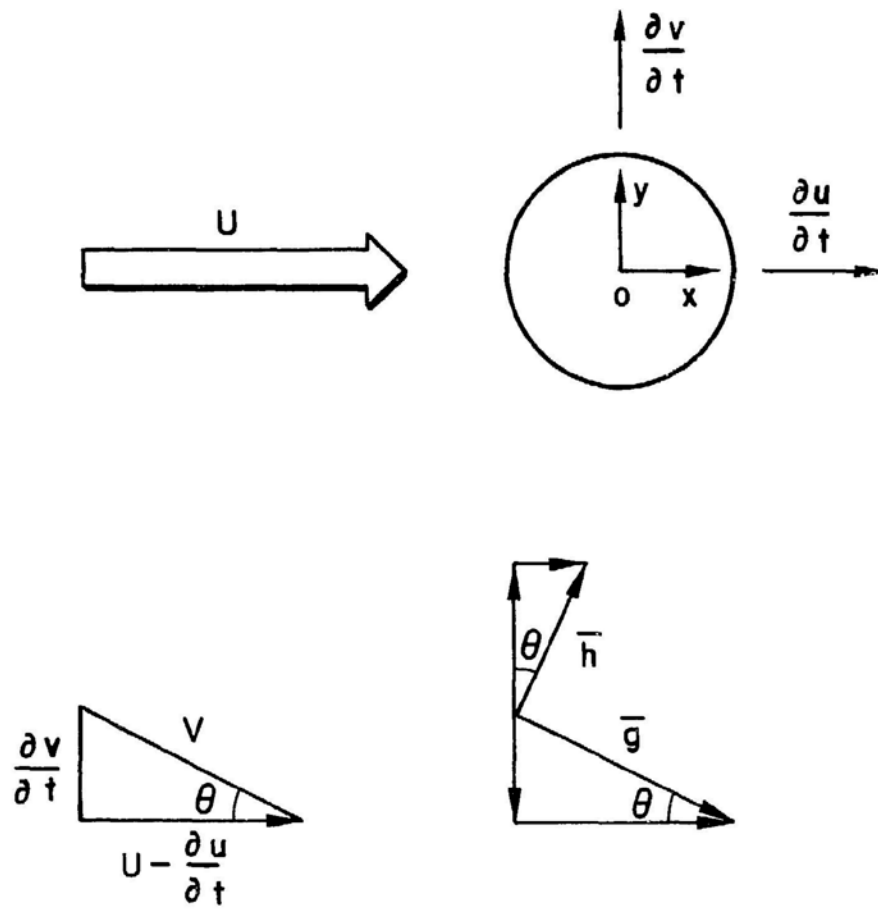


Fig. 7.17. Drag and Lift Force Components Acting on a Cylinder

$$g = \frac{1}{2} \rho U D \left[C_D \left(v - \frac{v}{U} \frac{\partial u}{\partial t} \right) + C_L \frac{v}{U} \frac{\partial v}{\partial t} \right] \quad \text{and} \quad (7.9)$$

$$h = \frac{1}{2} \rho U D \left[C_L \left(v - \frac{v}{U} \frac{\partial u}{\partial t} \right) - C_D \frac{v}{U} \frac{\partial v}{\partial t} \right]$$

In addition to the steady fluid-force components, the fluctuating drag and lift forces are

$$g = \frac{1}{2} \rho U^2 D C_D' \sin(\Omega_D t) \quad \text{and} \quad (7.10)$$

$$h = \frac{1}{2} \rho U^2 D C_L' \sin(\Omega_L t) ,$$

where Ω_D and Ω_L are the frequencies of vortex shedding and, in general, $\Omega_D = 2\Omega_L$.

The equations of motion for the cylinder in the drag and lift direction are

$$\begin{aligned} EI \frac{\partial^4 u}{\partial z^4} + C_v \frac{\partial u}{\partial t} + (m + C_m M_d) \frac{\partial^2 u}{\partial t^2} - \frac{1}{2} \rho U D \left[C_D \left(v - \frac{v}{U} \frac{\partial u}{\partial t} \right) \right. \\ \left. - C_L \frac{v}{U} \frac{\partial v}{\partial t} \right] = \frac{1}{2} \rho U^2 D C_D' \sin(\Omega_D t) + g' \end{aligned} \quad \text{and} \quad (7.11)$$

$$\begin{aligned} EI \frac{\partial^4 v}{\partial z^4} + C_v \frac{\partial v}{\partial t} + (m + C_m M_d) \frac{\partial^2 v}{\partial t^2} - \frac{1}{2} \rho U D \left[C_L \left(v - \frac{v}{U} \frac{\partial u}{\partial t} \right) \right. \\ \left. + C_D \frac{v}{U} \frac{\partial v}{\partial t} \right] = \frac{1}{2} \rho U^2 D C_L' \sin(\Omega_L t) + h' , \end{aligned}$$

where C_v is the viscous damping coefficient in stationary fluid, and g' and h' are turbulent excitations.

Let $\phi_1(z)$ and $\phi_2(z)$ be the normalized modal function of the cylinder in the x and y directions and

$$u(z, t) = q_1(t) \phi_1(z) \quad \text{and} \quad (7.12)$$

$$v(z, t) = q_2(t) \phi_2(z) .$$

Using Eqs. 7.11 and 7.12 gives

$$\begin{aligned} & \ddot{q}_1 + 2\xi_1 \omega_1 \dot{q}_1 + \omega_1^2 q_1 \\ & + \frac{\rho U D}{2(m + C M_d) \ell} \left[(C_D \int_0^\ell \frac{V}{U} \phi_1^2 dz) \dot{q}_1 - (C_L \int_0^\ell \frac{V}{U} \phi_1 \phi_2 dz) \dot{q}_2 \right] \\ & = \frac{\rho U D C_D}{2(m + C M_d) \ell} \int_0^\ell V \phi_1^2 dz + \frac{\rho U^2 D C'_D}{2(m + C M_d) \ell} \sin(\Omega_D t) \int_0^\ell \phi_1 dz + g_1 \end{aligned}$$

(7.13)

and

$$\begin{aligned} & \ddot{q}_2 + 2\xi_2 \omega_2 \dot{q}_2 + \omega_2^2 q_2 \\ & + \frac{\rho U D}{2(m + C M_d) \ell} \left[(C_L \int_0^\ell \frac{V}{U} \phi_1 \phi_2 dz) \dot{q}_1 + (C_D \int_0^\ell \frac{V}{U} \phi_2^2 dz) \dot{q}_2 \right] \\ & = \frac{\rho U D C_L}{2(m + C M_d) \ell} \int_0^\ell V \phi_2 dz + \frac{\rho U^2 D C'_L}{2(m + C M_d) \ell} \sin(\Omega_L t) \int_0^\ell \phi_2 dz + g_2 , \end{aligned}$$

where

$$\begin{aligned} \xi_j &= \frac{C_v}{2\omega_j(m + C M_d)} , \\ \omega_j &= \frac{\lambda_j^2}{\ell^2} \left(\frac{EI}{m + C M_d} \right)^{0.5} , \\ g_1 &= \frac{1}{(m + C M_d) \ell} \int_0^\ell g'(z, t) \phi_1(z) dz , \\ g_2 &= \frac{1}{(m + C M_d) \ell} \int_0^\ell h'(z, t) \phi_2(z) dz , \quad \text{and} \\ V &= [(U - \dot{q}_1 \phi_1)^2 + (\dot{q}_2 \phi_2)^2]^{0.5} , \end{aligned} \quad (7.14)$$

and λ_j is the modal constant.

Equations 7.13 are coupled nonlinear differential equations. The general solution is difficult to obtain in closed form. However, some special cases are amenable to closed-form solution.

When the flow velocity U is much larger than cylinder oscillations ($U \gg \dot{u}$ and \dot{v}),

$$V = U \left(1 - \frac{\dot{q}_1}{U} \phi_1 \right) . \quad (7.15)$$

Substituting Eq. 7.15 into 7.13 and neglecting higher order contributions yields

$$\ddot{q}_1 + 2(\zeta_1 + \zeta_{11})\omega_1 \dot{q}_1 + \omega_1^2 q_1 - 2\zeta_{12}\omega_2 \dot{q}_2 = g_1^o + g_1^v + g_1$$

(7.16)

and

$$\ddot{q}_2 + 2(\zeta_2 + \zeta_{22})\omega_2 \dot{q}_2 + \omega_2^2 q_2 + 2\zeta_{21}\omega_1 \dot{q}_1 = g_2^o + g_2^v + g_2 ,$$

where

$$\begin{aligned} \zeta_{11} &= \frac{C_D}{\pi} \left(\frac{M_d}{m + C M_d} \right) \left(\frac{U}{f_1 D} \right) , \\ \zeta_{12} &= \frac{C_L}{2\pi} \left(\frac{M_d}{m + C M_d} \right) \left(\frac{U}{f_2 D} \right) \int_0^1 \phi_1(\xi) \phi_2(\xi) d\xi , \\ \zeta_{21} &= \frac{C_L}{\pi} \left(\frac{M_d}{m + C M_d} \right) \left(\frac{U}{f_1 D} \right) \int_0^1 \phi_1(\xi) \phi_2(\xi) d\xi , \\ \zeta_{22} &= \frac{C_D}{2\pi} \left(\frac{M_d}{m + C M_d} \right) \left(\frac{U}{f_2 D} \right) , \\ g_1^o &= \frac{\rho D U^2 C_D}{2(m + C M_d)} \int_0^1 \phi_1(\xi) d\xi \\ g_2^o &= \frac{\rho D U^2 C_L}{2(m + C M_d)} \int_0^1 \phi_2(\xi) d\xi , \end{aligned} \quad (7.17)$$

$$g_1^v = \frac{\rho D U^2 C_D'}{2(m + C_{M_d})} \int_0^1 \phi_1(\xi) d\xi \sin(\Omega_D t) , \quad \text{and} \quad (7.17)$$

$$g_2^v = \frac{\rho D U^2 C_L'}{2(m + C_{M_d})} \int_0^1 \phi_2(\xi) d\xi \sin(\Omega_L t) . \quad (\text{Contd.})$$

Furthermore, the steady lift coefficient is, in general, equal to zero. The motion in the lift and drag directions are uncoupled and modal damping ratios are given by

$$\zeta_{f1} = \zeta_1 + \zeta_{11} = \zeta_1 + \frac{C_D}{\pi} \left(\frac{M_d}{m + C_{M_d}} \right) \left(\frac{U}{f_1 D} \right) \quad \text{and} \quad (7.18)$$

$$\zeta_{f2} = \zeta_2 + \zeta_{22} = \zeta_2 + \frac{C_D}{2\pi} \left(\frac{M_d}{m + C_{M_d}} \right) \left(\frac{U}{f_2 D} \right) .$$

ζ_{11} and ζ_{22} are attributed to drag force and are proportional to drag coefficient, mass ratio, and reduced flow velocity.

Different mechanisms of crossflow-induced vibrations of a cylinder can be evaluated using the equations of motion (7.13):

Wake Excitation: The natural vortex shedding induces periodic forces on the cylinder, perpendicular to the flow and in line with the flow, which are contained in these terms associated with C_D' and C_L' on the right side of Eq. 7.13. Wake excitation is, in general, a periodic forced excitation.

Self-Excitation: When the periodic flow excitation frequency is very close to the cylinder natural frequency, "lock-in" can occur and the vibration controls the vortex shedding and phasing necessary to continue the vibration. In this case, all the terms associated with C_L and C_L' (crossflow direction) or C_D and C_D' (in-line direction) become important.

Turbulence Excitation: Turbulence in the incoming flow or in flow across the cylinder can be expected to excite a random motion of the cylinder; this is controlled by the forcing terms g_1 and g_2 .

In addition to the dynamic response, the steady drag or lift forces can cause static displacement. This is associated with the steady fluid forces.

7.9 RESPONSE OF A CIRCULAR CYLINDER IN CROSSFLOW

Theoretically, the response of a cylinder subjected to crossflow can be calculated using Eqs. 7.13. In reality, the solution of these two equations is difficult for several reasons:

- The fluid force coefficients are not constants in general (i.e., C_D , C_D' and C_L' depend on cylinder response),
- The equations are nonlinear, and
- The fluid fields associated with turbulence g' , h' are not known in general.

Therefore, different simplified models have been developed for applications in different parameter ranges.

Consider a typical example of a single cylinder in water flow. Figure 7.18 shows the tube displacements and spectral density in the lift and drag directions and Fig. 7.19 summarizes the general response characteristics (Chen and Jendrzejczyk 1979). The cylinder response can be divided into several regions:

- $U_r < 1.25$ - Very small oscillations occur in both the lift and drag directions. Motion is excited predominantly by turbulence in the flow. The cylinder responds at the natural frequency in both the lift and drag directions. Occasionally, the cylinder may also be excited by vortex shedding; the response is in the lift direction and the response frequency is the vortex shedding frequency.

- $1.25 < U_r < 2.7$ - The cylinder performs steady oscillations in the drag direction with a small amplitude in the lift direction. The dominant frequencies in both the lift and drag directions are at the cylinder natural frequency.

- $2.7 < U_r < 4.5$ - The path of the cylinder motion is Lissajou's figure with the ratio of frequencies in the drag and lift directions equal to two.

- $U_r > 4.5$ - The cylinder motion is predominantly in the lift direction. Based on these observations, the cylinder response can be considered according to the following three conditions:

(1) Synchronization of Vortex Shedding in the Drag Direction: When the cylinder natural frequency is equal to twice the vortex shedding frequency, cylinder response in the drag direction is centered at the cylinder natural frequency. In this range of reduced flow velocity ($1.25 < U_r < 4.5$), the vortex shedding is controlled by cylinder motion in the drag direction; this response is called lock-in in the in-line direction.

(2) Synchronization of Vortex Shedding in the Lift Direction: When the vortex shedding frequency is close to the cylinder natural frequency, vortex-excited oscillations in the lift direction become dominant. In this range of reduced flow velocity ($4.5 < U_r < 10$), the response is called lock-in in the lift direction.

(3) Turbulence-induced Vibration: Tube response to turbulence excitation increases with reduced flow velocity and the response is centered at the cylinder natural frequency. Turbulence excitations occur for all values of U_r .

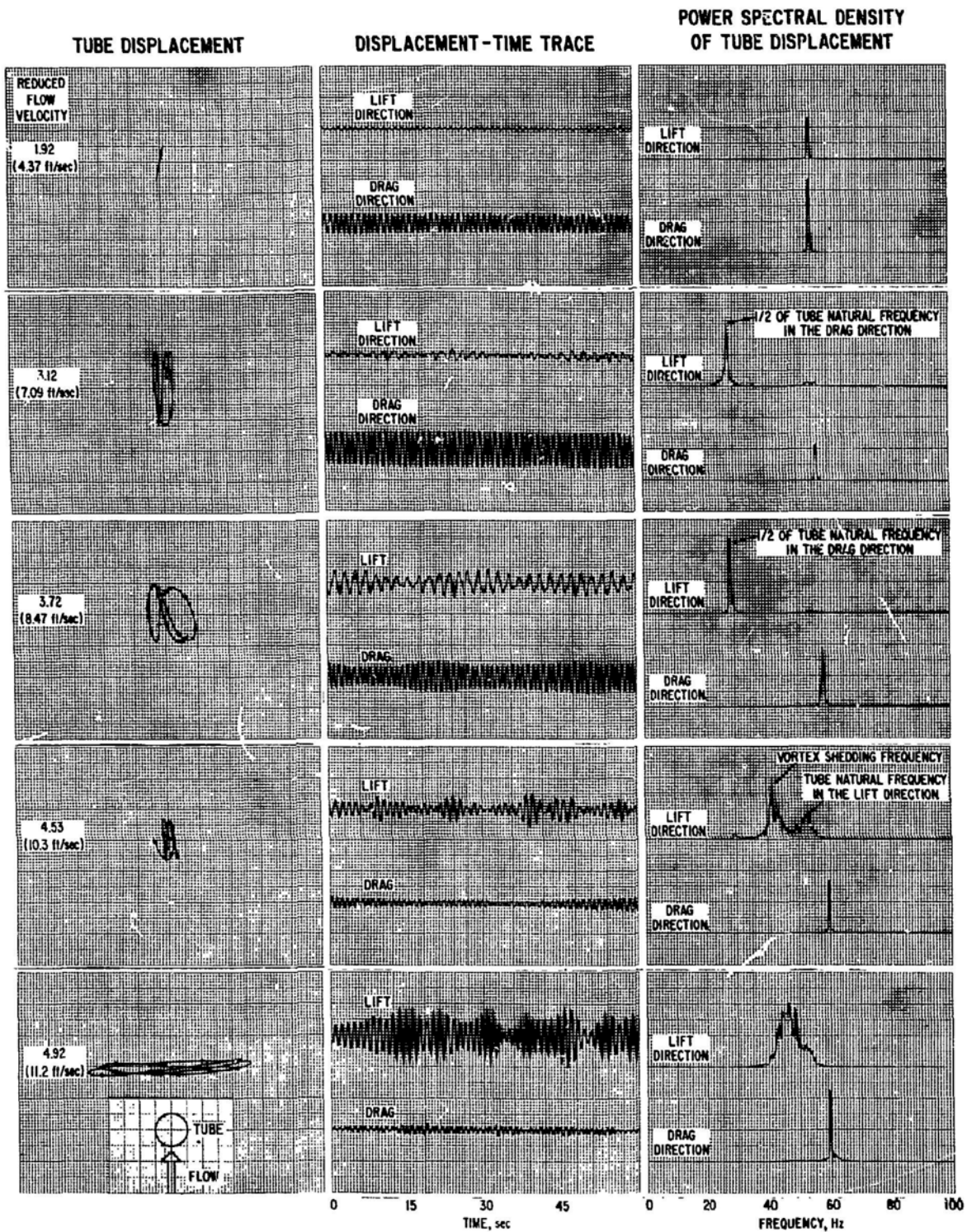


Fig. 7.18. Tube Displacement and Spectral Density of Tube Displacement in Water (Chen and Jendrzejczyk 1979)

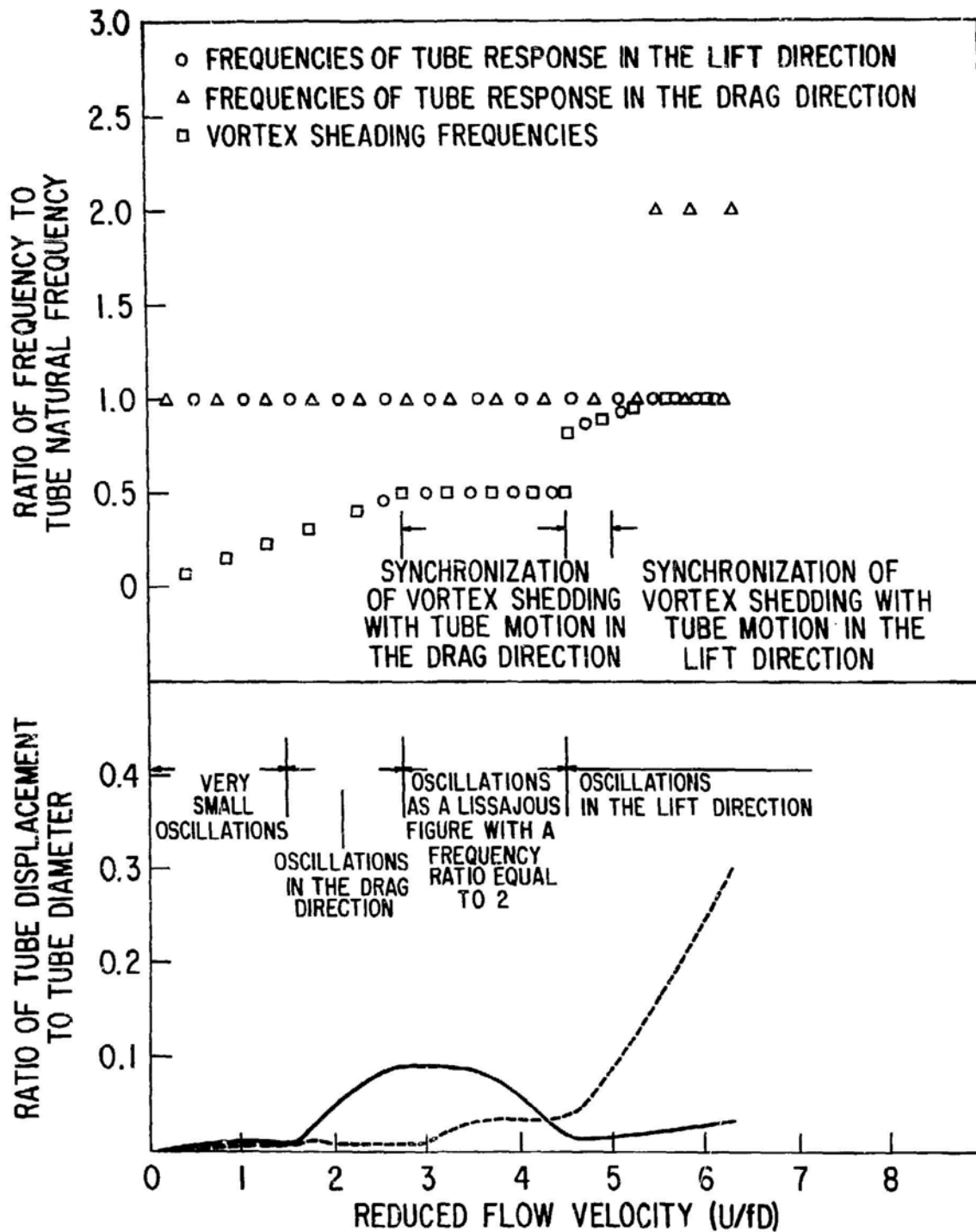


Fig. 7.19. Tube Response Characteristics

In-Line Oscillations

The in-line component of the periodic force, which occurs at twice the Strouhal frequency, is typically an order of magnitude less than the crossflow component (see Table 7.3). In a light fluid, it rarely excites the structure to a large amplitude. With the increased use of lightly damped structures in water, the potential for in-line oscillations has increased because of the larger fluid density and because of the lower flow velocities at which the resonant vibrations are initiated.

Oscillations in the in-line direction are contained within two adjacent but sometimes separate regions. The response in each region depends strongly on the mass-damping parameter δ_s . Figure 7.20 shows typical results from laboratory-scale measurements (King 1974). The first region covers the range approximately $1.25 < U/fD < 2.5$. The excitation is initiated at velocities only about a quarter of those necessary for crossflow excitation. The maximum amplitudes occur at $U/fD \sim 2.1$. The second region is $2.5 < U/fD < 3.8$, with the maximum amplitudes at $U/fD \sim 3.2$. These values are affected by the values of the mass-damping parameter δ_s . The cylinder response amplitudes in the two regions are approximately equal. However, the flow fields in the wake are different. The first region is characterized by the shedding of two vortices of opposing signs from opposite sides of the cylinder during one motion cycle, and in the second region a single vortex is shed during each cycle of oscillations and a street of alternately rotating vortices is formed downstream of the cylinder as shown in Fig. 7.21 (King 1977a). In some cases, there is no clear separation of the two regions (Chen and Jendrzejczyk 1979).

The in-line oscillations reach displacements of only about $0.25 D$ peak-to-peak at very low damping. All available evidence suggests that in-line oscillations do not occur for values of $\delta_s > 0.6$. Also, a limiting lower Reynolds number for the onset of vortex-excited, in-line oscillations in water is about $Re = 1200$ to 1500 (King 1977a).

Crossflow Oscillations

When the natural frequency of the cylinder is considerably greater than the frequency of vortex shedding for a stationary cylinder, the cylinder excites very small-amplitude vibrations at the natural frequency of the cylinder and at the Strouhal frequency. This is called the zone of constant Strouhal number and increasing forcing frequency. As the flow velocity is slowly increased, the cylinder amplitude also increases with the frequency of the vortex shedding, which is now controlled by the natural frequency of the structure. This process continues until a maximum amplitude is reached, at which point the input energy from the flow just balances that absorbed by the cylinder. A further increase in flow velocity causes the amplitude to fall off until eventually control of the shedding frequency is lost. At this

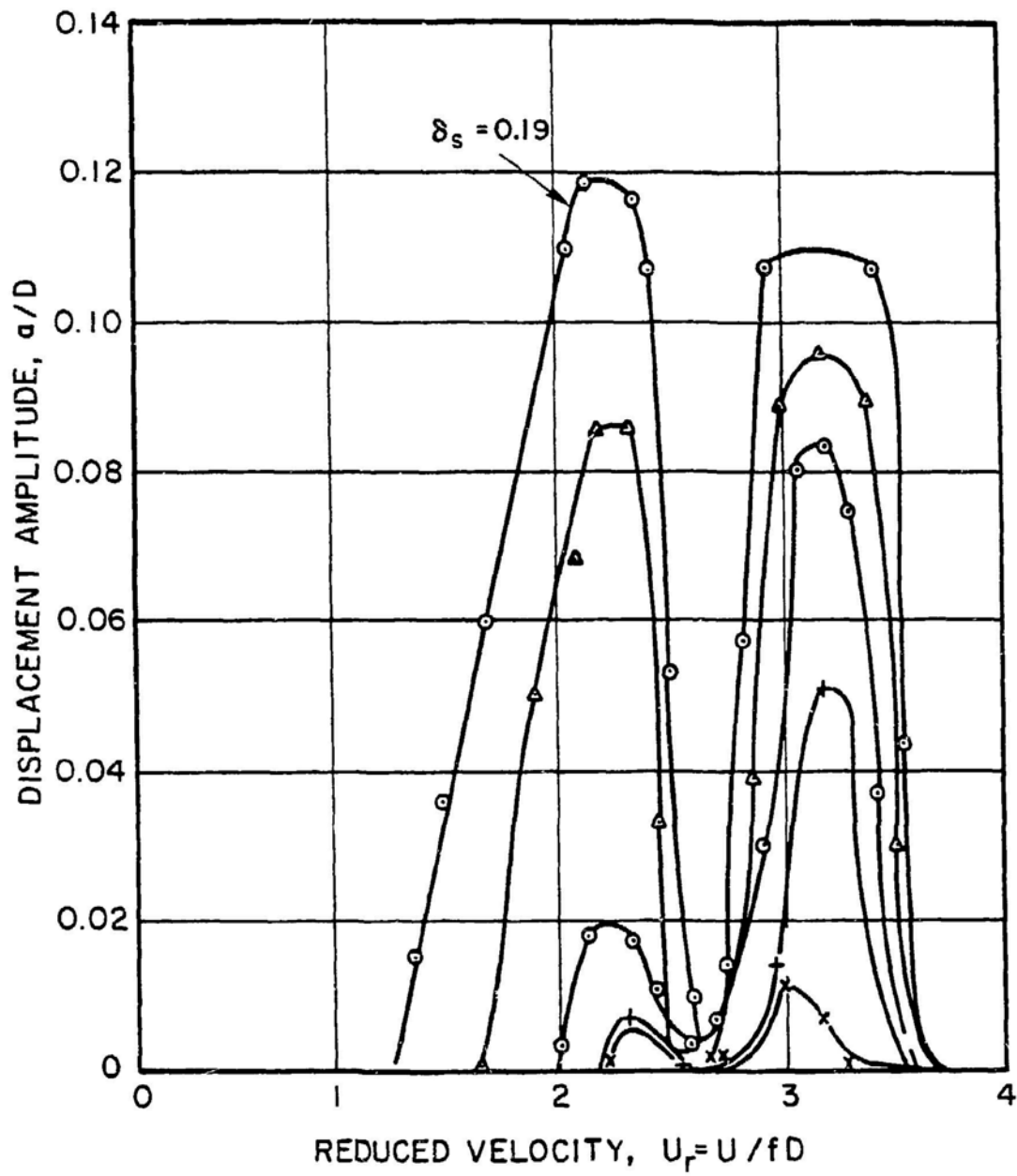


Fig. 7.20. Vortex-excited Displacement of a Cylinder in the In-line Direction (from King 1974, with permission--see Credits)

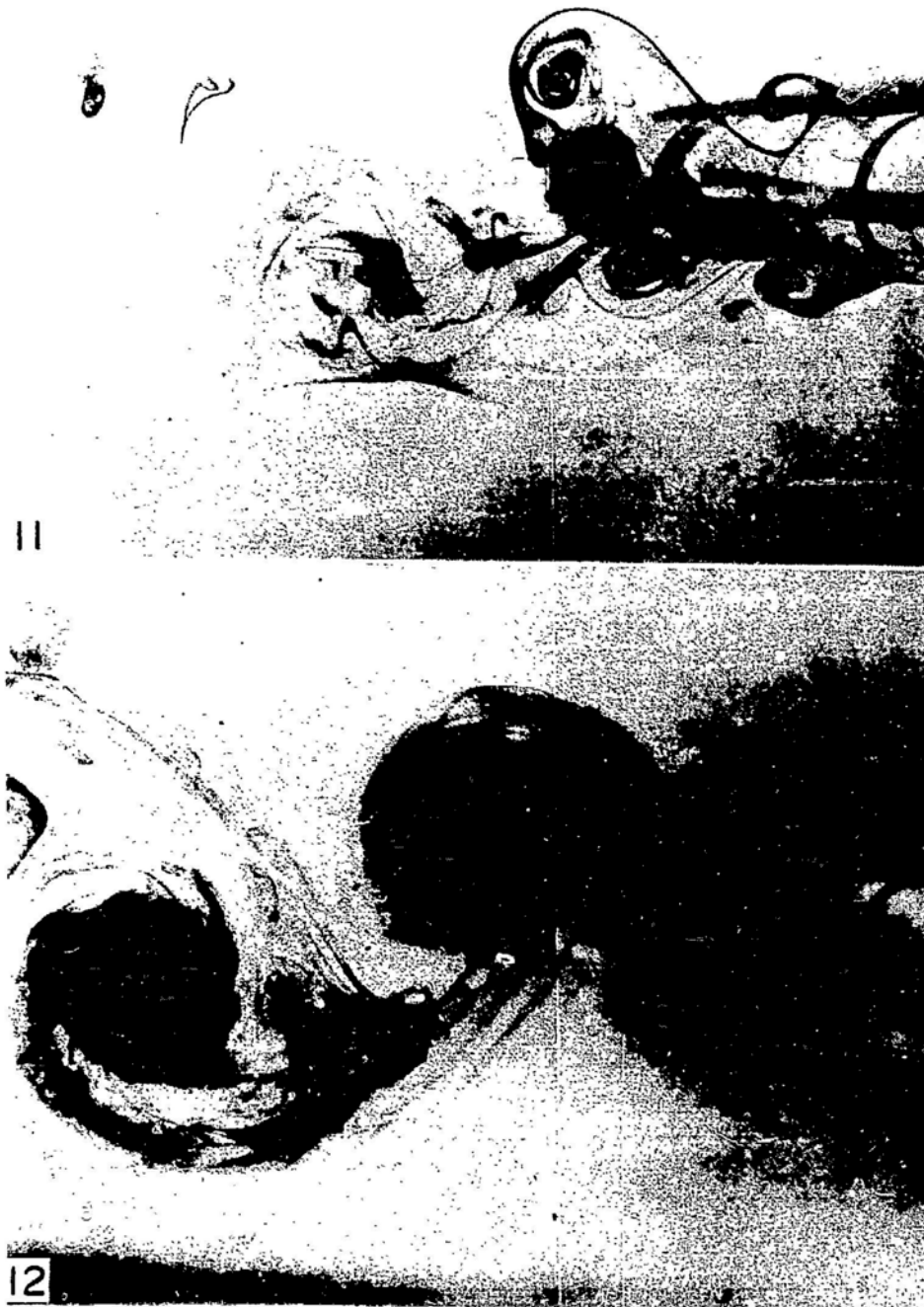


Fig. 7.21. Symmetric and Alternate Vortex Shedding (from King 1977a, with permission--see Credits)

point, if the natural frequency of higher modes and the damping are sufficiently high, the cylinder response amplitude becomes small. On the other hand, there is a possibility that a small range of flow velocity exists where two or more modes overlap.

Figure 7.22 shows the typical cylinder response in the lock-in region in the lift direction. Initially, as the flow velocity is increased from zero, the cylinder is stationary and the vortex shedding frequency follows the $St = 0.198$ straight-line relationship. However, as the lower critical flow velocity is approached, the cylinder begins to oscillate and the dominant wake frequency shifts from the $St = 0.198$ line and remains nominally equal to the cylinder natural frequency. Note that lock-in occurs over a range of velocities and the vortex shedding frequency coincides approximately with the natural frequency of the cylinder. At a velocity slightly above the critical value, the cylinder large-amplitude motion ceases and the vortex shedding frequency returns to the value predicted by the $St = 0.198$ straight-line relationship for a stationary cylinder.

The characteristics in the lock-in region can be summarized as follows:

- Capture of Vortex-Shedding Frequency by the Cylinder Frequency - Usually, the cylinder starts to capture the vortex frequency at approximately the flow speed for which the vortex shedding frequency for a stationary cylinder coincides with the cylinder natural frequency. Throughout the lock-in range, there is very little modulation of either cylinder displacement or pressure acting on the cylinder. This indicates a much more highly organized wake vortex system induced by the cylinder motion. The range of capture over which the vortex-shedding frequency is locked to the cylinder frequency depends on oscillation amplitude, which in turn depends on mass-damping parameter--the larger the amplitude, the larger the range of capture. The range of capture always encompasses the reduced velocity, which is equal to the inverse of the Strouhal number measured for the corresponding stationary cylinder.

- Increase of Correlation Length - The movement of the cylinder provides a means of synchronizing the movement of shedding along its length. The threshold oscillation amplitude to cause large increases in the correlation is approximately $a/D \approx 0.05 \sim 0.1$ (see Fig. 7.10).

- Variation in Lift Coefficient - Within the lock-in range, experimental data show an increase in the fluctuating lift coefficient at low oscillation amplitudes (see Fig. 7.8). This is associated with the increase of the strength of shed vortices over their fixed-cylinder values associated with the improved two-dimensionality of the flow and the direct effect of the cylinder movement on the flow field. A typical set of data by Sarpkaya (1978) for a cylinder oscillating in flow with the amplitude $a/D = 0.5$ is given in Fig. 7.23. The in-phase component is related to inertia and stiffness forces

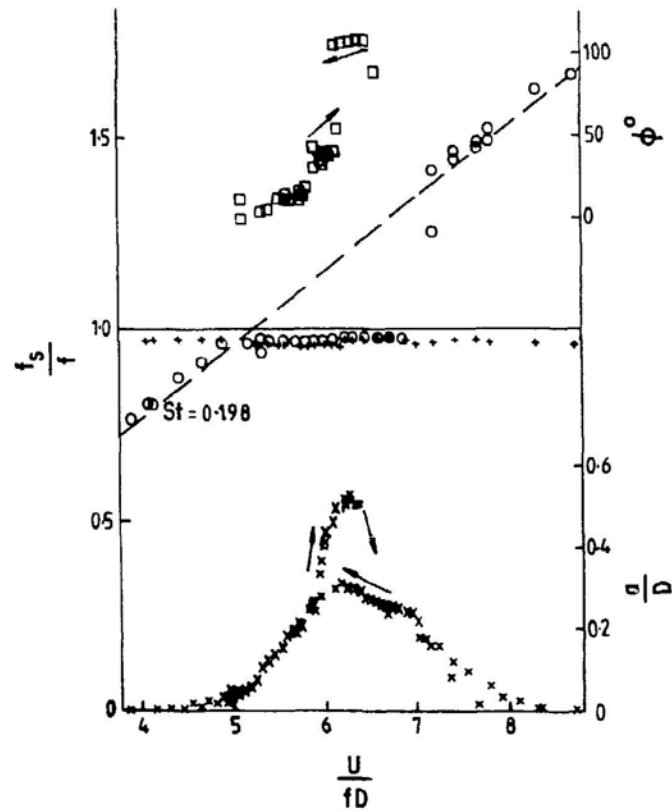


Fig. 7.22. Oscillation Characteristics for a Circular Cylinder for $\delta_s = 0.2$ (from Bearman 1984, with permission--see Credits; original source from Feng 1968)

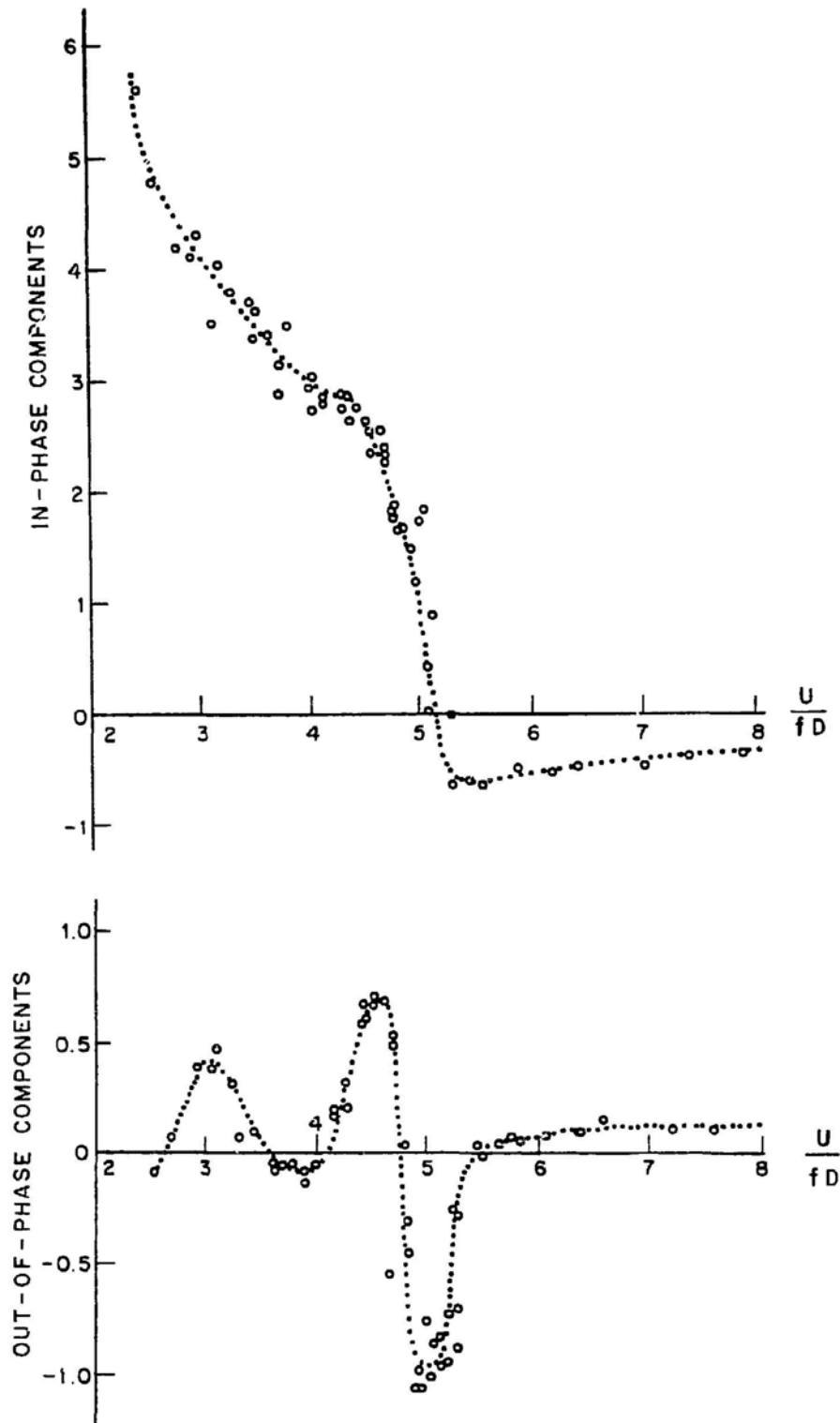


Fig. 7.23. Lift Coefficient vs. Reduced Flow Velocity for Forced Oscillation of a Circular Cylinder at $a/D = 0.5$ (from Sarpkaya 1978, with permission--see Credits)

and the out-of-phase component is related to damping mechanism. The drastic change of the components at $U_r \approx 5$ is connected with the vortex shedding as pointed out by Zdravkovich (1981). In the lower U_r , the vortex, formed on one side of the cylinder, is shed when the cylinder is near the maximum amplitude on the opposite side. With the increase in U_r , the vortex with the same circulation is shed when the cylinder reaches the maximum amplitude on the same side. Bearman and Currie (1979), using controlled forced-vibration experiments at fixed amplitudes, have shown that although the significant change occurs over a small range of U_r , it is progressive and not a discontinuity.

The characteristics of the two lock-in regions in the in-line direction and one lock-in region in the crossflow direction are summarized in Table 7.5.

7.10 PREDICTION METHODS FOR LOCK-IN RESPONSES

Prediction methods for both in-line and transverse oscillations of the cylinders are important for design evaluations as well as for understanding of the basic interaction process of cylinder and flow. Ideally, the methods should be based on the solution of the Navier-Stokes equation for the flow around a cylinder at high Reynolds numbers. At this point in time, no such techniques appear to be available to solve the problem. Researchers have developed different models to quantify the response under different conditions.

7.10.1 Lock-in Region for In-line Vibration

A quasisteady representation of the fluctuating drag on a cylinder in the critical Reynolds number is proposed by Martin et al. (1981) and Ribeiro (1983) as the mechanism for self-excited in-line oscillations. The mechanism can be explained qualitatively in terms of the instantaneous Reynolds number on the relative velocity between the incoming flow and moving cylinder. In the transition Reynolds numbers (see Fig. 7.6), the drag force varies drastically with Reynolds number. During the half cycle over which the cylinder is moving against the flow, the instantaneous Reynolds number is greater than that determined by the incoming flow alone. Therefore, during this half cycle, the drag force acting on the cylinder is smaller than the mean value and the difference between the mean value and the instantaneous drag is in the direction of the cylinder motion. Similarly, over the other half cycle, the difference in drag is also in the direction of cylinder motion. Because of the variation of drag, a periodic drag is produced by the cylinder motion. Under the quasisteady condition, energy from the flow stream will be transferred to the cylinder until an equilibrium amplitude is established.

Table 7.5. Characteristics of Lock-in Regions

Direction of Motion	In-Line Oscillation		Crossflow Oscillation
	First Region	Second Region	
Region	1	2	3
U_r	1.25 ~ 2.5	2.5 ~ 3.8	3.8 ~ 10
Value of U_r corresponding to the maximum response amplitude	2.4	3.2	5.5 ~ 8
Excitation frequency	Variable input frequency	Fixed frequency	Fixed frequency
Maximum cylinder response amplitude, a/D	0.25	0.25	2.0
Vortices	Symmetric vortex	Alternate vortex	Alternate vortex
Upper limit of δ_s in which lock-in occurs	0.6	0.6	32

Let the instantaneous drag force acting on the cylinder be g and the instantaneous flow velocity relative to the oscillating cylinder V . The cylinder will be unstable if the drag decreases when it is moving against the flow; i.e.,

$$\frac{dg}{dV} < 0 . \quad (7.19)$$

Note that

$$g = \frac{1}{2} C_D \rho D V^2 = \frac{1}{2} C_D \rho D \left(\frac{V}{D}\right)^2 Re^2 . \quad (7.20)$$

Then

$$\frac{dg}{dV} = \frac{D}{V} \frac{dg}{dRe} . \quad (7.21)$$

Thus the condition for instability becomes

$$\frac{d}{dRe} (C_D Re^2) < 0 . \quad (7.22)$$

Since C_D is a function of Re ,

$$-\frac{dC_D}{dRe} > 2 \frac{C_D}{Re} . \quad (7.23)$$

The condition requires that the slope of the C_D vs. Re curve be negative, and the magnitude of this slope must exceed twice the ordinate of the drag coefficient divided by the Reynolds number.

The condition of instability also can be investigated using the equation of motion. Consider the in-line motion only. Referring to Fig. 7.17 and Eqs. 7.10 to 7.14,

$$v = 0 , \quad \theta = 0 , \quad C_D^i = 0 , \quad g_1 = 0 . \quad (7.24)$$

Assume $\phi_1(z) = 1$; the first equation of Eq. 7.13 becomes (dropping the subscript 1):

$$\ddot{q} + 2\zeta\omega\dot{q} + \omega^2 q = \alpha C_D (U - \dot{q})^2 \quad (7.25)$$

$$\alpha = \frac{\rho D}{2(m + C_m M_d)} .$$

For small oscillations about the equilibrium position, the C_D vs. Re curve can be approximated in the neighborhood of Re_o and C_{Do} by

$$C_D = C_{Do} - \beta(Re - Re_o) , \quad (7.26)$$

where

$$C_{Do} = C_D(Re_o) = C_D\left(\frac{UD}{\nu}\right) . \quad (7.27)$$

Therefore,

$$C_D = C_{Do} + \beta \frac{D}{\nu} \dot{q} . \quad (7.28)$$

Equation 7.25 becomes

$$\ddot{q} + 2\zeta\omega\dot{q} + \omega^2 q = \left(C_{Do} + \frac{\beta D}{\nu} \dot{q}\right) \alpha (U - \dot{q})^2 . \quad (7.29)$$

The static deflection

$$q_o = \frac{C_{Do} \alpha U^2}{\omega^2} . \quad (7.30)$$

For stability of the system, consider small oscillations about the static equilibrium position. Let

$$q = \delta q \cos \omega t + q_o . \quad (7.31)$$

Using Eqs. 7.29 and 7.31, we obtain

$$\delta \ddot{q} = \left(\frac{\alpha \beta D U^2}{\alpha \nu} - \alpha C_{Do} U - \zeta \omega \right) 2 \delta \dot{q} \quad \text{and} \quad (7.32)$$

$$\delta \dot{q} = \left(\frac{\alpha \beta D U^2}{\alpha \nu} - \alpha C_{Do} U - \zeta \omega \right) \delta q .$$

Thus the condition of stability is

$$\frac{\alpha \beta D U^2}{\alpha \nu} - \alpha C_{Do} U - \zeta \omega < 0 \quad (7.33)$$

or

$$\beta < \frac{2 C_{Do}}{Re_o} + \frac{4 \delta_s}{Re_o U_r} . \quad (7.34)$$

When the second term in Eq. 7.34 is neglected, it is reduced to Eq. 7.23.

Using the quasisteady representation of the fluctuating drag on a circular cylinder, Martin et al. (1981) have predicted that the response amplitude in the drag direction depends on Re_o , δ_s , and U_r . The analytical predictions are in fair agreement with the experimental data by Hardwick and Wootton (1973).

The development of the mathematical models for the lock-in region in the drag direction is still in its infancy. Note that the drag coefficient is a function of cylinder oscillation amplitude, as shown in Fig. 7.9. Considerations must be given to including the motion-dependent effect of the drag force in a more refined model. Much more detailed study is needed. For practical applications, oscillation amplitude can be estimated using experimental data; e.g., King (1977a) presents the amplitude of oscillation as a function of the mass-damping parameter δ_g given in Fig. 7.24.

7.10.2 Lock-in Region for Crossflow Vibration

Two types of models have been proposed to describe the lock-in phenomena--self-excited oscillation models and forced-vibration models.

Self-Excited Oscillation Models

1. **Lift Oscillator Model** - The lift coefficient is assumed to satisfy a van der Pol-type equation (Hartlen and Currie 1970) based on observation by Bishop and Hassan (1964). The model has been refined and has successfully predicted the lock-in characteristics (Skop and Griffin 1973; Iwan and Blevins 1974; Landl 1975).

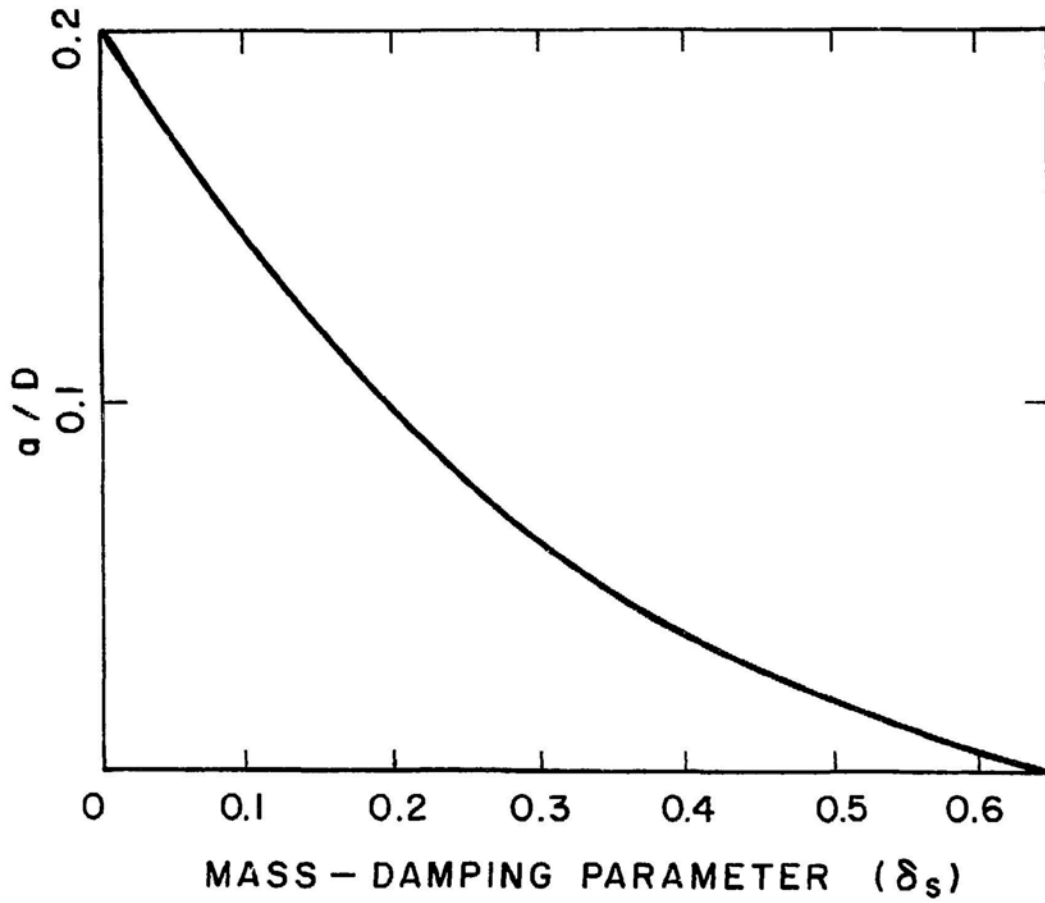


Fig. 7.24. Response Amplitude of a Cylinder in In-Line Direction
(from King 1977a, with permission--see Credits)

2. Birkhoff's Oscillation Model - The added fluid region behind the cylinder is modeled as Birkhoff's oscillator (Funakawa 1969). It is shown that flutter is possible in a limited range of flow velocity.

3. Variable Vortex-Wake Width Model - The vortex-wake width depends on cylinder amplitude and vortex origin time (Di Silvio 1969); the model is able to reproduce a certain narrowing of the wake and agrees well with experimental data.

Forced-vibration Models

The vortex-induced force is taken as the excitation. The problem is solved as a forced-vibration problem, with the excitation being the lift force. Two approaches are used--a correlation model and a variable-phase model.

1. Correlation Model: The cylinder motion is excited by the fluctuating lift force (Blevins and Burton 1976). The equation of motion can be reduced from the second Eq. of Eq. 7.13, assuming that $C_D = C_L' = 0$ and the excitation is a random forcing function:

$$\ddot{q}_2 + 2\xi_2\omega_2\dot{q}_2 + \omega_2^2 q_2 = \frac{1}{(m + C_{M_d})L} \int_0^L h'(z,t)\phi_2(z)dz. \quad (7.35)$$

The excitation is associated with the fluctuating lift coefficient, which is considered a function of oscillation amplitude (see Fig. 7.8). From Eq. 7.35, the cylinder displacement can be calculated.

2. Variable-phase Model: Sarpkaya (1978) and Staubli (1983) use the measured values of the in-phase and out-of-phase fluctuating lift forces (see Fig. 7.23) to calculate the response of the vibrating cylinder. The results obtained from the model agree reasonably well with the data.

All these approaches are similar in that model parameters are chosen on the basis of experimental observations or assumptions. Although all models are capable of reproducing some general characteristics of the cylinder responses, the basic interaction mechanisms remain unresolved.

In practical applications, the lock-in (synchronization) range, as well as the cylinder response amplitude, is of particular interest. Figures 7.25 and 7.26 show the synchronization range and vibration amplitude a/D as a function of δ_g (King et al. 1973). Note that for $\delta_g > 32$, no synchronization in the lift direction occurs. Different expressions of the response amplitude in the lock-in region have also been developed based on different models as summarized in Table 7.6, where δ_g^* is measured in still fluid; and γ is the mode shape factor ($= 1.31$ for a cantilevered cylinder). In addition, experimental data for $2a/D$ have been compiled by Griffin (1980) (Fig. 7.27) encompassing a wide range of single cylinders at Reynolds number from 300

Table 7.6. Predictions of Resonant Vortex-induced Vibration Amplitude of Circular Cylindrical Structures as a Function of Mass-damping Parameter

Author	Predicted Resonant Amplitude
Griffin et al.(1975)	$\frac{a}{D} = \frac{1.29\gamma}{[1 + 0.43(2\pi St^2 \delta_s^*)]^{3.35}}$
Iwan and Blevins (1974)	$\frac{a}{D} = \frac{0.07\gamma}{(\delta_s + 1.9)St^2} \left\{ 0.3 + \frac{0.72}{(\delta_s + 1.9)St} \right\}^{1/2}$
Sarpkaya (1978)	$\frac{a}{D} = \frac{0.32}{[0.06 + (2\pi St^2 \delta_s)^2]^{1/2}}$

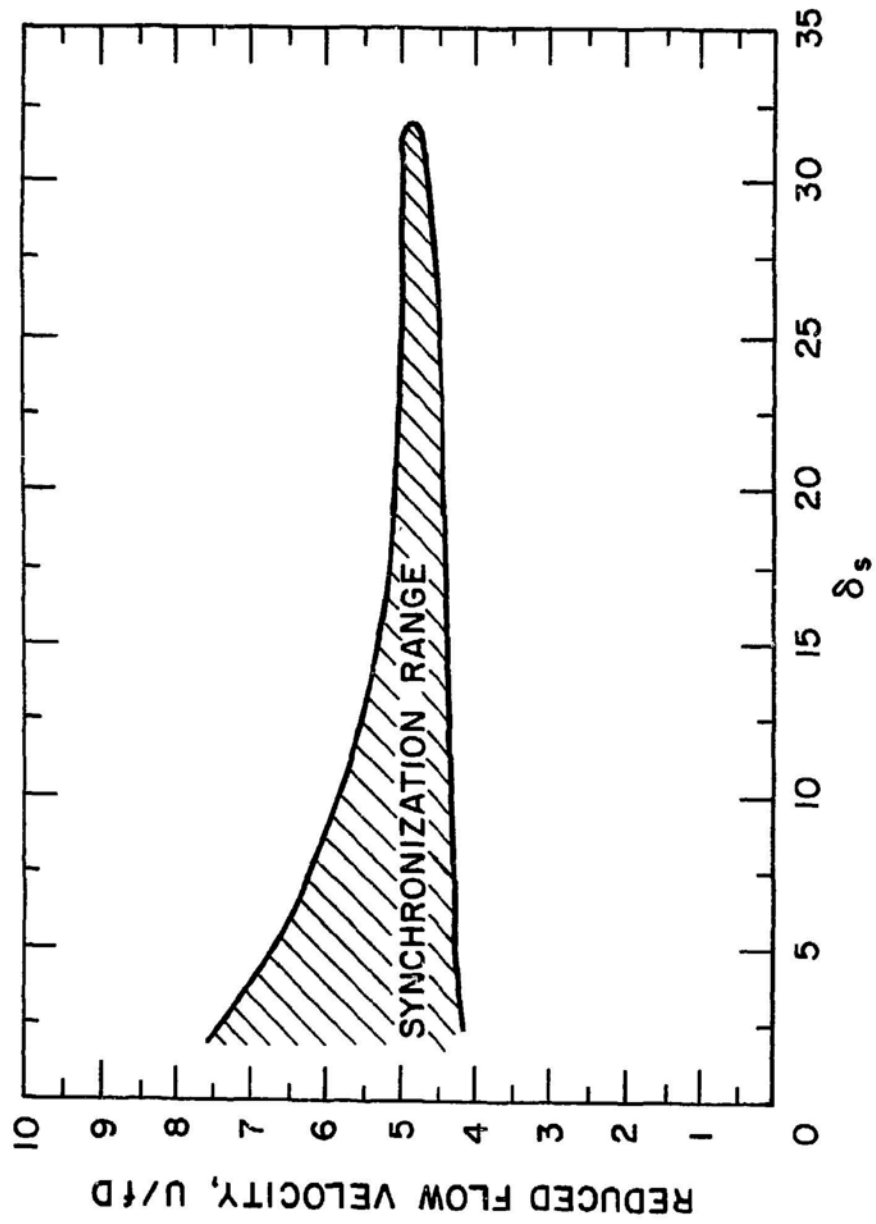


Fig. 7.25. Synchronization Range in Crossflow Direction

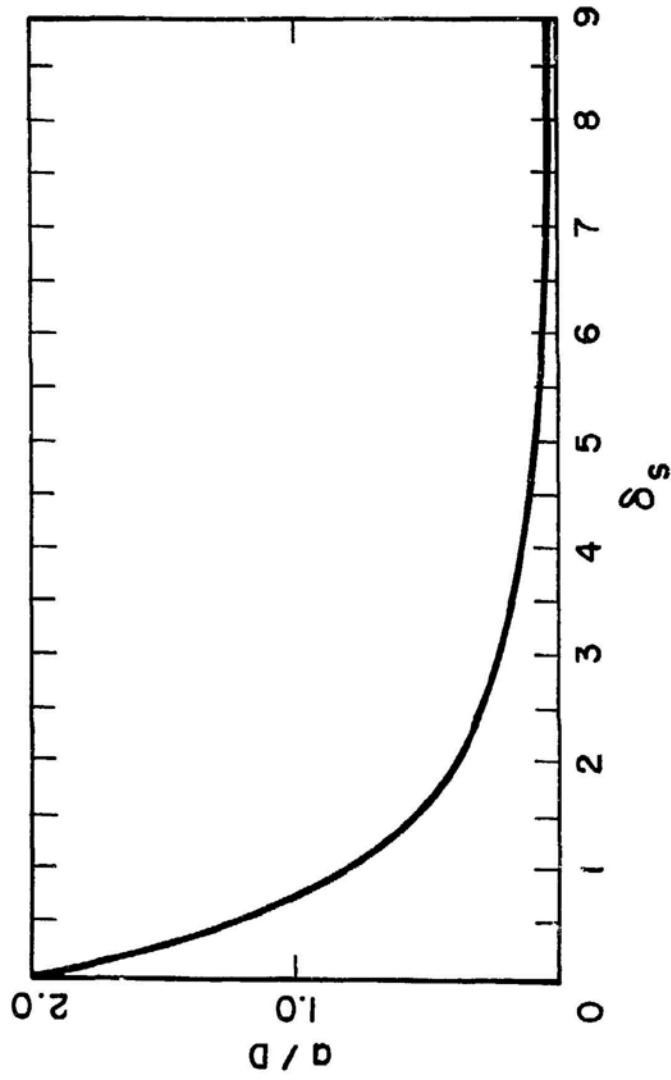


Fig. 7.26. Response Amplitude of a Cylinder in Crossflow Direction (from King 1977a, with permission--see Credits)

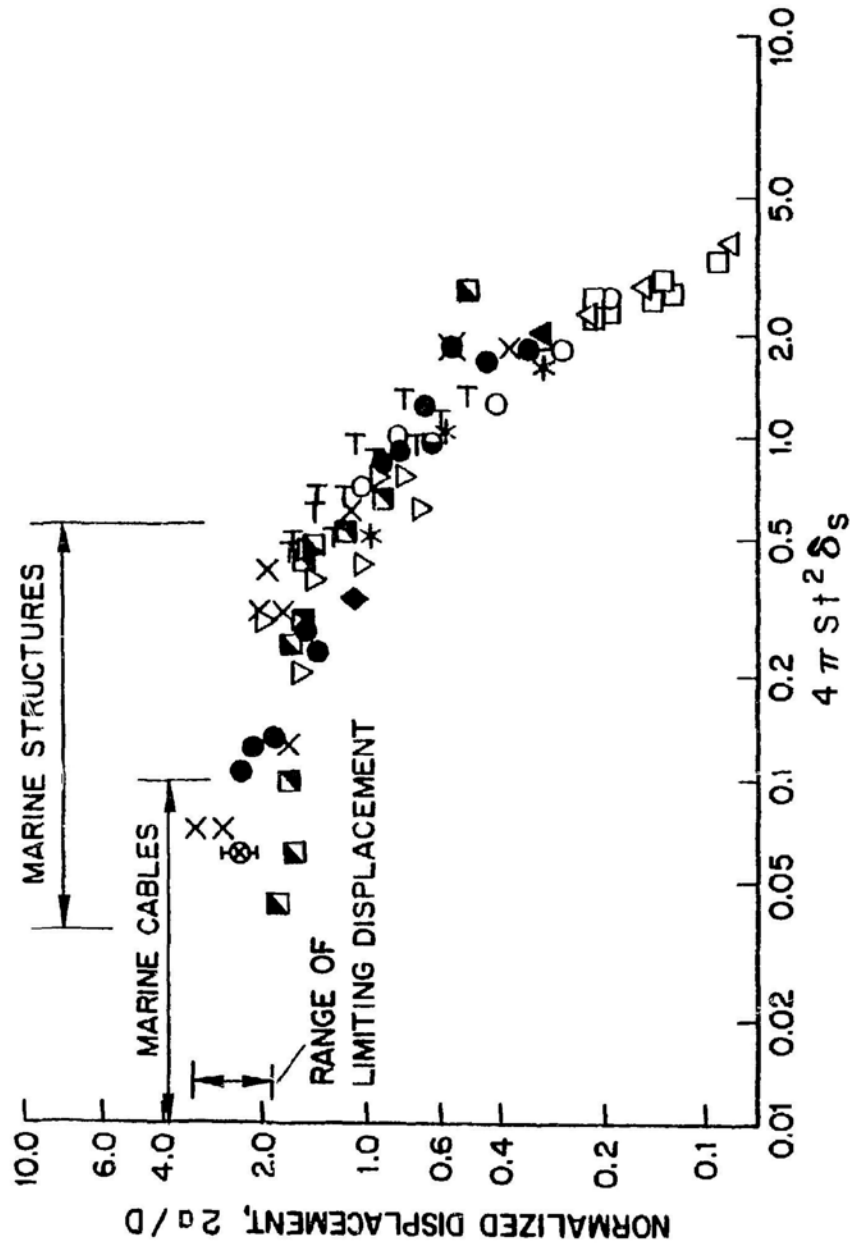


Fig. 7.27. Maximum Vortex-excited Crossflow Displacement Amplitude $2a/D$ of Circular Cylinder (from Griffin 1980, with permission--see Credits)

to 10^6 . All available experimental data indicate that the limiting unsteady displacement of a flexible cylinder is about $a/d \approx 1$ to 1.5 at low values of δ_s .

7.11 EFFECTS OF DIFFERENT SYSTEM PARAMETERS

The response of a cylinder in crossflow is affected by different system parameters: high Reynolds number, turbulence, yawed flow, blockage effect, surface roughness, etc. Some of the effects of these parameters are still not well understood.

High Reynolds Number

Vibrations at high Reynolds numbers are of particular interest with respect to the vibration of some structural components. Full-scale data on crossflow response of cylinders are quite limited because large-amplitude motions lead to failure within a short time of oscillations.

Flow characteristics at high Reynolds number are discussed in Sections 7.6 and 7.7. The response of a cylinder at high Reynolds number is not well documented. Based on the limited available data, some general observations are valuable in the assessment of the structural response.

- In contrast to stationary cylinders (see Fig. 7.5), there is no discernible Reynolds number effect on the Strouhal number for Re from 3×10^5 to 1.4×10^6 obtained from a full-scale experiment with a 30 inch diameter pipe (Wootton et al. 1974).

- The universal wake Strouhal number St^* --

$$St^* = St \left(\frac{U}{U_s} \right) \left(\frac{D}{D_s} \right) \quad (7.36)$$

where

D_s = the distance between two shear layers and

U_s = the flow speed just outside the shear layers--

is plotted in Fig. 7.28; the results span five decades of the Reynolds number from Re^* ($= U_s D_s / \nu$) = 10^2 to 10^7 . St^* collapses the characteristic wake scales onto a single curve (Griffin 1981).

- The overall pattern of behavior of a cylinder in water is similar at all Reynolds numbers where vortex shedding takes place. Some typical crossflow motions of several full-scale cylinders are given in Fig. 7.29 from the results of Sainsbury and King (1971). The Reynolds numbers were somewhat larger than 10^6 . Crossflow oscillations greater than 0.1 diameter were initiated at $U_r \approx 3.5$ to 4; the maximum crossflow response was near $U_r \approx 6$.

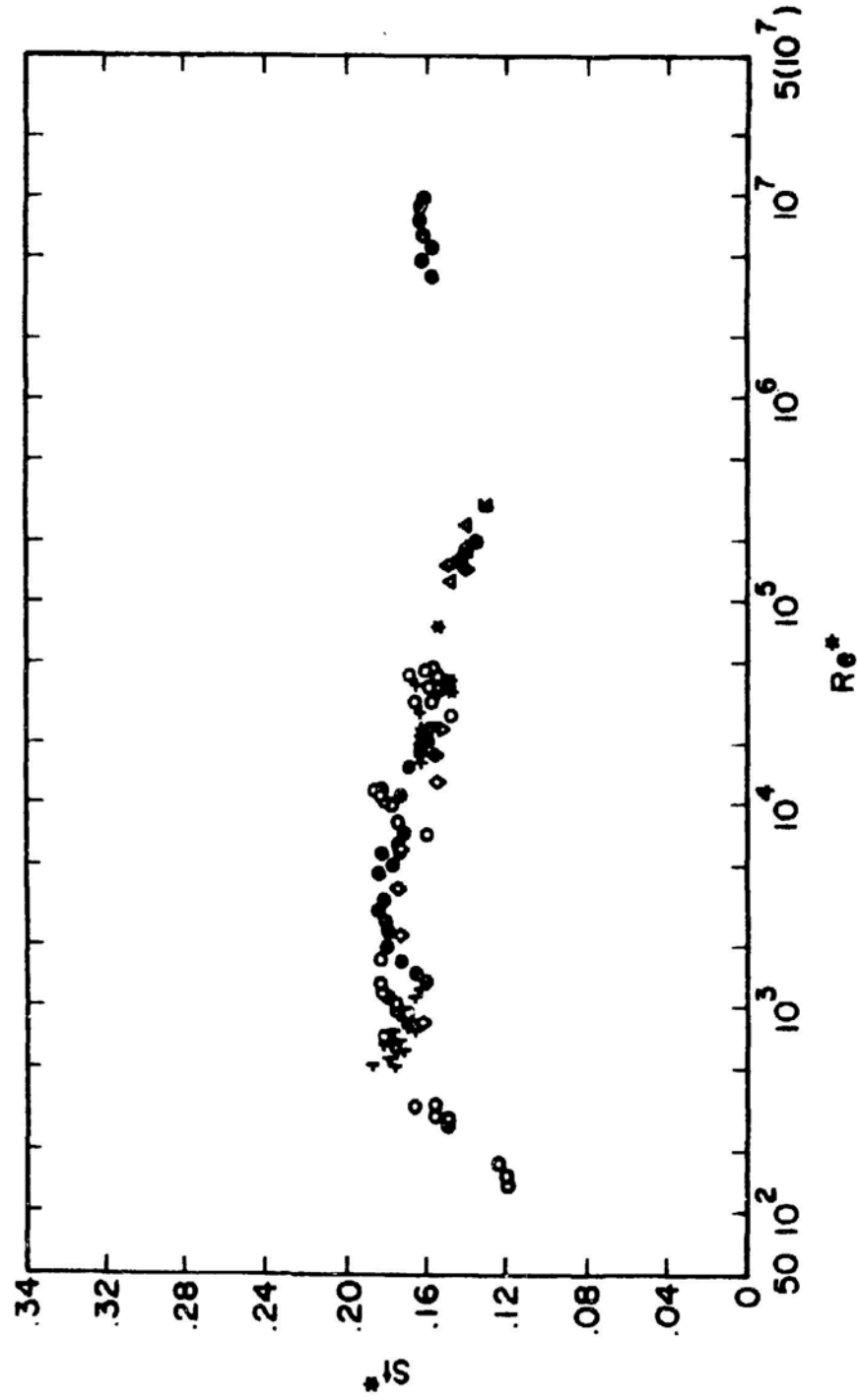


Fig. 7.28. Universal Strouhal Number St^* Plotted Against Wake Reynolds Number Re^* (from Griffin 1981, with permission--see Credits)

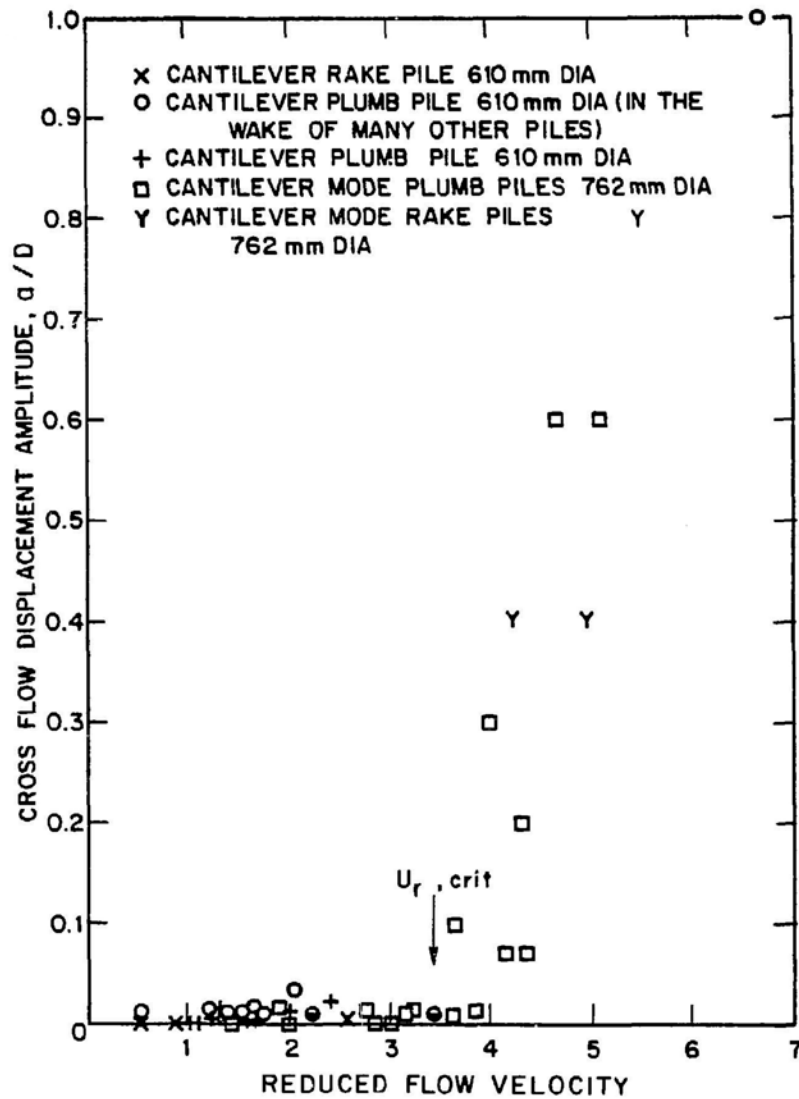


Fig. 7.29. Crossflow Displacement Amplitude a/D as a Function of U_r for Full-scale Marine Piles (from Griffin 1980, with permission--see Credits; original source from Sainsbury and King 1971)

Surface Roughness

A comprehensive study of the effect of surface roughness on steady drag was made by Miller (1976) for the case of stationary cylinders. However, there are very limited data for the fluctuating fluid force coefficients on roughed cylinders. Sarpkaya (1979b) notes a substantial increase in total fluid force for rough cylinders. Nakamura (1976) has measured the steady drag forces and Strouhal frequencies of rough cylinders at supercritical Reynolds numbers and has observed strong regular vortex shedding at $Re \approx 4 \times 10^6$ and above. In this Reynolds number range, the vortex-excited crossflow displacement amplitude of a rough cylinder increased substantially from the corresponding smooth cylinder. More tests are needed to quantify the effect of roughness of cylinder response in different flow regions.

Yawed Flow

If the cylinder is yawed to the flow direction with an angle ϕ , both the effective fluid force and the reduced flow velocity are reduced:

$$g = \frac{1}{2} \rho D [C_D (U \cos \phi)^2 + C_D' (U \cos \phi)^2 \cos(\omega t)] \quad \text{and} \quad (7.37)$$

$$U_r = \frac{U \cos \phi}{fD}.$$

This is based on the assumption that the normal component of the flow velocity can be taken as the effective flow velocity on a yawed cylinder; the use of the normal component of velocity is called the independence principle. Studies have been reported to verify the validity of the principle (e.g., King 1977b and Ramberg 1983).

King's results show that yawing the cylinder provides no protection against vortex-excited oscillations and sustained oscillations; both in-line and crossflow oscillations were recorded for yaw angles up to $\phi = 45^\circ$. The critical reduced flow velocities for the onset of in-line and crossflow oscillations were similar to those for the normal crossflow. King also found that the drag coefficient C_D is equal to the equivalent value of a cylinder at normal incidence. These illustrate that the independence principle is applicable. Ramberg undertook a detailed investigation of the flow around yawed cylinders and its responses. His main conclusion is that although the Independence Principle fails for the stationary cylinders, measurements of the bounds of the lock-in regime for yawed cylinders compare well with the normal-incidence case in terms of the effects of vibration on characteristic wake dimensions. The findings by King and Ramberg imply that various methodologies

for predicting vortex-excited oscillation at normal incidence can be applied to a cylinder at different yawed angles.

Blockage Effects

In many engineering problems of a cylinder in crossflow, the flow field is contained between parallel walls. The walls have significant effects on the response of the cylinders. Studies have been reported for a cylinder placed symmetrically in a channel (Richter and Naudascher 1976; Ramamurthy and Ng 1973; Suzuki and Hirano 1979) and a cylinder near a plane boundary (Bearman and Zdravkovich 1978; Angrilli et al. 1982).

For a cylinder in a channel, the Strouhal number is increased by increasing the flow confinement throughout the supercritical range of Reynolds numbers. Near transition, the rise in Strouhal number is very sudden, although the changes in drag and lift characteristics are more gradual. Flow confinement increases the steady drag because of higher separation velocities. The drop in the steady drag at the transition region becomes pronounced with greater confinement. Although flow confinement reduces the fluctuating drag in the subcritical range, it increases the fluctuating lift.

Vortex-induced vibration of a cylinder near a plane boundary is important in off-shore pipeline applications. Figure 7.30 shows the response amplitude and oscillation frequency (Tsahalis 1983), with G being the gap between the cylinder and the plane boundary. The effects of the plane boundary are: (1) the amplitude vs. flow velocity curve assumes an S shape in contrast to the "bell" shape for the isolated cylinder, (2) the maximum amplitude is reduced, (3) the response frequency is reduced, and (4) the critical flow velocity at which large oscillations occur increases.

7.12 RESPONSE OF CIRCULAR CYLINDRICAL SHELLS IN CROSSFLOW

In addition to a circular cylindrical rod, a circular cylindrical shell in crossflow can be subjected to "ovalling oscillations" in addition to the beam mode oscillations. The phenomenon of ovalling oscillation for a circular cylindrical shell is generally referred to as the circumferential mode with $n > 1$ (see Fig. 4.1). This type of vibration was first noted in the mid 1950s (Dickey and Woodruff 1956; Dockstader et al. 1956).

For beam mode response, the cylindrical shell can be treated as a beam; therefore, the general response characteristics is the same as a circular rod. The main excitation is the vortex shedding.

For ovalling oscillations, until the mid 1970s the excitation was considered to be vortex shedding (Dockstader et al. 1956; Johns and Sharma 1974). At the onset of large-amplitude oscillations, the frequency of ovalling oscillations of the shell f_{nm} (n is referred to circumferential wave number and m is referred to the axial wave number) is an integer multiple of the vortex shedding frequency f_s ; i.e., $f_{nm}/f_s = r_s$, where r_s is an integer ranging from 1 to 6.

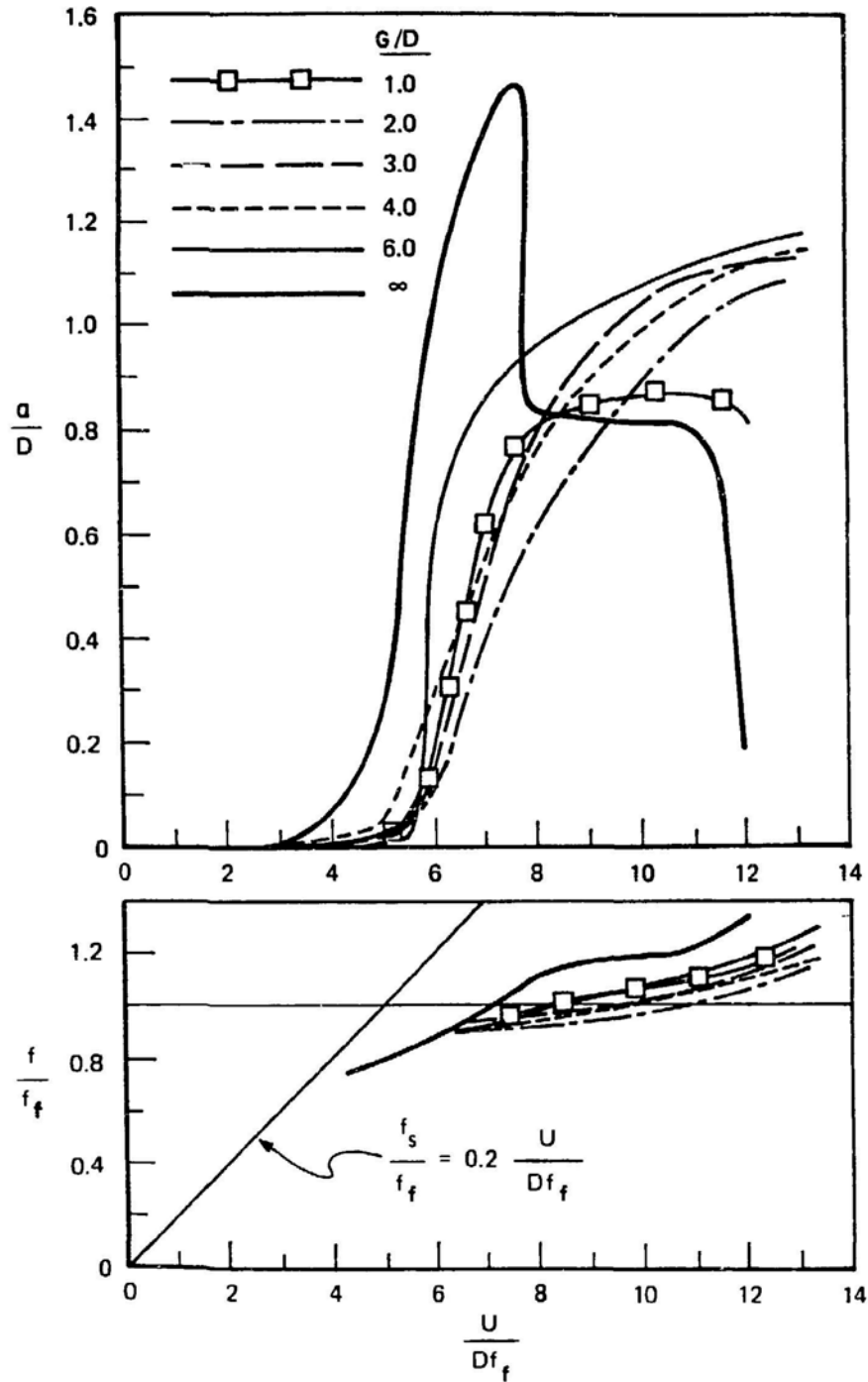


Fig. 7.30. Maximum Amplitude and Frequency Response vs. Reduced Flow Velocity of a Circular Cylinder for Different Gap to Diameter Ratios (from Tsahalis 1983, with permission--see Credits)

Most recently, in a series of experiments by Paidoussis and his colleagues (Paidoussis and Helleur 1979; Paidoussis et al. 1982a), several important observations were noted: (1) Beyond the onset of ovaling oscillations, r_s ceases to be an integer, f_{nm} remaining constant with U , while f_s increases in accordance with a constant Strouhal number St . (2) Ovaling oscillations can be excited even when a splitter plate is placed behind the shell. These observations show that the vortex shedding is not a necessary mechanism for ovaling oscillations, and that when there is a periodic wake, r_s is not necessarily an integer.

Figure 7.31 shows the response of cylindrical shells with $R = 38.1$ mm, $h = 0.48$ mm of different lengths. In general, more than one circumferential mode can be excited and the modes with respect to flow direction can change with flow speed.

Analytical modeling of the ovaling oscillations is far from complete. A quasi-static theory based on the superposition of the viscous mean flow and a potential flow associated with deformation of the shell is developed by Paidoussis et al. (1982b). The principal observed characteristics are qualitatively predicted by the theory, but the predicted critical flow velocity is too high by a factor of 1.6 to 5.

Based on the available data, it appears that vortex shedding and fluidelastic instability are the two main excitation mechanisms. In addition, there appears to be a significant interaction between the two mechanisms. More systematic studies are needed to clarify the matter.

7.13 CLOSING REMARKS

A single cylinder subjected to crossflow is one of the most extensively studied problems in the area of fluid mechanics. Nevertheless, the interaction of cylinder movement and flow field remains unsolved. Progress is being made in the characterization of flow field around an oscillating cylinder, numerical simulation of the flow field, and development of techniques to solve the coupling problem. Although complete analysis of the problem based on the fundamental principle of fluid dynamics and the theory of elasticity is still not possible, the gap between theory and experiment is getting closer.

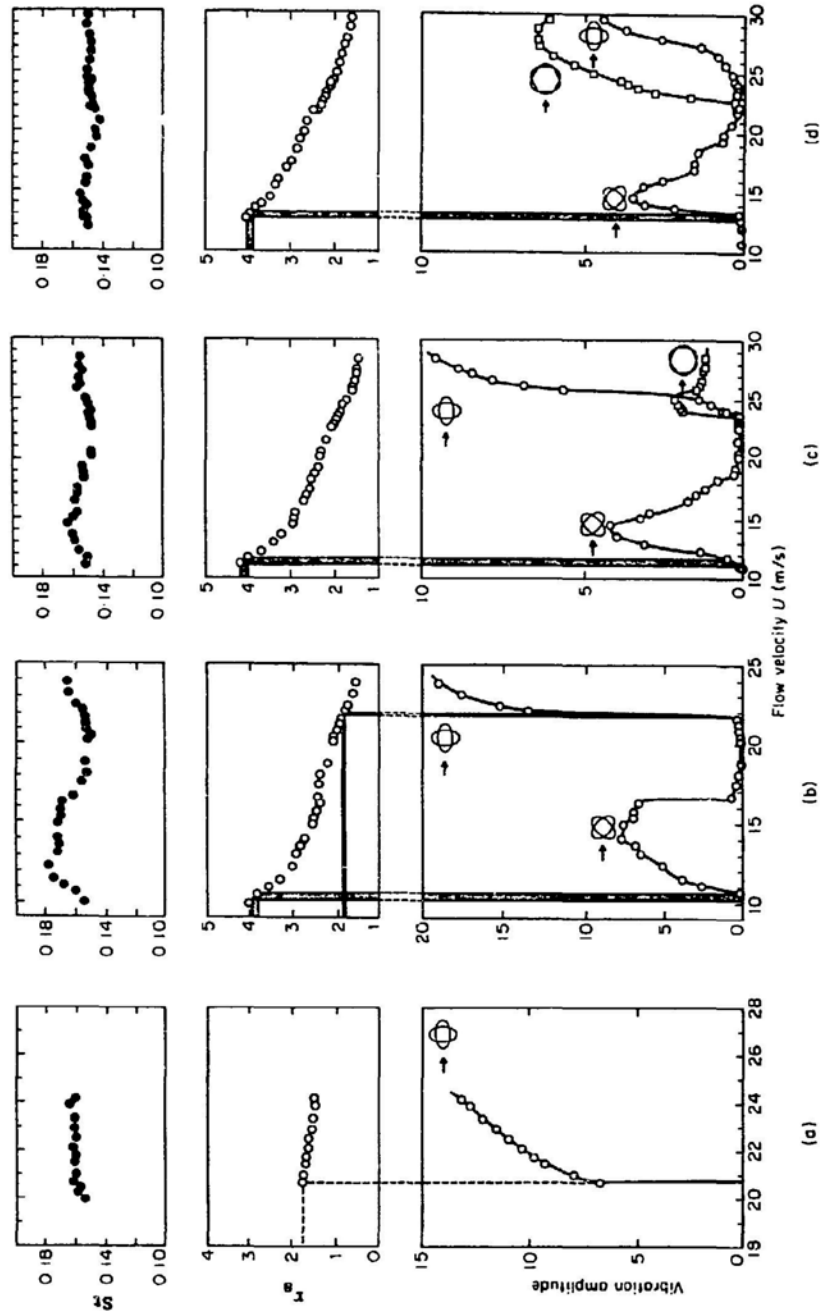


Fig. 7.31. Measured Vibration and Wake Characteristics of a Clamped-Free Shell in Crossflow: (a) $L = 479$ mm, (b) $L = 413$ mm, (c) $L = 362$ mm, (d) $L = 311$ mm (from Paidoussis et al. 1982a, with permission--see Credits)

REFERENCES--Sec. 7

- Achenbach, E. 1968. Distribution of Local Pressure and Skin Friction Around a Circular Cylinder in Cross Flow up to $R = 5 \times 10^6$. J. Fluid Mech. 34, 625-639.
- Achenbach, E. 1975. Total and Local Heat Transfer from a Smooth Circular Cylinder in Cross Flow at High Reynolds Number. Int. J. of Heat and Mass Transfer 18, 1387-1396.
- Angrilli, F., Bergamaschi, S., and Cossalter, V. 1982. Investigation of Wall Induced Modifications to Vortex Shedding from a Circular Cylinder. J. Fluids Eng. 104, 518-522.
- Bearman, P. W. 1969. On Vortex Shedding from a Circular Cylinder in the Critical Reynolds Number Regime. J. Fluid Mech. 37, 577-585.
- Bearman, P. W. 1984. Vortex Shedding from Oscillating Bluff Bodies. Ann. Rev. Fluid Mech. 16, 195-222.
- Bearman, P. W., and Currie, I. G. 1979. Pressure-Fluctuation Measurements on an Oscillating Circular Cylinder. J. Fluid Mech. 91, 661-677.
- Bearman, P. W., and Zdravkovich, M. M. 1978. Flow Around a Circular Cylinder Near a Plane Boundary. J. Fluid Mech. 89, 33-47.
- Berger, E., and Wille, R. 1972. Periodic Flow Phenomena. Ann. Rev. Fluid Mech. 4, 313-340.
- Bishop, R. E. D., and Hassan, A. Y. 1964. The Lift and Drag Forces on a Circular Cylinder in a Flowing Fluid. Proc. of the Royal Soc. Series A277, 51-75.
- Blevins, R. D., and Burton, T. E. 1976. Fluid Forces Induced by Vortex Shedding. J. Fluids Eng. 95, 19-24.
- Chen, S. S., and Jendrzejczyk, J. A. 1979. Dynamic Response of a Circular Cylinder Subjected to Liquid Cross Flow. J. Pressure Vessel Technol. 101, 106-112 (1979).
- Cheung, J. C. K., and Melbourne, W. H. 1983. Turbulence Effects on Some Aerodynamic Parameters of a Circular Cylinder at Supercritical Reynolds Numbers. J. Wind Eng. and Industrial Aerodynamics 14, 399-410.
- Dickey, W. L., and Woodruff, G. B. 1956. The Vibration of Steel Stacks. Trans. ASCE 121, 1054-1070.
- Di Silvio, G. 1969. Self-Controlled Vibration of Cylinder in Fluid Stream. ASCE J. Eng. Mech. Div. 95(EM2), 347-361.
- Dockstader, E. A., Swiger, W. F., and Ireland, E. 1956. Resonant Vibration of Steel Stacks. Trans. ASCE 121, 1088-1112.

- El-Baroudi, M. Y. 1960. Measurement of Two-Point Correlations of Velocity near a Circular Cylinder Shedding a Karman Vortex Street. University of Toronto, UTIAS, TN31.
- Farell, C. 1981. Flow Around Fixed Circular Cylinders: Fluctuating Loads. Proc. of ASCE, EM3, Paper No. 16330, 565-588.
- Farell, C., and Blessmann, J. 1983. On Critical Flow Around Smooth Circular Cylinders. J. Fluid Mech. 136, 375-391.
- Feng, C. L. 1968. The Measurement of Vortex-Induced Effects in Flow Past Stationary and Oscillating Circular and D-Section Cylinders. MASC Thesis, University of British Columbia, Vancouver.
- Funakawa, M. 1969. The Vibration of a Cylinder Caused by a Wake Force in a Flow. Bulletin of the JSME 12(53), 1003-1010.
- Gerlach, C. R., and Dodge, F. T. 1970. An Engineering Approach to Tube Flow-Induced Vibrations. Proc. Conf. on Flow-Induced Vibrations in Reactor System Components, pp. 205-225, Argonne National Laboratory.
- Griffin, O. M. 1980. OTEC Cold Water Pipe Design for Problems Caused by Vortex-Excited Oscillations. NRL Memorandum Report 4157, Naval Research Laboratory, Washington, D.C.
- Griffin, O. M. 1981. Universal Similarity in the Wakes of Stationary and Vibrating Bluff Structures. J. Fluids Eng. 103, 52-58.
- Griffin, O. M. 1982. Vortex Streets and Patterns. Mechanical Engineering, March 1982, 56-61.
- Griffin, O. M., Skop, R. A., and Ramberg, S. E. 1975. The Resonant Vortex-Excited Vibrations of Structures and Cable Systems. Offshore Technology Conference, Paper OTC-2319, Houston, Texas.
- Güven, O., Farell, C., and Patel, V. C. 1980. Surface Roughness Effects on the Mean Flow Past Circular Cylinders. J. Fluid Mech. 98, 673-701.
- Hardwick, J. D., and Wootton, L. R. 1973. The Use of Model and Full-Scale Investigations on Marine Structures. Proc. of the Int. Sym. on Vib. Prob. in Industry, Paper No. 127.
- Hartlen, R. T., and Currie, I. G. 1970. Lift-Oscillator Model of Vortex-Induced Vibration. ASCE, J. Eng. Mech. Div. 96(EM5), 577-591.
- Humphreys, J. S. 1960. On a Circular Cylinder in a Steady Wind at Transition Reynolds Numbers. J. Fluid Mech. 9, 603-612.
- Iwan, W. D., and Blevins, R. D. 1974. A Model for Vortex Induced Oscillation of Structures. J. Appl. Mech., Trans. ASME 41, 581-586.
- James, W. D., Paris, S. W., and Malcolm, G. N. 1980. Study of Viscous Crossflow Effects on Circular Cylinders at High Reynolds Numbers. AIAA Journal 18(9), 1066-1072.

- Jendrzejczyk, J. A., and Chen, S. S. 1985. Fluid Forces on Two Circular Cylinders in Crossflow. Argonne National Lab. ANL-85-35.
- Johns, D. J., and Sharma, C. B. 1974. On the Mechanism of Wind-Excited Ovaling Vibrations of Thin Circular Cylindrical Shells. In Flow-Induced Structural Vibrations, Ed. by E. Naudascher, Springer-Verlag, Berlin, pp. 650-662.
- King, R. 1974. Vortex-Excited Oscillations of a Circular Cylinder in Steady Currents. Offshore Technology Conference Preprint OTC 1948.
- King, R. 1977a. A Review of Vortex Shedding Research and Its Application. Ocean Engineering 4, 141-171.
- King, R. 1977b. Vortex Excited Oscillations of Yawed Circular Cylinders. J. Fluids Eng. 99, 495-502.
- King, R., and Johns, D. J. 1976. Wake Interaction Experiments with Two Flexible Circular Cylinders in Flowing Water. J. Sound Vib. 45(2), 259-283.
- King, R., Prosser, M. J., and Johns, D. J. 1973. On Vortex Excitation of Model Piles in Water. J. Sound Vib. 29, 169-188.
- Ko, S. C., and Graf, W. H. 1972. Drag Coefficient of Cylinders in Turbulent Flow. J. of the Hydraulics Division, Proc. ASCE, HY5, 897-912.
- Koopmann, G. H. 1967. The Vortex Wakes of Vibrating Cylinders at Low Reynolds Numbers. J. Fluid Mech. 28, 501-512.
- Landl, R. 1975. A Mathematical Model for Vortex-Excited Vibrations of Bluff Bodies. J. Sound Vib. 42(2), 219-234.
- Lienhard, J. H. 1966. Synopsis of Lift, Drag and Vortex Frequency Data for Rigid Circular Cylinders. Washington State University, College of Eng. Research Division Bulletin 300.
- Mair, W. A., and Maull, O. J. 1971. Bluff Bodies and Vortex Shedding - A Report on Euromech 17. J. Fluid Mech. 45(Part 2), 209-224.
- Marris, A. W. 1964. A Review on Vortex Streets, Periodic Wakes and Induced Vibration Phenomena. J. Basic Eng. 86, 185-196.
- Martin, W. W., Currie, I. G., and Naudascher, E. 1981. Streamwise Oscillations of Cylinders. ASCE J. Eng. Mech. Div. 107(3), 589-607.
- McGregor, D. M. 1957. An Experimental Investigation of the Oscillating Pressures on a Circular Cylinder in a Fluid Stream. UTIAS Tech. Note 14.
- Miller, B. L. 1976. The Hydrodynamic Drag of Roughened Circular Cylinders. Paper 9, Roy. Instn. Nav. Arch., Spring Meeting.

- Morkovin, M. V. 1964. Flow Around Circular Cylinders. A Kaleidoscope of Challenging Fluid Phenomena. ASME Symposium on Fully Separated Flows, Philadelphia, Pa., 102-118.
- Mulcahy, T. M. 1982. Design Guide for Single Circular Cylinder in Turbulent Crossflow. ANL-CT-82-7, Argonne National Laboratory, Argonne, IL.
- Nakamura, Y. 1976. Some Research on Aeroelastic Instabilities of Bluff Structural Elements. Proc. 4th Int. Conf. on Wind Effects on Buildings and Structures, Heathrow (UK), 359-368.
- Paidoussis, M. P., and Helleur, C. 1979. On Ovaling Oscillations of Cylindrical Shells in Cross-Flow. J. Sound Vib. 63, 527-542.
- Paidoussis, M. P., Price, S. J., and Suen, H.-C. 1982a. Ovaling Oscillations of Cantilevered and Clamped-Clamped Cylindrical Shells in Cross Flow: An Experimental Study. J. Sound Vib. 83, 533-553.
- Paidoussis, M. P., Price, S. J., and Suen, H.-C. 1982b. An Analytical Model for Ovaling Oscillation of Clamped-Clamped Cylindrical Shells in Cross Flow. J. Sound Vib. 83, 555-572.
- Parkinson, G. V. 1974. Mathematical Models of Flow-Induced Vibration of Bluff Bodies. In Flow-Induced Structural Vibrations, Ed. by E. Naudascher, Springer-Verlag, pp. 81-127.
- Perry, A. E., Chong, M. S., and Lim, T. T. 1982. The Vortex-Shedding Process Behind Two-Dimensional Bluff Bodies. J. Fluid Mech. 116, 77-90.
- Ramamurthy, A. S., and Ng, C. P. 1973. Effect of Blockage on Steady Force Coefficients. Proc. ASCE EM4, 755-772.
- Ramberg, S. E. 1983. The Effects of Yaw and Finite Length Upon the Vortex Wakes of Stationary and Vibrating Circular Cylinders. J. Fluid Mech. 128, 81-107.
- Ramberg, S. E., and Griffin, O. M. 1976. Velocity Correlation and Vortex Spacing in the Wake of a Vibrating Cable. Trans. ASME, J. Fluids Eng. 98, 10-18.
- Ribeiro, S. V. G. 1983. Mechanisms of Flow-Induced Vibrations of Circular Cylinders in Crossflow. Proc. 7th Int. Conf. on Structural Mechanics in Reactor Technology, 1983, Paper No. B5/7.
- Richter, A., and Naudascher, E. 1976. Fluctuating Forces on a Rigid Circular Cylinder in Confined Flow. J. Fluid Mech. 78, 561-576.
- Roshko, A. 1961. Experiments on the Flow Past a Circular Cylinder at Very High Reynolds Number. J. Fluid Mech. 10, 345-356.
- Sachs, P. 1978. Wind Forces in Engineering. Pergamon Press, Inc., New York, NY.

- Sainsbury, R. N., and King, D. 1971. The Flow Induced Oscillation of Marine Structures. Proc. Inst. Civil Engrs. 49, 269-302.
- Sarpkaya, T. 1978. Fluid Forces on Oscillating Cylinders. J. Waterway, Port, Coastal and Ocean Div. ASCE 104, 275-290.
- Sarpkaya, T. 1979a. Vortex-Induced Oscillations - A Selective Review. J. Appl. Mech. 46, 241-258.
- Sarpkaya, T. 1979b. Effect of Surface Roughness on the Transverse Oscillations of a Circular Cylinder. Naval Postgraduate School Report NRS-69SL79085-IR.
- Schewe, G. 1983. On the Force Fluctuations Acting on a Circular Cylinder in Crossflow from Subcritical up to Transcritical Reynolds Numbers. J. Fluid Mech. 133, 265-285.
- Shin, Y. S., and Wambsganss, M. W. 1977. Flow-Induced Vibration in LMFBR Steam Generators: A State-of-the-Art Review. Nucl. Eng. Des. 40, 235-284.
- Skop, R. A., and Griffin, O. M. 1973. A Model for the Vortex-Excited Resonant Response of Bluff Cylinders. J. Sound Vib. 27(2), 225-233.
- Staubli, T. 1983. Calculation of the Vibration of an Elastically Mounted Cylinder Using Experimental Data from Forced Oscillation. J. Fluids Eng. 105, 225-229.
- Suzuki, T., and Hirano, T. 1979. Effects of the Channel Height on the Flow Past a Circular Cylinder. Bulletin of the JSME 22(167), 661-668.
- Szechenyi, E. 1975. Supercritical Reynolds Number Simulation for Two-Dimensional Flow Over Circular Cylinders. J. Fluid Mech. 70, 523-542.
- Tsahalis, D. T. 1983. The Effect of Seabottom Proximity of the Vortex-Induced Vibrations and Fatigue Life of Offshore Pipelines. J. Energy Resources Technol. 105, 464-468.
- Toebe, G. H. 1969. The Unsteady Flow and Wake Near an Oscillating Cylinder. Trans. ASME J. Basic Eng. 91, 831-838.
- Wootton, L. R., Warner, M. H., and Cooper, D. H. 1974. Some Aspects of the Oscillations of Full-Scale Pipes. In Flow-Induced Structural Vibrations, Ed. by E. Naudascher, Springer-Verlag, Berlin, pp. 587-601.
- Zdravkovich, M. M. 1981. Modification of Vortex Shedding in the Synchronization Range. ASME Paper 81-WA/FE-25.

8. AN ARRAY OF CIRCULAR CYLINDERS IN CROSSFLOW

8.1 INTRODUCTION

When a fluid flows across a cylinder array, a fraction of the fluid energy is transmitted to the cylinder, resulting in cylinder vibration. Cylinder vibrations resulting from crossflow generally are much more severe than vibrations resulting from axial flow. Crossflow vibrations are caused by one or more of the following mechanisms:

- **Turbulent Excitation:** In a cylinder array, there exist random noises, including turbulent pressure fluctuations and far-field flow noises with some or little coherence; these randomly varying pressures on the surfaces of the cylinders generally produce relatively low-amplitude cylinder vibration.

- **Vortex-Induced Vibration:** These vibrations are induced by periodic vortex shedding from cylinders. Within the cylinder array, the regular vortex shedding of the first few rows becomes disorganized and turbulent. Although the vortex shedding process can be modified by cylinder motions and is synchronized with cylinder oscillations, it is the vortex shedding that initiates cylinder vibration.

- **Fluidelastic Instability:** At a certain flow velocity, fluid energy may feed into cylinders, resulting in large cylinder vibrations. The dominant fluid forces are the motion-dependent fluid forces. Severe damage can result in a short period of time.

- **Acoustic Excitation:** Acoustic excitation causes cylinder vibration, generally normal to flow direction and cylinder axis. When the natural frequency of vortex shedding at a particular flowrate coincides with the acoustic frequencies, two systems (fluid flow and acoustic field) are coupled and reinforce each other. The worst case is that in which the acoustic frequency, the cylinder frequency, and the vortex-shedding frequency are the same.

Typical response curves of a cylinder array in crossflow are sketched in Fig. 8.1 for different conditions.

At low U_r (Fig. 8.1a), turbulent buffeting is dominant; when U_r is increased to a critical value, dynamic instability occurs. In a certain range of U_r , vortex excitation is dominant as shown in Fig. 8.1b. The cylinder array becomes dynamically unstable for large U_r , and in other regions the response is attributed to turbulent buffeting. The conditions represented in Fig. 8.1c are similar to those in Fig. 8.1a except that instability occurs at a much smaller U_r .

In this chapter, turbulent buffeting, vortex shedding, and acoustic excitation are discussed. Fluidelastic instability is discussed in Chapter 10.

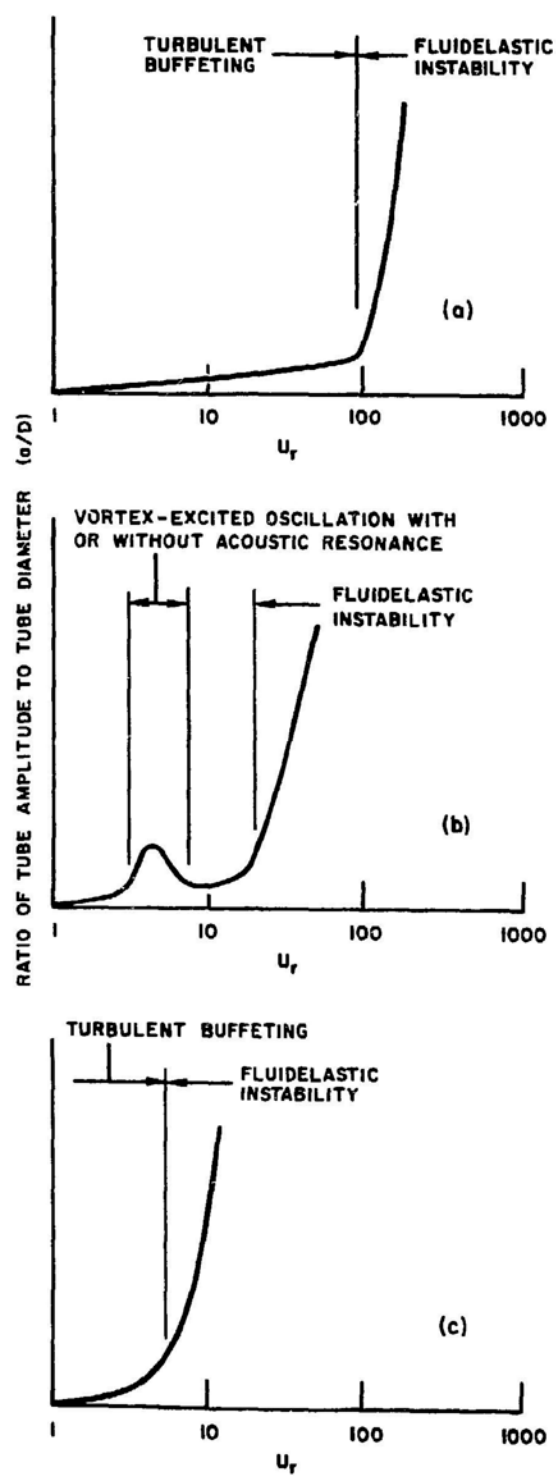


Fig. 8.1. Typical Response Curves of a Cylinder Array in Crossflow

8.2 FLOW REGIMES

Flow patterns across cylinder arrays depend on cylinder arrangement as well as other parameters. Cylinder spacing is an important parameter. Detailed classification of flow patterns remains a subject of current research. Based on limited data (Ishigai et al. 1973; Chen 1977), flow patterns for in-line and staggered cylinder arrays can be classified in five regimes, as shown in Fig. 8.2:

- Pattern A: All cylinders shed Karman vortices.
- Pattern B: Jet swing associated with Karman vortex shedding.
- Pattern C: The free shear layers of the front cylinder attach to the downstream cylinder and thus Karman vortices cannot be formed.
- Pattern D: Jet deflection.
- Pattern E: Karman vortex streets which are the same as those shed by isolated cylinders.

The flow pattern is the same within a range of cylinder pitches, and an abrupt change can be observed at the boundary of the cylinder spacing separating different regimes. The border lines dividing the flow pattern on Fig. 8.2 should not be considered rigorously fixed but they are influenced by Re and other parameters.

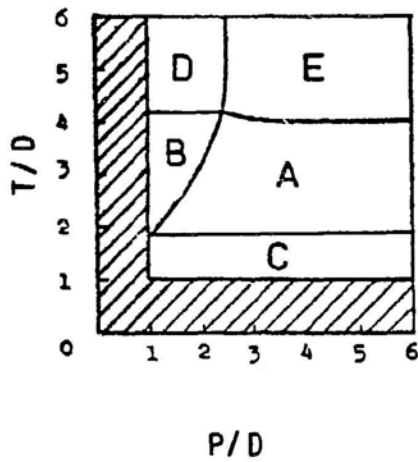
8.3 VORTEX SHEDDING FREQUENCY

Depending on cylinder spacings, as well as other system parameters, vortex shedding may or may not exist in a cylinder array. Early studies on vibration of cylinder arrays proceeded on the assumption that vortex shedding was the dominant mechanism. Therefore the main objective was to determine the vortex shedding frequency. Unfortunately, the precise determination of vortex shedding in a cylinder array proved complicated, for the following reasons:

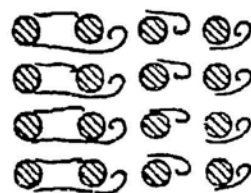
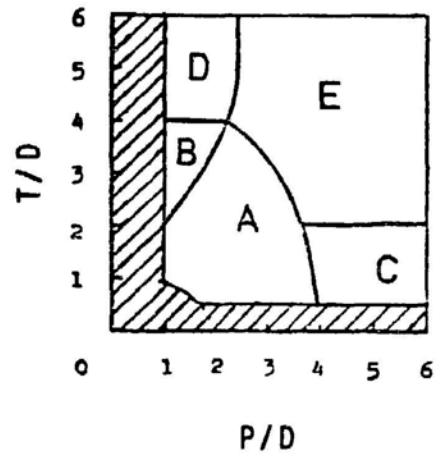
- The flow field across a cylinder array is not as easy to measure as flow across a single cylinder.
- In a test section, acoustic resonance can interfere with vortex shedding.
- Other flow parameters such as turbulence and Reynolds number affect the Strouhal number.
- Some of the vortex shedding frequencies were determined from cylinder response.

Even at subcritical Reynolds numbers, it is not possible to give a precise value of Strouhal number for each cylinder arrangement. However, based on the available experimental data, Strouhal numbers have been compiled by several investigators (Fitz-Hugh 1973; Chen 1968). Figures 8.3 and 8.4 show the Strouhal numbers compiled by Fitz-Hugh. For cylinder arrays, the

(a) IN-LINE ARRAY



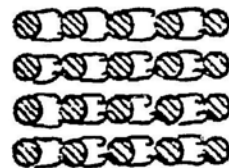
(b) STAGGERED ARRAY



Pattern A



Pattern B



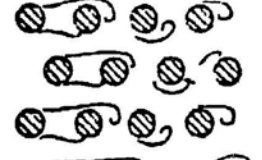
Pattern C



Pattern A



Pattern B



Pattern C

Fig. 8.2. Flow Patterns for In-Line and Staggered Arrays
(from Ishigai et al 1973, with permission--see Credits)

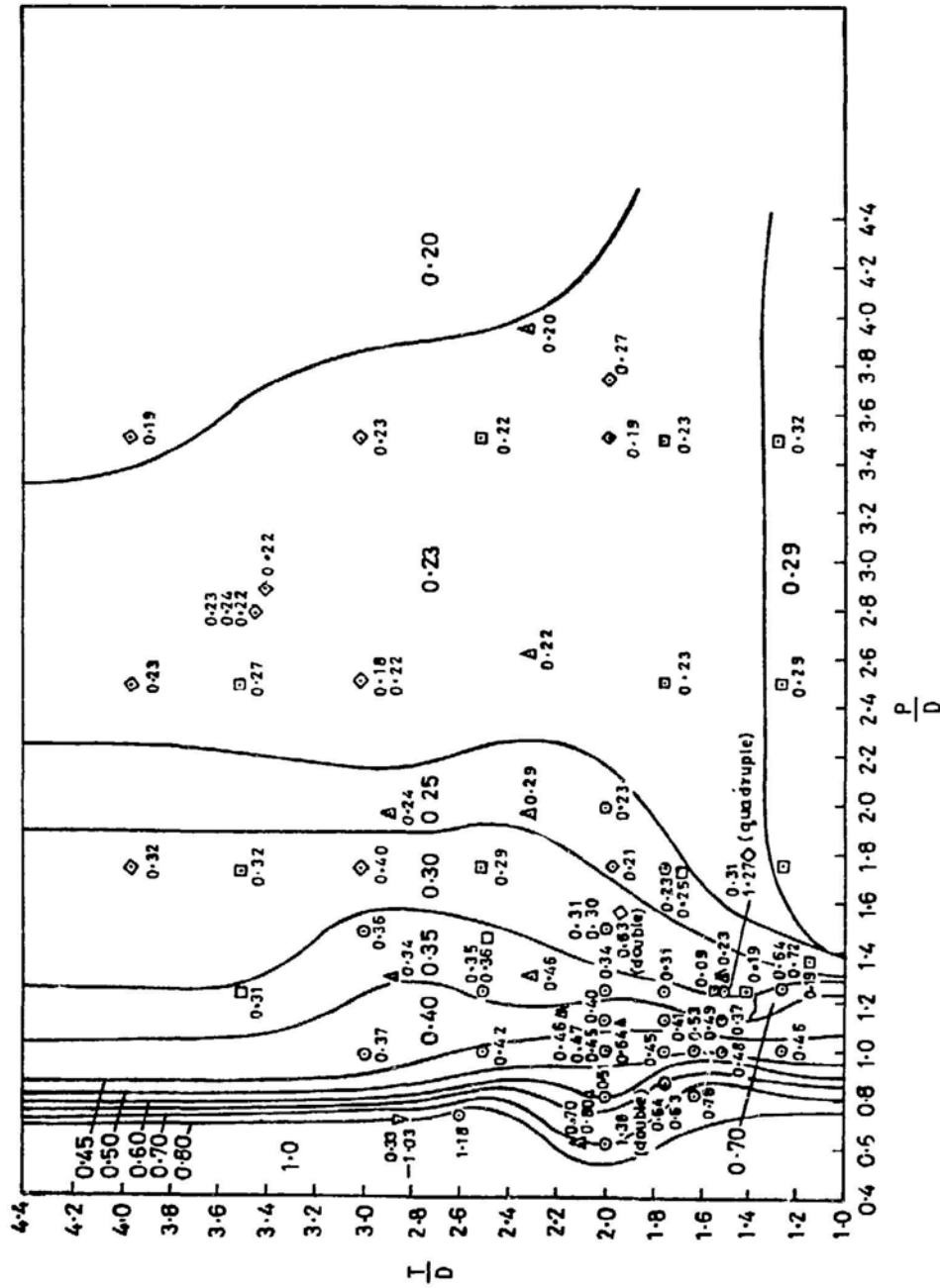


Fig. 8.3. Strouhal Number for In-Line Arrays (from Fitz-Hugh 1973, with permission--see Credits)

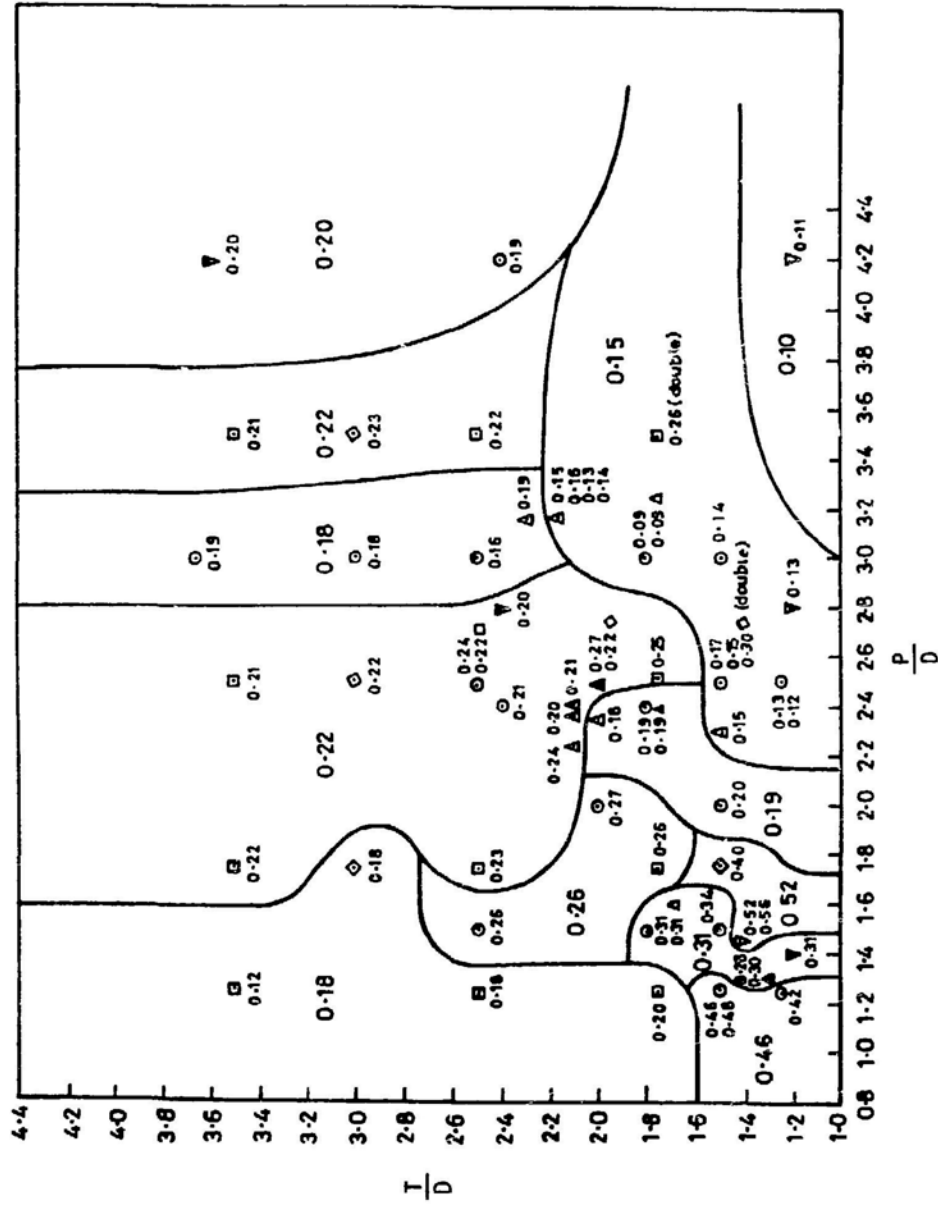


Fig. 8.4. Strouhal Number for Staggered Arrays (from Fitz-Hugh 1973, with permission--see Credits)

Strouhal number is defined the same way as that for a single cylinder; however, the flow velocity is based on the gap velocity:

$$U = \frac{U_{\text{approach velocity}}}{1 - D/T} \quad (8.1)$$

It should be pointed out that, although the Strouhal numbers given in Figs. 8.3 and 8.4 are widely used, some of the data are contradictory with results from elsewhere. A more detailed examination of the data to establish more reliable Strouhal numbers in cylinder arrays is needed.

8.4 PRESSURE AND FLOW VELOCITY DISTRIBUTIONS

Pressure distribution around a cylinder in array is very complex, and depends on the incoming-flow properties and cylinder arrangements. Very limited data are available. However, these data are important in understanding the flow field as well as obtaining the necessary force coefficients for response calculations.

In a wind tunnel, Zdravkovich and Namork (1979) reported the fluctuating and time-average pressure distribution around a tube located in different rows of a triangular array having a transverse pitch ratio of 1.375 (see Fig. 8.5) for $Re = 1.1 \times 10^5$. The plots are the measured differences between the local pressure on the tube and free-stream static pressure. The steady pressure distributions of the first three rows were replotted (Fig. 8.6) with a common start at the stagnation point. The actual pressure difference between the three stagnation points and the free stream was not the same due to a significant pressure drop along the tube bank.

It is evident in the first two rows of the cylinder array that both pressure distributions are distinctly different. The differences in pressure distribution are attributed to the changes of the structure of the interstitial flow: (1) The cylinder in the first row is subjected to interference by the adjacent side cylinders and low-turbulence free-stream flow. A steep pressure gradient around the upstream part of the cylinder is accompanied by low-intensity pressure fluctuations. (2) The cylinder in the second row is affected not only by the adjacent side cylinders but also by the wide wakes produced behind the first row of cylinders. The result is a steeper pressure gradient than in the first row and a huge increase of pressure fluctuations around both sides of the cylinder. The wake behind the cylinder in the second row is narrow. (3) The cylinders in the third and subsequent rows are exposed to a highly turbulent interstitial flow, which produces a sharp increase in pressure fluctuations around the stagnation point. The pressure gradient is less steep than in the second row, owing to the narrower wake behind the second row. The pressure fluctuations around the sides of the cylinder are also markedly reduced. The latter, however, gradually increases and reaches a pronounced peak around the separation point in the last row.

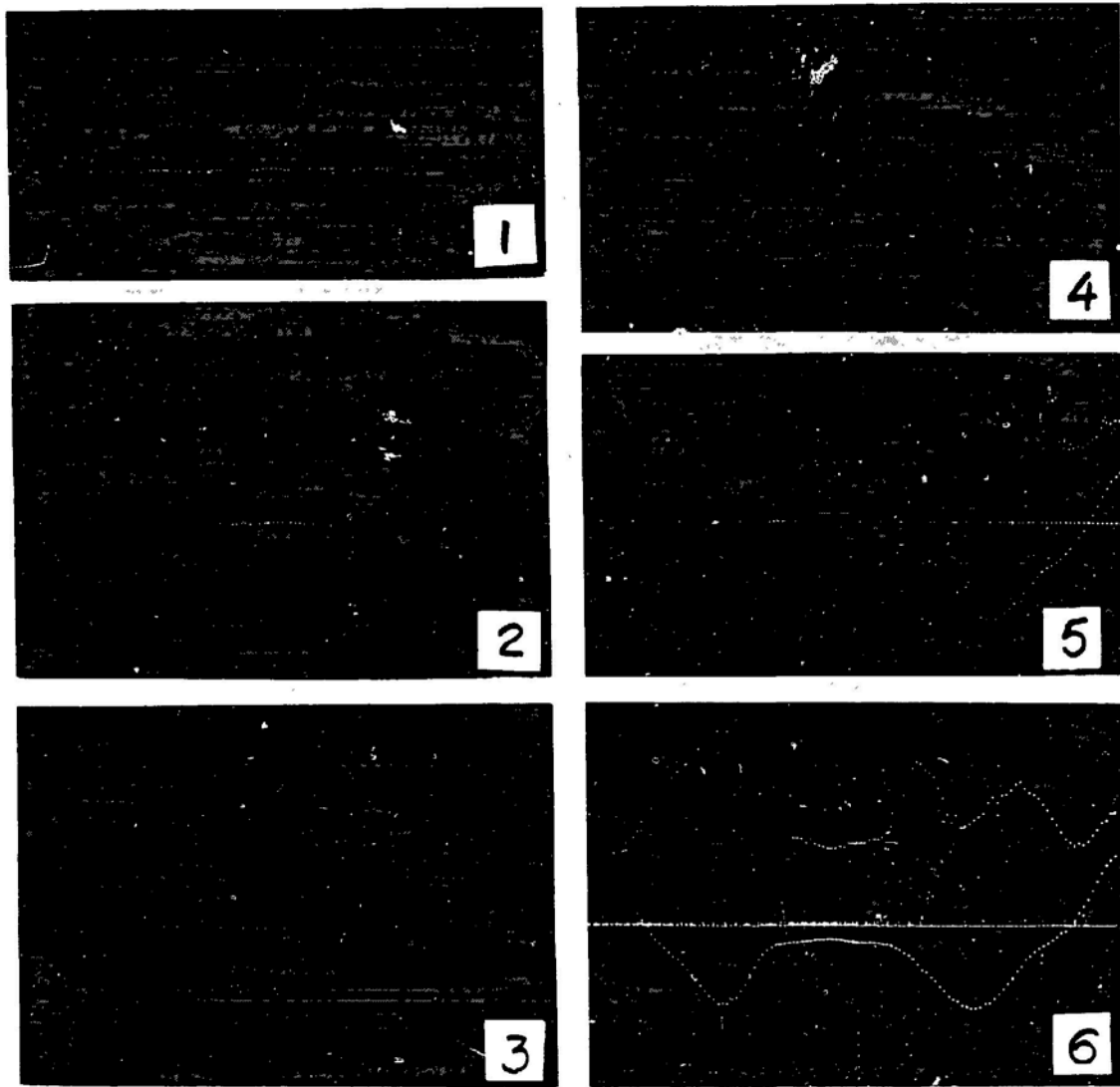


Fig. 8.5. Fluctuating (Top Curves) and Time-Average (Bottom Curves) Pressure Distribution Around the Tubes in Rows 1-6. Vertical scale arbitrary; horizontal scale 0-360° (one square = 36°) (from Zdravkovich and Namork 1979, with permission--see Credits)

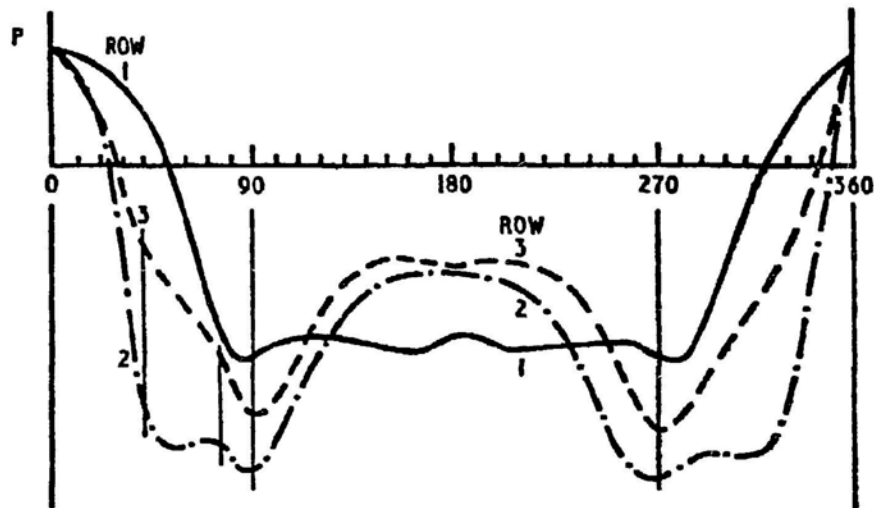


Fig. 8.6. Time-Average Pressure Distribution in First Three Rows
(from Zdravkovich and Namork 1979, with permission--
see Credits)

Figure 8.7(a) shows measured velocity and turbulence profiles across one pitch length behind a cylinder located in the middle. Very low velocity and high turbulence intensity were found within the wake. The velocity peaks were not found behind the gaps but did appear adjacent to separated shear layers. The minimum velocity behind the gap center was caused in the vicinity of the stagnation region in front of the cylinders in the second row. The shear layers did not affect the turbulence intensity, which remained low and constant.

Figure 8.7(b) shows velocity and turbulence profiles between the second and third rows. Again, the low velocity and high turbulence showed the position and width of the wake. The wake was narrower than that found behind the first row. Both velocity peaks were significantly lower compared with the corresponding peaks behind the first row of cylinders. This reduction was in direct proportion to the narrowing of the wake. The two time-average velocity peaks coincided with the minima of intensity of turbulence. The minimum velocity behind the gap center was coupled with the maximum turbulence intensity so that one profile appeared as the mirror image of the other. This feature remained typical for all subsequent rows.

Other measurements (Morsy 1975; Aiba et al. 1982a) for staggered arrays show similar results. However, for in-line arrays, the pressure distribution around the circumference is frequently asymmetric. This asymmetry originates from a deflection of the flow through the array (Aiba 1982b; Heinecke and Mohr 1982).

The turbulence intensity depends on the location of the cylinder. Figure 8.8 shows a plot of turbulence vs. depth into the cylinder array (Sandifer and Bailey 1984). The turbulence was measured in the center of the gap of a staggered array with a pitch-to-diameter ratio of 1.5. The turbulence intensity starts at a low level at the entrance to the array (about 4% in Fig. 8.8) and gradually increases to about 23% in the middle of the array. At a particular location of a cylinder array the turbulence intensity is fairly constant with increasing gap velocity. In addition, the power spectral of turbulence excitation does not change significantly through the cylinder array at a particular gap velocity.

8.5 FLUID EXCITATION FORCE COEFFICIENTS

Fluid excitation force coefficients are very limited for general cylinder arrays. There have been few systematic studies to measure those coefficients. In addition, these coefficients depend on cylinder arrangement, Reynolds number, upstream turbulence, etc.

The fluctuating lift coefficients for various cylinder arrays by Chen (1972) and Pettigrew and Ko (1980), for application to heat exchanger tubes, as given are presented in Tables 8.1 and 8.2. Some of the coefficients are

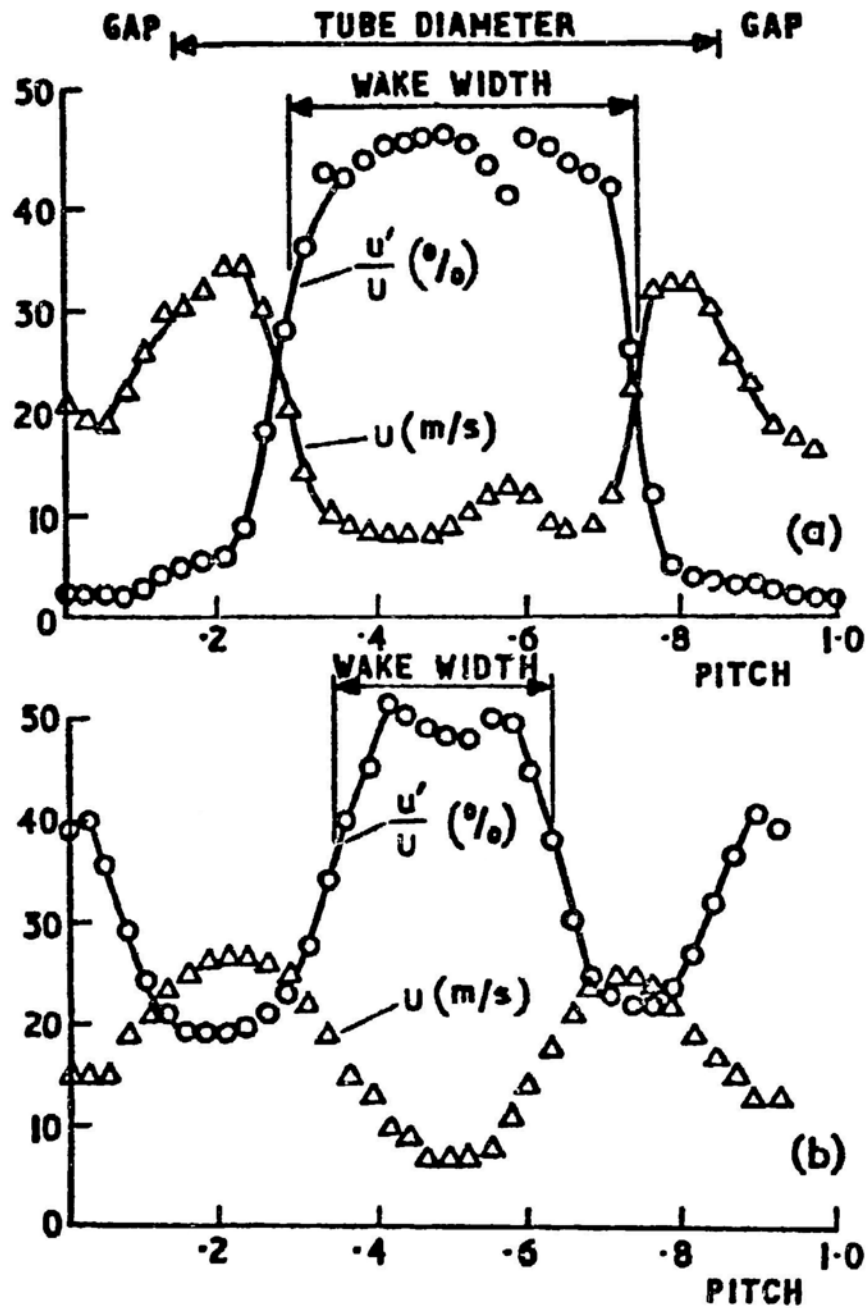


Fig. 8.7. Velocity and Turbulence Profiles Between Rows Along One Pitch (a) Behind First Row and (b) Behind Second Row (from Zdravkovich and Namork 1979, with permission--see Credits)

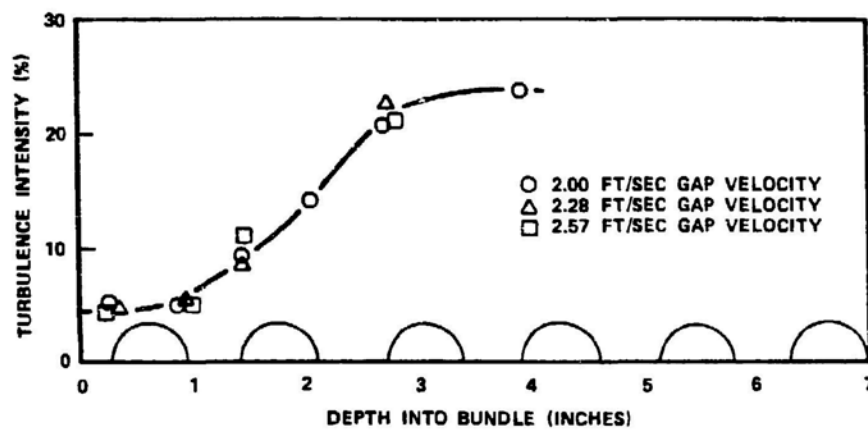


Fig. 8.8. Turbulence Intensity vs. Depth Into Array (from Sandifer and Bailey 1984, with permission--see Credits)

Table 8.1. Fluctuating Lift Coefficient (C_L') of Cylinder Arrays
(from Chen 1972, with permission--see Credits)

Cylinder Arrangement	Transverse Ratio (T/D)	Longitudinal Ratio (P/D)	Reynolds Number $\times 10^{-3}$	C_L'
In-line	1.2	1.4	10.8	0.035
	1.42	1.46	1.36	0.078
	2.4	1.4	15.4	0.035
	1.2	2.8	23.3	0.064
	2.4	2.8	14.3	0.358
	1.2	4.2	26.6	0.038
	2.4	4.2	15.8	0.295
	3.6	4.2	14.0	0.445
Staggered	1.46	2.84	0.79	0.63
	2.31	3.94	20.2	0.58
	4.62	2.63	42.5	0.87

Table 8.2. Fluctuating Lift Coefficient (C_L') and Strouhal Numbers
(from Pettigrew and Ko 1980, with permission--see Credits)

Cylinder Array	P/D	Cylinder Location	Periodic Wake Shedding Resonance			
			In Flow Direction*		Normal†	
			$St = \frac{fD}{U}$	C_L' (RMS)	$St = \frac{fD}{U}$	C_L' (RMS)
Normal triangle (30°)	1.23	1st row	None‡		None	
		2nd row	None		None	
		Interior	None		None	
		Downstream	None		None	
	1.33	1st row	None		0.44	0.046
		2nd row	0.42/0.30	0.020/(0.006)	0.45	0.011
		Interior	None			
		Downstream	0.48			
	1.36	1st row	None		0.67	0.064
		2nd row	0.45	0.023	None	
		Interior	0.61	0.008	0.61	0.007
		Downstream	0.67	(0.023)?	None	
	1.54	1st row	0.36	(0.018)	None	
		2nd row	0.37	(0.011)	None	
		Interior	None		None	
		Downstream	None		None	
	1.57	1st Row	0.57	0.027	0.42	0.019
		2nd Row	0.55	0.028	0.42	0.016
		Interior	None		None	
		Downstream	None		None	
Parallel triangle (60°)	1.23	1st row				
		2nd row	0.42	(0.025)	0.44	0.064
		Interior	0.54/0.44	0.033/0.015	0.49	0.020
		Downstream	0.46	0.016	0.46	0.016
	1.33	1st row			None	
		2nd row				
		Interior	None		None	
		Downstream	None		None	
	1.36	1st row	None		None	
		2nd row	None		0.48	(0.012)
		Interior	None		None	
		Downstream	None		None	

	1.54	1st row	0.45	0.033	0.45	(0.018)
		2nd row	0.45	(0.030)		
		Interior				
		Downstream	None		None	
	1.57	1st row	0.42	0.057	0.40	(0.021)
		2nd row	0.52	0.023	None	
		Interior	0.52	(0.006)	0.52	(0.007)
		Downstream	0.45	0.014	0.45	0.014
Normal square (90°)	1.30	1st row	None		None	
		2nd row	None		None	
		Interior	None		None	
		Downstream	None		None	
	1.47	1st row	0.48	0.048	0.63	0.025
		2nd row	0.45	0.047	0.63	0.018
		Interior	0.55	0.031	0.61/0.41	0.017/(0.012)
		Downstream	0.42	0.025	None	
Rotated square (45°)	1.30	1st row	0.43	0.007	None	
		2nd row				
		Interior	0.41	0.006	None	
		Downstream	None		None	
	1.50	1st Row			0.37	0.035
		2nd Row	None		None	
		Interior	None		None	
		Downstream	0.34	0.019	None	

* Resonant vibration in flow direction.

† Resonant vibration normal to flow direction.

‡ "None" indicates that no resonance was observed; a blank space indicates that the tests were not done or were inconclusive.

? Parenthesis indicate less prominent resonance peak (i.e., resonance peak < 2 x random turbulence response).

deduced from tube response, not from force measurements. Note that resonance is more likely and more severe in upstream tubes and highly nonuniform flow or gross turbulence can prevent the formation of correlated periodic wake shedding.

Fluctuating fluid force coefficients C_L' and C_D' for equilateral staggered arrays and square pitch in-line arrays were measured by Savkar (1983) for different pitch ratios ($T/D = 1.2, 1.5$, and 1.71) and upstream turbulence characteristics ($u'/U = 0.5\%$ and 8.5%). The flow patterns between the two types of arrays were considerably different. Flow through the staggered array followed a zig-zag path with the wakes more or less closed, while flow through the in-line arrays was channeled in the open lanes.

Arrays of four rows deep were employed in the tests by Savkar (1983). Typical RMS C_L' for equilateral staggered arrays are given in Fig. 8.9 for two different turbulence intensities (0.5% for no grid and 8.5% for a 154.22 mm grid). Several features can be noted: (1) For $T/D = 1.5$, the progression of the measured C_L' as a function of the row is more or less monotonic. However, this is not necessarily valid for other arrays. (2) The flows can change drastically and result in a large variation of C_L' . For example, at $Re = 8 \times 10^4$, there is a sudden drop in C_L' for the second-row cylinder, apparently as a result of early flow transition.

The order of magnitude of the lift and drag coefficients for the in-line arrays is comparable to that for the staggered arrays but the basic trends are somewhat different. Figures 8.10 and 8.11 show the RMS C_L' and C_D' for $T/D = 1.2$. The data show a decrease in the coefficients with increasing Re in uniform flow and turbulent flow. In general, the force coefficients for the trailing rows are higher than those for the leading rows.

The steady drag and lift forces acting on a cylinder in the middle of an array were obtained using the measured pressure for several different arrangements by Zdravkovich et al. (1976). The transverse pitch was 1.66 , and the coefficients were based on the free stream velocity. The values are presented in Table 8.3.

Steady drag coefficients also were measured by Morsy (1975) for a staggered array (30°) with a pitch ratio of 1.5 in a wind tunnel. Figure 8.12 shows the form drag coefficient at different Reynolds numbers for cylinders in different rows. In general, the drag coefficient decreased with Reynolds number. The first row offered the highest form resistance to flow. This is expected, due to the severe circumferential pressure gradients measured on this row of cylinders and the big difference between the pressures on the front and rear halves of its cylinders. The drag coefficient for the first row of cylinders is about 4.5 times the values recorded for a single cylinder in crossflow.

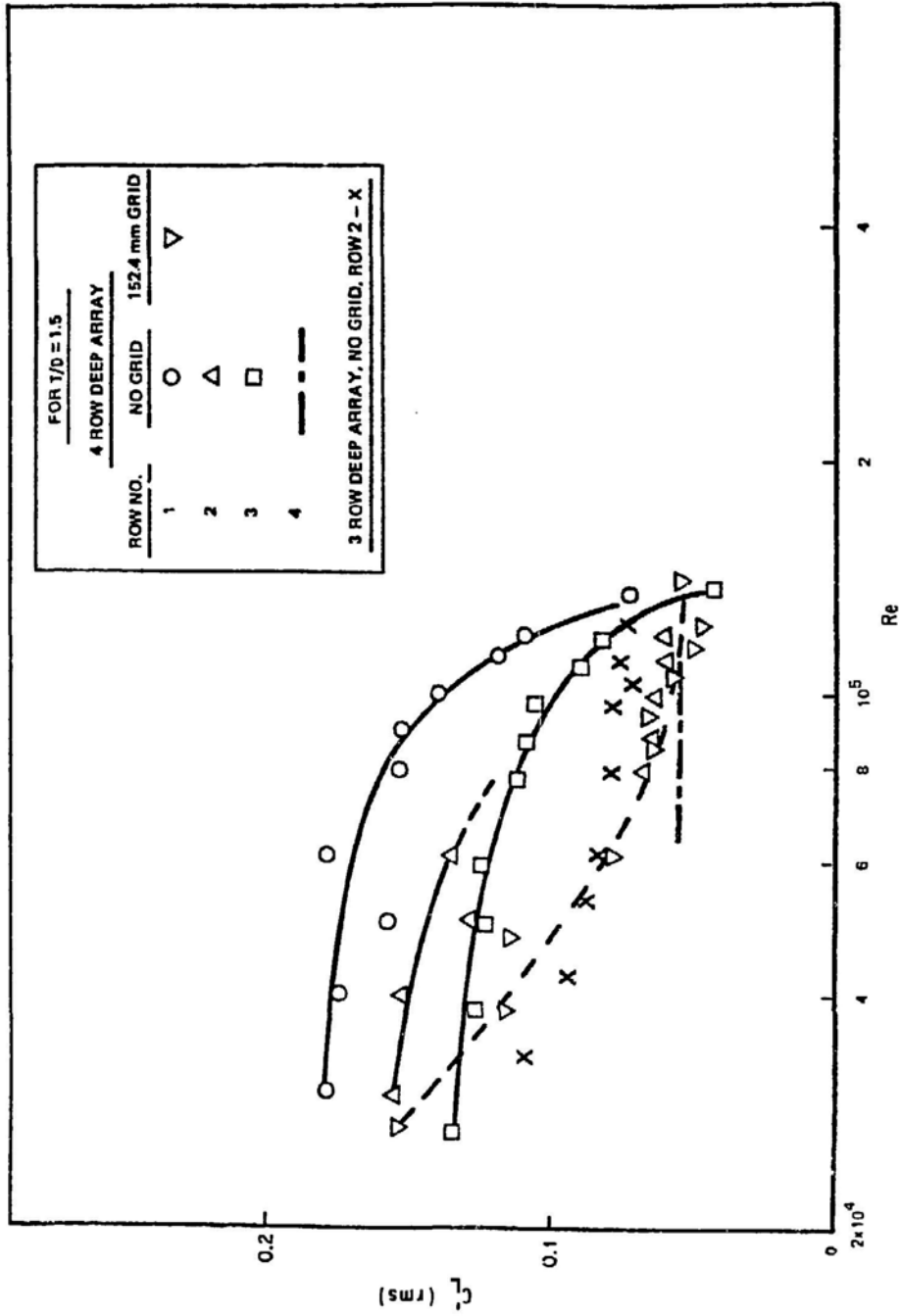


Fig. 8.9. Row-by-Row Fluctuating Lift Coefficient for an Equilateral Staggered Array (Savkar 1983)

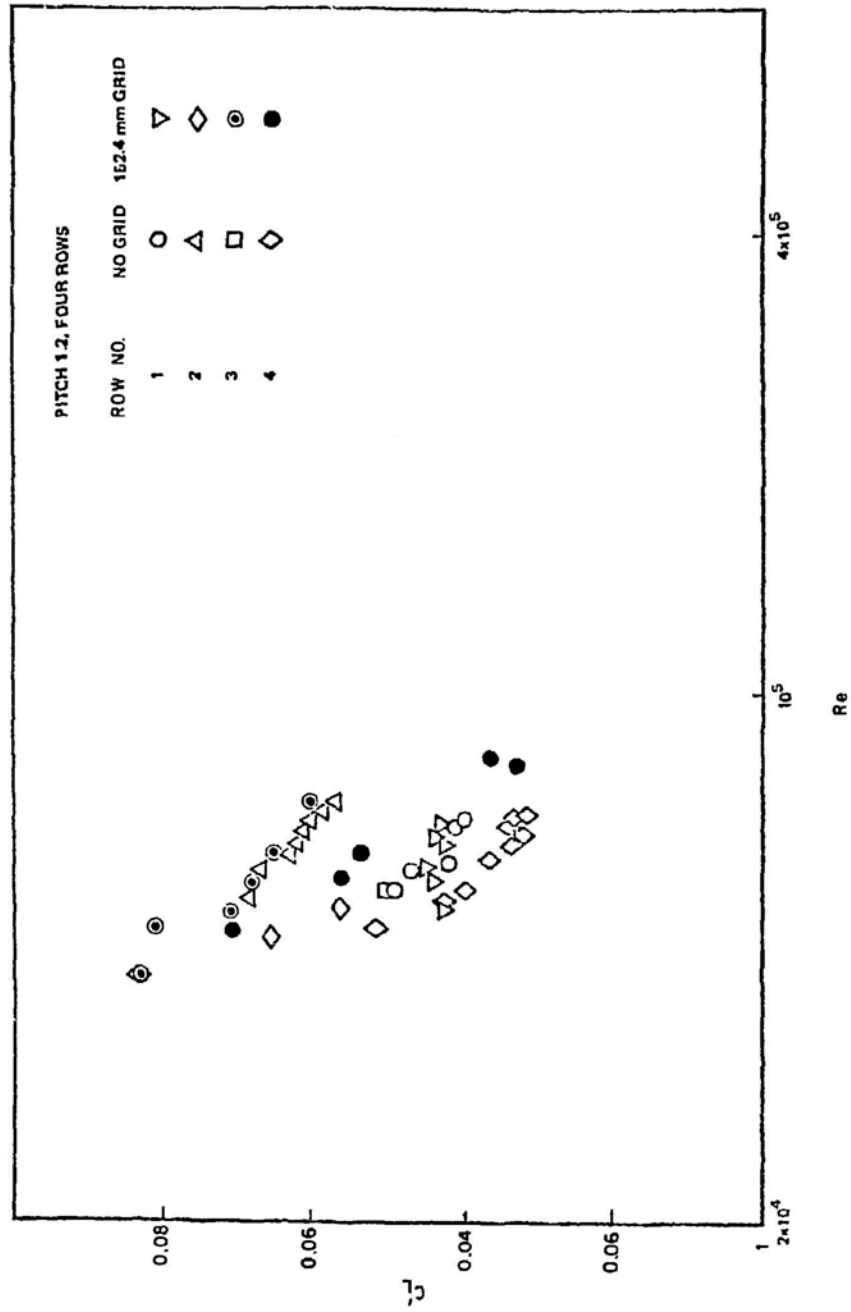


Fig. 8.10. Fluctuating Lift Coefficient for an In-Line Array (Savkar 1983)

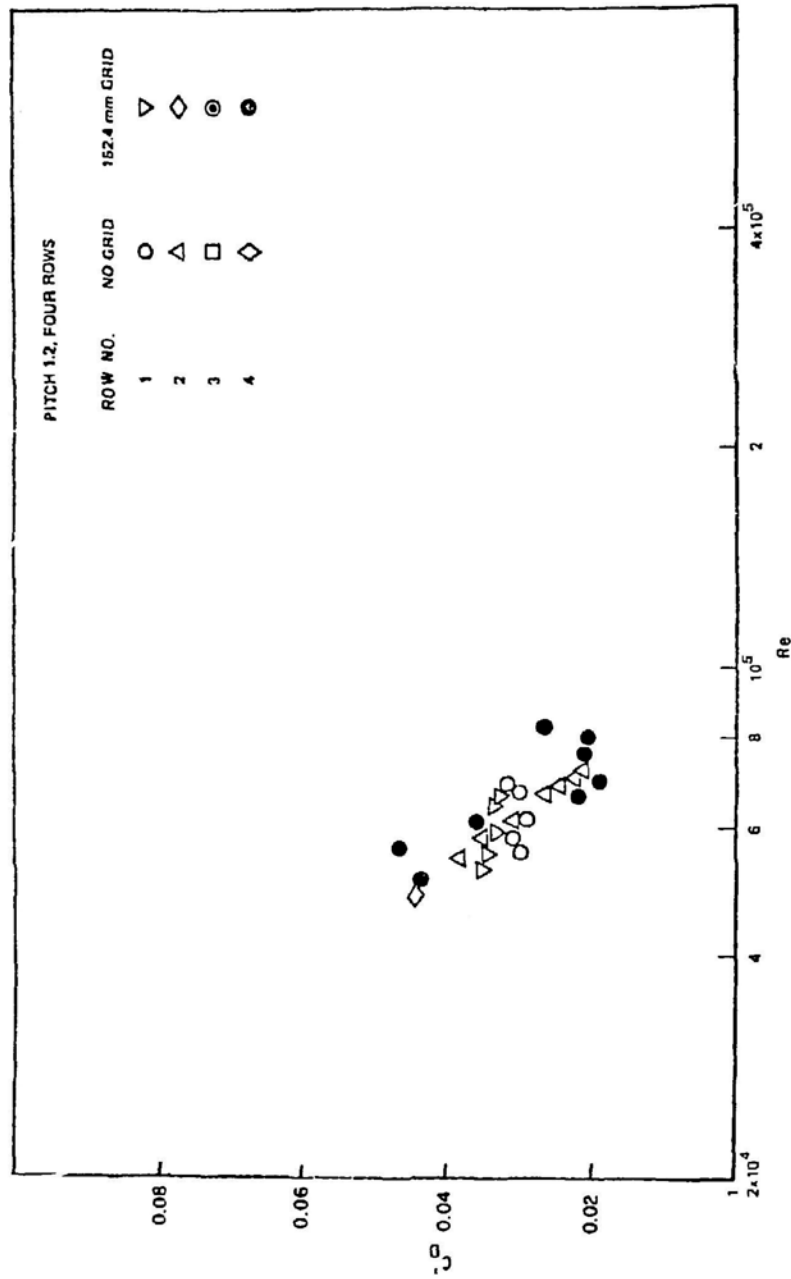


Fig. 8.11. Fluctuating Drag Coefficient for an In-Line Array (Savkar 1983)

Table 8.3. Steady Lift and Drag Coefficients (from Zdravkovich et al. 1976, with permission--see Credits)

Arrangement	P/D = 1.2		P/D = 2.0		P/D = 2.5	
	C_L	C_D	C_L	C_D	C_L	C_D
In-line	0.03	-0.12	0.0	-0.07	0.01	0.09
1/3 staggered	0.52	0.03	0.48	0.21	0.30	0.16
2/3 staggered	0.70	0.50	0.81	0.48	0.77	0.34
Staggered	0.03	0.43	0.21	0.59	0.26	0.40

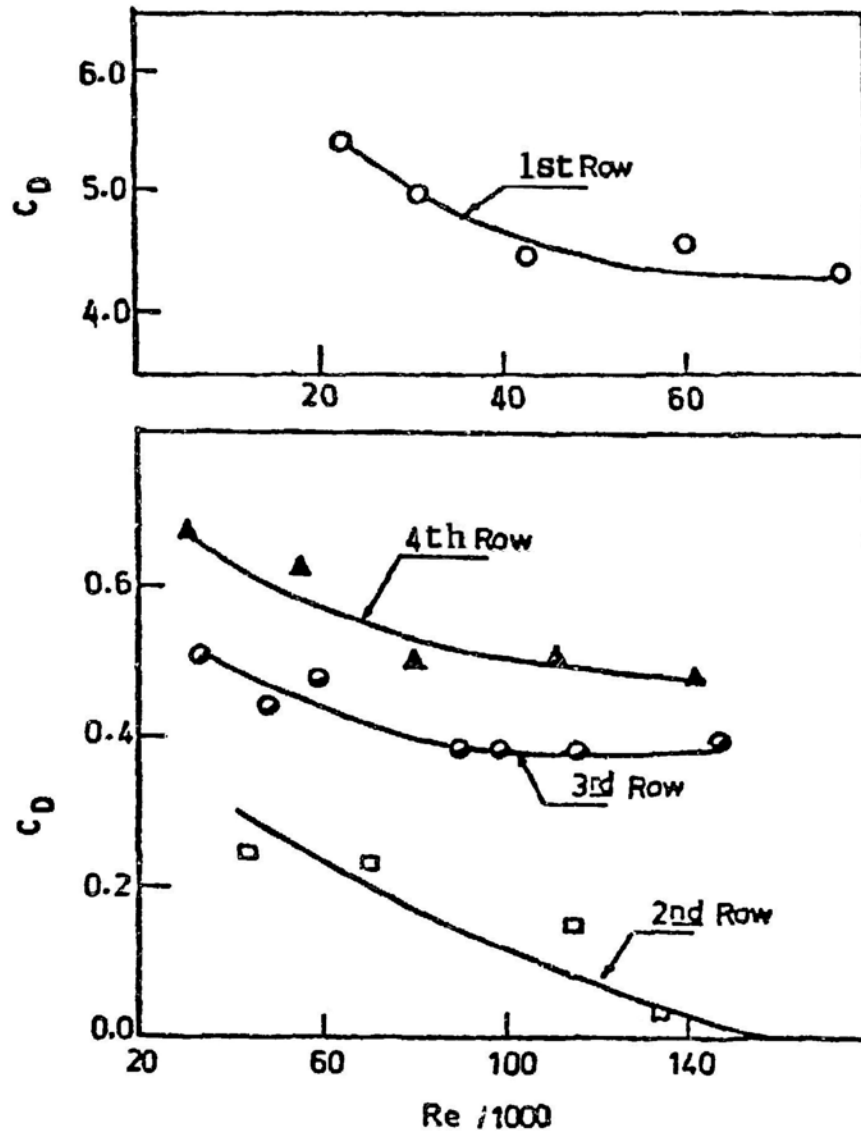


Fig. 8.12. Form Drag Coefficient for Tube Bank (from Morsy 1975, with permission--see Credits)

Both steady and unsteady drag and lift coefficients based on the gap velocity were obtained by Heinecke and Mohr (1982) for square arrays in a range of Reynolds numbers $10^4 < Re < 10^5$. Heinecke and Mohr showed that (1) the unsteady lift coefficient is almost independent of Reynolds number and the coefficient for the second row is larger than the first row, and (2) the steady drag and lift coefficients show that for different spacings the pressure distribution around the circumference is asymmetric.

The turbulence pressure field for cylinder arrays is not well characterized. A complete description of the pressure for application to vibration theory requires power spectral density of pressure at different locations and the correlation. There is no complete set of data for any cylinder array. However, several different forms of approximation have been suggested to render the turbulence pressure field practicable for simple use.

Pettigrew and Gorman (1981) assumed that the random force field is homogeneous and spatially correlated. The power spectral density of the random force acting on a cylinder is expressed

$$\Phi = \left(\frac{1}{2} C_R \rho U^2 D \right)^2, \quad (8.2)$$

where C_R is called the random turbulence excitation coefficient. Values of C_R from the results of different experiments show that the random force field depends on the location of the cylinder in an array.

Blevins, Gibert, and Villard (1981) measured both power spectral density and correlation of coherence along the axis of the cylinder in a wind tunnel for an in-line array. The results are given in Figs. 8.13 and 8.14. Figure 8.13 gives the spectrum in row 1 for four velocities. The four nondimensionalized spectra fall on the same curve, which indicates that the suggested nondimensionalization appears to be a valid representation of the spectra. Figure 8.14 gives the spectrum at five different points within the array. The turbulence rises from the inlet to a maximum value about six rows back; this turbulence level then persists to the back of the arrays and is consistent with the results by Sandifer and Bailey (1984).

The correlation length for the first row is about 3.4 cylinder diameters, which is comparable to the values obtained for a single cylinder (Toebes 1969). The correlation drops within the cylinder and increases sharply with cylinder vibration.

8.6 ANALYSIS OF FLOW-INDUCED VIBRATION

An array of N cylinders subjected to a cross flow is shown in Fig. 1.3. The axes of the cylinders are parallel to the z axis and flow is parallel to the x axis. The subscript j is used to denote variables associated with cylinder j . The variables associated with cylinder motion in the x direction

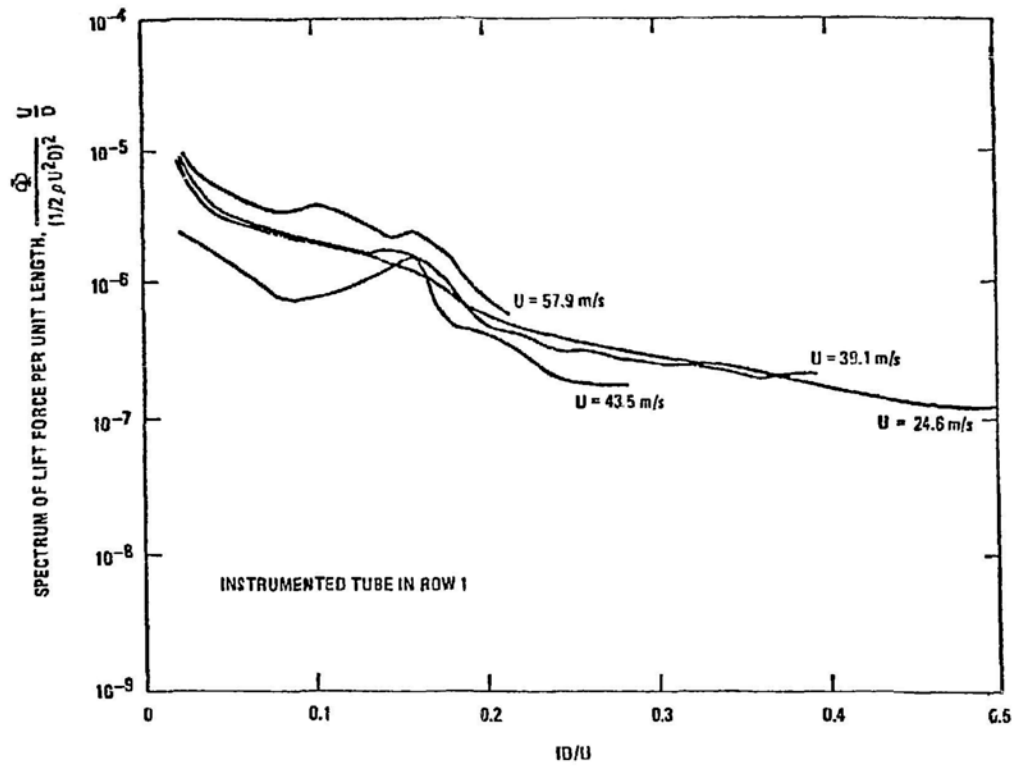


Fig. 8.13. Power Spectra of Turbulent Fluid Force for the Front Row
(from Blevins et al. 1981, with permission--see Credits)

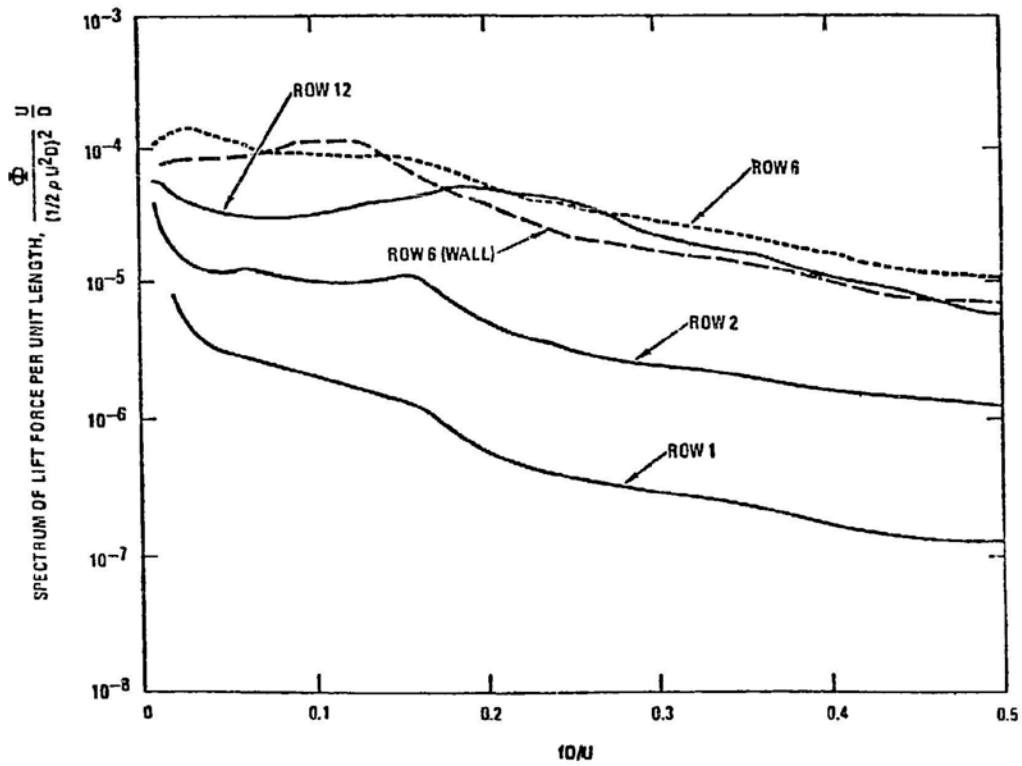


Fig. 8.14. Power Spectra of Turbulent Fluid Force for Different Rows
(from Blevins et al. 1981, with permission--see Credits)

are flexural rigidity $E_j I_j$, cylinder mass per unit length m_j , structural damping coefficient C_{sj} , and displacement u_j . The equation of motion for cylinder j in the x direction is

$$E_j I_j \frac{\partial^4 u_j}{\partial z^4} + C_{sj} \frac{\partial u_j}{\partial t} + m_j \frac{\partial^2 u_j}{\partial t^2} = g_j, \quad j = 1, 2, 3, \dots, N, \quad (8.3)$$

where g_j is given in Eqs. 1.4 and 1.5, including motion-dependent fluid forces and fluid excitation forces. Similarly, the equation of motion in the y direction is

$$E_j I_j \frac{\partial^4 v_j}{\partial z^4} + C_{sj} \frac{\partial v_j}{\partial t} + m_j \frac{\partial^2 v_j}{\partial t^2} = h_j, \quad j = 1, 2, 3, \dots, N, \quad (8.4)$$

where $E_j I_j$, C_{sj} , v_j , and h_j are flexural rigidity, structural damping coefficient, cylinder displacement, and the force per unit length in the y direction, which is given in Eqs. 1.4 and 1.5.

Substituting Eqs. 1.4 and 1.5 into 8.3 and 8.4 yields

$$\begin{aligned} E_j I_j \frac{\partial^4 u_j}{\partial z^4} + C_{sj} \frac{\partial u_j}{\partial t} + m_j \frac{\partial^2 u_j}{\partial t^2} + \sum_{k=1}^N \left(\bar{\alpha}_{jk} \frac{\partial^2 u_k}{\partial t^2} + \bar{\sigma}_{jk} \frac{\partial^2 v_k}{\partial t^2} \right) \\ + \sum_{k=1}^N \left(\bar{\alpha}'_{jk} \frac{\partial u_k}{\partial t} + \bar{\sigma}'_{jk} \frac{\partial v_k}{\partial t} \right) + \sum_{k=1}^N \left(\bar{\alpha}''_{jk} u_k + \bar{\sigma}''_{jk} v_k \right) \\ = \frac{1}{2} \rho U^2 D C_{Dj} + \frac{1}{2} \rho U^2 D C'_{Dj} \sin(\Omega_{Dj} + \phi_{Dj}) + g'_j \end{aligned} \quad (8.5)$$

and

$$\begin{aligned} E_j I_j \frac{\partial^4 v_j}{\partial z^4} + C_{sj} \frac{\partial v_j}{\partial t} + m_j \frac{\partial^2 v_j}{\partial t^2} + \rho \pi \sum_{k=1}^N \left(\bar{\tau}_{jk} \frac{\partial^2 u_k}{\partial t^2} + \bar{\beta}_{jk} \frac{\partial^2 v_k}{\partial t^2} \right) \\ + \sum_{k=1}^N \left(\bar{\tau}'_{jk} \frac{\partial u_k}{\partial t} + \bar{\beta}'_{jk} \frac{\partial v_k}{\partial t} \right) + \sum_{k=1}^N \left(\bar{\tau}''_{jk} u_k + \bar{\beta}''_{jk} v_k \right) \\ = \frac{1}{2} \rho U^2 D C_{Lj} + \frac{1}{2} \rho U^2 D C'_{Lj} \sin(\Omega_{Lj} + \phi_{Lj}) + h'_j. \end{aligned} \quad (8.6)$$

Equations 8.5 and 8.6 are the equations of motion for cylinder j in an array of cylinders subjected to a crossflow. In a group of N cylinders, there are $2N$ equations of motion.

In most practical situations all cylinders are of the same length and have the same type of boundary conditions in the x and y directions. In this case the modal functions for cylinders vibrating in the x and y directions are the same; thus let

$$\begin{aligned} u_j(z,t) &= \sum_{m=1}^{\infty} a_{jm} \phi_m(z) \quad \text{and} \\ v_j(z,t) &= \sum_{m=1}^{\infty} b_{jm} \phi_m(z) , \end{aligned} \quad (8.7)$$

where $\phi_m(z)$ is the mth orthonormal function of the cylinder in vacuo. Assume that the flow velocity distribution is given by

$$U(z) = \bar{U} \psi(z) . \quad (8.8)$$

Using Eqs. 8.5, 8.6, 8.7, and 8.8 yields

$$\begin{aligned} & \frac{d^2 a_{jm}}{dt^2} + \zeta_{vjm} \omega_{vjm} \frac{da_{jm}}{dt} + \omega_{vjm}^2 a_{jm} \\ & + \frac{1}{m_j} \sum_{k=1}^N \left(\bar{\alpha}_{jk} \frac{d^2 a_{km}}{dt^2} + \bar{\sigma}_{jk} \frac{d^2 b_{km}}{dt^2} \right) \\ & + \frac{1}{m_j} \sum_{k=1}^N \left(\bar{\alpha}'_{jkm} \frac{da_{km}}{dt} + \bar{\sigma}'_{jkm} \frac{db_{km}}{dt} \right) \\ & + \frac{1}{m_j} \sum_{k=1}^N \left(\bar{\alpha}''_{jkm} a_{km} + \bar{\sigma}''_{jkm} b_{km} \right) \\ & = \frac{1}{2m_j} \rho_{DC} \bar{U}^2 + \frac{1}{2m_j} \rho_{DC}' \bar{U}^2 \sin(\Omega_{Djm} + \phi_{Djm}) + \frac{1}{m_j} g'_{jm} \end{aligned} \quad (8.9)$$

and

$$\begin{aligned}
& \frac{d^2 b_{jm}}{dt^2} + \zeta_{vjm} \omega_{vjm} \frac{db_{jm}}{dt} + \omega_{vjm}^2 b_{jm} \\
& + \frac{1}{m_j} \sum_{k=1}^N \left(\bar{\tau}_{km} \frac{d^2 a_{km}}{dt^2} + \bar{\beta}_{jk} \frac{d^2 b_{km}}{dt^2} \right) \\
& + \frac{1}{m_j} \sum_{k=1}^N \left(\bar{\tau}'_{jkm} \frac{da_{km}}{dt} + \bar{\beta}'_{jkm} \frac{db_{km}}{dt} \right) \\
& + \frac{1}{m_j} \sum_{k=1}^N \left(\bar{\tau}''_{jkm} a_{km} + \bar{\beta}''_{jkm} b_{km} \right) \\
& = \frac{1}{2m_j} \rho_{DLC} \bar{U}^2 + \frac{1}{2m_j} \rho_{DC'} \bar{U}^2 \sin(\Omega_{Ljm} + \phi_{Ljm}) + \frac{1}{m_j} h'_{jm} \quad (8.10)
\end{aligned}$$

where

$$\begin{aligned}
\bar{\alpha}'_{jkm} &= \frac{1}{\ell} \int_0^\ell \bar{\alpha}'_{jk} \phi_m^2 \psi^2 dz, & \bar{\alpha}''_{jkm} &= \frac{1}{\ell} \int_0^\ell \bar{\alpha}''_{jk} \phi_m^2 \psi^2 dz, \\
\bar{\sigma}'_{jkm} &= \frac{1}{\ell} \int_0^\ell \bar{\sigma}'_{jk} \phi_m^2 \psi^2 dz, & \bar{\sigma}''_{jkm} &= \frac{1}{\ell} \int_0^\ell \bar{\sigma}''_{jk} \phi_m^2 \psi^2 dz, \\
\bar{\tau}'_{jkm} &= \frac{1}{\ell} \int_0^\ell \bar{\tau}'_{jk} \phi_m^2 \psi^2 dz, & \bar{\tau}''_{jkm} &= \frac{1}{\ell} \int_0^\ell \bar{\tau}''_{jk} \phi_m^2 \psi^2 dz, \\
\bar{\beta}'_{jkm} &= \frac{1}{\ell} \int_0^\ell \bar{\beta}'_{jk} \phi_m^2 \psi^2 dz, & \bar{\beta}''_{jkm} &= \frac{1}{\ell} \int_0^\ell \bar{\beta}''_{jk} \phi_m^2 \psi^2 dz, \\
C_{Djm} &= \frac{1}{\ell} \int_0^\ell C_{Dj} \phi_m^2 \psi^2 dz, & C_{Ljm} &= \frac{1}{\ell} \int_0^\ell C_{Lj} \phi_m^2 \psi^2 dz, \\
C'_{Djm} &= \frac{1}{\ell} \int_0^\ell C'_{Dj} \phi_m^2 \psi^2 dz, & C'_{Ljm} &= \frac{1}{\ell} \int_0^\ell C'_{Lj} \phi_m^2 \psi^2 dz, \\
g'_{jm} &= \frac{1}{\ell} \int_0^\ell g'_j \phi_m dz, & h'_{jm} &= \frac{1}{\ell} \int_0^\ell h'_j \phi_m dz,
\end{aligned} \quad (8.11)$$

and ω_{vjm} and ζ_{vjm} are the circular frequency and modal damping ratio of the j th cylinder of m th modes in vacuum.

The responses of an array of cylinders can be calculated fairly easily from Eqs. 8.9 and 8.10 if various fluid forces in the equations are known.

Equations 8.9 and 8.10 can be written in the standard form

$$[M]\{\ddot{Q}\} + [C]\{\dot{Q}\} + [K]\{Q\} = \{Q\} . \quad (8.12)$$

For a cylinder array in crossflow, the matrices C and K are not necessarily symmetric. However, M in general is symmetric. The properties of these matrices depend on different flow conditions.

A complete analysis of a cylinder array in crossflow requires knowledge of all fluid forces. Unfortunately, at this time, complete information is not available for any specific cylinder arrays. This suggests that for practical applications, simplifications or assumptions must be made in order to solve the problem.

8.7 RESPONSE OF CYLINDER ARRAYS

Many parameters affect the response of cylinder arrays: cylinder arrangement, damping value, reduced flow velocity, Reynolds number, Scruton's number, turbulence characteristics, etc. Cylinder response can be calculated based on Eqs. 8.5 and 8.6 provided that both fluid excitation forces and motion-dependent fluid forces are known. In practice, these forces are not known and the complicated cylinder response is difficult to predict.

To illustrate the complexity of cylinder response in crossflow, consider a typical example examined by Weaver and Abd-Rabbo (1984). A square array with $T/D = 1.5$ was tested in a low-turbulence ($< 0.5\%$) water tunnel. The cylinder natural frequency in air is about 25.5 Hz and damping about 1.4%. The tube response, frequency spectra, and flow field are given in Figs. 8.15 and 8.16. Examination of the results leads to the conclusion that the tube response can be separated into three regions: 0-0.45 m/s, 0.45-1.05 m/s, and greater than 1.05 m/s.

(a) $0 \leq U \leq 0.45$ m/s - The RMS tube response is very small both in the lift and drag directions. The frequency spectra contain the cluster of coupled natural frequencies in the range of 15-21 Hz. These are the coupled modes, as discussed in Section 3.4. The wakes shown in Fig. 8.17 consist of two stable vortices with straight flow lanes between tube columns at $U \approx 0.013$ m/s. The vortices may become unstable with flow crossing the wake region and vortices periodically being swept into the mainstream flows; at $U \sim 0.018$ m/s, the turbulence developed in the wakes appears to have little effect on the mainstream flow. At $U \sim 0.057$ m/s and 0.36 m/s, the wake regions become turbulent and the turbulent wakes perturb the mainstream flows. Also, the flow pattern surrounding the first row tubes is different from that seen by the other rows. In this range, the excitation is due to turbulence buffeting.

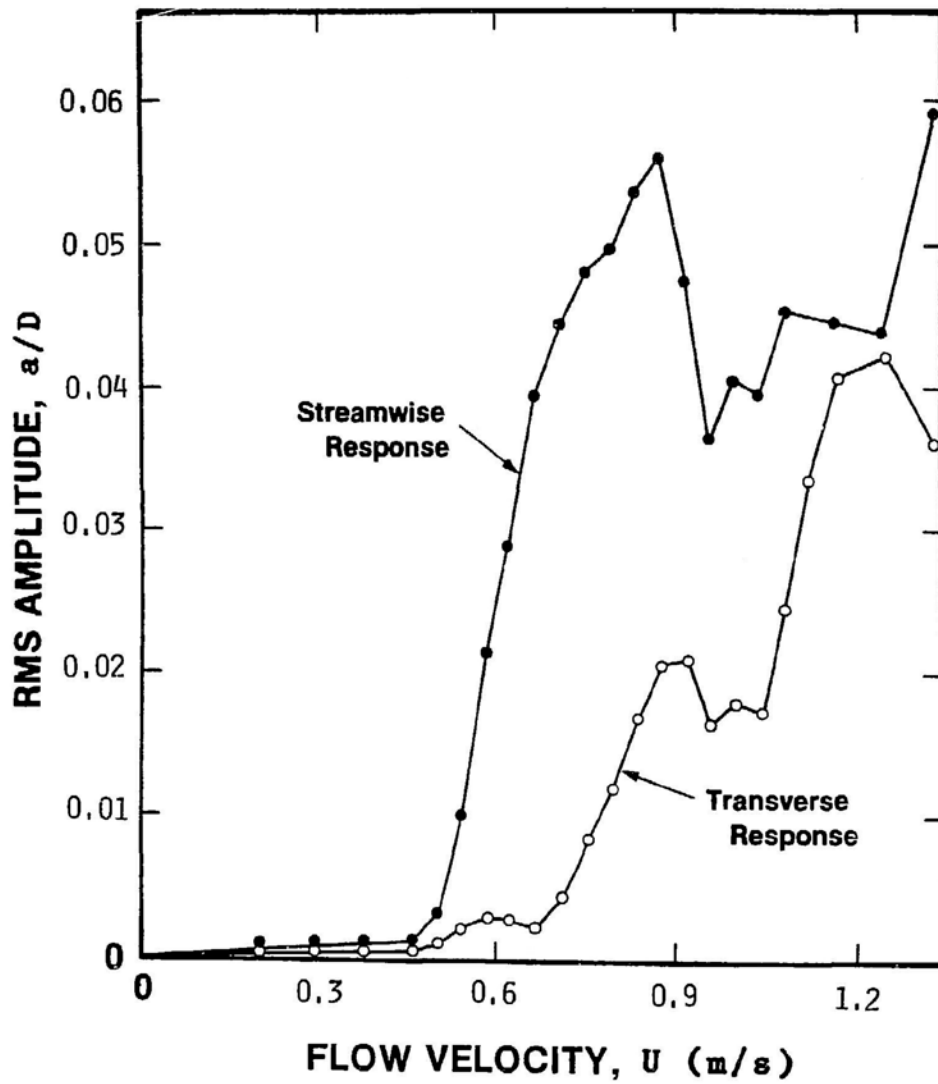


Fig. 8.15. Response of the Second Row Tube (from Weaver and Abd-Rabbo, with permission--see Credits)

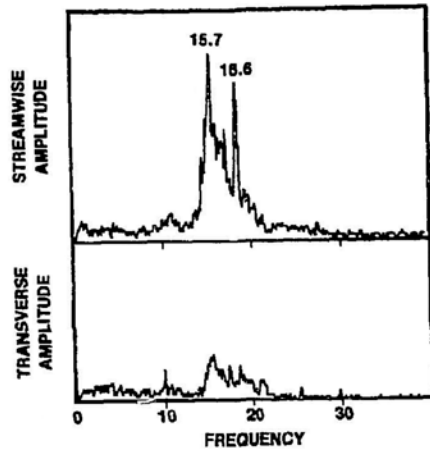
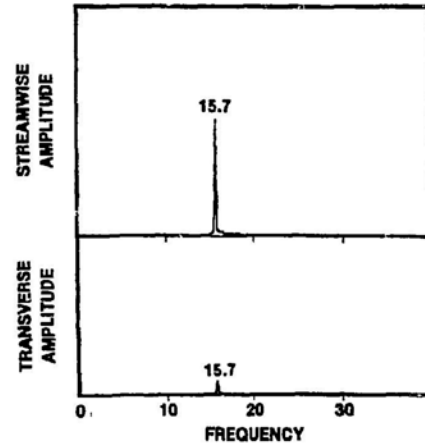
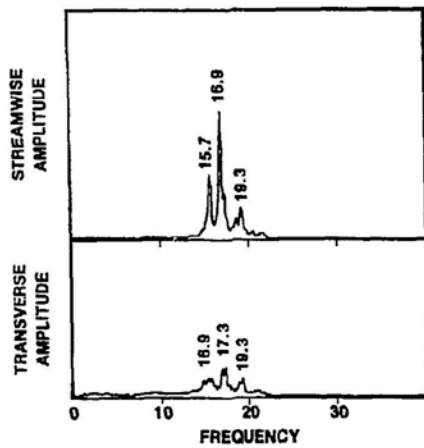
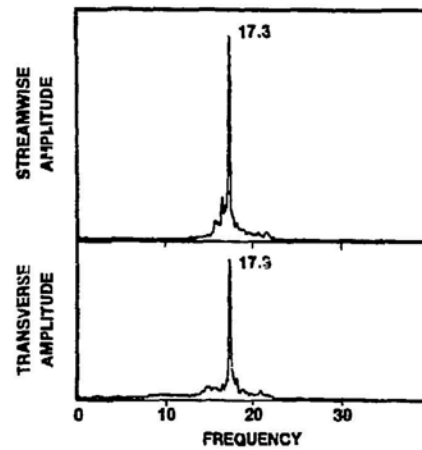
(a): $U = 0.45$ m/s(b): $U = 0.57$ m/s(c): $U = 1.05$ m/s(d): $U = 1.11$ m/s

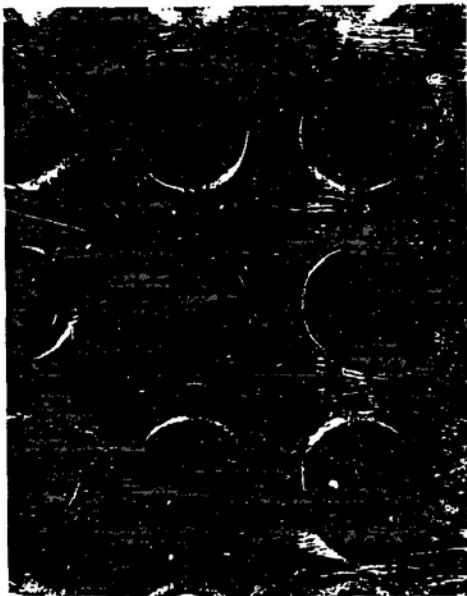
Fig. 8.16. Tube Response Spectra of the Second Row (from Weaver and Abd-Rabbo, with permission--see Credits)



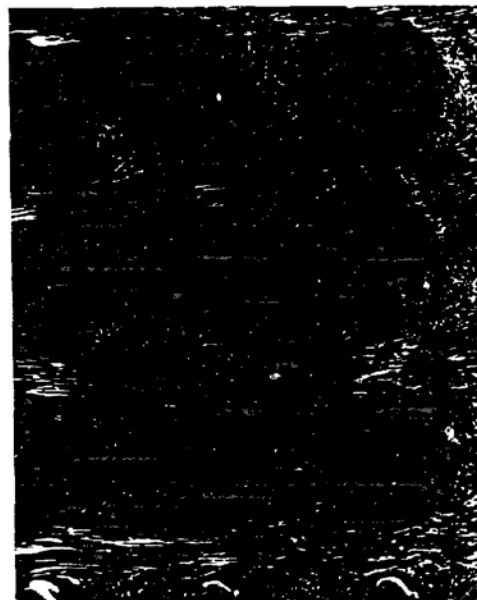
(a): $U = 0.013 \text{ m/s}$, $Re = 330$



(b): $U = 0.018 \text{ m/s}$, $Re = 450$



(c): $U = 0.057 \text{ m/s}$, $Re = 1470$



(d): $U = 0.36 \text{ m/s}$, $Re = 9.3 \times 10^3$

Fig. 8.17. Flow Field for $0 < U < 0.45 \text{ m/s}$ (from Weaver and Abd-Rabbo, with permission--see Credits)

(b) $0.45 \text{ m/s} < U \leq 1.05 \text{ m/s}$ - There is an abrupt increase in RMS amplitude, with the predominant response being in the drag direction. This response peaks at $U \sim 0.9 \text{ m/s}$ and falls off sharply to a trough at about 1.05 m/s . The predominantly drag response at $U = 0.57 \text{ m/s}$ can be seen in Fig. 8.16b. Note the absence of other coupled mode frequencies. At $U \sim 1.05 \text{ m/s}$, the response is characterized by a much less well organized behavior, as indicated in Fig. 8.16c, with several response frequencies: All tubes in a given row oscillate in phase with one another and approximately 180° out of phase with tubes in adjacent rows. The coherent vortices were being shed in symmetric pairs from the first row tubes, with all vortex pairs being in phase with one another. This can be seen in Fig. 8.18, which shows the effect of a stream of aluminum tracer particles released just upstream of the first tube row. In this region, the motion is excited by vortex shedding and the peak response at $U \sim 0.9 \text{ m/s}$ represents the lock-in in the drag direction.

(c) $1.05 \text{ m/s} < U$ - Tube amplitudes rise sharply in a whirling mode in which the drag and lift amplitudes are of the same order. The responses are highly modulated and the relative modes unsteady, with a single frequency being dominant, as shown in Fig. 8.16d. The tube bundle is in the fluidelastic instability region. Sometimes the tube motion is primarily transverse, with tubes in a column in phase with one another and 180° out of phase with the adjacent columns, as shown in Fig. 8.19a and b. However, at other times, the relative mode pattern changes entirely, usually accompanied by a shift in the dominant response frequency. The flow field is given in Fig. 8.19c.

This example illustrates the three different excitations being dominant in different flow velocity ranges. Many other studies have been conducted (e.g., Blevins et al. 1981; Heinecke and Mohr 1982; Pettigrew and Gorman 1981) to determine the response of an array of cylinders in crossflow. However, no detailed data are available for general cylinder arrays.

The prediction method for fluidelastic instability is given in Chapter 10. Response of cylinder arrays to excitations due to turbulent buffeting and vortex shedding remains difficult to predict, for two reasons. First, most of the experimental studies have been spotty. There is no systematic investigation to quantify the turbulent pressure field and vortex shedding in different cylinder arrays. Second, at this time, it is impossible to calculate the detailed flow field across a cylinder array. Therefore assumptions have to be included in the solution of the problem governed by Eqs. 8.5 and 8.6.

The common assumptions used in the prediction of turbulence-induced responses are:

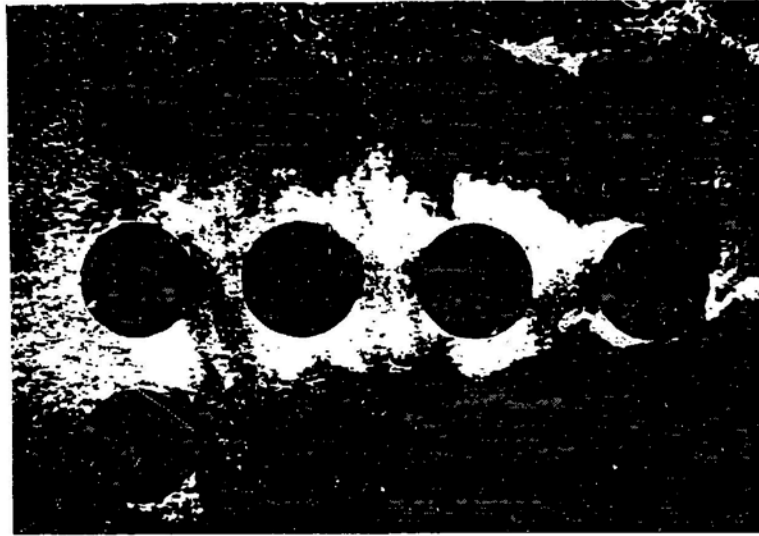


Fig. 8.18. Flow Field for $U \approx 0.75$ m/s (from Weaver and Abd-Rabbo 1984, with permission--see Credits)

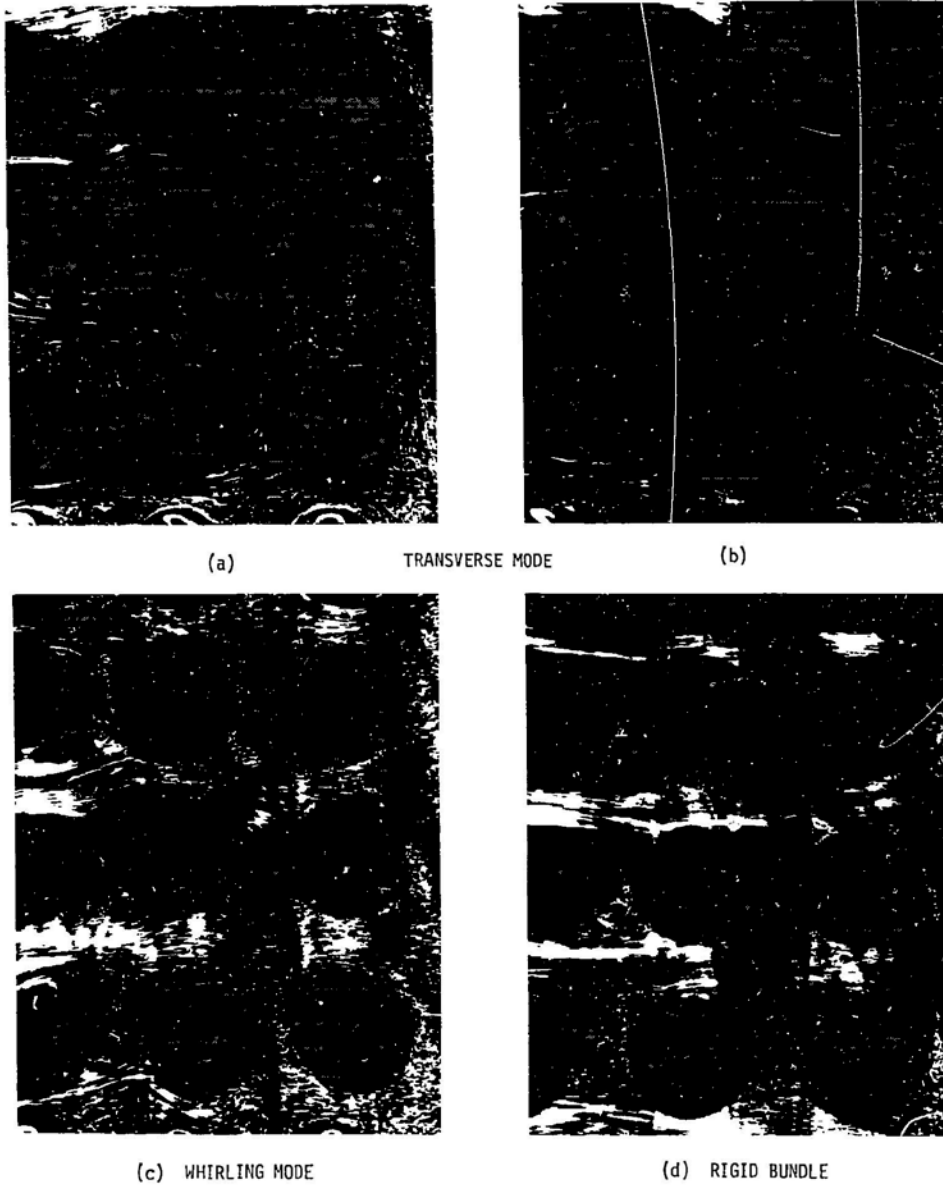


Fig. 8.19. Flow Field for $U = 1.32$ m/s (from Weaver and Abd-Rabbo 1984, with permission--see Credits)

(1) The motion of the cylinders does not significantly affect the pressure fluctuations; i.e., g_j^i and h_j^i in Eq. 8.5 and 8.6 are independent of u_j and v_j .

(2) The pressure fluctuations are independent of other flow excitations such as vortex shedding.

(3) Prediction of the cylinder arrays can be based on that of a single cylinder in a rigid cylinder array.

Based on these assumptions, the response of the cylinder array can be calculated by applying the random vibration theory and the technique developed in Section 6.3. Simplified analyses have been presented by different investigators (Pettigrew and Gorman 1981; Blevins et al. 1981).

The response to vortex shedding can be calculated once the vortex excitation forces are known. Ideally, the coupled motion of cylinder arrays should be considered; i.e., the response should be calculated from Eqs. 8.5 and 8.6. However, because of the lack of information on fluid force coefficients, a single cylinder approximation has been used in applications.

8.8 ACOUSTIC RESONANCE

A fluid surrounding an array of circular cylinders can vibrate in a resonant manner. This type of oscillation, commonly called acoustic vibration, can cause failures of the cylinders if it occurs at a frequency that is close to one of the natural frequencies of the cylinders. Even if the resonant vibration of the fluid does not produce failures in cylinders, it can generate an intense noise. It also can induce fatigue damage to the casing of the cylinder array, such as a heat exchanger.

There have been many reported cases of flow-induced vibration of an array of circular cylinders associated with acoustic excitation (e.g., Grotz and Arnold 1956; Putnam 1964; Byrne 1983). In this section, acoustic frequencies, excitation mechanisms, and prevention of acoustic resonance in heat exchanger tube arrays are discussed.

8.8.1 Propagation of Sound Waves along Fluid Cylinders

The wave equation relevant to acoustic propagation in a circular cylindrical duct is given by

$$\phi = \psi(r, \theta, z) \exp(i\omega t) , \quad (8.13)$$

$$\nabla^2 \psi + k^2 \psi = 0 , \quad k^2 = \omega^2 / c^2 .$$

The solution of Eq. 8.13 is

$$\phi = [A_1 J_n(k_r r) + A_2 Y_n(k_r r)] \cos n\theta \exp[-i(k_z z - \omega t)] \quad (8.14)$$

$$k_r^2 + k_z^2 = k^2 ,$$

where n is an integer. If the propagation constant k_z is real, Eq. 8.14 represents a wave with phase velocity ω/k_z along the z axis. If k_z is imaginary, no propagation occurs.

First, consider a fluid cylinder along the z axis with a rigid wall at $r = R$. The boundary condition is that the radial component of velocity must vanish at the wall. The propagation constant must satisfy the condition

$$\left. \frac{\partial}{\partial r} [J_n(k_{rnm} r)] \right|_{r=R} = 0 . \quad (8.15)$$

The velocity potential for the (n,m) mode is

$$\phi_{nm} = A_{nm} J_n(k_{rnm} r) \cos n\theta \exp[-i(k_z z - \omega t)] . \quad (8.16)$$

The integers m and n indicate the number of pressure nodal diameters and circles, respectively, associated with each mode shape. Each mode also has an associated cut-off frequency. Thus, if the radian frequency ω is high enough,

$$k = \omega/c > k_{rnm} \quad \text{and} \quad k_z > 0 ,$$

and the (n,m) th mode will propagate down the duct. At the cut-off frequency,

$$k = k_{rnm} , \quad \text{and} \quad k_z = 0 , \quad (8.17)$$

and there is no longitudinal acoustic wave motion in that mode. Below this frequency $k_z^2 < 0$ and the acoustic mode does not propagate. Its amplitude decays exponentially with distance from the sound sources.

For a fluid cylinder with pressure-release wall, the pressure must vanish at the wall, so that the characteristic values are determined by the equation

$$J_n(k_{rnm} R) = 0 . \quad (8.18)$$

If the fluid in the cylinder is moving with constant velocity U , the equation of acoustic pressure is given by

$$\nabla^2 p = \frac{1}{c^2} \frac{\partial^2 p}{\partial t^2} + \frac{2M}{c} \frac{\partial^2 p}{\partial z \partial t} + M_c^2 \frac{\partial^2 p}{\partial z^2} . \quad (8.19)$$

If we assume the same type of solution as for Eq. 8.13, the wave number relationship now becomes

$$k_z^2 + k_{rnm}^2 = (k - M_c k_z)^2 . \quad (8.20)$$

The cut-off frequency is defined by

$$k = k_{rnm} (1 - M_c^2)^{0.5} . \quad (8.21)$$

Therefore, the frequency will be reduced irrespective of the direction of propagation.

Next consider a compressible Newtonian fluid undergoing very small oscillations. The governing equations are given in Eqs. 6.11. To illustrate the essential feature, consider the axisymmetric waves. The equations of motion in this case are

$$\left[\left(1 + \frac{1}{\omega_o} \frac{\partial}{\partial t} \right) \nabla^2 - \frac{1}{c^2} \frac{\partial^2}{\partial t^2} \right] \phi = 0 \quad (8.22)$$

and

$$\left[\nabla^2 - \frac{1}{2} \frac{1}{v_o} \frac{\partial}{\partial t} \right] \psi_\theta = 0 . \quad (8.23)$$

The solution of Eqs. 8.22 and 8.23 is in the form

$$\bar{f}(r, z, t) = \text{Re} [f(r) e^{-i(k_z z - \omega t)}] , \quad (8.24)$$

where ω is the circular frequency, and k_z is the propagation constant, which is complex.

Application of Eq. 8.24 to Eq. 8.22 and the bounded condition at $r = 0$ gives

$$\phi(r, z, t) = \text{Re}[A_1 J_0(k_r r) e^{-i(k_z z - \omega t)}] , \quad (8.25)$$

where the complex constant k_r is the principal square root of

$$k_r^2 = \left[k_z^2 + \frac{\omega^2}{c^2} \frac{1}{1 + i\omega/\omega_0} \right]^{0.5} . \quad (8.26)$$

Application of Eq. 8.24 to Eq. 8.23 and the bounded condition at $r = 0$ gives

$$\psi_\theta(r, z, t) = \text{Re}[A_2 J_1(k'_r r) e^{-i(k_z z - \omega t)}] , \quad (8.27)$$

where the complex constant k'_r is the principal square root of

$$k'_r^2 = [k_z^2 - i\omega/\nu_0]^{0.5} . \quad (8.28)$$

Therefore,

$$\begin{aligned} v_r(r, z, t) &= -\text{Re}\{[A_1 k_r J_1(k_r r) + A_2 k_z J_1(k'_r r)] e^{-i(k_z z - \omega t)}\} \\ v_z(r, z, t) &= \text{Re}\{[A_1 k_z J_0(k_r r) + A_2 k'_r J_0(k'_r r)] e^{-i(k_z z - \omega t)}\} \end{aligned} \quad (8.29)$$

$$p(r, z, t) = \text{Re}\{-A_1 i\rho_0 \omega / (1 + i\omega/\omega_0) J_0(k_r r) e^{-i(k_z z - \omega t)}\}$$

and

$$\rho(r, z, t) = \frac{1}{c^2} p(r, z, t) .$$

The two homogeneous zero-speed boundary conditions at the wall are

$$v_r(R, r, t) = 0 \quad \text{and} \quad (8.30)$$

$$v_z(R, r, t) = 0 .$$

Using Eqs. 8.29 and 8.30 yields

$$\begin{bmatrix} k_r J_1(k_r R) & k_z J_1(k'_r R) \\ k_z J_0(k_r R) & k'_r J_0(k_r R) \end{bmatrix} \begin{Bmatrix} A_1 \\ A_2 \end{Bmatrix} = \begin{Bmatrix} 0 \\ 0 \end{Bmatrix}. \quad (8.31)$$

Therefore the dispersion relation is

$$k_r k'_r \frac{J_1(k_r R)}{J_0(k_r R)} - k_z^2 \frac{J_1(k'_r R)}{J_0(k'_r R)} = 0, \quad (8.32)$$

which provides the relationship between the complex eigenvalue k_z and circular frequency ω . Given the parameters ω , ν , ν' , the dispersion relation can be solved for all the eigenvalues (Scarton and Rouleau 1973).

Based on the frequency equations, (Eqs. 8.15, 8.18, and 8.32), the acoustic frequencies can be calculated. It should be pointed out that if a fluid contains a number of circular cylinders whose dimensions are small relative to the wavelength of sound at the frequencies of interest, the effective speed of sound in the composite media will be reduced. It can be shown that the effective speed of sound is given as follows (Meyer and Neumann 1972):

$$\frac{\text{Effective speed of sound}}{\text{Actual speed of sound}} = \frac{1}{(1 + \sigma)^{0.5}}, \quad (8.33)$$

where σ is the fraction of the space occupied by solid bodies. The effective speed of sound should be used in appropriate situations.

8.8.2 Criteria for Acoustic Resonance

In general, the turbulent buffeting and vortex shedding in an array of circular cylinders will not be synchronized. However, at a certain frequency it is possible for these fluctuating quantities to become synchronized. Two criteria have been proposed to predict the condition of acoustic resonance--one by Chen (1968) and another by Bryce et al. (1978).

Chen Criterion

The first requirement of Chen's (1968) criterion is that the Strouhal frequency f_s be equal to the acoustic frequency f_a ; i.e.,

$$f_s = f_a . \quad (8.34)$$

The second requirement is that the parameter Ψ_c exceed a certain value where Ψ_c is defined as

$$\Psi_c = \frac{Re}{St} \left(\frac{P - D}{P} \right)^2 \frac{D}{T} . \quad (8.35)$$

The critical value for Ψ_c is 600 for wind tunnels and 2000 for practical applications (Chen and Young 1974). Therefore, in Chen's criteria, frequency coincidence is a necessary but insufficient condition for acoustic resonance. Even if Eq. 8.34 is satisfied, when Ψ_c is smaller than the critical value, the acoustic resonance will be damped out.

Bryce et al. Criterion

Several authors have proposed a simplified criterion which provides for an acoustic Strouhal number

$$St_a = \frac{D}{2P} . \quad (8.36)$$

Bryce et al. (1978) proposed a lower bound for acoustic resonance given by

$$St_a = \frac{1}{2\left(\frac{P}{D} - 0.5\right)} . \quad (8.37)$$

Equation 8.37 is proposed as a general guideline for avoidance of acoustic resonance up to $P/D = 3.0$.

The sequence used to predict whether an acoustic resonance can occur is as follows:

- Calculate the dominant flow excitation frequency.
- Predict the acoustic natural frequency most apt to be excited.
- Compare the excitation frequency with the predicted acoustic frequency.
- Meet any other requirements according to the criterion used.

The technique is straightforward; however, the calculations of dominant flow excitation frequency and acoustic natural frequencies in practical system components are fraught with difficulties.

The criteria by Chen and by Bryce et al. are not developed from the fundamental principles of fluid dynamics and acoustics. Additional research is needed to firmly set these criteria.

8.8.3 Avoidance of Acoustic Resonances

If acoustic resonance is predicted, there are several techniques to eliminate the problem.

- **Detuning Baffles:** Introducing baffles in an array of cylinders raises the acoustic frequency above the fluid excitation frequencies. The baffles are installed parallel to the axis of the cylinders and the flow. Different types of baffles and several baffles can be used; including solid baffles and porous baffles (Eisinger 1979; Byrne 1983). This method increases the pressure drop through the array.

- **Reposition or Removal of Cylinders:** Removing cylinders located at the pressure modes in standing acoustic waves may eliminate the resonance. The full bank tested by Walker and Keising (1968) produced noise of 140 dB at a distance of 3 ft. Complete elimination of the noise was achieved by the omission of a single cylinder at each pressure node position. Tests by Zdravkovich and Nuttall (1974) show that acoustic resonance can be eliminated by unequal longitudinal pitches in two successive rows.

- **Fin Barriers and Helical Spacers (Eisinger 1979):** The fin barrier is made up of fins welded to the tubes forming a fin "wall" parallel to the direction of flow and perpendicular to the direction of propagation of longitudinal waves. The helical spacer can be inserted in the cylinder array at different locations.

8.9 CLOSING REMARKS

The dynamics of an array of circular cylinders subjected to crossflow is very complex. Its dynamic characteristics and response to flow noises remain difficult to predict. In the past, tests have been used heavily for design evaluations. At this time, there is a sound basis for analyzing the response of a cylinder array in crossflow. However, the main task is in the characterization of flow field, such as vortex shedding and turbulent excitation. Detailed characterization of a cylinder array subjected to crossflow is much more difficult. As pointed out in Chapter 7, it is not possible to solve the coupled fluid-cylinder response for an isolated cylinder at this time based on the fundamental principles of fluid dynamics and theory of elasticity; much more study will be required to solve the multiple cylinder problem in a rigorous manner.

REFERENCES--Sec. 8

- Aiba, S., Tsuchida, H., and Ota, T. 1982a. Heat Transfer Around Tubes in Staggered Tube Banks. Bulletin of the JSME 25(204), 927-933.
- Aiba, S., Tsuchida, H., and Ota, T. 1982b. Heat Transfer Around Tubes in In-line Tube Banks. Bulletin of the JSME 25(204), 919-926.
- Blevins, R. D., Gibert, R. J., and Villard, B. 1981. Experiment on Vibration of Heat Exchanger Tube Arrays in Cross Flow. Trans. 6th Int. Conf. on Structural Mechanics in Reactor Technology, Paris, Paper No. B6/9.
- Bryce, W. B., Wharmby, J. S., and Fitzpatrick, J. 1978. Duct Acoustic Resonances Induced by Flow Over Coiled and Rectangular Heat Exchanger Test Banks in Plain and Finned Tubes. Proc. BNES Sym. on Vibration in Nuclear Plant, Keswick, Paper No. 3.5
- Byrne, K. P. 1983. The Use of Porous Baffles to Control Acoustic Vibrations in Crossflow Tubular Heat Exchangers. J. Heat Transfer 105, 751-758.
- Chen, Y. N. 1968. Flow-Induced Vibration and Noise in Tube Bank Heat Exchangers due to von Karman Streets. ASME J. Engineering for Industry 90, 134-146.
- Chen, Y. N. 1972. Fluctuating Lift Forces of the Karman Vortex Streets on Single Circular Cylinders and in Tube Bundles, Part 3 - Lift Forces in Tube Bundles. Trans. ASME, J. Eng. for Industry 94, 603-628.
- Chen, Y. N. 1977. The Sensitive Tube Spacing Region of Tube Bank Heat Exchangers for Fluid-Elastic Coupling in Cross Flow. Fluid Structure Interaction Phenomena in Pressure Vessel and Piping Systems, ASME PVP-PB-026, pp. 1-18.
- Chen, Y. N., and Young, W. C. 1974. The Orbital Movement and the Damping of the Fluidelastic Vibration of Tube Banks Due to Vortex Formation, Part 3 - Damping Capability of the Tube Bank Against Vortex Excited Sonic Vibration in the Fluid Column. J. Eng. for Industry 96, 1072-1075.
- Eisinger, F. L. 1979. Prevention and Cure of Flow-Induced Vibration Problems in Tubular Heat Exchangers. Flow Induced Vibrations, ASME Publications 47-55.
- Fitz-Hugh, J. S. 1973. Flow-induced Vibration in Heat Exchangers. Proc. Int. Sym. on Vibration Problems in Industry, Keswick, U.K., Paper No. 427.
- Grotz, B. J., and Arnold, R. R. 1956. Flow Induced Vibration in Heat Exchanger. TN No. 31 to Office of Naval Research for Stanford, AD104568.
- Heinecke, E. P., and Mohr, K. H. 1982. Investigations on Fluid Borne Forces in Heat Exchangers with Tubes in Cross Flow. Proc. Int. Conf. on Vibration in Nuclear Plant, Keswick, U.K.

- Ishigai, S., Nishikawa, E., Yagi, E. 1973. Structures of Gas Flow and Vibration in Tube Banks with Tube Axes Normal to Flow. Int. Sym. on Marine Engineering, Tokyo, pp. 1-5-23 to 1-5-33.
- Meyer, E., and Neumann, E. G. 1972. Physical and Applied Acoustics. New York, Academic Press, pp. 191-192.
- Morsy, M. G. 1975. Skin Friction and Form Pressure Loss in Tube Bank Condensers. Proc. Instn. Mech. Engr. 189, 49/75.
- Pettigrew, M. J., and Gorman, D. J. 1981. Vibration of Heat Exchanger Tube Bundles in Liquid and Two-Phase Cross-Flow. ASME Publication, Flow-Induced Vibration Design Guidelines, PVP Vol. 52, 89-109.
- Pettigrew, M. J., and Ko, P. L. 1980. A Comprehensive Approach to Avoid Vibration on Fretting in Shell and Tube Heat Exchangers. Flow-Induced Vibration of Power Plant Components, PVP-41, ASME, pp. 1-18.
- Putnam, A. A. 1964. Flow-Induced Noise and Vibration in Heat Exchangers. ASME Paper No. 64-WA/HT-21.
- Sandifer, J. B., and Bailey, R. T. 1984. Turbulent Buffeting of Tube Arrays in Liquid Crossflow. Symposium on Flow-Induced Vibrations, Vol. 2, ASME Publication, 211-226.
- Savkar, S. D. 1983. Flow-Induced Vibration of Cylinders in Cross Flows. General Electric Report No. GEAP-22274, pp. 3.1-3.81.
- Scarton, H. A., and Rouleau, W. T. 1973. Axisymmetric Waves in Compressible Newtonian Liquids Contained in Rigid Tubes: Steady-Periodic Mode Shapes and Dispersion by the Method of Eigenvalleys. J. Fluid Mech. 58, 595-621.
- Toebe, G. H. 1969. The Unsteady Flow and Wake Near an Oscillating Cylinder. J. Basic Eng. 91, 493-505.
- Walker, E. M., and Reising, G. F. S. 1968. Flow-Induced Vibrations in Cross-Flow Heat Exchangers. Chemical Process and Engineering 49, 95-103.
- Weaver, D. S., and Abd-Rabbo, A. 1984. A Flow Visualization Study of a Square Array of Tubes in Water Cross-Flow. Symposium on Flow-Induced Vibrations, Vol. 2, ASME Publication, 165-177.
- Zdravkovich, M. M., and Namork, J. E. 1979. Structure of Interstitial Flow Between Closely Spaced Tubes in Staggered Array. Flow Induced Vibrations, ASME Publications, 41-46.
- Zdravkovich, M. M., and Nuttall, J. A. 1974. On the Elimination of Aerodynamic Noise in a Staggered Tube Bank. J. Sound and Vibration 34, 173-177.
- Zdravkovich, M. M., Singh, S., Nuttall, J. A., and Causon, D. M. 1976. Flow Induced Vibration in Staggered Tube Banks. Sixth Thermodynamics and Fluid Mechanics Convention, University of Durham, April 1976.

9. TWO CYLINDERS IN CROSSFLOW

9.1 INTRODUCTION

The flow field around a pair of rigid circular cylinders is very complex, and has been studied extensively. Some objectives of those studies have been to measure the fluid force and/or pressure distribution acting on each cylinder, flow velocity profile, and vortex shedding, and to understand the resultant flow patterns. An excellent review was published recently by Zdravkovich (1977).

When one or both cylinders are elastic and vibrate, the flow field becomes significantly more complicated because of the interaction of the fluid flow and the cylinder motion. Efforts have been made to understand the phenomena involved. Motivated by concern over the large oscillations frequently occurring in transmission lines exposed to high wind, most of the studies of elastic cylinders have focused on characterizing the motion of two cylinders in tandem. The disturbed flow caused by the windward cylinder striking the leeward cylinder can induce dynamic instability, called wake-induced flutter. Cylinders are also subjected to other fluctuating forces associated with vortex shedding and turbulence generated by the cylinder motion. These phenomena have been studied experimentally and analytically by Wilson and Caldwell (1971), Tanida et al. (1973), King and Johns (1976), Simpson and Flower (1977), Tsui (1977) and Zdravkovich (1974) and others. In contrast to two cylinders in tandem, there is very limited information on two cylinders normal to flow; Livesey and Dye (1962), Dye (1973), and Jendrzejczyk et al. (1979) have conducted experimental investigations into the possible modes of two cylinders normal to flow. A review of the response of two cylinders was reported most recently by Zdravkovich (1984).

9.2 FLUID-FORCE COMPONENTS

Consider two cylinders, 1 and 2 (see Fig. 9.1), subjected to crossflow. Fluid-force components acting on the two cylinders are g_1 and g_2 in the drag direction and h_1 and h_2 in the lift direction. If the cylinders are rigid, these fluid force components can be written

$$\begin{aligned}
 g_j &= \frac{1}{2} \rho U^2 DC_{Dj} + \frac{1}{2} \rho U^2 DC'_{Dj} \sin(\Omega_{Dj} t + \phi_{Dj}) + g'_j \quad \text{and} \\
 h_j &= \frac{1}{2} \rho U^2 DC_{Lj} + \frac{1}{2} \rho U^2 DC'_{Lj} \sin(\Omega_{Lj} t + \phi_{Lj}) + h'_j, \\
 j &= 1, 2.
 \end{aligned}
 \tag{9.1}$$

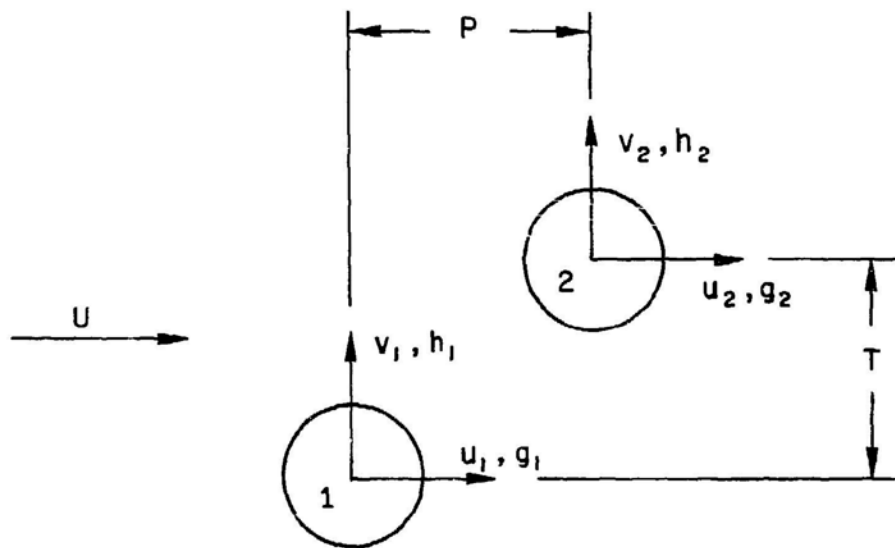


Fig. 9.1. Two Cylinders in Crossflow

The fluid-force components given in Eq. 9.1 are fluid excitation forces. If the cylinders are movable, additional fluid-force components will result from cylinder oscillations. These are the motion-dependent fluid forces, which are given as follows:

$$g_j = \sum_{k=1}^2 \left(\bar{\alpha}_{jk} \frac{\partial^2 u_k}{\partial t^2} + \bar{\sigma}_{jk} \frac{\partial^2 v_k}{\partial t^2} + \bar{\alpha}'_{jk} \frac{\partial u_k}{\partial t} + \bar{\sigma}'_{jk} \frac{\partial v_k}{\partial t} + \bar{\alpha}''_{jk} u_k + \bar{\sigma}''_{jk} v_k \right) \quad (9.2)$$

and

$$h_j = \sum_{k=1}^2 \left(\bar{\tau}_{jk} \frac{\partial^2 u_k}{\partial t^2} + \bar{\beta}_{jk} \frac{\partial^2 v_k}{\partial t^2} + \bar{\tau}'_{jk} \frac{\partial u_k}{\partial t} + \bar{\beta}'_{jk} \frac{\partial v_k}{\partial t} + \bar{\tau}''_{jk} u_k + \bar{\beta}''_{jk} v_k \right).$$

Different types of motion can be classified according to the dominant fluid-force components given in Eqs. 9.1 and 9.2.

9.3 FLOW REGIMES

The interference between the two cylinders will occur either when they are sufficiently close to each other or when the rear cylinder is adjacent to or within the wake of the front one. Based on the arrangement of the two cylinders, we can group the different situations into three regions, as shown in Fig. 9.2 (Zdravkovich 1982).

- **Coupled Region:** The flow field or motion of either cylinder affects the other.

- **Wake Interference Region:** The flow field or motion of the front one affects the one in the wake.

- **No Interference Region:** The flow field and motion of either one is not affected by the other.

The boundaries of different regions are affected by different system parameters. At this time, the precise boundaries are not known. Figure 9.2 is included only to illustrate the general location of the three major regions. The two cylinders can be arranged side-by-side relative to the incoming flow, one behind the other in tandem arrangement or staggered relative to the flow velocity. The coupled regions encompass all three arrangements up to a certain pitch-to-diameter ratio. The wake interference region extends very far downstream but it is limited to the tandem and slightly staggered arrangements.

9.3.1 Two Cylinders Side-by-Side

One of the methods to characterize the interference is the measurement of interference drag, which is defined as the difference between the drag

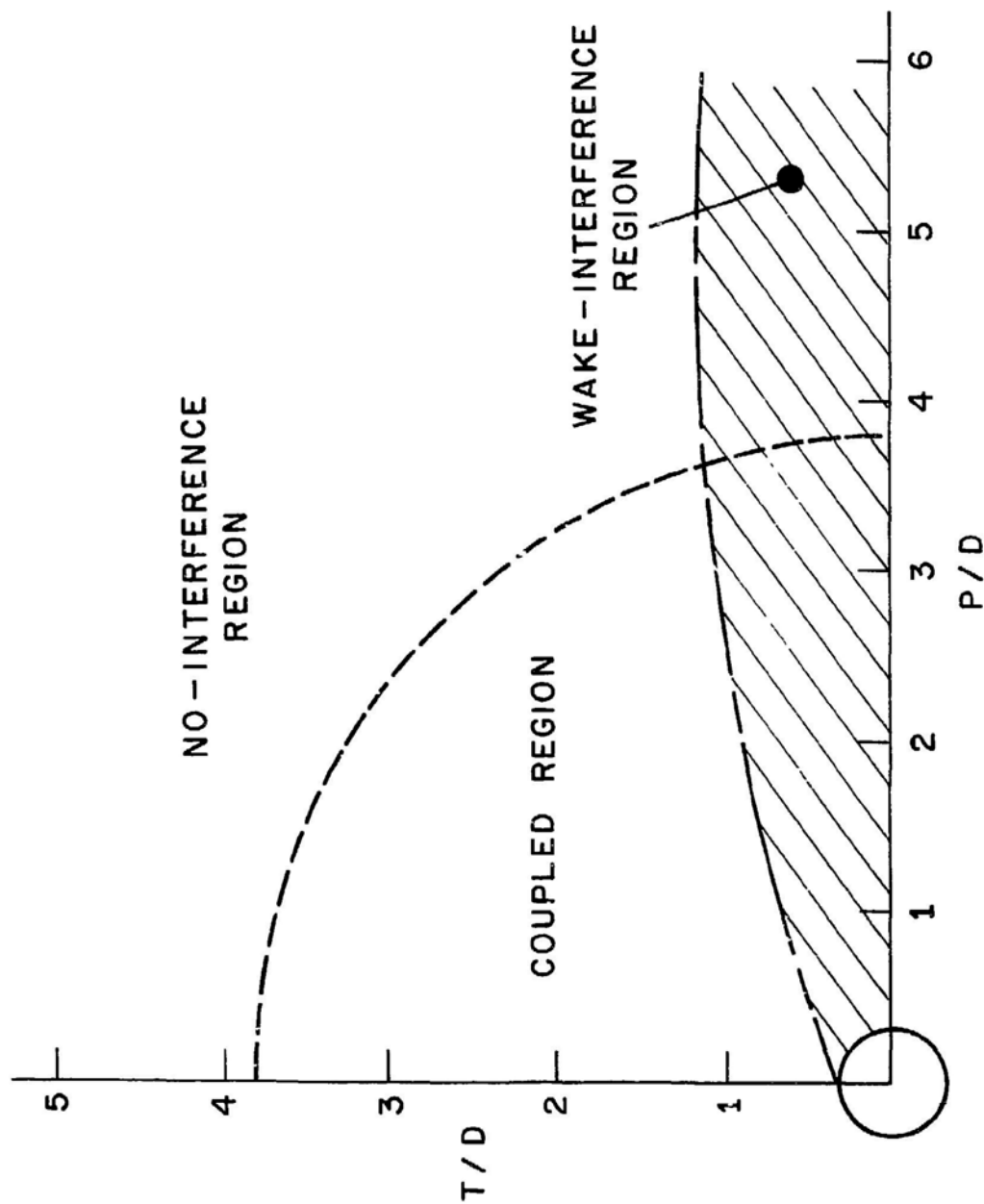


Fig. 9.2. Interference Regions for Two Cylinders (from Zdravkovich 1982, with permission--see Credits)

coefficient measured on one of the cylinders, and the drag coefficient of the single cylinder at the same Reynolds number.

Figure 9.3 shows the interference drag as a function of the pitch-to-diameter ratio (Biermann and Herrnstein 1933). Note that the interference drag was zero for all spacings greater than five diameters; it increases as the spacing decreases but only down to about two diameters. For small spacings, the interference drag changes drastically.

The Strouhal number based on that measured by Spivak (1946) is shown in Fig. 9.4 as a function of pitch-to-diameter ratio. Similar results have been obtained by Bearman and Wadcock (1973) and Jendrzejczyk and Chen (1982). For T/D larger than 2.0, the Strouhal frequency is the same as for the single cylinder. For $T/D < 2.0$, two frequencies are noted. The upper frequency disappears for small spacings and the lower frequency continues down to the two cylinders in contact.

One of the distinct features of the flow field is the bistable nature of the biased flow pattern. For $1.1 < T/D < 2.3$, Bearman and Wadcock (1973) have found that the base pressure on the two cylinders is different and changes from one steady value to another, or fluctuates between the two extremes. In this range of spacing, two bistable forces are experienced by the two cylinders.

The steady lift and drag coefficients, compiled by Zdravkovich (1977), are shown in Fig. 9.5, in which repulsive lift force between the cylinders is taken as positive. The general trend of the different curves is the same. The sum of the bistable low drag and the high drag is always smaller than twice the drag of an isolated cylinder.

A detailed study of the fluid force coefficients was conducted for $T/D = 1.5$ for different upstream turbulence intensities (TIs). The various coefficients are given in Figs. 9.6-9.9 (Jendrzejczyk and Chen 1982). The steady drag coefficient increases with turbulence intensity in the range of Reynolds numbers tested; however, its effect is small. The results agree well with those by Zdravkovich and Pridden (1977). The lift force tends to push the two cylinders apart. The results are consistent with those by Bearman and Wadcock (1973).

The fluctuating drag and lift force coefficients given in Figs. 9.8 and 9.9 show distinct features. Both fluctuating drag and lift forces increase with turbulence intensity in the Reynolds numbers tested and they can increase or decrease with Reynolds number. There is incomplete information on C_D' and C_L' . More data are needed.

Based on the interference drag (Biermann and Herrnstein 1933), photographic studies of the wake behind the cylinders (Landweber 1942; Ishigai et al. 1972), vortex shedding frequency (Spivak 1946), and base pressure (Hori 1959; Bearman and Wadcock 1973) the flow field for two identical cylinders

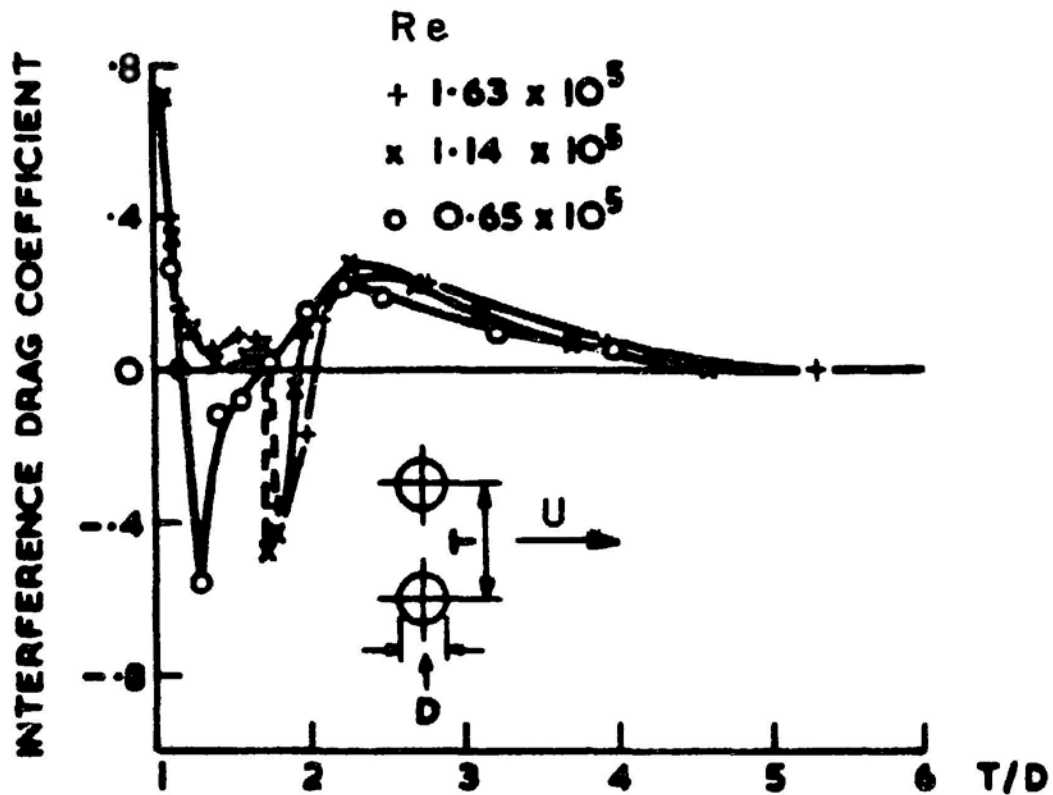


Fig. 9.3. Interference Drag Coefficient for Side-by-Side Arrangement (from Zdravkovich 1977 with permission--see Credits; original source from Biermann and Herrnstein 1933)

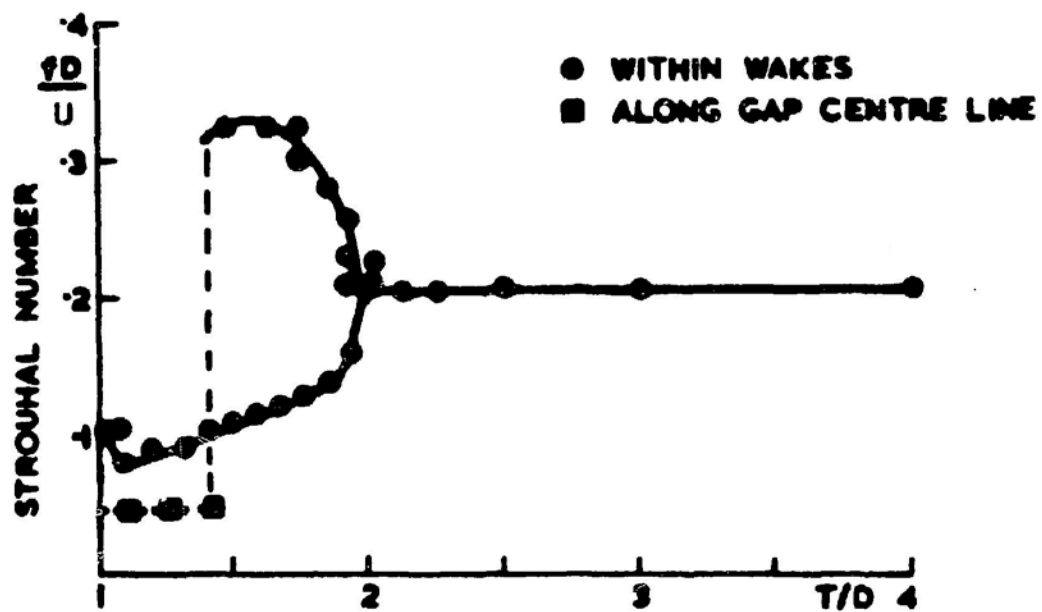


Fig. 9.4. Strouhal Number for Side-by-Side Arrangement (from Zdravkovich 1977, with permission--see Credits; original source from Spivak 1946)

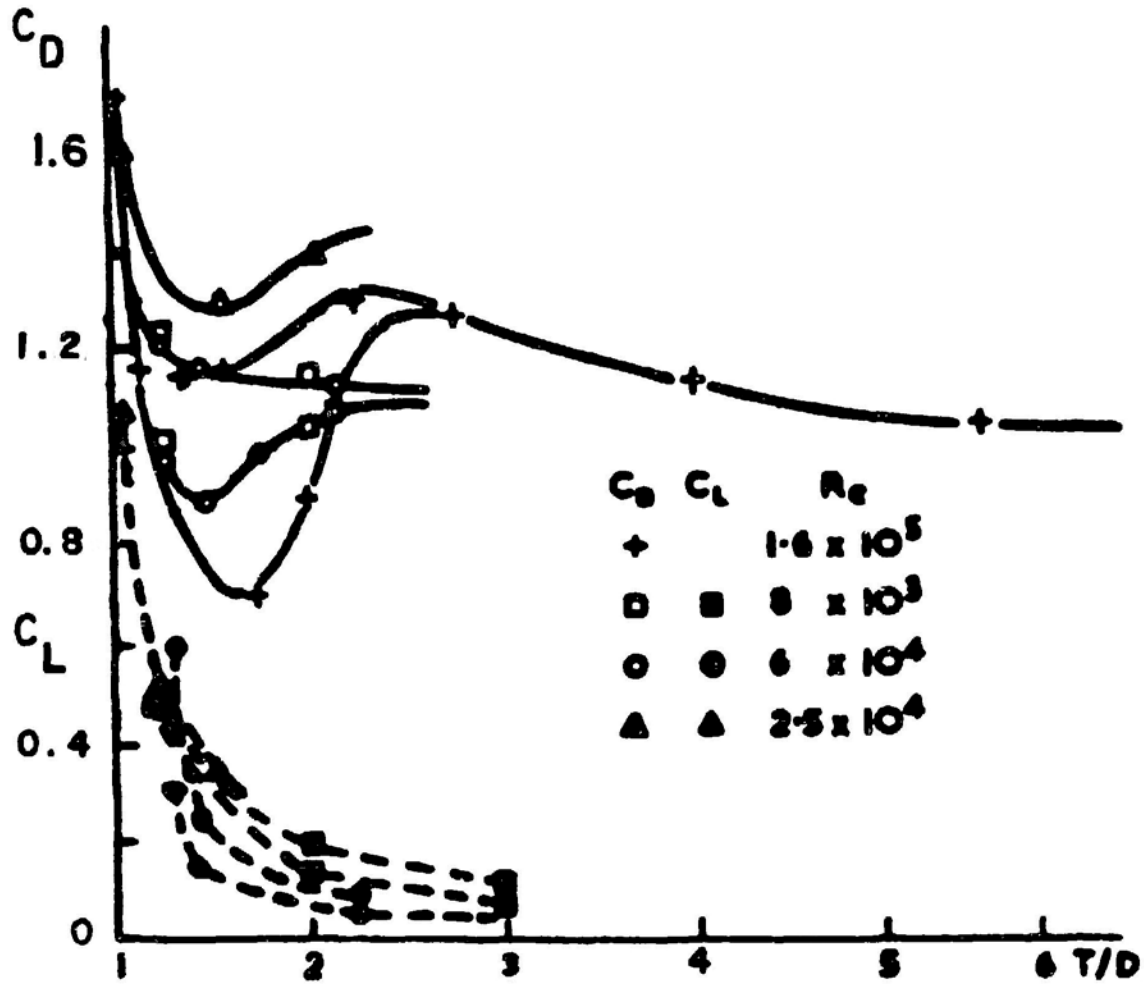


Fig. 9.5. Steady Drag and Lift Coefficients for Side-by-Side Arrangement
(from Zdravkovich 1977 with permission--see Credits; original
source from Zdravkovich and Pridden 1977)

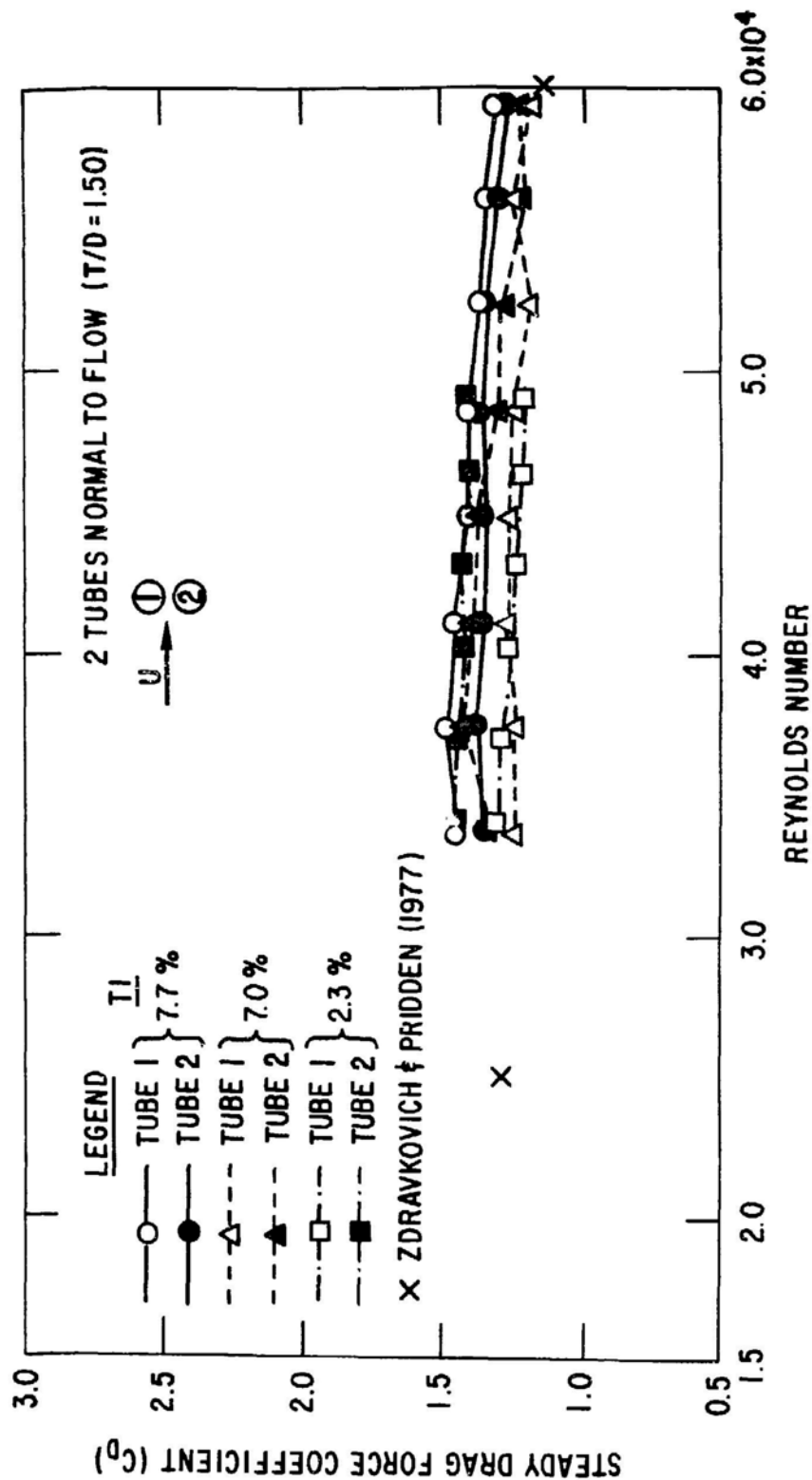


Fig. 9.6. Steady Drag Force Coefficient for Side-by-Side Arrangement with $T/D = 1.5$
(Jendrzejczyk and Chen 1982)

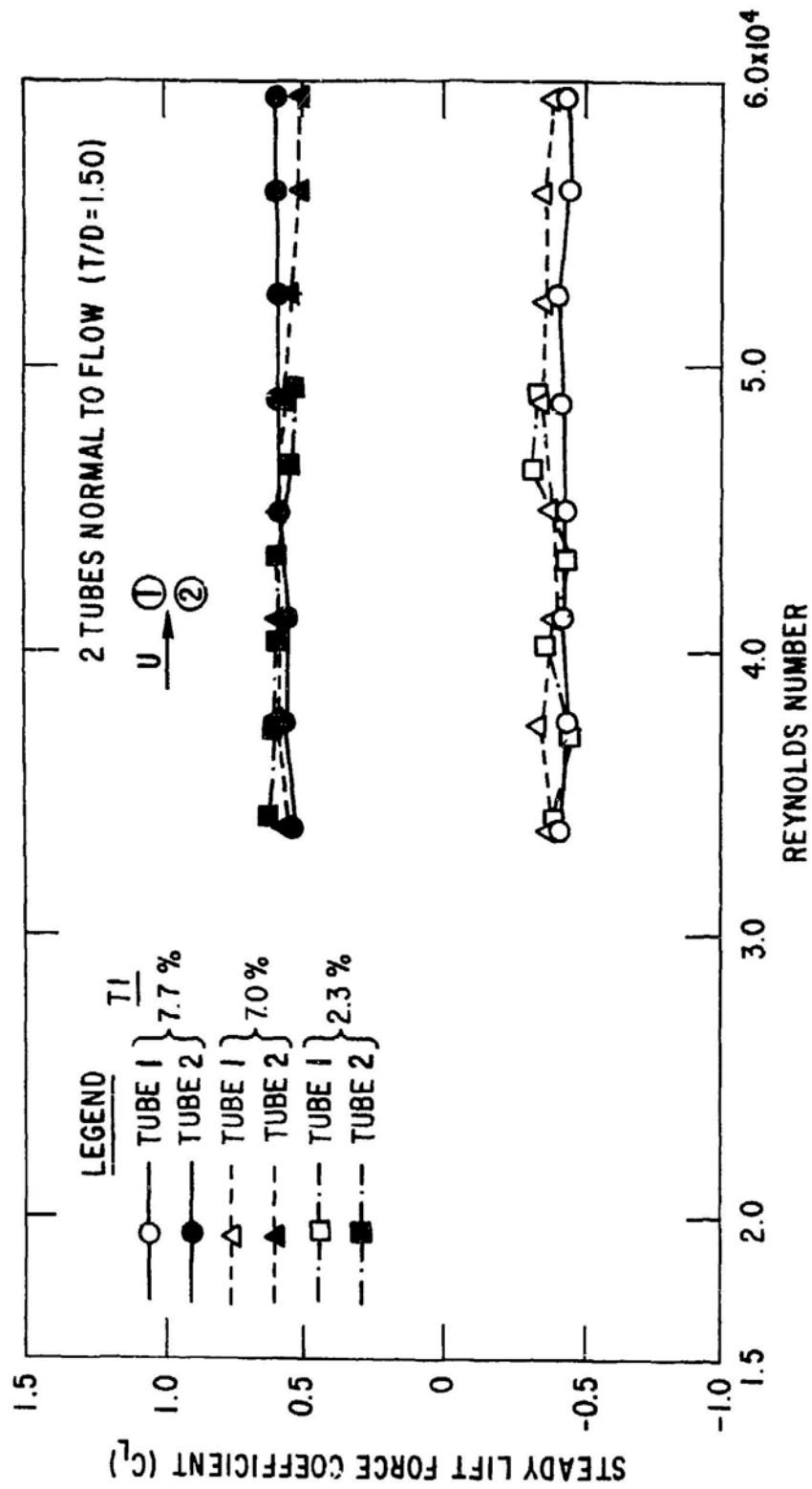


Fig. 9.7. Steady Lift Force Coefficient for Side-by-Side Arrangement with $T/D = 1.5$
(Jendrzejczyk and Chen 1982)

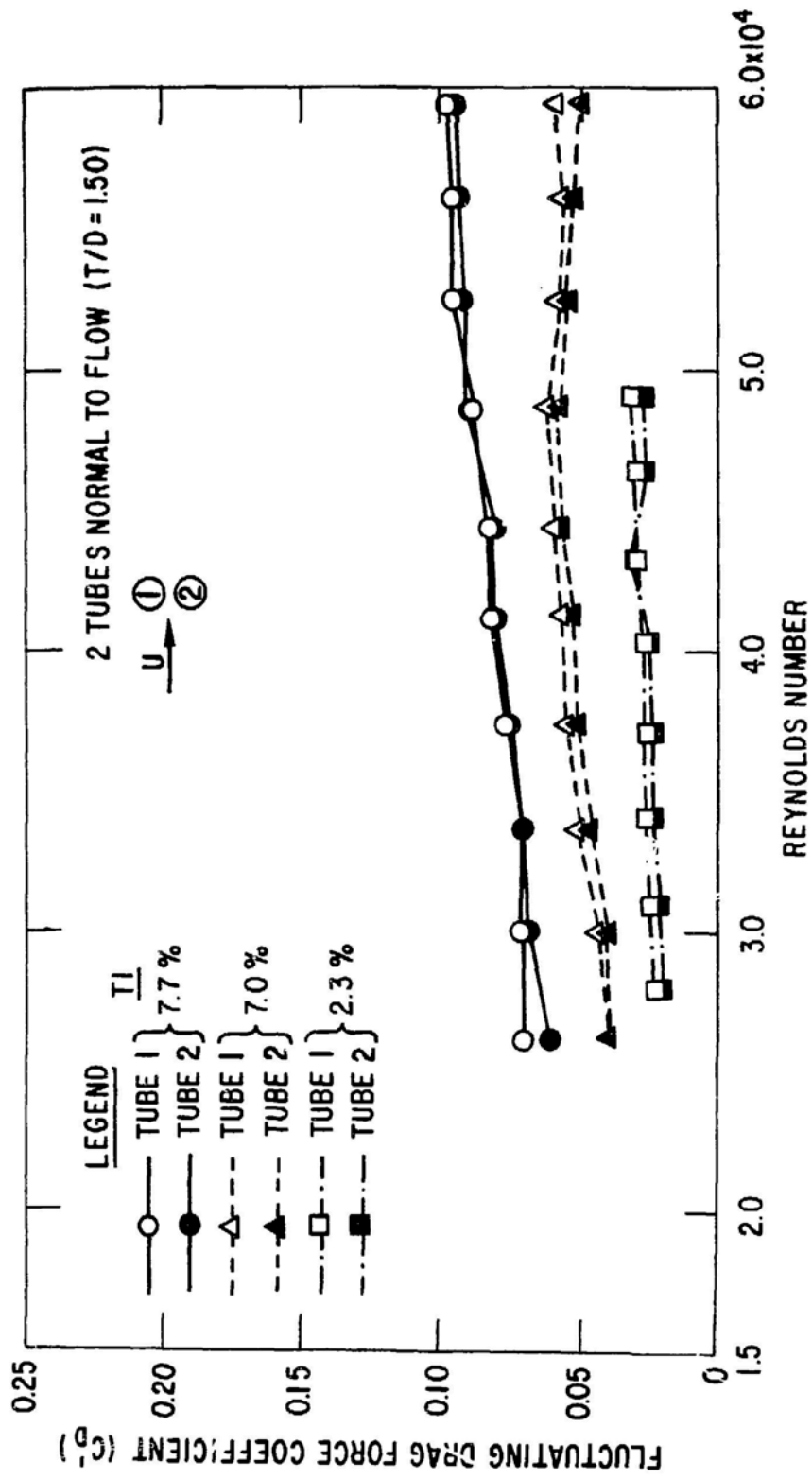


Fig. 9.8. Fluctuating Drag Force Coefficient for Side-by-Side Arrangement with $T/D = 1.5$
(Jendrzejczyk and Chen 1982)

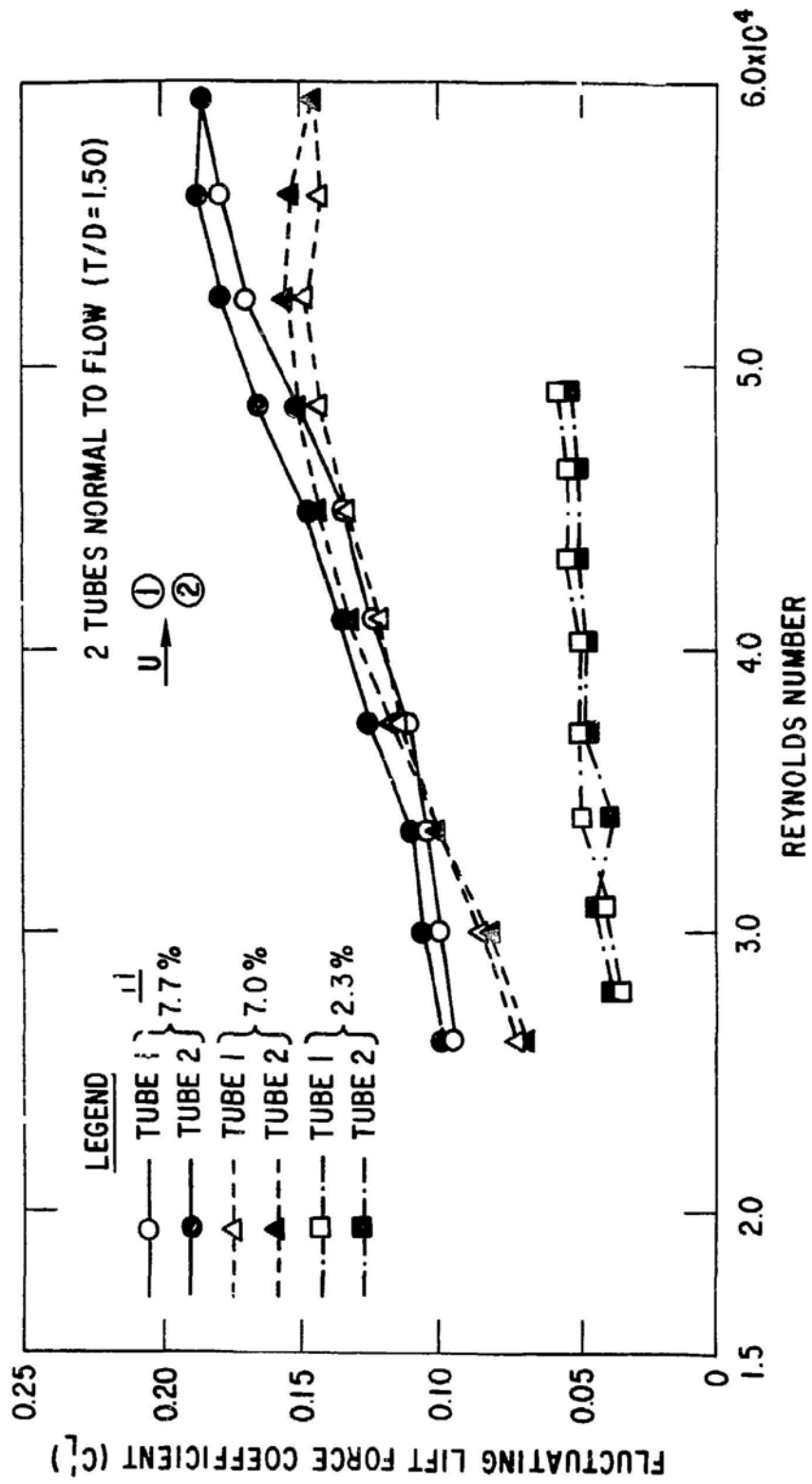


Fig. 9.9. Fluctuating Lift Force Coefficient for Side-by-Side Arrangement with $T/D = 1.5$
(Jendrzejczyk and Chen 1982)

normal to flow can be divided into four regions (see Fig. 9.10). In this case, because the two cylinders are identical,

$$\begin{aligned} C_{D1} = C_{D2} = C_D, \quad C_{L1} = -C_{L2} = C_L, \\ C'_{D1} = C'_{D2} = C'_D, \quad C'_{L1} = C'_{L2} = C'_L. \end{aligned} \quad (9.3)$$

Equations 9.3 are valid except in the bistable flow region.

No-Interference ($T/D > 4$): The flow around the cylinders is the same as that around an isolated cylinder. Therefore $C_L = 0$, and the steady drag coefficient C_D , fluctuating drag and lift coefficients C'_D and C'_L , and Strouhal frequency are the same as those for an isolated cylinder. The dominant excitation mechanism is the vortex shedding.

Coupled Vortex Streets ($2.0 < T/D < 4$): The interference drag increases with decreasing T/D , the Strouhal number is the same as that of an isolated cylinder, and both C_D and C_L decrease with increasing T/D . Although both vortex streets have the same frequency, they are coupled in an out-of-phase mode; i.e., the vortices are simultaneously formed and shed on the gap side and then simultaneously on the other sides. In this region, vortex shedding is the dominant excitation, although there is some interaction between the two cylinders.

Biased Flow Pattern ($1.2 < T/D < 2.0$): The gap flow is biased to one side; consequently, wide and narrow wakes are formed behind the cylinders. The biased flow in the gap is bistable and intermittently changes from one side to the other. Two Strouhal frequencies are associated with the two wakes and the drag and lift forces are not steady because of the bistable nature of the biased flow pattern. In this region, in addition to the vortex excitation, fluidelastic instability is important.

Single Vortex Street ($1.2 < T/D$): When two cylinders are fairly close, a single vortex street is formed downstream. Two cylinders behave as a single bluff body. The drag and lift coefficients C_D and C_L increase with decreasing T/D . Because of the small gap, the two cylinders are strongly coupled by the flow field. Both vortex-excited oscillation and fluidelastic instability can cause cylinders to impact with each other.

9.3.2 Two Cylinders in Tandem

Figure 9.11 shows the interference drag for both cylinders and the combined interference drag, obtained by adding the interference drag coefficients of both cylinders (Biermann and Herrnstein 1933). Note that the minimum interference drag coefficient of the upstream cylinder coincides with

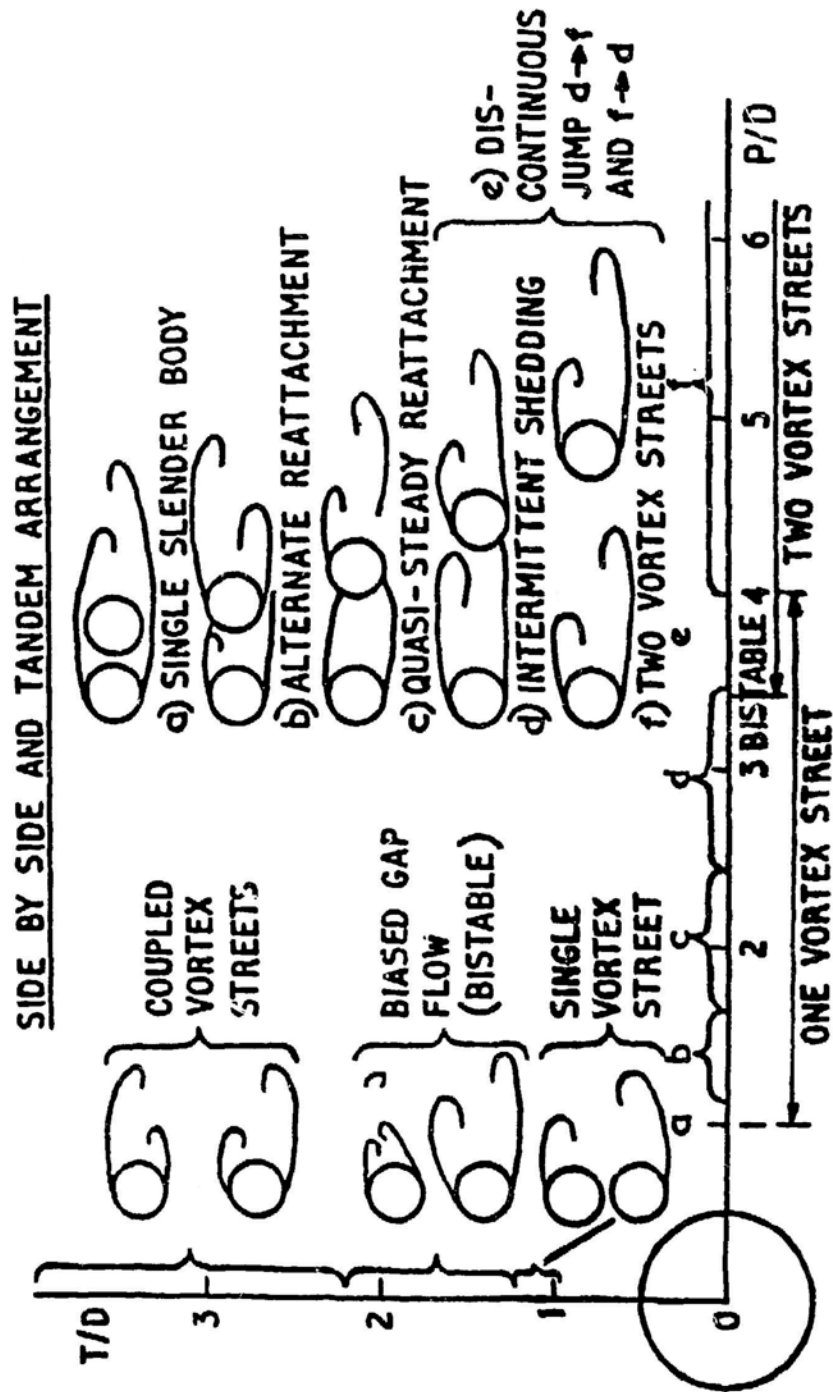


Fig. 9.10. Classification of Flow Regimes in Side-by-Side and Tandem Arrangements for Stationary Cylinders (from Zdravkovich 1982, with permission--see Credits)

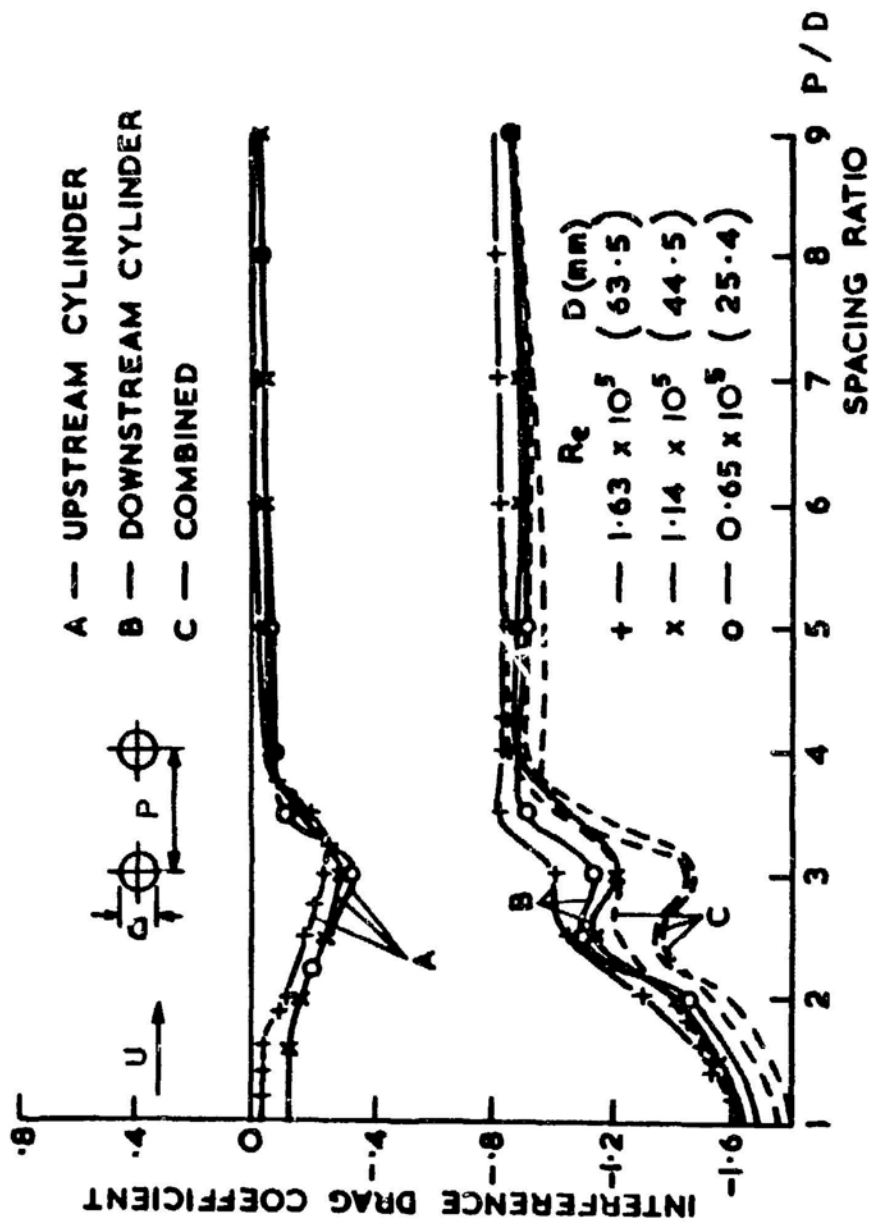


Fig. 9.11. Interference Drag Coefficient for Tandem Cylinders (from Zdravkovich 1977, with permission--see Credits; original source from Biermann and Herrnstein 1933)

the "s" portion of the interference drag coefficient of the downstream cylinder.

The Strouhal frequency measured by Oka et al. (1972) is given in Fig. 9.12. In general, the vortex shedding frequencies behind the two cylinders are different. No distinct vortex shedding is found behind the upstream cylinders up to $P/D = 3.8$. For $P/D > 3.8$, the vortex shedding frequency reaches the value for an isolated cylinder. The vortex shedding exists in the whole range of spacing behind the downstream cylinder. It decreases with P/D for $1 < P/D < 3.8$, then jumps to higher values at $P/D \sim 3.8$, which is the same spacing at which the vortex shedding appears behind the upstream cylinder.

Figure 9.13 shows the drag coefficients compiled by Zdravkovich (1977) for various Reynolds numbers. It shows the discontinuous jump of the drag coefficient at P/D between 3 and 4 for the upstream cylinder. Regardless of the Reynolds number, the drag coefficient reaches the value for a single cylinder once the spacing is larger than the critical P/D . The downstream cylinder shows a stronger dependence on the Reynolds number.

Figures 9.14-9.16 show the steady and fluctuating drag and lift coefficients for $P/D = 1.5$ for different turbulence intensities (Jendrzejczyk and Chen 1982). In these figures,

- The steady drag coefficient increases with turbulence intensity,
- Fluctuating lift force is larger than fluctuating drag force (this is mainly attributed to vortex shedding),
- Both fluctuating lift and drag forces increase with turbulence intensity, and
- Both fluctuating force components in lift and drag directions acting on the upstream cylinders are smaller than those on the downstream one.

Based on experimental data, the flow field can be divided into the following regions (Zdravkovich 1982):

- Single Slender Body ($1 < P/D < 1.1$): The two cylinders behave as a single slender body with high Strouhal number (~ 0.24). The shear layers separated from the front cylinder do not reattach onto the downstream cylinder. The drag force acting on the downstream cylinder is to push it upstream.
- Alternate Reattachment ($1.1 < P/D < 1.6$): An alternate reattachment of the shear layers takes place on the front side of the rear cylinder in the rhythm of vortex shedding of the latter. The drag force acting on the downstream still acts to push it upstream. Both Strouhal number and the absolute value of the drag coefficients decrease with increasing P/D .
- Quasi-Steady Reattachment ($1.6 < P/D < 2.4$): Quasi-steady reattachment of separated shear layers is noted. Strouhal number and the absolute value of the drag coefficients decrease with P/D .

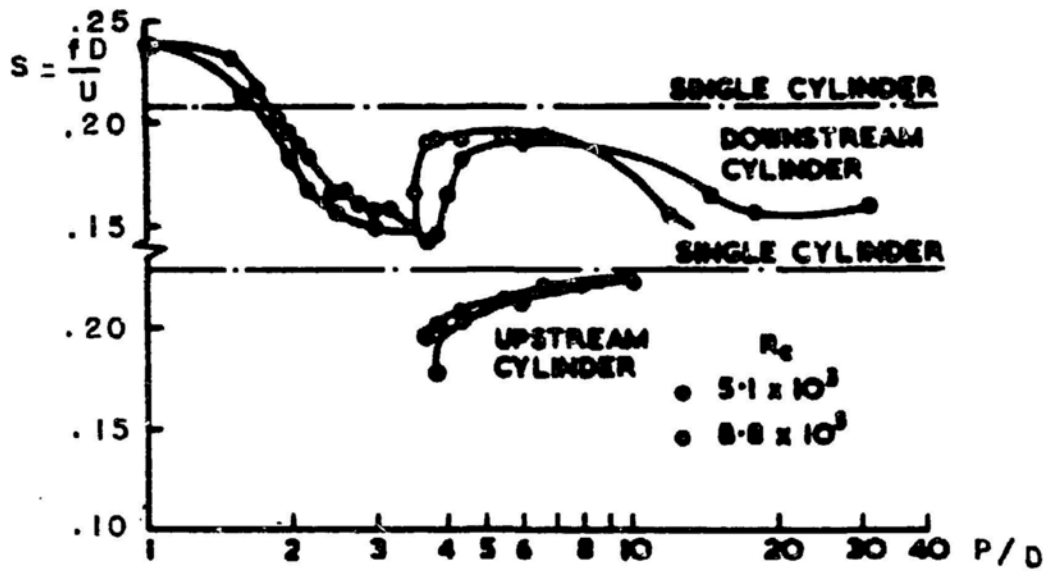


Fig. 9.12. Strouhal Number Behind Cylinders in Tandem Arrangement
(from Zdravkovich 1977 with permission--see Credits;
original source from Oka et al. 1972)

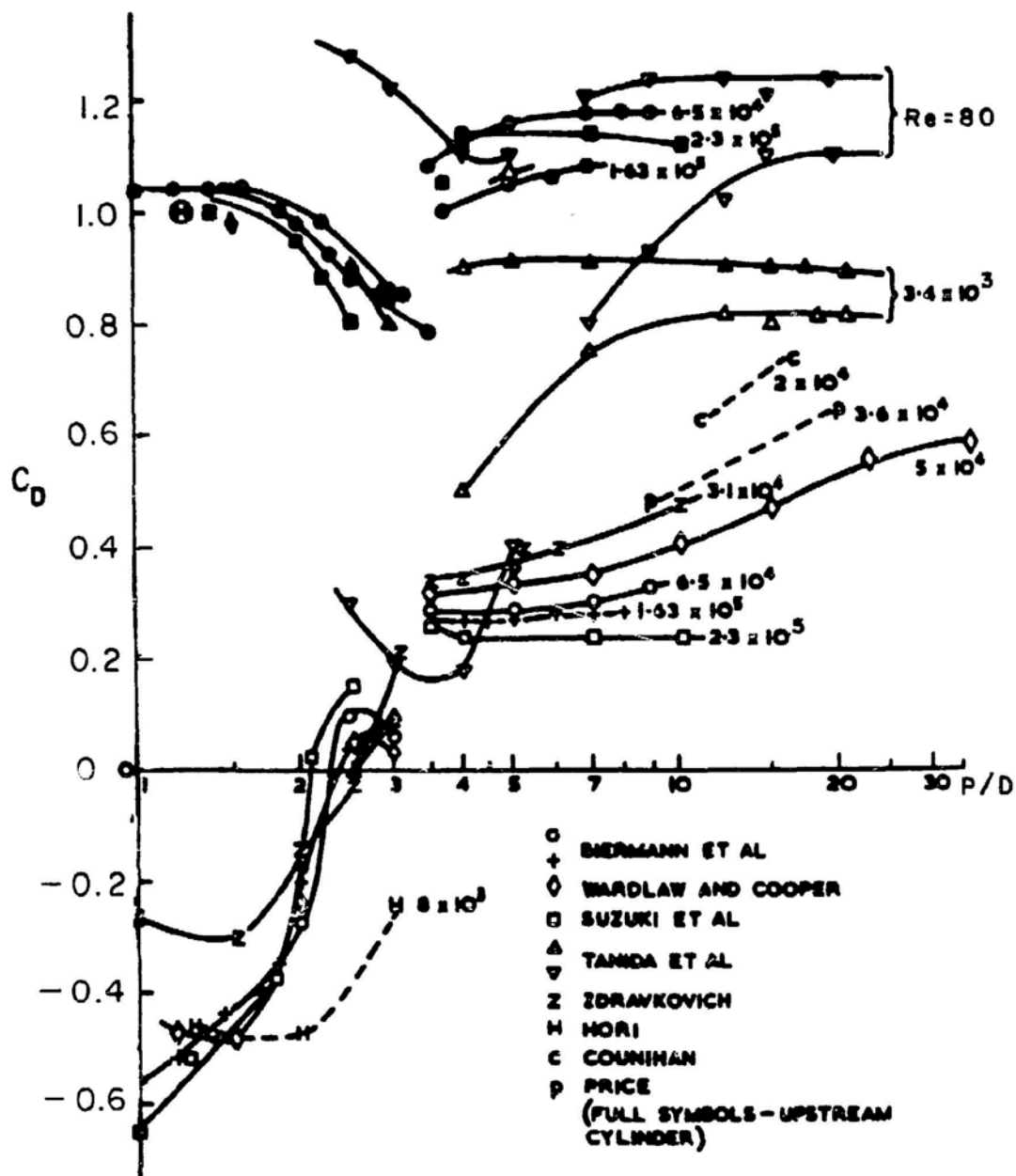


Fig. 9.13. Steady Drag Coefficient for Two Cylinders in Tandem Arrangement (from Zdravkovich 1977, with permission--see Credits)

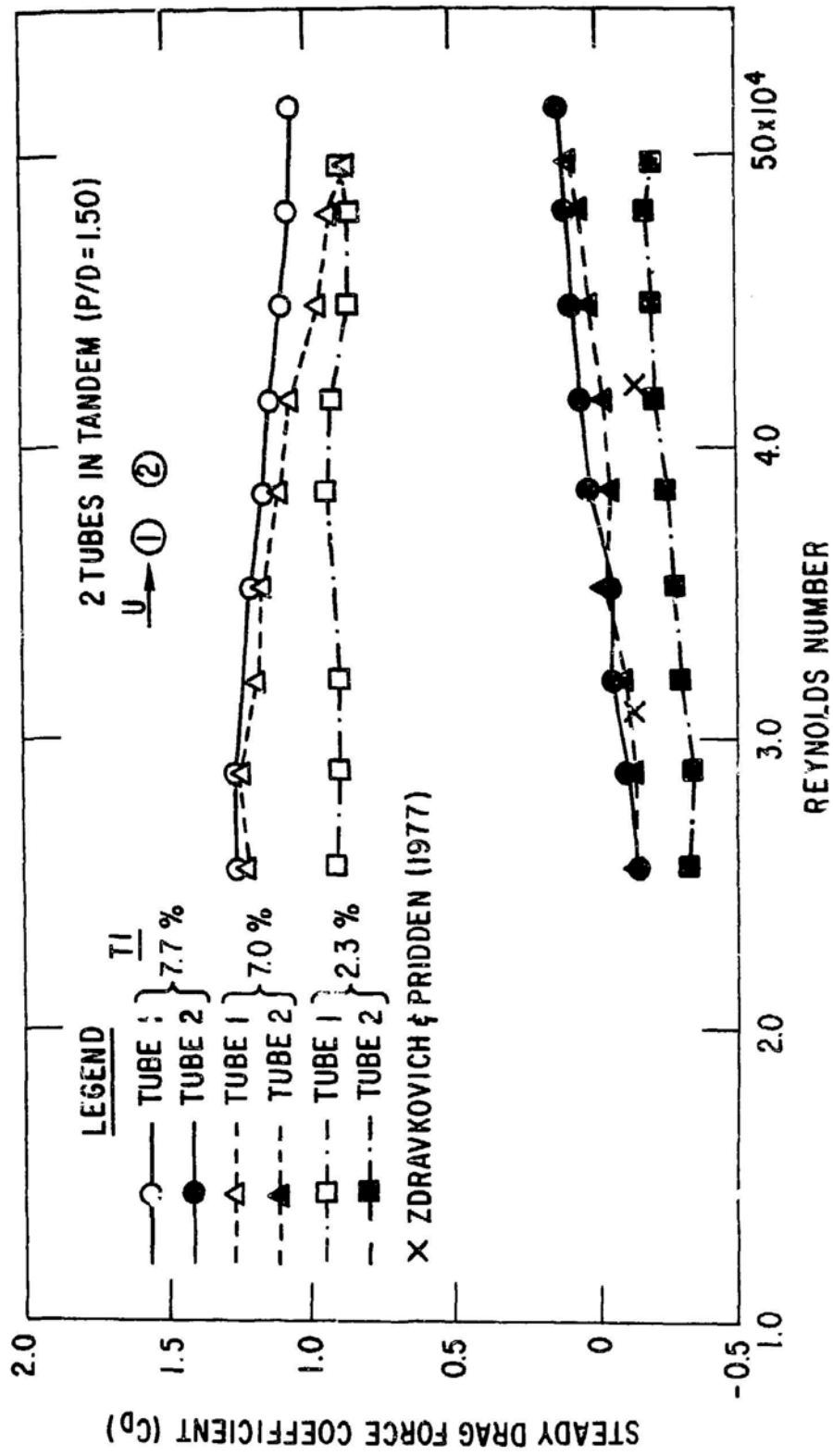


Fig. 9.14. Steady Drag Coefficients for Two Cylinders in Tandem with P/D = 1.5
(Jendrzejczyk and Chen 1982)

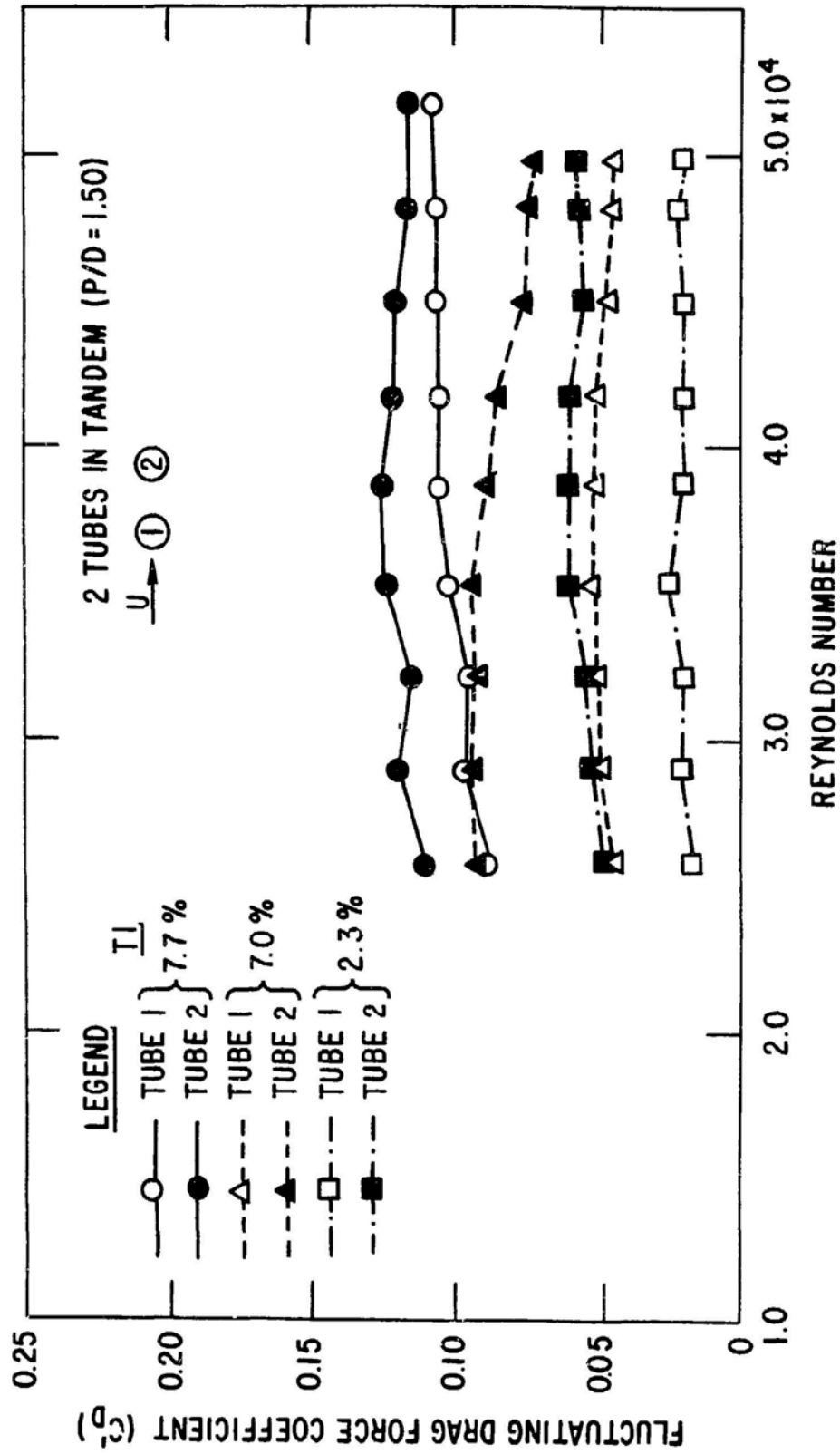


Fig. 9.15. Fluctuating Drag Coefficient for Two Cylinders in Tandem with $P/D = 1.5$
(Jendrzejczyk and Chen 1982)

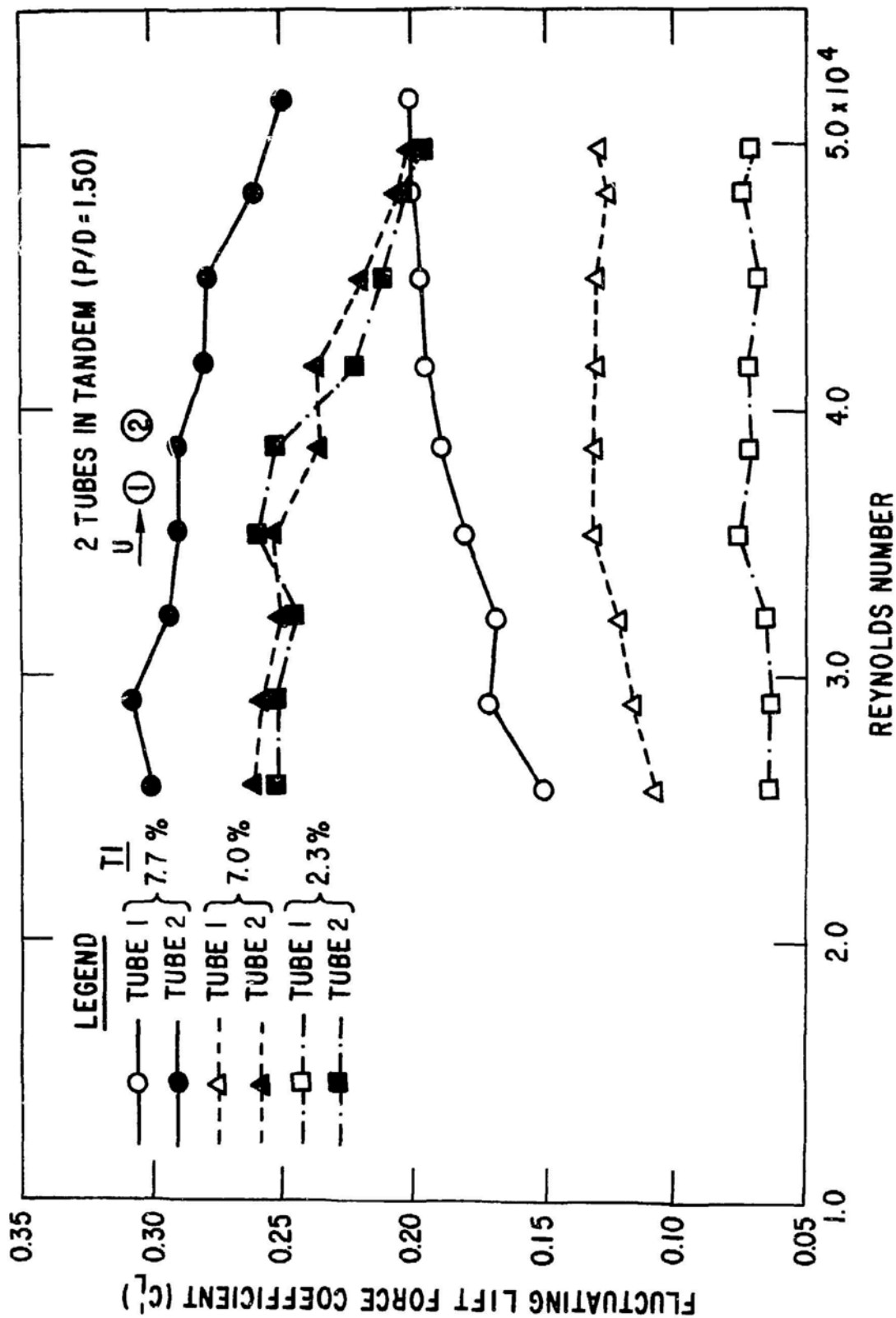


Fig. 9.16. Fluctuating Lift Coefficient for Two Cylinders in Tandem with $P/D = 1.5$
(Jendrzejczyk and Chen 1982)

- Intermittent Shedding ($2.4 < P/D < 3.5$): One of the reattachments is disturbed but no regular vortex shedding behind the front cylinder. The Strouhal number and the drag coefficient for the front cylinder continue to decrease, while the drag coefficient for the downstream one changes direction.

- Unstable Region ($3.5 < P/D < 4$): The vortex shedding behind the front cylinder persists for some time and then it is intermittently suppressed and replaced by the reattachment flow regime. There is a sharp increase of Strouhal number of the downstream cylinder. No distinct vortex shedding is detectable behind the front cylinder. Jump of the drag coefficients takes place for both cylinders.

- Two Vortex Streets ($P/D > 4$): Beyond the unstable region, both cylinders form vortex streets. The Strouhal number for the front cylinder first increases with P/D approaching the value found for the single cylinder and then decreases again for $P/D > 8$ and, for the downstream cylinder, it soon reaches the value for a single cylinder. The drag coefficient for the front cylinder is always larger than the downstream one.

9.3.3 Two Cylinders in Staggered Arrangement

The staggered arrangement is most likely to occur in practical situations; nevertheless, there are only a few published systematic studies of the flow field. Measurements have been made for base pressure, interference force coefficients, lift and drag forces, and Strouhal numbers for different arrangements (Hori 1959; Mair and Maull 1971; Zdravkovich 1977; Kiya et al. 1980; Arie et al. 1983; and Layoub 1982).

The Strouhal numbers obtained by Arie and his colleague (Kiya et al. 1980) for a Reynolds number of 1.58×10^4 are given in Fig. 9.17, in which the curves of constant Strouhal numbers are drawn by linear interpolation of the measured values. All possible arrangements of the two cylinders are divided into several regions denoted by 1, 2, 3, 4, and 5 for a particular Reynolds number. The general features of the flow are summarized by Kiya et al. (1980).

- With respect to vortex shedding, the cylinders behave as a single body when $(T^2 + P^2)^{0.5} < 1.4 D$.

- The bistable side-by-side arrangement, which represents the transition from the upstream to the downstream stagger with respect to one of the two cylinders, results in large changes in Strouhal number.

- There exists a region in which the Strouhal number for the upstream cylinder is much higher than that for the single cylinder.

- The Strouhal number for the downstream cylinder is generally lower than that for the single cylinder except when the spacing is less than $1.4 D$ in a tandem arrangement.

- (1) Region where the Strouhal number is higher than that for the single cylinder.
- (2) Region where the Strouhal number is less than that for the single cylinder.
- (3) Region where the bistable vortex shedding occurs.
- (4) Region where the pair of the cylinders behaves as a single body with regard to the vortex shedding.
- (5) Region where weak or no vortex shedding occurs.

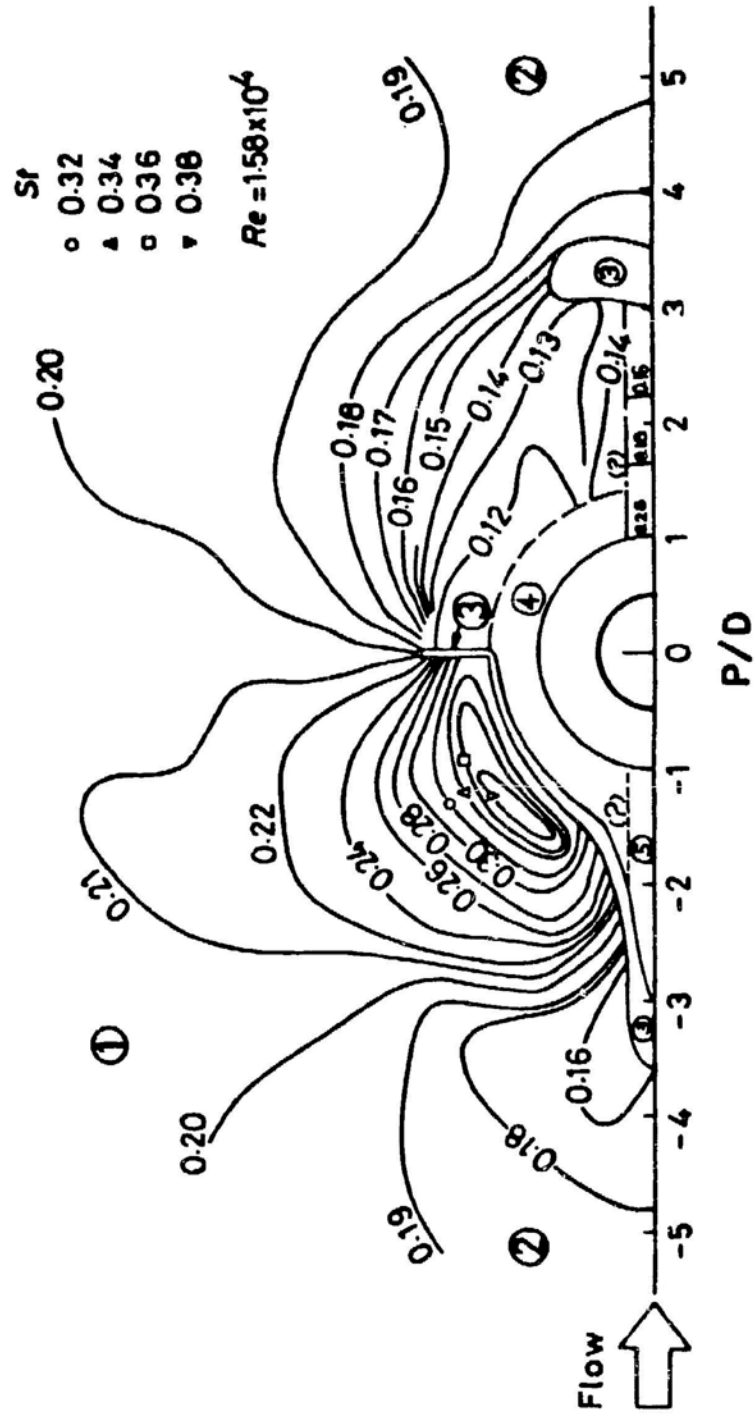


Fig. 9.17. Strouhal Number for Two Cylinders in Staggered Arrangement (from Kiya et al. 1980, with permission--see Credits)

- The gap flow between the cylinders is biased to the side of the upstream cylinder, thus forming a much narrower wake behind the upstream cylinder than that behind the downstream cylinder. Narrower wakes correspond to higher Strouhal numbers and wider wakes to lower Strouhal numbers.

Figure 9.18 shows the steady drag and lift coefficients for the downstream cylinders for $Re \ 6 \times 10^4$ (Zdravkovich and Pridden 1977). The oncoming flow field is responsible for variations in the dynamic effect on the downstream cylinder. The drag variation is symmetric about zero lateral displacement. These variations occur mainly as a result of the total pressure defect in the wake as well as the high turbulence level of the oncoming flow. The minimum drag curve is given by the chain-dot line.

The lift coefficients show a positive repulsive force in the vicinity of side-by-side arrangements; the remainder of the staggered arrangements have a negative force directed toward the wake center. The negative lift force increases gradually towards the maximum value, shown as the chain-dot lines. There are two separate curves representing the maximum lift coefficient; one inside the wake for pitches up to 3 diameters and the other near the wake boundary for pitches greater than 2.7.

There is very limited information regarding fluctuating force coefficients. In general, available information is sufficient for predicting cylinder response from these force components.

The front cylinder is stable in the staggered arrangements except when the downstream cylinder is fairly close to the upstream one. Therefore, for a relatively large spacing, the main excitation mechanism for the front cylinder is vortex shedding. For small spacings, the two cylinders are coupled by fluid inertia forces. When the downstream cylinder is in the wake of the upstream one, large oscillations can occur; this is called wake-induced flutter, wake-induced oscillation, or wake-induced galloping.

9.4 RESPONSE OF TWO CYLINDERS IN FLOW

The method presented in Section 8.6 can be used for two cylinders. Once the fluid force components are known, the analysis is straightforward, but generally the analysis cannot be made because of the lack of fluid-force data.

The response of two cylinders in flow is very complex, depending on pitch ratio, flow direction, and mass ratio. Corresponding to a single mode for an isolated cylinder, there are four coupled modes, as discussed in Section 3.2. All four modes contribute to cylinder response. In addition, flow affects the four modes. Cylinder response has been investigated experimentally (e.g., Jendrzejczyk et al. 1979; King and Johns 1976; Livesey and Dye 1962; and Tanida et al. 1973).

There are very few systematic studies characterizing response characteristics. A detailed investigation was conducted by Zdravkovich (1982); vortex

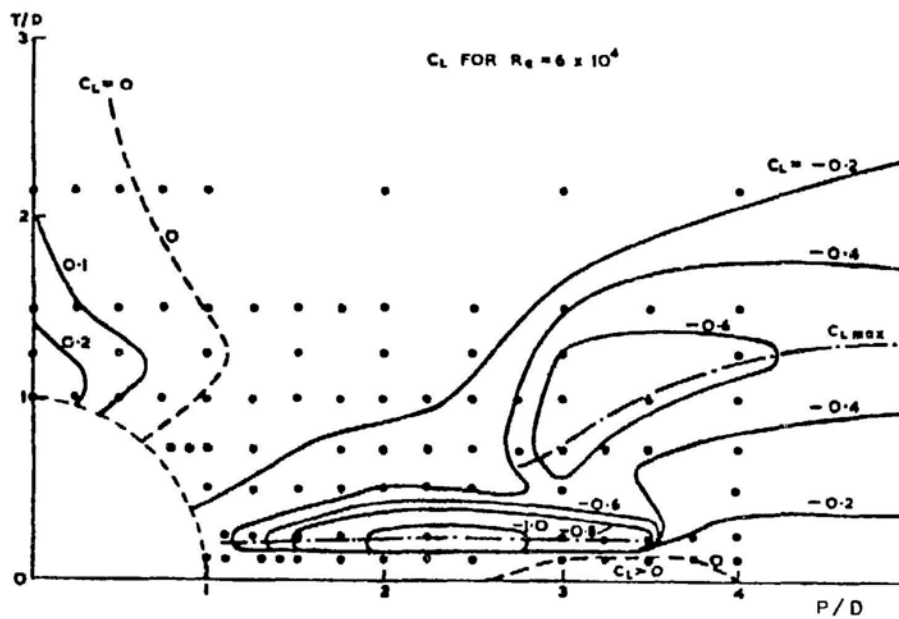
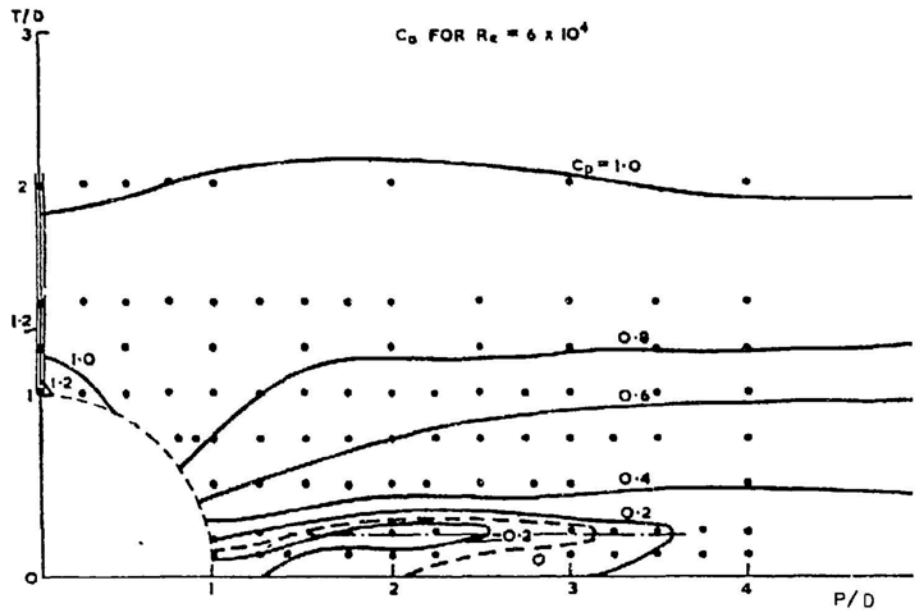


Fig. 9.18. Steady Drag and Lift Coefficients for Two Cylinders in Staggered Arrangement (from Zdravkovich and Pridden 1977, with permission--see Credits)

excitation and fluidelastic instability were investigated for different cylinder arrangements.

Figure 9.19 shows the synchronization region for $\delta_g = 23$ for different cylinder arrangements. The reduced flow velocities for the threshold and end of synchronization are given within each circle; the reduced flow velocity where maximum amplitude developed is given in parentheses. The frequency of vortex shedding depends on the arrangement, and Strouhal number can vary from 0.1 to 0.38 (see Fig. 9.17). This means that the synchronization region can begin from $U_r = 2.6$ to 10. In addition, the oscillation of one cylinder can strongly affect vortex shedding and the synchronization of the other cylinder. These effects are illustrated in Fig. 9.19. Figure 9.20 shows the typical maximum amplitude of vortex excitation. It is apparent that the oscillation amplitudes depend strongly on the arrangement. In some cases, the displacement of the front cylinder (denoted by F) is larger than that of the rear one (denoted by R); however, in most cases, the displacement of the rear one is much larger.

Fluidelastic instability for two cylinders in crossflow is also very important. The instability may be fluid-damping-controlled or fluid-stiffness-controlled. Several mechanisms associated with different flow field are of particular interest.

Jet Switch Mechanism: For small flow velocities, the two cylinders are subject to the same drag and lift forces as in a side-by-side arrangement. As flow velocity increases, the biased flow forms narrow and wide wakes, resulting in different fluid forces (which may be in phase with the cylinder displacement). The biased flow can lead to a steep rise in amplitude in both directions. This jet-switch mechanism of excitation was also found for a row of cylinders (Roberts 1966).

Discontinuities of Flow Field: The drag force coefficients and fluid pressure acting on two cylinders in crossflow show discontinuous "jump" at some critical spacings. The cylinder oscillations can trigger and control the change of flow regimes. The discontinuous change of the fluid force can build up and maintain a large amplitude of oscillations.

Wake-induced Flutter: The wake flow behind the front cylinder is complex, containing periodicities and general turbulence. When such disturbed flow strikes the rear cylinder, dynamic instability of the rear cylinder can occur; however, the dynamic instability is not necessarily affected by the turbulence and periodicities in the flow.

9.4.1 Two Cylinders Side by Side

Two cylinders mounted at varying spacing in air flow were tested by Livesey and Dye (1962). For $T/D > 2.4$, the cylinders vibrate as an isolated cylinder. For $T/D < 2$, two distinct modes are found; at lower speeds, the

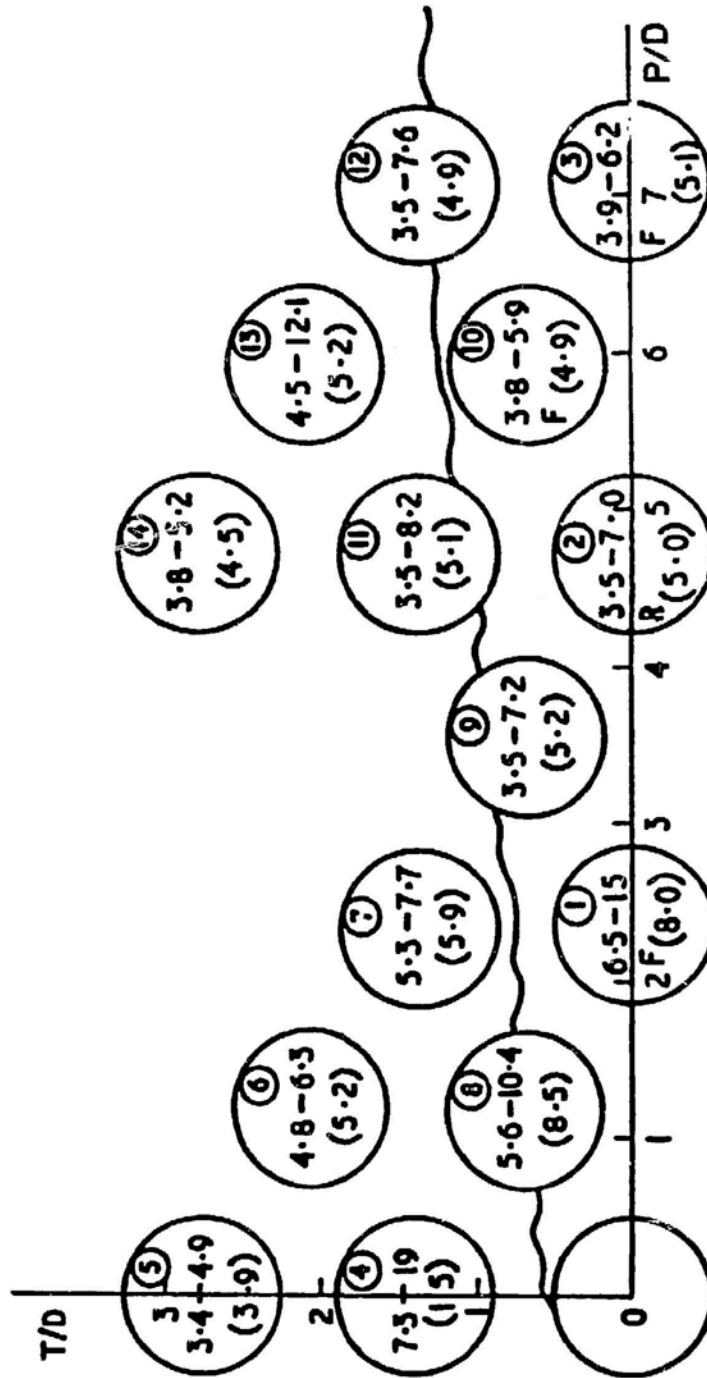


Fig. 9.19. Vortex Shedding Excited Oscillations for Two Cylinders (from Zdravkovich 1982, with permission--see Credits)

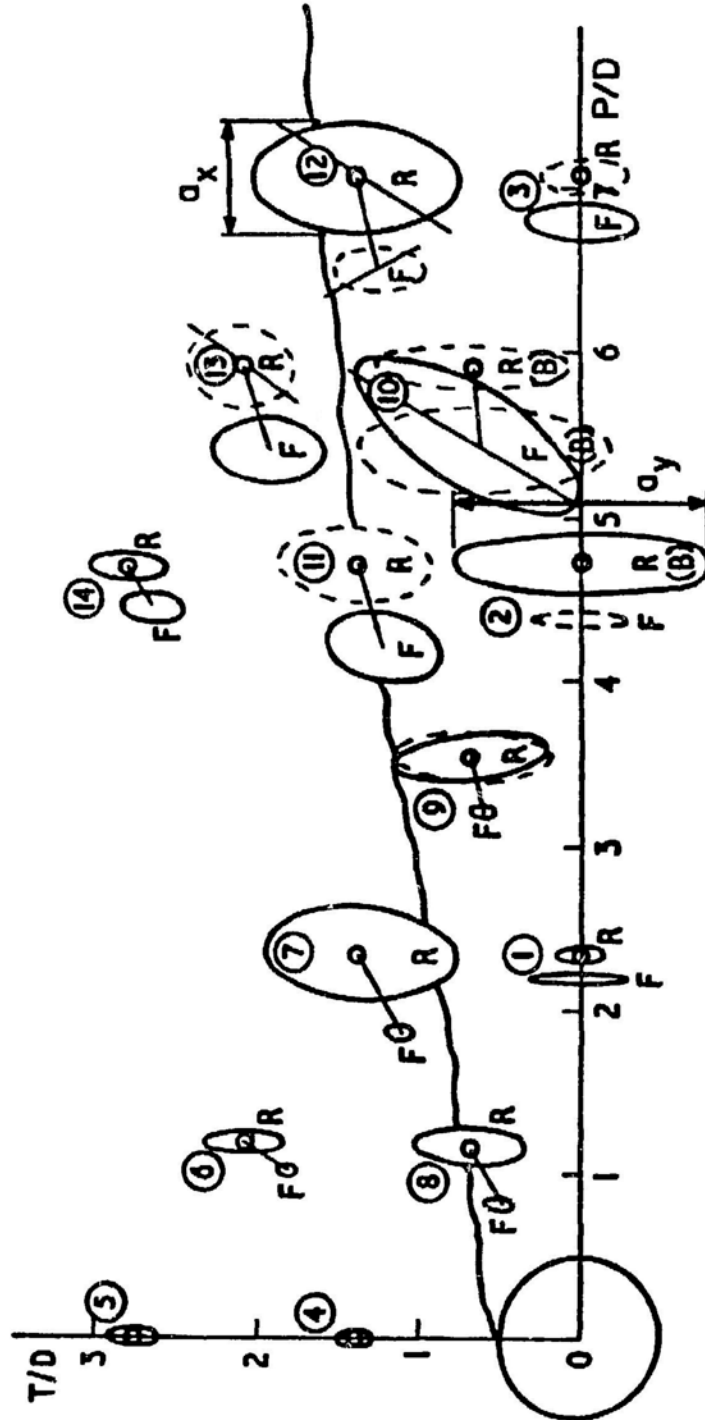


Fig. 9.20. Typical Oscillations at Maximum Amplitude for Vortex Shedding Oscillations (from Zdravkovich 1982, with permission--see Credits)

cylinders moved out of phase, while at higher speeds they vibrate in phase. For $2.0 < T/D < 2.4$, both modes were found. These observations are generally consistent with the flow pattern shown in Fig. 9.10. For large spacings, the coupling due to air flow is very small; therefore, the cylinder responds basically the same as an isolated cylinder. For $T/D < 2$, there are multiple vortex shedding frequencies, and the out-of-phase and in-phase modes are associated with the resonance of the corresponding vortex shedding.

A detailed study of two cylinders in crossflow with $T/D = 1.5$ and 1.75 , which corresponds to the bistable flow regime, was conducted in water by Jendrzejczyk et al. (1979). The study measured cylinder response characteristics, including natural frequencies, damping, displacements, and vibration orbit.

The response characteristics of a particular case ($T/D = 1.515$) are given in Figs. 9.21-9.24 for two tubes with the characteristics shown in Table 9.1. Figure 9.21 shows the tube displacement in the drag and lift directions as a function of flow velocity. Tube displacement in the drag direction begins to increase at a certain value of flow velocity. The peak of the drag-direction displacement curve is characterized by reduced flow velocities in the range of $U_r = 2.25$ to 3.0 . This peak is attributed to the synchronization of vortex shedding with tube motion in the drag direction. In this range of flow velocity, vortex shedding is controlled by tube motion. The general behavior is similar to that of a single cylinder. Tube displacements in the lift direction are small at low flow velocities. As the flow velocity is increased to a certain value, tube oscillations in the lift direction increase drastically. With the coupled natural frequency of the out-of-phase mode of in-plane motion used as the basis, the reduced flow velocity at which significant oscillations in the lift direction occur is about 4.6 .

Tube response frequencies in the lift and drag directions are given in Fig. 9.22. At low flow velocities, tube natural frequencies in the drag and lift direction are the same. As the flow velocity increases, tube natural frequencies in the lift direction decrease while those in the drag direction increase. The cause for the increase and reduction is not known, but it is believed to be attributable to three factors: (1) the drag-force induced displacement tends to change the end condition of the tubes, (2) the added mass matrix is not constant but varies with flow velocity, and (3) the effect of fluid damping and fluid stiffness forces may be important.

From the frequency spectra of tube displacements, major frequency contents of the tube displacement can easily be identified. Tube responses in the drag direction are essentially at the natural frequency of the tubes. However, tube responses in the lift direction contain several components: (1) tube natural frequency, (2) vortex shedding frequency with Strouhal number

Table 9.1. Natural Frequencies (Hz) in Air and Water
of Two Tubes in Side-by-Side Arrangement

<u>Natural Frequency in Air</u>	
Lift direction	
Tube A	67.87
Tube B	75.05
Drag direction	
Tube A	68.41
Tube B	75.05
<u>Coupled Natural Frequency in Water</u>	
Lift direction	
Out-of-phase mode	59.91 Hz
In-phase mode	63.57 Hz
Drag direction	
Out-of-phase mode	59.52
In-phase mode	63.95

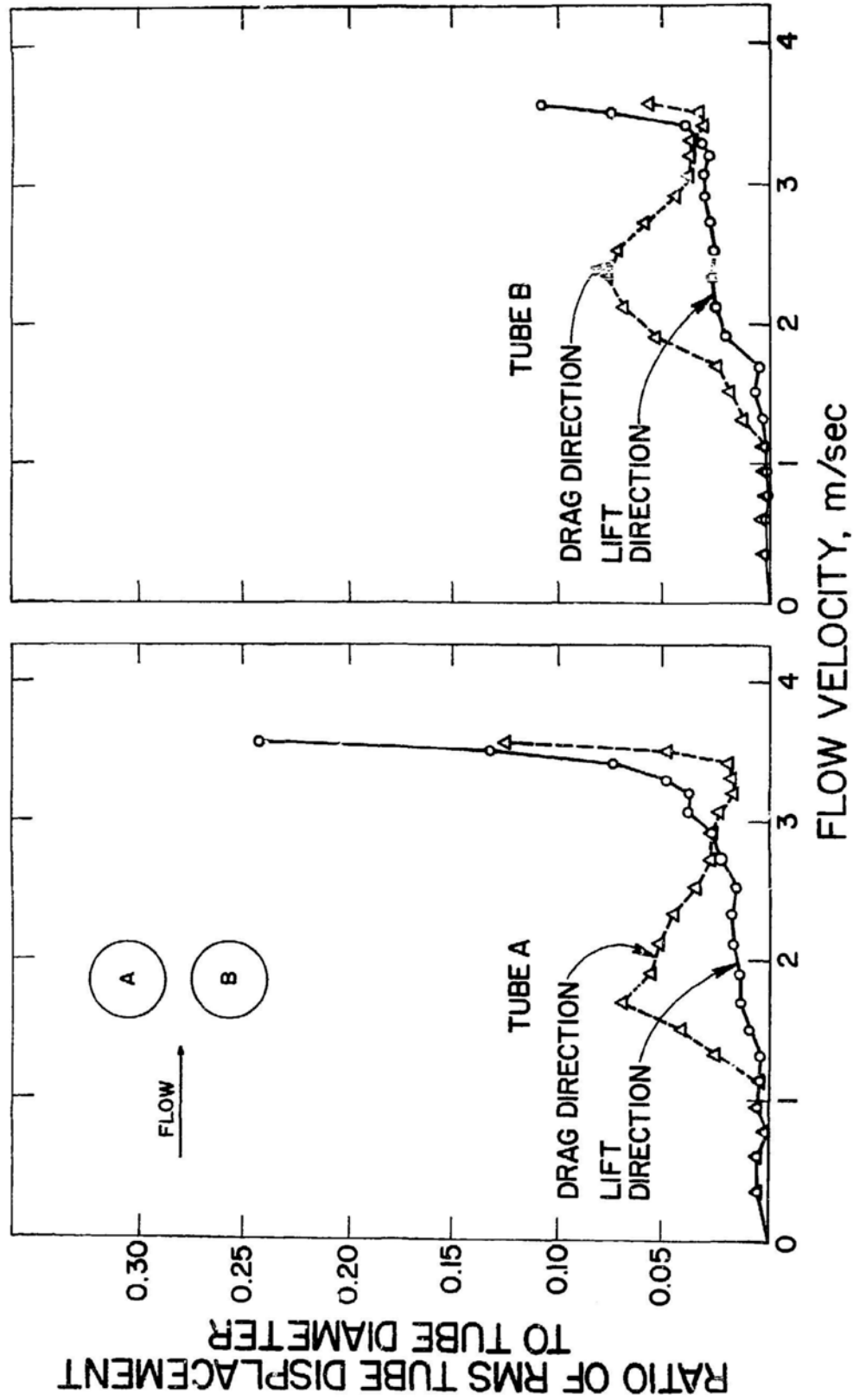


Fig. 9.21. Tube Displacement Component for Two Tubes in Side-by-Side Arrangement
(Jendrzeczyk et al. 1979)

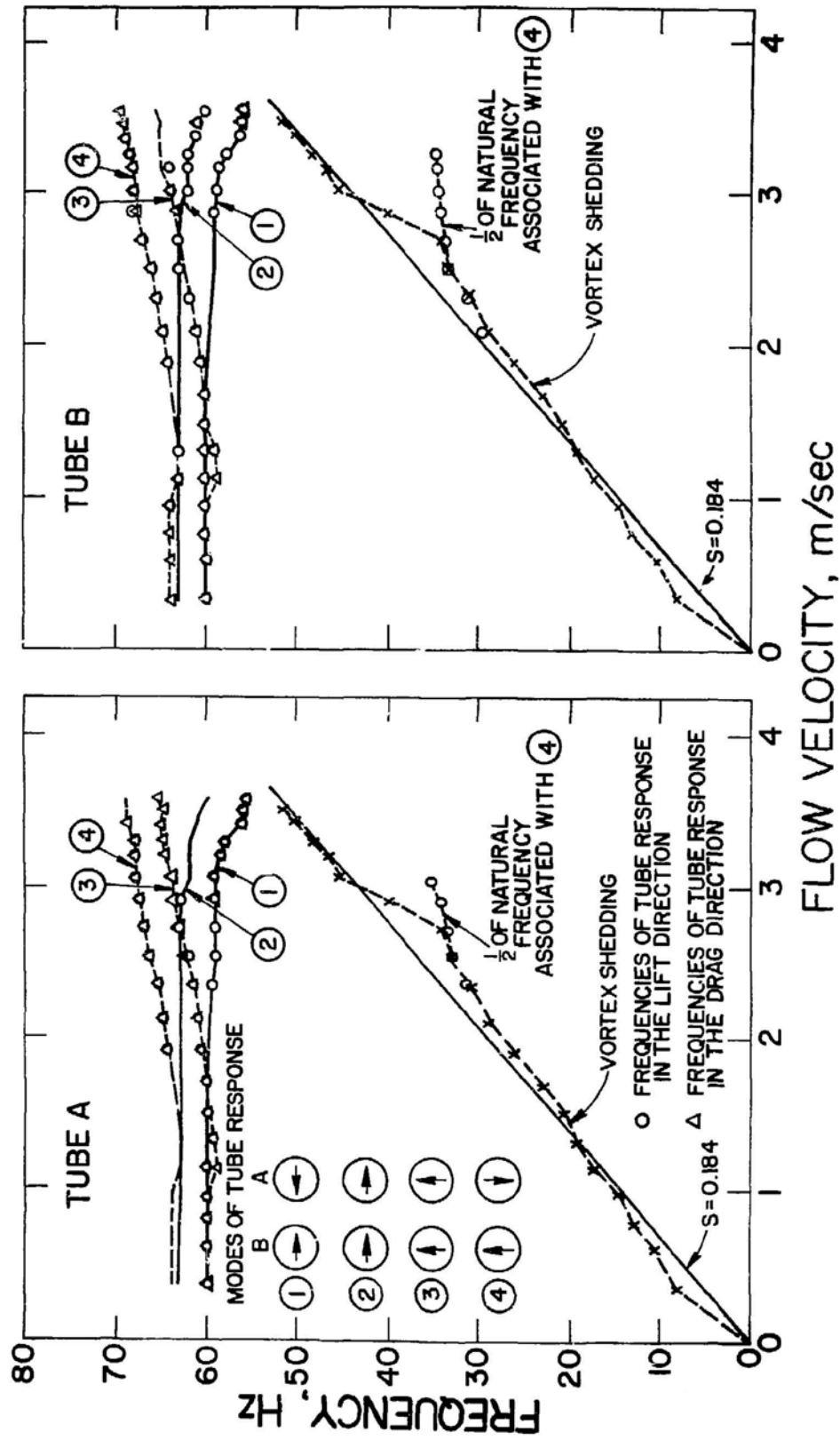


Fig. 9.22. Tube Response Frequencies as a Function of Flow Velocity for Two Tubes in Side by Side Arrangement (Jendrzeczyk et al. 1979)

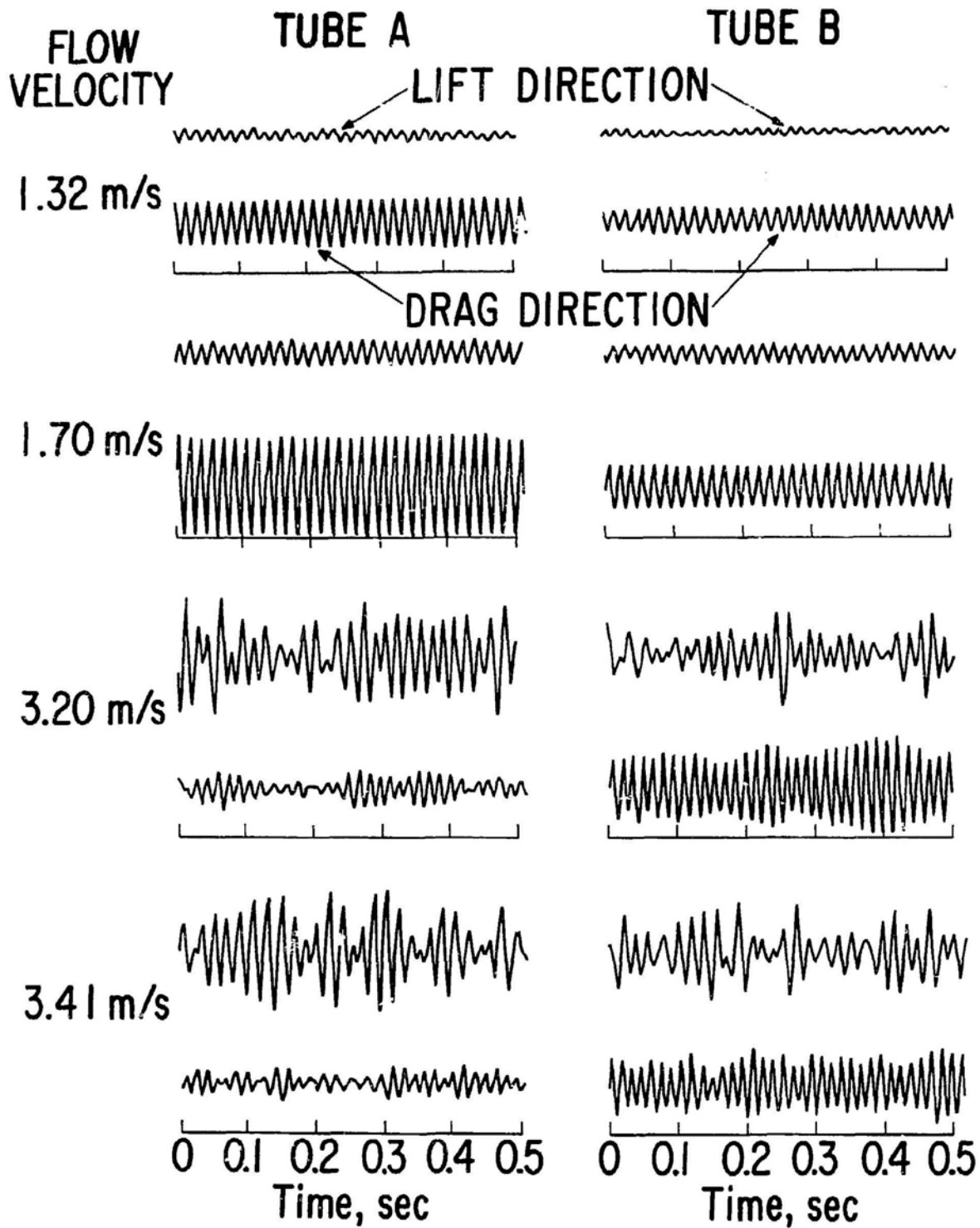


Fig. 9.23. Tube Displacement at Different Flow Velocities for Two Tubes in Side-by-Side Arrangements (Jendrzejczyk et al. 1979)

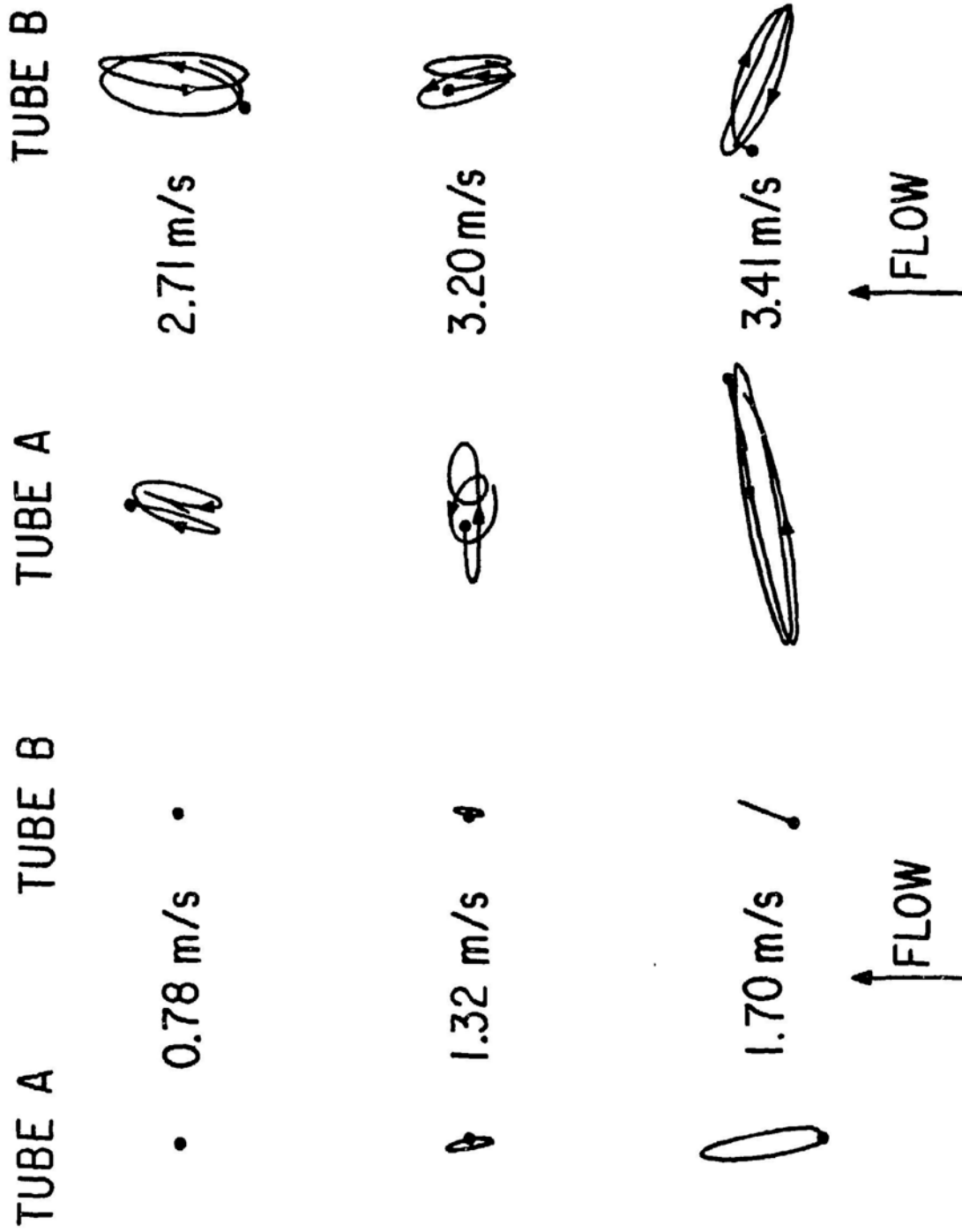


Fig. 9.24. Tube Orbital Paths for Two Tubes in Side-by-Side Arrangement (Jendrzejczyk et al. 1979)

equal to about 0.18, and (3) half the natural frequency in the drag direction. These characteristics are similar to those for a single tube.

Figure 9.23 shows tube displacement-time traces and Fig. 9.24 shows the orbital paths of tube motion at various flow velocities. At low flow velocities, the motion is sinusoidal with a single frequency component and the tube oscillates predominantly in the drag direction. When the tube motion in the drag direction is synchronized with vortex shedding, such as at 2.71 m/s in Fig. 9.24, the contribution to lift direction from the frequency equal to half the natural frequency in the drag direction motion is significant (this can also be seen from the frequency curve in Fig. 9.22). The maximum tube displacement in Fig. 9.24 is about 0.15 tube diameter for tube A at a flow velocity of 3.41 m/s. The two tubes move out of phase and the motion is predominantly in the lift direction. At these flow velocities, the vortex shedding frequency is close to the tube natural frequency. Once vortex shedding causes a tube to oscillate, the gap between the two tubes changes, as does the fluid field. In turn, the fluid force acting on the tubes changes and causes the tubes to oscillate more violently.

9.4.2 Two Cylinders in Tandem

The flow field for two cylinders is extremely complex, as shown in Fig. 9.10; therefore, the cylinder response is also very complex, depending on spacing, mass ratio, and Reynolds number. At this time, many more studies are needed for an understanding of the response for different conditions. Some of the known characteristics are discussed here.

A detailed study of two cylinders in tandem immersed in a water flow and spaced at between 0.20 and 4 diameters was made by King and Johns (1976) (Figs. 9.25 and 9.26). They found that complex mutual interactions can arise between the flow, vortex shedding, and the motion of the cylinders. The dynamic response of the cylinders is a function of pitch ratio, reduced flow velocity, mass ratio, and damping value. Reynolds number also is important; Re must exceed 1200-1500 for in-line oscillation to occur and must exceed 100 for crossflow oscillation to occur. The responses, which depend strongly on P/D , can be summarized as follows:

- $P/D < 2.75$: Symmetric vortices are shed from both cylinders in the range $1.25 < U_r < 2.5$ and both cylinders oscillate in the in-line direction provided the mass-damping parameter is less than 2.4.
- $P/D > 2.75$: For $1.25 < U_r < 2.5$, the upstream cylinder oscillates in-line and sheds symmetric vortices but the downstream cylinders do not oscillate and a wide turbulent wake is formed.
- $1.5 < P/D < 7$: For $2.7 < U_r < 3.8$, the alternate wake from the upstream cylinder generally reinforces that from the downstream cylinder.



Fig. 9.25. Flow Field for Two Cylinders Oscillating in the In-Line Direction with $P/D = 2.0$ for $U_r < 2.5$ (from King and Johns 1976, with permission--see Credits)

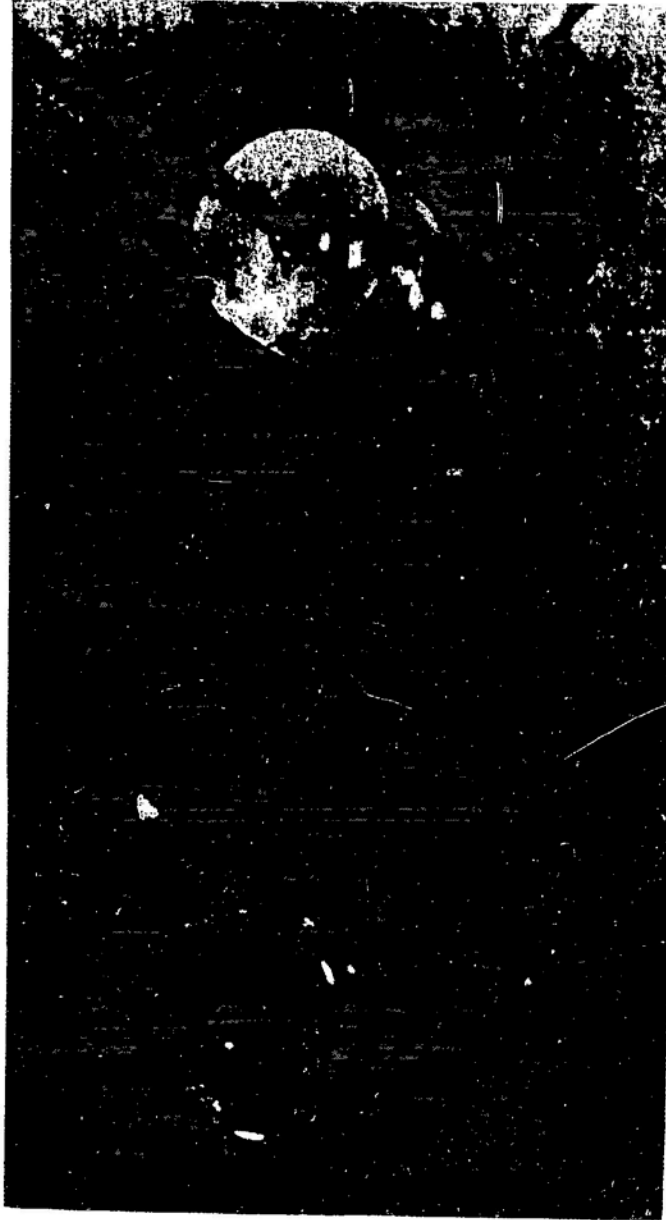


Fig. 9.26. Flow Field for Two Cylinders Oscillating in the In-Line Direction with $P/D = 4.0$ for $U_r < 2.5$ (from King and Johns 1976, with permission--see Credits)

- $1.25 < P/D < 7$: The alternate vortex shedding associated with the oscillating upstream cylinder generally reinforces that from the downstream cylinder.

Figures 9.27 and 9.28 show typical cylinder displacements for $P/D = 1.75$ (Jendrzeczyk et al. 1979). There are two peaks in the response curves in the drag direction. The peaks correspond to the reduced flow velocities equal to 1.7 and 3.0, respectively. This is consistent with the experimental results by King and Johns (1976). Figure 9.28 shows the orbital paths of two cylinders at several flow velocities. As the flow velocity increases, predominant cylinder motion changes from the drag direction to the lift direction. At large oscillations, the upstream cylinder vibrates more severely than the downstream one. The two cylinders vibrate out of phase when they execute large oscillations. The orbital paths bend in the downstream direction. This can be attributed to the drag variation--that is, when the cylinders are farthest from the equilibrium position, the drag force acting on the cylinders becomes larger. The large amplitude oscillations given in Figs. 9.27 and 9.28 are associated with the "interference galloping," discussed in Section 9.6.

Most investigations consider the cases in which the cylinders are free to move in both the drag and lift directions. Several studies are focused on the constrained mode, in which the cylinders are allowed to move only in the drag or the lift direction. Simpson (1977) shows that a pair of smooth cylinders, mounted in tandem in an airstream and free to oscillate in the drag direction, can exhibit flutter. However, the flutter exists only when there is a mechanical coupling between the cylinders. This flutter is most likely to be experienced along the wake centerline at low values of cylinder spacing. In contrast, Bokaian and Geoola (1984a, 1984b) study two cylinders in different arrangements with either the upstream one or the downstream one oscillating in the lift direction only. When the upstream cylinder is rigid, depending on the cylinder separation, damping, the downstream cylinder exhibits vortex-excited resonance, a flutter, a combined vortex-excited resonance and flutter, or a separated vortex-excited resonance and flutter. When the downstream cylinder is rigid, the upstream cylinder exhibits a vortex-excited resonance or flutter. The vortex shedding frequency was found to be related to oscillation frequency. Although the vibration characteristics remained essentially unaffected with changes in incoming turbulence intensity, the flutter amplitudes were sensitive to cylinder aspect ratio.

Most recently, Zdravkovich (1984) has attempted to summarize the response of two cylinders according to three flow regimes, illustrated in Fig. 9.29, which is a more detailed description of flow regimes as shown in Fig. 9.2. His results are given in Table 9.2. It can be seen that there is still incomplete knowledge of the cylinder response characteristics. In addition,

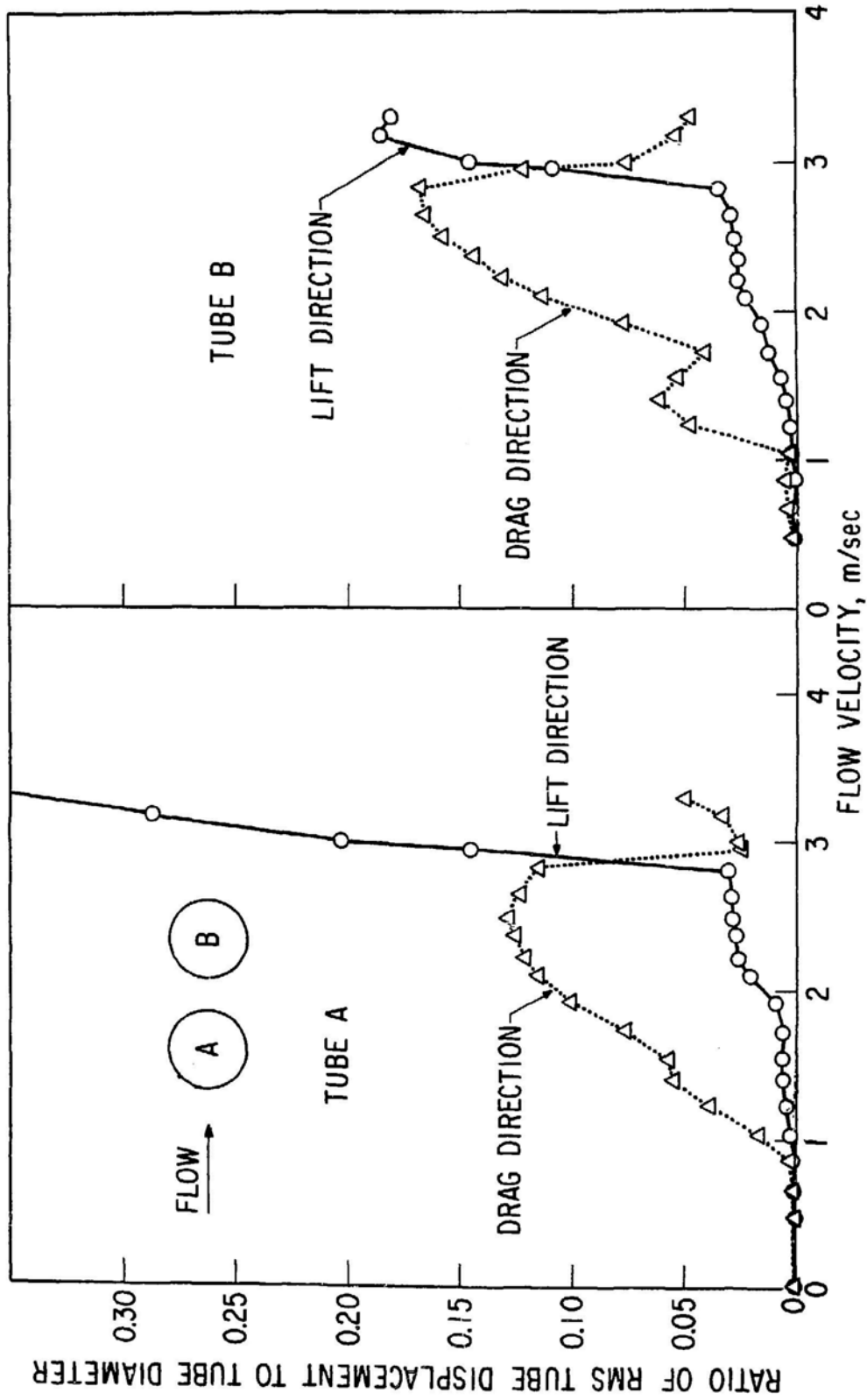


Fig. 9.27. Tube Displacement Components for Two Tubes in Tandem (Jendrzejczyk et al. 1979)

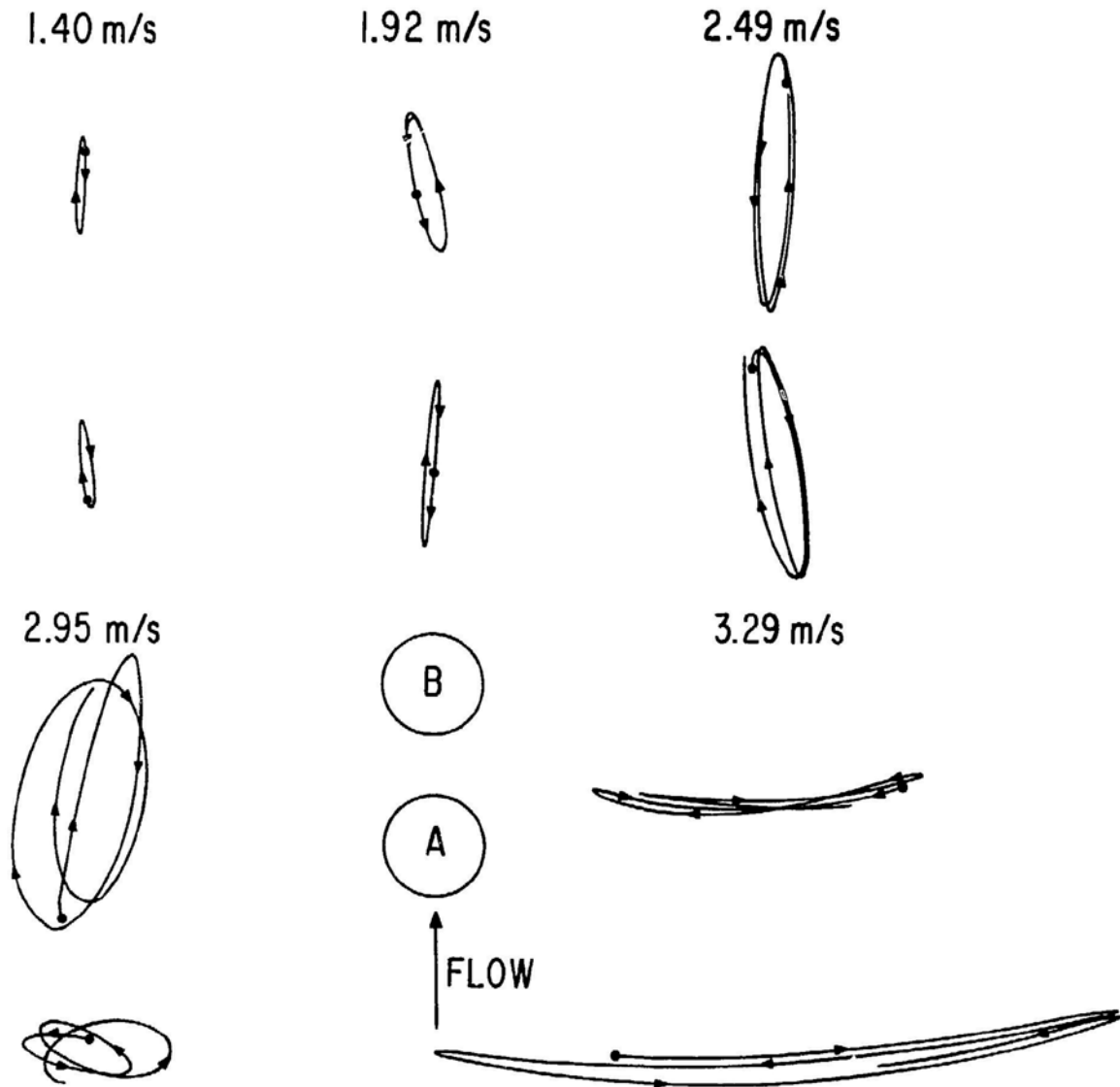


Fig. 9.28. Tube Orbital Paths for Two Tubes in Tandem (Jendrzeczyk et al. 1979)

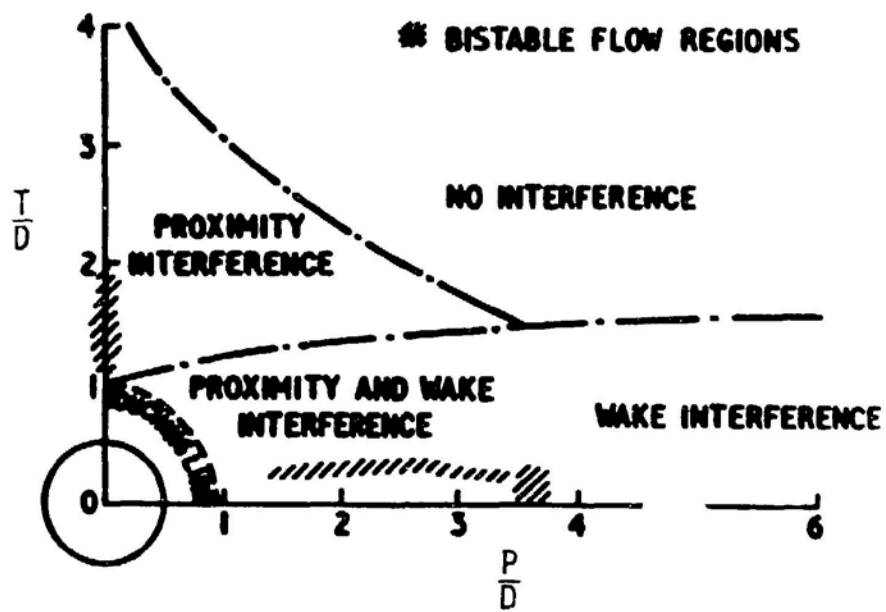


Fig. 9.29. Interference Regions (from Zdravkovich 1984, with permission--see Credits)

Table 9.2. Classification of Interfering Flow-Induced Oscillations *

CATEGORY	INITIAL ARRANGEMENT	STREAM WISE P/D	TRANS VERSE T/D	FLOW REGIMES FOR STATIONARY CYLINDERS	TYPE OF EXCITATION		
					LOW U_r	MED. U_r	HIGH U_r
P R O X I M I T Y	SIDE BY SIDE	0	1-0 1-2	SINGLE VORTEX STREET	?	?	
		0	1-1 2-2	BIASED JET	⊖ ⊖	⊖ ⊖	
		0	2-0 4-0	COUPLED	?	?	
	STAGGERED	<3-8	< I_B	VORTEX STREETS	?	?	
P R O X I M I T Y	TANDEM	1-1 1-5	0	SYNCHRONIZED REATTACHMENT	⊖ ⊖	⊖ ⊖	
		1-5 3-8	0	QUASI-STEADY REATTACHMENT	⊖ ⊖	⊖ ⊖	
	STAGGERED	1-1 3-2	0-2 0-3	GAP FLOW	?	?	
	TANDEM	>3-8	0	COUPLED VORTEX STREETS	?	?	
W A K E	STAGGERED	>8	0	DISTURBED VORTEX STREET	⊖ ⊖	?	
		>3-2	> $C_{L,max}$	DISPLACED WAKE	⊖ ⊖	?	
	STAGGERED	>8	< I_B	OUTSIDE WAKE BOUNDARY	⊖ ⊖	?	
I _B - INTERFERENCE BOUNDARY					NO INTERFERENCE		
					WAKE GALLOPING		
					WAKE DISPLACEMENT		
					NONE		
					GAP FLOW SWITCH		
					JET SWITCH		

*From Zdravkovich (1984) with permission--see Credits.

the precise boundaries separating different regions are not well defined because they are affected by various system parameters. Considerable work remains to be done before one can describe the dynamic behavior in detail.

9.5 WAKE-INDUCED FLUTTER

The wake behind the upstream cylinder contains periodicities and general turbulence. When this wake strikes the downstream cylinder, large oscillations can be excited in the rear cylinder; this motion moves downstream near the outer edge of the wake and upstream near wake center. This is called wake-induced flutter, wake galloping or wake-induced oscillation. In transmission lines, wake-induced flutter has been observed with arrangements of two, three, four, or more conductors. Because the oscillation can be wholly within a subspan bound by the conductor spacers, it is also referred to as a subspan oscillation.

The mathematical model for wake-induced flutter is commonly based on two cylinders. Different forms of fluid forces acting on cylinders have been proposed (Hardy and Cloutier 1973; Rawlins 1976; Simpson and Flower 1977; Tsui and Tsui 1979). A summary of these models is given in Table 9.3. The models have been developed for cylinders in air; therefore, the added mass of fluid is neglected. Fluid damping and fluid stiffness forces are derived from the steady drag and lift forces.

9.5.1 Motion-dependent Fluid Forces on the Downstream Cylinder

Figure 9.30 depicts the wake of the upstream cylinder, which is assumed to be fixed. The fluid forces acting on the downstream cylinder are calculated based on the quasi-static fluid dynamic theory.

At equilibrium, when the free-stream velocity is U , the position of the downstream cylinder relative to the upstream cylinder is defined by the transverse pitch T and longitudinal pitch P . In motion, at some instant t , the velocity of the cylinders are \dot{u}_2 and \dot{v}_2 . Let C_{D2} and C_{L2} be the hydrodynamic coefficients based on the local velocity V in the wake. The fluid forces acting on cylinder 2 are

$$\begin{aligned} g_2 &= \frac{1}{2} \rho V D \left[C_{D2} \left(U - \frac{\partial u_2}{\partial t} \right) + C_{L2} \frac{\partial v_2}{\partial t} \right] \quad \text{and} \\ h_2 &= \frac{1}{2} \rho V D \left[C_{L2} \left(U - \frac{\partial u_2}{\partial t} \right) - C_{D2} \frac{\partial v_2}{\partial t} \right] . \end{aligned} \quad (9.4)$$

The coefficients C_{D2} and C_{L2} depend on the position of the cylinder. When U_F is very large, the quasi-static hydrodynamics are justified. Consider

Table 9.3 Comparison of Four Mathematical Models for the Fluid Dynamic Forces on Tandem Conductors in Motion

Parameter	Hardy Model (1973)	Rawlins Model (1976)	Simpson-Flower Model (1977)	Tsui & Tsui Model (1979)
Includes effect of the motion of the upstream conductor on the wake velocity distribution	Yes	Yes	Yes	No
Includes time lag between the upstream and downstream conductors experiencing fluid dynamic forces	No	No	Yes, but in very complicated way	No
Requires lift and the drag coefficient of upstream conductor	No; $C_D = 1.2$ for laminar flow, $C_D = 0.8$ for turbulent flow, $C_L = 0$	Yes	Yes	No, lift coefficient $C_L = 0$, drag coefficient $C_D = 0$
Includes variation of lift and drag coefficients with respect to flow velocity.	No	Yes	Yes	No
Provides means to include buoyancy force	No	No	Yes	No
Includes fluid dynamic forces on upstream conductor	Linearized fluid dynamic force	Differs from Hardy model because of lift and drag coefficients of upstream conductor and derivatives of these coefficients with respect to flow velocity	Same as Rawlins model	Same as Hardy model
Includes fluid dynamic forces on downstream conductor	Only difference between Hardy and Tsui & Tsui is in fluid dynamic cross-damping terms attributed to velocity of upstream conductor	Difference between Rawlins and Hardy is in derivatives of fluid dynamic coefficients with respect to flow velocity	Difference between Simpson and Rawlins lies in at least two aspects--time lag and buoyancy force	Linearized fluid dynamic force

*From Tsui and Tsui (1979) with permission--see Credits.

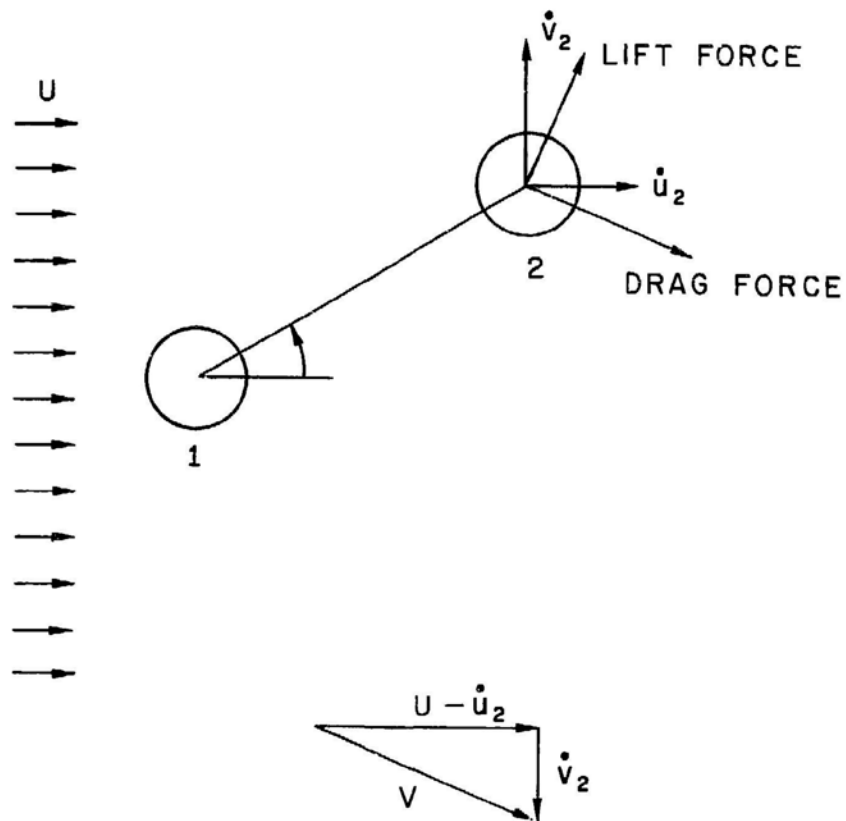


Fig. 9.30. Schematic of Two Cylinders in Crossflow

u_2 , v_2 and their time derivative small. Let

$$C_{D2} = C_{D2}(u_2, v_2) = \bar{C}_{D2} + \frac{\partial C_{D2}}{\partial u_2} u_2 + \frac{\partial C_{D2}}{\partial v_2} v_2$$

and

$$C_{L2} = C_{L2}(u_2, v_2) = \bar{C}_{L2} + \frac{\partial C_{L2}}{\partial u_2} u_2 + \frac{\partial C_{L2}}{\partial v_2} v_2 . \quad (9.5)$$

where \bar{C}_{D2} and \bar{C}_{L2} are the steady drag and lift coefficients at the equilibrium position. Substituting Eq. 9.5 into Eq. 9.4 and neglecting higher-order terms yields

$$g_2 = \frac{1}{2} \rho U^2 D \left\{ \frac{\partial C_{D2}}{\partial u_2} u_2 + \frac{\partial C_{D2}}{\partial v_2} v_2 + \frac{1}{U} \left(-2\bar{C}_{D2} \frac{\partial u_2}{\partial t} + \bar{C}_{L2} \frac{\partial v_2}{\partial t} \right) \right\} + \frac{1}{2} \rho U^2 D \bar{C}_{D2}$$

and

$$h_2 = \frac{1}{2} \rho U^2 D \left\{ \frac{\partial C_{L2}}{\partial u_2} u_2 + \frac{\partial C_{L2}}{\partial v_2} v_2 + \frac{1}{U} \left(-2\bar{C}_{L2} \frac{\partial u_2}{\partial t} - \bar{C}_{D2} \frac{\partial v_2}{\partial t} \right) \right\} + \frac{1}{2} \rho U^2 D \bar{C}_{L2} . \quad (9.6)$$

The last terms in both equations 9.6 are the steady drag and lift forces, which generally do not affect the stability of the cylinder. The others are the motion-dependent forces, which are obtained from the quasi-static theory. Note that the motion-dependent fluid forces include fluid stiffness and fluid damping forces. Complete static force coefficient data for the downstream cylinder are needed for predicting the instability regions. Not only the magnitudes of the coefficients, but also their derivatives with respect to both coordinates, are required.

Figure 9.31 depicts the wake of the downstream cylinder, in which lift coefficients C_{L2} and C_{D2} are required to the free-stream velocity. Measurements of these coefficients by Price (1975) for typical cases are shown in Fig. 9.32. Figure 9.33 shows derivative in the transverse direction for lift and drag. The profiles for different cases are similar, the lift coefficient profile being antisymmetric, with the lift force toward the center of the wake, and the drag coefficient being symmetric, with the minimum drag on the wake centerline. Turbulence decreased the magnitudes of the forces, but did not destroy their profiles. Of course, turbulence also lowered the Reynolds number for transition of the flow around the cylinders.

Figure 9.32 shows that the lift and drag curves are still significant when the pitch is greater than 20 diameters. Lift and drag curves for different Reynolds numbers show no dependence on Reynolds number.

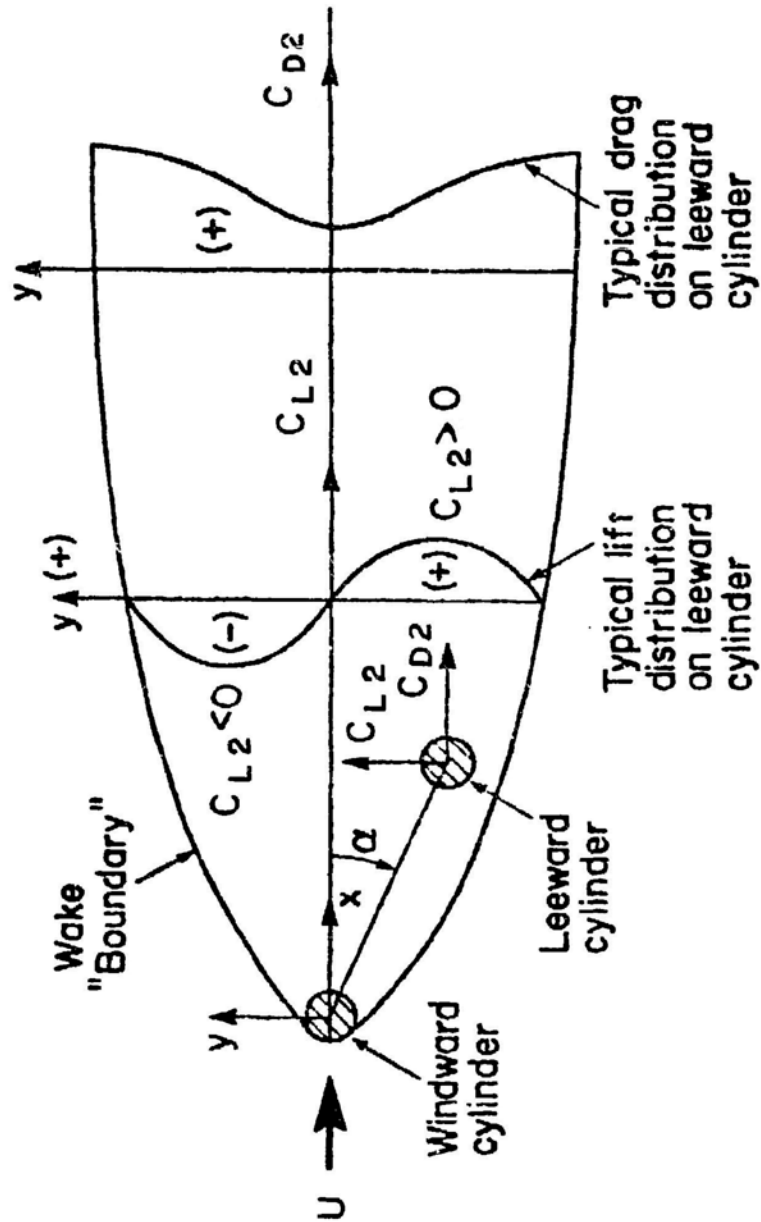


Fig. 9.31. Spatial Distribution of Steady Lift and Drag Coefficients in a Wake

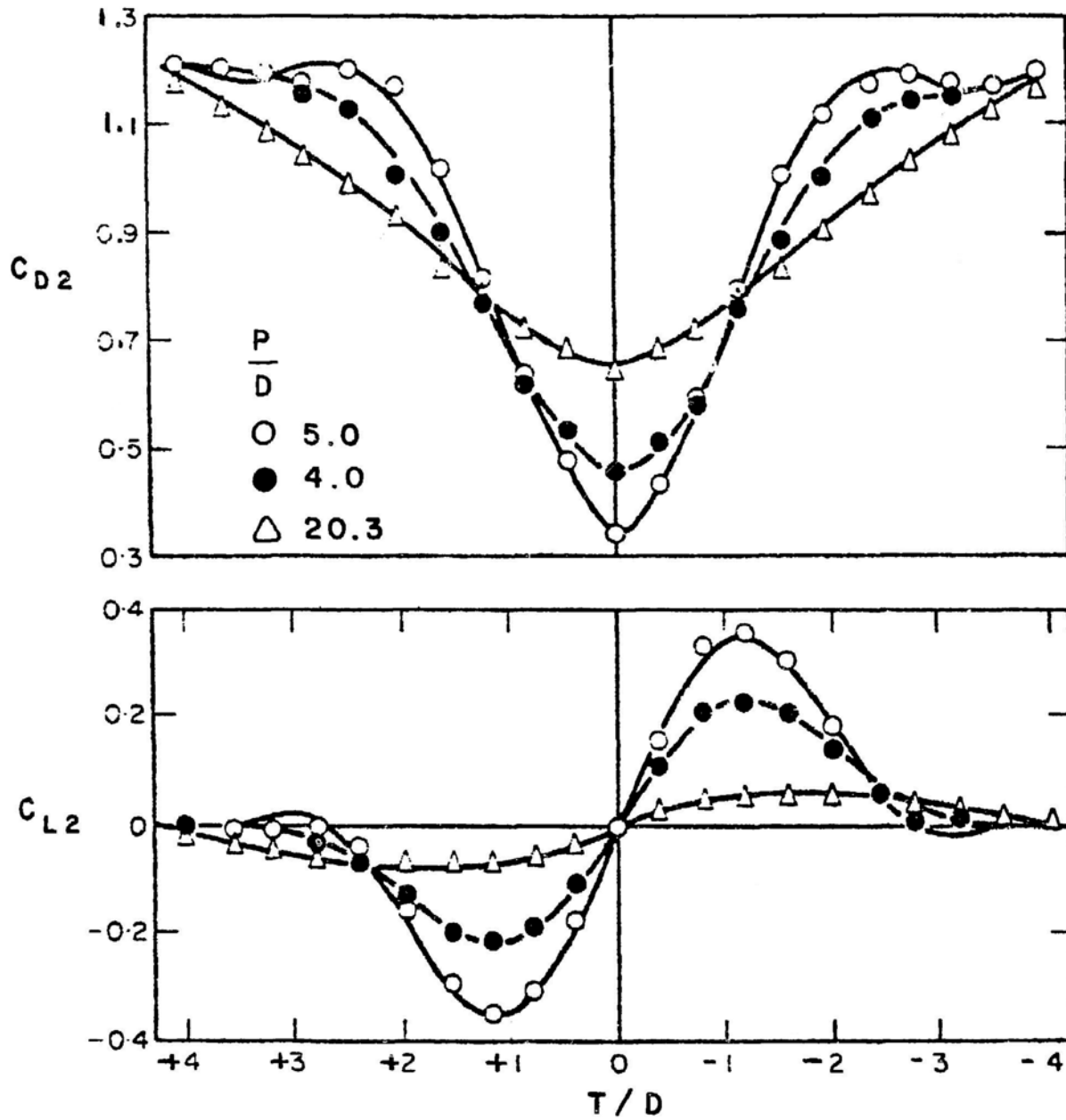


Fig. 9.32. Steady Drag and Lift Coefficients for $Re = 3.58 \times 10^4$ and $TI = 1.5\%$ (from Price 1975, with permission--see Credits)

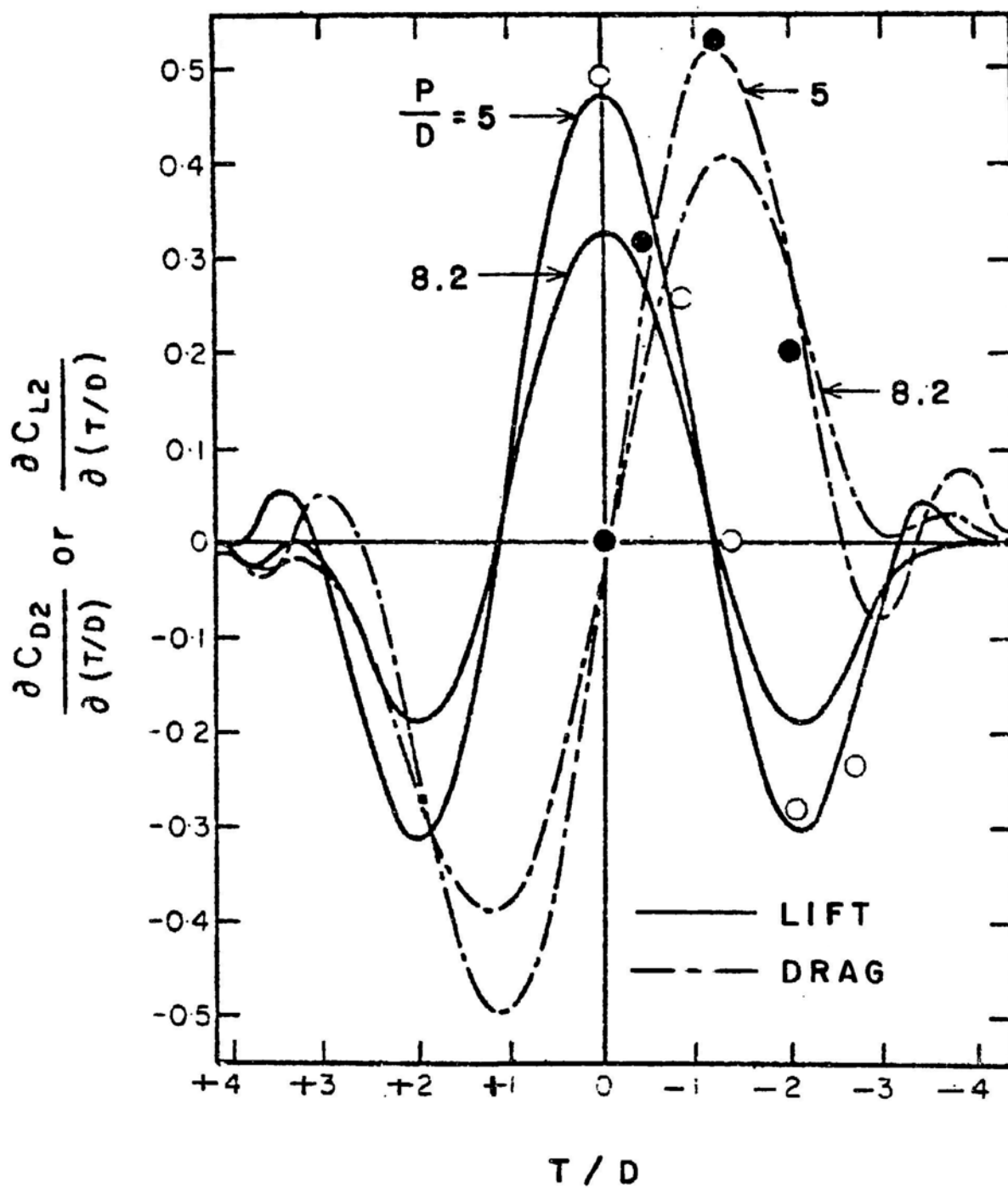


Fig. 9.33. Derivatives for Steady Lift and Drag Curves ($\partial C_{D2}/\partial(T/D)$ and $\partial C_{L2}/\partial(T/D)$) for $P/D = 5$ (from Price 1975, with permission--see Credits)

9.5.2 Stability Analysis

Wake-induced flutter is a special case of fluidelastic instability of cylinder arrays, as discussed in Section 10.6; therefore, the method presented in Section 10.6 can be applied to wake-induced flutter. Once the motion-dependent fluid forces given in Eq. 9.6 are known, the analysis is straightforward.

A typical trace of the buildup is shown in Fig. 9.34 (Wardlaw 1972). The relationship between wind speed and the vertical and horizontal final limit cycle amplitude is also given in Fig. 9.34. Using the measured quasi-static fluid force coefficients, the motion can be predicted with a reasonable degree of accuracy using quasi-static analysis.

Equations 9.6 are used in the analysis of stability boundary; both fluid-damping and fluid-stiffness forces are taken into account. However, the effect of fluid damping is small (Simpson 1971). The basic instability mechanism is of the fluid-stiffness-controlled type.

Most of the analysis is based on the assumption that the upstream cylinder is rigid; i.e., the effect of the motion of the upstream cylinder in the wake velocity distribution is neglected. Experimental data for both cylinders movable are not available. Simple models have included the effect of the upstream cylinder; e.g., Tsui and Tsui (1979) have studied the stability for two flexible cylinders. In this case, the motion-dependent fluid forces acting on the two cylinders are given by

$$\begin{aligned}
 g_1 &= \frac{1}{2} \rho U^2 D \left(1 - \frac{2}{U} \frac{\partial u_1}{\partial t} \right), \\
 h_1 &= -\frac{1}{2} \rho U D \frac{\partial v_1}{\partial t}, \\
 g_2 &= \frac{1}{2} \rho U^2 D \left\{ \frac{\partial C_{D2}}{\partial u_2} (u_2 - u_1) + \frac{\partial C_{D2}}{\partial v_2} (u_2 - v_1) \right. \\
 &\quad \left. + \frac{1}{U} \left(-2\bar{C}_{D2} \frac{\partial u_2}{\partial t} + \bar{C}_{L2} \frac{\partial v_2}{\partial t} \right) \right\}, \quad \text{and} \\
 h_2 &= \frac{1}{2} \rho U^2 D \left\{ \frac{\partial C_{L2}}{\partial u_2} (u_2 - u_1) + \frac{\partial C_{L2}}{\partial v_2} (v_2 - v_1) \right. \\
 &\quad \left. + \frac{1}{U} \left(-2\bar{C}_{L2} \frac{\partial u_2}{\partial t} - \bar{C}_{D2} \frac{\partial v_2}{\partial t} \right) \right\}.
 \end{aligned} \tag{9.7}$$

Based on Eq. 9.7, the flutter of coupled mode can be calculated.

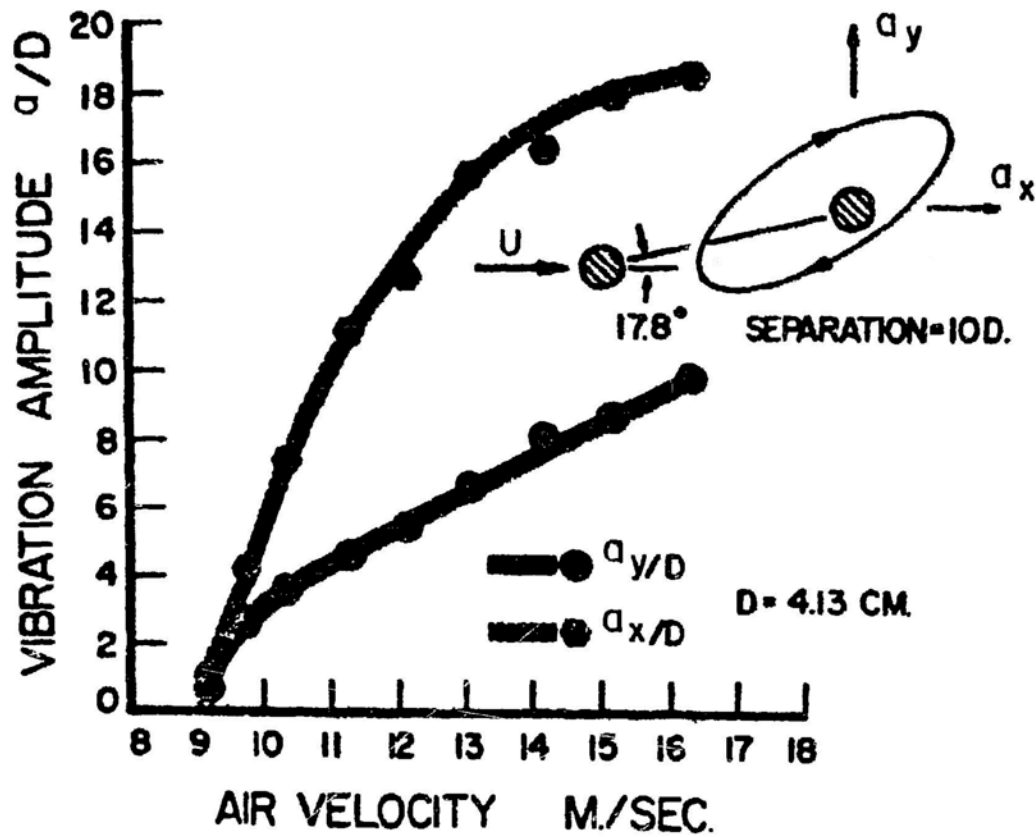


Fig. 9.34. Amplitude Response of Leeward Cylinder of Twin Cylinders
(from Scanlan and Wardlaw 1973 with permission--see Credits;
original source from Wardlaw 1972)

9.6 INTERFERENCE GALLOPING

In contrast to wake-induced flutter, which is generally important for relatively large longitudinal pitch P/D , two cylinders with a small longitudinal pitch ratio can be subjected to "interference galloping," which is similar to the galloping of a single cylinder with rectangular shape in crossflow (Blevins 1977). As shown by Ruscheweyh (1983), two different flow conditions occur around two cylinders (see Fig. 9.35). At the flow velocity below the critical angle, the downstream cylinder is completely in the wake of the upstream cylinder and no lift force exists. If the critical angle is attained or exceeded, the flow streams through the gap at high speed and produces a lift force on the downstream cylinder. The lift force coefficient C_{L2} is shown in Fig. 9.36 for different pitch ratio P/D . Near the critical angle, the values of C_{L2} vary drastically. This is associated with the change of flow conditions given in Fig. 9.35. In this range, interference galloping is observed.

The analysis of interference galloping is similar to the classical galloping of a single cylinder (Blevins 1977). The equation of motion of cylinder 2 in the y direction is

$$m_2 \frac{d^2 v_2}{dt^2} + C_{s2} \frac{dv_2}{dt} + k_{s2} v_2 = \frac{1}{2} \rho U^2 D C_{L2} , \quad (9.8)$$

where the added mass is ignored and the fluid force is based on the quasi-steady fluid-dynamic force. For the harmonic motion,

$$v_2 = \bar{v}_2 \sin \omega t ,$$

$$\frac{dv_2}{dt} = \bar{v}_2 \omega \cos \omega t , \quad \text{and} \quad (9.9)$$

$$\frac{d^2 v_2}{dt^2} = -\bar{v}_2 \omega^2 \sin \omega t .$$

The phase lag between the lift force and displacement is θ .

$$C_{L2} = C_{L2} \sin(\omega t + \theta) . \quad (9.10)$$

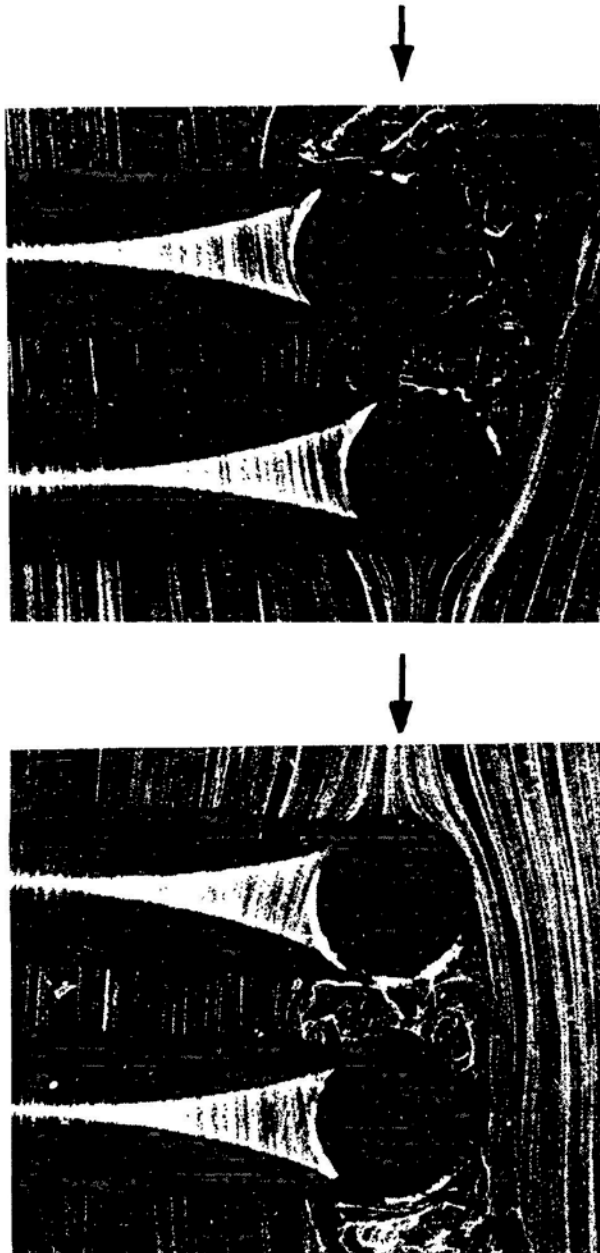


Fig. 9.35. Flow Patterns for Two Cylinders in Tandem (from Ruscheweyh 1983, with permission---see Credits)

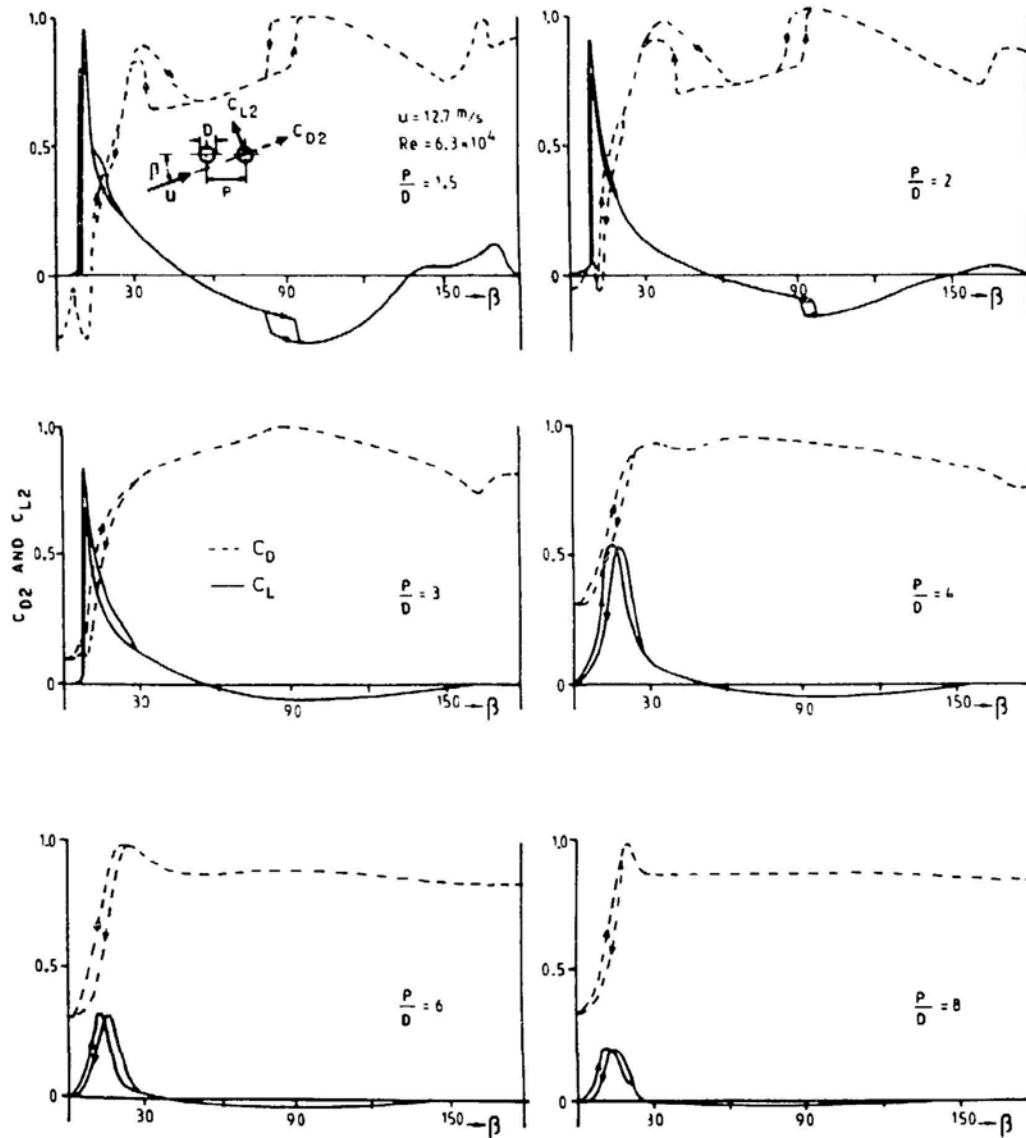


Fig. 9.36. Steady Drag Coefficient C_{D2} and Lift Coefficient C_{L2} for the Downstream Cylinder of Two Cylinders with $Re = 6.3 \times 10^4$ (from Ruscheweyh 1983, with permission--see Credits)

For small angle of attack β ,

$$\bar{C}_{L2} = \frac{\partial C_{L2}}{\partial \beta} \left(-\frac{\bar{v}_2}{P} \right) . \quad (9.11)$$

Using Eqs. 9.8-9.11 yields

$$\begin{aligned} (k_{s2} - m_2 \omega^2 - \frac{1}{2} \rho U^2 D \bar{C}_{L2} \cos \theta) \bar{v}_2 \sin \omega t \\ + (C_{s2} \omega - \frac{1}{2} \rho U^2 D \bar{C}_{L2} \sin \theta) \bar{v}_2 \cos \omega t = 0 . \end{aligned} \quad (9.12)$$

The expression in the first bracket describes the natural frequency of the system with the interference coupling effect and the expression in the second expression describes the damping. When the latter becomes zero, the system loses stability by galloping; i.e.,

$$C_{s2} \omega - \frac{1}{2} \rho U^2 D \bar{C}_{L2} \sin \theta = 0 . \quad (9.13)$$

Neglecting the effect of the interference coupling on the natural frequency in Eq. 9.13 yields

$$\frac{U}{fD} = 3.54 \left(\frac{P/D}{\frac{\partial C_{L2}}{\partial \beta} \sin \theta} \right)^{0.5} \left(\frac{2\pi r_m}{\rho D^2} \right)^{0.5}$$

where

$$\begin{aligned} f &= \frac{1}{2\pi} \left(\frac{k_{s2}}{m_2} \right)^{0.5} \quad \text{and} \\ \zeta &= \frac{C_{s2}}{4\pi m_2 f} . \end{aligned} \quad (9.14)$$

The onset flow velocity depends on the square root of the mass-damping parameter δ_g ; this is contrary to the classical galloping, in which the critical flow velocity is proportional to δ_g . The sign of the phase lag θ is

normally negative; therefore, for instability to occur, $\partial C_{L2}/\partial \beta$ must be positive. This is also contrary to that of classical galloping, in which the derivative is negative.

9.7 CLOSING REMARKS

The flow field around two circular cylinders is very complex. It depends on Reynolds number, cylinder arrangement, and incoming flow conditions. The interaction of fluid flow with cylinder oscillation is even more complicated. The excitation mechanisms can be classified as vortex shedding, turbulent buffeting, and fluidelastic instability. A general procedure to determine the response for different excitations is presented in this chapter and various available experimental data are reviewed.

At this time, it is not possible generally to predict the response of two cylinders in crossflow because the fluid forces acting on the cylinders cannot be calculated. Therefore, techniques to obtain the fluid forces need to be developed. Several approaches can be used, including analytical methods, numerical techniques, and experimental methods. It is expected that more research will be directed toward this area.

Based on the available information, the general characteristics of cylinder response in crossflow are not well understood in various parameter ranges. Most of the experimental data were obtained for specific applications. A systematic study is needed to quantify the response of two cylinders under different flow conditions.

Flow discontinuities and the resulting effects are important and interesting. No systematic study to investigate their characteristics has been reported. Detailed characterization of the flow discontinuities and cylinder responses deserves further attention.

Most of the research has been conducted in the subcritical Reynolds number range. However, in many engineering applications, Reynolds numbers are in the postcritical range. Flow characteristics and cylinder response in a high Reynolds number range should be studied.

REFERENCES--Sec. 9

- Arie, M., et al. 1983. Pressure Fluctuations on the Surface of Two Circular Cylinders in Tandem Arrangement. *J. Fluids Eng.* 105, 161-167.
- Bearman, P. W., and Wadcock, A. J. 1973. The Interaction between a Pair of Circular Cylinders Normal to a Stream. *J. Fluid Mech.* 61(Part 3), 499-511.
- Biermann, D., and Herrnstein, W. H., Jr. 1933. The Interference between Struts in Various Combinations. National Advisory Committee for Aeronautics, Technical Rep. 468.
- Blevins, R. D. 1977. Flow Induced Vibration. Van Nostrand Reinhold Co.
- Bokaian, A., and Geoola, F. 1984a. Proximity-Induced Galloping of Two Interfering Circular Cylinders. *J. Fluid Mech.* 146, 417-449.
- Bokaian, A., and Geoola, F. 1984b. Wake-Induced Galloping of Two Interfering Circular Cylinders. *J. Fluid Mech.* 146, 383-415.
- Dayoub, A. 1962. Aerodynamic Forces on a Cylindrical Structure in a Wake of Another Cylindrical Structure. *Applied Scientific Research* 39 3-20.
- Dye, R. C. F. 1973. Vortex-excited Vibration of a Heat Exchanger Tube Row in Cross-flow. *Proc. of Conference on Vibration Problems in Industry*, Keswick, Paper No. 417.
- Hardy, C., and Cloutier, L. J. 1973. Analyse Linéaire de la Stabilité d'un faisceau de conducteurs sous le vent. Report No. 73-952-01, Institut de Recherche de d'Hydro-Quebec, Varennes, P.Q., Canada (November 2, 1973).
- Hori, E. 1959. Experiments on Flow Around a Pair of Parallel Circular Cylinders. *Proc. 9th Japan National Congress for Appl. Mech.*, Tokyo, pp. 231-234.
- Ishigai, S., Nishikawa, E., Nishimura, K., and Cho, K. 1972. Experimental Study on Structure of Gas Flow in Tube Banks with Tube Axes Normal to Flow (Part 1, Karman Vortex Flow Around Two Tubes at Various Spacings). *Bulletin of the JSME* 15(86), 949-956.
- Jendrzejczyk, J. A., and Chen, S. S. 1982. Fluid Forces Acting on Circular Cylinders in Liquid Cross-Flow. in *Flow-Induced Vibration of Circular Cylindrical Structure*, ASME PVP Vol. 63, pp. 31-44.
- Jendrzejczyk, J. A., Chen, S. S., and Wambsganss, M. W. 1979. Dynamic Response of a Pair of Circular Tubes Subjected to Liquid Cross Flow. *J. Sound Vib.* 67(2), 263-273.
- King, R., and Johns, D. J. 1976. Wake Interaction Experiments with Two Flexible Circular Cylinders in Flowing Water. *J. Sound Vib.* 45(2), 259-283.

- Kiya, M., et al. 1980. Vortex Shedding from Two Circular Cylinders in Staggered Arrangement. Trans. ASME, J. Fluids Eng. 102, 166-173.
- Landweber, L. 1942. Flow About a Pair of Adjacent Parallel Cylinders Normal to a Stream. Navy Department, The David W. Taylor Model Basin Report 485 (July 1942).
- Livesey, J. L., and Dye, R. C. F. 1962. Vortex Excited Vibration of a Heat Exchanger Tube Row. J. Mech. Eng. Sci. 4, 349-352.
- Mair, W., and Maull, D. J. 1971. Aerodynamic Behavior of Bodies in the Wakes of Other Bodies. Phil. Trans. Roy. Soc. Lond. A 269, 425-437.
- Oka, S., Kostic, Z. G., and Sikmanovic, S. 1972. Investigation of the Heat Transfer Processes in Tube Banks in Cross Flow. Int. Seminar on Recent Developments in Heat Exchangers, Trogir, Yugoslavia, 1972.
- Price, S. J. 1975. Wake Induced Flutter of Power Transmission Conductors. J. Sound Vib. 38(1), 125-147.
- Rawlins, C. B. 1976. Fundamental Concepts in the Analysis of Wake-Induced Oscillation of Bundled Conductors. IEEE Trans. Power Apparatus Syst., Vol. Pas-97 (4), 1377-1393.
- Roberts, B. W. 1966. Low Frequency, Aeroelastic Vibrations in a Cascade of Circular Cylinders. Mech. Eng. Sci. Monograph No. 4 (September 1966).
- Ruscheweyh, H. P. 1983. Aeroelastic Interference Effects between Slender Structures. J. of Wind Engineering and Industrial Aerodynamics 14, 129-140.
- Scanlan, R. H., and Wardlaw, R. L. 1973. Reduction of Flow-Induced Structural Vibrations. In Isolation of Mechanical Vibration, Impact, and Noise, ASME Publication, pp. 35-63.
- Simpson, A. 1971. Wake Induced Flutter of Circular Cylinders: Aeronautical Aspects. Aeronautical Quarterly 23, 101-118 (1971).
- Simpson, A. 1977. In-Line Flutter of Tandem Cylinders. J. Sound Vib. 54(3), 379-387.
- Simpson, A., and Flower, J. W. 1977. An Improved Mathematical Model for the Aerodynamic Forces on Tandem Cylinders in Motion with Aeroelastic Applications. J. Sound Vib. 51, 183-217.
- Spivak, H. M. 1946. Vortex Frequency and Flow Pattern in the Wake of Two Parallel Cylinders at Varied Spacings Normal to an Air Stream. J. Aeronautical Sciences 13, 289-297.
- Tanida, Y., Okajima, A., and Watanabe, Y. 1973. Stability of a Circular Cylinder Oscillating in Uniform Flow or in a Wake. J. Fluid Mech. 61, 769-784.

- Tsui, Y. T. 1977. On Wake-Induced Flutter of a Circular Cylinder in the Wake of Another. Trans. ASME, J. Appl. Mech. 99, 194-200.
- Tsui, Y. T., and Tsui, C. C. 1979. On Wake-Induced Flutter of a Circular Conductor in the Wake of Another. Proc. ASME Symp. Flow-Induced Vib., San Francisco, pp. 19-33.
- Wardlaw, R. L. 1972. Wind Tunnel Investigation in Industrial Aerodynamics. Canadian Aeronautical and Space Journal 18(3).
- Wilson, J. F., and Caldwell, H. M. 1971. Force and Stability Measurements on Models of Submerged Pipelines. J. Eng. for Industry 93, 1290-1298.
- Zdravkovich, M. M. 1974. Proceedings of an International Symposium on Flow Induced Structural Vibrations, Karlsruhe, 1972. Springer Verlag, pp. 631-639.
- Zdravkovich, M. M. 1977. Review of Flow Interference between Two Circular Cylinders in Various Arrangements. J. Fluids Eng. 99, 618-633.
- Zdravkovich, M. M. 1982. Flow Induced Oscillations of Two Interfering Circular Cylinders. Int. Conf. on Flow Induced Vibrations in Fluid Engineering, Reading, England, Sept. 14-16, 1982, Paper No. D2.
- Zdravkovich, M. M. 1984. Classification of Flow-Induced Oscillations of Two Parallel Circular Cylinders in Various Arrangement. in Sym. on Flow-Induced Vibration, Vol. 2, ASME, pp. 1-13.
- Zdravkovich, M. M., and Pridden, D. L. 1977. Interference between Two Circular Cylinders; Series of Unexpected Discontinuities. J. of Industrial Aerodynamics 2, 255-270.

10. FLUIDELASTIC INSTABILITY OF A GROUP OF CIRCULAR CYLINDERS IN CROSSFLOW

10.1 INTRODUCTION

The displacement of one cylinder in an array alters the flow field, upsetting the neighboring cylinders and causing them to change their displacements. If during a cycle of oscillation the energy extracted from the flow by the cylinder exceeds the energy dissipated by the damping, an instability will result from the interaction of flow and cylinder. Connors (1970) developed a simple stability criterion based on the quasi-steady theory; the critical velocity above which large-amplitude cylinder vibration initiates is given by

$$\frac{U}{fD} = \alpha \left(\frac{2\pi \zeta m}{\rho D^2} \right)^{0.5}, \quad (10.1)$$

where α is the threshold instability constant. The original work by Connors (1970) has provided great impetus for numerous innovative studies of cylinder arrays subjected to crossflow. The mechanism described by Connors has been used to interpret different phenomena, and Connors' stability criterion has been used extensively and misused occasionally. Furthermore, erroneous interpretations of Connors' criterion by some investigators have been published in different journals, illustrating the lack of understanding of this subject.

10.2 DEFINITION OF CRITICAL FLOW VELOCITY AND SYSTEM PARAMETERS

The displacement of a cylinder in an array subjected to crossflow is shown in Fig. 8.1. The critical flow velocity is defined as the flow velocity above which large cylinder oscillations occur. Mathematically, this is generally described as follows: Let the displacement of a particular location of the cylinder be

$$u(t) = a \exp(\lambda + i\omega)t. \quad (10.2)$$

The stability of the cylinder is determined by λ , which is a function of flow velocity:

If $\lambda < 0$, the cylinder motion is damped.

If $\lambda > 0$, the cylinder displacement increases with time.

$\lambda = 0$ is the condition that separates the stable and unstable regions. Therefore, the critical flow velocity can be determined from the condition $\lambda = 0$.

Based on Eq. 10.2, once the cylinder becomes unstable, the displacement will increase with time without limit. Practically, other nonlinear effects

will become important as soon as the cylinder motion becomes large, and the cylinder displacement will be limited to a certain value. The increase in response amplitude with flow velocity is gradual, as shown in Fig. 8.1, unlike that described in Eq. 10.2, which shows that the cylinder response amplitude is infinite for $\lambda > 0$. It is apparent that using the response curves given in Fig. 8.1 to establish the critical flow velocity based on the linear theory given in Eq. 10.2 will encounter some difficulty.

A number of methods have been used to define the critical flow velocity in laboratory tests and practical equipment tests (Wambsganss et al. 1981). These are discussed below:

Sensory Observations: Tube vibration amplitudes are determined visually or auditorially. When the cylinder array can be viewed from the end or at a particular section, the amplitude increase can generally be detected visually. If, in addition, cylinder impacting results, a distinctive loud noise associated with the impacting is readily audible. This method does not precisely determine critical flow velocity in most cases, because the method is subjective and requires a fair amount of engineering judgment and experience.

Vibration Amplitude vs. Flow Velocity: The cylinder RMS amplitude or peak amplitude is plotted as a function of flow velocity, as shown, for example, in Fig. 10.1. The flow velocity at which the cylinder experiences a rapid increase in response is defined as the critical flow velocity. Using this definition, different investigators define the critical flow velocity in different manners. For example, Weaver and El-Kashlan (1981) define the threshold flow velocity as the point on the curve where there is a sudden change in slope, while Soper (1980) defines the threshold flow velocity as the intersection of the velocity axis and the tangent to that portion of the curve which is rapidly rising (see Fig. 10.1a).

The example given in Fig. 10.1a is ideal for defining critical flow velocity. However, even in this case, the critical flow velocities determined by different investigators are different. For other cases, the situation becomes more difficult. For example, in Fig. 10.1b, there is uncertainty as to whether or not the first peak indicates instability. Difficulty also arises when the response curve exhibits a gradual increase.

Vibration Amplitude vs. Flow: The critical flow velocity is defined as the velocity at which the threshold displacement is first exceeded. Values of 2-2.5% of cylinder diameter have been suggested (Yeung and Weaver 1983). Once the threshold amplitude is established, determination of the critical flow velocity is straightforward. This method is attractive for practical applications but it is not theoretically correct.

Frequency Response Data: When a cylinder array is subjected to a flow, there are many natural frequencies of coupled modes (see Sec. 3.4). At flow

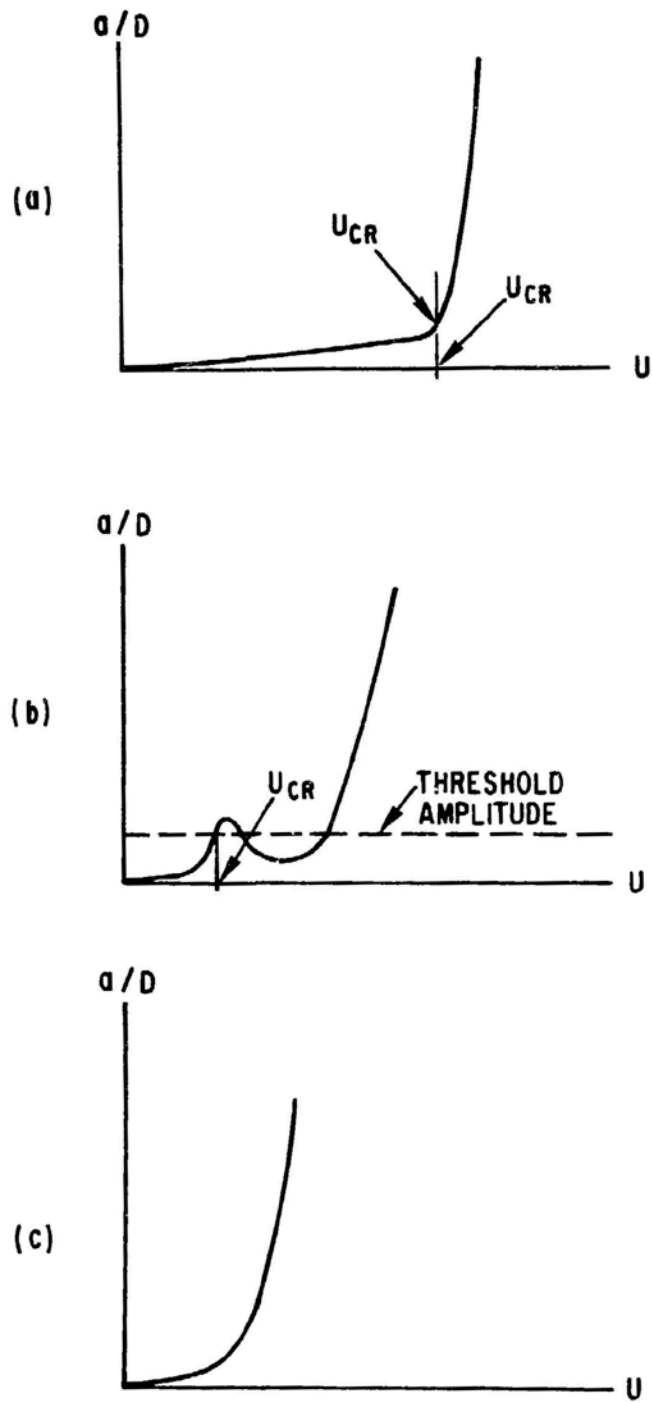


Fig. 10.1. Critical Flow Velocity

velocities below the threshold value, turbulent buffeting or other excitation source is the dominant excitation mechanism. It excites, in general, a broad range of coupled frequencies. On the other hand, the vibration at instability typically is at a well-defined single frequency corresponding to a particular instability mode. Therefore, the critical flow velocity can be defined as the flow velocity at which the response PSD changes from a relatively broad-band spectrum to a narrow-band spectrum (see Fig. 10.2). This method is accurate in general. However, difficulty arises for light fluid in which the natural frequencies of coupled modes are in a narrow band as well as for the case in which either there is a gradual transition from broad band to narrow band spectra or instability is too abrupt, such that it results in impacting with broad-band spectra above the critical flow velocity.

There is no single method that can be used to predict critical flow velocity precisely in all cases. According to the definition of the critical flow velocity associated with $\lambda = 0$ given in Eq. 10.2, the method that appears to be most useful is a combination of two methods--vibration amplitude vs. flow velocity, and frequency response data. In practical applications, from the vibration amplitude-flow velocity curve, the critical flow velocity can be established approximately. Then with the frequency response data at different flow velocities near the critical region, the critical flow velocity can be determined more precisely. In light fluids, the critical flow velocity is associated with high values of U_r and can generally be determined from the amplitude velocity curve alone, such as that given in Fig. 10.1a. The response spectra will be used to verify the existence of instability. In heavy fluids, the frequency spectra can be used as the primary tool in determining the critical flow velocity such as that given in Eq. 10.2. The vibration amplitude-flow velocity curve can be used supplementally to verify the critical flow velocity.

The three important parameters used in the stability criteria are mass per unit length m , natural frequency f , and damping ratio ζ (see Eq. 10.1). For a cylinder array vibrating in flow, the definitions of these three parameters vary widely. System parameters can be measured under four conditions:

- In vacuum (practically, in air), where the effect of the surrounding fluid is ignored,
- In a quiescent fluid, with uncoupled vibration, for an elastic cylinder vibrating in a fluid with the surrounding cylinder being held rigid and the coupling effect of fluid not taken into account,
- In quiescent fluid, with coupled vibration, for an array of cylinders vibrating in a fluid with the coupling effect of fluid included, and

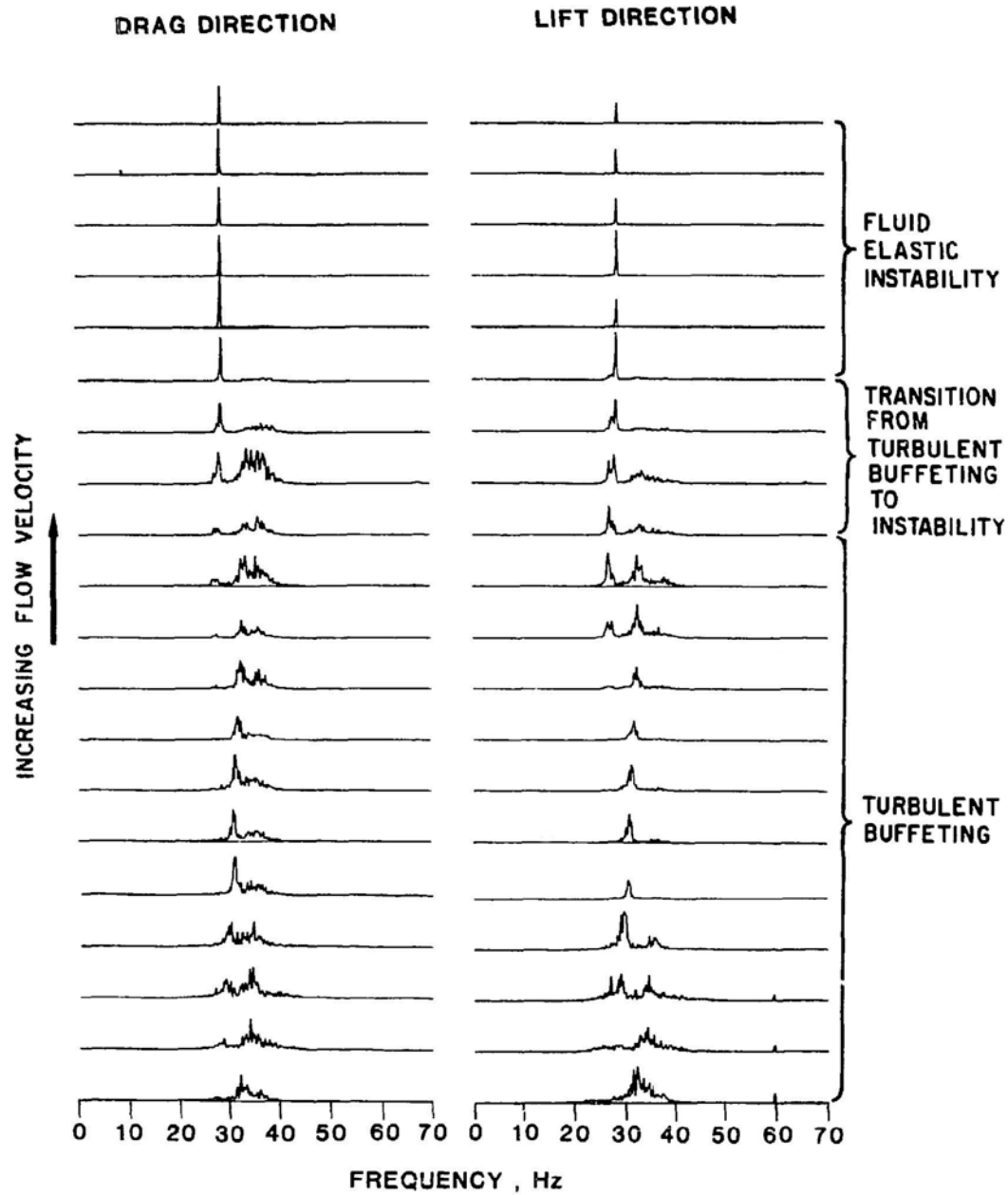


Fig. 10.2. Cylinder Response PSDs for Various Flowrates (ordinate not to scale) (Chen and Jendrzejczyk 1984)

- In flow, for uncoupled and/or coupled modes; in general, they depend on the flow velocity.

These parameters under different conditions are summarized in Table 10. Different sets of parameters have been used by different investigators in the stability criteria.

10.3 EMPIRICAL STABILITY CRITERIA

From a practical point of view, there is a great demand for design tool in predicting critical flow velocity. Various stability criteria have been proposed based on experimental data. Most of these criteria can be grouped into two classes:

1. The critical flow velocity U/fD is a function of the mass damping parameter,

$$\frac{U}{fD} = \alpha_1 \left(\frac{2\pi m \zeta}{\rho D^2} \right)^{\alpha_2} . \quad (10.1)$$

2. The critical flow velocity is a function of mass ratio $(m/\rho D^2)$ and damping $(2\pi \zeta)$,

$$\frac{U}{fD} = \beta_1 \left(\frac{m}{\rho D} \right)^{\beta_2} (2\pi \zeta)^{\beta_3} . \quad (10.2)$$

Models based on these two classes of criteria have been adopted by various investigators; the studies are summarized in Tables 10.2 and 10.3.

Experimental data for the critical flow velocity obtained by various experimentalists are not in agreement, and various stability criteria do not correlate well. This is attributed to the following reasons:

- Different parameters are used by different investigators; some use in-vacuum parameters, and some use in-fluid parameters or in-flow parameters. Even with the same stability criterion, the results will be different using two different sets of parameters, as illustrated in Table 10.1.
- Instability may be caused by different instability mechanisms. In the past, the fluid-stiffness-controlled instability mechanism has been used exclusively. It is not expected that the stability criterion for fluid-stiffness-controlled instability can be used to correlate data for fluid-damping-controlled instability (see Section 10.6).

Table 10.1. Effective Mass, Natural Frequency, and Modal Damping Ratio under Different Conditions

Parameters	In Vacuum	In Quiescent Fluid		In Flow (uncoupled and/or coupled modes)
		Uncoupled Vibration	Coupled Vibration	
Effective mass (m)	m_v	m_u	m_c	m_f
Natural frequency (f)	f_v	f_u	f_c	f_f
Modal damping ratio (ζ)	ζ_v	ζ_u	ζ_c	ζ_f

Table 10.2. Values of α_1 and α_2 in Studies Where Critical Flow Velocity Is a Function of Mass Damping Parameter

Investigators	α_1	α_2	Remarks
Connors (1970)	9.9	0.5	Tube row with T/D = 1.42
Blevins (1974)	$\frac{2(2\pi)^{0.5}}{(C_x C_y)^{0.25}}$	0.5	C_x and C_y are fluid-elastic-stiffness force coefficients
Y. N. Chen (1974)	$\alpha Re^{-0.25}$	0.5	Re = Reynolds number, α = constant
Gross (1975)	$4/\alpha$	1.0	For square array and α determined from fluid force
Gorman (1976)	3.3	0.5	Suggested design guideline
Savkar (1977)	$4.95(T/D)^2$	0.5	For triangular arrays
Connors (1978)	$0.37 + 1.76 \frac{P}{D}$	0.5	For square array, $1.41 < \frac{P}{D} < 2.12$
Pettigrew et al. (1978)	3.3	0.5	Suggested design guideline
Weaver and Grover (1978)	7.1	0.21	Rotated triangular array P/D = 1.375
Chen and Jendrzejczyk (1981)	2.49 to 6.03	0.2 to 1.08	For various rectangular arrays and mixed array in water flow
Tanaka and Takahara (1981)	3.0	0.75	For square array, P/D = 2.0

Table 10.3. Values of β_1 , β_2 , and β_3 in Studies Where Critical Flow Velocity Is a Function of Mass Ratio and Damping

Investigators	β_1	β_2	β_3	Remarks
Paidoussis (1980b)		0.5	0.25	Using published data
Paidoussis (1980b)	$2.3\left(\frac{P}{D} - 1\right)$	0.4	0.4	Including all data
	$5.8\left(\frac{P}{D} - 1\right)$			Excluding some data
Tanaka and Takahara (1981)		0.5	0.5	For square array, $P/D = 1.33$
		0.333	0.2	Low-density fluid High-density fluid

- The gap flow velocities defined by different investigators are not consistent with one another, and the critical flow velocities are not determined with the same method.
- Critical flow velocities of tube arrays depend on tube arrangement, spacing, and other parameters.

It is apparent that developing a universal stability criterion applicable to all cases will be difficult, if not impossible.

10.4 MATHEMATICAL MODELS

The development of mathematical models has been very exciting. A summary of the published models is presented in Table 10.4--Additional models are not listed in Table 10.4; for example, the quasi-static model by Whiston and Thomas (1982), which is basically the extension of Blevins' model and the empirical correlation by Pettigrew et al. (1978), which is the same as Connors' model.

Table 10.4 shows that these models do not agree in certain aspects:

Instability Mechanisms: Before 1980, the displacement mechanism was used exclusively; therefore, instability was caused by fluid-stiffness forces. If instability is attributed to the displacement mechanism, the coupling of fluid-stiffness forces with the neighboring tubes is one of the requirements for instability to occur. During that period, it was thought that a single elastic tube among an array of rigid tubes would not become unstable. Although experimental results showed the contrary, no plausible explanation was given. One of the keys in resolving this issue was the publication of fluid-force data by Tanaka et al. (1981, 1982). Using Tanaka's fluid-force data, Chen (1983a, 1983b) has shown that, in addition to the displacement mechanism, the velocity mechanism is also very important. Based on the two mechanisms, the discrepancy among different models can now be resolved reasonably well.

Stability Criteria and System Parameters: Table 10.4 shows that different investigators have developed different stability criteria and that different parameters are used in different correlations. In some cases, the system parameters are not defined in sufficient detail.

Equations of Motion: Different approaches are used in solving the equations of motion; these include a single equation of motion, multiple equations of motion with assumed modes, and general solution of multiple equations.

It is recognized that each model has its merits and deficiency. These can be summarized as follows:

Table 10.4. Summary of Models for Stability of a Group of Circular Cylinders in Crossflow

Author	Name of Instability	Instability Mechanism	Dominant Fluid Force	Instability Criterion	Parameters Used in Stability Criterion	Method to Obtain Stability Criterion
Connors (1970)	Fluidelastic vibration	Displacement mechanism	Fluid-stiffness force	$\frac{U}{fD} = \alpha \left(\frac{2\pi\zeta m}{\rho D^2} \right)^{0.5}$	f_u, m_u, ζ_u	Energy consideration of a single tube and experimental measurement of fluid-stiffness forces
Blevins (1974, 1979)	Fluidelastic whirling	Displacement mechanism	Fluid-stiffness force	$\frac{U}{fD} = \alpha \left(\frac{2\pi\zeta m}{\rho D^2} \right)^{0.5}$	f_u, m_u, ζ_u or ζ_f	Equations of motion for tube rows with assumed mode shapes
Tanaka et al. (1981, 1982)	Fluidelastic vibration	Displacement and velocity mechanisms	Fluid dynamic force including fluid-stiffness force and flow-velocity-dependent damping force	Light fluid: $\frac{U}{fD} = \alpha \left(\frac{2\pi\zeta m}{\rho D^2} \right)^{0.5}, (P/D = 1.33)$ Heavy fluid: $\frac{U}{fD} = \alpha_1 (2\pi\zeta)^2 \left(\frac{m}{\rho D^2} \right)^{0.75}, (P/D = 1.33)$ $\frac{U}{fD} = \alpha_1 \left(\frac{2\pi\zeta m}{\rho D^2} \right)^{0.75}, (P/D = 2.0)$	f_u, m_u, ζ_u or ζ_f f_v, m_v, ζ_v	Equations of motion using measured fluid-force data
Chen et al. (1983a, 1983b)	Dynamic instability: Fluid-damping-controlled or fluid-stiffness-controlled instability	Displacement mechanism and/or velocity mechanism	Fluid-stiffness force and flow-velocity-dependent damping force	Light fluid: $\frac{U}{fD} = \alpha \left(\frac{2\pi\zeta m}{\rho D^2} \right)^{0.5}$ Heavy fluid: $\frac{U}{fD} = \alpha_1 (2\pi\zeta)^2 \left(\frac{m}{\rho D^2} \right)^{0.75}$	f_u, m_u, ζ_u or f_c, m_c, ζ_c	Equations of motion using measured fluid-damping and fluid-stiffness forces
Price and Paidoussis (1983)	Fluidelastic instability	Displacement mechanism	Fluid-stiffness force (flow-velocity-dependent force taken into account partially)	$\frac{U}{fD} = \alpha_1 [1 + (1 + \alpha_2 \frac{2\pi\zeta m}{\rho D^2})^{0.5}]$	f^*, m^*, ζ^*	Equations of motion using measured fluid-stiffness forces
Lever and Weaver (1982)	Fluidelastic instability	Velocity mechanism	Flow-velocity-dependent damping force	$\frac{U}{fD} = F \left(\frac{2\pi\zeta m}{\rho D^2} \right)$	f^*, m^*, ζ^*	Equation of motion of a single tube among a rigid tube array

*Not clearly specified. In most cases, these parameters are defined as follows: m = mass or mechanical mass; f = tube natural frequency; and ζ = tube damping ratio or mechanical damping ratio.

$\alpha, \alpha_1, \alpha_2, \alpha_3$ in different equations denote constants, which have different values in different equations, and F denotes a function.

Quasi-static models (Connors, Blevins, and Price and Paidoussis) are applicable for fluid-stiffness-controlled instability only. Although flow-velocity-dependent damping forces have been considered partially in some models, these models do not appear to be applicable for fluid-damping-controlled instability.

The analytical model (Lever and Weaver) is based on the velocity mechanism for a single elastic tube, surrounded by rigid tubes, moving in a specific direction. The model requires only three empirical constants and has demonstrated the existence of the "jump" phenomenon in the critical flow velocity at a certain value of mass-damping parameter. For heavy fluid, the results qualitatively agree well with test results; for light fluid, the model predicts that the critical flow velocity U/fD is proportional to the first power of the mass-damping parameter. The model looks very promising; extending the theory to incorporate the coupling fluidelastic-stiffness forces for multiple elastic tubes will probably improve the model significantly.

General semi-analytical models (Chen et al. and Tanaka et al.) require measurements or computations to determine the fluid-force coefficients. However, this type of model predicts very well all the observed characteristics of instability for both light and heavy fluids.

At this time, it appears that the Chen (1983a, 1983b) model provides the most detailed insights of the instability phenomena by (1) identifying two different instability mechanisms, (2) resolving the controversy among different investigators, (3) identifying proper parameters to be used in stability criteria, (4) comparing well with experimental data, (5) demonstrating the existence of the jump in the critical flow velocity at a certain value of mass-damping parameter and multiple stable and unstable regions, (6) developing different stability criteria for light and heavy fluids, and (7) predicting the effect of different system parameters. Therefore, the Chen model is being used as the basis for development of the mathematical model.

10.5 FLUID FORCE COEFFICIENTS

Consider a group of N cylinders vibrating in a flow, as shown in Fig. 1.3. The motion-dependent fluid-force components acting on cylinder j in the x and y directions are g_j and h_j respectively; g_j and h_j are given as (see Eq. 1.4)

$$g_j = - \sum_{k=1}^N \left\{ [\bar{\alpha}_{jk} \frac{\partial^2 u_k}{\partial t^2} + \bar{\alpha}'_{jk} \frac{\partial u_k}{\partial t} + \bar{\alpha}''_{jk} u_k] \right. \\ \left. + [\bar{\sigma}_{jk} \frac{\partial^2 v_k}{\partial t^2} + \bar{\sigma}'_{jk} \frac{\partial v_k}{\partial t} + \bar{\sigma}''_{jk} v_k] \right\} \quad \text{and} \quad (10.5)$$

$$h_j = - \sum_{k=1}^N \left\{ [\bar{\tau}_{jk} \frac{\partial^2 u_k}{\partial t^2} + \bar{\tau}'_{jk} \frac{\partial u_k}{\partial t} + \bar{\tau}''_{jk} u_k] \right. \\ \left. + [\bar{\beta}_{jk} \frac{\partial^2 v_k}{\partial t^2} + \bar{\beta}'_{jk} \frac{\partial v_k}{\partial t} + \bar{\beta}''_{jk} v_k] \right\} . \quad (10.6)$$

Experimental data have shown that the fluid-damping and fluid-stiffness matrices are a function of the reduced flow velocity. Equations 10.5 and 10.6 can be written in terms of dimensionless force coefficients:

$$\bar{\alpha}_{jk} = \rho \pi R^2 \alpha_{jk}, \quad \bar{\alpha}'_{jk} = - \frac{\rho U^2}{\omega} \alpha'_{jk}, \quad \bar{\alpha}''_{jk} = -\rho U^2 \alpha''_{jk} \\ \bar{\sigma}_{jk} = \rho \pi R^2 \sigma_{jk}, \quad \bar{\sigma}'_{jk} = - \frac{\rho U^2}{\omega} \sigma'_{jk}, \quad \bar{\sigma}''_{jk} = -\rho U^2 \sigma''_{jk} \\ \bar{\tau}_{jk} = \rho \pi R^2 \tau_{jk}, \quad \bar{\tau}'_{jk} = - \frac{\rho U^2}{\omega} \tau'_{jk}, \quad \bar{\tau}''_{jk} = -\rho U^2 \tau''_{jk} \\ \bar{\beta}_{jk} = \rho \pi R^2 \beta_{jk}, \quad \bar{\beta}'_{jk} = - \frac{\rho U^2}{\omega} \beta'_{jk}, \quad \bar{\beta}''_{jk} = -\rho U^2 \beta''_{jk} . \quad (10.7)$$

Using Eqs. 10.5, 10.6 and 10.7 yields

$$g_j = -\rho \pi R^2 \sum_{k=1}^N \left(\alpha_{jk} \frac{\partial^2 u_k}{\partial t^2} + \sigma_{jk} \frac{\partial^2 v_k}{\partial t^2} \right) \\ + \frac{\rho U^2}{\omega} \sum_{k=1}^N \left(\alpha'_{jk} \frac{\partial u_k}{\partial t} + \sigma'_{jk} \frac{\partial v_k}{\partial t} \right) \\ + \rho U^2 \sum_{k=1}^N \left(\alpha''_{jk} u_k + \sigma''_{jk} v_k \right) \quad \text{and} \quad (10.8)$$

$$\begin{aligned}
h_j = & -\rho\pi R^2 \sum_{k=1}^N \left(\tau_{jk} \frac{\partial^2 u_k}{\partial t^2} + \beta_{jk} \frac{\partial^2 v_k}{\partial t^2} \right) \\
& + \frac{\rho U^2}{\omega} \sum_{k=1}^N \left(\tau'_{jk} \frac{\partial u_k}{\partial t} + \beta'_{jk} \frac{\partial v_k}{\partial t} \right) \\
& + \rho U^2 \sum_{k=1}^N \left(\tau''_{jk} u_k + \beta''_{jk} v_k \right) .
\end{aligned} \tag{10.9}$$

α_{jk} , σ_{jk} , τ_{jk} , and β_{jk} are called added mass coefficients, α'_{jk} , σ'_{jk} , τ'_{jk} and β'_{jk} are called fluid-damping coefficients, and α''_{jk} , σ''_{jk} , τ''_{jk} and β''_{jk} are called fluid-stiffness coefficients.

Equations 10.8 and 10.9 describe the fluid force components for arbitrary cylinder displacements. When the cylinder is oscillating in a particular pattern, simplified results can be obtained. For example, let the cylinder displacements be

$$u_k = a_k u \quad \text{and} \tag{10.10}$$

$$v_k = b_k v ,$$

where a_k and b_k are constants. Using Eqs. 10.8, 10.9, and 10.10 yields

$$\begin{aligned}
g_j = & \rho\pi R^2 \left(\alpha_j \frac{\partial^2 u}{\partial t^2} + \sigma_j \frac{\partial^2 v}{\partial t^2} \right) \\
& + \frac{\rho U^2}{\omega} \left(\alpha'_j \frac{\partial u}{\partial t} + \sigma'_j \frac{\partial v}{\partial t} \right) \\
& + \rho U^2 (\alpha''_j u + \sigma''_j v) \quad \text{and}
\end{aligned} \tag{10.11}$$

$$\begin{aligned}
h_j = & -\rho\pi R^2 \left(\tau_j \frac{\partial^2 u}{\partial t^2} + \beta_j \frac{\partial^2 v}{\partial t^2} \right) \\
& + \frac{\rho U^2}{\omega} \left(\tau'_j \frac{\partial u}{\partial t} + \beta'_j \frac{\partial v}{\partial t} \right) \\
& + \rho U^2 (\tau''_j u + \beta''_j v) ,
\end{aligned} \tag{10.12}$$

where

$$\begin{aligned}
 \alpha_j &= \sum_{k=1}^N \alpha_{jk} a_k, & \alpha'_j &= \sum_{k=1}^N \alpha'_{jk} a_k, & \alpha''_j &= \sum_{k=1}^N \alpha''_{jk} a_k, \\
 \sigma_j &= \sum_{k=1}^N \sigma_{jk} b_k, & \sigma'_j &= \sum_{k=1}^N \sigma'_{jk} b_k, & \sigma''_j &= \sum_{k=1}^N \sigma''_{jk} b_k, \\
 \tau_j &= \sum_{k=1}^N \tau_{jk} a_k, & \tau'_j &= \sum_{k=1}^N \tau'_{jk} b_k, & \tau''_j &= \sum_{k=1}^N \tau''_{jk} a_k, \\
 \text{and} \\
 \beta_j &= \sum_{k=1}^N \beta_{jk} b_k, & \beta'_j &= \sum_{k=1}^N \beta'_{jk} b_k, & \beta''_j &= \sum_{k=1}^N \beta''_{jk} b_k.
 \end{aligned} \tag{10.13}$$

When $a_k = b_k = 1$ ($k = 1$ to N), all cylinders oscillate with the same amplitude; this corresponds to the case of a rigid body consisting of N cylinders. The displacement patterns given in Eq. 10.10 are called "constrained modes"; in general, these modes do not correspond to the coupled natural modes in flow.

Added Mass Coefficients: Added mass coefficients can be calculated by the method described in Section 3.3 for a quiescent fluid. In flowing fluid, the added mass coefficient can vary with flow velocity and may depend on period parameters (Keulegan and Carpenter 1958). If the motion of the cylinders is small (i.e., for small K_c), added mass based on the quiescent ideal fluid will be acceptable. Investigations of added masses for cylinders with relatively large amplitude in practical flow conditions remain to be made.

Fluid-Damping Coefficients: Fluid damping is conveniently divided into two parts: viscous damping and flow-velocity-dependent damping. Fluid viscous damping is defined as the damping at zero flowrate ($U = 0$); the flow-velocity-dependent damping is defined as the damping at a given flowrate ($U \neq 0$) minus that at zero flowrate. In practical applications, it may not always be possible to separate the two parts. In Eqs. 10.8 and 10.9, these two parts of damping are combined. Since at $U = 0$ the fluid damping is not equal to zero in general, the fluid damping coefficient multiplied by $\rho U^2 / \omega$ at $U = 0$ is a finite number. At this time, no analytical solutions are available for the fluid-damping coefficients for $U \neq 0$, and they can be obtained experimentally. In general, for $U \neq 0$, these coefficients are not symmetric.

Fluid-Stiffness Coefficients: Analytical solutions for fluid-stiffness coefficients are not available except for those based on the potential flow theory, which is not generally applicable. Systematic experiments can be

performed to obtain fluid-stiffness coefficients. Fluid-stiffness coefficients are not symmetric, in general.

Fluid forces acting on cylinder arrays were measured and reported by Tanaka and his colleagues (1980, 1981, 1982) for a row of cylinders and square arrays. In their tests, fluid force components are measured as a function of cylinder displacements. For example, cylinder k is excited in the y direction; its displacement in the y direction is given by

$$v_k = \bar{v}_k \exp(i\omega t) . \quad (10.14)$$

The fluid force acting on cylinder j in the x direction is given by

$$g_j = \frac{1}{2} \rho U^2 (c_{jk} \cos \psi_{jk} + i c_{jk} \sin \psi_{jk}) \bar{v}_k , \quad (10.15)$$

where c_{jk} is the fluid force amplitude and ψ_{jk} is the phase angle between the fluid force and the cylinder displacement. These values can be measured experimentally.

Using Eqs. 10.8 and 10.14, we can also write the fluid force component as

$$g_j = (\rho \pi R^2 \omega^2 \sigma_{jk}'' + \rho U^2 \sigma_{jk}'' + i \rho U^2 \sigma_{jk}') \bar{v}_k . \quad (10.16)$$

Comparing Eqs. 10.15 and 10.16 yields

$$\begin{aligned} \sigma_{jk}'' &= \frac{1}{2} c_{jk} \cos \psi_{jk} - \frac{\pi}{U_r^2} \sigma_{jk} \quad \text{and} \\ \sigma_{jk}' &= \frac{1}{2} c_{jk} \sin \psi_{jk} , \end{aligned} \quad (10.17)$$

where U_r is the reduced flow velocity ($= \pi U / \omega R$).

Values of α_{jk}' , σ_{jk}' , τ_{jk}' , β_{jk}' , α_{jk}'' , σ_{jk}'' , τ_{jk}'' , and β_{jk}'' for a row of cylinders and a square array reduced from Tanaka's data are given in Figs. 10.3-10.6 as a function of reduced flow velocity (U_r). At low U_r , variations of fluid force coefficients are more drastic. For large U_r , both fluid-damping and fluid-stiffness coefficients are almost independent of U_r .

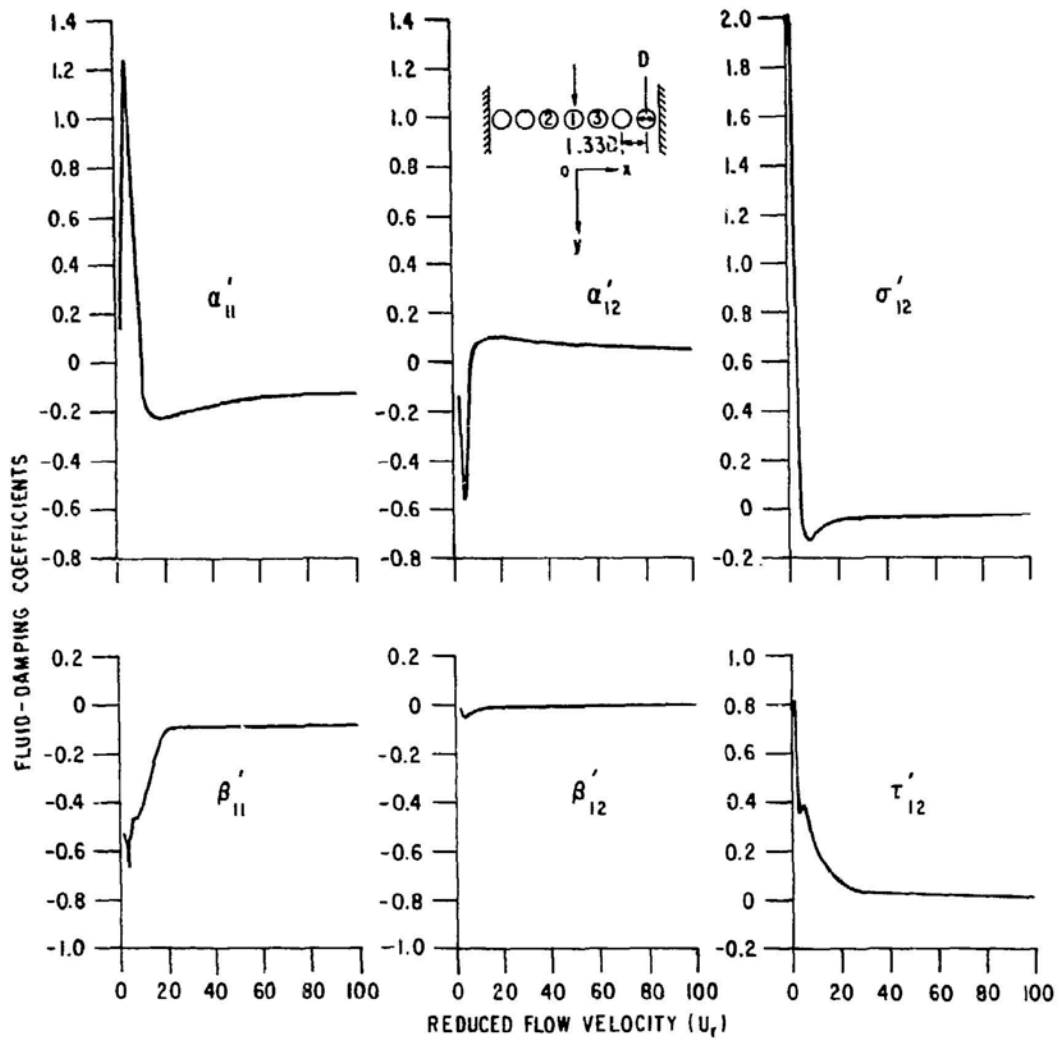


Fig. 10.3. Fluid-Damping Coefficients for a Row of Cylinders (Chen 1983b)

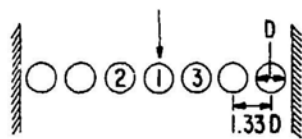
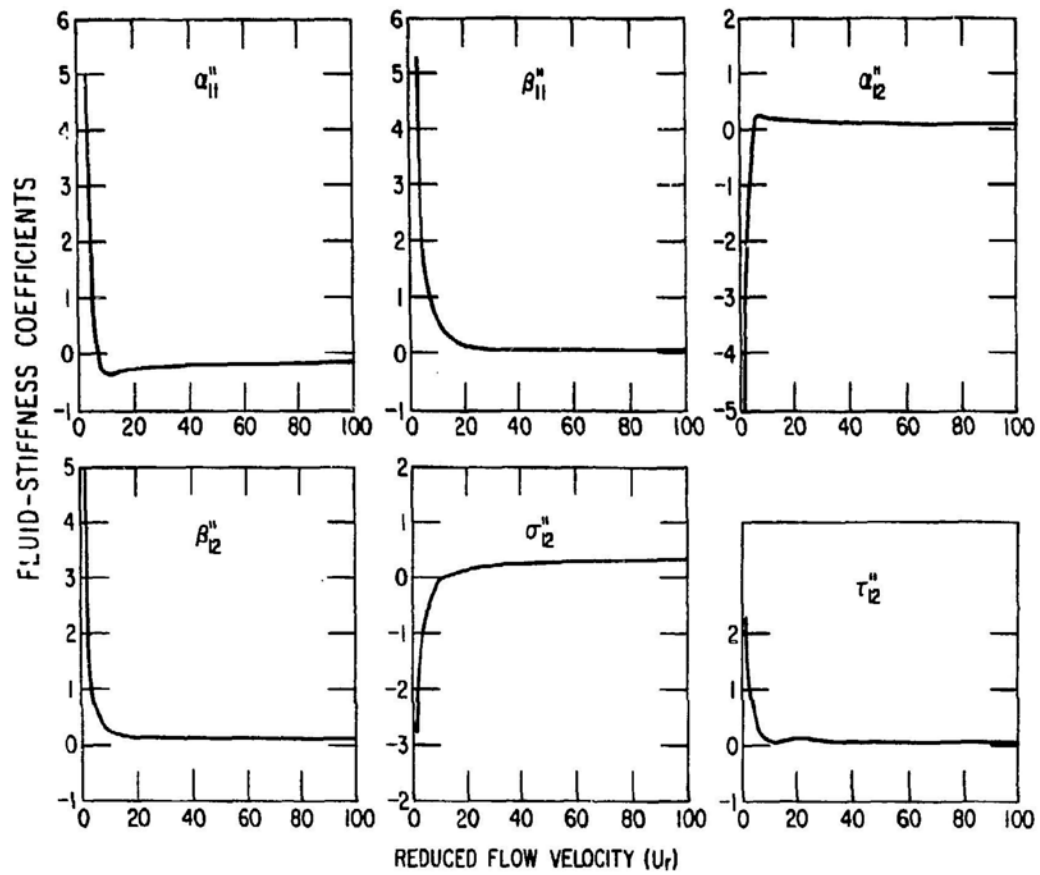


Fig. 10.4. Fluid-Stiffness Coefficients for a Row of Cylinders (Chen 1983b)

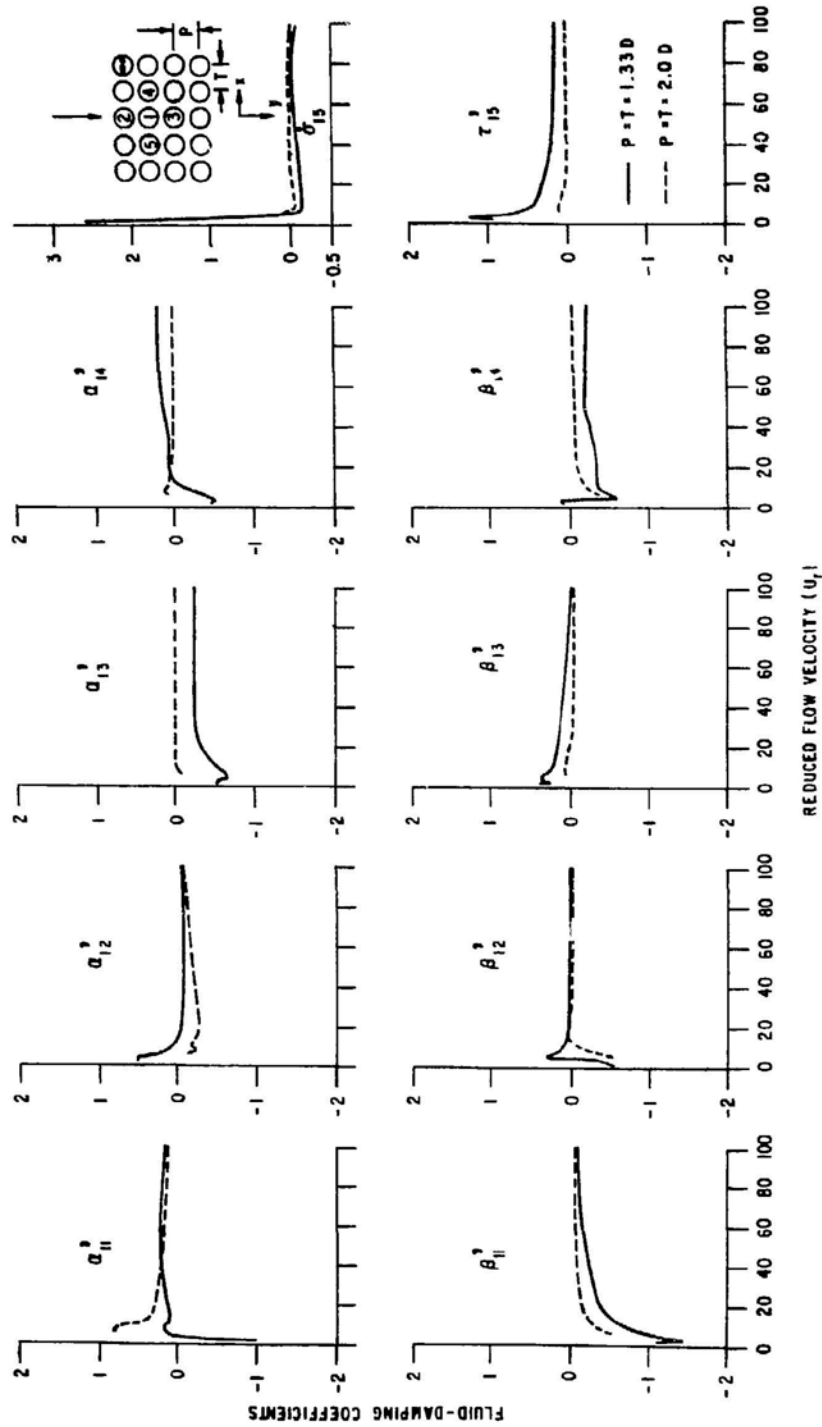


Fig. 10.5. Fluid-Damping Coefficients for a Square Array (Chen and Jendrzejczyk 1983)

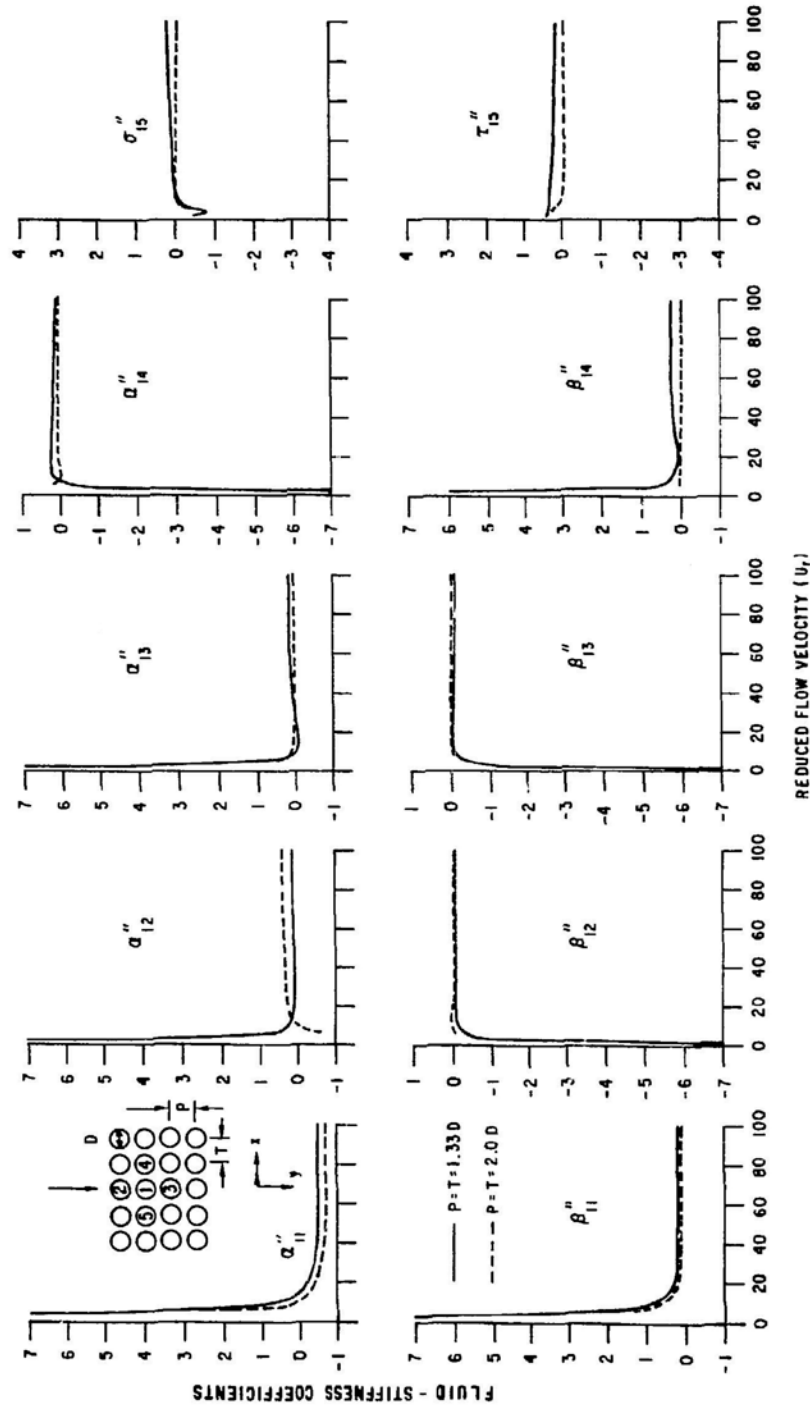


Fig. 10.6. Fluid-Stiffness Coefficient for a Square Array (Chen and Jendrzejczyk 1983)

10.6 PREDICTION OF THE CRITICAL FLOW VELOCITY

10.6.1 Analysis

Critical flow velocity can be calculated based on Eqs. 8.9 and 8.10 by setting the right side of the equations equal to zero. Using Eqs. 8.9, 8.10, 8.11 and 10.7, we obtain the equations of motion as follows:

$$\begin{aligned}
 & \frac{d^2 a_{jm}}{dt^2} + \zeta_{vjm} \omega_{vjm} \frac{da_{jm}}{dt} + \omega_{vjm}^2 a_{jm} \\
 & + \frac{\rho \pi R^2}{m_j} \sum_{k=1}^N \left(\alpha_{jk} \frac{d^2 a_{km}}{dt^2} + \sigma_{jk} \frac{d^2 b_{km}}{dt^2} \right) \\
 & - \frac{\rho \bar{U}}{m_j \omega} \sum_{k=1}^N \left(\alpha'_{jkm} \frac{da_{km}}{dt} + \sigma'_{jk} \frac{db_{km}}{dt} \right) \\
 & - \frac{\rho \bar{U}^2}{m_j} \sum_{k=1}^N \left(\alpha''_{jkm} a_{km} + \sigma''_{jk} b_{km} \right) = 0 \quad \text{and} \quad (10.18)
 \end{aligned}$$

$$\begin{aligned}
 & \frac{d^2 b_{jm}}{dt^2} + \zeta_{vjm} \omega_{vjm} \frac{db_{jm}}{dt} + \omega_{vjm}^2 b_{jm} \\
 & + \frac{\rho \pi R^2}{m_j} \sum_{k=1}^N \left(\tau_{jk} \frac{d^2 a_{km}}{dt^2} + \beta_{jk} \frac{d^2 b_{km}}{dt^2} \right) \\
 & - \frac{\rho \bar{U}}{m_j \omega} \sum_{k=1}^N \left(\tau'_{jkm} \frac{da_{km}}{dt} + \beta'_{jk} \frac{db_{km}}{dt} \right) \\
 & - \frac{\rho \bar{U}^2}{m_j} \sum_{k=1}^N \left(\tau''_{jkm} a_{km} + \beta''_{jk} b_{km} \right) = 0, \quad (10.19)
 \end{aligned}$$

where

$$\begin{aligned}
 \alpha'_{jkm} &= \frac{1}{\ell} \int_0^\ell \alpha'_{jk} \phi_m^2 \psi^2 dz, & \alpha''_{jkm} &= \frac{1}{\ell} \int_0^\ell \alpha''_{jk} \phi_m^2 \psi^2 dz, \\
 \sigma'_{jkm} &= \frac{1}{\ell} \int_0^\ell \sigma'_{jk} \phi_m^2 \psi^2 dz, & \sigma''_{jkm} &= \frac{1}{\ell} \int_0^\ell \sigma''_{jk} \phi_m^2 \psi^2 dz, \\
 \tau'_{jkm} &= \frac{1}{\ell} \int_0^\ell \tau'_{jk} \phi_m^2 \psi^2 dz, & \tau''_{jkm} &= \frac{1}{\ell} \int_0^\ell \tau''_{jk} \phi_m^2 \psi^2 dz, \\
 \beta'_{jkm} &= \frac{1}{\ell} \int_0^\ell \beta'_{jk} \phi_m^2 \psi^2 dz, & \beta''_{jkm} &= \frac{1}{\ell} \int_0^\ell \beta''_{jk} \phi_m^2 \psi^2 dz, \quad (10.20)
 \end{aligned}$$

Note that Eqs. 10.18 and 10.19 can be applied to all values of m . For each m , there are $2N$ equations that are coupled. However, there is no coupling among the equations for different m . This is true for a cylinder array having the same length and same type of boundary conditions, whether the cylinders are single span or multiple spans. If the cylinders have different types of end conditions, a similar method of analysis can be developed. In this case the equations for different m will be coupled.

Let ω_v be the reference circular frequency, which may be the natural frequency of a particular cylinder in vacuum. Using the dimensionless parameters

$$\tau = \omega_v t ,$$

$$U_v = \frac{\bar{U}}{f_v D} \quad (f_v = \frac{\omega_v}{2\pi}) , \quad \text{and} \quad (10.21)$$

$$\gamma_j = \frac{\rho \pi R^2}{m_j} ,$$

Equations 10.18 and 10.19 become

$$\begin{aligned} \ddot{a}_j + \gamma_j \sum_{k=1}^N (\alpha_{jk} \ddot{a}_k + \sigma_{jk} \ddot{b}_k) \\ + 2\zeta_{vjm} \left(\frac{\omega_{vjm}}{\omega_v} \right) \dot{a}_j - \frac{\gamma_j}{\pi} U_v^2 \sum_{k=1}^N (\alpha'_{jkm} \dot{a}_k + \sigma'_{jkm} \dot{b}_k) \\ + \left(\frac{\omega_{vjm}}{\omega_v} \right)^2 a_j - \frac{\gamma_j}{\pi^3} U_v^2 \sum_{k=1}^N (\alpha''_{jkm} a_k + \sigma''_{jkm} b_k) = 0 \quad \text{and} \end{aligned} \quad (10.22)$$

$$\begin{aligned} \ddot{b}_j + \gamma_j \sum_{k=1}^N (\tau_{jk} \ddot{a}_k + \beta_{jk} \ddot{b}_k) \\ + 2\zeta_{vjm} \left(\frac{\omega_{vjm}}{\omega_v} \right) \dot{b}_j - \frac{\gamma_j}{\pi} U_v^2 \sum_{k=1}^N (\tau'_{jkm} \dot{a}_k + \beta'_{jkm} \dot{b}_k) \\ + \left(\frac{\omega_{vjm}}{\omega_v} \right)^2 b_j - \frac{\gamma_j}{\pi^3} U_v^2 \sum_{k=1}^N (\tau''_{jkm} a_k + \beta''_{jkm} b_k) = 0 , \end{aligned} \quad (10.23)$$

where the dot denotes differentiation with respect to τ . Fluid-damping and fluid-stiffness coefficients are functions of the reduced flow velocity U_r ($= \bar{U}/fD$). The frequency of oscillation $f(= \omega/2\pi)$ is different from the reference frequency f_v .

The stability of a cylinder array is determined from Eqs. 10.22 and 10.23. The nondimensional parameters in Eqs. 10.22 and 10.23 are γ_j , ω_{vjm}/ω_v , ζ_{vjm} , U_v , α_{jk} , σ_{jk} , τ_{jk} , β_{jk} , α'_{jkm} , σ'_{jkm} , τ'_{jkm} , β'_{jkm} , α''_{jkm} , σ''_{jkm} , τ''_{jkm} and β''_{jkm} . Therefore, the critical flow velocity can be written in a functional form:

$$U_v = F(\gamma_j, \omega_{vjm}/\omega_v, \zeta_{vjm}, \alpha_{jk}, \sigma_{jk}, \tau_{jk}, \beta_{jk}, \alpha'_{jkm}, \sigma'_{jkm}, \tau'_{jkm}, \beta'_{jkm}, \alpha''_{jkm}, \sigma''_{jkm}, \tau''_{jkm}, \beta''_{jkm}). \quad (10.24)$$

These parameters can be divided into several groups.

Mass Ratio (γ_j): This represents the ratio of displaced mass of fluid to the cylinder mass. In most practical applications, all cylinders are identical; therefore

$$\gamma_j = \gamma_v, \quad j = 1, 2, 3, \dots, N. \quad (10.25)$$

Detuning in Frequency (ω_{vjm}): Frequency variations of different cylinders in an array can affect stability. For an in-tune cylinder array,

$$\omega_{vjm} = \omega_v, \quad j = 1, 2, 3, \dots, N. \quad (10.26)$$

Detuning in Damping (ζ_{vjm}): Detuning in damping can also affect stability. For a cylinder array without damping variation,

$$\zeta_{vjm} = \zeta_v, \quad j = 1, 2, 3, \dots, N. \quad (10.27)$$

Added Mass Coefficients (α_{ij} , σ_{ij} , τ_{ij} , and β_{ij}): These coefficients depend on cylinder arrangement only. For a given array, they are constants.

Effective Fluid-damping Coefficients (α'_{jkm} , σ'_{jkm} , τ'_{jkm} , and β'_{jkm}): These coefficients depend on flow-velocity distribution function $\psi(z)$ (see Eq. 8.8), cylinder mode shape $\phi_m(z)$, and fluid-damping coefficients α'_{jk} , σ'_{jk} , τ'_{jk} , and β'_{jk} . Fluid-damping coefficients are a function of the reduced flow velocity U_r for small U_r and approximately constants for large U_r .

Effective Fluidelastic-stiffness Coefficients (α''_{jkm} , σ''_{jkm} , τ''_{jkm} , and β''_{jkm}): These coefficients are functions of flow-velocity distribution function $\psi(z)$, tube mode shape $\phi_m(z)$ (see Eq. 8.7), and fluid-stiffness coefficients α''_{1j} , σ''_{1j} , τ''_{1j} , and β''_{1j} . In general, fluid-stiffness coefficients are functions of the reduced flow velocity U_r ; however, for large U_r , they are very weak functions of U_r and can be considered as constants.

For a cylinder array in which all cylinders are identical, having the same natural frequency and damping in both directions, using Eqs. 10.21-10.23 and 10.25-10.27 yields

$$\begin{aligned} \ddot{a}_j + \gamma_v \sum_{k=1}^N (\alpha_{jk} \ddot{a}_k + \sigma_{jk} \ddot{b}_k) \\ + 2\zeta_v \dot{a}_j - \frac{\gamma_v}{\pi} U_v^2 \sum_{k=1}^N (\alpha'_{jkm} \dot{a}_k + \sigma'_{jkm} \dot{b}_k) \\ + a_j - \frac{\gamma_v}{\pi} U_v^2 \sum_{k=1}^N (\alpha''_{jkm} a_k + \sigma''_{jkm} b_k) = 0 \quad \text{and} \end{aligned} \quad (10.28)$$

$$\begin{aligned} \ddot{b}_j + \gamma_v \sum_{k=1}^N (\tau_{jk} \ddot{a}_k + \beta_{jk} \ddot{b}_k) \\ + 2\zeta_v \dot{b}_j - \frac{\gamma_v}{\pi} U_v^2 \sum_{k=1}^N (\tau'_{jkm} \dot{a}_k + \sigma'_{jkm} \dot{b}_k) \\ + b_j - \frac{\gamma_v}{\pi} U_v^2 \sum_{k=1}^N (\tau''_{jkm} a_k + \sigma''_{jkm} b_k) = 0. \end{aligned} \quad (10.29)$$

The critical flow velocity can be calculated based on Eqs. 10.22 and 10.23 or 10.28 and 10.29.

Approximate solutions based on constrained mode provide significant insight into the system characteristics. Consider cylinder 1 oscillating in the x direction. The equation of motion is

$$\ddot{a}_1 + 2\zeta_{f1} \omega_{f1} \dot{a}_1 + \omega_{f1}^2 a_1 = 0,$$

where

$$\omega_{f1} = \omega_v \left(\frac{1 - \frac{1}{\pi} \gamma_v U_v^2 \alpha''_{11m}}{1 + \alpha_{11} \gamma_v} \right)^{1/2} \quad (10.30)$$

and

$$\zeta_{f1} = \frac{\zeta_v - \frac{1}{2\pi^3} \gamma_v U_v^2 \alpha'_{11m}}{\left[(1 + \gamma_v \alpha_{11}) \left(1 - \frac{1}{\pi^3} \gamma_v U_v^2 \alpha''_{11m} \right) \right]^{1/2}},$$

where ω_{f1} and ζ_{f1} are the circular natural frequency and modal damping ratio of the constrained mode in flow. The critical flow velocity can be determined from Eq. 10.30:

$$\zeta_{f1} = 0; \quad \text{i.e., } U_v = \left(\frac{2\pi^3 \zeta_v}{\gamma_v \alpha'_{11m}} \right)^{1/2} \quad (10.31)$$

$$\text{or } \frac{\bar{U}}{f_v D} = \left(\frac{4\pi}{\alpha'_{11m}} \right)^{0.5} \left(\frac{2\pi \zeta_v m_v}{\rho D^2} \right)^{0.5}. \quad (10.32)$$

Similarly, oscillations in the y direction can be analyzed; the results are similar to those given in Eqs. 10.30 to 10.32.

For constrained modes involving multiple cylinders oscillating in a particular pattern, similar results are obtained. For example, consider the case in which all cylinders are moving in the x direction with the same amplitude. The equation of motion becomes

$$\ddot{x}_1 + 2\zeta_{f1} \omega_{f1} \dot{x}_1 + \omega_{f1}^2 x_1 = 0, \quad (10.33)$$

where

$$\omega_{f1} = \omega_v \left(\frac{1 - \frac{1}{\pi^3} \gamma_v U_v^2 \alpha''_{11m}}{1 + \alpha_1 \gamma_v} \right)^{1/2},$$

$$\zeta_{f1} = \frac{\zeta_v - \frac{1}{2\pi^3} \gamma_v U_v^2 \alpha'_{11m}}{\left[(1 + \gamma_v \alpha_1) \left(1 - \frac{1}{\pi^3} \gamma_v U_v^2 \alpha''_{11m} \right) \right]^{1/2}}, \quad (10.34)$$

$$\alpha_1 = \sum_{j=1}^N \alpha_{1j},$$

$$\alpha''_{lm} = \frac{1}{\ell} \int_0^{\ell} \left(\sum_{j=1}^N \alpha_{lj} \right) \phi_m^2 \psi^2 dz ,$$

and

$$\alpha'_{lm} = \frac{1}{\ell} \int_0^{\ell} \left(\sum_{j=1}^N \alpha'_{lj} \right) \phi_m^2 \psi^2 dz .$$

The critical flow velocity is given by

$$\frac{\bar{U}}{f_v D} = \left(\frac{4\pi}{\alpha'_{lm}} \right)^{0.5} \left(\frac{2\pi \zeta_v m_v}{\rho D^2} \right)^{0.5} . \quad (10.35)$$

For light fluids, the fluid inertia can be neglected; Eqs. 10.28 and 10.29 can be written

$$\begin{aligned} \ddot{a}_j + 2\zeta_v \dot{a}_j + a_j \\ - \frac{\gamma_v}{\pi} U_v^2 \sum_{k=1}^N (\alpha'_{jkm} \dot{a}_k + \sigma'_{jkm} \dot{b}_k + \alpha''_{jkm} a_k + \sigma''_{jkm} b_k) = 0 \end{aligned} \quad (10.36)$$

and

$$\begin{aligned} \ddot{b}_j + 2\zeta_v \dot{b}_j + b_j \\ - \frac{\gamma_v}{\pi} U_v^2 \sum_{k=1}^N (\tau'_{jkm} \dot{a}_k + \beta'_{jkm} \dot{b}_k + \tau''_{jkm} a_k + \beta''_{jkm} b_k) = 0 . \end{aligned} \quad (10.37)$$

In light fluids, instability occurs at large U_v , and the fluid-force coefficients α'_{ijm} , σ'_{ijm} , τ'_{ijm} , β'_{ijm} , α''_{ijm} , σ''_{ijm} , τ''_{ijm} , and β''_{ijm} are approximately independent of U_v ($U_v \approx U_r$). In Eqs. 10.36 and 10.37, the variables controlling the system stability are the parameters ζ_v and $\gamma_v U_v^2$. Note that the role of $\gamma_v U_v^2$ is the same as ζ_v . The terms associated with ζ_v and $\gamma_v U_v^2$ in Eqs. 10.36 and 10.37 are contributing to system damping; the modal damping of a mode can be written as

$$\zeta_{fl} = \zeta_v - C \gamma_v U_v^2 , \quad (10.38)$$

where C depends on the fluid-force coefficients. The instability occurs if $\zeta_{f1} = 0$; i.e.,

$$U_v = \frac{1}{C} \left(\frac{\zeta_v}{\gamma_v} \right)^{0.5} \quad (10.39)$$

or

$$\frac{\bar{U}}{f_v D} = \left(\frac{2\pi \zeta_v m_v}{\rho D^2} \right)^{0.5} \quad (10.40)$$

Thus for light fluid, the critical reduced flow velocity is proportional to the half-power of the mass-damping parameter. This is true in both fluid-damping-controlled and fluid-stiffness-controlled instability as long as the critical reduced flow velocity is relatively large. At low reduced flow velocity U_v , since both fluid-damping and fluid-stiffness coefficients are functions of U_r , no such conclusions can be made.

10.6.2 Two Instability Mechanisms

Based on the results of this model, instability can be caused by a velocity mechanism or a displacement mechanism.

Velocity Mechanism: The dominant fluid force is proportional to the velocity of the cylinders. Depending on the reduced flow velocity, fluid-damping force can act as an energy-dissipation mechanism or an excitation mechanism for cylinder oscillations. When it acts as an excitation mechanism, the system damping is reduced. Once the modal damping of a mode becomes negative, the cylinders lose stability. This type of instability is called fluid-damping-controlled instability. The instability criterion is given by

$$\frac{U}{f_v D} = \alpha_v \left(\frac{2\pi \zeta_v m_v}{\rho D^2} \right)^{0.5}, \quad (10.41)$$

where α_v is a function of fluid damping coefficients.

Displacement Mechanisms: The dominant fluid force is proportional to the displacements of the cylinders. The fluid-stiffness force can affect natural frequencies as well as modal damping. As the flow velocity increases, the fluid-stiffness force can reduce modal damping. When the modal damping of a mode becomes negative, the cylinders become unstable; this type of instability is called fluid-stiffness-controlled instability. The instability criterion is given by

$$\frac{U}{f_v D} = \beta_v \left(\frac{2\pi \zeta_v m_v}{\rho D^2} \right)^{0.5}, \quad (10.42)$$

where β_v is a function of fluid-stiffness coefficients.

In general cases, the two mechanisms are superimposed on each other. Then the stability criterion can be written

$$\frac{U}{f_v D} = F \left(\zeta_v, \frac{m_v}{\rho D^2}, \frac{P}{D}, \text{turbulence characteristics} \right). \quad (10.43)$$

The main differences between the two basic instability mechanisms are summarized in Table 10.5.

It should be emphasized that, in general, both fluid-damping coefficients and fluid-stiffness coefficients are functions of the reduced flow velocity $U_r (= U/f_v D)$. Therefore, the parameters α_v in Eq. (10.41) and β_v in Eq. (10.42) are functions of the reduced flow velocity U_r . For light fluids, the instability occurs at large values of U_r . It has been shown that for large U_r , both fluid damping coefficients and fluid-stiffness coefficients are approximately independent of U_r ; therefore, for a given cylinder array, α_v and β_v are constants.

10.6.3 Numerical Examples

For this presentation, calculations for a standard case of a row of cylinders with a pitch-to-diameter ratio of 1.33 are based on $\zeta_v = 2\%$, $\phi(z) = 1$ and all cylinders being in tune.

Figure 10.7 shows the critical flow velocity as a function of the number of cylinders in a row for several values of $\delta_s (= 2\pi \zeta_v m_v / \rho D^2)$. For an array in which all cylinders are in tune, the critical flow velocity decreases with the number of cylinders; the decrease is more drastic for a small number of cylinders. Also, the effect of the number of cylinders on the fluid-stiffness-controlled instability ($\delta_s = 20, 40, \text{ and } 60$) is more significant than on the fluid-damping instability ($\delta_s = 1$). This effect can be explained qualitatively using the equations of motion and fluid-force coefficients. For small δ_s , cylinder instability is basically controlled by the coefficient α'_{ij} , while at large δ_s it is controlled by τ''_{ij} and σ''_{ij} . At low δ_s , instability can occur in an elastic cylinder surrounded by rigid cylinders. But at large δ_s , at least two cylinders are needed to cause instability.

Table 10.5. Comparison of Two Instability Mechanisms

	Fluid-damping- controlled Instability (velocity mechanism)	Fluid-stiffness- controlled Instability (displacement mechanism)
Instability criteria	$\frac{U}{\bar{f}_D} = \alpha_v(U_r) \left(\frac{2\pi m \zeta_v}{\rho D} \right)^{0.5}$	$\frac{U}{\bar{f}_D} = \beta_v(U_r) \left(\frac{2\pi m \zeta_v}{\rho D} \right)^{0.5}$
Dominant fluid force	Flow-velocity-dependent damping force	Fluid-stiffness force
Fluid coupling	Not necessary	Necessary
Phase relation- ship of tube oscillations	0, 180°	0, ±90°, 180°
Effect of detuning	Less significant	More significant

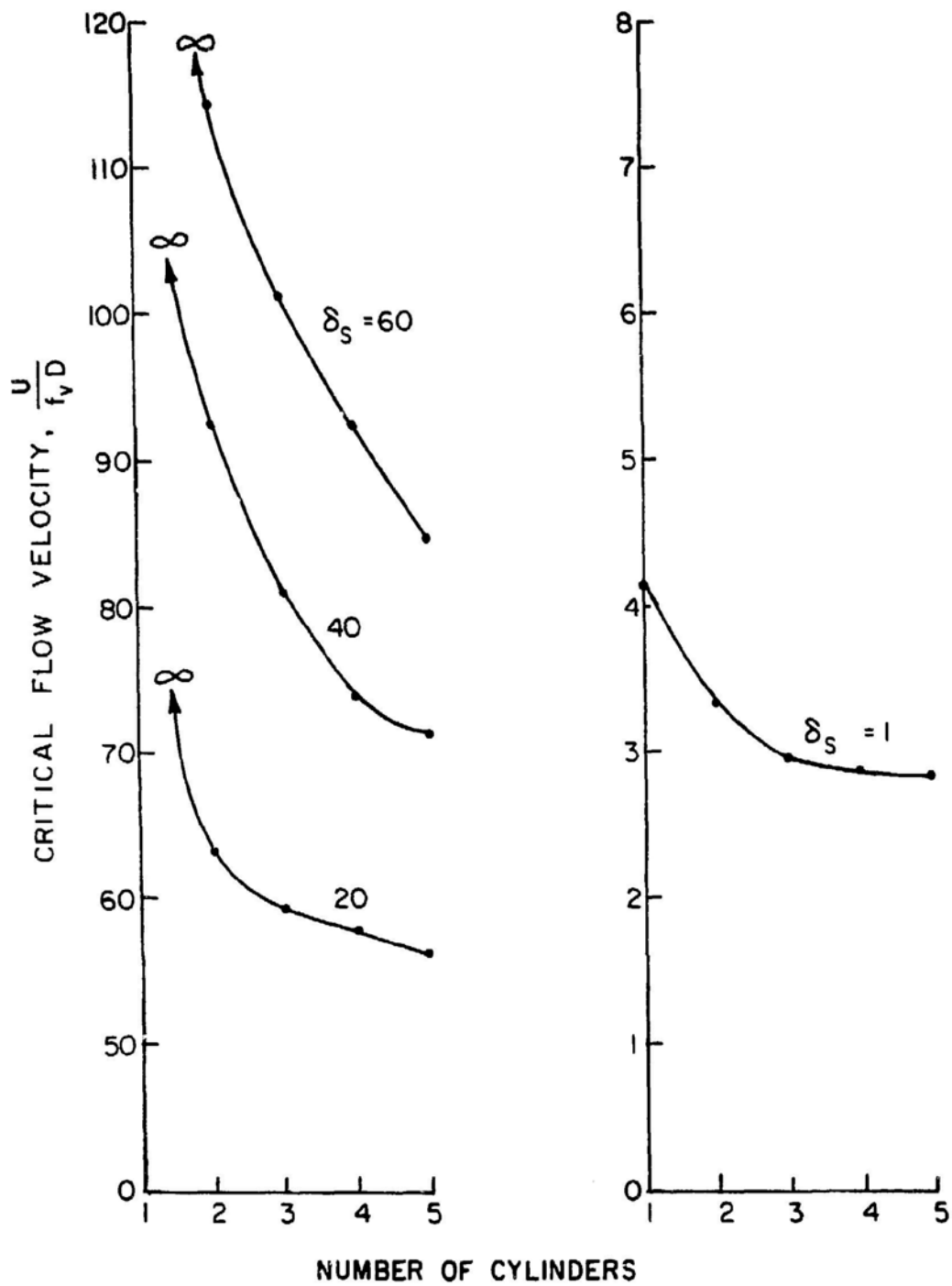


Fig. 10.7. Critical Flow Velocity as a Function of Number of Cylinders (Chen and Jendrzejczyk 1983)

In different experiments conducted by different investigators, the number of cylinders used is not the same. Therefore, even if all other parameters are the same, the instability flow velocity will be different.

Figures 10.8 and 10.9 show the stability map for a row of five and three cylinders. For large δ_s , the results calculated for different set of ζ_v and $m_v/\rho D^2$ are about the same; i.e., the instability is independent of the individual values of ζ_v and $m_v/\rho D^2$, but dependent on the product of ζ_v and $m_v/\rho D^2$. At low δ_s , the results for different sets of ζ_v and $m_v/\rho D^2$ are not the same. In Fig. 10.8, the critical flow velocities are determined for a fixed ζ_v with variable $m_v/\rho D^2$ at low δ_s . It is seen that for a fixed δ_s , the critical flow velocity increases with decreasing ζ_v . In Fig. 10.9, the mass ratio is kept constant while ζ_v is variable. For a fixed δ_s , the critical flow velocity increases with decreasing mass ratio.

The two parameters ζ_v and $m_v/\rho D^2$ are frequently combined as a single parameter. This is applicable for large δ_s . For small δ_s , the two parameters must be treated as two variables. Most of the experimental data reported are presented as a function of δ_s . Since different experiments are carried out for different sets of ζ_v and $m_v/\rho D^2$, even for the same δ_s , the critical flow velocity will be different. This is one of the reasons that there is more scattering in the data at low values of δ_s .

At δ_s equal to about 3 to 5, there is a finite jump in the critical flow velocity. The jump is attributed to the transition from fluid-damping-controlled instability to fluid-stiffness-controlled instability. The values of δ_s at which the jump occurs depends on the values of damping ζ_v and γ_v . For smaller ζ_v in Fig. 10.8 and smaller γ_v in Fig. 10.9, the jump occurs at higher δ_s , and vice versa.

Figure 10.10 shows the instability modes for two, three, four, and five cylinders in a row and for two values of δ_s . For $\delta_s = 1$, the instability is fluid-damping-controlled type. The motion is predominantly in the lift direction, and the cylinders are moving out of phase. For $\delta_s = 40$, the instability is fluid-stiffness-controlled type. The motion is a typically orbital path with some cylinders moving predominantly in the drag direction and some cylinders in the lift direction.

Figure 10.11 shows the ratio of critical flow velocities of a row of detuned cylinders to a row of in-tune cylinders. In the detuned row, natural frequencies in the two directions are the same, and cylinders 2 and 4 have higher natural frequency ω_B . In the in-tune row, all natural frequencies are ω_A . In this case, detuning tends to stabilize the system; i.e., the critical flow velocity increases with the increase in the frequency ratio ω_B/ω_A . Figure 10.11 shows that for $\delta_s = 20$, the critical flow increases significantly with ω_B/ω_A . However, for $\delta_s = 1$, the effect of detuning is not very important. The effect of detuning is much more significant in fluid-stiffness-controlled instability.

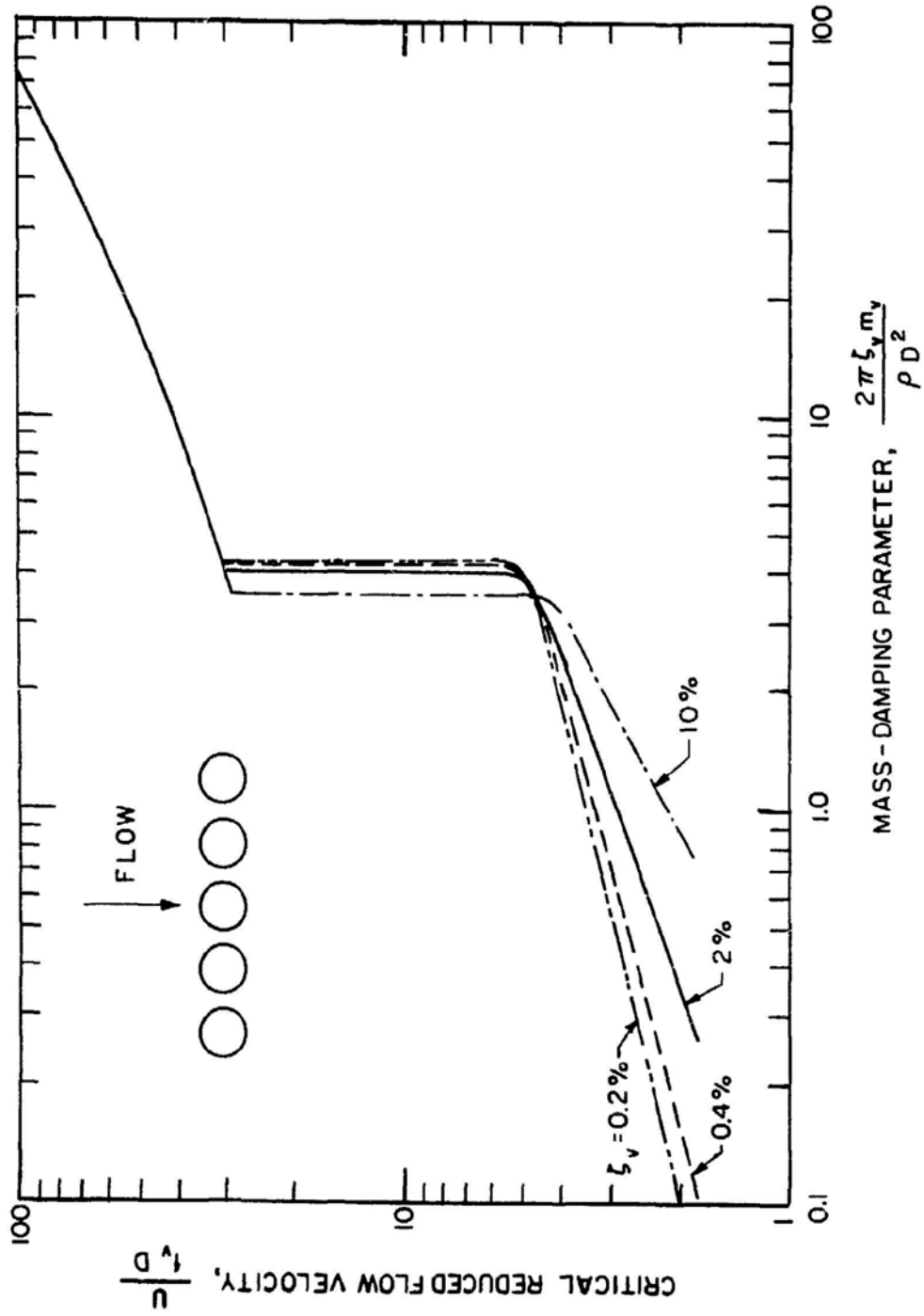


Fig. 10.8. Critical Flow Velocity for a Row of Five Cylinders (Chen and Jendrzejczyk 1983)

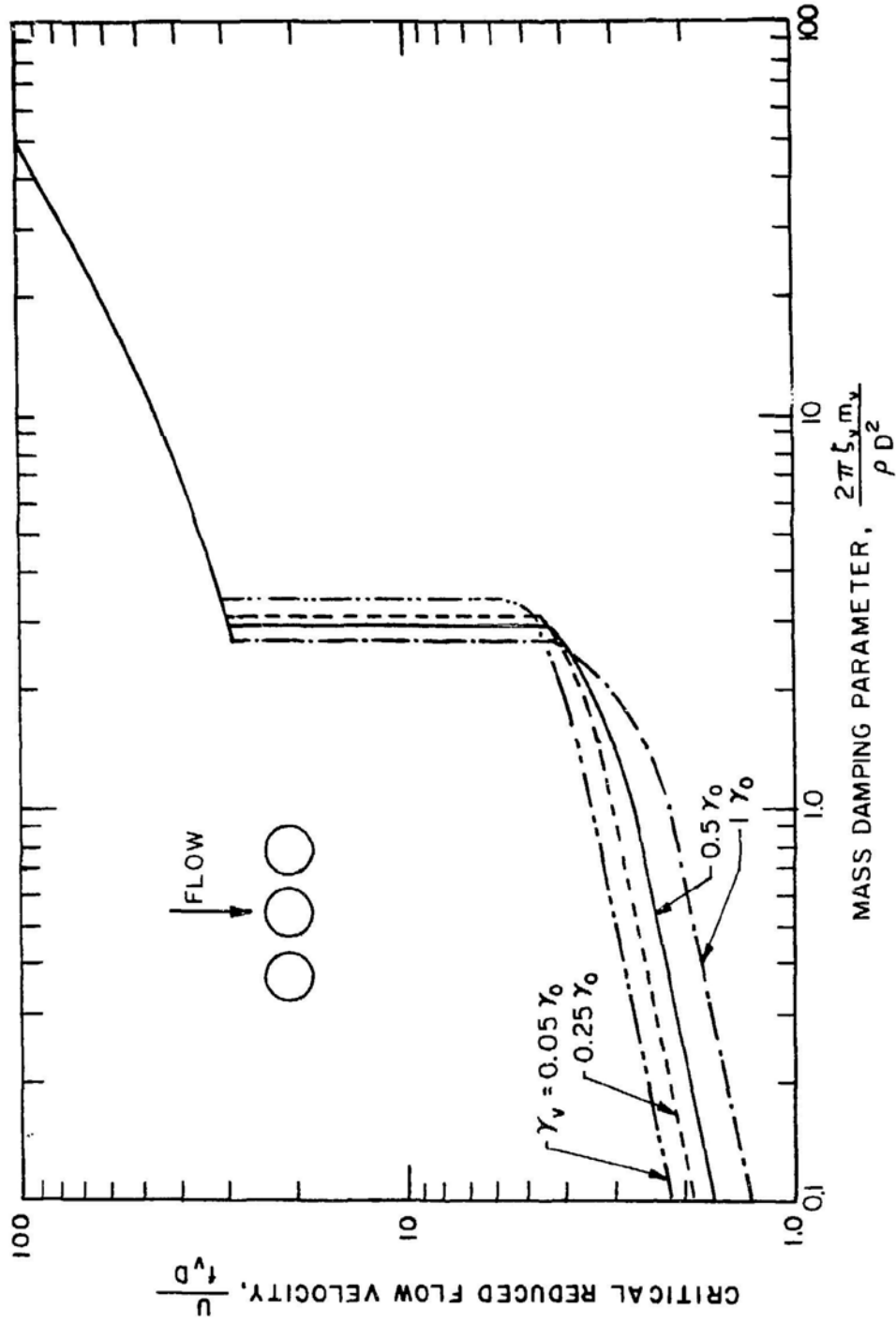


Fig. 10.9. Critical Flow Velocity for a Row of Three Cylinders (Chen and Jendrzejczyk⁺ 1983)

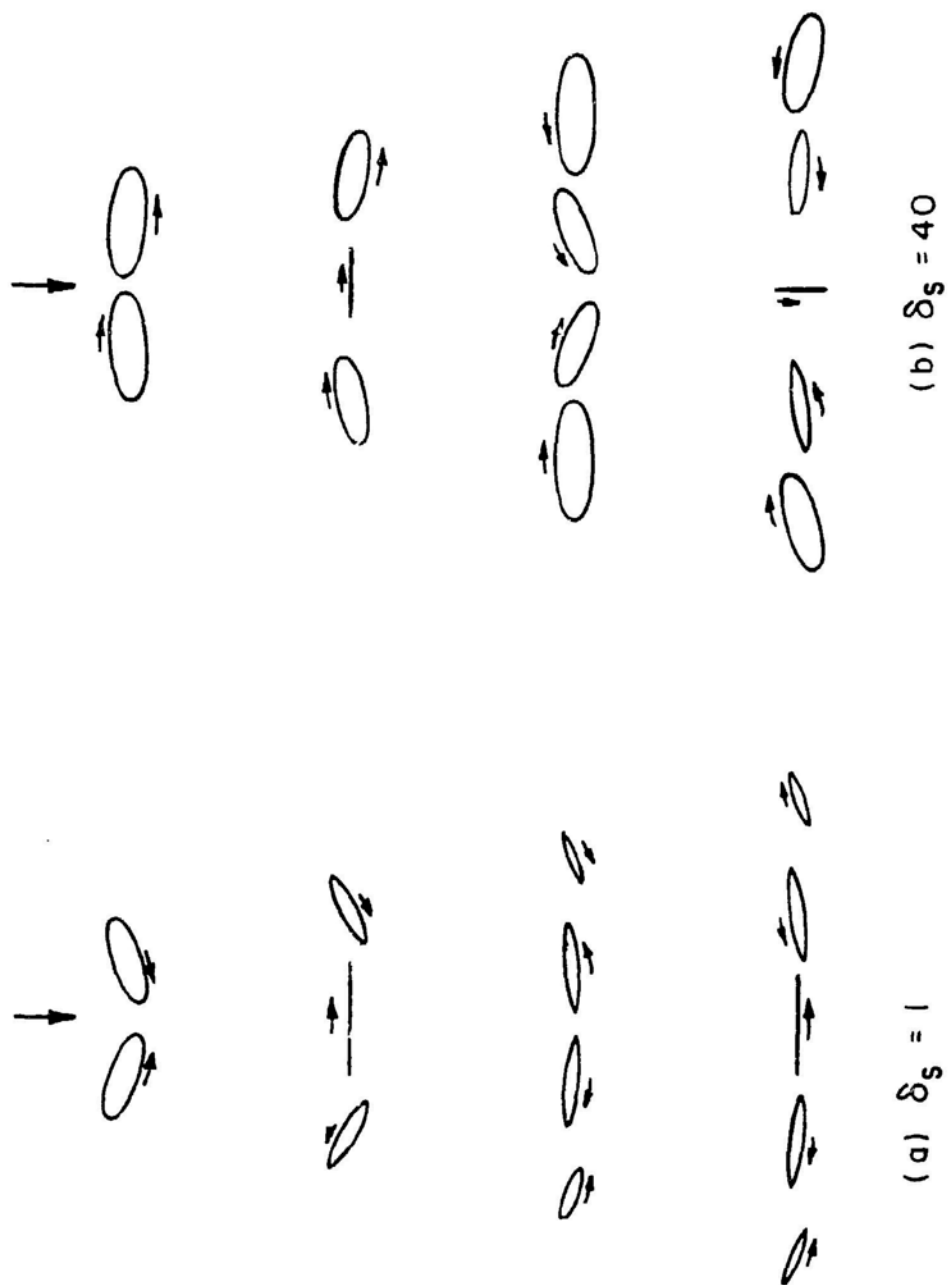


Fig. 10.10. Instability Modes for Rows of Cylinders with Two, Three, Four and Five Tubes
(Chen and Jendrzejczyk 1983)

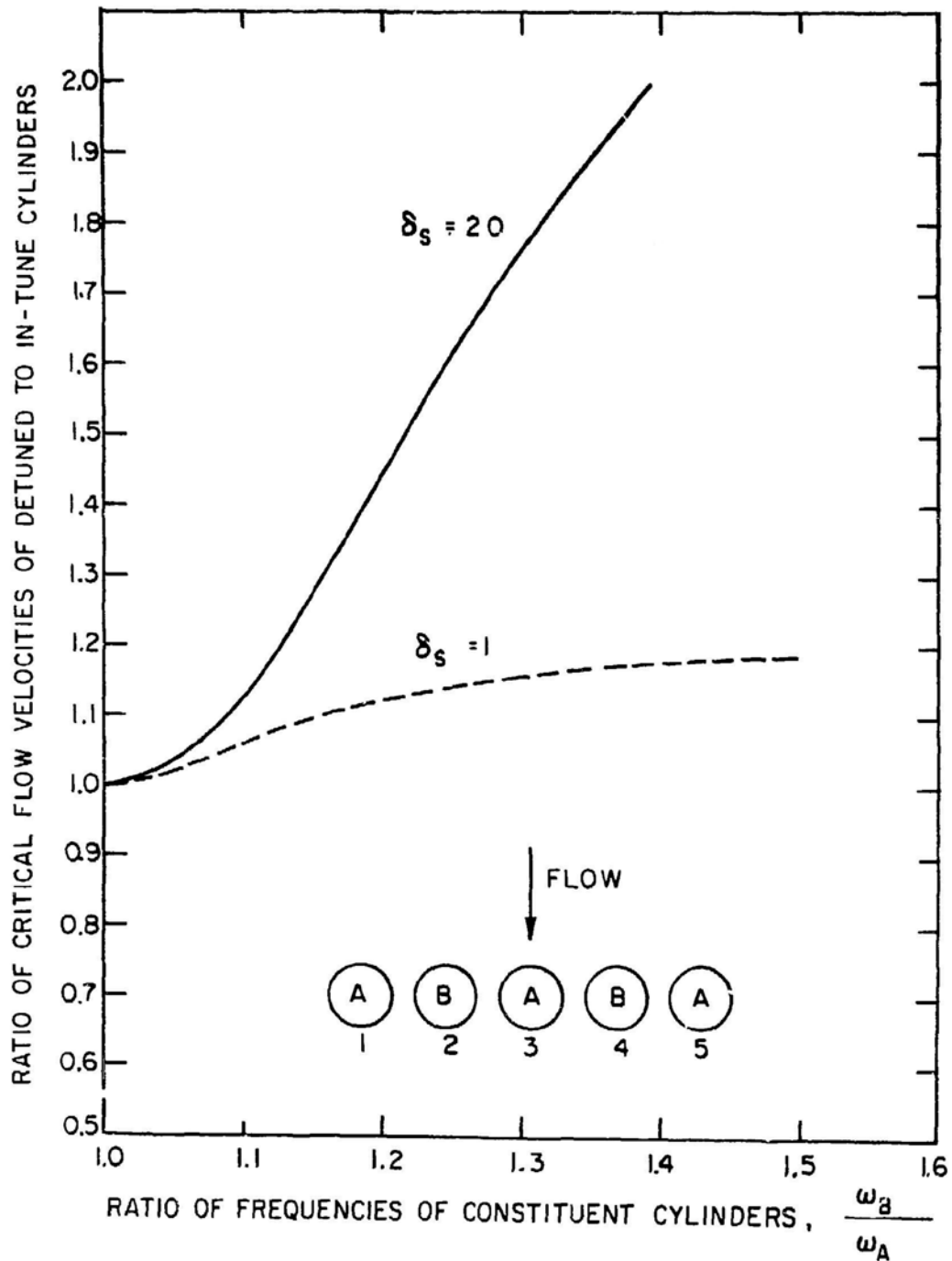


Fig. 10.11. Effect of Detuning in Frequency of Different Cylinders on Critical Flow Velocity (Chen and Jendrzejczyk 1983)

10.6.4 Comparison of Theoretical and Experimental Results

A row of brass tubes (Fig. 10.12) tested in a water tunnel is used to confirm the analytical results. Each tube element is suspended as a simply supported beam on two O-rings mounted 91.4 cm apart. The O-rings are seated in the compression plates. The tube outside diameter is 1.59 cm, the tube wall thickness is 0.318 cm, the transverse pitch-to-diameter ratio is 1.35, and the overhung length is 35.6 cm. Note that AD is in fluid, BC in flow, and DE in air.

During the test, the flow velocity is increased at small intervals. At each flow velocity, the displacement signals in the lift and drag directions are analyzed. The test is terminated when tube impact occurs.

There are multiple stable and unstable regions. The flow velocity is increased rapidly to reach to the second stable region. Then the flow is decreased or increased at small intervals to determine the lower and upper stability boundaries.

Tube damping depends on water temperature (this is attributed to O-rings, whose characteristics are a function of temperature); therefore, tube damping can be controlled by controlling water temperature. The tube row is tested under several temperatures.

The results of the tests are summarized in Table 10.6. There are two critical flow velocities, which correspond to the lower and upper bounds of the first unstable region. For $U < U_1$, (Fig. 10.13) the tube displacements are very small. As U is increased to U_1 , the tubes become unstable. Therefore, U_1 is the lowest critical flow velocity. At U_1 , the tube vibration amplitude increases rather slowly. If the flow velocity is increased rapidly from a value less than U_1 to that above U_2 , the tubes do not become unstable. However, if the flow velocity is decreased to U_2 , large tube motions occur. The increase of oscillation amplitude at U_2 is much more rapid than that at U_1 . For $U_1 < U < U_2$, tubes are unstable; in this region, tubes can impact with one another. For $U > U_2$, although tube motions may be relatively large, the tubes in general do not impact with the neighbor tubes. In most cases, the tubes move in phase for $U > U_2$.

The critical flow velocities ($U/f_v D$) are given in Fig. 10.14, plotted as functions of δ_s . Analytical results also are given in Fig. 10.14.

There are multiple stable and unstable regions. Once the flow velocity is increased to the lowest critical flow velocity, large tube oscillations develop, but this takes time. If the flow velocity is increased very rapidly passing through the unstable region, large tube oscillations do not occur and the tubes remain stable. On the other hand, if the flow velocity is increased slowly so that tubes execute large-amplitude oscillations in the unstable zone, the tubes may not regain stability because of nonlinear effects. For heavy tubes, the buildup of large oscillations is slow, for thin-wall tubes, instability develops much more rapidly.

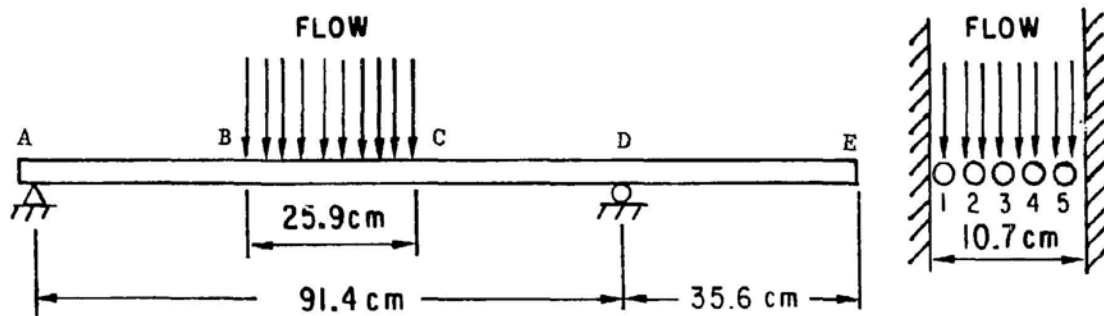


Fig. 10.12. Schematic of Tube Row in Crossflow

Table 10.6. Experimental Data for a Tube Row in Crossflow (Chen and Jendrzejczyk 1983)

Temperature, °C	Natural Frequency, Hz		Modal Damping Ratio, %		Oscillation Frequency at Instability, Hz	Critical Flow Velocity, m/s	$\frac{U}{f D}$	$\frac{2\pi \rho D^2 U}{\rho D^2}$
	In Air	In Water	In Air	In Water				
8.78	26.1	24.5	4.5	4.8	25.0 26.0	1.68 2.19	4.05 5.29	1.13
10.39	26.1	24.2	3.8	4.1	24.2 26.0	1.52 2.26	3.68 5.44	0.96
11.44	26.3	24.4	3.1	3.5	24.1 25.5	1.44 2.53	3.46 6.14	0.78
13.00	26.2	24.3	2.6	3.0	24.0 25.5	1.37 2.73	3.30 6.56	0.65
15.89	26.2	24.3	1.7	2.1	23.9 25.5	1.29 3.08	3.11 7.40	0.43
20.28	25.9	24.0	1.2	1.7	23.6 25.0	1.26 3.38	3.05 8.23	0.30
30.17	25.9	24.0	0.9	1.4	23.5	1.14	2.78	0.23

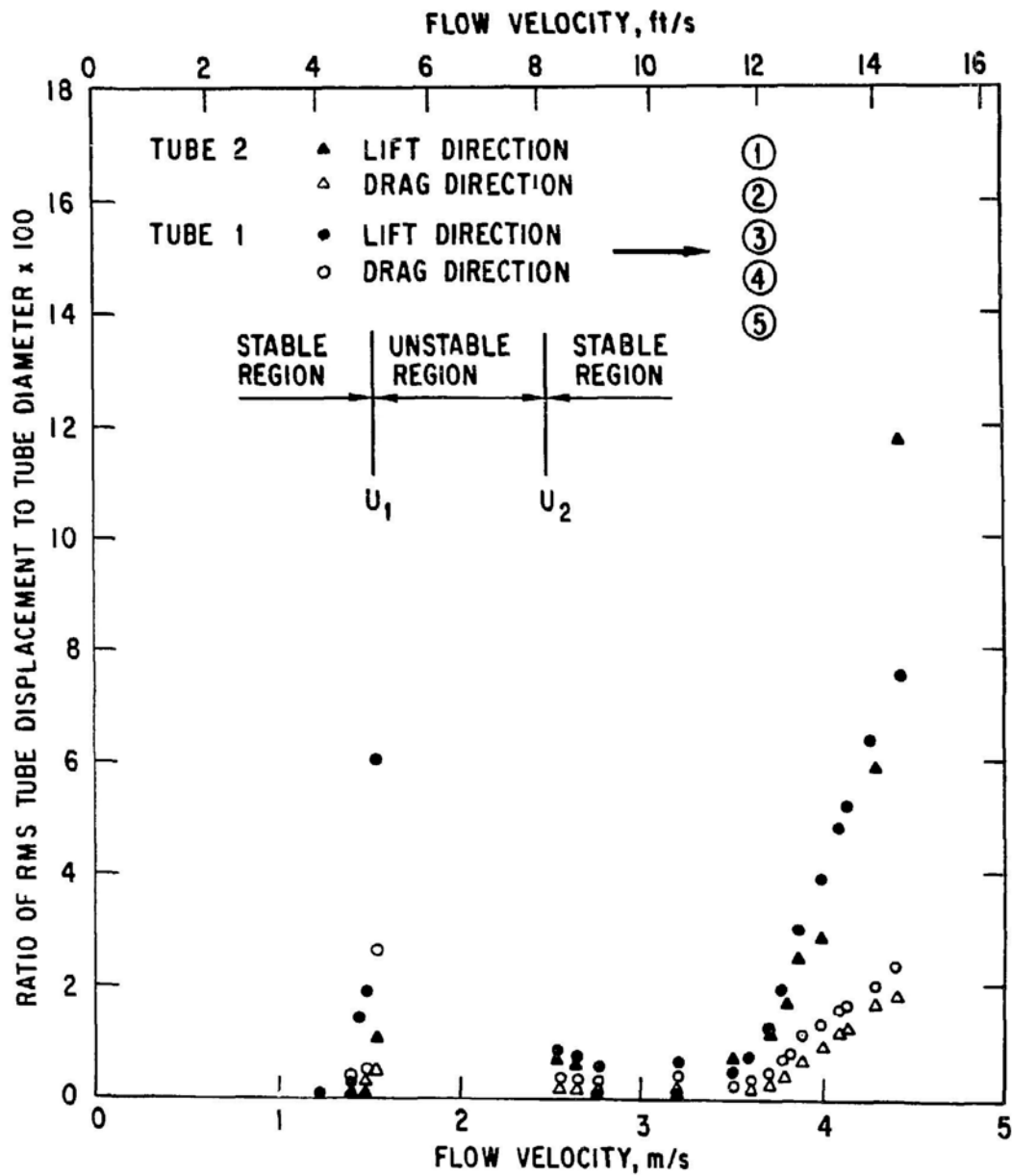


Fig. 10.13. Tube Displacement as a Function of Flow Velocity (Chen and Jendrzejczyk 1983)

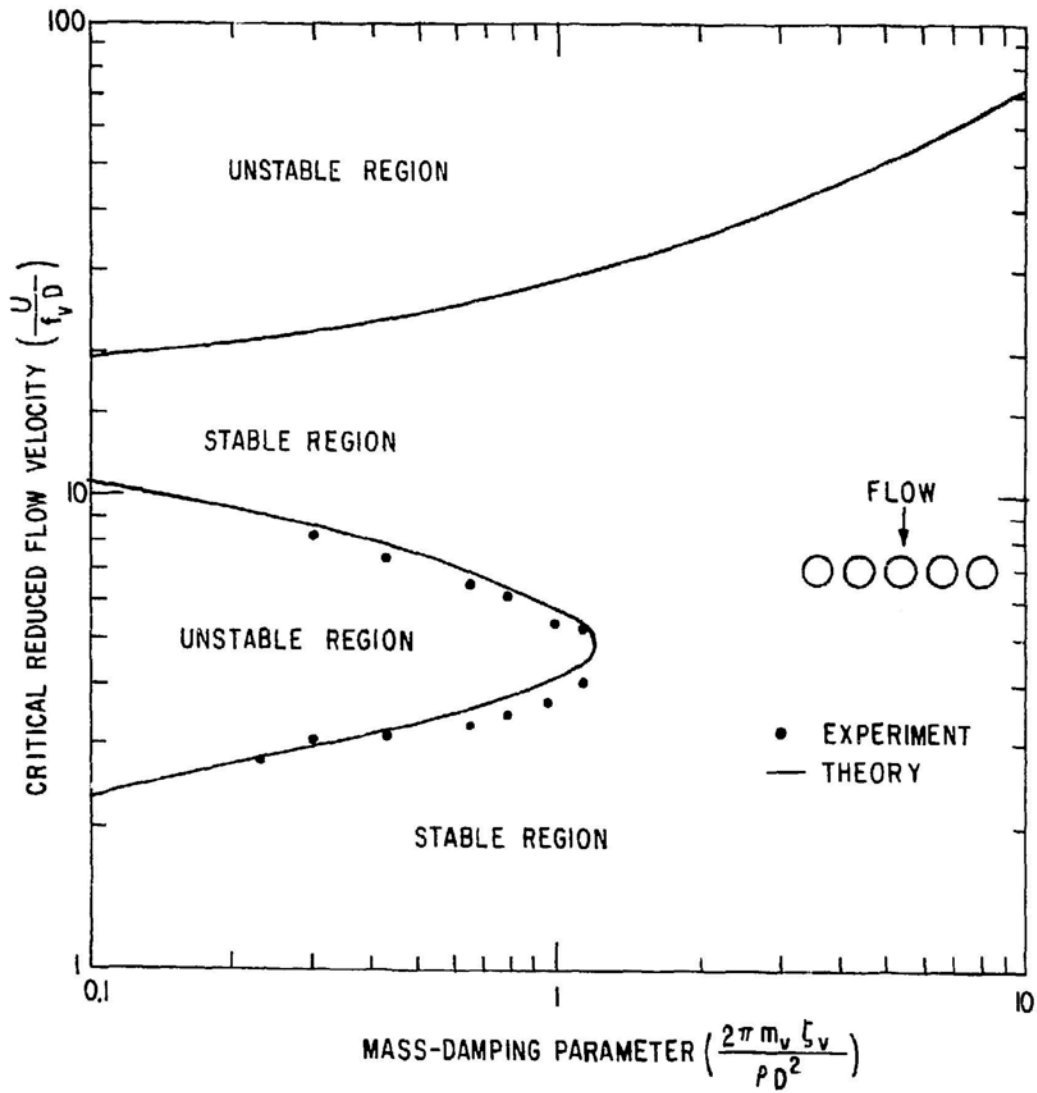


Fig. 10.14. Stability Map (Chen and Jendrzejczyk 1983)

The upper and lower bounds of the instability regions in Fig. 10.14 are associated with the same mode in which the tubes oscillate, predominantly in the lift direction and out of phase with respect to the neighboring tubes. Mathematically this can be explained by the fluid-damping coefficients. In this range of reduced flow velocity, fluid-damping coefficients α'_{11} and α'_{12} are the two dominant coefficients that cause the instability. In this range of U_r , α'_{11} and α'_{12} have opposite signs; therefore the tube motions of the two neighboring tubes must be out of phase. In the other flow-velocity range, α'_{11} and α'_{12} change sign and the tubes do not lose stability by the damping mechanism. For practical applications, the lower critical flow velocity is of importance. The higher instability boundaries are more of academic interest.

The jump of the lowest critical flow velocity at a certain value of δ_s is demonstrated in the tests. The jump is attributed to the transition from one instability mechanism to another. At low δ_s the instability is attributed to the fluid-damping-controlled type, while at higher δ_s it is attributed to the fluid-stiffness-controlled type. The experimental and analytical values of δ_s at which the jump in the critical flow velocity occurred agree reasonably well.

Figure 10.15 shows the lowest critical flow velocities for tubes with different wall thicknesses. The theoretical results and experimental data agree reasonably well. Comparison of these two tests demonstrates several features:

- The jump in the critical flow velocity (the transition of one instability mechanism to another) occurs at a δ_s that depends on the mass ratio. Both experimental and analytical results show that the transition for heavy-wall tubes occurs at larger δ_s .
- Except near the transition region, for a fixed δ_s the critical flow velocity for the thin-wall tube is lower. Both theoretical results and experimental data agree well.
- The mechanism for the two tests are basically the same, although at instability, the tube motion for thin-wall tubes is much larger.

10.7 STABILITY MAPS

Critical flow velocities can be predicted by using the method described in Section 10.6. To carry out the analysis, various fluid-force coefficients must be known. Unfortunately, at this time, fluid-damping and fluid-stiffness coefficients are difficult to compute. Except for a few cases in which fluid-force coefficients have been measured, a stability analysis cannot be made. Under such circumstances, stability maps based on the experimental data are available for applications.

In the empirical correlations for critical flow velocities, different system parameters measured in vacuum or in quiescent fluid are used. Most

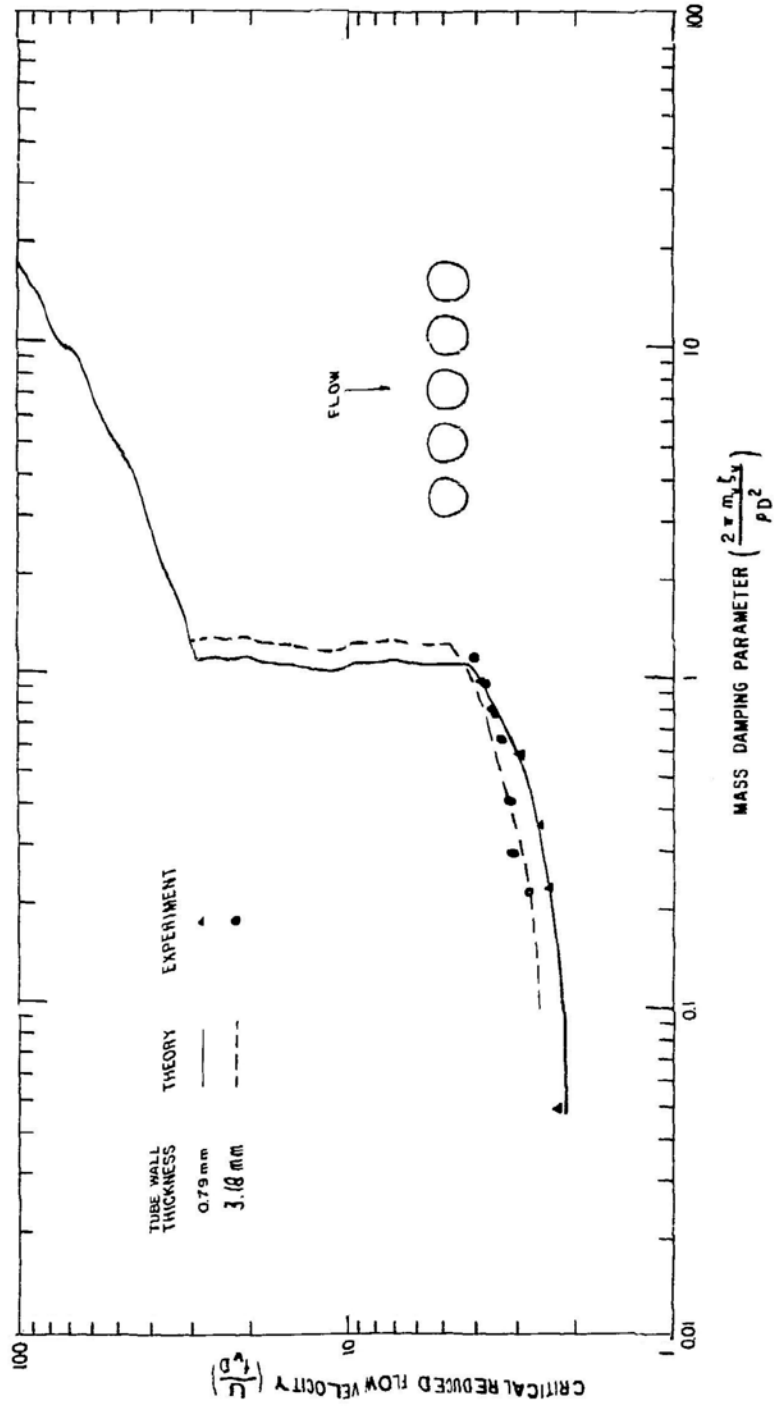


Fig. 10.15. Effect of Tube Mass on Critical Flow Velocity (Chen and Jendrzeyczyk 1983)

investigators use the modal damping value ζ , mass per unit length m , and natural frequency f measured in quiescent fluid, but some use those measured in vacuum (actually in air), or in flowing fluid. From the analysis of the model, it is clear that one can use those parameters determined either in vacuum or in quiescent fluid, provided that appropriate fluid-damping coefficients are used (Chen 1983a). However, the two types of stability criteria are not identical. For practical applications, it is more convenient to use the in-vacuum parameters, since they are well defined. In-fluid parameters are more difficult to determine. In particular, for heavy fluid, inertia and viscous coupling become important; coupled-mode frequencies, f_c , effective mass m_c , and modal damping ζ_c are more difficult to measure (see Table 10.1).

The stability criteria, Equations 10.41 and 10.42, are expressed in terms of in-vacuum parameters. The effects of various parameters are as follows:

1. $2\pi\zeta_v m_v / \rho D^2$: This is the most important parameter. The critical flow velocity increases with this parameter.
2. $m_v / \rho D^2$: This parameter determines the role of added mass. For heavy fluids, it cannot generally be combined with the damping $2\pi\zeta$ as a single parameter.
3. P/D : Fluid-force coefficients depend on tube arrangement; therefore, the critical flow velocity will depend on P/D .
4. Turbulence Characteristics: Fluid-force coefficients depend on incoming characteristics (intensity and scale). Again, the critical flow velocity depends on the turbulence characteristics.

Available experimental data for the reduced flow velocity $U_r (= U/fD)$ are plotted as a function of the mass-damping parameter $\delta_s (= 2\pi\zeta m / \rho D^2)$ for different tube arrangements (Figs. 10.16-10.20). Chen (1983a) showed that either the in-vacuum parameters (m_v , f_v and ζ_v) or the in-fluid parameters (m_c , f_c and ζ_c) can be used in the stability criteria. In most experiments the in-vacuum parameters are actually measured in air. The effect of air on those parameters is small. Therefore, m_v , f_v , and ζ_v will be based on those measured in air. In liquid-flow tests, the values of in-fluid parameters m_u , f_u , and ζ_u are generally measured and, in most cases, in-vacuum parameters m_v , f_v , and ζ_v , and in-fluid parameters m_c , f_c , and ζ_c , are not measured. Under such circumstances, the in-fluid parameters of uncoupled modes m_u , f_u , and ζ_u are used.

In the stability diagrams (Figs. 10.16-10.20) the data for air flow are denoted by open symbols, liquid flow by solid symbols, and two-phase flow by semi-solid symbols (Chen 1984). The stability diagrams summarize the published data for different tube arrangements obtained by different investigators.

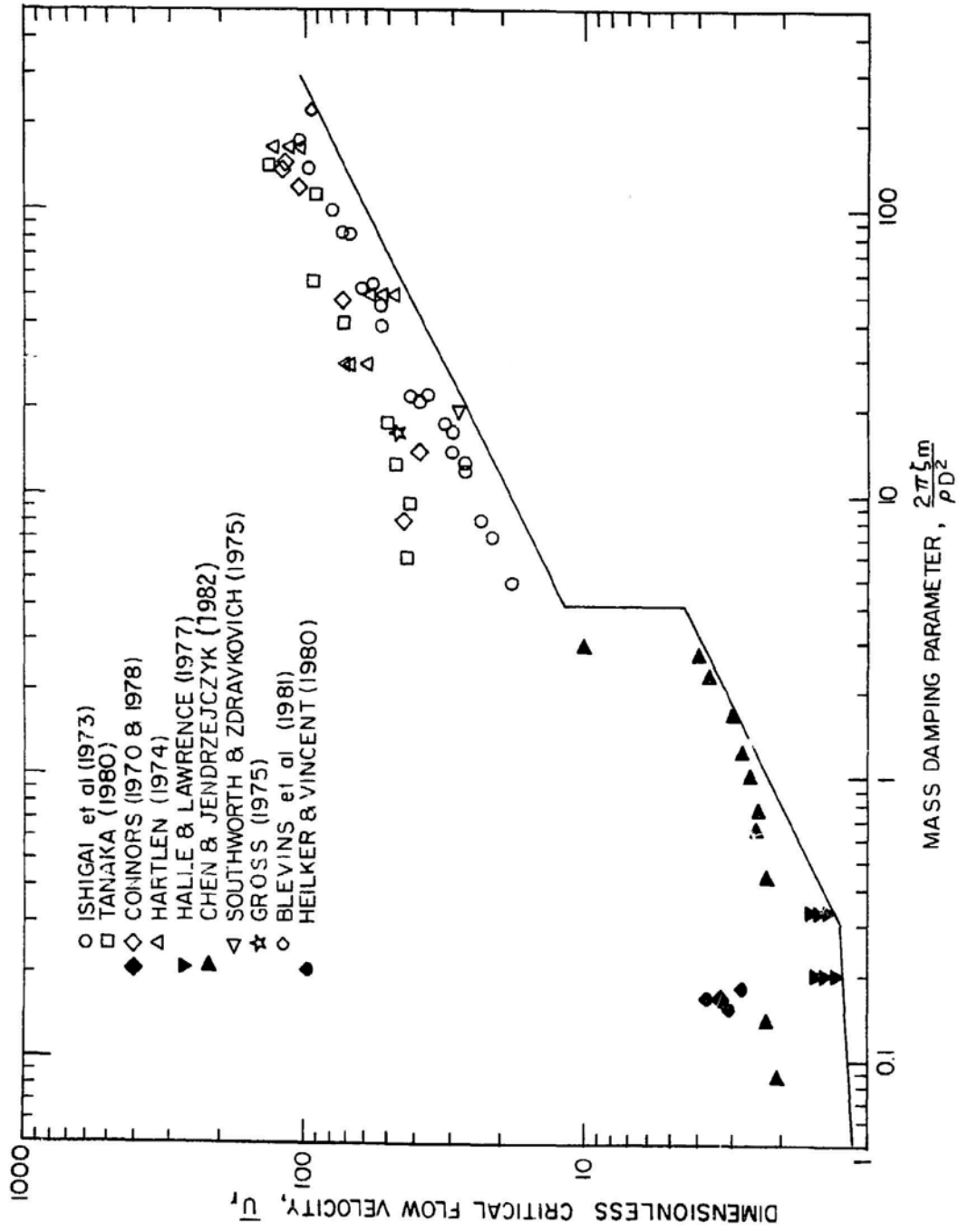


Fig. 10.16. Stability Map for a Row of Cylinders (Chen 1984)

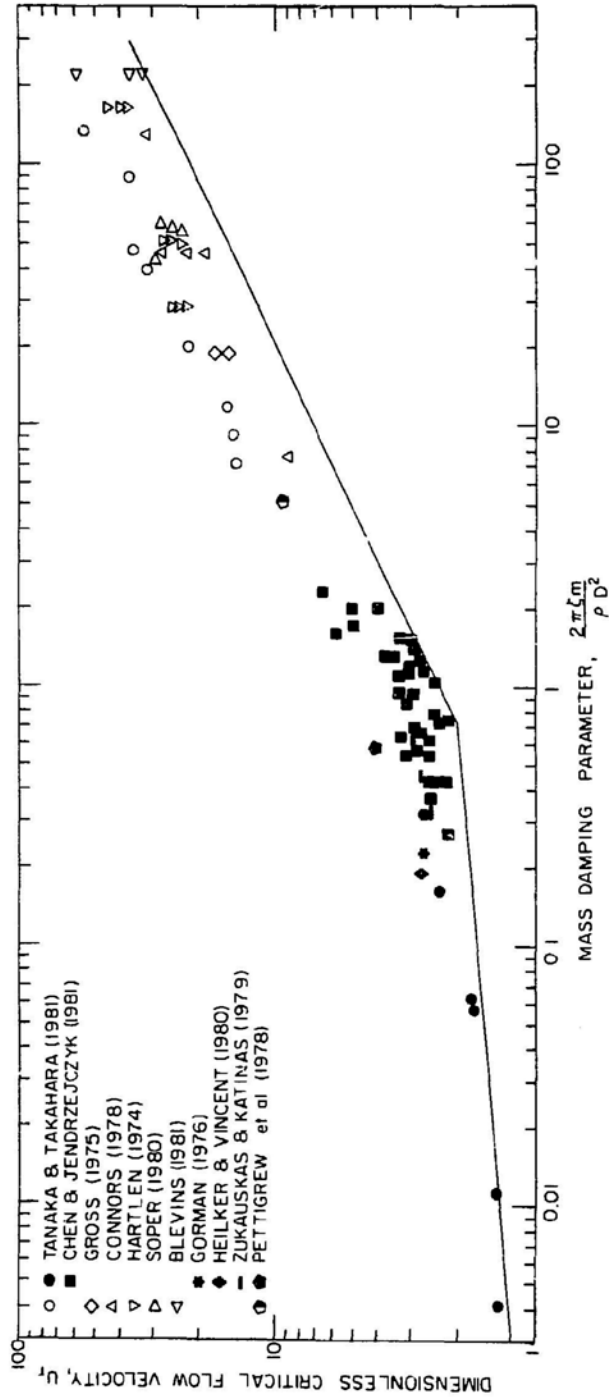


Fig. 10.17. Stability Map for Square Arrays (Chen 1984)

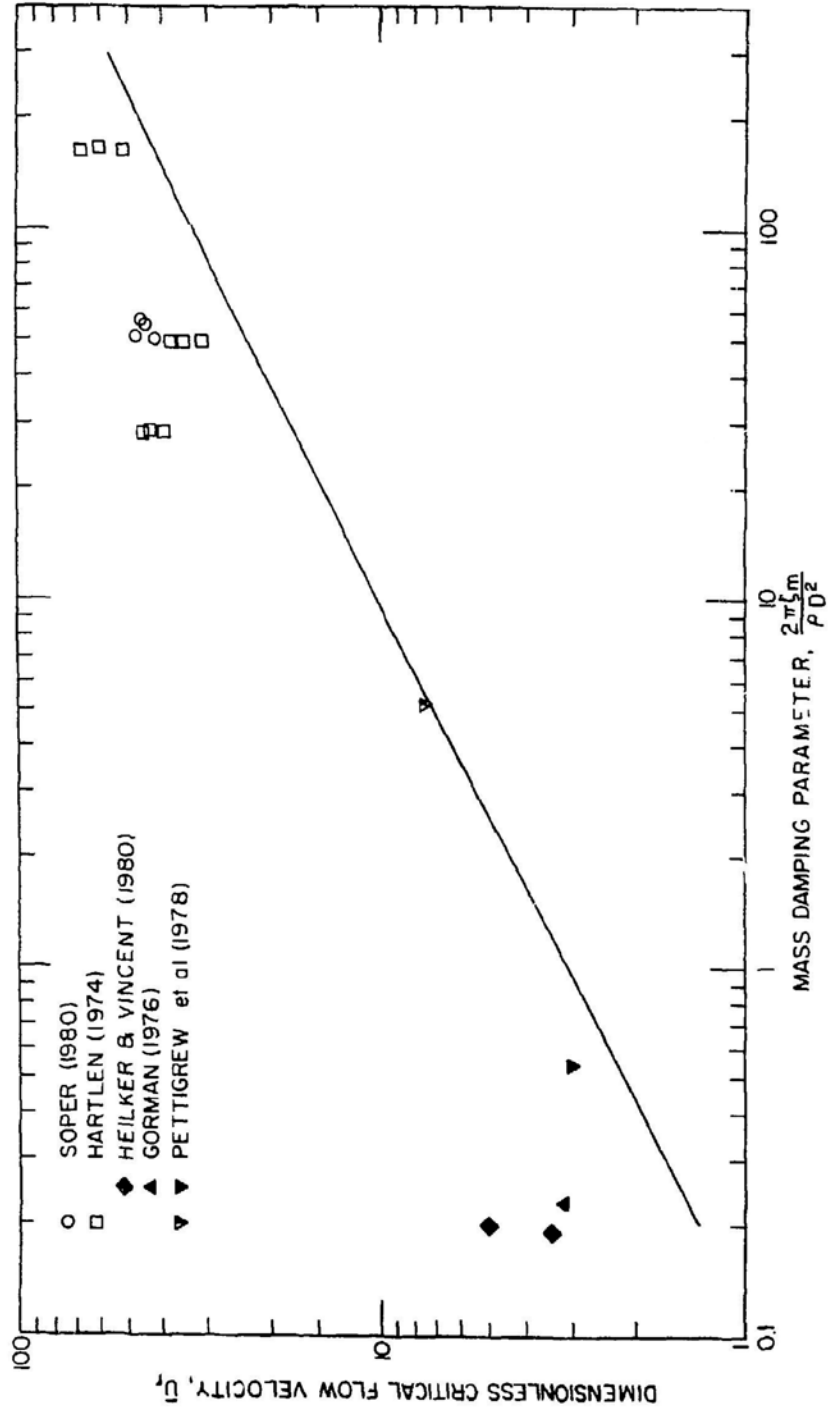


Fig. 10.18. Stability Map for Rotated Square Arrays (Chen 1984)

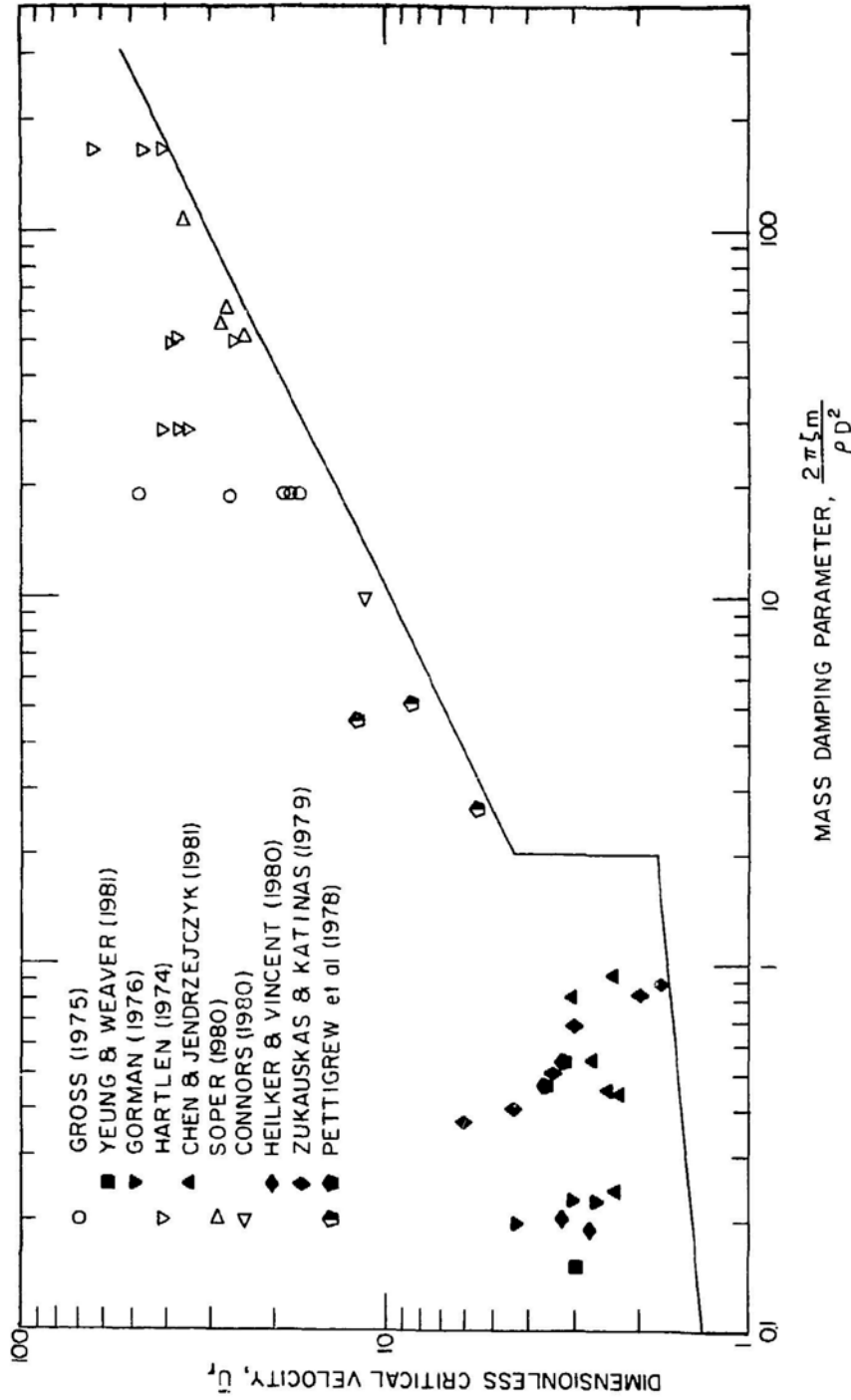


Fig. 10.19. Stability Map for Triangular Arrays (Chen 1984)

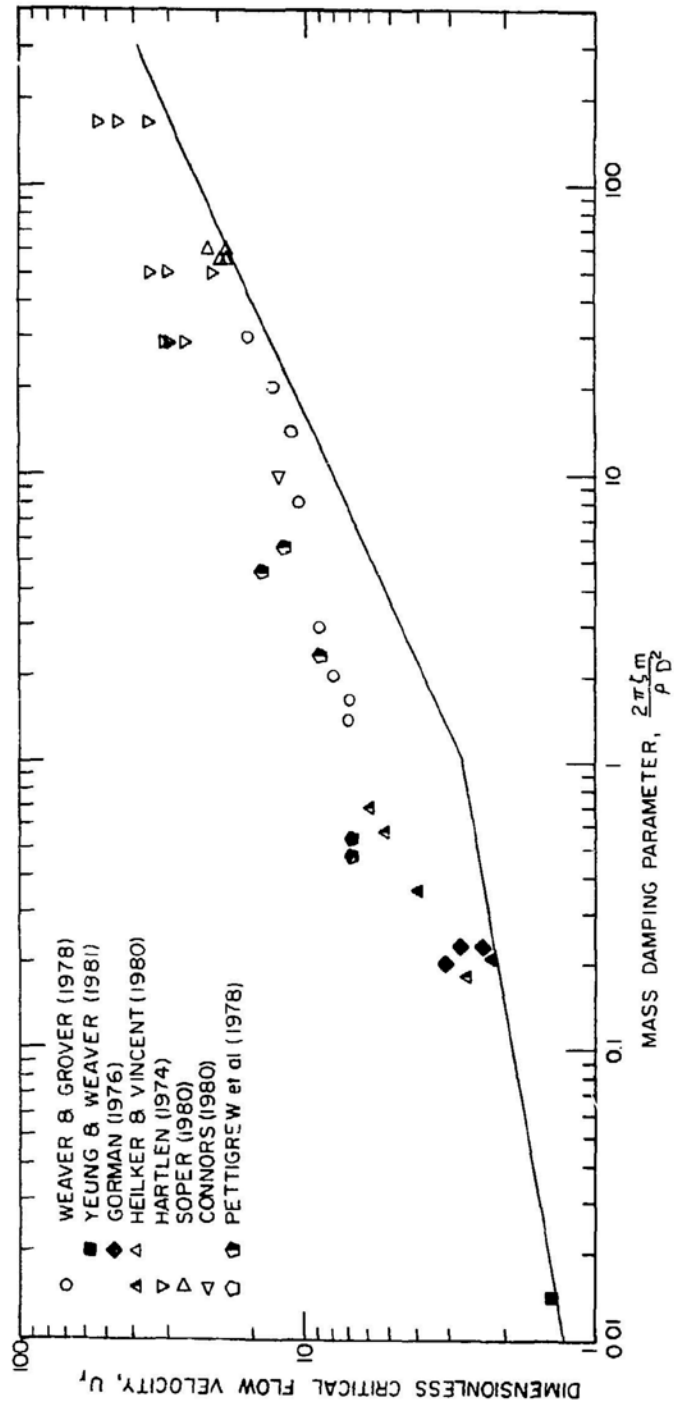


Fig. 10.20. Stability Map for Rotated Triangular Arrays (Chen 1984)

10.7.1 A Row of Cylinders

The critical flow velocity for a row of cylinders depends on the pitch-to-diameter ratio T/D . Several studies have been made to investigate the effect of T/D on the critical flow velocity. Blevins (1977) shows that

$$\alpha_1 = \frac{2(2\pi)^{0.5}}{\left[\left(\frac{D}{T}\right)^2 \left\{2\left(\frac{D}{T}\right)^3 - \left(\frac{D}{T}\right)^2 - 0.25\right\}\right]} \quad (10.44)$$

Equation 10.44 is applicable for $T/D < 2$ only. In a systematic investigation, Ishigai et al. (1983) show that for a row of cylinders,

$$\alpha_1 = 8 \left(\frac{T}{D} - 0.375 \right) \quad (10.45)$$

Therefore, the critical flow velocity is proportional to $(T/D - 0.375)$. A new reduced critical flow velocity incorporating the effect of tube spacing is defined as follows:

$$\bar{U}_r = \frac{\frac{U}{fD}}{\frac{T}{D} - 0.375} \quad (10.46)$$

Then \bar{U}_r is independent of tube spacing T/D .

Figure 10.16 shows the critical flow velocity of \bar{U}_r as a function of the mass-damping parameter $2\pi\zeta m/\rho D^2$. The in-vacuum parameters are used whenever they are available. Experimental data obtained in air correlate reasonably well for tube rows with different pitch-to-diameter ratios ranging from 1.19 to 2.68. In liquid flow, except for Chen and Jendrzejczyk (1982), who use in-vacuum parameters, other investigators use different parameters: Connors (1978) and Halle and Lawrence (1977) use f_u , m_u , and ζ_u , while Heilker and Vincent (1980) use f_f , m_u and ζ_f .

10.7.2 Square Array (90°)

Square tube arrays with different spacing are tested in air by Soper (1980) and in water by Chen and Jendrzejczyk (1981). The results of these tests show that critical flow velocity is not very sensitive to the variation of tube spacing. Therefore, for square arrays, the critical flow velocity \bar{U}_r is plotted as a function of δ_s regardless of the spacing. The results are given in Fig. 10.17.

Although different tests are performed for different flow conditions and cylinder spacing, the data correlate fairly well. In particular, for in-water tests, different investigators use different parameters: Tanaka and Takahara (1981) use in-vacuum parameters, Heilker and Vincent (1980) use in-flow parameters, and the others use in-fluid parameters.

10.7.3 Rotated Square Array (45°)

Based on Soper's data (1980), the critical flow velocity is approximately proportional to $(T/D - 0.5)$. Note that in Eq. 10.46, $U_r = \bar{U}_r$ for $T/D = 1.375$. To make $\bar{U}_r = U_r$ at $P/D = 1.375$, for this case, we define U_r as follows:

$$U_r = \frac{\frac{U}{fD}}{1.143 \left(\frac{T}{D} - 0.5 \right)} \quad (10.47)$$

The results are given in Fig. 10.18.

10.7.4 Triangular Array (30°)

Following the same procedure as that for rotated square arrays, \bar{U}_r is defined as follows:

$$\bar{U}_r = \frac{\frac{U}{fD}}{2.105 \left(\frac{T}{D} - 0.9 \right)} \quad (10.48)$$

At $T/D = 1.375$, $\bar{U}_r = U_r$. Figure 10.19 summarizes the results. There is more scattering of the data at low values of δ_g . This is attributed to different parameters used by different investigators and may be caused by different spacings. Note that Eq. 10.48 is based on Soper's data obtained in a wind tunnel. The variation of the critical flow velocity with tube spacing in water may be different from that in air. For example, the variation of \bar{U}_r with tube spacing in the data by Zukauskas and Katinas (1980) is different from those by Soper (1980).

10.7.5 Rotated Triangular Arrays (60°)

Soper's data show that the critical flow velocity varies insignificantly with tube spacing. All available experimental data are plotted in Fig. 10.20 regardless of tube spacing. They agree reasonably well.

The stability diagrams given in Figs. 10.16-10.20 can be used in design evaluation.

Calculation of Mass-Damping Parameter ($\delta_s (= 2\pi m_v \zeta_v / \rho D^2)$): Fluid density ρ , tube diameter D , and cylinder mass per unit length m_v , are relatively easy to determine. The modal damping ratio ζ_v can be estimated or measured.

Determination of the Lower Bound of the Critical Flow Velocity: The lower bounds for different cylinder arrays are given in Figs. 10.16-10.20 by solid lines and summarized in Table 10.7. The critical flow velocity calculated from Table 10.7 can be compared with the actual flow velocity.

The lower bounds are established based on the following results:

- According to the analytical and experimental results, the exponent of the mass-damping parameter is always positive; i.e., the slopes of all solid lines given in Figs. 10.16-10.20 are positive.

- The slope for large values of the mass-damping parameter is 0.5.

- No experimental data are larger than the values given by the lower bound.

It is recognized that the lower bounds are not uniquely determined by this procedure; nevertheless, these bounds are established based on current available information. It would be desirable to establish an error margin for each case. Unfortunately, the data obtained by different investigators are not analyzed in the same manner, so it is difficult to establish such an error margin at this time.

10.8 EFFECT OF VARIOUS PARAMETERS ON DYNAMIC INSTABILITY

The critical flow velocity of a cylinder array is affected by many parameters. Some of these effects are qualitatively known, but most of them are still difficult to evaluate quantitatively.

10.8.1 Detuning

The frequency variation of a cylinder array in vacuum is called detuning. Once a cylinder array is submerged in a fluid, all cylinders are coupled by fluid. Therefore, in defining detuning, the natural frequencies of each individual cylinder in vacuum must be employed. In general, the detuning of a cylinder array increases the critical flow velocity. Fluid-damping-controlled instability is attributed predominantly to the motion of the cylinder itself. Coupling with neighboring cylinders is not necessary for this type of instability to occur. Therefore, the effect of detuning is not very significant. On the contrary, fluid-stiffness-controlled instability is attributed to the coupling effect; detuning plays a more significant role (see Fig. 10.11).

The effect of detuning on fluid-stiffness-controlled instability has been demonstrated by Southworth and Zdravkovich (1975) for a row of cylinders. In a wind-tunnel test, they obtained the critical flow velocity of a row of

Table 10.7 Lower Bounds on Critical Flow Velocities

Array	Parameter Range for δ_s	$\frac{U_m}{fD}$
Tube Row	$0.05 < \delta_s < 0.3$	$1.35(T/D - 0.375)\delta_s^{0.06}$
	$0.3 < \delta_s < 4.0$	$2.30(T/D - 0.375)\delta_s^{0.5}$
	$4.0 < \delta_s < 300$	$6.00(T/D - 0.375)\delta_s^{0.5}$
Square (90°)	$0.03 < \delta_s < 0.7$	$2.10 \delta_s^{0.15}$
	$0.7 < \delta_s < 300$	$2.35 \delta_s^{0.5}$
Rotated Square (45°)	$0.1 < \delta_s < 300$	$3.54(T/D - 0.5)\delta_s^{0.5}$
Triangular (30°)	$0.1 < \delta_s < 2$	$3.58(T/D - 0.9)\delta_s^{0.1}$
	$2 < \delta_s < 300$	$6.53(T/D - 0.9)\delta_s^{0.5}$
Rotated	$0.01 < \delta_s < 1$	$2.8 \delta_s^{0.17}$
Triangular (60°)	$1 < \delta_s < 300$	$2.8 \delta_s^{0.5}$

in-tune cylinders at about $U_r = 45$. However, when only one of the cylinders in a row was flexible they did not observe instability for U_r up to 100. This is consistent with the theoretical prediction. Tests also have been done for rows with three adjacent tubes flexible, and alternating tubes flexible. At a given flow velocity, tube response is largest for all tubes flexible and smallest for one tube flexible. This also illustrates that detuning tends to stabilize the system.

In a water-loop test, Chen and Jendrzejczyk (1981) demonstrate the effect of detuning on fluid-damping-controlled-instability. They show that an elastic tube surrounded by rigid tubes in water flow can lose stability; the motion is predominantly in the lift direction. This agrees with the theory that a single elastic tube in a square array can lose stability by fluid-damping force in the lift direction (Chen 1983b).

Other experimental data (Gross 1975; Blevins et al. 1981; Soper 1980; Weaver and Lever 1977) basically agree with those of Southworth and Zdravkovich (1975) as well as analytical results (Tanaka and Takahara 1981). However, Weaver and Lever (1977) show that tests on a rotated triangular array produce an increase in critical flow velocity of up to 46% for a 3% difference in frequency and no significant effect for a frequency difference greater than 10%. Larger detuning might cause the critical mode with the lowest critical flow velocity to change to some other mode. For a particular mode, detuning is expected to be beneficial in stabilizing the tubes.

A series of tests with the difference in streamwise and transverse frequencies ranging from 6.3 to 57% for a rotated triangular array with a pitch ratio of 1.375 was conducted by Weaver and Koroyannakis (1985). They found that the critical reduced flow velocity based on the lower frequency was increased only slightly over the symmetric case, being about 20% higher than that for tubes with identical stiffness in the transverse and streamwise directions. The effect is essentially independent of the difference in frequency and "direction" of the lower frequency relative to flow. Note that the results are applicable for the particular tube arrangement only; for different tube arrays, the effect is not the same. For example, for a tube row in water flow, the lowest critical flow velocity is associated with the out-of-phase mode in the lift direction (Chen and Jendrzejczyk 1981); in this case, an increase in the natural frequency in the drag direction has little effect on the critical flow velocity.

10.8.2 Upstream Turbulence

Upstream turbulence can affect critical flow velocity. Wind-tunnel experiments (Gross 1975; Southworth and Zdravkovich 1975) have shown that turbulence produces a shift in the initiation of fluidelastic instability to higher flow velocities. Gorman (1980) carried out tests in water for typical

heat-exchanger tubes. He found that the existence of upstream grids and screens had no appreciable effect on the critical liquid approach velocity. However, other wind-tunnel experiments (Franklin and Soper 1977) have shown that turbulence tends to reduce critical flow velocity. A water-tunnel test has been used to resolve the discrepancy (Chen and Jendrzejczyk 1981); turbulence can stabilize or destabilize the cylinder array depending on the characteristics of the turbulence. This conclusion is verified by Soper in his wind-tunnel tests (Soper 1981). In practical situations, the turbulence characteristics are not known; it is difficult to account for the effect of turbulence.

10.8.3 Nonuniform Flow Distribution

In general, flow velocity is not uniform either in the axial direction along the cylinder or perpendicular to the cylinder. Most experiments are conducted for uniform flow. In practice, nonuniform flow distribution must be considered.

Nonuniform Flow in the Transverse Direction: Gorman (1977) considered the effect of open tube lanes on instability of tubes adjacent to these lanes and found that there was no evidence of local triggering of instabilities. Connors (1980) shows that the skimming flows created in the vicinity of inlet-nozzle impingement plates can cause instability; the critical flow velocity depends on tube pattern and spacing and on the clearance between the tube array and the wall. In a large cylinder array, the cylinders do not become unstable at the same time; this is attributed to the nonuniform flow distribution as well as other effects. In practical applications, it is difficult to assess the effect of the nonuniform flow in the transverse direction, but it is reasonable to consider an equivalent uniform-flow case, with the flow velocity being the maximum flow of the nonuniform case.

Nonuniform Flow in the Axial Direction: Empirical correlations are developed for the case in which the entire cylinder length is subjected to the same flow velocity. In many structural components or experiments, the flows are not uniform. A general practice is to reduce the general case of nonuniform flow to the ideal case of uniform flow. An equivalent uniform flow velocity is defined by

$$U_e^2 = \frac{\int U^2(z) \psi_m^2(z) dz}{\int \psi_m^2(z) dz}, \quad (10.49)$$

where $\psi_m(z)$ is the m th orthonormal function of the cylinders. Equation 10.49 has been used by various investigators (Connors 1978; Pettigrew et al. 1978; Franklin and Soper 1977). It can be shown that an equivalent flow velocity

(defined in Eq. 10.49) is applicable provided that fluid-damping and fluid-stiffness coefficients are constants. At high reduced flow velocities, this condition is satisfied; therefore, Eq. 10.49 is applicable. At low reduced flow velocities, both fluid-stiffness coefficients and fluid-damping coefficients vary with the reduced flow velocity and Eq. 10.49 is not strictly applicable. A more rigorous analysis requires the solution of the complete equations given in Eqs. 10.18 and 10.19.

10.8.4 Tube Location

In a cylinder array, cylinder responses depend on cylinder location and types of fluid. In water flow, the upstream cylinder row is usually the critical one. Experiments in water (Gorman 1976; Chen and Jendrzeczyk 1981; Soper 1981) have shown that the upstream tubes are most susceptible to instability. The concept of "prison bars" in the upstream has been proposed on the basis of this observation (Mirza and Gorman 1975).

Cylinder responses in gas flow have been investigated for different arrangements (Gross 1975; Weaver and El-Kashlan 1981). For in-line arrays (60° and 90°), the first three rows in the upstream might be the critical ones; for out-of-line arrays (30° and 45°), the first two rows might lose stability at the lowest flow velocity. The critical row is shifted in the direction of flow as the pitch ratio becomes larger.

Little work has been reported for two-phase flow (Heilker and Vincent 1980; Pettigrew and Gorman 1973). Pettigrew and Gorman (1973) conducted an experiment in a simulated two-phase flow. Their main results are as follows: upstream cylinders vibrate most; vibration amplitudes are maximum at roughly 15% steam quality; an in-line rectangular array vibrates most; and vibration amplitude is generally larger in the drag direction than in the lift direction.

10.9 CLOSING REMARKS

To improve the stability criteria given in Table 10.7, the key step is to predict the fluid-force coefficients. The fluid-inertia coefficients can be calculated based on the potential flow theory (see Section 3.3). In most practical applications, the results from the potential flow theory will be acceptable. However, the potential flow solutions for fluid-damping coefficients and fluid-stiffness coefficients are generally unacceptable. Therefore, the main task is to develop an analytical method to compute these coefficients. This is one of the problems that is certain to be pursued in the field of computational fluid dynamics. These fluid-force coefficients can also be measured using the technique demonstrated by Tanaka and Takahara (1981), but this is a very tedious process. Furthermore, fluid-force coefficients are a function of geometry. A large number of experiments will

be required before one can quantify the fluid force for all practical cylinder arrangements.

In addition to the prediction techniques, understanding of the basic fluid dynamics for flow across a vibrating cylinder array remains a difficult task. Detailed flow measurements and theoretical study of the flow field must be carried out before the basic flow effect and the effect of cylinder motion on flow field can be identified. The interaction process of cylinder array and crossflow is certain to receive more attention in the future (Weaver and Abd-Rabbo 1984).

Based on the Chen model (1983a), the inconsistency among experimental data obtained by different investigators as well as different phenomena reported in literature can now be resolved reasonably well. Although it is still not possible to predict the critical flow velocity analytically, because of the difficulty to calculate the fluid-force coefficients, there is a sound basis for further development to quantify the instability flow velocity.

REFERENCES--Sec. 10

- Blevins, R. D. 1974. Fluid Elastic Whirling of a Tube Row. *Journal of Pressure Vessel Technology* 96, 263-267.
- Blevins, R. D. 1977. Fluid Elastic Whirling of Tube Rows and Tube Arrays. *Journal of Fluids Engineering* 99, 457-461.
- Blevins, R. D. 1979. Fluid Damping and the Whirling Instability of Tube Arrays. in *Flow Induced Vibrations*, Chen, S. S., and Bernstein, M. D., Eds., ASME, New York, pp. 35-39.
- Blevins, R. D., Gibert, R. J., Villard, B. 1981. Experiments on Vibration of Heat Exchanger Tube Arrays in Cross Flow. 6th Int. Conf. on Structural Mechanics in Reactor Technology, Paris, Paper No. B6/9.
- Chen, S. S. 1983a. Instability Mechanism and Stability Criteria of a Group of Circular Cylinders Subjected to Crossflow. Part I: Theory. *J. of Vibration, Acoustics, Stress and Reliability in Design* 105, 51-58.
- Chen, S. S. 1983b. Instability Mechanism and Stability Criteria of a Group of Circular Cylinders Subjected to Crossflow. Part II: Numerical Results and Discussions. *J. of Vibration, Acoustics, Stress and Reliability in Design* 105, 253-260.
- Chen, S. S. 1984. Guidelines for the Instability Flow Velocity of Tube Arrays in Crossflow. *J. Sound and Vibration* 93, 439-455.
- Chen, S. S., and Jendrzejczyk, J. A. 1981. Experiments on Fluid Elastic Instability in Tube Banks Subjected to Liquid Cross Flow. *Journal of Sound and Vibration* 78(3), 355-381.
- Chen, S. S., and Jendrzejczyk, J. A. 1982. Experiment and Analysis of Instability of Tube Rows Subject to Liquid Crossflow. *Journal of Applied Mechanics* 48, 704-709.
- Chen, S. S., and Jendrzejczyk, J. A. 1983. Stability of Tube Arrays in Crossflow. *Nucl. Eng. and Design* 75(3), 351-374.
- Chen, S. S., and Jendrzejczyk, J. A. 1984. Flow-Induced Vibration of the SSME LOX Pests. ANL-84-75, Argonne National Laboratory, Argonne, IL.
- Chen, Y. N. 1974. The Orbital Movement and the Damping of the Fluidelastic Vibration of Tube Banks Due to Vortex Formation, Part 2, Criterion for the Fluidelastic Orbital Vibration of Tube Arrays. *Transactions American Society of Mechanical Engineers* 96, Series B, 1065-1071.
- Connors, H. J. 1970. Fluidelastic Vibration of Tube Arrays Excited by Cross Flow. in *Flow-Induced Vibration of Heat Exchangers*, Reiff, D. D., Ed., ASME, New York, pp. 42-56.
- Connors, H. J. 1978. Fluidelastic Vibration of Heat Exchanger Tube Arrays. *Journal of Mechanical Design* 100, 347-353.

- Connors, H. J. 1980. Fluidelastic Vibration of Tube Arrays Excited by Nonuniform Cross Flow. in Flow-Induced Vibration of Power Plant Components, Au-Yang, M. K., Ed., ASME, New York, pp. 93-107.
- Franklin, R. E., and Soper, B. M. H. 1977. An Investigation of Fluidelastic Instabilities in Tube Banks Subjected to Fluid Cross-Flow. Proc. 4th Int. Conf. on Structural Mechanics in Reactor Technology, Paper No. F6/7.
- Gorman, D. J. 1976. Experimental Development of Design Criteria to Limit Liquid Cross-flow-induced Vibration in Nuclear Reactor Heat Exchange Equipment. Nuclear Science and Engineering 61, 324-336.
- Gorman, D. J. 1977. Experimental Study of Peripheral Problems Related to Liquid Flow Induced Vibration in Heat Exchangers and Steam Generators. Proc. 4th Int. Conf. on Structural Mechanics in Reactor Technology, Paper No. F6/2.
- Gorman, D. J. 1980. The Effects of Artificially Induced Up-Stream Turbulence on the Liquid Cross-Flow Induced Vibration of Tube Bundles. ASME Publication PVP-41, pp. 33-43.
- Gross, H. 1975. Investigations in Aeroelastic Vibration Mechanisms and Their Application in Design of Tubular Heat Exchangers. Technical University of Hanover, Ph.D. dissertation.
- Halle, H., Lawrence, W. P. 1977. Crossflow-induced Vibration of a Row of Circular Cylinders in Water. Presented at the ASME-IEEE Joint Power Generation Conference, ASME Paper No. 77-JPGC-NE-4, Long Beach, CA.
- Hartlen, R. T. 1974. Wind Tunnel Determination of Fluidelastic Vibration Thresholds for Typical Heat Exchanger Tube Patterns. Ontario Hydro, Report No. 74-309-K, Toronto, Canada.
- Heilker, W. J., and Vincent, R. Q. 1980. Vibration in Nuclear Heat Exchangers Due to Liquid and Two-phase Flow. Presented at the Century 2 Nuclear Engineering Conference, San Francisco, CA, ASME Paper No. 80, C2-NE-4.
- Ishigai, S., Nishikawa, E., and Yagi, E. 1973. Structure of Gas Flow and Vibration in Tube Bank with Tube Axes Normal to Flow. International Symposium on Marine Engineering, Tokyo, pp. 1-5-23 to 1-5-33.
- Keulegan, G. H., and Carpenter, L. H. 1958. Forces on Cylinders and Plates in an Oscillating Fluid. J. of Research, NBS, 60(5), 423-440.
- Lever, J. H., and Weaver, D. S. 1982. A Theoretical Model for Fluidelastic Instability in Heat Exchanger Tube Bundles. Journal of Pressure Vessel Technology 104, 147-158.
- Mirza, S. and Gorman, D. J. 1975. Experimental and Analytical Correlation of Local Driving Forces and Tube Response in Liquid Flow-Induced Vibration of Heat Exchangers. Proc. 2nd Int. Conf. on Structural Mechanics in Reactor Technology, Paper No. F6/5.

- Paidoussis, M. P. 1980a. Flow Induced Vibrations in Nuclear Reactors and Heat Exchangers. Proceedings of IUTAM-IAHR Symposium on Practical Experiences with Flow Induced Vibrations, Karlsruhe, Naudascher, E., and Rockwell, D., Eds, pp. 1-80, Springer-Verlag, Berlin.
- Paidoussis, M. P. 1980b. Fluidelastic Vibration of Cylinder Arrays in Axial and Cross Flow, State of the Art. in Flow-Induced Vibration Design Guidelines, Chen, P. Y., Ed., ASME, New York, pp. 11-46.
- Pettigrew, M. J., and Gorman, D. J. 1973. Experimental Studies on Flow Induced Vibration to Support Steam Generator Design, Part III - Vibration of a Small Tube Bundle in Liquid and Two-Phase Cross Flow. Proc. Int. Sym. on Vibration Problems in Industry, Keswick, U.K., Paper No. 4-24.
- Pettigrew, M. J., Sylvestre, Y., and Campagna, A., O. 1978. Vibration Analysis of Heat Exchanger and Steam Generator Designs. Nuclear Engineering and Design 48, 97-115.
- Price, S. J., and Paidoussis, M. P. 1983. Fluidelastic Instability of an Infinite Double Row of Circular Cylinders Subjected to a Uniform Crossflow. J. of Vibration, Acoustics, Stress and Reliability in Design 105, 59-66.
- Savkar, S. D. 1977. A Brief Review of Flow Induced Vibration of Tube Arrays in Cross-Flow. Journal of Fluids Engineering 99, 517-519.
- Soper, B. M. H. 1980. The Effect of Tube Layout on the Fluidelastic Instability of Tube Bundles in Cross Flow. in Flow-Induced Heat Exchanger Tube Vibration - 1980, Chenoweth, J. M., and Stenner, J. R., Eds., ASME, New York, pp. 1-9.
- Soper, B. M. H. 1981. The Effect of Grid Generated Turbulence on the Fluidelastic Instability of Tube Bundle in Cross Flow. Dubrovnik, Sept. 7-12, 1981, Paper No. P10.6.
- Southworth, P. J., and Zdravkovich, M. M. 1975. Cross-flow-induced Vibrations of Finite Tube Banks in in-line Arrangements. Journal of Mechanical Engineering Science 17(4), 190-198.
- Tanaka, H. 1980. Study on Fluidelastic Vibrations of Tube Bundle. Japan Society of Mechanical Engineers, Transaction, Section B 46(408), 1398-1407.
- Tanaka, H., and Takahara, S. 1981. Fluid Elastic Vibration of Tube Array in Cross Flow. Journal Sound and Vibration, 77(1), 19-37.
- Tanaka, H., Takahara, S., and Ohta, K. 1982. Flow-induced Vibration of Tube Arrays with Various Pitch-to-diameter Ratio. Journal Pressure Vessel Technology 104, 168-176.
- Wambsganss, M. W., Halle, H., and Lawrence, W. P. 1981. Tube Vibration in Industrial Size Test Heat Exchanger. ANL-CT-81-42, Argonne National Laboratory, Argonne, IL.

- Weaver, D. S., and Abd-Rabbo, A. 1984. A Flow Visualization Study of a Square Array of Tubes in Water Cross-Flow. Sym. on Flow-Induced Vibrations, ASME Publication V.2, 165-177.
- Weaver, D. S., and El-Kashlan, M. 1981. The Effect of Damping and Mass Ratio on the Stability of a Tube Bank. J. Sound and Vibration 76(2), 283-294.
- Weaver, D. S., and Grover, L. K. 1978. Cross-flow Induced Vibrations in a Tube Bank - Turbulent Buffeting and Fluid Elastic Instability. Journal of Sound and Vibration 59(2), 277-294.
- Weaver, D. S., and Koroyannakis, D. 1985. Flow Induced Vibrations of Heat Exchanger U-Tubes, A Simulation to Study the Effects of symmetric Stiffness. J. Vibration, Acoustics, Stress and Reliability in Design 105, 67-75.
- Weaver, D. S., and Lever, J. 1977. Tube Frequency Effects on Cross Flow Induced Vibrations in Tube Arrays. Proc. 5th Biennial Sym. on Turbulence, Univ. of Missouri-Rolla, Missouri.
- Whiston, G. S., Thomas, G. D. 1982. Whirling Instabilities in Heat Exchanger Tube Arrays. Journal of Sound and Vibration 81(3), 1-31.
- Yeung, H., and Weaver, D. S. 1981. The Effect of Approach Flow Direction on the Flow Induced Vibrations of a Triangular Tube Array. ASME Paper No. 81-DET-25, J. Vibration, Acoustics, Stress and Reliability in Design 105, 76-82 (1983).
- Yeung, H., and Weaver, D. S. 1983. The Effect of Approach Flow Direction on the Flow Induced Vibrations of a Triangular Tube Array. Journal of Mechanical Design 105, 76-82.
- Zukauskas, A., and Katinas, V. 1979. Flow-Induced Vibration in Heat-Exchanger Tube Banks. Sym. on Practical Experiences with Flow-Induced Vibration, Karlsruhe, Germany, Sept. 3-6, 1979.
- Zukauskas, A., and Katinas, V. 1980. Flow-induced Vibration in Heat-exchanger Tube Banks. Proceedings of IUTAM-IAHR Symposium on Practical Experiences with Flow Induced Vibrations, Naudascher, E., and Rockwell, D., Eds., Springer-Verlag, Berlin.

11. DESIGN CONSIDERATIONS

11.1 INTRODUCTION

Flow-induced vibration can be found in a whirlpool, but it can be extremely detrimental to structural and mechanical components subjected to high-velocity flow. Therefore any mechanical and structural components subjected to flow should be designed to control flow-induced vibration to an acceptable level.

In the last two decades, significant progress has been made in the development of design analysis methods. However, a lot of work remains to be done. There are design guidelines available for different applications. But in many cases, the assessment of the flow-induced vibration problem is still not an exact science.

In this chapter, the techniques to evaluate the design of components from the standpoint of flow-induced vibration are reviewed, available design guidelines are presented, and design analysis methods and techniques to control flow-induced vibration are discussed.

11.2 ASSESSMENT OF FLOW-INDUCED VIBRATION

In the evaluation of a structural or mechanical component, several issues must be resolved:

- What are the flow-induced vibration phenomena that have to be considered and how are the responses determined?
- What are the acceptance criteria and can the component meet the criteria?
- If the component cannot meet the criteria, what fixes can be made to reduce the vibration amplitude to an acceptable level?

These are the simple questions but complete answers are difficult to provide.

Some general procedures for evaluating the potential for flow-induced vibration of a component subject to flow, as illustrated in Fig. 11.1, are as follows:

- Identification of Flow Distribution and Problem Areas: From design drawings, design data, and knowledge of the component operating characteristics, estimate the expected flow distribution through the component and identify regions of predominantly crossflow or axial flow. From the estimated flow distributions and component geometries and locations within the flow field, identify potential vibration problem areas.

- Calculations of Flow Velocities: Compute the flow velocities--particularly in areas of potential flow-induced vibration problems--using analytical techniques, computer codes, results from related calculations, and experimental techniques.

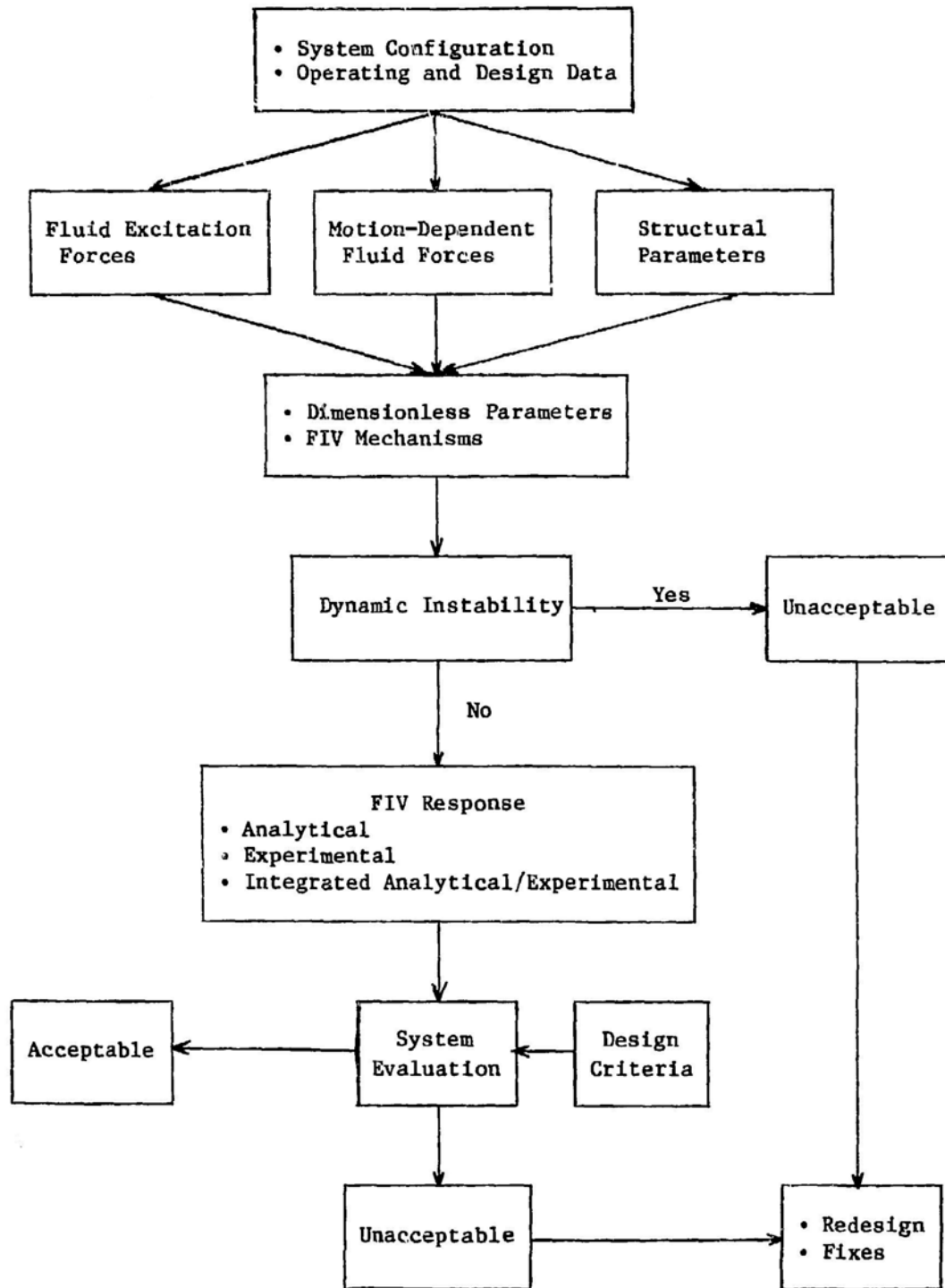


Fig. 11.1. Flow-induced Vibration Evaluation Flow Chart

- **Determination of Dynamic Characteristics of the Components:** Determine the natural frequencies and modal damping ratios of the components in vacuum and in fluid. The general method given in Chapters 2-4 can be employed.

- **Dimensionless Numbers:** Computer different dimensionless numbers, as given in Section 1.2. These dimensionless numbers are useful in determining the significance of different excitation mechanisms.

- **Dynamic Instability:** From the dimensionless numbers and stability criteria, determine if the component is in the stable region.

- **Response Amplitude:** If the system is in the stable region, calculate the response amplitudes in the operating flow-velocity range.

- **Acceptance Criteria:** If the system is in the unstable region, in most cases, dynamic instability is unacceptable. For low-level vibrations, assess the fatigue and wear life of components.

- **Modifications:** Based on the predicted response as well as experimental data, decide whether to accept the design, recommend testing, direct a redesign, or propose modifications.

In applying the general assessment procedures, one can rely on available design guidelines, analytical methods, numerical techniques, and experimental method. Design guidelines developed at Argonne National Laboratory as well as other organizations are given in the references. At this time, there are no complete design guides applicable to all cases. In many instances, it is still difficult to determine the acceptance criteria. Improvements of the design guides require further work.

Because of the complexities associated with the flow field and general structural components, it is generally necessary to resort to some form of testing to verify design adequacy from the standpoint of flow-induced vibration. Prototype testing is most desirable because it provides the direct information. However, such testing is often impossible or prohibitively expensive. The alternative, then, is to perform experiments on scale models. But the resulting information must be correlated with the prototype. The scale models do not always simulate all features of the prototype equipment; frequently, important features are omitted from the model tests. This tends to reduce the usefulness of the test results.

11.3 METHODS OF SUPPRESSING VIBRATION

From a practical point of view, designers need either a simple procedure that will assure that the design life of a structure will not be affected by flow-induced vibration or a simple method that can be adapted to vibration problems in a unit already in operation. Because of the complexity of the problem, no single solution will solve all vibration problems. But three methods are generally used to eliminate detrimental vibration:

- Fluid-Dynamic Attenuation: Modify the flow field so that fluid excitation forces are eliminated, weakened, or modified.

- Structural-Dynamic Attenuation: Modify the structural component so that it is less susceptible to vibration.

- A Combination of Fluid-Dynamic and Structural-Dynamic Attenuation: Modify both flow field and structure to reduce the vibration to a tolerable level.

For example, consider the case of vortex-excited oscillations. A wide variety of fluid dynamic means can be employed for suppressing vortex-shedding excitations. An excellent review was published recently by Zdravkovich (1981). The different means can be grouped into three categories, shown in Fig. 11.2. The first category, surface protrusions, can be further subdivided into omnidirectional and unidirectional. Omnidirectional are those not affected by the direction of flow velocity--helical strakes, helical wires, rectangular plates forming a helix, helical wires forming a herringbone pattern, etc. Unidirectional are those effective only in one direction of flow velocity--straight fins, straight wires, rectangular fins, spherical turbulence promoters, etc.

The second category includes all shapes of shrouds. The full shrouds are omnidirectional, while incomplete shrouds become unidirectional. These include perforated shrouds with circular or square holes, fine mesh gauze, parallel axial rods, straight slats, etc.

The third category includes a variety of nearwake stabilizers, which possess only unidirectional effectiveness, such as sawtooth fins, splitter plate, guiding plates, guiding vanes, etc.

The techniques presented in Fig. 11.2 can be applied for isolated cylinder and multiple cylinders. The effectiveness of different means depends not only on the Reynolds number, structural parameters, and flow regime, but also on the displacement of the cylinder itself. It should be pointed out that the vortex shedding mechanism appears indestructible; however, it can be delayed and weakened but never totally destroyed.

When flows or obstacle configuration cannot be modified to eliminate flow excitations, recourse may be structural stiffening or increasing structural damping. Increasing frequency is a problem; it requires consideration of both stiffness and inertia, parameters which in practice are far from independently adjustable. As to structural or mechanical damping, it is a much sought-after attribute, and one not easily achieved in practice.

In most practical cases, both modifications to flow field as well as structural parameters are needed to reduce the vibration to an acceptable range.

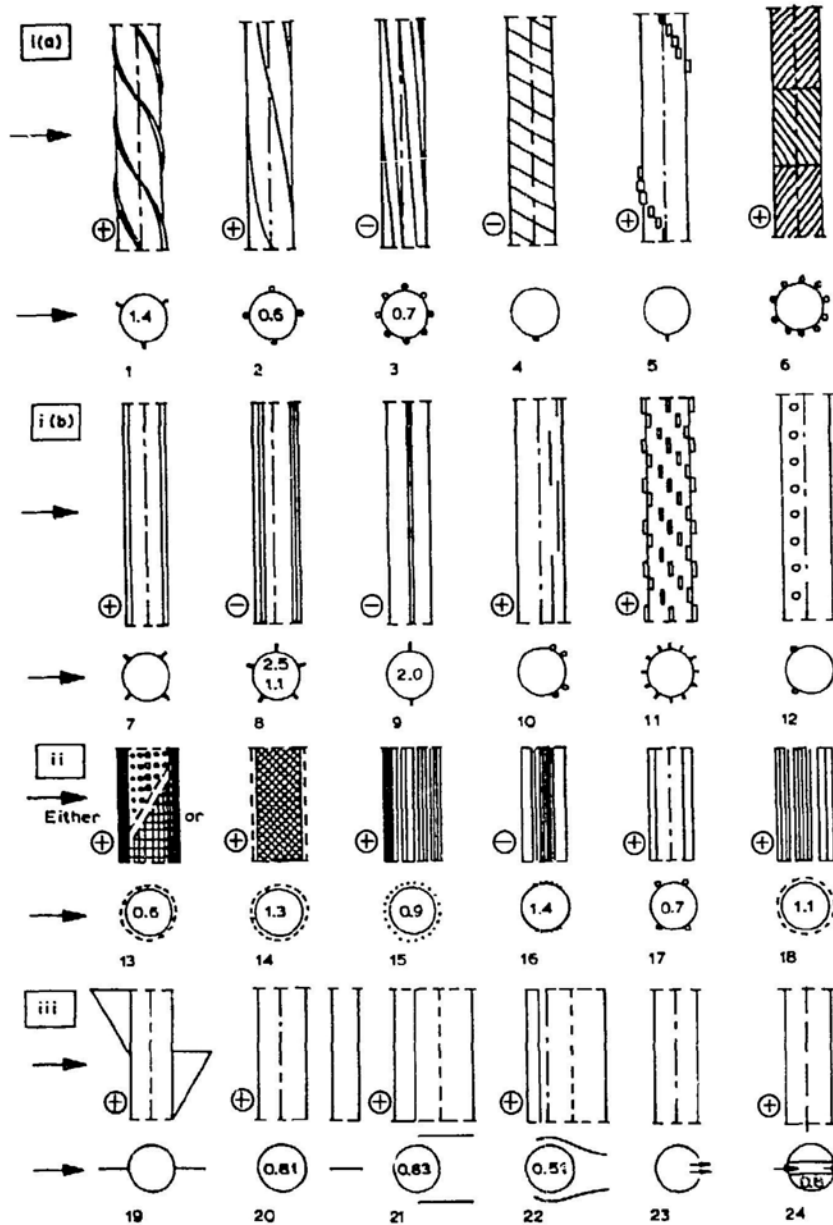


Fig. 11.2. Fluid Dynamic Means for Interfering with Vortex Shedding
 (i) Surface Protrusion (a, Omnidirectional; b, Unidirectional), (ii) Shrouds, (iii) Nearwake Stabilizers
 (from Zdravkovich 1981, with permission--see Credits)

11.4 CLOSING REMARKS

Even though there are significant gaps in codified knowledge, designers have been able to put together many system components that have provided useful service without significant problems. In many cases, without detailed consideration of the flow-induced vibration calculation, some of the obvious flow-induced effects can be avoided with common sense and experience. Of course, in the past some spectacular failures, as documented by Paidoussis (1980), were attributed to totally ignoring the flow-induced vibration effects or insufficiently considering flow-induced vibration effects.

Methods are available for solving flow-induced vibration problems, but it is better to avoid the problem in the first place. However, design with a large margin of safety factors increases costs and decreases performance. Furthermore, the method used to reduce vibration frequently requires a compromise to satisfy other requirements. Therefore structural design should be optimized with respect to cost performance and safety. The current state-of-the-art design procedures leave much to be desired; this points out the need for in-depth studies. Until such time as all significant design parameters can be identified and quantified, the engineer charged with design must avoid detrimental vibrations by relying on existing information and sound judgment in modeling and testing.

REFERENCES CITED--Sec. 11

- Paidoussis, M. P. 1980. Flow-Induced Vibrations in Nuclear Reactors and Heat Exchangers: Practical Experiences and State of Knowledge, in Practical Experiences with Flow-Induced Vibrations, eds. Naudascher, E., and Rockwell, D. Springer-Verlag, Berlin, pp. 1-81.
- Zdravkovich, M. M. 1981. Review and Classification of Various Aerodynamic and Hydrodynamic Means for Suppressing Vortex Shedding. J. of Wind Eng. and Industrial Aerodynamics 7, 145-189.

ADDITIONAL REFERENCES--Sec. 11

- Ananthanarayanan, K. S. 1978. Preliminary Design Handbook for Flow-Induced Vibration of Light Water Reactors. GEAP-24158, General Electric Co.
- Au-Yang, M. K. 1984. Flow-Induced Vibration: Guidelines for Design, Diagnosis, and Troubleshooting of Common Power Plant Components. ASME Sym. on Flow-Induced Vibrations, Vol. 3, pp. 119-138.
- Chen, S. S. 1981. Design Guide for Calculating the Instability Flow Velocity of Tube Arrays in Crossflow. ANL-CT-81-40, Argonne National Laboratory, Argonne, IL.
- Chen, S. S. 1983. Design Guide for Calculating Fluid Damping for Circular Cylindrical Structures. ANL-83-54, Argonne National Laboratory, Argonne, IL.
- Chen, S. S., and Chung, H. 1976. Design Guide for Calculating Hydrodynamic Mass; Part I: Circular Cylindrical Structures. ANL-CT-76-45, Argonne National Laboratory, Argonne, IL.
- Chen, S. S., and Wambsganss, M. W. 1974. Design Guide for Calculating Natural Frequencies of Straight and Curved Beams on Multiple Supports. ANL-CT-74-06, Argonne National Laboratory, Argonne, IL.
- Mulcahy, T. M. 1982. Design Guide for Single Circular Cylinder in Turbulent Crossflow. ANL-CT-82-7, Argonne National Laboratory, Argonne, IL.
- Safety Guide 20 - Vibration Measurements on Reactor Internals. Dec. 29, 1971. Wash-1226-20 Directorate of Regulatory Standards AEC.
- Wambsganss, M. W., and Chen, S. S. 1971a. Tentative Design Guide for Calculation Procedures for Vibration of Tubes with Transverse Stops. ANL-ETD-71-01, Argonne National Laboratory, Argonne, IL.
- Wambsganss, M. W., and Chen, S. S. 1971a. Tentative Design Guide for Calculating the Vibration Response of Flexible Cylindrical Elements in Axial Flow. ANL-ETD-71-07, Argonne National Laboratory, Argonne, IL.

APPENDIX A. VIBRATION OF DAMPED LINEAR SYSTEMS

For a system of N degrees of freedom, the equation of motion in matrix form is

$$[M]\{\ddot{Q}\} + [C]\{\dot{Q}\} + [K]\{Q\} = \{G\} , \quad (A.1)$$

where M , C , and K are N by N real matrices.

Consider the free vibration with $G = 0$. The solution of (A.1) is represented in the form

$$Q = \sum_{j=1}^{2N} \bar{q}_j \exp(\lambda_j t) . \quad (A.2)$$

λ_j 's are $2N$ roots to the equation

$$\text{Det}[\lambda^2 M + \lambda C + K] = 0 . \quad (A.3)$$

In general, the roots of (A.3) can be stated as

$$\lambda_j = \gamma_j \pm i\beta_j . \quad (A.4)$$

The stability of the system is determined by γ_j :

- $\gamma_j < 0$, the system is asymptotically stable.
- $\gamma_j = 0$, the system is marginally stable.
- $\gamma_j > 0$, the system is unstable.

A.1 CLASSICAL NORMAL MODES

In each mode, the various parts of a system vibrate in the same phase, passing through their equilibrium configuration at the same instant of time; this type of normal mode is called the classical normal mode. The necessary and sufficient conditions for the existence of the classical normal modes were investigated by Caughey and O'Kelley (1965) and subsequently discussed by several investigators (e.g., Lin 1966; Fawzy 1977; Müller 1979; Nicholson 1979).

If M , C , and K are real and symmetric and M is positive definite, the necessary and sufficient condition for the existence of classical normal modes

is the commutativity of $M^{-1}K$ and $M^{-1}C$; i.e.,

$$CM^{-1}K = KM^{-1}C . \quad (A.5)$$

The necessary and sufficient condition for a system of N degrees of freedom to satisfy the commutativity condition in Eq. A.5 is to select the damping matrix in such a manner that

$$[M]^{-1}[C] = \sum_{j=0}^{N-1} \alpha_j [M^{-1}[K]]^j , \quad (A.6)$$

where α_j 's are constants. The condition given in Eq. A.6 was originally developed by Caughey and O'Kelley (1965) and can also be derived as a direct consequence of the Cayley-Hamilton theorem (Lin 1966). If the first two terms in Eq. A.6 are retained in its expression, Eq. A.6 is reduced to the Rayleigh condition of proportional damping,

$$[C] = \alpha_0 [M] + \alpha_1 [K] . \quad (A.7)$$

Equation A.7 has been used extensively in practical applications.

A.2 FORCED VIBRATION OF SYSTEM WITH CLASSICAL NORMAL MODES

For a system of N degrees of freedom the eigenvalues and eigenvectors of the system are easily computed from the undamped homogeneous equation,

$$[K - \omega^2 M] \{\bar{Q}\} = \{0\} . \quad (A.8)$$

We can normalize Eq. A.8 using the weighted modal matrix $[E]$ formed from the columns of eigenvectors. Letting

$$\{\bar{Q}\} = [E] \{W\} , \quad (A.9)$$

and premultiplying by the transpose $[E]^T$, we obtain

$$[E^T M E] \{\ddot{W}\} + [E^T C E] \{\dot{W}\} + [E^T K E] \{W\} = [E^T] \{G\} . \quad (A.10)$$

The matrices $[E^T M E] = [I]$ and $[E^T K E] = [\Lambda]$ are diagonal, where $[I]$ is an identity matrix and $[\Lambda]$ is a diagonal matrix with the diagonal elements being the eigenvalues.

When the damping matrix $[C]$ is a Rayleigh damping,

$$[E^{TCE}] = \alpha_0 [I] + \alpha_1 [A] = [\bar{C}] , \quad (A.11)$$

where $[\bar{C}]$ is diagonal. Equation A.11 is then completely uncoupled and can be solved sequentially for the element of $\{W\}$. The physical coordinates $\{Q\}$ can be recovered from Eq. A.9.

Equating the elements of $[\bar{C}]$ to the term $2\zeta_j \omega_j$, which appears in the equation of motion of a single-degree-of-freedom oscillation, gives

$$\zeta_j = \frac{\alpha_0}{2\omega_j} + \frac{\alpha_1 \omega_j}{2} , \quad j = 1, 2, \dots, N , \quad (A.12)$$

where ζ_j is the equivalent viscous modal damping ratio for the j th mode. The more general case of Eq. A.6 results in

$$[\bar{C}] = \sum_{k=0}^{N-1} \alpha_k \omega^{2k} \quad (A.13)$$

and

$$\zeta_j = \frac{1}{2} \left(\frac{\alpha_0}{\omega_j} + \alpha_1 \omega_j + \alpha_2 \omega_j^3 + \dots \right) , \quad j = 1, 2, \dots, N . \quad (A.14)$$

A.3 FORCED VIBRATION OF SYSTEM WITH NONCLASSICAL NORMAL MODES

When the damping matrix does not satisfy the condition given in Eq. A.6, the following technique can be used. If Eq. A.1 is augmented with the trivial equation $[M]\{\ddot{Q}\} - [M]\{\ddot{Q}\} = \{0\}$, it becomes

$$[U]\{\dot{\Psi}\} + [V]\{\Psi\} = \{r\} , \quad (A.15)$$

$$[U] = \begin{pmatrix} 0 & M \\ M & C \end{pmatrix} ; \quad [V] = \begin{pmatrix} -M & 0 \\ 0 & K \end{pmatrix} ; \quad \{\Psi\} = \begin{Bmatrix} \dot{Q} \\ Q \end{Bmatrix} ; \quad \{r\} = \begin{Bmatrix} 0 \\ G \end{Bmatrix} . \quad (A.16)$$

Equations A.16 are the basic equations which are to be used in the studies of free vibration, stability, and forced vibration.

The damped free vibration mode shapes and mode values are obtained by applying solutions

$$\{\Psi\} = \{\bar{X}\} \exp(\lambda t) \quad (\text{A.17})$$

to the homogeneous form of Eq. A.15:

$$[\lambda U + V] \{\bar{X}\} = \{0\} . \quad (\text{A.18})$$

The adjoint form to Eq. A.18 is

$$[\lambda U' + V'] \{\bar{Y}\} = \{0\} , \quad (\text{A.19})$$

where ' denotes the transport of a matrix. The solutions of Eqs. A.18 and A.19 can be achieved by standard procedures. Assume that the modal matrices obtained from Eqs. A.18 and A.19 are $[X]$ and $[Y]$, respectively. Let

$$\{\Psi\} = [X] \{Z\} . \quad (\text{A.20})$$

Substituting Eq. A.20 into A.15 and using the biorthogonality condition yields

$$[E] \{\dot{Z}\} + [F] \{Z\} = [Y'] \{T\} , \quad (\text{A.21})$$

where E and F are diagonal and hence Eq. A.21 is uncoupled and easily solved.

REFERENCES--Appendix A

- Caughey, T. K., and O'Kelley, M. E. J. 1965. Classical Normal Modes in Damped Linear Dynamic System. ASME J. Appl. Mech. 32, 583-588.
- Fawzy, I. 1977. A Theorem on the Free Vibration of Damped Systems. ASME J. Appl. Mech. 44, 132-134.
- Lin, Y. K. 1966. Discussion of the Paper by Caughey and O'Kelley (1965), ASME J. Appl. Mech. 33, 471-472.
- Müller, P. C. 1979. Remarks on Vibrations of Damped Linear Systems. Mech. Res. Comm. 6(1), 7-15.
- Nicholson, D. W. 1979. Comments on Damped Response in Linear System. Mech. Res. Comm. 6(1), 17-25.

APPENDIX B. GENERAL FLUID EQUATIONS

The motion of a continuous medium is governed by the principles of classical mechanics for conservation of mass and momentum. If the properties of the fluid medium are continuous in some domain of space and time, the equations of motion become (Schlichting 1968):

Conservation of Mass:

$$\frac{D\rho}{Dt} + \rho \vec{\nabla} \cdot \vec{U} = 0 \quad (B.1)$$

Conservation of Momentum:

$$\rho \frac{D\vec{U}}{Dt} - \vec{\nabla} \cdot \vec{\sigma} = \vec{f} \quad (B.2)$$

where

$$\sigma = -p\vec{I} + \lambda(\vec{\nabla} \cdot \vec{U})\vec{I} + 2\mu(\vec{\nabla}\vec{U} + \vec{U}\vec{\nabla}) . \quad (B.3)$$

In these equations, t is the time, ρ is the density, \vec{U} is the velocity of a material particle in the frame of reference, $\vec{\sigma}$ is the stress tensor, p is the pressure, λ and μ are the two coefficients of viscosity, and \vec{f} is the internal force per unit volume. Equations B.1 to B.3 can be simplified to different forms for different conditions in cylindrical coordinates. The cylindrical coordinates (r, θ, z) are related to the Cartesian (x, y, z) by

$$x = r \cos \theta , \quad y = r \sin \theta , \quad \text{and} \quad z = z , \quad (B.4)$$

and the convective time derivative and Laplacian operator are

$$\begin{aligned} \vec{U} \cdot \vec{\nabla} &= u_r \frac{\partial}{\partial r} + \frac{1}{r} u_\theta \frac{\partial}{\partial \theta} + u_z \frac{\partial}{\partial z} \quad \text{and} \\ \nabla^2 &= \frac{1}{r^2} \frac{\partial}{\partial r} \left(r \frac{\partial}{\partial r} \right) + \frac{1}{r^2} \frac{\partial^2}{\partial \theta^2} + \frac{\partial^2}{\partial z^2} . \end{aligned} \quad (B.5)$$

E.1 INCOMPRESSIBLE FLUID

The equations of motion are:

$$\begin{aligned}
 \rho \left(\frac{\partial u_r}{\partial t} + u_r \frac{\partial u_r}{\partial r} + \frac{u_\theta}{r} \frac{\partial u_r}{\partial \theta} - \frac{u_\theta^2}{r} + u_\theta \frac{\partial u_r}{\partial z} \right) \\
 = f_r - \frac{\partial p}{\partial r} + \mu \left(\frac{\partial^2 u_r}{\partial r^2} + \frac{1}{r} \frac{\partial u_r}{\partial r} - \frac{u_r}{r^2} + \frac{1}{r^2} \frac{\partial^2 u_r}{\partial \theta^2} - \frac{2}{r^2} \frac{\partial u_\theta}{\partial \theta} + \frac{\partial^2 u_r}{\partial z^2} \right), \\
 \rho \left(\frac{\partial u_\theta}{\partial t} + u_r \frac{\partial u_\theta}{\partial r} + \frac{u_\theta}{r} \frac{\partial u_\theta}{\partial \theta} + \frac{u_r u_\theta}{r} + u_z \frac{\partial u_\theta}{\partial z} \right) \\
 = f_\theta - \frac{1}{r} \frac{\partial p}{\partial \theta} + \mu \left(\frac{\partial^2 u_\theta}{\partial r^2} + \frac{1}{r} \frac{\partial u_\theta}{\partial r} - \frac{u_\theta}{r^2} + \frac{1}{r^2} \frac{\partial^2 u_\theta}{\partial \theta^2} + \frac{2}{r^2} \frac{\partial u_r}{\partial \theta} + \frac{\partial^2 u_\theta}{\partial z^2} \right), \quad (B.6)
 \end{aligned}$$

and

$$\begin{aligned}
 \rho \left(\frac{\partial u_z}{\partial t} + u_r \frac{\partial u_z}{\partial r} + \frac{u_\theta}{r} \frac{\partial u_z}{\partial \theta} + u_z \frac{\partial u_z}{\partial z} \right) \\
 = f_z - \frac{\partial p}{\partial z} + \mu \left(\frac{\partial^2 u_z}{\partial r^2} + \frac{1}{r} \frac{\partial u_z}{\partial r} + \frac{1}{r^2} \frac{\partial^2 u_z}{\partial \theta^2} + \frac{\partial^2 u_z}{\partial z^2} \right).
 \end{aligned}$$

The continuity equation is.

$$\frac{\partial u_r}{\partial r} + \frac{u_r}{r} + \frac{1}{r} \frac{\partial u_\theta}{\partial \theta} + \frac{\partial u_z}{\partial z} = 0. \quad (B.7)$$

The stress components are:

$$\begin{aligned}
 \sigma_{rr} &= -p + 2\mu \frac{\partial u_r}{\partial r}; & \tau_{r\theta} &= \mu \left[r \frac{\partial}{\partial r} \left(\frac{u_\theta}{r} \right) + \frac{1}{r} \frac{\partial u_r}{\partial \theta} \right]; \\
 \sigma_{\theta\theta} &= -p + 2\mu \left(\frac{1}{r} \frac{\partial u_\theta}{\partial \theta} + \frac{u_r}{r} \right); & \tau_{\theta z} &= \mu \left(\frac{\partial u_\theta}{\partial z} + \frac{1}{r} \frac{\partial u_z}{\partial \theta} \right); \\
 \sigma_{zz} &= -p + 2\mu \frac{\partial u_z}{\partial z}; & \tau_{rz} &= \mu \left(\frac{\partial u_r}{\partial z} + \frac{\partial u_z}{\partial r} \right).
 \end{aligned} \quad (B.8)$$

B.2 LINEARIZED COMPRESSIBLE VISCOUS FLUID

Consider a compressible Newtonian fluid undergoing very small amplitude oscillation. For a density perturbation ρ much smaller than the constant steady-state density ρ_0 , and for a fluid perturbation velocity \vec{U} whose modulus is much smaller than the speed of sound $c = (K/\rho_0)^{0.5}$, where K is the isothermal bulk modulus, the continuity, state and momentum equations reduce to the linear acoustic equations

$$\frac{\partial \rho}{\partial t} + \rho_0 \nabla \cdot \vec{U} = 0 ,$$

$$\frac{\partial p}{\partial \rho} = c^2 , \quad \text{and} \quad (B.9)$$

$$\frac{\partial \vec{U}}{\partial t} = -\frac{1}{\rho} \nabla p - \nu_0 \nabla \times \nabla \times \vec{U} + \left(\nu' + \frac{4}{3} \nu_0 \right) \nabla (\nabla \cdot \vec{U}) ,$$

where ν_0 and ν' are the kinetic and second viscosities of the fluid. The velocity field can be represented as

$$\vec{U} = \nabla \phi + \nabla \times \vec{\psi} . \quad (B.10)$$

Using Eqs. B.9 and B.10 yields

$$\left(\frac{\partial}{\partial t} - \nu_0 \nabla^2 \right) \vec{\psi} = 0 \quad \text{and}$$

$$p = p_0 - \rho_0 \frac{\partial \phi}{\partial t} + \rho_0 \left(\frac{4}{3} \nu_0 + \nu' \right) \nabla^2 \phi \quad (B.11)$$

$$\left[\left(1 + \frac{1}{\omega_0} \frac{\partial}{\partial t} \right) \nabla^2 - \frac{1}{c^2} \frac{\partial^2}{\partial t^2} \right] \phi = 0 ,$$

where

$$\omega_0 = \frac{c^2}{\frac{4}{3} \nu_0 + \nu'} .$$

B.3 LINEARIZED INCOMPRESSIBLE FLUID EQUATIONS

For small-amplitude motion, the equations of incompressible fluid can be reduced from Eqs. B.9-B.11;

$$\vec{\nabla} \cdot \vec{U} = 0 \quad \text{and} \quad \frac{\partial \vec{U}}{\partial t} = -\frac{1}{\rho} \vec{\nabla} p + \frac{1}{\nu} \nabla^2 \vec{U} . \quad (\text{B.12})$$

The solution of Eqs. B.12 is given by

$$\begin{aligned} \vec{U} &= \vec{\nabla} \phi + \vec{\nabla}_x \vec{\psi} , \\ p &= -\rho \frac{\partial \phi}{\partial t} , \\ \nabla^2 \phi &= 0 , \quad \text{and} \\ (\nabla^2 - \frac{1}{\nu} \frac{\partial}{\partial t}) \vec{\psi} &= 0 . \end{aligned} \quad (\text{B.13})$$

B.4 LINEARIZED COMPRESSIBLE INVISCID FLUID

For small-amplitude motion, the equation of inviscid fluid reduced from Eqs. B.12 and B.13 are

$$\begin{aligned} \vec{U} &= \nabla \phi , \\ p &= -\rho \frac{\partial \phi}{\partial t} , \quad \text{and} \\ (\nabla^2 - \frac{1}{c^2} \frac{\partial^2}{\partial t^2}) \phi &= 0 , \end{aligned} \quad (\text{B.14})$$

where c is the speed of sound.

REFERENCES--Appendix B

Schlichting, H. 1968. Boundary-Layer Theory, McGraw-Hill Book Company.

APPENDIX C. CHARACTERISTIC EQUATIONS, EIGENFUNCTIONS, AND ADJOINT EIGENFUNCTIONS

The eigenfunctions $\phi_n(\xi)$ for beam vibration are obtained from the following eigenvalue problem:

$$L\phi = \lambda\phi \quad L = \frac{d^4}{d\xi^4} + \alpha \frac{d^2}{d\xi^2}, \quad (C.1)$$

$$\left. \begin{aligned} \phi + a_1 \frac{d^3\phi}{d\xi^3} - \frac{d\phi}{d\xi} - b_1 \frac{d^2\phi}{d\xi^2} &= 0 & \text{at } \xi = 0, \\ \phi - a_2 \frac{d^3\phi}{d\xi^3} - \frac{d\phi}{d\xi} + b_2 \frac{d^2\phi}{d\xi^2} &= 0 & \text{at } \xi = 1, \end{aligned} \right\} \quad (C.2)$$

and

where α , a_1 , a_2 , b_1 , and b_2 are constants. Employing Green's identity, we can define the adjoint eigenvalue problem. Green's identity is

$$\langle \psi(\xi), L\phi(\xi) \rangle - \langle \phi(\xi), L^* \psi(\xi) \rangle = K[\phi(\xi), \psi(\xi)], \quad (C.3)$$

where L^* is the adjoint operator and $\psi(\xi)$ is the adjoint eigenfunction. On substituting Eq. C.1 into C.3, utilizing Eqs. C.2, and requiring that the bilinear concomitant $K[\phi, \psi]$ vanishes, we obtain the following adjoint eigenvalue problem:

$$L^* \psi = \lambda \psi \quad L^* = \frac{d^4}{d\xi^4} + \alpha \frac{d^2}{d\xi^2}, \quad (C.4)$$

$$\left. \begin{aligned} \psi + a_1 \alpha \frac{d\psi}{d\xi} + a_1 \frac{d^3\psi}{d\xi^3} - b_1 \alpha \psi - \frac{d\psi}{d\xi} + b_1 \frac{d^2\psi}{d\xi^2} &= 0 & \text{at } \xi = 0, \\ \psi - a_2 \alpha \frac{d\psi}{d\xi} - a_2 \frac{d^3\psi}{d\xi^3} - b_2 \alpha \psi + \frac{d\psi}{d\xi} + b_2 \frac{d^2\psi}{d\xi^2} &= 0 & \text{at } \xi = 1. \end{aligned} \right\} \quad (C.5)$$

and

In general, the eigenvalue problem specified by Eqs. C.1 and C.2 is non-self-adjoint, since the boundary conditions in C.2 and C.5 are different. However, if $a_1 = a_2 = 0$, then the eigenvalue problem is self-adjoint.

The solution of Eq. C.1 is taken as

$$\phi(\xi) = C_1 \sin p\xi + C_2 \cos p\xi + C_3 \sinh q\xi + C_4 \cosh q\xi, \quad (C.6)$$

where

$$p = \left(\sqrt{\frac{\alpha^2}{4} + \lambda^2} + \frac{\alpha}{2} \right)^{1/2} \quad \text{and} \quad q = \left(\sqrt{\frac{\alpha^2}{4} + \lambda^2} - \frac{\alpha}{2} \right)^{1/2}. \quad (C.7)$$

On substituting Eq. C.6 into Eqs. C.2 we obtain

$$\begin{bmatrix} -a_1 p^3 & 1 & a_1 q^3 & 1 \\ p & b_1 p^2 & q & -b_1 q^2 \\ \sin p + a_2 p^3 \cosh q & \cosh p - a_2 p^3 \sinh q & \sinh q - a_2 q^3 \cosh q & \cosh q - a_2 q^3 \sinh q \\ p(\cosh p - b_2 p \sinh q) & -p(\sinh p + b_2 p \cosh q) & q(\cosh q + b_2 q \sinh q) & q(\sinh q + b_2 q \cosh q) \end{bmatrix} \begin{bmatrix} C_1 \\ C_2 \\ C_3 \\ C_4 \end{bmatrix} = \begin{bmatrix} 0 \\ 0 \\ 0 \\ 0 \end{bmatrix}. \quad (C.8)$$

Setting the coefficient matrix in Eq. C.8 equal to zero yields the characteristic equation, which can be written as

$$\Delta(a_1, a_2, b_1, b_2, \alpha, \lambda) = 0. \quad (C.9)$$

Next, the solution of Eq. C.4 is taken as

$$\psi(\xi) = C_1^* \sin p\xi + C_2^* \cos p\xi + C_3^* \sinh q\xi + C_4^* \cosh q\xi. \quad (C.10)$$

which, substituting Eq. C.10 into Eqs. C.5, gives

$$\begin{bmatrix}
 a_1 \alpha p - a_1 p^3 & 1 & a_1 \alpha q + a_1 q^3 & 1 \\
 -p & b_1 \alpha - b_1 p^2 & -q & b_1 \alpha + b_1 \alpha^2 \\
 \sin p - a_2 \alpha p \cosh q & \cosh q + a_2 \alpha p \sin p & \sinh q - a_2 \alpha q \cosh q & \cosh q - a_2 \alpha q \sinh q \\
 + a_2 p^3 \cosh q & -a_2 p^3 \sin p & -a_2 q^3 \cosh q & -a_2 q^3 \sinh q \\
 b_2 \alpha \sin p + p \cosh q & b_2 \alpha \cosh q - p \sin p & b_2 \alpha \sinh q + q \cosh q & b_2 \alpha \cosh q + q \sinh q \\
 -b_2 p^2 \sin p & -b_2 p^2 \cosh q & +b_2 q^2 \sinh q & +b_2 q^2 \cosh q
 \end{bmatrix}
 \begin{bmatrix}
 C_1^* \\
 C_2^* \\
 C_3^* \\
 C_4^*
 \end{bmatrix}
 =
 \begin{bmatrix}
 0 \\
 0 \\
 0 \\
 0
 \end{bmatrix}
 \quad (C.11)$$

Setting the determinant of the coefficient matrix of Eqs. C.11 equal to zero, we also obtain Eq. C.9, which can be solved numerically. Once the eigenvalues are obtained, we can find C_n ($n = 1, 2, 3$) in terms of C_4 , and C_n^* ($n = 1, 2, 3$) in terms of C_4^* .

The characteristic equations, eigenfunctions, and adjoint eigenfunctions of the most common assumed end conditions are summarized as follows:

Fixed-fixed end conditions ($a_1 = a_2 = b_1 = b_2 = 0$)

Characteristic equation:

$$1 - \cos p \cosh q - \frac{q}{2\sqrt{\lambda}} \sin p \sinh q = 0$$

Eigenfunctions:

$$\phi(\xi) = C_1 \sin p\xi + C_2 \cos p\xi + C_3 \sinh q\xi + C_4 \cosh q\xi$$

$$C_1 = (\cosh q - \cos p) / \left(\frac{p}{q} \sinh q - \sin p \right)$$

$$C_2 = -1$$

$$C_3 = -(\cosh q - \cos p) / \left(\sinh q - \frac{q}{p} \sin p \right)$$

$$C_4 = 1$$

Adjoint eigenfunctions:

$$\psi(\xi) = \phi(\xi)$$

Hinged-hinged end conditions ($a_1 = a_2 = 0$, $b_1 = b_2 = \infty$)

Characteristic equation:

$$\sin p = 0$$

Eigenfunctions:

$$\phi(\xi) = \sin n\pi\xi, \quad n = 1, 2, 3, \dots,$$

Adjoint eigenfunctions:

$$\psi(\xi) = \phi(\xi)$$

Fixed-free end conditions ($a_1 = b_1 = 0$, $a_2 = b_2 = \infty$)

Characteristic equation:

$$\alpha^2 + 2\lambda(1 + \cos p \cosh q) + \alpha\sqrt{\lambda} \sin p \sinh q = 0$$

Eigenfunctions:

$$\phi(\xi) = C_1 \sin p\xi + C_2 \cos p\xi + C_3 \sinh q\xi + C_4 \cosh q\xi$$

$$C_1 = 1$$

$$C_2 = -(p^2 \sin p + pq \sinh q) / (p^2 \cos p + q^2 \cosh q)$$

$$C_3 = -p/q$$

$$C_4 = (p^2 \sin p + pq \sinh q) / (p^2 \cos p + q^2 \cosh q)$$

Adjoint eigenfunctions:

$$\psi(\xi) = C_1^* \sin p\xi + C_2^* \cos p\xi + C_3^* \sinh q\xi + C_4^* \cosh q\xi$$

$$C_1^* = 1$$

$$C_2^* = -[(\alpha - p^2) \sin p - \frac{p}{q} (\alpha + q^2) \sinh q] / [(\alpha - p^2) \cos p - (\alpha + q^2) \cosh q]$$

$$C_3^* = -p/q$$

$$C_4^* = [(\alpha - p^2) \sin p - \frac{p}{q} (\alpha + q^2) \sinh q] / [(\alpha - p^2) \cos p - (\alpha + q^2) \cosh q]$$

Based on these results, the eigenvalues and eigenfunctions can be calculated.

In most practical applications, the system is self-adjoint. Table C.1 show the angular natural frequencies and mode shapes for six types of end conditions (Harris and Crede 1976).

REFERENCES--Appendix C

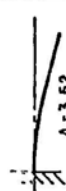
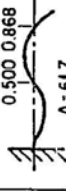
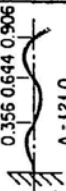
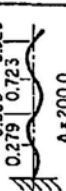
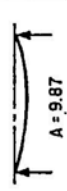
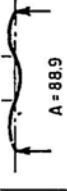

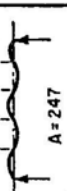
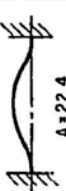
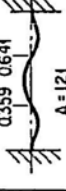


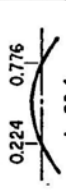
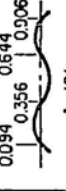
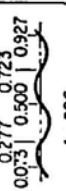
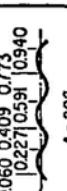




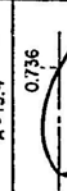
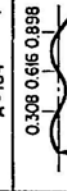
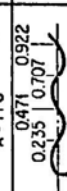

Harris, C. M., and Crede, C. E. 1976. Shock and Vibration Handbook. McGraw-Hill Book Co., Second Ed.

Table C.1. Beams of Uniform Section*

$$\text{Angular Natural Frequency } \omega_n = \lambda_n \sqrt{\frac{EI}{m\ell^4}}$$

E = Young's modulus
 I = Area moment of inertia
 ℓ = Length of beam
 m = mass per unit length of beam
 λ_n = Coefficient from Table below

NODES ARE INDICATED IN TABLE BELOW AS A PROPORTION OF LENGTH ℓ MEASURED FROM LEFT END

FIXED-FREE (CANTILEVER)	 0.774 A = 22.4	 0.500 0.868 A = 61.7	 0.355 0.644 0.906 A = 200.0	 0.279 0.723 0.926 A = 247
HINGED-HINGED (SIMPLE)	 0.500 A = 39.5	 0.333 0.667 A = 88.9	 0.25 0.50 0.75 A = 158	 0.20 0.40 0.60 0.80 A = 298
FIXED-FIXED (BUILT-IN)	 0.132 0.868 A = 61.7	 0.094 0.544 0.906 A = 121	 0.277 0.723 0.927 A = 200	 0.060 0.409 0.773 0.940 A = 298
FREE-FREE	 0.224 0.776 A = 15.4	 0.384 0.616 A = 104	 0.294 0.706 0.922 A = 178	 0.190 0.581 0.937 A = 272
FIXED-HINGED	 0.446 A = 50.0	 0.308 0.692 A = 104	 0.277 0.723 0.927 A = 200	 0.238 0.619 0.810 A = 272
HINGED-FREE	 0.736 A = 15.4	 0.446 0.554 A = 50.0	 0.277 0.723 0.927 A = 200	 0.381 0.763 0.937 A = 272

*Table from Harris and Crede (1976), with permission--see Credits.

APPENDIX D: ~~AMASS~~—FLUID DYNAMIC MASS COEFFICIENTS OF A GROUP OF CIRCULAR CYLINDERS IN A FLUID

```

C THIS PROGRAM CALCULATES HYDRODYNAMIC MASS COEFFICIENTS OF A GROUP
C OF CIRCULAR CYLINDERS IMMERSED IN A FLUID CONTAINED IN A CYLINDER
C OR IN AN INFINITE FLUID.
C
C ON INPUT:
C
C   NNN: NUMBER OF TERMS USED (IN GENERAL, NNN=10 WILL GIVE RESULTS
C         WITH SUFFICIENT ACCURACY).
C   KKI: TOTAL NUMBER OF CYLINDERS INCLUDING THE OUTER CYLINDER.
C   ICHK: IF ICHK=1, GENERAL CASE, ONE INNER CYLINDER IS CONCENTRIC
C         WITH THE OUTER CYLINDER (IK=0).
C         IF ICHK=2, NO INNER CYLINDER IS CONCENTRIC WITH THE OUTER
C         CYLINDER (IK=1).
C         IF ICHK=3, A GROUP OF CYLINDERS IN AN INFINITE FLUID (IK=2).
C   RA(I),XA(I),YA(I): RADIUS AND COORDINATES OF CYLINDER I.
C   * INPUT SEQUENCE OF CYLINDER GEOMETRIES *
C     OUTER CYLINDER, CONCENTRIC INNER CYLINDER & OTHER CYLINDERS.
C
C ON OUTPUT:
C
C   GAM(I,J): HYDRODYNAMIC MASS COEFFICIENT MATRIX.
C   PADD(I): PRINCIPAL VALUES OF HYDRODYNAMIC MASS MATRIX DIVIDED BY
C            FLUID DENSITY AND BY PHI=3.1416 (SHOULD BE MULTIPLIED
C            BY FLUID DENSITY AND BY PHI TO YIELD THE EFFECTIVE
C            HYDRODYNAMIC MASS PER UNIT LENGTH OF CYLINDERS).
C   ZZ(I,J): EIGENVECTORS OF THE HYDRODYNAMIC MASS MATRIX.
C
C ** DIMENSION SPECIFICATIONS **
C   (KKI)           RA,XA,YA
C   (KKK)           R,X,Y
C   (KKI*2)         PADD,D
C   (KKI,KKI)       RAIJ,PHYA,ALP,BET,SIG,TAU
C   (KKK,KKK)       RIJ,PHY
C   (KKI*2,KKI*2)   GAM,RAI,ZZ
C   (KKI,NNN,KKI)   AL,BE,SI,TA,H
C   (KKK,NNN,KKK,NNN) AA,BB,CC,DD
C   (KKI*NNN*2,KKI*NNN*2) E
C   (KKI*NNN*2,KKI) F
C   WHERE KKK=KKI+IK.
C
C   * THIS SUBROUTINE IS FOR NNN=10 AND KKI=4 *
C
C -----
C
C SUBROUTINE AMASS(NNN,KKI,ICLK,RA,XA,YA,GAM,PADD,ZZ)
C
C REAL*8 CNA,CMA,CNMA,CNA1,CMA1,CNMMA,CNA2,CMA2,CMMNA
C REAL*8 AGG,BGG,CGG,DGG,AGG1,AGG2

```

```

REAL*8 AA,BB,CC,DD,H,E,F,DETERM
REAL*8 AG1,BG1,CG1,DG1,AG11,BG11,CG11,DG11
REAL*8 RAM,ZZ,PADD,D

C
  DIMENSION RA(4),XA(4),YA(4),R(6),X(6),Y(6)
  DIMENSION RAIJ(4,4),PHYA(4,4),RIJ(6,6),PHY(6,6)
  DIMENSION AA(6,10,6,10),BB(6,10,6,10)
  DIMENSION CC(6,10,6,10),DD(6,10,6,10)
  DIMENSION H(4,10,4),E(80,80),F(80,4)
  DIMENSION AL(4,10,4),SI(4,10,4),TA(4,10,4),BE(4,10,4)
  DIMENSION ALP(4,4),SIG(4,4),TAU(4,4),BET(4,4)
  DIMENSION GAM(8,8),RAM(8,8),ZZ(8,8),PADD(8),D(8)

C
  KKI2=KKI*2
C ::::: SET UP CONTROL VARIABLES :::::
  GO TO (4001,4002,4003),ICLK
4001  IK=0
      IKK=2
      GO TO 4004
4002  IK=1
      IKK=1
      GO TO 4004
4003  IK=2
      IKK=0
4004  KKK=KKI+IK
C ::::: COMPUTE RAIJ(I,J) AND PHYA(I,J) :::::
      DO 201 I=1,KKI
        DO 201 J=1,KKI
          GO TO (4011,4012,4013),ICLK
4011  IF (I-2) 4013,4013,4012
4013  IF (J-2) 4014,4014,4012
4014  RAIJ(I,J)=0.0
      PHYA(I,J)=0.0
      GO TO 201
4012  IF (I-J) 4015,4014,4015
4015  ARG=(XA(J)-XA(I))**2+(YA(J)-YA(I))**2
      RAIJ(I,J)=SQRT(ARG)
      ARG1=YA(J)-YA(I)
      ARG2=XA(J)-XA(I)
      PHYA(I,J)=ATAN2(ARG1,ARG2)
201  CONTINUE
C ::::: CLEAR WORK SPACES :::::
      DO 4005 I=1,KKK
        R(I)=0.0
        X(I)=0.0
        Y(I)=0.0
      DO 4005 J=1,KKK
        RIJ(I,J)=0.0
        PHY(I,J)=0.0
      DO 4005 N=1,NNN
        DO 4005 M=1,NNN
          AA(I,N,J,M)=0.0
          BB(I,N,J,M)=0.0
          CC(I,N,J,M)=0.0
          DD(I,N,J,M)=0.0
4005
C ::::: GO TO INDEX KKK FROM KKI :::::
      GO TO (4031,40331,4033),ICLK
4031  DO 4032 I=1,KKK
      X(I)=XA(I)

```

```

      Y(I)=YA(I)
      R(I)=RA(I)
      DO 4032 J=1, KKK
      RIJ(I,J)=RAIJ(I,J)
4032  PHY(I,J)=PHYA(I,J)
      GO TO 4040
40331 X(1)=XA(1)
      Y(1)=YA(1)
      R(1)=RA(1)
      RIJ(1,1)=RAIJ(1,1)
      PHY(1,1)=PHYA(1,1)
4033  DO 4036 I=3, KKK
      IIK=I-IK
      X(I)=XA(IIK)
      Y(I)=YA(IIK)
      R(I)=RA(IIK)
      GO TO (4034,4035), IK
4034  IM1=I-1
      RIJ(I,1)=RAIJ(IM1,1)
      RIJ(1,I)=RAIJ(1,IM1)
      PHY(I,1)=PHYA(IM1,1)
      PHY(1,I)=PHYA(1,IM1)
4035  DO 4036 J=3, KKK
      JJK=J-IK
      RIJ(I,J)=RAIJ(IIK,JJK)
4036  PHY(I,J)=PHYA(IIK,JJK)
4040  CONTINUE
C ::::: FORM AA, BB, CC, DD MATRICES :::::
      GO TO (4050,4050,5010), ICHK
4050  DO 5000 I=1, IKK
      DO 5000 N=1, NNN
      GO TO (8881,8882), I
8881  MMM=N
      GO TO 8883
8882  MMM=NNN
8883  CONTINUE
      DO 5000 J=1, KKK
      IF(ICHK.EQ.1) GO TO 4051
      IF(J.EQ.2) GO TO 5000
4051  CONTINUE
      DO 5000 M=1, MMM
      GO TO (4052,7770), I
4052  CONTINUE
      IF (J-2) 4053,4053,4100
4053  IF (N-M) 4061,4054,4061
4054  IF (I-J) 4058,4055,4058
4055  AA(I,N,J,M)=N
      BB(I,N,J,M)=N
      CC(I,N,J,M)=0.0
      DD(I,N,J,M)=0.0
      GO TO 5000
4058  AA(I,N,J,M)=-N*(R(2)/R(1))**(N+1)
      BB(I,N,J,M)=-N*(R(2)/R(1))**(N+1)
      CC(I,N,J,M)=0.0
      DD(I,N,J,M)=0.0
      GO TO 5000
4061  AA(I,N,J,M)=0.0
      BB(I,N,J,M)=0.0
      CC(I,N,J,M)=0.0

```

```

DD(I,N,J,M)=0.0
GO TO 5000
4100 MM1=M-1
    NMM=N-M
    ARG11=(M-1)*PHY(1,J)
    AGG1=R(I)*R(J)/(R(I)*RIJ(1,J))
    DO 4101 MC=1,M
4101 AGG1=AGG1*RIJ(1,J)/R(J)
    CNA1=1.0
    DO 4102 MC=1,N
    CNA1=CNA1*MC
4102 AGG1=AGG1*R(J)/R(I)
    CMA1=1.0
    IF (M-1) 4103,4105,4103
4103 DO 4104 MC=1,MM1
4104 CMA1=CMA1*MC
4105 CNMMA=1.0
    IF (NMM) 4106,4108,4106
4106 DO 4107 MC=1,NMM
4107 CNMMA=CNMMA*MC
4108 AA(I,N,J,NMM+1)=-AGG1*CNA1*COS(ARG11)/(CMA1*CNMMA)
    BB(I,N,J,NMM+1)=AA(I,N,J,NMM+1)
    CC(I,N,J,NMM+1)=AGG1*CNA1*SIN(ARG11)/(CMA1*CNMMA)
    DD(I,N,J,NMM+1)=-CC(I,N,J,NMM+1)
    GO TO 5000
7770 CONTINUE
    IF(J.GT.2) GO TO 7774
    IF(N.NE.M) GO TO 7772
    IF(I.EQ.J) GO TO 7771
    IF(N.EQ.1) GO TO 7773
    AA(I,N,J,M)=N*(R(2)/R(1))**(N-1)
    BB(I,N,J,M)=N*(R(2)/R(1))**(N-1)
    CC(I,N,J,M)=0.0
    DD(I,N,J,M)=0.0
    GO TO 5000
7771 AA(I,N,J,M)=-N
    BB(I,N,J,M)=-N
    CC(I,N,J,M)=0.0
    DD(I,N,J,M)=0.0
    GO TO 5000
7772 AA(I,N,J,M)=0.0
    BB(I,N,J,M)=0.0
    CC(I,N,J,M)=0.0
    DD(I,N,J,M)=0.0
    GO TO 5000
7773 AA(I,N,J,M)=1.0
    BB(I,N,J,M)=1.0
    CC(I,N,J,M)=0.0
    DD(I,N,J,M)=0.0
    GO TO 5000
7774 IN1=N-1
    IM1=M-1
    INM1=N+M-1
    ARG1=(N+M)*PHY(I,J)
    AGG=R(I)/RIJ(I,J)*R(J)/R(I)
    DO 15051 MC=1,M
15051 AGG=AGG*(-1)**MC*R(J)/R(I)
    CNA=1.0
    IF (IN1) 15052,15054,15052

```



```

15052 DO 15053 MC=1,IN1
15053 CNA=CNA*MC
15054 CMA=1.0
      IF (IM1) 15055,15057,15055
15055 DO 15056 MC=1,IM1
15056 CMA=CMA*MC
15057 CNMA=1.0
      DO 15058 MC=1,INM1
15058 CNMA=CNMA*MC/(RIJ(I,J)/R(I))
      AA(I,N,J,M)=AGG*CNMA/CNA/CMA*COS(ARG1)
      BB(I,N,J,M)=-AA(I,N,J,M)
      CC(I,N,J,M)=AGG*CNMA/CNA/CMA*SIN(ARG1)
      DD(I,N,J,M)=CC(I,N,J,M)
5000 CONTINUE
      IF (KKK-2) 206,206,5010
5010 CONTINUE
      DO 205 I=3,KKK
      DO 205 N=1,NNN
      DO 205 J=1,KKK
      GO TO (5011,5012,5013),ICLK
5012 IF (J-2) 5011,205,5011
5013 IF (J-2) 205,205,5011
5011 CONTINUE
      DO 205 M=1,NNN
      IF (I-J) 5017,5014,5017
5014 IF (N-M) 5016,5015,5016
5015 AA(I,N,J,M)=-N
      BB(I,N,J,M)=-N
      CC(I,N,J,M)=0.0
      DD(I,N,J,M)=0.0
      GO TO 205
5016 AA(I,N,J,M)=0.0
      BB(I,N,J,M)=0.0
      CC(I,N,J,M)=0.0
      DD(I,N,J,M)=0.0
      GO TO 205
5017 IN1=N-1
      IM1=M-1
      INM1=N+M-1
      MMN=M-N
      IF (J-1) 5050,5018,5050
5018 IF (M-N) 5019,5020,5020
5019 AA(I,N,J,M)=0.0
      BB(I,N,J,M)=0.0
      CC(I,N,J,M)=0.0
      DD(I,N,J,M)=0.0
      GO TO 205
5020 ARG12=(M-N)*PHY(1,I)
      AGG2=R(1)/RIJ(1,I)
      CMA2=1.0
      DO 5021 MC=1,M
      AGG2=AGG2*RIJ(1,I)/R(1)
5021 CMA2=CMA2*MC
      CNA2=1.0
      IF (N-1) 5022,5024,5022
5022 DO 5023 MC=1,IN1
      AGG2=AGG2*R(I)/RIJ(1,I)
5023 CNA2=CNA2*MC
5024 CMMNA=1.0

```

```

      IF (MMN) 5025,5027,5025
5025 DO 5026 MC=1,MMN
5026 CMMNA=CMMNA*MC
5027 AA(I,N,J,M)=AGG2*CMA2*COS(ARG12)/(CNA2*CMMNA)
      BB(I,N,J,M)=AA(I,N,J,M)
      CC(I,N,J,M)=AGG2*CMA2*SIN(ARG12)/(CNA2*CMMNA)
      DD(I,N,J,M)=-CC(I,N,J,M)
      GO TO 205
5050 ARG1=(N+M)*PHY(I,J)
      AGG=R(I)/RIJ(I,J)*R(J)/R(I)
      DO 5051 MC=1,M
5051 AGG=AGG*(-1.)*R(J)/R(I)
      CNA=1.0
      IF (IN1) 5052,5054,5052
5052 DO 5053 MC=1,IN1
5053 CNA=CNA*MC
5054 CMA=1.0
      IF (IM1) 5055,5057,5055
5055 DO 5056 MC=1,IM1
5056 CMA=CMA*MC
5057 CNMA=1.0
      DO 5058 MC=1,INM1
5058 CNMA=CNMA*MC/(RIJ(I,J)/R(I))
      AA(I,N,J,M)=AGG*CNMA/CNA/CMA*COS(ARG1)
      BB(I,N,J,M)=-AA(I,N,J,M)
      CC(I,N,J,M)=AGG*CNMA/CNA/CMA*SIN(ARG1)
      DD(I,N,J,M)=CC(I,N,J,M)
205 CONTINUE
206 CONTINUE
      GO TO (5200,5100,5100),ICLK
5100 DO 50 N=1,NNN
      DO 50 M=1,NNN
      DO 50 I=3,KKK
      II1=I-1
      I1K=I-1K
      GO TO (11,12),IK
11 AA(II1,N,1,M)=AA(I,N,1,M)
      BB(II1,N,1,M)=BB(I,N,1,M)
      CC(II1,N,1,M)=CC(I,N,1,M)
      DD(II1,N,1,M)=DD(I,N,1,M)
12 DO 50 J=3,KKK
      GO TO (21,23),IK
21 IF (I-4) 22,23,23
22 JJ1=J-1
      EA(1,N,JJ1,M)=AA(1,N,J,M)
      BB(1,N,JJ1,M)=BB(1,N,J,M)
      CC(1,N,JJ1,M)=CC(1,N,J,M)
      DD(1,N,JJ1,M)=DD(1,N,J,M)
23 JJK=J-1K
      AA(I1K,N,JJK,M)=AA(I,N,J,M)
      BB(I1K,N,JJK,M)=BB(I,N,J,M)
      CC(I1K,N,JJK,M)=CC(I,N,J,M)
      DD(I1K,N,JJK,M)=DD(I,N,J,M)
50 CONTINUE
5200 KN=KKI*NNN
C :::: PREPARE TO SOLVE SYSTEM OF EQUATIONS FOR X-AXIS :::::
      DO 230 I=1,KKI
      DO 230 N=1,NNN
      IN=(I-1)*NNN+N

```

```

      II=IN+KN
      DO 230 J=1,KKI
      DO 230 M=1,NNN
      JM=(J-1)*NNN+M
      JJ=JM+KN
      E(IN,JM)=AA(I,N,J,M)
      E(II,JJ)=BB(I,N,J,M)
      E(IN,JJ)=CC(I,N,J,M)
      E(II,JM)=DD(I,N,J,M)
230  CONTINUE
      DO 220 I=1,KKI
      DO 220 N=1,NNN
      DO 220 L=1,KKI
      IF (N-1) 62,60,62
60    IF (I-L) 62,61,62
61    H(I,N,L)=1.0
      GO TO 220
62    H(I,N,L)=0.0
220  CONTINUE
      DO 240 I=1,KKI
      DO 240 N=1,NNN
      IN=(I-1)*NNN+N
      II=IN+KN
      DO 240 L=1,KKI
      F(IN,L)=H(I,N,L)
240  F(II,L)=0.0
      KNKN=2*KN
C ::::: SOLVE SYSTEM OF EQUATIONS :::::
      CALL CROUT(E,KNKN,F,KKI,DETERM,80)
      DO 250 I=1,KKI
      DO 250 N=1,NNN
      IN=(I-1)*NNN+N
      II=IN+KN
      DO 250 L=1,KKI
      AL(I,N,L)=F(IN,L)
      TA(I,N,L)=F(II,L)
250  CONTINUE
C ::::: PREPARE TO SOLVE SYSTEM OF EQUATIONS FOR Y-AXIS :::::
      DO 270 I=1,KKI
      DO 270 N=1,NNN
      IN=(I-1)*NNN+N
      II=IN+KN
      DO 270 L=1,KKI
      F(IN,L)=0.0
270  F(II,L)=H(I,N,L)
      DO 231 I=1,KKI
      DO 231 N=1,NNN
      IN=(I-1)*NNN+N
      II=IN+KN
      DO 231 J=1,KKI
      DO 231 M=1,NNN
      JM=(J-1)*NNN+M
      JJ=JM+KN
      E(IN,JM)=AA(I,N,J,M)
      E(II,JJ)=BB(I,N,J,M)
      E(IN,JJ)=CC(I,N,J,M)
231  E(II,JM)=DD(I,N,J,M)
C ::::: SOLVE SYSTEM OF EQUATIONS :::::
      CALL CROUT(E,KNKN,F,KKI,DETERM,80)

```

```

DO 280 I=1,KKI
DO 280 N=1,NNN
IN=(I-1)*NNN+N
II=IN+KN
DO 280 L=1,KKI
SI(I,N,L)=F(IN,L)
BE(I,N,L)=F(II,L)
280 CONTINUE
C :::: CALCULATE ADDED MASS COEFFICIENTS ::::
GO TO (6001,6002,6003),ICHK
6001 I=1
R21=RA(2)*RA(2)/(RA(1)*RA(1))
DO 600 L=1,KKI
ALP(1,L)=AL(1,1,L)+AL(2,1,L)*R21
SIG(1,L)=SI(1,1,L)+SI(2,1,L)*R21
TAU(1,L)=TA(1,1,L)+TA(2,1,L)*R21
BET(1,L)=BE(1,1,L)+BE(2,1,L)*R21
IF (KKI.LE.2) GO TO 600
DO 6000 J=3,KKI
RJI2=RA(J)*RA(J)/(RA(I)*RA(I))
ALP(1,L)=ALP(1,L)+AL(J,1,L)*RJI2
SIG(1,L)=SIG(1,L)+SI(J,1,L)*RJI2
TAU(1,L)=TAU(1,L)+TA(J,1,L)*RJI2
6000 BET(1,L)=BET(1,L)+BE(J,1,L)*RJI2
600 CONTINUE
I=2
DO 7004 L=1,KKI
ALP(2,L)=AL(1,1,L)+AL(2,1,L)
SIG(2,L)=SI(1,1,L)+SI(2,1,L)
TAU(2,L)=TA(1,1,L)+TA(2,1,L)
BET(2,L)=BE(1,1,L)+BE(2,1,L)
IF (KKI.LE.2) GO TO 7004
DO 7003 J=3,KKI
AGG=0.0
BGG=0.0
CGG=0.0
DGG=0.0
RJIJ=RA(J)/RA(IJ(2,J))
DO 7002 N=1,NNN
ARG=(N+1)*PHYA(2,J)
AG1=N*RJIJ*(COS(ARG)*AL(J,N,L)+TA(J,N,L)*SIN(ARG))
BG1=N*RJIJ*(COS(ARG)*SI(J,N,L)+BE(J,N,L)*SIN(ARG))
CG1=N*RJIJ*(SIN(ARG)*AL(J,N,L)-TA(J,N,L)*COS(ARG))
DG1=N*RJIJ*(SIN(ARG)*SI(J,N,L)-BE(J,N,L)*COS(ARG))
DO 7001 MC=1,N
AG1=-AG1*RJIJ
BG1=-BG1*RJIJ
CG1=-CG1*RJIJ
7001 DG1=-DG1*RJIJ
AGG=AGG+AG1
BGG=BGG+BG1
CGG=CGG+CG1
7002 DGG=DGG+DG1
ALP(2,L)=ALP(2,L)+AGG
SIG(2,L)=SIG(2,L)+BGG
TAU(2,L)=TAU(2,L)+CGG
7003 BET(2,L)=BET(2,L)+DGG
7004 CONTINUE
DO 605 L=1,KKI

```

```

ALP(2,L)=-ALP(2,L)
SIG(2,L)=-SIG(2,L)
TAU(2,L)=-TAU(2,L)
605 BET(2,L)=-BET(2,L)
GO TO 6003
6002 DO 700 L=1,KKI
ALP(1,L)=AL(1,1,L)
SIG(1,L)=SI(1,1,L)
TAU(1,L)=TA(1,1,L)
BET(1,L)=BE(1,1,L)
DO 700 J=2,KKI
RJ12=RA(J)*RA(J)/(RA(1)*RA(1))
ALP(1,L)=ALP(1,L)+AL(J,1,L)*RJ12
SIG(1,L)=SIG(1,L)+SI(J,1,L)*RJ12
TAU(1,L)=TAU(1,L)+TA(J,1,L)*RJ12
700 BET(1,L)=BET(1,L)+BE(J,1,L)*RJ12
6003 ISS=IKK+1
IF(KKI-ISS) 899,6004,6004
6004 CONTINUE
DO 800 I=ISS,KKI
DO 800 L=1,KKI
ALP(I,L)=AL(I,1,L)
SIG(I,L)=SI(I,1,L)
TAU(I,L)=TA(I,1,L)
BET(I,L)=BE(I,1,L)
DO 790 J=1,KKI
AGG=0.0
BGG=0.0
CGG=0.0
DGG=0.0
IF (I-J) 801,770,801
801 GO TO (802,802,805),ICLK
802 IF (J-1) 805,803,805
803 DO 750 N=1,NNN
ARG1=(N-1)*PHYA(1,I)
R1IJ=RA(1)/RAIJ(1,I)
RIJ1=RAIJ(1,I)/RA(1)
AG11=N*R1IJ*(COS(ARG1)*AL(1,N,L)+TA(1,N,L)*SIN(ARG1))
BG11=N*R1IJ*(COS(ARG1)*SI(1,N,L)+BE(1,N,L)*SIN(ARG1))
CG11=N*R1IJ*(-SIN(ARG1)*AL(1,N,L)+TA(1,N,L)*COS(ARG1))
DG11=N*R1IJ*(-SIN(ARG1)*SI(1,N,L)+BE(1,N,L)*COS(ARG1))
DO 804 MC=1,N
AG11=AG11*RIJ1
BG11=BG11*RIJ1
804 CG11=CG11*RIJ1
DG11=DG11*RIJ1
AGG=AGG+AG11
BGG=BGG+BG11
CGG=CGG+CG11
750 DGG=DGG+DG11
GO TO 770
805 RJIJ=RA(J)/RAIJ(I,J)
DO 760 N=1,NNN
ARG=(N+1)*PHYA(I,J)
AG1=N*RJIJ*(COS(ARG)*AL(J,N,L)+TA(J,N,L)*SIN(ARG))
BG1=N*RJIJ*(COS(ARG)*SI(J,N,L)+BE(J,N,L)*SIN(ARG))
CG1=N*RJIJ*(SIN(ARG)*AL(J,N,L)-TA(J,N,L)*COS(ARG))
DG1=N*RJIJ*(SIN(ARG)*SI(J,N,L)-BE(J,N,L)*COS(ARG))
DO 806 MC=1,N

```

```

      AG1=-AG1*RJIJ
      BG1=-BG1*RJIJ
      CG1=-CG1*RJIJ
806   DG1=-DG1*RJIJ
      AGG=AGG+AG1
      BGG=BGG+BG1
      CGG=CGG+CG1
760   DGG=DGG+DG1
770   CONTINUE
      ALP(I,L)=ALP(I,L)+AGG
      SIG(I,L)=SIG(I,L)+BGG
      TAU(I,L)=TAU(I,L)+CGG
790   BET(I,L)=BET(I,L)+DGG
800   CONTINUE
      DO 299 I=ISS,KKI
      DO 299 L=1,KKI
      ALP(I,L)=-ALP(I,L)
      SIG(I,L)=-SIG(I,L)
      TAU(I,L)=-TAU(I,L)
299   BET(I,L)=-BET(I,L)
899   CONTINUE
      DO 8800 I=1,KKI
      DO 8800 L=1,KKI
      ALP(I,L)=ALP(I,L)*RA(I)*RA(I)
      SIG(I,L)=SIG(I,L)*RA(I)*RA(I)
      TAU(I,L)=TAU(I,L)*RA(I)*RA(I)
8800  BET(I,L)=BET(I,L)*RA(I)*RA(I)
      DO 900 I=1,KKI
      DO 900 L=1,KKI
      RAM(I,L)=ALP(I,L)
      RAM(I,KKI+L)=SIG(I,L)
      RAM(KKI+I,L)=TAU(I,L)
900   RAM(KKI+I,KKI+L)=BET(I,L)
      DO 810 I=1,KKI
      DO 810 L=1,KKI
      RIL=4./((RA(I)+RA(L))**2)
      ALP(I,L)=ALP(I,L)*RIL
      SIG(I,L)=SIG(I,L)*RIL
      TAU(I,L)=TAU(I,L)*RIL
      BET(I,L)=BET(I,L)*RIL
      GAM(I,L)=ALP(I,L)
      GAM(I,KKI+L)=SIG(I,L)
      GAM(KKI+I,L)=TAU(I,L)
810   GAM(KKI+I,KKI+L)=BET(I,L)
      CALL TRED2(KKI2,KKI2,RAM,PADD,D,ZZ)
      CALL IMTQL2(KKI2,KKI2,PADD,D,ZZ,IER)
      RETURN
      END
C *****
C *
C *      *** SUBROUTINE CROUT ***
C *
C *****
C
C THIS PROGRAM SOLVES MATRIX EQUATION AX=B BY THE CROUT METHOD.
C
C ON INPUT:
C
C      A:      MATRIX.

```

```

C      N:      ORDER OF MATRIX A.
C      B:      COLUMN MATRIX.
C      M:      NUMBER OF COLUMN VECTOR B.
C      DETERM:  RETURN CODE, IF ZERO A IS SINGULAR.
C      NMAX:    ROW DIMENSION FOR MATRIX A AND COLUMN VECTOR B.

```

```

C      ON OUTPUT:

```

```

C      B:      SOLUTION VECTOR X STORED.

```

```

C      -----
C
C      SUBROUTINE CROUT (A,N,B,M,DETERM,NMAX)
C      REAL*8 A,B,DETERM,DOTP,V,AMAX,TEMP
C      DIMENSION A (NMAX,N) ,B (NMAX,M)
C      DIMENSION V (80)
C      DETERM=1.0D0
C      DO 1000 K=1,N
C      KP1=K+1
C      KM1=K-1
C      TEMP=0.0
C      DO 20 I=K,N
C      DO 2 L=1,K
2      V(L)=A(I,L)
C      A(I,K)=A(I,K)-DOTP(V,A(1,K),KM1)
C      IF (DABS(A(I,K)).LT.TEMP) GO TO 20
3      TEMP=DABS(A(I,K))
C      IMAX=I
20      CONTINUE
C      AMAX=A(IMAX,K)
C      IF (DETERM.EQ.0.0) RETURN
C      IF (IMAX.EQ.K) GO TO 600
C      DETERM=-DETERM
C      DO 50 J=1,M
C      TEMP=A(K,J)
C      A(K,J)=A(IMAX,J)
C      A(IMAX,J)=TEMP
50      CONTINUE
C      IF (M.LE.0) GO TO 600
C      DO 400 J=1,M
C      TEMP=B(K,J)
C      B(K,J)=B(IMAX,J)
C      B(IMAX,J)=TEMP
400      CONTINUE
600      DO 666 L=1,K
666      V(L)=A(K,L)
C      IF (K.EQ.N) GO TO 850
C      DO 700 I=KP1,N
700      A(I,K)=A(I,K)/AMAX
C      DO 800 J=KP1,N
800      A(K,J)=A(K,J)-DOTP(V,A(1,J),KM1)
850      IF (M.LE.0) GO TO 1000
C      DO 900 J=1,M
900      B(K,J)=B(K,J)-DOTP(V,B(1,J),KM1)
1000     CONTINUE
C      IF (M.LE.0) RETURN
C      DO 8000 I=1,N
C      K=N+1-I

```

```

DO 6666 L=K, N
6666 V(L)=A(K, L)
DO 7000 J=1, M
7000 B(K, J)=(B(K, J)-DOTP(V(K+1), B(K+1, J), I-1))/A(K, K)
8000 CONTINUE
RETURN
END

```

```

C *****
C *
C *
C *** FUNCTION DOTP ***
C *
C *****

```

```
C  THIS IS A MATRIX MULTIPLICATION SUBPROGRAM.
```

```

      FUNCTION DOTP(A,B,N)
      REAL*8 A,B,DOTP
      DIMENSION A(1),B(1)
      DOTP=0.0
      IF (N.EQ.0) RETURN
      DO 100 I=1,N
      DOTP=DOTP+A(I)*B(I)
      RETURN
      END
100

```

```

C      ****
C      *
C      *      *** SUBROUTINE  TRED2 ***
C      *
C      ****

```

```
C THIS SUBROUTINE IS A TRANSLATION OF THE ALGOL PROCEDURE TRED2,
C NUM. MATH. 11, 181-195 (1968) BY MARTIN, REINSCH, AND WILKINSON.
C HANDBOOK FOR AUTO. COMP., VOL.II-LINEAR ALGEBRA, 212-226 (1971).
```

```

C      THIS SUBROUTINE REDUCES A REAL SYMMETRIC MATRIX TO A
C      SYMMETRIC TRIDIAGONAL MATRIX USING AND ACCUMULATING
C      ORTHOGONAL SIMILARITY TRANSFORMATIONS.

```

C ON INPUT:

```

C      NM MUST BE SET TO THE ROW DIMENSION OF TWO-DIMENSIONAL
C      ARRAY PARAMETERS AS DECLARED IN THE CALLING PROGRAM
C      DIMENSION STATEMENT:

```

C N IS THE ORDER OF THE MATRIX:

```

C      A CONTAINS THE REAL SYMMETRIC INPUT MATRIX.  ONLY THE
C      LOWER TRIANGLE OF THE MATRIX NEED BE SUPPLIED.

```

C ON OUTPUT:

C D CONTAINS THE DIAGONAL ELEMENTS OF THE TRIDIAGONAL MATRIX:

```

C      E CONTAINS THE SUBDIAGONAL ELEMENTS OF THE TRIDIAGONAL
C      MATRIX IN ITS LAST N-1 POSITIONS.  E(1) IS SET TO ZERO:

```



```

      G=E(J)-HH*F
      E(J)=G
      DO 260 K=1,J
      Z(J,K)=Z(J,K)-F*E(K)-G*Z(I,K)
260   CONTINUE
290   D(I)=H
300   CONTINUE
320   D(1)=0.0D0
      E(1)=0.0D0
C   :::: ACCUMULATION OF TRANSFORMATION MATRICES ::::
      DO 500 I=1,N
      L=I-1
      IF(D(I).EQ.0.0D0) GO TO 380
      DO 360 J=1,L
      G=0.0D0
      DO 340 K=1,L
340   G=G+Z(I,K)*Z(K,J)
      DO 360 K=1,L
      Z(K,J)=Z(K,J)-G*Z(K,I)
360   CONTINUE
380   D(I)=Z(I,I)
      Z(I,I)=1.0D0
      IF(L.LT.1) GO TO 500
      DO 400 J=1,L
      Z(I,J)=0.0D0
      Z(J,I)=0.0D0
400   CONTINUE
500   CONTINUE
      RETURN
      END
C   *****
C   *
C   *      *** SUBROUTINE INTQL2 ***
C   *
C   *****
C
C   THIS SUBROUTINE IS A TRANSLATION OF THE ALGOL PROCEDURE INTQL2,
C   NUM. MATH. 12, 377-383 (1968) BY MARTIN AND WILKINSON,
C   AS MODIFIED IN NUM. MATH. 15, 450 (1970) BY DUBRULLE.
C   HANDBOOK FOR AUTO. COMP., VOL. II-LINEAR ALGEBRA, 227-240 (1971).
C
C   THIS SUBROUTINE FINDS THE EIGENVALUES AND EIGENVECTORS
C   OF A SYMMETRIC TRIDIAGONAL MATRIX BY THE IMPLICIT QL METHOD.
C   THE EIGENVECTORS OF A FULL SYMMETRIC MATRIX CAN ALSO
C   BE FOUND IF TRED2 HAS BEEN USED TO REDUCE THIS
C   FULL MATRIX TO TRIDIAGONAL FORM.
C
C   ON INPUT:
C
C   NM MUST BE SET TO THE ROW DIMENSION OF TWO-DIMENSIONAL
C   ARRAY PARAMETERS AS DECLARED IN THE CALLING PROGRAM
C   DIMENSION STATEMENT;
C
C   N IS THE ORDER OF THE MATRIX;
C
C   D CONTAINS THE DIAGONAL ELEMENTS OF THE INPUT MATRIX;
C
C   E CONTAINS THE SUBDIAGONAL ELEMENTS OF THE INPUT MATRIX
C   IN ITS LAST N-1 POSITIONS. E(1) IS ARBITRARY;

```

C Z CONTAINS THE ORTHOGONAL TRANSFORMATION MATRIX
 C PRODUCED IN THE REDUCTION;
 C
 C A AND Z MAY COINCIDE. IF DISTINCT, A IS UNALTERED.
 C
 C -----

```

C      SUBROUTINE TRED2(NM,N,A,D,E,Z)
C
C      INTEGER I,J,K,L,N,II,NM,JP1
C      REAL*8 A(NM,N),D(N),E(N),Z(NM,N)
C      REAL*8 F,G,H,HH,SCALE
C      REAL*8 DSQRT,DABS,DSIGN
C
C      DO 100 I=1,N
C      DO 100 J=1,I
100    Z(I,J)=A(I,J)
C      IF(N.EQ.1) GO TO 320
C      ::::: FOR I=N STEP -1 UNTIL 2 DO -- :::::
C      DO 300 II=2,N
C      I=N+2-II
C      L=I-1
C      H=0.0D0
C      SCALE=0.0D0
C      IF(L.LT.2) GO TO 130
C      ::::: SCALE ROW (ALGOL TOL THEN NOT NEEDED) :::::
C      DO 120 K=1,L
120    SCALE=SCALE+DABS(Z(I,K))
C      IF(SCALE.NE.0.0D0) GO TO 140
130    E(I)=Z(I,L)
C      GO TO 290
140    DO 150 K=1,L
C      Z(I,K)=Z(I,K)/SCALE
C      H=H+Z(I,K)*Z(I,K)
150    CONTINUE
C      F=Z(I,L)
C      G=-DSIGN(DSQRT(H),F)
C      E(I)=SCALE*G
C      H=H-F*G
C      Z(I,L)=F-G
C      F=0.0D0
C      DO 240 J=1,L
C      Z(J,I)=Z(I,J)/H
C      G=0.0D0
C      ::::: FORM ELEMENT OF A*U :::::
C      DO 180 K=1,J
180    G=G+Z(J,K)*Z(I,K)
C      JP1=J+1
C      IF(L.LT.JP1) GO TO 220
C      DO 200 K=JP1,L
200    G=G+Z(K,J)*Z(I,K)
C      ::::: FORM ELEMENT OF P :::::
220    E(J)=G/H
C      F=F+E(J)*Z(I,J)
240    CONTINUE
C      HH=F/(H+H)
C      ::::: FORM REDUCED A :::::
C      DO 260 J=1,L
C      F=Z(I,J)
  
```

```

C
C      Z CONTAINS THE TRANSFORMATION MATRIX PRODUCED IN THE
C      REDUCTION BY TRED2, IF PERFORMED. IF THE EIGENVECTORS
C      OF THE TRIDIAGONAL MATRIX ARE DESIRED, Z MUST CONTAIN
C      THE IDENTITY MATRIX.
C
C      ON OUTPUT:
C
C      D CONTAINS THE EIGENVALUES IN ASCENDING ORDER. IF AN
C      ERROR EXIT IS MADE, THE EIGENVALUES ARE CORRECT BUT
C      UNORDERED FOR INDICES 1,2,...,IERR-1;
C
C      E HAS BEEN DESTROYED;
C
C      Z CONTAINS ORTHONORMAL EIGENVECTORS OF THE SYMMETRIC
C      TRIDIAGONAL (OR FULL) MATRIX. IF AN ERROR EXIT IS MADE,
C      Z CONTAINS THE EIGENVECTORS ASSOCIATED WITH THE STORED
C      EIGENVALUES;
C
C      IERR IS SET TO
C      ZERO      FOR NORMAL RETURN,
C      J         IF THE J-TH EIGENVALUE HAS NOT BEEN
C               DETERMINED AFTER 30 ITERATIONS.
C
C      -----
C
C      SUBROUTINE IMTQL2(NM,N,D,E,Z,IERR)
C
C      INTEGER I,J,K,L,M,N,II,NM,MML,IERR
C      REAL*8 D(N),E(N),Z(NM,N)
C      REAL*8 B,C,F,G,H,P,R,S,MACHEP
C      REAL*8 DSQRT,DABS,DSIGN
C      :::::::::: MACHEP IS A MACHINE DEPENDENT PARAMETER SPECIFYING
C      THE RELATIVE PRECISION OF FLOATING POINT ARITHMETIC.
C      MACHEP = 16.0D0**(-13) FOR LONG FORM ARITHMETIC
C      ON S360 ::::::::::
C      DATA MACHEP/Z3#100000000000000/
C
C      IERR=0
C      IF(N.EQ.1) GO TO 1001
C      DO 100 I=2,N
100    E(I-1)=E(I)
C      E(N)=0.0D0
C      DO 240 L=1,N
C      J=0
C      :::::::::: LOOK FOR SMALL SUB-DIAGONAL ELEMENT ::::::
105    DO 110 M=L,N
C      IF(M.EQ.N) GO TO 120
C      IF(DABS(E(M)).LE.MACHEP*(DABS(D(M))+DABS(D(M+1)))) GO TO 120
110    CONTINUE
120    P=D(L)
C      IF(M.EQ.L) GO TO 240
C      IF(J.EQ.30) GO TO 1000
C      J=J+1
C      :::::::::: FORM SHIFT ::::::
C      G=(D(L+1)-P)/(2.0D0*E(L))
C      R=DSQRT(G*G+1.0D0)
C      G=D(M)-P+E(L)/(G+DSIGN(R,G))
C      S=1.0D0

```

```

      C=1.0D0
      P=0.0D0
      MML=M-L
C  ::::: FOR I=M-1 STEP -1 UNTIL L DO -- :::::
      DO 200 II=1,MML
      I=M-II
      F=S*E(I)
      B=C*E(I)
      IF (DABS(F).LT.DABS(G)) GO TO 150
      C=G/F
      R=DSQRT(C*C+1.0D0)
      E(I+1)=F*R
      S=1.0D0/R
      C=C*S
      GO TO 160
150   S=F/G
      R=DSQRT(S*S+1.0D0)
      E(I+1)=G*R
      C=1.0D0/R
      S=S*C
160   G=D(I+1)-P
      R=(D(I)-G)*S+2.0D0*C*B
      P=S*R
      D(I+1)=G+P
      G=C*R-B
C  ::::: FORM VECTOR :::::
      DO 180 K=1,N
      F=Z(K,I+1)
      Z(K,I+1)=S*Z(K,I)+C*F
      Z(K,I)=C*Z(K,I)-S*F
180   CONTINUE
200   CONTINUE
      D(L)=D(L)-P
      E(L)=G
      E(M)=0.0D0
      GO TO 105
240   CONTINUE
C  ::::: ORDER EIGENVALUES AND EIGENVECTORS :::::
      DO 300 II=2,N
      I=II-1
      K=I
      P=D(I)
      DO 260 J=II,N
      IF (D(J).GE.P) GO TO 260
      K=J
      P=D(J)
260   CONTINUE
      IF (K.EQ.I) GO TO 300
      D(K)=D(I)
      D(I)=P
      DO 280 J=1,N
      P=Z(J,I)
      Z(J,I)=Z(J,K)
      Z(J,K)=P
280   CONTINUE
300   CONTINUE
      GO TO 1001
C  ::::: SET ERROR -- NO CONVERGENCE TO AN EIGENVALUE
C      AFTER 30 ITERATIONS :::::

1000  IERR=L
1001  RETURN
      END

```

Distribution for ANL-85-51Internal:

C. E. Till	S. K. Zussman
R. S. Zeno	R. A. Valentin
P. R. Huebotter	S. H. Fistedis
M. W. Wambsganss (5)	R. A. Lewis
S. S. Chen (25)	Y. I. Chang
H. Halle	D. J. Malloy
B. J. Hsieh	R. W. Seidensticker
J. A. Jendrzeczyk	ANL Patent Dept.
T. M. Mulcahy	ANL Contract File
H. H. Chung	ANL Libraries (2)
W. P. Lawrence	TIS Files (6)

External:

DOE-TIC (30)
 Manager, Chicago Operations Office, DOE
 Director, Technology Management Div., DOE-CH
 E. Gallagher, DOE-CH
 M. K. Au-Yang, B&W
 E. B. Baumeister, Rocketdyne Div.
 C. C. Bigelow, DOE/Nuclear Energy
 A. S. Cakmak, Princeton Univ.
 C. C. Chamis, LeRC/NASA
 C. A. Chandley, TVA
 S. Chandra, Northeast Utilities
 P. Y. Chen, NRC
 J. M. Chenoweth, HTRI
 W. K. Dahm, MSFC/NASA
 E. H. Dowell, Duke Univ.
 W. Edelstein, IIT
 F. L. Eisinger, FWEC
 R. J. Fritz, GE/KAPL
 M. J. Gabler, Rocketdyne Div.
 E. L. Gluekler, GE
 O. K. Goetz, MSFC/NASA
 N. Grossman, DOE/Nuclear Energy
 J. E. Haas, LeRC/NASA
 R. J. Hansen, NRL
 W. J. Heilker, CE
 R. A. Johnson, Rocketdyne Div.
 E. Kiss, General Electric Co.
 O. P. Manley, DOE/BES
 E. Moody, Rocketdyne Div.
 R. J. Neuhold, DOE/Nuclear Energy
 E. E. Olich, GE
 P. R. Pluta, GE
 L. Povinelli, LeRC/NASA
 J. Rajan, NRC
 M. M. Reischmann, ONR
 E. L. Reiss, Northwestern Univ.

B. J. Rock, DOE/Nuclear Energy
J. B. Sandifer, B&W/ARC
M. Sax, W-Bettis
J. Schwab, LeRC/NASA
K. P. Singh, Joseph Oat Co.
N. R. Singleton, W
N. Sondergaard, DTNSRDC
D. Steininger, EPRI
H. Struck, MSFC/NASA
R. Volin, Shock & Vibration Center
G. H. Weidenhamer, NRC/RES
F. R. Wiltshire, GE
Components Technology Division Review Committee:
P. Alexander, Flopetrol Johnston Schlumberger, Houston
D. J. Anthony, General Electric Co., San Jose
A. A. Bishop, U. Pittsburgh
B. A. Boley, Northwestern U.
R. N. Christensen, Ohio State U.
R. Cohen, Purdue U.
R. E. Scholl, URS, San Francisco, CA
J. Weisman, U. Cincinnati